

High-Throughput Methods For Reaction Development Using The Mosquito[®] Liquid Handling Robot

David James Battersby

St. Catharine's College
University of Cambridge



This dissertation is submitted for the degree of Doctor of Philosophy

September 2018

Department of Chemistry

University of Cambridge

Lensfield Road

Cambridge

CB2 1EW

United Kingdom

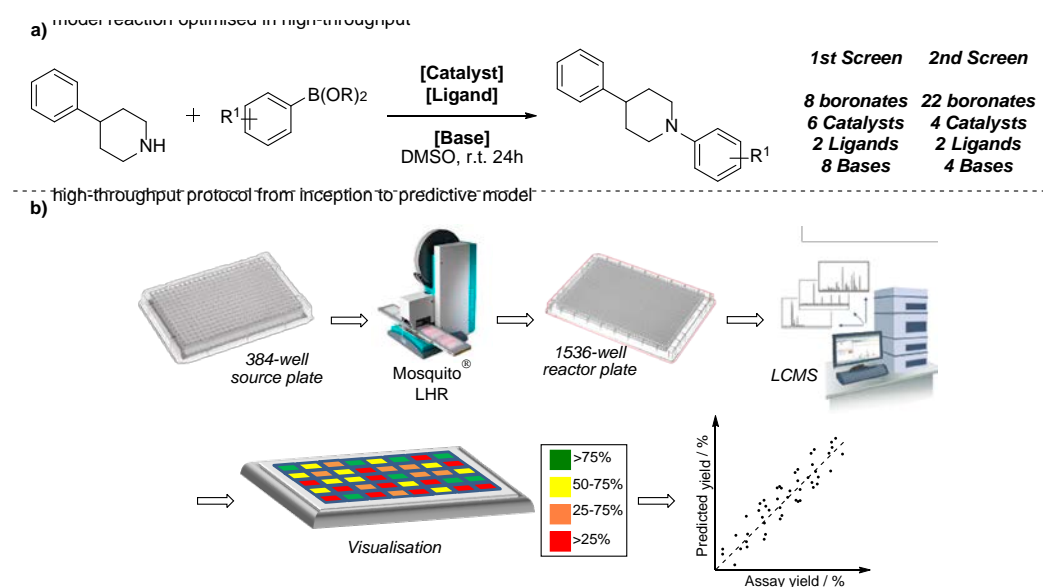
*This page has been
intentionally left blank*

High-Throughput Methods For Reaction Development Using The Mosquito[®] Liquid Handling Robot

David Battersby

High-throughput technologies have dramatically advanced processes such as drug screening and protein crystallisation. Application of related high-throughput experimentation practices have the potential to revolutionise chemical synthesis. This thesis describes the standardisation and implementation of high-throughput protocols in the Gaunt group using the Mosquito[®] liquid-handling robot.

An automated high-throughput protocol was established for quantitative data generation. The Chan-Lam reaction of an amine and aryl boronates was used as an initial proof-of-concept reaction to standardise the high-throughput protocol. All parts of the protocol were optimised including the creation of an Excel spreadsheet and Mosquito[®] dosing protocols. Quantitative data was achieved using high-throughput LCMS analysis with internal standards and calibration curves. Data were tested by statistical methods integrated into the Excel Spreadsheet.



Using the standardised high-throughput protocol, reaction conditions for the Chan-Lam were assessed using multi-parallel arrays. A total of 30 boronic esters were screened against eight bases, six copper catalysts and two ligands, totaling 5,888 reactions. All reaction components were parameterised using experimental and computational descriptors to generate a predictive model, in collaboration with computational chemists. To rapidly triage reaction conditions, high-throughput TLC was developed. Three transformations were investigated using this technique, reducing the total analysis time to less than 2 hours for 1536-reactions.

This study demonstrates the potential of automated equipment in reaction optimisation and discovery.

Declaration

This thesis is submitted in partial fulfilment of the requirements for the degree of Doctor of Philosophy. It describes the work carried out in the Department of the Chemistry from October 2014 to April 2018. This dissertation is the result of my own work and includes nothing which is the outcome of work done in collaboration except where specifically indicated in the text.

David James Battersby

Statement of Length

This thesis does not exceed the word limit of 60 000 as set by the Degree Committee for the faculty of physics and Chemistry

David James Battersby

Dedicated to my Grandad - Alan Rushton Battersby

1925 - 2018

“Tight lines”

i. Acknowledgements

To start, I would like to thank Prof. Matthew Gaunt. Firstly, for giving me the opportunity to work in your group and work on a very new area. Secondly, thank you for giving me belief in my own skills and understanding as well as putting your faith in this new area of research. Thank you for always having an open door and giving me time out of your very busy schedule to mentor me and keep me focused on the bigger picture. Thank you for all your effort in getting grants and funding for the lab so we can pursue cutting edge research without hesitation or limits. I hope going forward we can maintain a strong working relationship.

Secondly, I would like to thank Dr Scarlett Walton, Dr Jaime Cabrera-Pardo, Dr Amanda Kennedy and Antonio Pedrina-McCarthy for taking time out of their work schedules to proofread this thesis in part or entirety. Without your meticulousness and diligence this thesis wouldn't have been half what it is now.

I would like to express my gratitude to TTPLabTech for kindly donating the Mosquito[®] liquid handling robot to the Gaunt group. Thank you Dr Gillian Lewis and Dr Greta Miksaite for giving me 4.5mm and 9.0mm pipettes so I could complete this research.

Thanks to the technicians Nic Davies, Matt Pond and Naomi Campbell for the endless support. Thanks Duncan Howe, Andrew Mason and Peter Grice, for all their help with my NMR problems. I would like to thank Dr Atty Rullay at Shimadzu. You put me into contact with many mass spectrometry experts to help me problem solve and give me new ideas.

Over my 4 years in the Gaunt group I have made many great friends whom I will keep close to my heart. Thanks to all the group for putting up with my bad habits in the lab as well as my singing and bad music taste. Dr Manuel Nappi thank you for teaching me what it takes to be a good synthetic chemist and for showing me the more colourful side of the Italian language. Dr Jaime Cabrera-Pardo, I was so sad to see you leave Cambridge and I miss you dearly. I will be visiting you in Chile at some point and there will also be a sofa at mine for you to crash on when you return to the UK. Aaron Trowbridge, words cannot describe the fun that we have had over the past 4 years. The infamous "rage-quit" prank, freezing my stir bars, food poisoning and Burrito-joggers are only a few of the great times we have shared together. You have a contagious enthusiasm for chemistry and are always full of ideas, both of which will serve you well when you become an academic yourself.

Thanks to all the friends I have made in Catz too. "Top-floor-crew" was a great initiation into Cambridge and, because of this strong friendship group I can look back on my time here as

some of the greatest of my life so far. Thank you to all the fellows in Catz for making my time here even more memorable.

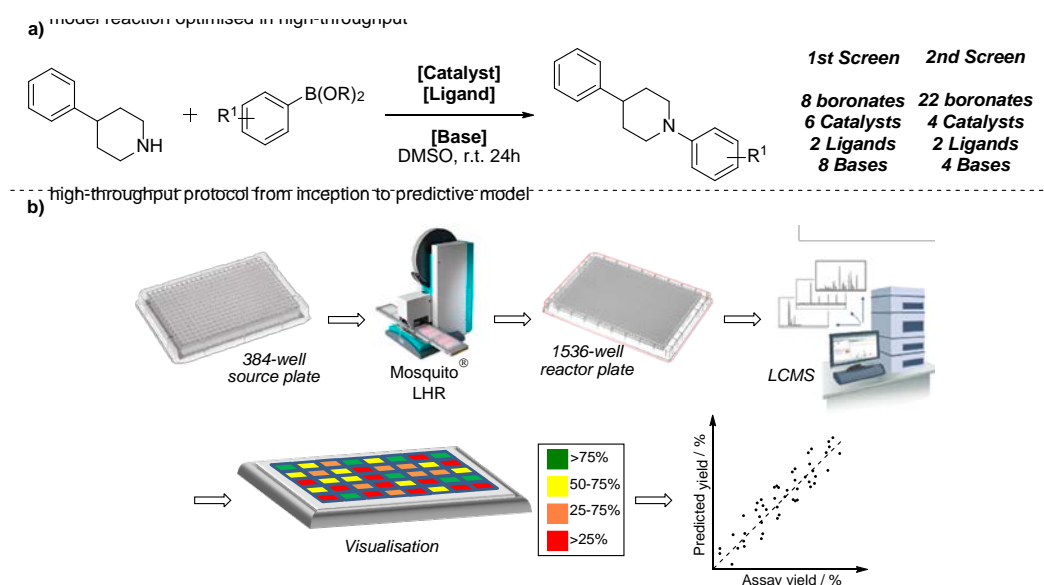
I would like to thank my family for their continuously and never-ending support. Dad and Mum, I know the last 4 years have been tough and, now you're out of the woods, keep aiming high and taking small steps (literally) on the road to recovery. Amanda Kennedy thank you for keeping me sane through my Ph.D. and time in Cambridge. You have been the best support I could have asked for over the last four years. The trips to Sweden have also been a welcome escape from the Cambridge-bubble.

Grandad, I miss you immensely. Every day I wake up in Barrow Road hoping to hear your voice or see you coming down the hallway to say "hello". You were the inspiration for me taking up chemistry: from the first chemical reaction in the kitchen to your interest in my education, culminating in a Ph.D. in chemistry in the same college. Although the chemistry I have researched was atypical in your opinion, I hope that I have done you proud.

ii. Abstract

High-throughput technologies have dramatically advanced processes such as drug screening and protein crystallisation. Application of related high-throughput experimentation practices have the potential to revolutionise chemical synthesis. This thesis describes the standardisation and implementation of high-throughput protocols in the Gaunt group using the Mosquito[®] liquid-handling robot.

An automated high-throughput protocol was established for quantitative data generation. The Chan-Lam reaction of an amine and aryl boronates was used as an initial proof-of-concept reaction to standardise the high-throughput protocol. All parts of the protocol were optimised including the creation of an Excel spreadsheet and Mosquito[®] dosing protocols. Quantitative data was achieved using high-throughput LCMS analysis with internal standards and calibration curves. Data were tested by statistical methods integrated into the Excel Spreadsheet.



Using the standardised high-throughput protocol, reaction conditions for the Chan-Lam were assessed using multi-parallel arrays. A total of 30 boronic esters were screened against eight bases, six copper catalysts and two ligands, totaling 5,888 reactions. All reaction components were parameterised using experimental and computational descriptors to generate a predictive model, in collaboration with computational chemists. To rapidly triage reaction conditions, high-throughput TLC was developed. Three transformations were investigated using this technique, reducing the total analysis time to less than 2 hours for 1536-reactions.

This study demonstrates the potential of automated equipment in reaction optimisation and discovery.

iii. Abbreviations

μL – Microlitres
2-MeTHF – 2-Methyltetrahydrofuran
 \AA – Angstrom
a.u. – Arbitrary Units
Abs - Absorption
Ac – Acetyl
Acac – Acetylacetone
ACN - Acetonitrile
ADH – Alcohol Dehydrogenase
Aliq. ERR – Aliquot Error
APCI – Atmospheric Pressure Chemical Ionisation
API – Active Pharmaceutical Ingredient
Ar – Unspecified Aromatic group
ASAP – Atmospheric Solids Analysis Probe
AY – Assay Yield
b.p. – Boiling Point
BINOL – 1,1'-Bi-2-naphthol
Bn – Benzyl
Boc – *tert*-Butyloxycarbonyl
BSA – Bovine Serum Albumin
BTMG – 2-*tert*-Butyl-1,1,3,3-tetramethylguanidine (Barton's Base)
CAS – Chemical Abstract Service Number
Cat. No. – Catalogue Number
BTTP – Phosphazene base *tert*-Butylimino-tri(pyrrolidino)phosphorane
 cm^{-1} – Wavenumber
COC – Cyclic Olefin Co-polymer
cod – Cyclooctadiene
COSY – Homonuclear Correlation Spectroscopy
CPME – Cyclopentyl Methyl Ether
CuAAC – Copper-Catalysed Azide-Alkyne Cycloaddition
CuSAC – Copper-Catalysed Sydnone-Alkyne Cycloaddition
CV – Coefficient of Variance
d.r. – Diastereomeric Ratio
DABCO – 1,4-Diazabicyclo[2,2,2]octane
dba - Dibenzylideneacetone
DBU – 1,8-Diazabicyclo(5.4.0)undec-7-ene
DCE – 1,1,2,2-Tetrachloroethane
DEPT – Distortionless Enhancement By Polarisation Transfer
DFT – Density-Functional Theory
DIEA - *N,N*-Diisopropylethylamine
DMF – *N,N*-Dimethylformamide
DMSO – Dimethylsulfoxide
DNA – Deoxyribose nucleic acid
DoE – Design of Experiment
dppb - 1,4-Bis(diphenylphosphino)butane
DUIS – Dual Ionisation Source
e.e. – Enantiomeric Excess
E:Z : Entgegen:Zusammen Alkene Isomer Ratio
ELISA – Enzyme-linked Immunosorbent Assay
equiv. – Equivalent

ESI – Electrospray Ionisation
 Et – Ethyl group
 FID – Flame Ionisation Detector
 FRET – Förster resonance energy transfer
 FW – Formula Weight
 GC – Gas Chromatography
 GC-FID – Gas Chromatography tandem Flame Ionisation Detector
 GCMS – Gas Chromatography tandem Mass Spectrometry
 GDP – Gross Domestic Product
 h – Hour
 hERG – Human Ether-à-go-go-Related Gene
 HMBC – Heteronuclear Multiple Bond Correlation
 HOMO – Highest Occupied Molecular Orbital
 HPLC – High-Performance Liquid Chromatography
 HRMS – High-Resolution Mass Spectrometry
 HSQC – Heteronuclear Single Quantum Coherence
 HT – High-throughput
 HTS – High-throughput Screening
 HT-TLC – High-throughput Thin Layer Chromatography
 IC₅₀ – Half Maximal Inhibitory Concentration
 INT – Intermediate
 IS – Internal Standard
 ISES – In-situ Enzymatic Screening
J – Coupling Constant
 LC – Liquid Chromatography
 LCMS – Liquid Chromatography tandem single quadrupolar Mass Spectrometry
 LCMS-MS – Liquid Chromatography tandem triple quadrupolar Mass Spectrometry
 LED – Light emitting diode
 LHR – Liquid Handling Robot
 LiHMDS – Lithium Bis(trimethylsilyl)amide
 LogP – Octanol:Water partition coefficient
 LUMO – Lowest Unoccupied Molecular Orbital
 m.p. – Melting Point
 mAb – Monoclonal Antibody
 MAD – Median Absolute Deviation
 MALDI – Matrix Assisted Laser Desorption/Ionisation
 MALDI-TOF – Matrix Assisted Laser Desorption/Ionisation tandem time-of-flight mass spectrometry
 Me – Methyl group
 MHz – Megahertz
 mins – Minutes
 MISER – Multiple Injections in a single experimental run
 mL – Millilitre
 mmol – Millimole
 MS – Mass Spectrometry
 MSD – Merck Sharp and Dohme
 MTBD – 1,3,4,6,7,8-Hexahydro-1-methyl-2H-pyrimido[1,2-a]pyrimidine
 MTP – Microtitre plate
 NAD – Nicotinamide adenine dinucleotide
 NADH – Reduced Nicotinamide Adenine Dinucleotide
 NHC – *N*-heterocyclic Carbene
 nL – Nanolitre

NMP – *N*-Methyl-2-pyrrolidone
NMR – Nuclear Magnetic Resonance
NSI – Nanospray Ionisation
OTIPS – Oxygen protected with triisopropylsilane group
PDA – Photodiode Array
Ph – Unsubstituted Phenyl Ring
PhMe - Toluene
 pK_a – Logarithm of Acid Dissociation Constant
PMDTA - *N,N,N',N'',N'''*-Pentamethyldiethylenetriamine
PMP – 4-Methoxyphenyl
PN – Product Number
ppm – Parts-per-million
PreCat – Pre-catalyst
PS – Proton Sponge
QLCMS – Quantitative liquid chromatography tandem mass spectrometry
R – Unspecified Functional Group
RV – Range Variance
SAMDI – Self-Assembled Monolayers for Desorption/Ionisation
SFC – Supercritical Fluid Chromatography
SIM – Selective Ion Monitoring
TFA – Trifluoromethyl acetic acid
TfOH – Triflic Acid
THF - Tetrahydrofuran
TIC – Total Ion Count
TLC – Thin Layer Chromatography
TMU – Tetramethylurea
UPLC – Ultra-performance Liquid Chromatography
UPLCMS – Ultra-performance Liquid Chromatography tandem single quadrupolar Mass Spectrometry
UPLCMS-MS – Ultra-performance Liquid Chromatography tandem triple quadrupolar Mass Spectrometry
UV – Ultra-violet
UV/Vis – Ultra-violet/visible
v/v – Volume by volume
vol - Volume
w/w – Weight by Weight
X – Unspecified Heteroatom
Y – Unspecified Heteroatom

iv. Contents

Chapter 1: Introduction	1
1.1. Evolution of Synthetic Chemistry	1
1.2. Technological Advances in Synthetic Chemistry	2
1.2.1. Flow Chemistry	2
1.3. Miniaturisation in Synthetic Chemistry	4
1.4. High-Throughput Analysis Techniques	7
1.4.1. Imaging Assays	7
1.4.2. Biochemical Assays	11
1.4.3. Direct Mass-Spectrometry	18
1.4.4. Chromatographic Coupled UV/Vis Assaying	23
1.4.5. Chromatographic Coupled Mass Spectrometry	30
1.5. Conclusion and Outlook	39
1.6. Aim of Research	40
Chapter 2: High-Throughput Protocol Standardisation	41
2.1. Introduction	41
2.2. How the Mosquito [®] Works	44
2.3. Reaction Setup on Mosquito [®]	46
2.4. Dosing the reactor plate	54
2.5. High-Throughput Experimentation using Mosquito [®]	57
2.5.1. 384-Well Reactor Plates	57
2.5.2. 1536-Well Reactor Plates	59
2.6. High-Throughput Analysis by LCMS	61
2.6.1. Early LCMS Optimisation for High-Throughput Analysis	64
2.6.2. Removal of Ion-Suppression	66
2.6.3. Selection of Internal Standard	68
2.6.4. Effects of DMSO	72
2.6.5. LCMS Conditioning	77

2.7.	Calibration Curves for Quantification of Yields.....	80
2.8.	Quality Control, Data Visualisation and Validation.....	84
2.9.	Summary.....	88
Chapter 3:	High-throughput experimentation of the Chan-Lam reaction to model reactivity	
	89	
3.1.	Introduction.....	89
3.1.1.	Application of Machine Learning in Synthetic Chemistry.....	89
3.2.	Parameter Screening of the Chan-Lam Reaction Using QLCMS	92
3.2.1.	Initial Screening – 8 boronic esters	92
3.2.2.	Substrate Scope Screening for Library Diversification.....	102
3.2.3.	Summary of High-Throughput Data	113
3.3.	Computational Modelling of the Chan-Lam Reaction	114
3.3.1.	Reactant Parameterisation	114
3.3.2.	Construction of Computational Model.....	116
3.4.	Summary of Computational Model	121
Chapter 4:	Reaction Discovery Using the High-Throughput Protocol	122
4.1.	Introduction.....	122
4.2.	Development of High-Throughput Thin Layer Chromatography for Reaction Triage	
	123	
4.3.	Reaction Discovery using HT-TLC.....	124
4.3.1.	Palladium-Catalysed Miyaura borylation.....	124
4.3.2.	Cobalt-Catalysed Borylation	126
4.3.3.	Silver-Decarboxylation Minisci-Coupling	129
4.4.	Summary.....	130
Chapter 5:	Conclusions and Future Work.....	132
Chapter 6:	References	137
Chapter 7:	Chan-Lam Experimental.....	143
7.1.	General Considerations.....	143
7.2.	General Procedures	146

7.2.1.	Nanoscale General Procedures.....	146
7.2.2.	Milliscale General Procedures	149
7.3.	Three Variable Optimisation of the Chan-Lam Reaction. 96 to 384-well plate	150
7.4.	Four Variable Optimisation of the Chan-Lam Reaction. 384- to 1536-well plate..	158
7.5.	High-Throughput Quantitative Analysis of Chan-Lam Reaction	183
7.6.	High-Throughput Substrate Scope	209
7.7.	Commercial Boronic Ester Experimental Parameterisation.....	250
7.8.	Synthesised Boronic Esters and Parameterisation.....	254
7.9.	Chan-Lam Product Characterisation	266
Chapter 8:	Reaction Discovery Experimental	282
8.1.	Palladium Borylation.....	283
8.2.	Cobalt Borylation	289
8.3.	Silver-Decarboxylation Minisci-Coupling.....	295

Chapter 1: Introduction

1.1. Evolution of Synthetic Chemistry

Synthetic chemistry is responsible for the invention, creation and development of many pharmaceutical compounds,¹⁻³ agrochemical agents⁴⁻⁶ and petrochemical supplies.⁷ In the 1950s, many of the early drug pharmaceutical leads relied upon the isolation of natural products and secondary metabolites.⁸ Today, their subsequent synthesis and derivatisation have produced thousands of active pharmaceutical ingredients (APIs), many of these are still available to this day.^{9,10} Even though the synthetic chemist's toolbox of transformations has expanded, drug candidate synthesis remains a major bottleneck for drug discovery projects.⁹

Linear batch optimisation, a one-variable-at-a-time process, is the most commonly used optimisation protocol in both drug discovery and academic labs.¹¹ Each parameter of a reaction is independently assessed to establish an optimal set of reaction conditions. The iterative process is the standout protocol used in synthetic chemistry and its impact cannot be underestimated. Critically, the optimisation protocol suffers from the following limitations. Firstly, the entire process can take months or years to complete. Secondly, screening one-variable-at-a-time can return high yielding conditions for the model substrate used but lower yields for the scope. Lastly, multiple grams of material or precious metal catalysts are utilised that could be used in other optimisation protocols.

Over the last 20 years, technology has improved at an incredible rate to the point where computers and automated equipment are now commonplace in laboratories.¹² While synthetic chemistry has been slow to adapt to new technology, biochemistry and life sciences have leveraged automated liquid handling robotics to complete daily routine laboratory tasks.^{13,14} High-throughput compound screening in pharmaceutical companies uses automated machinery to rapidly assess new therapeutic targets.^{15,16} Automated serial dilution and protein crystallisation experiments in biochemical laboratories are accurate and less prone to human error.¹⁷

The integration of automated robotics and computerised data capture is paving the way for a new approach to reaction discovery and optimisation. The use of automated systems can drastically improve throughput and accuracy by performing miniaturised reactions on a micro/nano molar scale. This concept not only increases efficiency of reaction optimisation, but also reduces chemical waste and minimises error.^{18,19} The application of robotics in synthesis would allow chemists to fully assess all reaction parameters simultaneously, generating vast amounts of data.²⁰

Although life sciences have benefitted greatly from the application of automated machinery, the area of chemical sciences still rely on traditional methods that were developed as early as the beginning of the 20th century. During this time new and improved analytical techniques have been developed, for example: gas chromatography (GC), liquid chromatography (LC) and nuclear magnetic resonance spectroscopy (NMR). Only recently has automated machinery been used to successfully facilitate and automate reaction discovery and optimisation.^{21,22}

1.2. Technological Advances in Synthetic Chemistry

1.2.1. Flow Chemistry

Although the field of flow chemistry is outside the scope of this document, its impact as a technological advancement in synthetic chemistry must not be overlooked. Flow chemistry, the synthesis or manufacturing of compounds in continuous flow through small diameter tubes, has received significant attention in both academia and industry over the last decade.²³ A reaction in flow can be subjected to different reaction conditions, for example, heating and cooling. As the reaction proceeds through the tubes, the product can be collected in a flask after a set time, known as the “residence-time” (Figure 1). Flow chemistry offers many benefits for synthetic chemical transformations such as fast reactant mixing, simple flow-parameter optimisation, improved control of exotherms, as well as safe containment of dangerous chemicals.²³

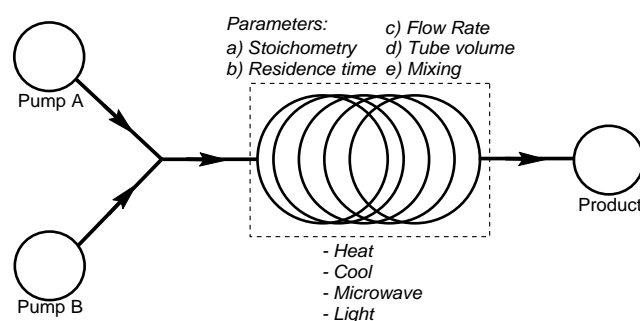


Figure 1: Flow chemistry reactor setup. Different overall reaction parameters can be tuned to give the best overall yield.

Flow chemistry was first used in synthesis to automate the preparation of key synthetic intermediates in the production of drug targets in the early 2000s.^{24,25} Since then, more advanced synthetic techniques have been adapted to flow chemistry protocols in the preparation of APIs,^{26,27} natural products²⁸ and other fine chemical intermediates.^{29,30} Reactions using highly reactive Grignard reagents³¹ and organolithium^{32–35} species have been adapted for flow chemistry reaction as either a single step or over a multi-step synthesis. Along with these advancements, new machinery has been created to enable biphasic gas reactions such as hydrogenation, ozonolysis and carboxylations.³⁶

Due to flow chemistry's versatility for synthesis, the field has seen little development for reaction optimisation. However, in 2018 Pfizer reported a flow-chemistry based platform for the optimisation of a Suzuki-Miyaura coupling of heterocyclic compounds (Figure 2).³⁷ The setup included a three HPLC pump format in combination with a HPLC autosampler to inject different reagent stock solutions into the flow system. Two UPLC-MS machines were set up in parallel to maximise analysis, so that whilst one sample was running, the second could be prepared for the next sample. This setup analysed over 5000 different nanoscale reaction conditions in 24 hours. Each reaction was performed in a total of 4 μL of solvent and each different set of conditions was segmented in 45 second intervals, preventing reaction cross-contamination.

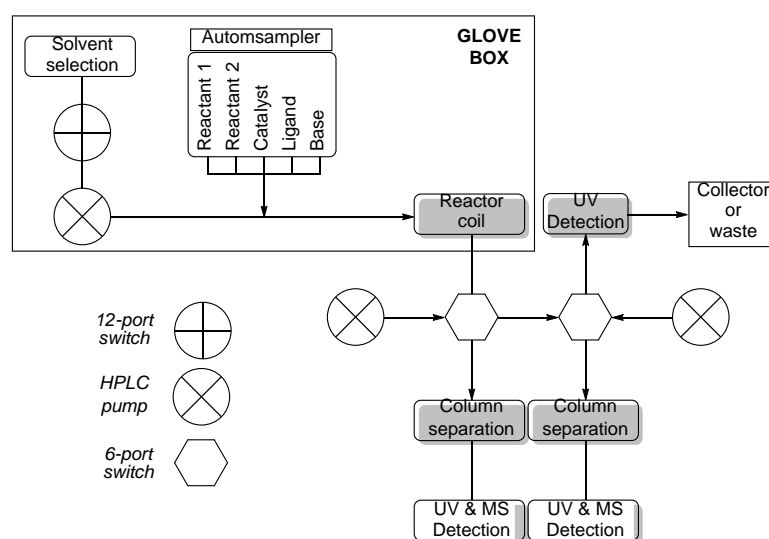
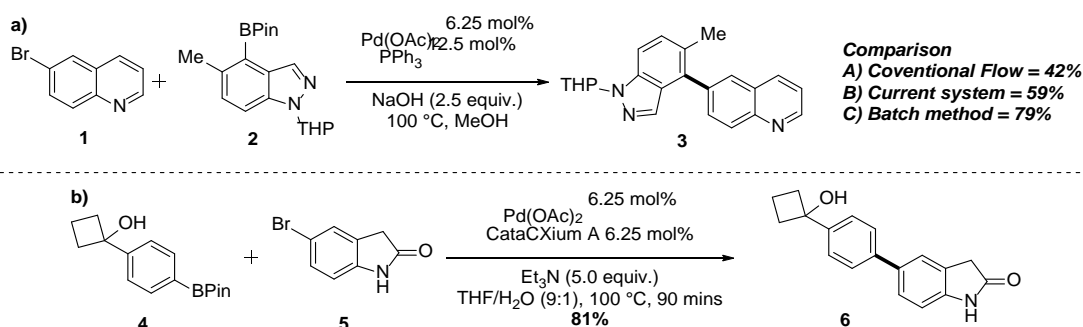


Figure 2: Pfizer flow chemistry for reaction optimisation of Suzuki-Miyaura coupling. a) Flow diagram for optimisation.

Semi-quantitative data was obtained by integration of product peaks from UV-chromatogram. A total of 5760 different reaction conditions were assessed using this strategy, testing eleven substrates against twelve ligands (including a control), eight organic and inorganic bases (including a control) and four solvents mixtures. The authors reported good correlation between the nanoscale reactions in flow reactors (59%) and conventional batch scale (79%) (Figure 2a) as well as the millimole scale reaction of **4** and **5**, taken as an initial hit from the nanoscale reaction flow-optimisation returning **6** in 81% isolated yield (Figure 2b).



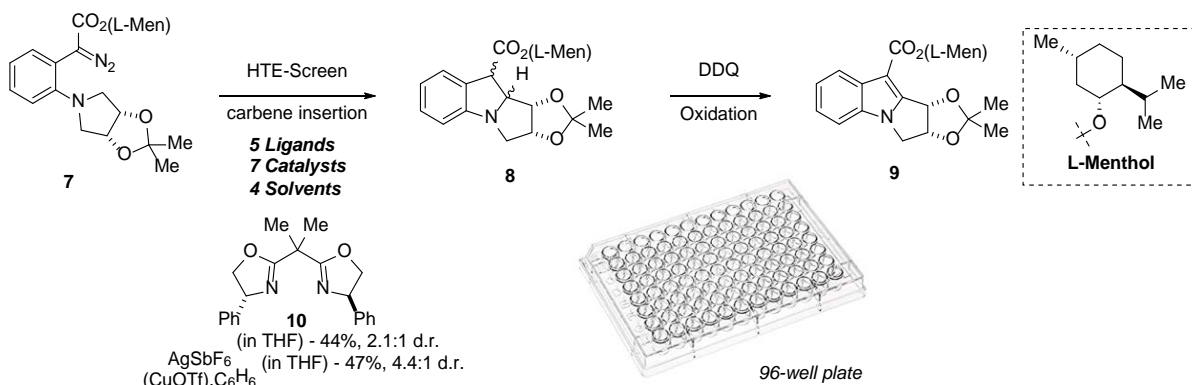
Scheme 1: Comparison of the current system to previous flow work and batch scale up. Example of reaction optimised using a flow reactor and scaled to 0.41 mmol.

Although flow chemistry has been widely applied in industry and academia, there are several disadvantages that need to be considered before adapting a transformation from batch to flow or visa-versa.³⁸ Flow chemistry requires dedicated equipment such as pumps, PEEK tubing and heaters, therefore changing reagents and reaction conditions becomes time-consuming. Additionally, whilst microfluidic mixing is beneficial in flow, correlation of these observed yields on a macro-scale is sometimes unachievable.

1.3. Miniaturisation in Synthetic Chemistry

High-throughput protocols in synthetic chemistry saw a surge in interest since Merrifield won the Nobel Prize in 1984 for solid supported and peptide synthesis.³⁹ Buoyed by the promise of rapid drug discovery in a matter of weeks, industry heavily invested in combinatorial synthesis to solve a diminishing drug pipeline.⁴⁰ Data deconvolution from thousands of unique compounds, all within the same assay, was time-consuming and fundamentally limited the expedient application of this technique. Although this previous attempt at quickening chemical synthesis has retreated from the limelight of pharmaceutical and academic chemistry, the technology that developed alongside it has remained and evolved.⁴¹ Liquid handling robotics developed for HTS are used for a myriad of processes: nanolitre liquid handling, dosing of complex biological assays, as well as cell incubation using a totally automated workflow.⁴²

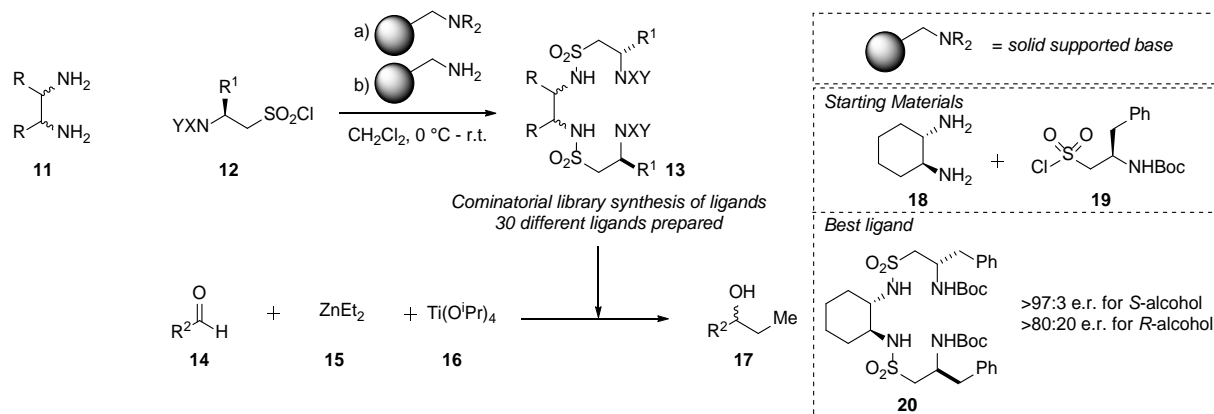
The application of miniaturised techniques in synthetic chemistry was first reported by in 1996 by Burgess, who described a multi-variate screening platform investigating a C–H insertion reaction of different metal carbenes (Scheme 2).⁴³ Reactions were screened on a 10 mg scale in 100 μ L of solvent in 96-well microtiter plates, screening seven metal catalysts against five ligands in four different solvents. Using HPLC-UV spectroscopy and naphthalene as an internal standard, conditions were found within one week to furnish **9** in 44% and 2:1 d.r. when using silver(I) hexafluoroantimonate and BOX-ligand **10**. An improved yield and d.r. was also found when copper(I) triflate.benzene complex was used with the same ligand.



Scheme 2: Metal carbene cyclisation furnishing dihydropyrroloindole **9**. Screening seven different metal catalysts against dive nitrogen-based ligands and four solvents.

Shortly after this seminal publication, Gennari proposed a parallel ligand synthesis strategy to identify novel ligand and catalyst combinations for Lewis-acid **16** assisted asymmetric addition of diethylzinc **15** to aldehydes **14** (Scheme 3).⁴⁴ A combinatorial synthesis of 30 different ligands were prepared in discrete wells using sulfonyl chloride **12** (derived from chiral pool amino acids) and commercial diamines **11**.

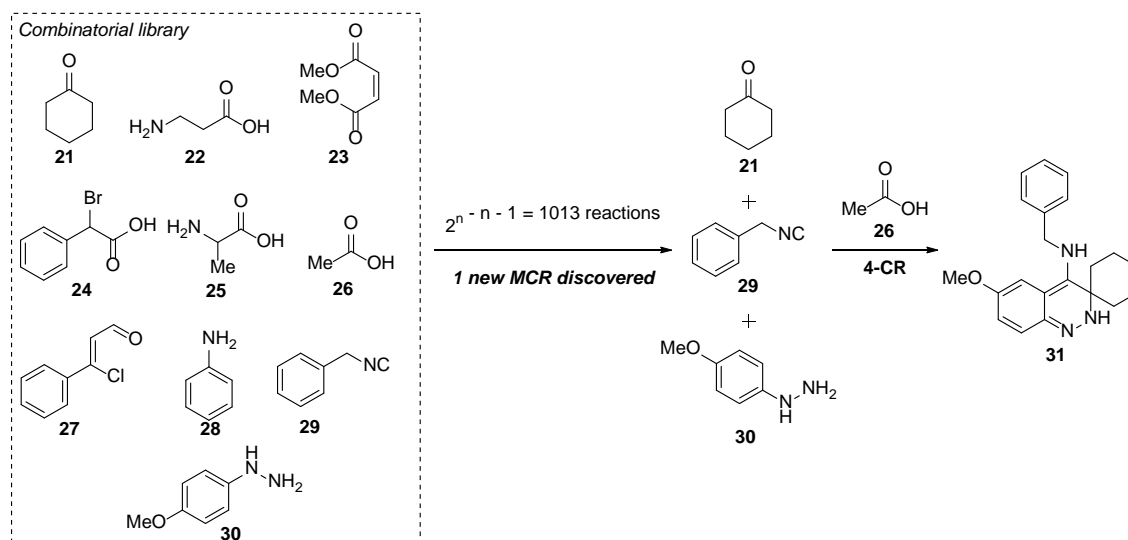
The synthesised ligands were screened against a mixture of four aldehydes in the presence of **16** and **15** and experiments were analysed using chiral GC. The strategy discovered chiral diamine **18** with sulfonyl chloride **19** derived from phenylalanine returned the enantioenriched secondary alcohol **17** in >97:3 e.r. for (*S*)-alcohol and >80:20 e.r. for the (*R*)-alcohol.



Scheme 3: Combinatorial synthesis of ligands for the enantioselective addition of diethylzinc to various aldehydes. Ligands derived from cyclohexyldiamines and phenylalanine performed the best.

The previous two reports are early examples of multi-variate screening that efficiently assess reaction conditions in microtiter plates. Automated liquid-handling robots were not employed to assist in reaction setup, as each microtiter plate was prepared manually, using a variety of air displacement pipettes. The first automated high-throughput reaction discovery platform was published by Weber in 1999 while investigating multi-component Ugi reactions.⁴⁵ A liquid-handling robot was used to dispense reagent stock solutions into microtiter plates to assess combinations between two-component and ten-component reactions using **21-30** (Scheme 4). Of the 1013 unique reactions, a new four-component reaction was discovered; the coupling of

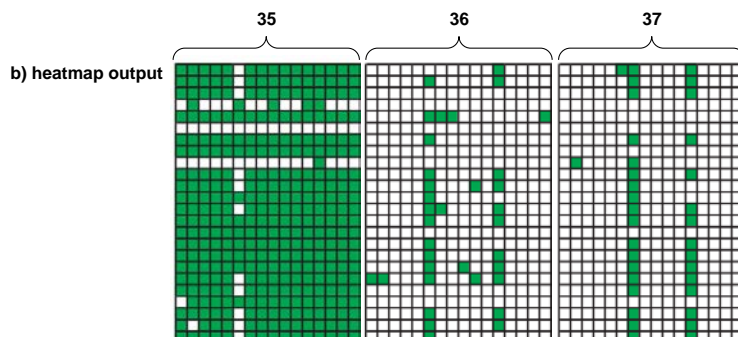
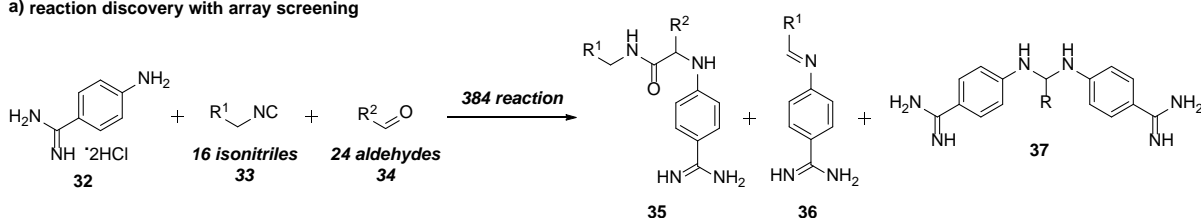
cyclohexanone **21** with benzylnitrile **29** and phenylhydrazine **30** in the presence of acetic acid forming spiro-cinnoline **31**.



Scheme 4: Combinatorial library of compounds screened to assess ten-component Ugi reactions, discovering a 4-component reaction to synthesise **31**.

Additionally, the same strategy was used to investigate a structure-activity relationship for a known three-component Ugi reaction (Scheme 5a). All reaction components were dosed into 384-well plates using an automated robot covering 44 amines, 16 isonitriles and 24 aldehydes totalling 16,896 unique reaction conditions. All reactions were assessed using an automated mass spectrometer. When, for example, 4-amino-benzamidine dihydrochloride **32** was tested in the high-throughput multi-variate screen, automated mass spectroscopy could rapidly identify three key products from the screen and, more importantly, combinations which only gave one product. The heatmap output (Scheme 5b) was coloured green for the presence of one of three outcomes, **35** from the expected three-component Ugi reaction, **36** for the condensation of **32** with an aldehyde, and finally, **37** where two equivalents of **32** condensed with an aldehyde.

a) reaction discovery with array screening



Scheme 5: Three-component reaction discovered. Coupling aniline **32** with isonitriles and aldehydes found three products. B) Three 384-well plates with coloured cells with the first identifying product **35**, middle showing product **36** and last showing product **37**. (Image use with permission from Synlett, RightsLink: 4534221105817).

The seminal work described by Burgess, Gennari and Weber in the 1990s showcased the potential impact miniaturised and automated protocols can have on chemistry. Performing hundreds of reactions within a single screen using milligrams of material or synthesising tens of thousands of unique compounds is simplified using parallel screening and automated robotics. The long analysis times, however, limit the generality and utility of this technique for the greater synthetic community. Since these pioneering publications, new analysis techniques have been reported to assist high-throughput analysis for qualitative, semi-quantitative and fully quantitative data capture.

1.4. High-Throughput Analysis Techniques

To fully realise the power of high-throughput protocols in synthetic chemistry, methods for the rapid assessment of reactions are key to their sustained use. A robust analytical technique requires simple and time-efficient methods that can be used on readily available equipment.

1.4.1. Imaging Assays

1.4.1.1. Colour-Change Triage

Some of the earliest tools for high-throughput analysis adopted thermal imaging (Figure 3) as a technique to identify exothermic reaction conditions.⁴⁶⁻⁴⁹ Other triaging assays based purely on visual identification have also been used for high-throughput reaction discovery. For example, use of radical cation dyes for easy reaction triage^{50,51} or colloidal gold nanoparticles.⁵² Iodine paper has also provided a quick triaging method to assess metal-catalysed reactions. This

colour-swatch style method, although purely qualitative, has assessed a host of different C–C, C–O and C–S bond forming reactions.⁵³

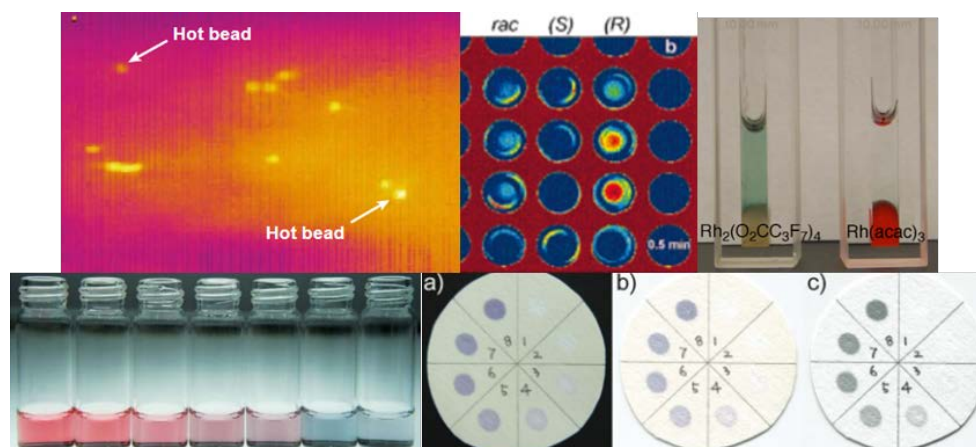
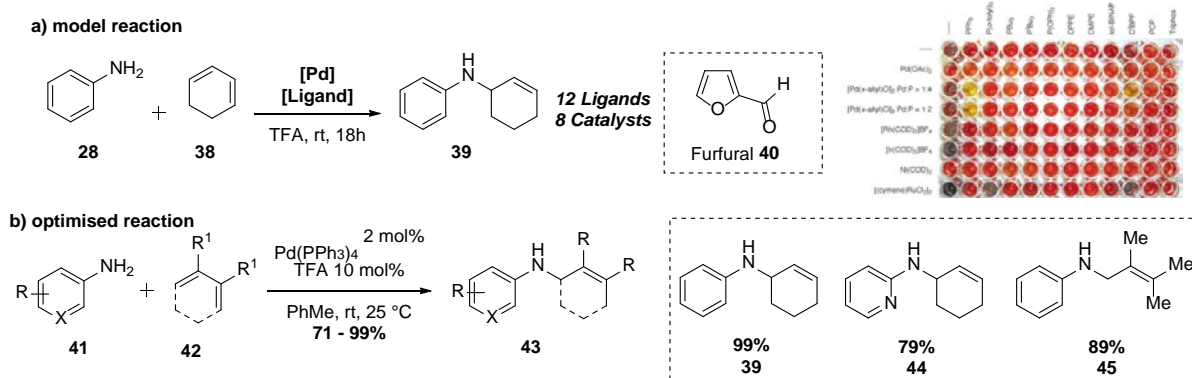


Figure 3: A - Thermal Imaging of solid supported catalysis (Image use with permission from Science, RightsLink: 4534230394540); B - Thermal imaging of cyclisation reactions (Image use with permission from Science, RightsLink: 4534221193041); C - Colour-based assay using radical acceptor (Image use with permission from ScienceAngew. Chemie, RightsLink: 4534221401828); D - Gold nanoparticle-based assay (Image use with permission from Angew. Chemie, RightsLink: 4534221497577); E: Iodine paper swatch assay (Image use with permission from Chem. Commn., RightsLink: 11793970).

In 2001, Hartwig used furfural, known to condense with aniline giving a red coloured solution,⁵⁴ to investigate new conditions for the hydroamination of cyclohexadiene (Scheme 6a).⁵⁵ Employing a model reaction between aniline **28** and cyclohexadiene **38**, a 96-well plate array was used to screen twelve different mono- and bidentate phosphine ligands against eight different metal catalysts including palladium, rhodium, ruthenium and nickel sources. Upon the addition of acidified furfural **40** solution to the crude reaction mixtures, the most reactive conditions (those with the least amount of aniline) turned into yellow coloured solutions, whereas the least active conditions remained red.



Scheme 6: a) Model reaction of aniline **28** with cyclohexadiene **38** with 11 different phosphine ligands against 7 different catalysts to furnish alkyaniline **39**. Furfural **40** was used to qualitatively show conversion of aniline. b) optimised reaction with tetrakis(triphenylphosphine)palladium(0) with catalytic TFA in toluene. (Image use with permission from Science, RightsLink: JACS).

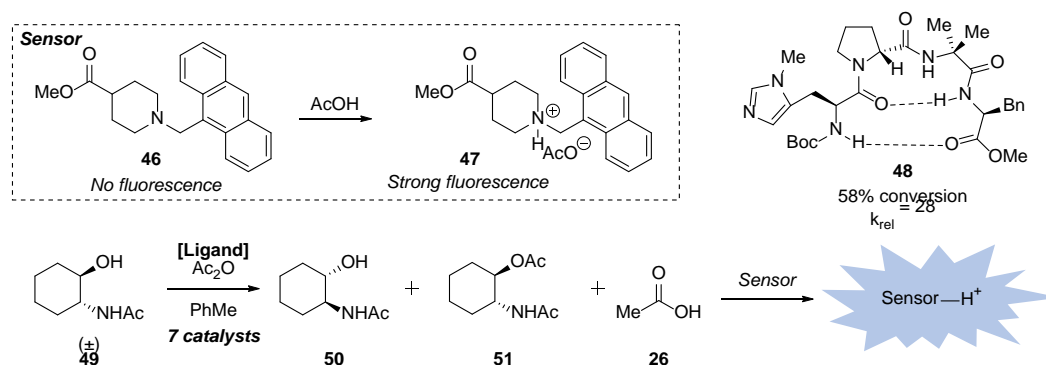
The triaging method quickly identified $[\text{Pd}(\text{allyl})\text{Cl}]_2$ in the presence of triphenylphosphine returned yellow solutions corresponding to reactive conditions with low aniline concentrations. Subsequent batch scale optimisation found $\text{Pd}(\text{PPh}_3)_4$ in the presence of catalytic TFA gave the

desired product in greater than 71% yield. The optimised conditions were applicable across a diverse substrate scope tolerant of heterocyclic anilines **41** and even non-cyclic alkenes **42** could be employed, returning **45** in 89% yield.

1.4.1.2. Fluorescence

Imaging assays can be further improved using fluorescence and colourimetry experiments and have been used in biochemical and pharmacological sciences for decades.⁵⁶ As a result, this well known analysis technique has been adapted to obtain semi- and fully quantitative data with automated plate readers that are now commonplace in many laboratories.

In 1999, Miller employed plate readers using an intense fluorescence sensor to obtain semi-quantitative data in minutes (Scheme 7).⁵⁷ The sensor, a benzylamine-anthracene derivative **46**, is non-fluorescent in its free-base form due to nitrogen lone pair quenching.⁵⁸ When protonated **47**, the lone pair can no longer quench the fluorescence and a strong reading can be obtained. The non-invasive nature of fluorescence spectroscopy means it can be used throughout the analysis to give a “snap-shot” of the reaction, important when comparing relative reaction rates.

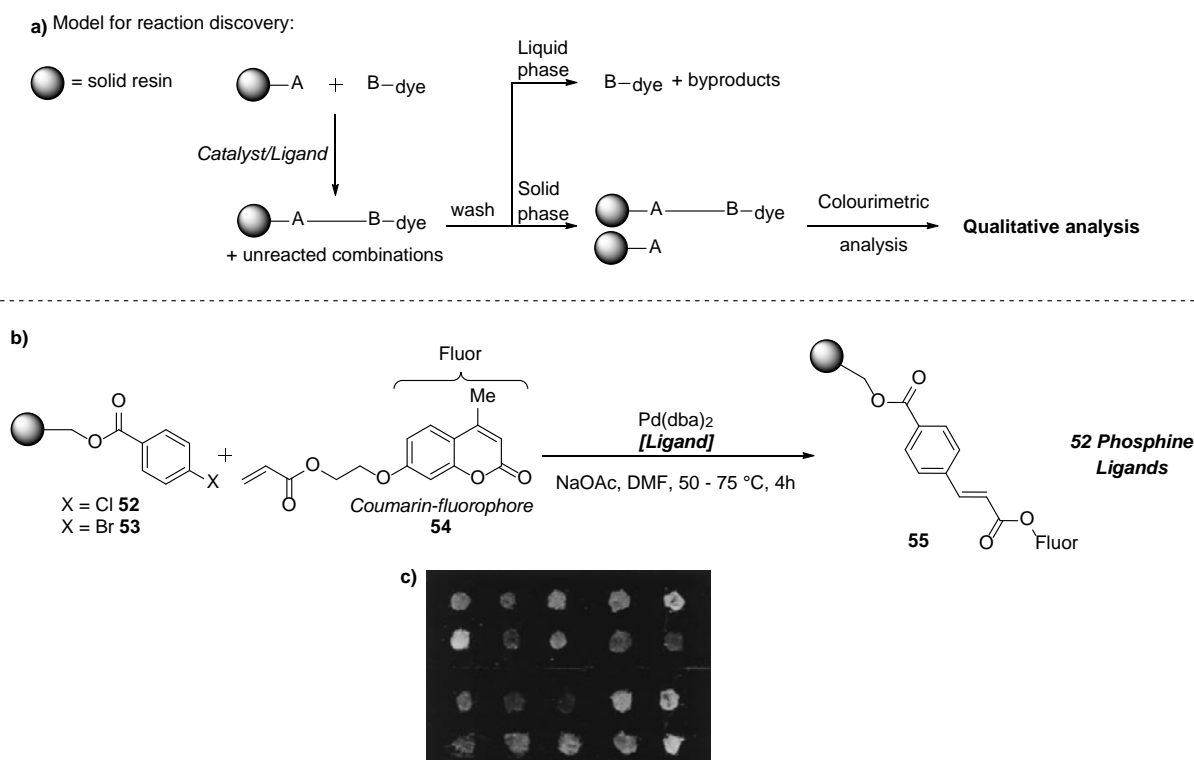


Scheme 7: Chemical sensor fluorescence imaging dynamic chiral resolution.

To showcase the applicability of this fluorescence sensor for high-throughput reaction discovery, Miller investigated a kinetic resolution of 2-hydroxycyclohexylacetamides **49** using seven nucleophilic catalysts at three different loadings. Known “super-acylation” catalysts⁵⁹ were found to give fast reaction rates but racemic products. Peptide derived catalyst **48** was found to give k_{rel} of 28 with 58% conversion over the course of the reaction. Solid-supported peptides, derivatised with the sensor, were synthesised to show the versatility of the fluorescence imaging technique for rapid assessment of screen newly synthesised catalysts.

Later, Hartwig identified the limitations of using an external sensor when measuring relative reaction rates, especially a sensor in equilibrium between on and off states. Employing a different strategy (Scheme 8), whereby one functional group is covalently linked to a fluorescent dye (Reagent B) and a complementary functionality attached to a solid supported matrix (Reagent A), bond forming reactions could be visualised using fluorescence imaging

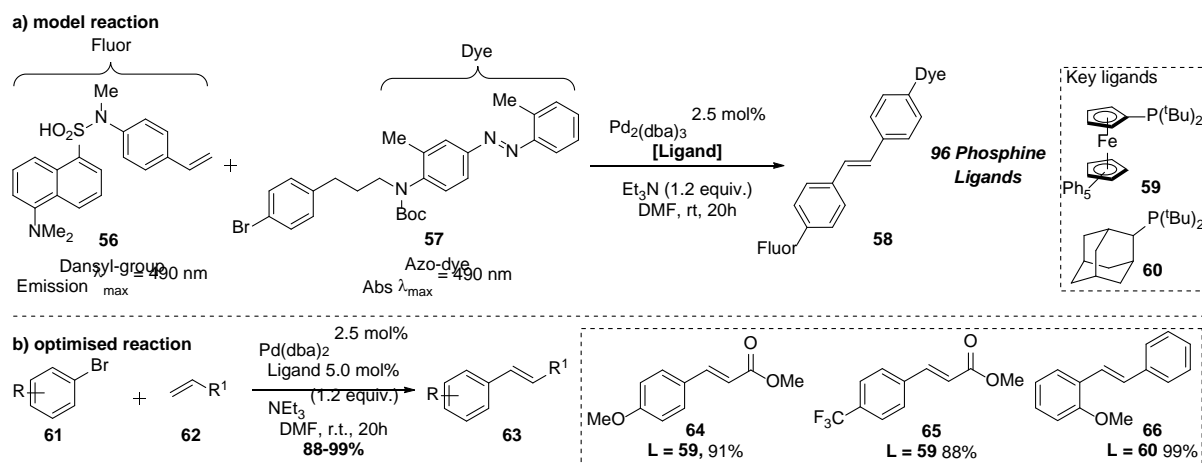
cameras.⁶⁰ This tagging strategy found mild conditions for the Heck-reaction of aryl halides **52/53** and acrylates **54** (Scheme 8b) by isolating each bead and visualising under UV-light; the brightest bead represented the best set of conditions (Scheme 8c).



Scheme 8: Tethered dye reaction discovery for Heck reactions. a) model analysis method for reaction discovery; b) Reaction screened using tagged dye; c) fluorescence image of isolated beads are the reaction conditions. Image use with permission from Science, RightsLink: JACS.

Although fluorescence imaging is useful to identify solid-supported reagents, the analysis of solution phase reactions can be problematic due to overlapping absorbance bands, resulting in false positives and false negatives. FRET-imaging can solve this issue by employing two fluorescent molecules covalently attached to each other and are therefore close in space. One emission (donor) is excited by light and the fluorescence energy absorbed by a dye (acceptor) fluorophore with overlapping emission and absorption bands. Once energy is absorbed by the donor it is instantaneously transferred from to the acceptor, resulting in no fluorescence transmission and an overall FRET-pair concentration can be observed.⁶¹

Hartwig installed an alkene appended to a dansyl fluorophore donor **56** and a complementary aryl bromide attached to the diazo-dye acceptor **57** to investigate a Heck-coupling reaction **58** (Scheme 9).⁶² Multi-variate screening was completed on 96-well microtiter plates to assess 96 structurally and electronically diverse phosphine ligands, with each reaction assessed semi-quantitatively using an automated fluorescence plate reader. Over 15 reaction conditions were found to give >70% product, but further investigation revealed phosphine **59** and **60** gave the best yields across electron rich and poor aryl bromides.



Scheme 9: First FRET imaging technique for reaction optimisation of Heck alkenylation by Hartwig.⁶²

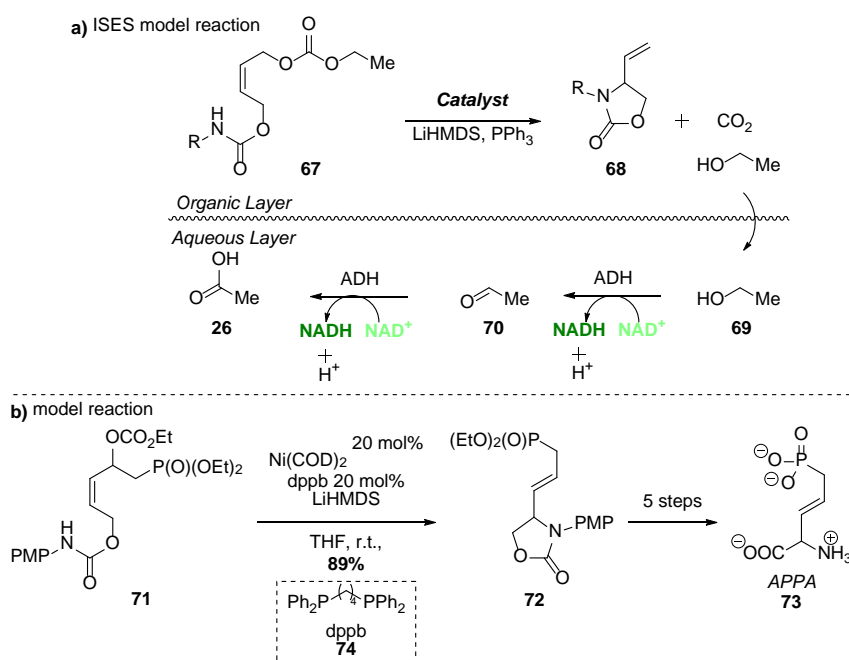
FRET imaging analysis has subsequently been employed to investigate and optimise cyanoacetate arylation by screening 119 phosphine ligands to initially identify hits.⁶³ Hartwig obtained quantitative data using calibration curves of FRET-pairs in the investigation of palladium-catalysed Buchwald-Hartwig arylation of amines.⁶⁴ In 2009, a separate publication by Plenio appended the FRET-pair to the ligand rather than the substrate which reduced lengthy substrate synthesis and large scale preparation.⁶⁵

Visual and colour-based assays are straightforward methods that enable rapid triaging of candidate reaction conditions and assessment of their relative performance. The step-change from purely qualitative analysis to a quantitative analysis marked a progression in the quality of data obtained. Lengthy synthesis of tagged compounds restricts the generality of this analytical method and therefore it has not seen further application in recent years. The fluorescence imaging analytical equipment, however, has been used more recently in different high-throughput reaction analysis.

1.4.2. Biochemical Assays

1.4.2.1. *In-situ* Enzymatic Screening

The Berkowitz group utilised a different colorimetric method for analysis. Rather than using fluorophores or chromophores in the reaction, they employed a biphasic reaction discovery manifold that facilitated rapid hit identification as well as elucidating relative rates. Their system utilised an alcohol dehydrogenase (ADH) enzymatic system⁶⁶ which they coined as *in-situ* enzymatic screening (ISES) (Scheme 10).⁶⁷⁻⁶⁹



Scheme 10: ISES protocol for reaction discovery evolving an equivalent of ethanol per catalytic turnover results in a two-fold product of green, fluorescent NADH.

The model reaction Berkowitz chose, a metal catalysed cyclisation of carbamate **67**, was tailored to the analysis protocol. The desired product, an oxazolidinone, was furnished alongside an equivalent of carbon dioxide and ethanol **69**. The ethanol diffused into the aqueous layer where enzyme-catalysed oxidation of ethanol to acetic acid **26** was achieved as well as production of two equivalents of fluorescent NADH from NAD⁺ (Scheme 10a). The reaction solvent, a complex mixture of THF, toluene, and hexane, was key to this analytical technique and was found to furnish the desired product without affecting the enzymic reaction in the aqueous layer. The production of two equivalents of NADH from one equivalent of ethanol underpins the analytical resolution of ISES which is capable of identifying nanomole quantities of product.

Berkowitz used this new colorimetric technique to assess the cyclisation of **67** with eight transition metal catalysts and triphenylphosphine. ISES and fluorescence spectroscopy found Ni(COD)₂ and triphenylphosphine produced a relative rate of NADH production of 58 units per minute. Batch scale confirmation gave the target product in 70% isolated yield. Further batch scale optimisation revealed para-methoxyphenyl (PMP) protected carbamate returned a relative rate of 35 units per second over 10 minutes. It was also found that replacement of monodentate triphenylphosphine with bidentate phosphine 1,4-bis(diphenylphosphino)butane **74** (dppb) gave a further improvement to the relative rate, 118 units per minute by ISES. These newly discovered conditions were subsequently applied to the synthesis of important drug targets vinylglycine and homoserine phosphate analogue **73**, with the key step returning target oxazolidinone in up to 89% isolated yield (Scheme 10b). Shortly after the seminal report

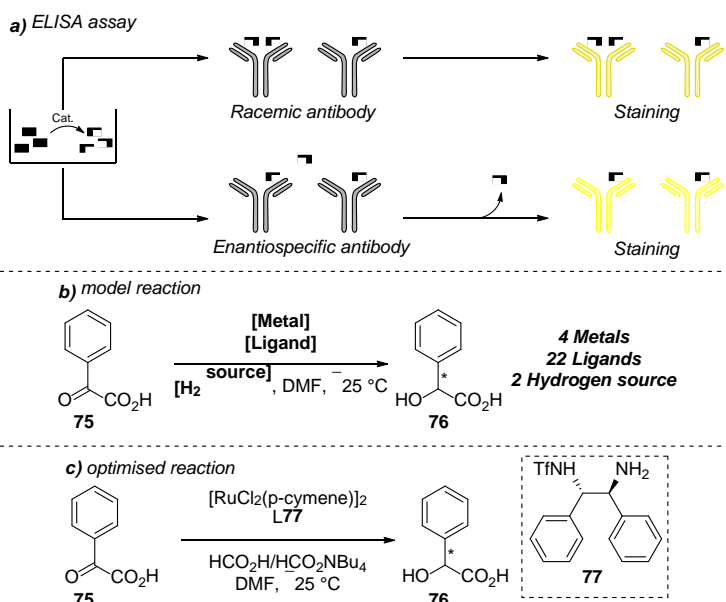
detailing ISES, Berkowitz utilised the technique to discover one of the first examples of asymmetric nickel-catalysed allylic amination.⁶⁷ The initial strategy has now been expanded by the same group to generate reaction yield and e.e. using a “double-cuvette” two-part analysis.^{68,69}

The ISES analysis technique represents a significant improvement for high-throughput analysis. The use of rapid spectroscopy techniques to assess yield and e.e. marked a major step towards a fully high-throughput reaction screening platform. The biphasic system employed by Berkowitz restricted the conditions that are assessed to those that are compatible with aqueous solvents and enzymes. The analytical sensor produced in the array needed to be polar enough to diffuse into the aqueous enzymatic-phase so that yield or e.e. determination can take place.

1.4.2.2. Enzymatic Immunoassay

Wagner and Mioskowski⁷⁰ published an enantioselective reduction of benzo- α -ketoacids using a combination of racemic and enantioselective enzymatic immunoassays (ELISA), an analytical technique that has been used in biology and pharmacology since the 1970s (Scheme 11).^{71,72} Product binding receptors were appended to a monoclonal antibody (mAb) target that either unselectively binds to both enantiomers (yield determining) or binds one enantiomer specifically (e.e. determining). Subsequent antibody staining can qualitatively determine the overall performance of each reaction. The ELISA assay is conducted independently of the screening array and is therefore compatible with reaction conditions, a beneficial advancement from ISES.

The first ELISA assay for high-throughput analysis was used to investigate the asymmetric reduction of benzoyl formic acid **75** to furnish enantiopure mandelic acid **76**. Four different metal catalysts (Ru, Rh, Ir) were screened against 22 enantiopure diamine-derived ligands and two hydrogen storage systems, totalling 176 reactions (Scheme 11b). Microliter reaction mixture aliquots were added to the ELISA assay and, after staining and absorbance spectroscopy, a semi-quantitative yield and e.e. could be determined. The ELISA absorption discovered $[\text{RuCl}_2(\text{p-cymene})]_2$ in combination with diamine ligand **77** furnished mandelic acid **76** in 98% yield and 79% e.e. in the presence of a known hydrogen release system⁷³ (Scheme 11c).



Scheme 11: ELISA assay to elucidate yield and e.e. for the asymmetric reduction of benzo- α -ketoacid. Using 96-well plates to effectively screen one ligand and one catalyst per reaction.

ELISA was subsequently employed in the optimisation of Heck reactions⁷⁴ and, more recently, a modified “sandwich” assay reported by Taran was used to discover new bioconjugations with a focus on chemoselectivity and fast kinetics (Figure 4).⁷⁵ The “sandwich” ELISA assay requires two reagents possessing specific mAb-binding moieties. The first mAb captures the first reagent on a solid support, while the second mAb (attached with acetylcholinesterase) acts as the detector. When bond formation occurs, staining with Ellman’s reagent reveals new reactions as yellow solutions.

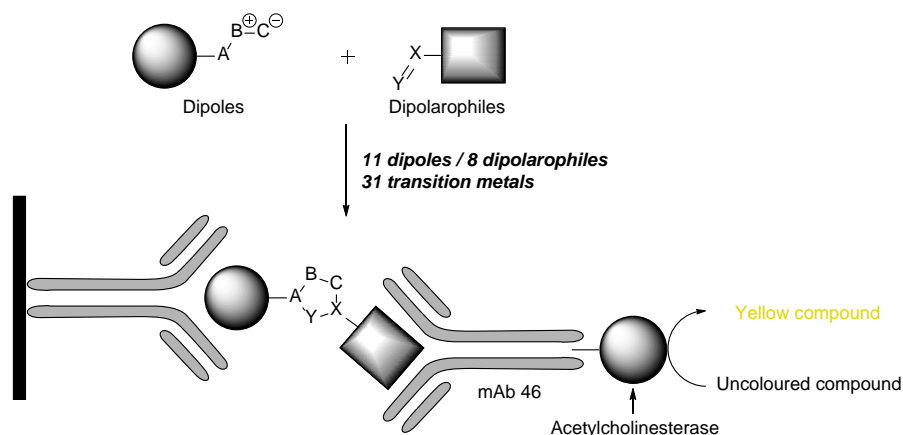
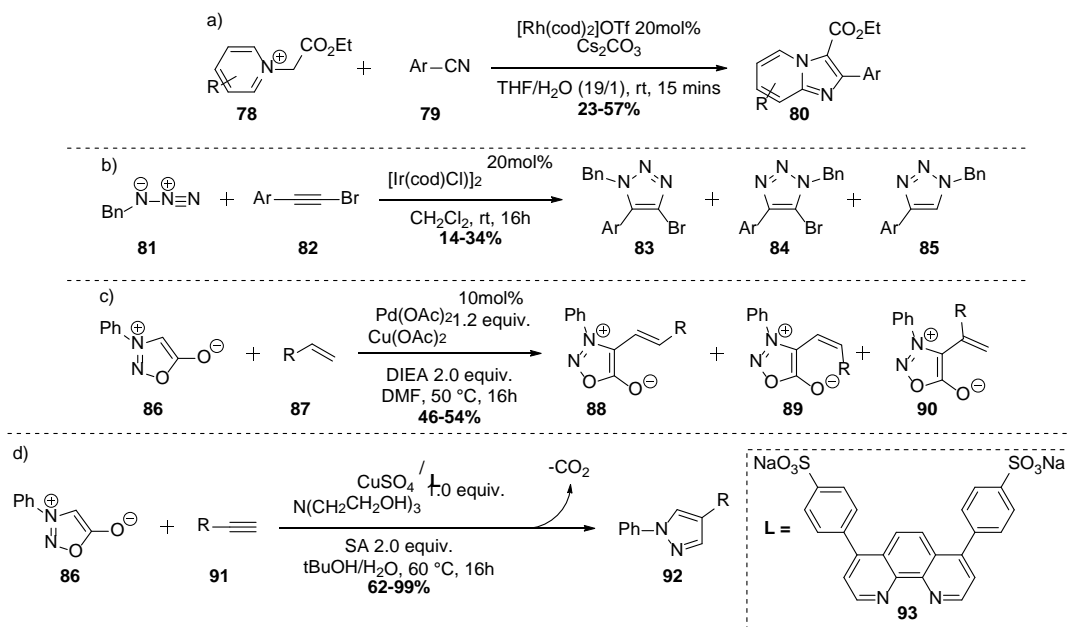


Figure 4: Basis of ELISA for the discovery of biocompatible dipolar cycloaddition reactions. Coordination of the dipole tag to a solid supported mAb and subsequent coordination of an acetylcholinesterase conjugated mAb to the dipolarophile end subsequently allows for quantitative analysis.

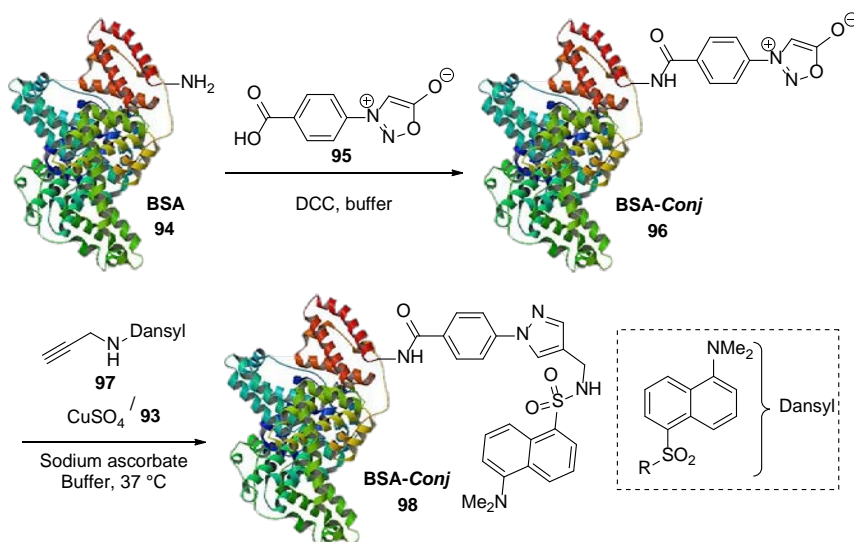
A series of 1,3-dipolar cycloadditions were investigated and analysed using sandwich-ELISA. A total of eleven dipoles and eight dipolarophiles and were screened against 31 different metals catalysts totalling 2,728 unique reactions. ELISA revealed over 51 reaction conditions that gave product, including nine known reactions such as Huisgen-cycloaddition⁷⁶, azide-bromoalkyne⁷⁷ and azomethidine-imine-alkyne.⁷⁸ The other 42 reaction conditions revealed unknown products

in less than 15% assay yield. A second high-throughput optimisation protocol was completed to investigate these new but low yielding reactions using sandwich-ELISA analysis. Four new metal catalysts were assessed against eight ligands, four bases and eight solvents. The second array found optimal conditions for four new cyclisation reactions including a rhodium-catalysed Knoevenagel reaction (A), iridium-catalysed Huisgen cyclisation (B) and palladium-catalysed Heck reaction (C) (Scheme 12).



Scheme 12: Reactions discovered with ELISA. A) Rhodium catalysed Knoevenagel condensation; B) Iridium catalysed azide-alkynebromide cyclisation; C) Palladium catalysed cyclisation. D) Biocompatible dipole-alkyne coupling using copper sulfate and water soluble phenanthroline ligand **93**.

Interestingly, the discovery of a copper-catalysed syndone-alkyne cycloaddition (CuSAC) furnished 1,4- and 1,5-substituted pyrazoles at 50 °C. The latter high-throughput screen showed the reaction was completed in 24 hours and was compatible with a range of complex biological media such as cell lysate and blood plasma. The replacement of phenanthroline with water-soluble sodium sulfate bathophenanthroline **93** improved the reaction yield and selectivity which furnished 1,4-substituted pyrazole **92** exclusively at room temperature in water. The newly optimised CuSAC reaction was even capable of dansylating a modified bovine serum albumin (BSA **94**), placing a strong fluorophore selectively on the *N*-terminus of the peptide **98** (Scheme 13).

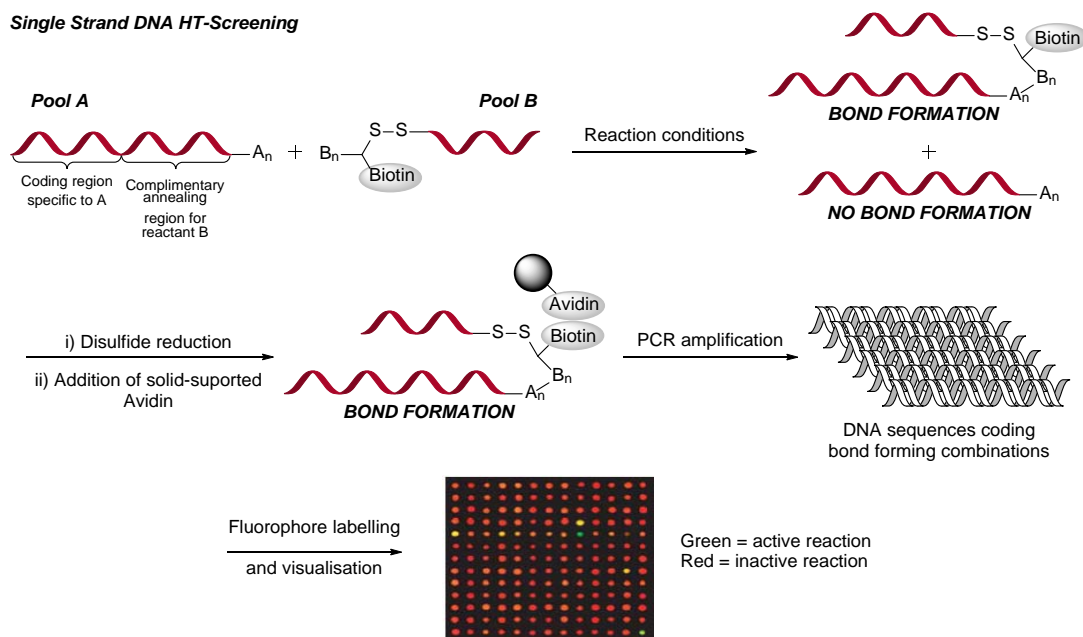


Scheme 13: CuSAC coupling of syndone with alkyne in the presence of BSA, tagging with a fluorogenic dansyl group.

The early deployment of ELISA by Wagner and Mioskowski, and the subsequent development of the sandwich assay by Taran, marked major advancements for high-throughput analysis. Validation of the assay in combination with HPLC assay underpinned this strategy for both yield and e.e. determination. The use of immunoassaying, while being extremely elegant solution to this problem, is empirically limited by the appended tag to the reaction centres (often involving lengthy synthesis before reaction screening can even begin) as well as a deep intellectual understanding of monoclonal antibodies and their preparation.

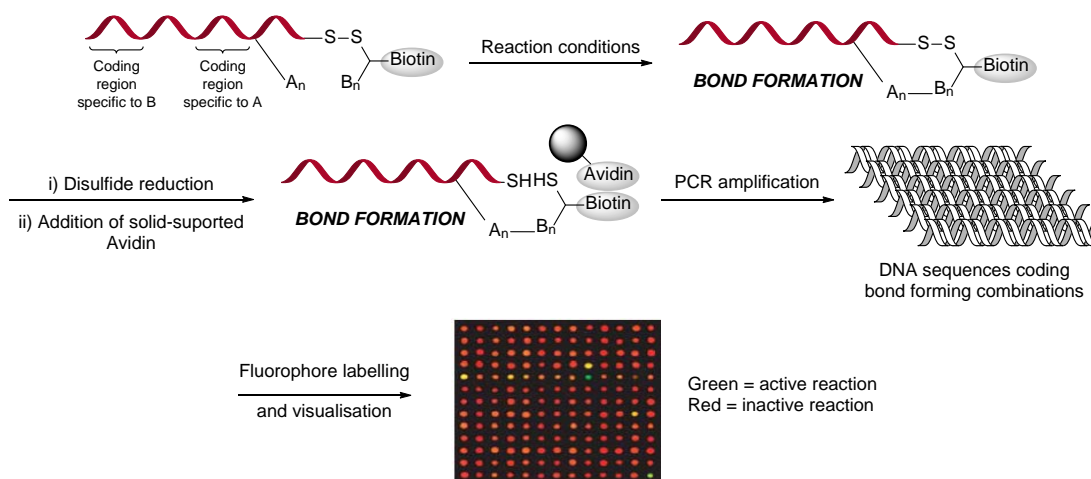
1.4.2.3. DNA Tethering

Using a similar known biochemical assaying approach, Liu employed DNA-tagged reagents to investigate a range of carbon-carbon bond forming reactions (Scheme 14).⁷⁹ One subset of coupling partners (A) were attached to a single strand of DNA and a complimentary Watson-Crick pairing-strand was attached to the other reactant subset (B) through a disulfide linker. Bond forming reaction conditions could be picked out of solution using the highly specific biotin-avidin affinity system⁸⁰ and analysed using PCR. The amplified DNA was labelled with red (pre-selection) or green (post-selection) fluorophores and analysed by a plate reader. Green wells indicated successful bond forming reactions, red cells highlight no reactivity.



Scheme 14: Fundamental of DNA assay. Appending reactive centre A to the first DNA pool A and reactive centre B to pool B. Watson-Crick pair formation and reaction of A with B leads to bond formation or no bond formation. Cleavage and exposure to solid supported Avidin binds only bond forming combinations which can be analysed by PCR and staining. (Image use with permission from ScienceNature, RightsLink: 4534220420384).

A further extension of the DNA assay, also developed by Liu, was reported using a single strand of DNA with both reagents covalently attached to the same strand (Scheme 15).⁸¹ When bond formation occurred between reagent A and B, the disulfide bond was cleaved by tris-carboxyethylphosphine hydrochloride⁸² and, using the same biotin-avidin system, bond forming conditions could be rapidly identified after PCR amplification.

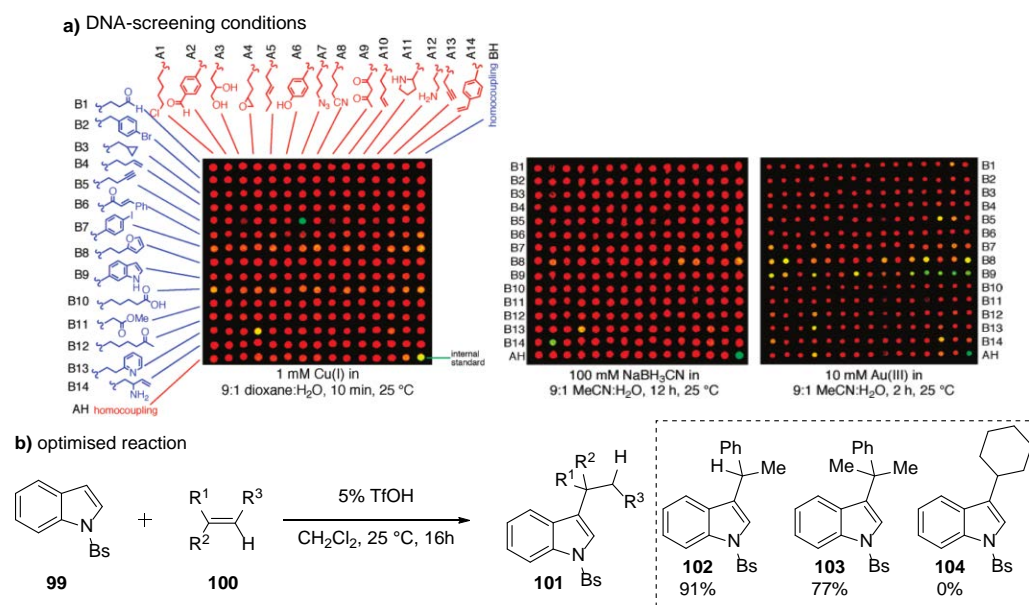


Scheme 15: Adapted DNA assay using only a single strand of DNA with both reactive centres attached. Disulfide bond cleavage then breaks reactive centre B from the DNA strand that can be removed preventing false positive results. The same process of Avidin capture, PCR amplification and staining reveals working reaction combinations. Image use with permission from ScienceNature, RightsLink: 4534220420384.

The single-strand DNA analysis technique was used to assess the reactivity of 14 “A-substrates” and 14 “B-substrates”, both containing a variety of nucleophilic and electrophilic functionalities (Scheme 16a). Three reactant systems were investigated: a copper (I) catalyst, a gold(III) catalyst and sodium borohydride in three different well plates. Post-PCR visualisation found

conditions corresponding to reductive amination and Husigen-cycloaddition reactions from the sodium borohydride and copper(I) catalyst screens respectively. Within the gold(III) catalyst array, a novel indole-alkene hydroalkylation was discovered with alkylation observed at the C3 position exclusively (Scheme 16b).

The hit reaction was confirmed without the DNA scaffold on scale to furnish the Markovnikov product **101** in 82% yield with stoichiometric gold(III) salts. Further batch-scale optimisation revealed triflic acid was sufficient to catalyse the reaction.



Scheme 16: Screening of 28 different reagents against copper(I) catalyst, sodium borohydride and gold catalyst. B) Optimised reaction of indoles with alkenes. Image use with permission from ScienceNature, RightsLink: 4534220420384.

The DNA-tethered analytical methods developed by Liu are another sophisticated solution for reaction discovery and condition screening. The combination of visual staining for instantaneous reaction triage, and automated plate readers for spectrochemical analysis underpins the generality and flexibility of the strategy. The single-stranded DNA analysis simplified the technique compared to the initial double-DNA method, but the required understanding of DNA synthesis and PCR limits the applicability of this method. Furthermore, reactions conditions analysed by DNA-tethering need to be tolerant of DNA-base pairs and subsequent Watson-Crick base pairing.

1.4.3. Direct Mass-Spectrometry

Since pioneering studies of gas discharges by Thomson⁸³ in the early 19th century, mass spectrometry has developed at an incredible rate with improved analyte resolution, ionisation and utility occurring in a matter of decades.^{84,85} The power of mass spectrometry for high-throughput lies in minimal analyte prefunctionalisation, meaning direct reaction analysis is possible. Detecting different analytes simultaneously by selective ion monitoring (SIM) not

only gives a relative conversion and yield, but also has the potential to reveal reaction selectivity. Normally used in combination with chromatographic techniques, direct injection mass spectrometry permitted high-throughput screening of forensic samples⁸⁶ and food products⁸⁷, but it has not been fully utilised in synthetic chemistry.

Mass spectrometry is dependent on analyte ionisation and there are many different types available such as electron bombardment (ESI) or acid/base chemical ionisation (CI).⁸⁵ ESI-MS has been used by Pfaltz^{88–93} to identify ligand/catalyst combinations for generating enantiospecific Tsuji-Trost intermediates which would otherwise be unobservable using conventional liquid-chromatography techniques. More recently, new ionisation techniques such as solvent-assisted (DESI) or laser-assisted (MALDI) ionisation have become available. MALDI, a relatively soft ionisation technique, is capable of rapidly assessing analytes using a high-power laser capable of firing 50-100 laser ionisations every second (50-100 Hz) and is especially attractive for high-throughput synthetic chemistry (Figure 5a).

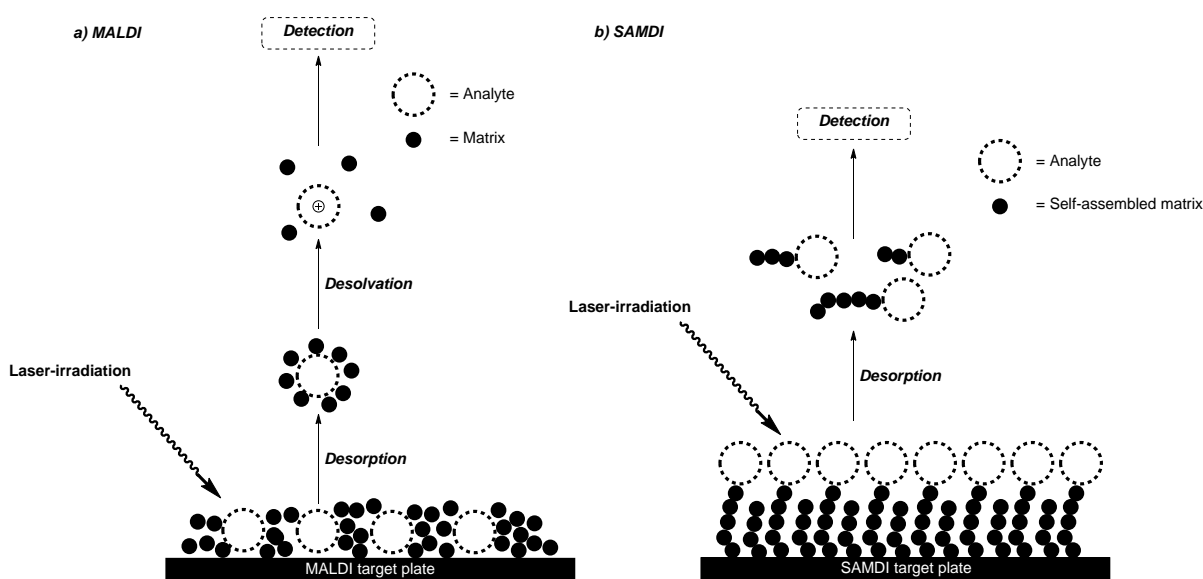
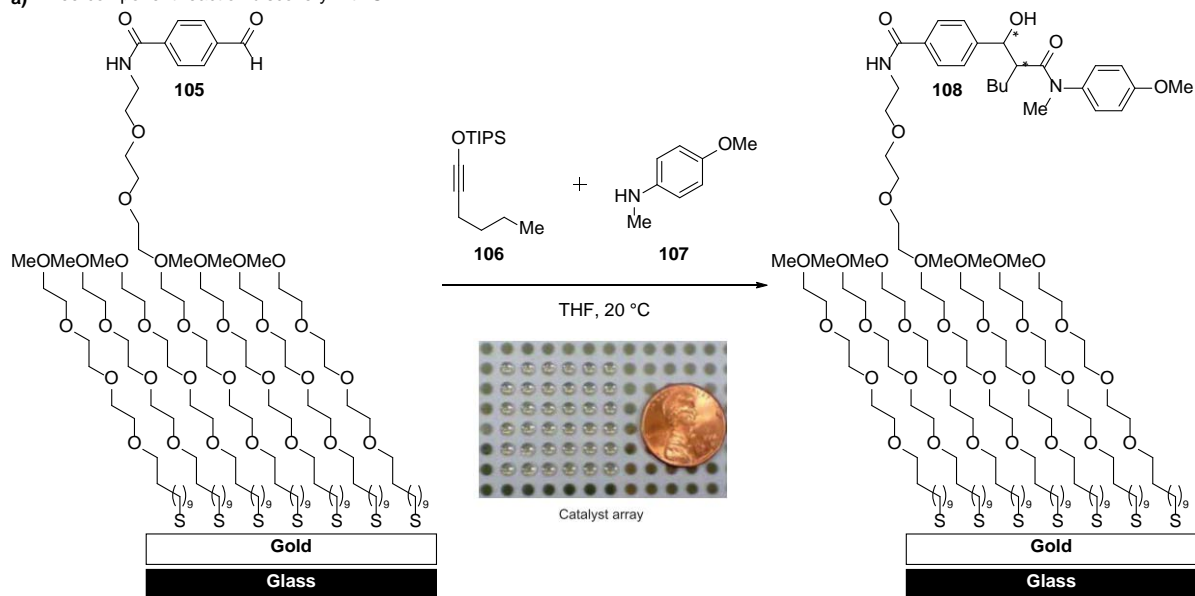


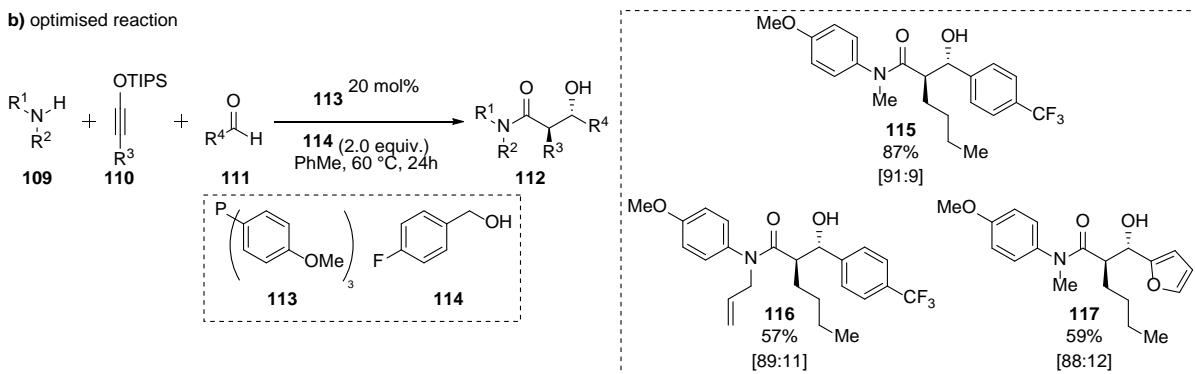
Figure 5: Basis of MALDI-MS and SAMDI-MS. MALDI-MS requiring a mix of matrix and analyte on the plate. SAMDI-MS requires the analyte adhered to a self-assembled monolayer of matrix.

A collaboration between Kozmin and Mrksich groups identified that a major drawback of MALDI is the need for an external matrix to facilitate analyte ionisation, which requires laborious MALDI-plate preparation.⁹⁴ Rather than adding an external matrix, a modified glass slide was prepared with “gold islands” adhered with an alkanethiolate matrix. The targeted MALDI laser subsequently induced ionisation by fragmentation of the alkanethiolate matrix. This process is known as self-assembled monolayers for matrix-assisted laser desorption/ionisation, or SAMDI (Figure 5b), a concept previously developed by Lloyd⁹⁵ and Mrksich.⁹⁶

a) Three-component reaction discovery with SAMDI



b) optimised reaction

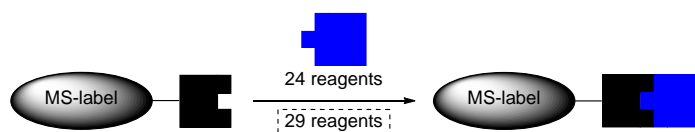


Scheme 17: SAMDI matrix high-throughput analysis of a three-component Ugi reaction to produce two contiguous stereocentres. A) SAMDI diagram of the target and reaction of interest. B) Optimised reaction. Image use with permission from ScienceNature, RightsLink: 4534230309675.

A three-component reaction was investigated between an aldehyde **105**, electron rich alkyne **106** and amine **107**. The SAMDI target appended with aldehyde **105** was reacted with a secondary amine and electron rich alkyne in the presence of 24 different metal, Lewis-acid and Brønsted-acid catalysts. The SAMDI analysis found an early hit when Pd(PPh₃)₄ was employed. Upon batch scale validation, a 50% conversion to **108** with 85:15 d.r. was observed. Subsequent batch-scale optimisation found electron rich tris(4-methoxyphenyl)phosphine **113** with 4-fluorobenzyl alcohol **114** in toluene at 60 °C was enough to furnish the desired product in 96% conversion and 91:9 d.r.

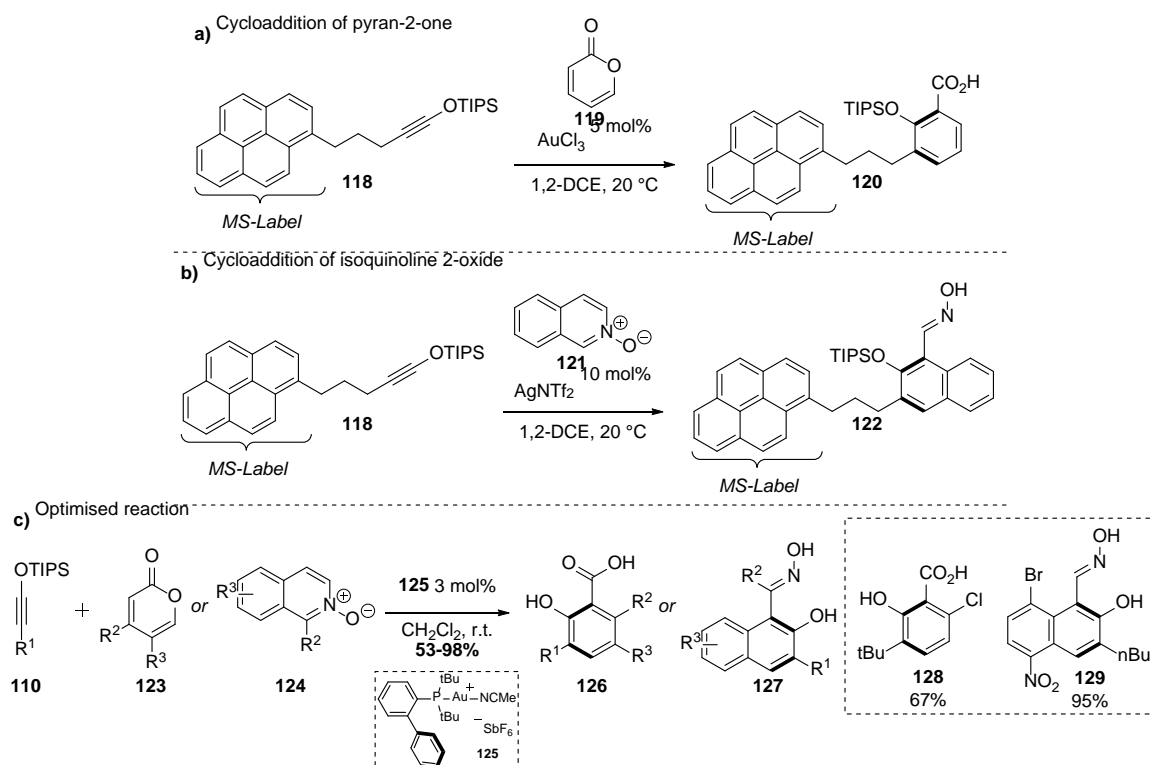
Scheme 17b). The scope of the reaction was investigated and found that electron rich amines could be coupled with electron deficient and heteroaromatic aldehydes to furnish the corresponding products **115** 87% (91:9 d.r.) and **117** 59% (88:12 d.r.) respectively. In addition, electron rich secondary allyl amines **116** were also tolerated in a slightly lower 57% yield (89:11 d.r.).

SAMDI targets require meticulous and time-consuming preparation as well as knowledge of self-assembling systems, potentially a discouraging issue for synthetic chemists. Rather than having the surface of a glass sheet appended with MALDI absorbing matrix, Kozmin attached the laser-absorbing group to the substrate, using simple synthetic chemical procedures (Scheme 18).⁹⁷ Pyrene was identified as a good candidate for laser absorption/desorption^{98,99} and was subsequently attached to a silyoxyalkyne **118** which served as a model substrate for the reaction. A liquid handling robot was employed to prepare 96-well plates, screening 24 different coupling partners (plus a control) against 28 different metal or organocatalysts (plus a control), a total of 725 combinations.



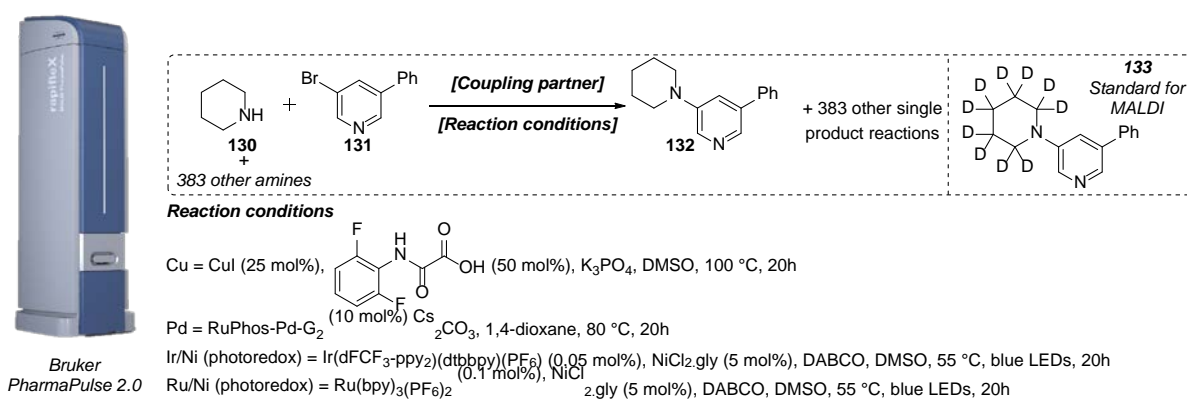
Scheme 18: Basis of Pyrene-labelling for MALDI analysis.

The same liquid handling robot prepared the MALDI target plate with only 800 nL of crude reaction mixture and were typically analysed within 2 hours. Direct analysis of the crude reaction mixtures revealed two [4+2]-cycloaddition reactions (Scheme 19). The first, cycloaddition of 2-pyrones **119** and silyoxyalkyne **118**, in the presence of a gold catalyst, gave poly-substituted benzoic acids at room temperature (Scheme 19a). The second cycloaddition of isoquinoline *N*-oxides **121** and silyoxyalkyne **118**, in the presence of silver(I) triflimide, furnished naphthaldehyde oximes (Scheme 19b). Batch-scale optimisation discovered both cycloaddition reactions could be catalysed by the same gold(I) pre-catalyst **125** to furnish poly-substituted benzoic acids and naphthaldehyde oximes in good yield (Scheme 19c).



Scheme 19: A) Cycloaddition of pyran-2-one with labelled alkyne **118**; B) Cycloaddition of isoquinoline-2-oxide with labelled alkyne **118**; C) Optimised reactions found from high-throughput screening.

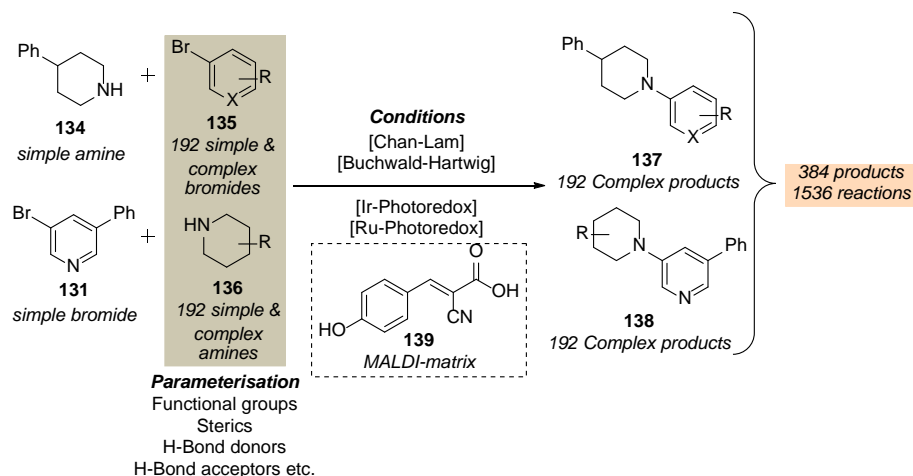
MALDI has recently been utilised by Merck to investigate four C–N bond forming reactions (Chan-Lam, Buchwald-Hartwig as well as ruthenium and iridium photoredox reactions), all without prior substrate functionalisation to aid ionisation (Scheme 20).¹⁰⁰ A state-of-the-art MALDI from Bruker (PharmaPulse 2.0 MALDI-TOF) capable of 1000s of samples per hour throughput, was utilised to rapidly assess multi-parallel arrays. As a proof of concept, model heterocyclic bromide **131** was screened against 384 simple and pharmaceutically relevant amines. A combination of UPLCMS and MALDI were required to validate the MALDI assay, incorporating a deuterated standard **133** to standardise each MALDI response.



Scheme 20: PharmaPulse 2.0 and the overall reaction discovery platform assessed using MALDI-TOF. Image use with permission from Bruker.

To further showcase the analytical power of the PharmaPulse 2.0 MALDI-TOF, a further 1536-reactions were prepared. 192 complex aryl bromides and 192 complex amines were reacted with 4-phenylpiperidine **134** and 3-bromo-5-phenylpyridine **131** respectively in the presence of

the four chosen C–N bond forming conditions (Scheme 21). The MALDI target plate was prepared with 175 μL of reaction mixture and α -cyano-4-hydroxycinnamic acid **138** as the matrix. The continuous variation screening platform, along with the semi-quantitative MALDI and UPLC, was subsequently modelled using computational methods to identify trends in reactivity based upon substrate parameters such as hydrogen bond donor/acceptors properties, sterics and functional group location to “map chemical space”.



Scheme 21: Further screening and parameterisation of simple and complex substrates for mapping chemical space and reactivity.

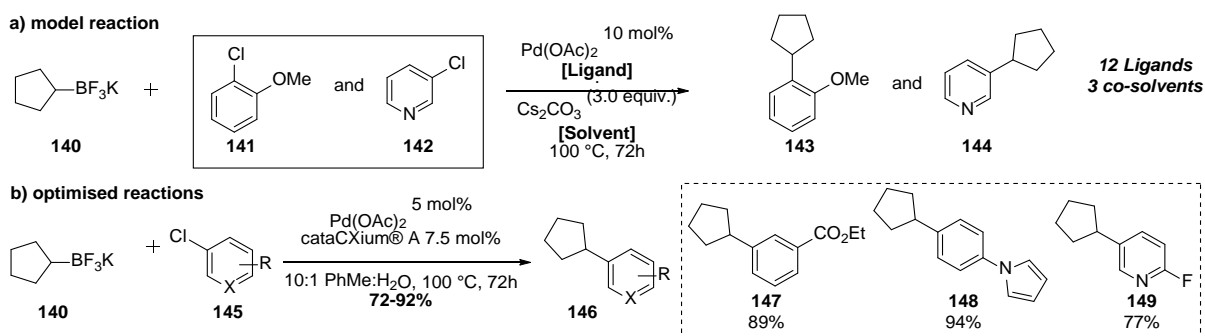
The MALDI assay technique described within this section is a powerful analytical tool for synthetic reaction development. The rapid sample speed and throughput makes this an attractive technique for high-throughput reaction development. The exemplary work of Kozmin underpinned this technology for reaction discovery and these efforts were subsequently expanded by Merck for complex pharmaceutical substrates. These advantages, however, are outweighed by the capital cost of the machinery, making it prohibitively expensive investment for institutions and academic groups. There are currently no methods for obtaining quantitative data which prevents MALDI from being utilised in chemical reaction optimisation protocols.

1.4.4. Chromatographic Coupled UV/Vis Assaying

Since chromatography was first applied for high-throughput reaction analysis by Burgess⁴³, Gennari⁴⁴ and Weber¹⁰¹, chromatographic machinery has developed to exhibit shorter analysis time per sample with increased analyte resolution. In combination with these improvements, UV/vis analysis post-separation by photo-diode arrays (PDA) can allow rapid semi- or fully quantitative determination of desired products. In addition, computer controlled autosamplers can automate data accumulation, increasing sample throughput.

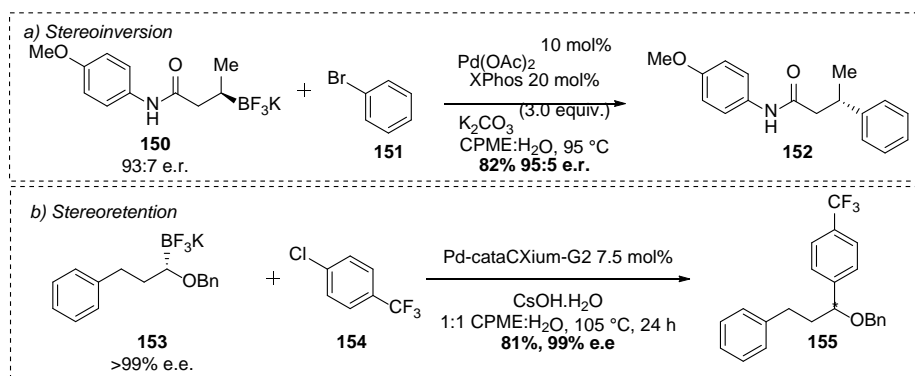
1.4.4.1. High-Performance Liquid Chromatography

In 2008, Dreher and Molander published a multi-variate microvial strategy¹⁰² to screen and optimise conditions for coupling of heteroaromatic halides with secondary alkyl tetrafluoroborate salts.¹⁰³ When secondary organopalladium salts were previously utilised palladium β -hydride elimination gave complex product mixtures.¹⁰⁴ High-throughput multi-parallel screening was subsequently employed to find conditions which did not undergo deleterious β -hydride elimination. Secondary trifluoroborate salt **140**, ortho-substituted aromatic halide **141** and heteroaromatic halide **142** all served as model substrates for the screen which assessed three solvent mixtures (5:1 water with either toluene, THF and CPME) against twelve different ligands. A total of 72 reaction unique reactions were assessed using 10 μ mol of substrate per reaction. HPLC equipment was analysed each reaction with 4-isopropylbiphenyl as the internal standard to obtain semi-quantitative data (Scheme 22).



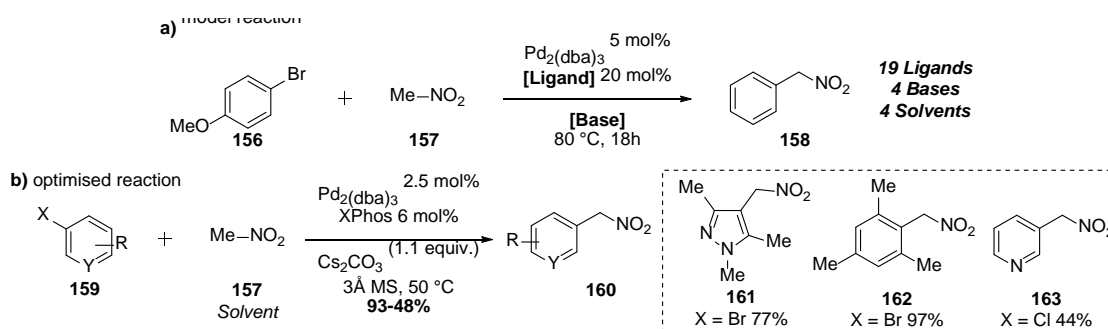
Scheme 22: Model reaction investigated using microvial assay. B) Optimised reaction conditions found with UV-Vis HPLC assay.

The high-throughput assay successfully identified phosphine ligand cataCXium® A in 10:1 toluene:water as the best conditions to transfer secondary trifluoroborate salts to aromatic **147/148** and heteroaromatic halides **149**. The conditions were shown to be broadly applicable across a range of different aromatic and heteroaromatic substrates. More impressively, acyclic trifluoroborate salts could be transferred in moderate yield with a slight preference for branched over linear products. The same multi-variate screening protocol and HPLC assay has also been applied to the enantiospecific transfer of enantioenriched trifluoroborate salts with both stereoinversion¹⁰⁵ and stereoretention¹⁰⁶ (Scheme 23).



Scheme 23: Arylation of enantioenriched secondary trifluoroborate salts using high-throughput platforms and HPLC assays. A) Stereoinvertive arylation; B) Stereoretentive arylation.

Kozlowski employed high-throughput multi-parallel screening arrays to investigate a palladium-catalysed nitromethylation of aryl halides with nitromethane, a cheap feedstock chemical (Scheme 24). Nitro-functional groups are highly versatile with the capability of delivering many functional groups including: aldehydes¹⁰⁷, oximes¹⁰⁸, amines¹⁰⁹ and carboxylates¹¹⁰ amongst others. A similar HPLC analysis method employed by Dreher and Molander was used to assess 304 different reactions, covering 19 structurally and electronically diverse phosphine ligands, four inorganic bases and four solvents. All reactions were performed on a 20 μ L scale. The internal standard (biphenyl) was used to obtain semi-quantitative information by analysing the ratio of UV peak area between the internal standard and product.

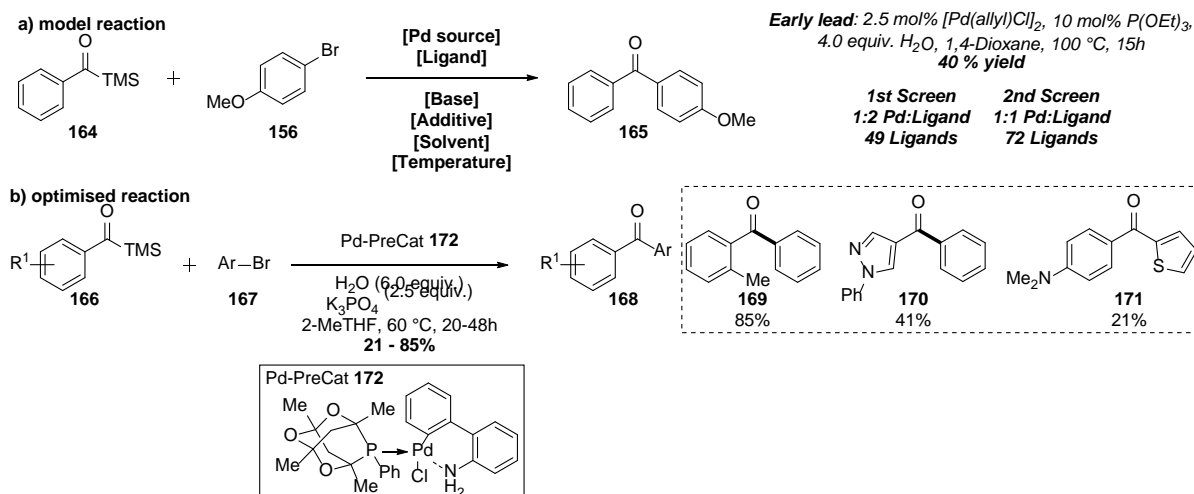


Scheme 24: A) Model reaction screened of 19 ligands against four bases and four solvents on 20-micromole scale; B) Optimised, batch reaction for the nitromethylation of aryl bromides.

The synthesis of unsymmetrical ketones can be difficult and lengthy, normally employing reactivity-controlled substrates such as Weinreb amides.¹¹¹ Merck improvised an Umpolung strategy whereby the nucleophilic moiety was appended to the carbonyl. Acylsilanes¹¹² were initially identified as suitable acyl-nucleophile precursors, exhibiting exemplary stability, solubility and functional group tolerance. Multi-parallel screening was used to efficiently vary conditions on a 10 μ mol scale (Scheme 25).¹¹³

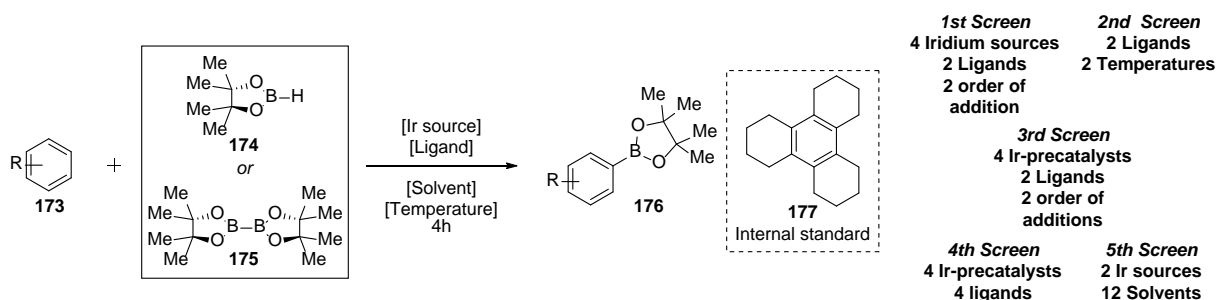
Prior to this study, an early lead was discovered when $[\text{Pd}(\text{allyl})\text{Cl}]_2$ was screened in combination with triethylphosphite, the desired unsymmetrical ketone **165** was furnished in 40% HPLC yield. Two further screens assessed 72 different ligands, with either 1:1 or 2:1 ligand:palladium ratio and revealed bulky phosphine ligands gave the most conversion to

product by HPLC. Batch-scale optimisation found that precatalyst **172**, appended with the best ligand from the multi-parallel array, furnished unsymmetrical benzophenones in generally good yield. Heterocyclic acylsilanes were tolerated in the reaction, furnishing ketone **170** in 41%. Electron rich ketones that would normally be difficult to prepare using traditional Grignard/organolithium chemistry, were prepared in 21% yield.



Scheme 25: A) Reaction modelled for the coupling of acylsilanes with aryl bromides; B) Optimised reaction conditions with precatalyst **172** with good scope, especially with product **171** where thiophenes are known to poison palladium catalysts.

The multi-variate screening strategies and HPLC assays were leveraged by Smith and Merck to complete a tutorial for C–H borylation reactions that fully assessed the dependence of all reaction components and external factors (Scheme 26).¹¹⁴ Although the number of reactions completed in a single screen was relatively small (maximum 32 in a single screen), over 200 unique sets of conditions were assessed using HPLC and dodecahydrotriphenylene **177** as an internal standard.

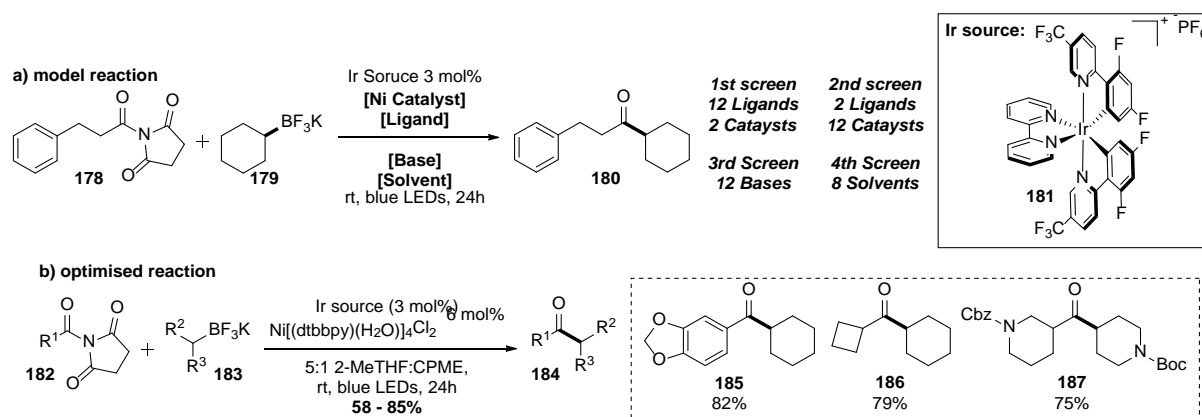


Scheme 26: C–H borylation of various aromatic compounds employing multi-variate reaction arrays to assess all parameters.

High-throughput parallel screening and semi-quantitative HPLC analysis has been utilised by several research groups to rapidly assess reaction outcomes. The Kozlowski group has used HPLC assays to optimise arylation reactions of both nitroacetates¹¹⁵ and phosphonoacetates.¹¹⁶ In addition, the Walsh group have used HPLC to investigate the C–H alkylation¹¹⁷ and arylation¹¹⁸ of activated benzylic C–H bonds¹¹⁹ as well as sulfoxide C–H arylation¹²⁰ and

cyclopropanol ring opening.¹²¹ Molander has also employed HPLC methods to investigate Suzuki-couplings with palladium^{122–125} or nickel,^{126,127} Kumada-coupling,¹²⁸ Sonogashira,¹²⁴ photoredox co-catalysis,^{129–133} borylation^{134–138} and amination.¹³⁹ The summation of all this work highlights the generality of HPLC for high-throughput multi-parallel reaction discovery and optimisation.

A newer analytical technique called UPLC, has surpassed HPLC with improved compound separation in shorter analytical run times. The Molander group has used UPLC to assess a multi-parallel high throughput array for the photoredox/nickel-catalysed synthesis of unsymmetrical ketones. Exploiting a single electron oxidation of trifluoroborate salts by iridium-photoredox catalysis,¹⁴⁰ as well as a known imide C–N insertion mechanism by nickel co-catalyst, new conditions using 4,4'-di-*tert*-butylbiphenyl as an internal standard were found.



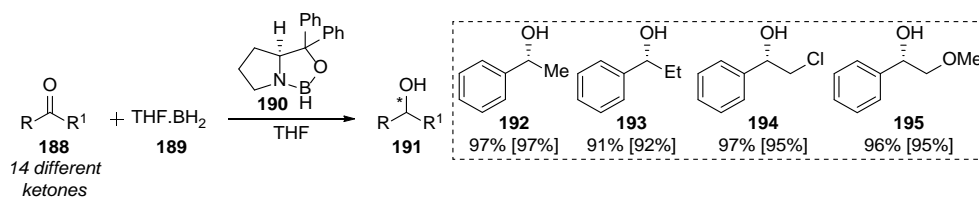
Scheme 27: Photoredox ipso-alkylation of amides. A) Model reaction screened in high-throughput; B) Initial two catalyst/ twelve ligand screen.

Early hits from the high-throughput screen and UPLC analysis identified $\text{NiCl}_2 \cdot \text{dme}$ precatalyst returned the desired product in the best UPLC assay yield. Further multi-parallel screening found that iridium catalyst **181** in combination with a nickel precatalyst, $\text{Ni}[(\text{dtbbpy})(\text{H}_2\text{O})_4]\text{Cl}_2$, in a mixed solvent system of 2-MeTHF and CPME furnished unsymmetrical ketones **184** in good yield. Electron rich aromatics **185** and cyclobutane **186** were tolerated as well as protected heterocycles **187**. The same UPLC assay has also been employed by Molander to optimise amide bond formation using alkyl-silicates with ruthenium/nickel photoredox co-catalysis.¹⁴¹

1.4.4.2. Chiral high-performance liquid chromatography

Kagan described the first combinatorial screening approach to investigate the asymmetric reduction of ketones using the Corey-Bakshi-Shibata (CBS) reagent using chiral HPLC (Scheme 28).¹⁴² Screening multiple different ketones in one-pot with the CBS reagent, chiral

analysis discovered the enantioselectivities correlated well when independently scaled in a single reaction mixture.



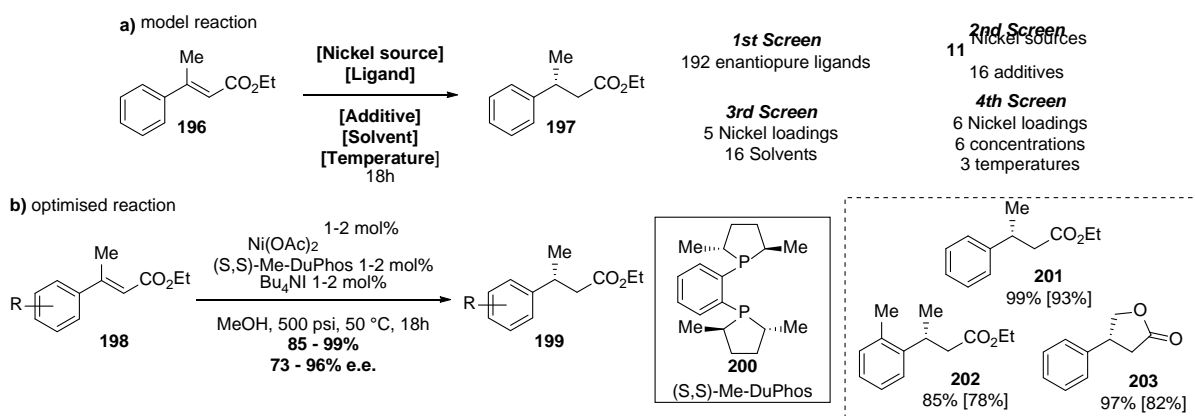
Scheme 28: High throughput reaction scope of CBS reduction of ketones. This method requires aromatic groups alpha to the ketone, so UV/vis absorption spectre can be obtained.

It was proposed that this approach could be used as an initial screen for new chiral reactions to speed up the rate of reaction discovery before moving into investigation in batch. There are however caveats to this approach, such as overlapping enantiomer peaks on chiral HPLC which can result in false positives/negatives, or productive participation of one of the other products in the screen. Previously, chiral HPLC required long assay run times and slow flow rates to tease enantiomers apart which has therefore limited its application in high-throughput analysis.

More recently, supercritical fluid chromatography (SFC) has come to the forefront of chiral compound analysis. Utilising similar principles to HPLC, but adopting supercritical carbon dioxide as the apolar mobile phase, SFC has improved analyte resolving power and subsequently correlated to improvements for analyte throughput.¹⁴³

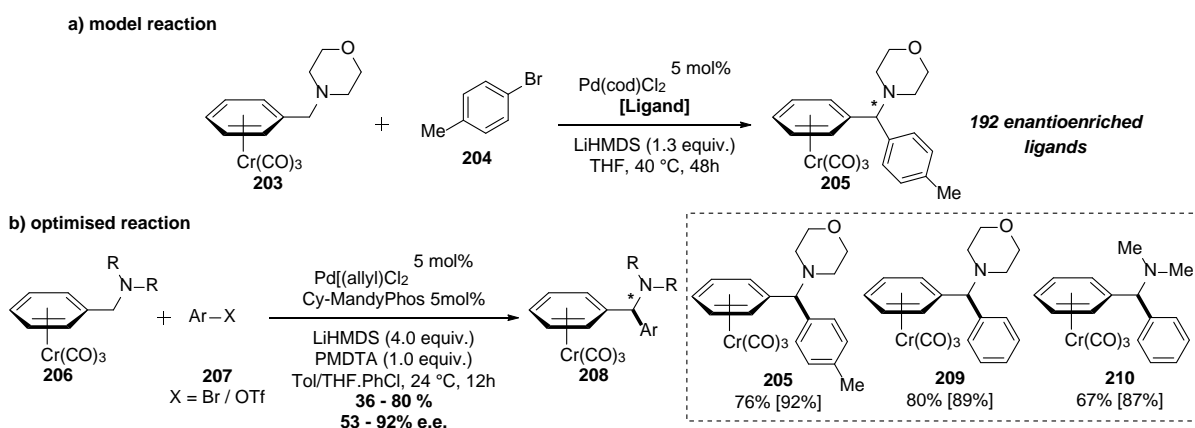
Noting a lack of first-row transition metal catalysts for asymmetric hydrogenation,¹⁴⁴ Chirik employed cobalt catalysts with discrete electronic structures to expand first-row transition metal catalysed asymmetric hydrogenation. Employing chiral SFC to rapidly assess the enantioselectivity of reactions in high-throughput, Chirik developed a the asymmetric hydrogenation of 2-acetamidoacrylates and, more impressively, trans-stilbenes.¹⁴⁵ Each reaction was assessed in less than 7 minutes, obtaining both relative starting material conversion and an overall reaction e.e.

In addition, Chirik also employed SFC and high-throughput parallel screening to discover a nickel-catalysed asymmetric hydrogenation of α,β -unsaturated esters (Scheme 29).¹⁴⁶ A diverse library of 192 different enantiopure ligands were screened with nickel(II) acetate in methanol under 500 psi of hydrogen. This approach found MeDuPhos **200** gave moderate conversion of **198** to **199** by SFC, with encouraging e.e., which served as a lead hit for further optimisation. Further multi-parallel screening revealed a combination of nickel(II) acetate and tetrabutylammonium iodide were key for high yielding transformation with excellent e.e.



Scheme 29: Nickel catalysed asymmetric hydrogenation screened in high-throughput. A) model reaction screened in three different assays screened on 20 μ mol of substrate; B) optimised reaction with select substrate scope.

The Walsh group continued their C–H functionalisation work to develop a dynamic kinetic resolution of activated benzylic C–H bonds to obtain enantiopure compounds **205** under strongly basic conditions.¹⁴⁷ A library of 192 structurally and electronically diverse enantioenriched mono- and bidentate ligands were screened for the coupling of dimethylbenzylamine-chromium complex **203** with bromotoluene **204**, all of which were analysed by chiral SFC (Scheme 30). The analytical strategy quickly found ferrocenylphosphine ligands returned the highest enantioselectivities, albeit with moderate yields. To improve the initial hit reaction, batch-scale optimisation was used to screen various additives which subsequently found the addition of chlorobenzene and PMDTA furnished asymmetric product **208** in good yield and excellent enantioselectivity. The substrate scope was tolerant of electron rich substrates and heterocycles but was unable to transfer electron poor aryl groups.



Scheme 30: Asymmetric arylation of tertiary benzylamines. A) Model reaction screened using high-throughput assay; B) Optimised reaction with selected substrate scope. Yield quoted and e.e. in [].

Chromatographic techniques, coupled with UV/Vis analysis, are extremely versatile analytical methods for high-throughput reaction development. Improved throughput can be obtained when employing current state-of-the-art UPLC machinery, which also comes with an associated increased capital cost. In addition, chiral SFC has made significant improvements for high-

throughput chiral analysis over conventional HPLC, although the assay lengths still limit sample throughput.

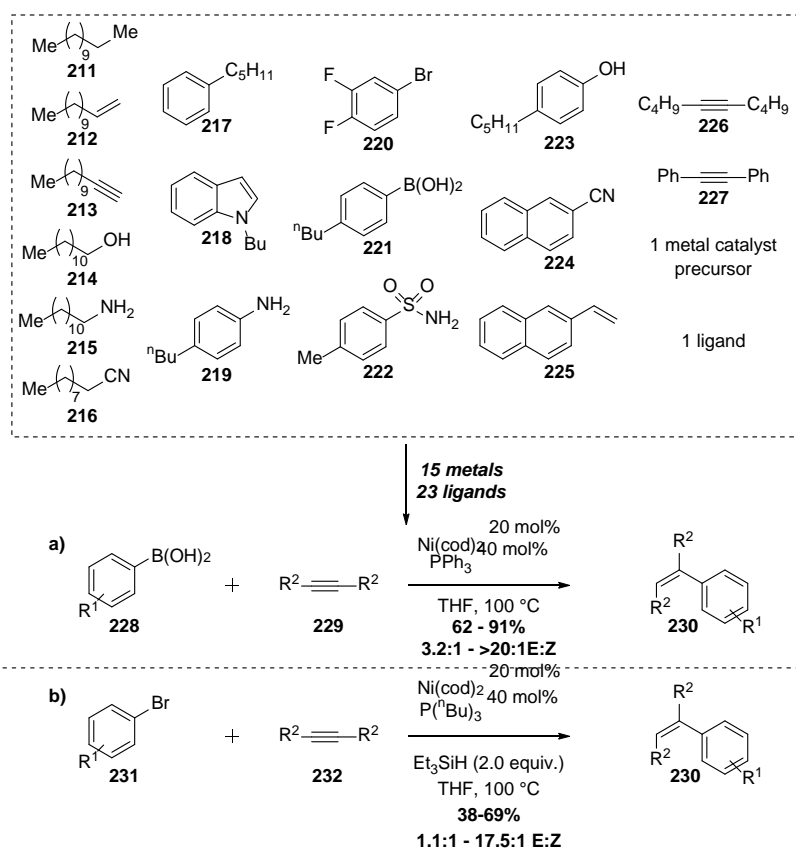
1.4.5. Chromatographic Coupled Mass Spectrometry

Chromatography coupled with mass spectrometry is commonplace in any synthetic chemical laboratory. The combination of chromatographic separation along with the detailed analytical power of mass spectrometry allows intricate sample analysis and, in combination with internal standards, semi-quantitative or even fully quantitative analysis can be achieved. Single quadrupolar LCMS¹⁴⁸ and triple quadrupolar LCMS-MS¹⁴⁹ have been used in high-throughput drug screening, but these machines have had limited use in high-throughput reaction discovery and optimisation thus far.

1.4.5.1. Gas-chromatography tandem mass spectrometry

In 2017, Hartwig published a combinatorial approach to reaction discovery that could greatly reduce the time it takes to find new bond forming reactions (Scheme 31).¹⁵⁰ A library of 17 reagents **211-227** with diverse functionalities were screened against 15 different earth-abundant metals (with a control) and 23 ligands (including a control) on a 384-well plate. Reactions were sealed and heated at 100 °C before GCMS analysis.

Hartwig proposed a simple deconvolution strategy to aid reaction discovery. All potential bimolecular products with or without simple leaving groups loss (hydrogen, water, halides etc.) were calculated prior to analysis. These products had larger and distinguishable masses compared to the starting materials and could be used to simplify the GCMS spectra. The deconvolution strategy was validated by three positive control reactions: a Ni-catalysed carbocyanation reaction between **227** and **224**,¹⁵¹ Cu-catalysed Chan-Lam of an **219** and **221**¹⁵² and a Ru-catalysed alkylation of a **222** and **214**.¹⁵³ More importantly, two hydroarylation reactions were discovered using both an aryl boronic acids **228** or a bromoarenes **231**. The discovered reaction furnished stereochemically specific trisubstituted alkenes **230**, a transformation previously known with more expensive rhodium or palladium catalysts.^{154,155} Batch-scale optimisation was subsequently employed to complete the optimisation.



Scheme 31: Reaction discovery using combinatorial library of 17 monofunctionalised compounds against 1 metal catalysts and 1 ligand. A) Boronic acid-alkyne coupling B) Arylbromide coupling with alkyne.

Although combinatorial screening methods were successfully demonstrated for reaction discovery, the deconvolution of each analytical sample means that a new discovery can take days or weeks. Hartwig developed an automated analysis and interpretation strategy termed “snap deconvolution” to quicken GCMS analysis-to-hit times for combinatorial mixtures (Figure 6).¹⁵⁶ This approach employed reactive functional groups ordered into clusters (α , β , γ), which possessed the same reactive functionalities appended to similar scaffolds with different masses. If bond formation occurred between the same functionalities within the clusters, their corresponding product masses could be rapidly identified using Excel-macros and compared to verify the predicted outcome.

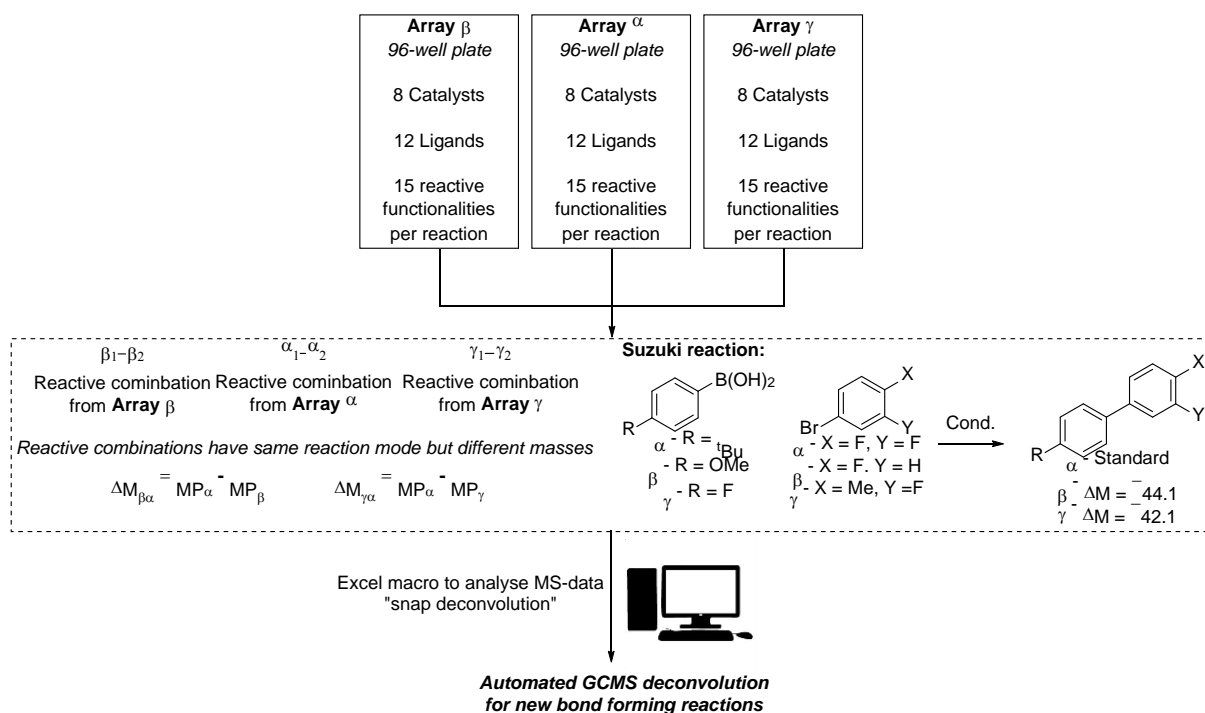
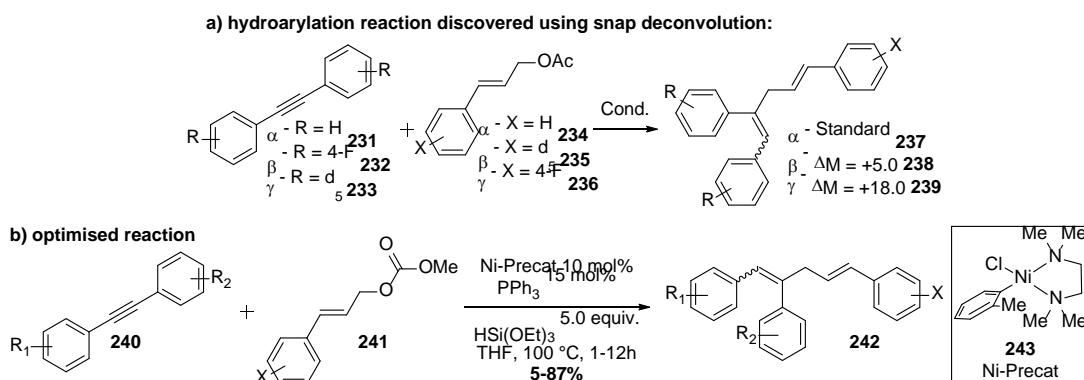


Figure 6: Snap-deconvolution strategy employed by Hartwig to automate GCMS analysis. Reactive functionalities were screened combinatorically in wells and the difference in masses were used to rapidly assess whether new reactions had taken place between arrays.

The “analytical suite” predicted and calculated product masses of bimolecular or trimolecular combinations, incorporating the corresponding loss of reactive functionalities such as bromides or boronic acids. Reaction products could then be identified from the reactant clusters to reveal complementary reactive functionalities and catalyst/ligand combinations. Assuming only bimolecular and trimolecular were to occur, over 1600 potential reactions were analysed by GCMS in three 96-well plates at 11-minutes per sample (a total of 53 hours of analysis). The snap deconvolution strategy automated analysis of the corresponding spectra, an otherwise prohibitively time-consuming bottleneck for reaction discovery.

A positive control reaction (Suzuki-Miyaura cross coupling) was integrated into the screen (Figure 6) to confirm the viability of snap deconvolution in discovering new reactive combinations. In addition to the positive control, a new nickel-catalysed hydroallylation of alkynes was found, albeit in low yield. Further optimisation using parallel multi-variate high-throughput screening returned an optimised set of conditions capable of furnishing a diverse range of hydroallylated products in 5-87% yield (Scheme 32).



Scheme 32: a) Hydroarylation discovered using snap deconvolution. b) Optimised reaction using conventional parallel multi-variate screening.

The snap deconvolution strategy is an attractive solution for high-throughput analysis of combinatorial reaction mixtures. The automated Excel ‘analytical suite’ used to rapidly deconvolute the data not only assesses exact substrate pairs but also the extract catalyst/ligand combination. These new hits were taken on for further optimisation, either using high-throughput platforms or conventional batch chemistry. The unautomated reaction setup process, however, requires manual 96-well reactor plate preparation which can be tedious and time-consuming.

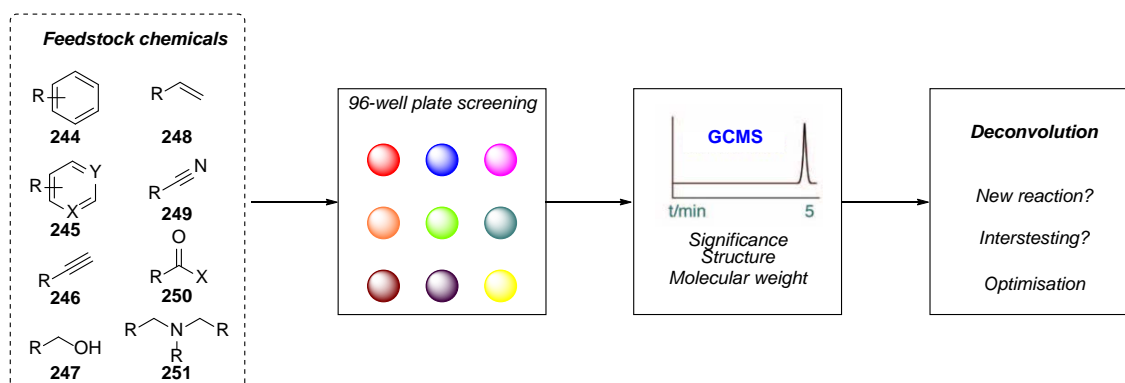
The MacMillan group hoped to “accelerate serendipity” in a similar way to Hartwig by employing a fully automated high-throughput reaction preparation robot from ChemSpeed.¹⁵⁷ The ChemSpeed synthesiser (Figure 7) is a versatile robot capable of automating workflows such as reagent preparation, solid weighing and liquid dispensing, multistep synthesis, reaction workup, purification and analysis.¹⁵⁸ Up to 96 reactions can be performed in one array in a variety of different solvents in less than 1.0 mL total reaction volume. The ChemSpeed synthesiser has been applied in automated library synthesis^{159–162} but there are limited reports of reaction screening, although, examples have been reported by BASF in a review by Jäkel¹⁵⁸



for high-throughput asymmetric hydrogenation.

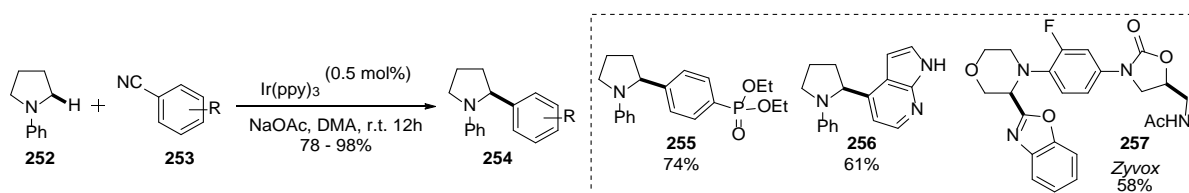
Figure 7: ChemSpeed SLT-100. Image copyright ChemSpeed®, Switzerland. Image use with permission from ChemSpeed.

Cheap and commercially available feedstock chemicals **244-251** were dosed into 96-well plates to assess whether the time taken to discover a new bond forming reaction could be accelerated by screening different transition metal complexes and ligands (Scheme 33). The authors discovered a novel C–H arylation with electron deficient arenes employing photoredox catalysis. The ChemSpeed was used to automate reaction set up in 96-well plates which required 0.1 mmol of reactant in 500 μ L of solvent. Once the plates were dosed and sealed, the array was taken to a conventional hotplate that either stirred, heated or attached with a CFL light. Crude reaction mixtures were aliquoted into vials and analysed by GCMS.



Scheme 33: High-throughput reaction screening using ChemSpeed robot. Feedstock chemicals were dosed into a 96-well plate in different combinations and screened. GCMS analysis of all reactions and subsequent deconvolution lead to batch scale optimisation.

To identify new products, a rapid method was developed to show samples only with substantial peak intensities and, using the NIST mass spectral structural database, identify novel structures. This method identified new metal catalysts for existing reactions which, although interesting, were deemed less important than the new photoredox reaction (Scheme 34). With the new reaction in hand, batch scale optimisation was completed giving a high yielding and mild arylation reaction with a white light. The overall scope of the reaction shows compatibility with various cyclic amines **252** and electron deficient arenes **255**, as well as heterocycles **256** and pharmaceutically relevant compounds **257**, including the antibiotic, Zyvox.

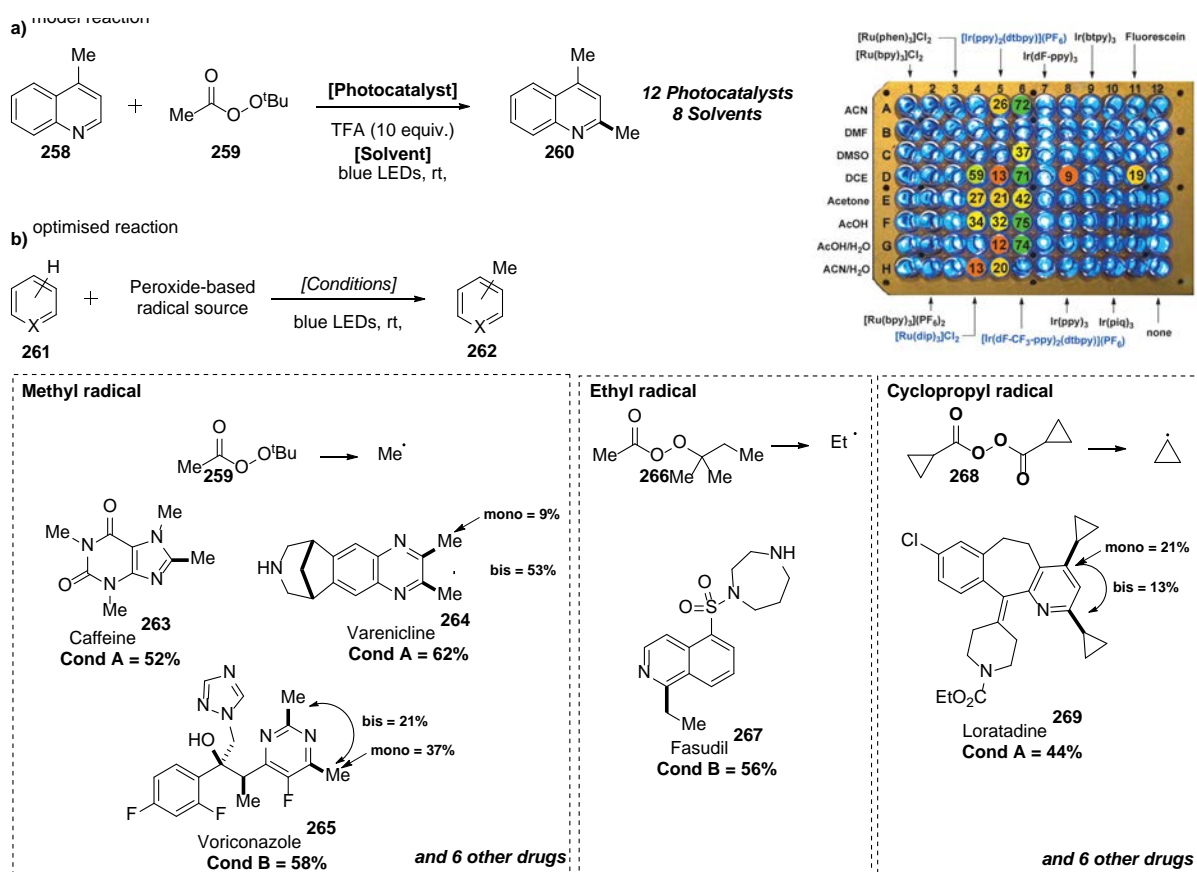


Scheme 34: C–H arylation of tertiary amines by photoredox catalysis discovered using accelerated serendipity high-throughput reaction discovery.

The Chemspeed robot leveraged to accelerate reaction discovery requires an overall capital cost of approximately \$1 million making it prohibitively expensive for most laboratories. The automated manner of reaction setup makes this approach very appealing for reaction discovery although, GCMS without a deconvolution strategy precludes a truly high-throughput method.

1.4.5.2. Liquid-Chromatography Tandem Mass Spectrometry

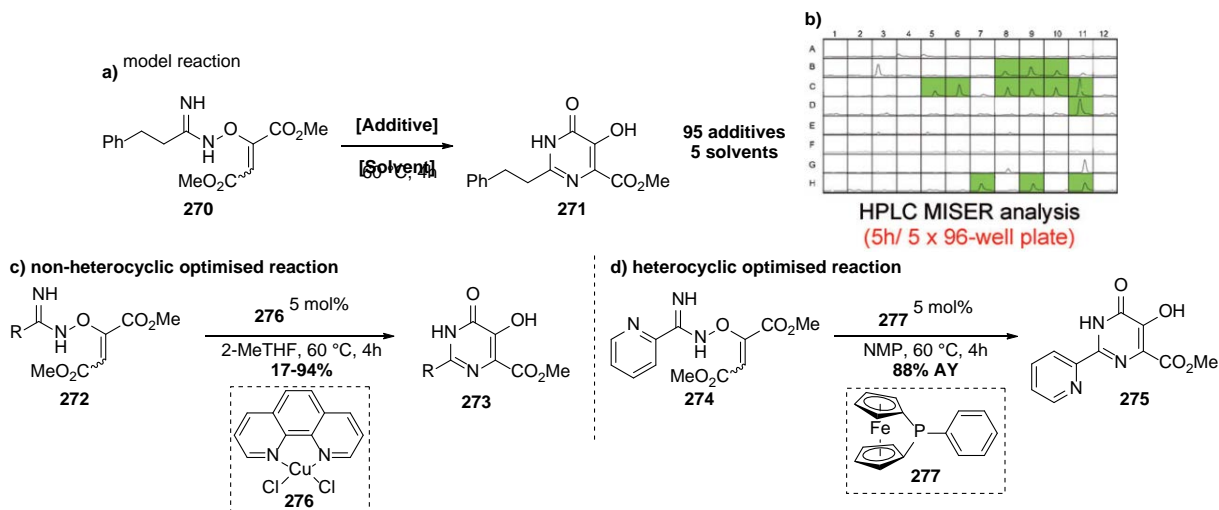
In 2014, Merck reported a photoredox Minisci reaction capable of methylating heterocycles **258** and late-stage drug fragments using *tert*-butylperacetate **259** as the methyl radical source. Using high throughput methodology, eight different solvents were screened against twelve different photocatalysts which rapidly identified conditions that gave the **260** in 75% assay yield (Scheme 32)¹⁶³ Each reaction was performed on 10 μ mol scale in 100 μ L of solvent per vial and a conversion for each reaction was obtained using UPLC-MS (biphenyl was employed as an internal standard).



Scheme 35: Minisci reaction optimisation in high-throughput using microvial array. A) Model reaction of lepidine **258** with *tert*-butylperacetate **259** with 96-well reactor array under blue LED lamp; B) Optimised reaction with selection of substrate scope covering methyl radicals, ethyl radicals and cyclopropyl radicals. Cond A = 2 mol% $[\text{Ir}(\text{ppy})_2(\text{dtbbpy})]\text{PF}_6$, TFA (1.0 equiv.), 1:1 AcOH:ACN (0.1M); Cond B = 2 mol% $[\text{Ir}(\text{ppy})_2(\text{dtbbpy})]\text{PF}_6$, 1:1 TFA:ACN (0.1M). Image use with permission from Angew. Chemie., RightsLink: 4534230025030.

Four different reaction conditions were reported to work well for the Minisci methylation across a range of pharmaceutically and agrochemically relevant molecules, in the presence of a variety of functional groups such as free alcohols, amines, amides and esters. Furthermore, by simply changing the peroxide reagent, different alkyl groups, such as ethyl **266** or cyclopropyl **268** could be added to late-stage drug targets as medicinally versatile bioisosteres.¹⁶⁴ This multi-variable screening strategy quickly assessed reaction conditions for these drug targets.

A new and rapid analytical technique was developed by Merck in 2010 called MISER which injects analytical samples in quick succession.¹⁶⁵ The samples can be passed through a chromatographic column or injected directly into a mass spectrometer to obtain a relative detector response (semi-quantitative yield). In 2012, Merck utilised MISER to analyse over 475 different reactions in five hours using 2.5 μmol of substrate per reaction, a total of only 370 mg for an entire optimisation.¹⁶⁶



Scheme 36: a) Model reaction investigated using MISER HPLC; b) MISER analysis of 96-well plate and “MISER-GRAM” output from HPLC. c) Optimised non-heterocyclic cyclisation; d) Optimised heterocyclic cyclisation. Image use with permission from Angew. Chemie, RightsLink: 4534230081698.

A range of solvents, catalysts, ligands, temperatures and reagent loadings were assessed to find a reaction for the synthesis of pyrimidinones **271**. A copper(II) chloride/phenanthroline complex **276** was found to furnish the pyrimidinone targets **273** in excellent yield. On the other hand, substituted heterocyclic substrates gave low yields, however addition of ferrocenyl phosphine **277** was enough to catalyse the cyclisation for the synthesis of heterocyclic product pyrimidines **275**.

Further synthetic utility was shown by Merck when MISER analysis was used in combination with an automated reaction discovery and optimisation platform leveraging a liquid handling robot, developed by TTPLabTech, called the Mosquito[®] (Figure 8).¹⁶⁷ The Mosquito[®] has previously been marketed as a solution for biochemical and pharmacological applications, with its remarkable accuracy and microtiter plate compatibility. Its niche has been in protein crystallisation experiments which require high accuracy, as well as for serial dilution experiments and other repetitive liquid handling tasks. Its overall capital cost of £50,000 makes it an accessible machine for industrial and academic laboratories.

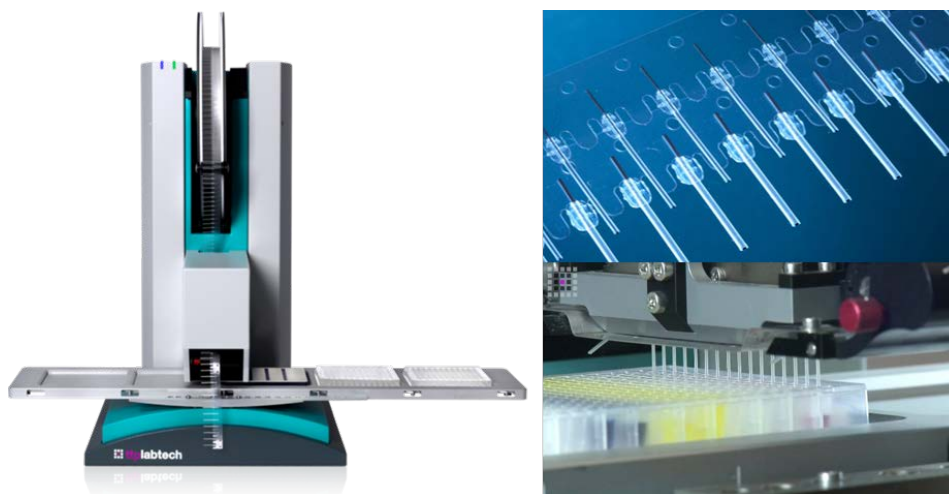
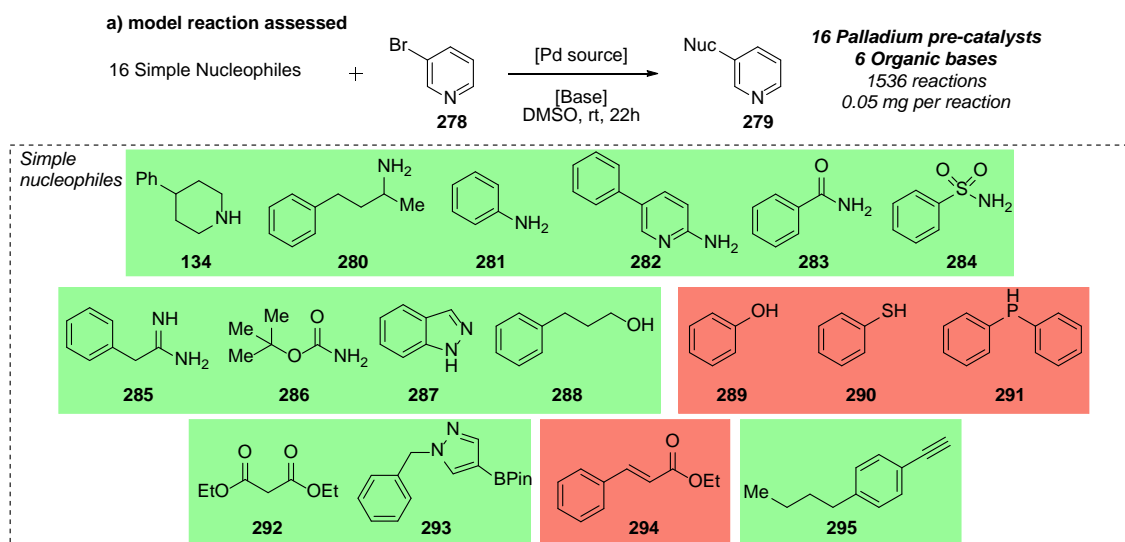


Figure 8: Mosquito[®] liquid handling robot. Image use with permission from TTPLabTech.

The team at Merck cited that approximately 50% of all palladium catalysed reactions attempted within the company failed, thus key drug candidates within SAR target libraries would be missed and therefore potentially vital information would be lost. In attempt to develop a platform to rapidly screen palladium-catalysed Buchwald-Hartwig reactions on late-stage drug fragments, Merck designed a parallel screening strategy on 1536-well plates. The Mosquito[®] was able to dose 1536 unique reaction combinations using small (1000 nL total reaction volume) quantities of material from millimolar reagent stock solutions.

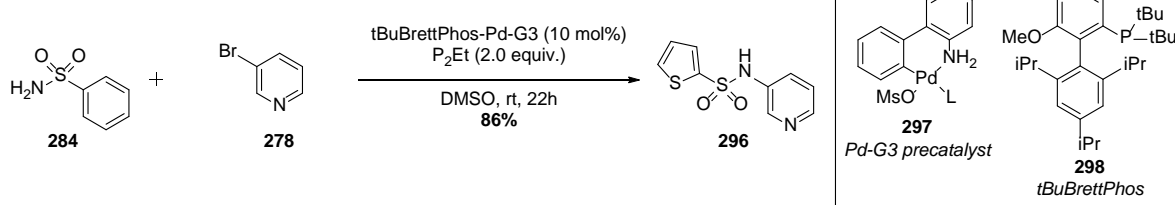
3-Bromopyridine **278** was chosen as a model coupling reagent as the pyridine motif is often found in pharmaceutically active compounds (Scheme 37). The Mosquito[®] dosed a 1536-well reactor plate with a combination of 16 different catalysts, six different strong organic bases and 16 different nucleophiles resulting in 1536 different reaction conditions in one single screen. Each reaction was performed in 1 μ L of solvent with 100 nmol of aryl halide. UPLC-MS analysis of these reactions was performed and, using a ratio of the total ion count of product compared to internal standard (4-isopropylbiphenyl) semi-quantitative yields were obtained.



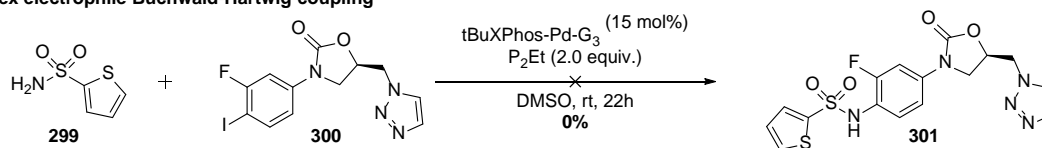
Scheme 37: Nano-mole reaction screened using Mosquito[®] liquid handling robot. A) Model reaction screened in 1536-well plate. Conditions were found for substrates in green, while those in red were not found.

Hit reactions from the UPLCMS were validated on millimole scale and found high yielding Buchwald-Hartwig arylation conditions for 13 of the original 16 substrates, for example the coupling of **284** with **278** gave secondary amine **296** in 91% isolated yield (Scheme 38a). A set of twelve more complex amines nucleophiles reacted with eight complex, drug-like aryl halides under the newly discovered conditions from the first screen. When amines with the same reactive functionalities such as **299** and **300** were tested using the newly discovered conditions, no product was observed by UPLCMS (Scheme 38b).

a) simple substrate Buchwald-Hartwig coupling



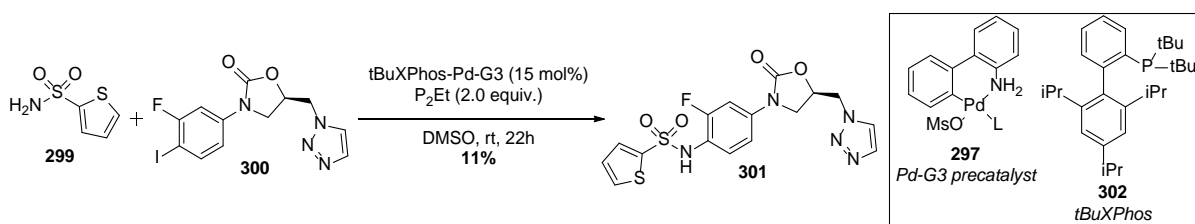
b) complex electrophile Buchwald-Hartwig coupling



Scheme 38: High-throughput optimised Buchwald-Hartwig amination. A) Simple substrate optimisation on the C–H arylation of malonate; B) Same conditions as the simple substrate were then exposed to more complex electrophiles but no product was observed.

Therefore, a secondary screen of six complex electrophiles and twelve nucleophiles were assessed with six palladium pre-catalysts and eight organic bases, constituting 1536 unique reactions. MISER was used rather than UPLCMS to rapidly analyse all reactions. Semi-quantitative data was obtained with a triple-quadrupolar mass spectrometer. As the MISER autosampler was compatible with 384-well plate only, one 1536-well reactor plate was dispensed into four separate 384-well analysis plates and were analysed in nine hours. The analysis protocol could be streamlined further by combining four reactions in one well of a 384-

well plate (only one 384-well analysis plate for 1536 reactions) and using selective ion monitoring, which reduced the analysis time to 2 hours. New conditions were found by MISER to furnish all 21 products in quantities sufficient for biological testing (Scheme 39).



Scheme 39: **299** and **300** reassessed using Mosquito[®] high-throughput optimisation. New conditions gave 11% isolated yield, enough for an enzymatic assay.

This strategy reported by Merck is the cutting edge of high-throughput reaction discovery and represents a substantial progression in the application of robotics for synthetic chemistry. Although the use of MISER-MS-MS is prohibitively expensive for academic laboratories, the fundamental concept is certainly appealing and could be adapted to normal LCMS. The automated Mosquito[®] liquid handling robot does come with a significant limitation that needs to be addressed for synthetic chemistry. Using microlitres of solvent in high-surface area:volume ratio microtiter plates limits what solvents are compatible with the technique. High-vapour pressure and low boiling point solvents such as dichloromethane and tetrahydrofuran evaporate too readily, but low-vapour pressure and high boiling point solvents such as dimethylsulfoxide and dimethylformamide are compatible.

1.5. Conclusion and Outlook

A plethora of analytical techniques have been applied to high-throughput reaction discovery and optimisation. Most of the techniques discussed have required prohibitively expensive equipment (MALDI, MS-MS), labour-intensive and esoteric tethering strategies (eIDA, ELISA) or prefunctionalisation of starting materials. The most promising technique discussed has been the work of Merck using MISER; this novel technique facilitates rapid analysis, without the need of analytical handles, using 96-well and 384-well plates albeit in only a semi-quantitative manner. Therefore, a rapid, fully quantitative analysis technique using cheaper analytical machinery represents a powerful and transformative strategy.

1.6. Aim of Research

The Gaunt group's high-throughput research is split into two areas: the application of large data sets and computational modelling methods for quantitative reaction prediction and to quicken the reaction development process by leveraging automated machinery. As the Mosquito[®] has shown potential in an industrial setting for reaction development, the aim was to translate this platform in the academic laboratory to aid reaction preparation. To achieve this, the following were considered:

1. Prepare Excel-based spreadsheets to automate stock solution calculation and source plate design.
2. Program the Mosquito[®] liquid handling robot to dispense nanolitre stock solutions.
3. Explore and implement LCMS for quantitative high-throughput analysis.
4. Implement statistical tests to automatically analyse data and exclude anomalous data.
5. Integrate calibration curves to obtain quantitative data and visualise each high-throughput array using heatmaps.
6. Apply the standardised protocol to a proof-of-concept reaction to generate quantitative data.
7. Model the data using machine learning algorithms for chemical reaction outcome prediction.
8. Investigate new triaging methods for reaction discovery

Chapter 2: High-Throughput Protocol Standardisation

2.1. Introduction

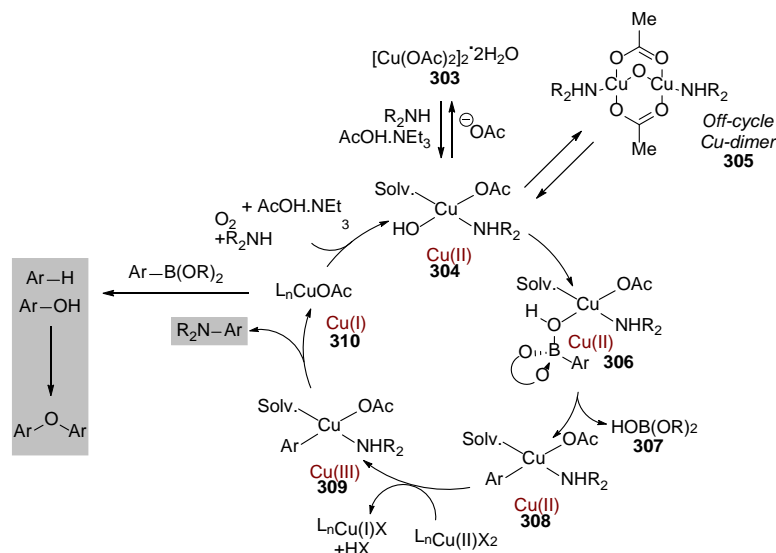
The exemplary work by MSD showed the potential impact that high-throughput machinery could have on synthesis.¹⁶⁷ Assessing thousands of reaction combinations rapidly, and in parallel, revealed new conditions for complex substrates in a shorter time compared to iterative procedures. The analytical equipment, UPLCMS-MS or MISER-MS-MS, improved sample throughput and, more importantly, required no prior substrate pre-functionalisation.¹⁶⁵ The prohibitive cost of these machines, however, restricts the general application of this strategy to institutions where the technology available. Although the initial results from the HTE protocol were performed in triplicate, later arrays were performed in singlet, increasing the chances of false positives or run-to-run error.

With the previous work by MSD in mind, a complementary study was proposed to benchmark the Mosquito[®] liquid handling robot for high-throughput reaction development in an academic laboratory. The new protocol would stand out from the seminal publication by leveraging simpler, automated single-quadrupolar LCMS to obtain quantitative data. To standardise the high-throughput protocol, a C–N bond-forming reaction, the Chan-Lam, was chosen which utilises cheap and readily available copper catalysts.

The Chan-Lam reaction was first discovered in the 1990 by Dominic Chan and Patrick Lam^{152,168}, two medicinal chemists at DuPont. Initially reported using stoichiometric copper, it has since been made catalytic by the addition of an oxygen atmosphere as the catalyst turnover reagent (Scheme 40).^{169,170} Employing either nitrogen- or oxygen-based nucleophiles and boronic acid or ester coupling partners, high-yielding reactions transfer of both heterocycle and arenes to primary or secondary amines can be obtained at elevated temperatures. This relatively simple protocol does not have a straightforward mechanism with multiple catalyst oxidation states and off-cycle species. Recent spectrochemical analysis for oxygen-based nucleophiles by Stahl¹⁷¹ and nitrogen-based nucleophiles by Watson¹⁷² has elucidated key intermediates as well as a general mechanism (Scheme 40).

An initial denucleation of the copper(II) acetate **303** by the amine starting material and conjugate acid of triethylamine results in a mononuclear and catalytically active copper(II) complex **304**. This complex **304** is also in dynamic equilibrium with a catalytically inactive dimeric complex **305** (tetrameric complexes were also observed). The boronate ester can engage with the copper-hydroxyl group leading to pre-transmetalation species **306**, which was computed to have a lower energy than complexation through the acetate ligand. Four-membered

transmetalation of the boronic ester with the concurrent expulsion of acid **307** gives the organocopper intermediate **308**. Disproportionation of **308** with copper(II) results in copper(III) intermediate **309** which undergoes product yielding reductive elimination. The furnished copper(I) species **310**, which was shown to be responsible for deleterious side reactions, was reoxidised with molecular oxygen in the presence of amine conjugate acid.

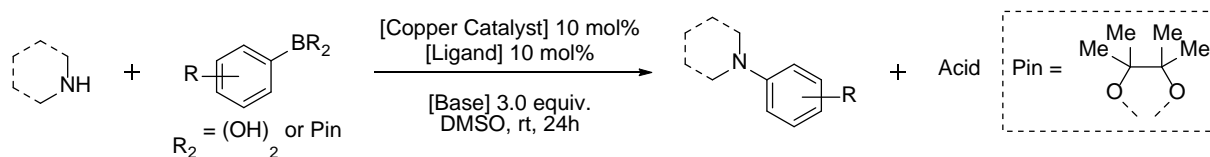


Scheme 40: Catalytic Chan-Lam amination of boronate esters as proposed by Watson¹⁷²

Although the Chan-Lam reaction has been known for more than twenty years¹⁷³ optimised conditions have not been found when DMSO has been used as the solvent even though it possesses attractive properties such as organic compound and oxygen solubility.¹⁷⁴ Stoichiometric quantities of both amine and boronic ester were also chosen in the effort to find an efficient set of conditions. As the Mosquito[®] would be housed outside a glove-box, air would be used as the terminal oxidant. Noted at the end of the previous section, all reactions take place at room temperature to minimise solvent evaporation. Carbon-nitrogen bond-forming reactions are a highly desirable class of transformations encompassing over 50% of all reactions performed in industry.¹⁷⁵ Therefore, mild conditions for the Chan-Lam amination would be a significant addition to this field.

Before high-throughput screening was started, all assessable reaction components were identified for the Chan-Lam reaction. Five-components were identified for assessment in high-throughput; 1) amine; 2) coupling partner; 3) copper catalyst, 4) ligand; 5) base (Scheme 41). In line with iterative optimisation protocols, the amine was kept constant throughout the protocol. Boronic acids or esters were chosen as the reactive species due to the commercial availability, stability and ease of synthesis. Catalyst and ligand were set to 10 mol% loading allowing facile differentiation between obvious hits low yielding conditions. Different bases with a range of pK_as would allow for complete reagent assessment. The base loading was

initially set to 3.0 equivalents as the reaction can generate between one and three equivalents of acid depending on whether boronic esters or acids are employed.



Scheme 41: Variable assessment of the Chan-Lam for high-throughput reaction optimisation with the Mosquito® LHR.

With each variable identified, the overall high-throughput optimisation protocol was broken into individual areas which required bespoke optimisation or new solutions (Figure 9).

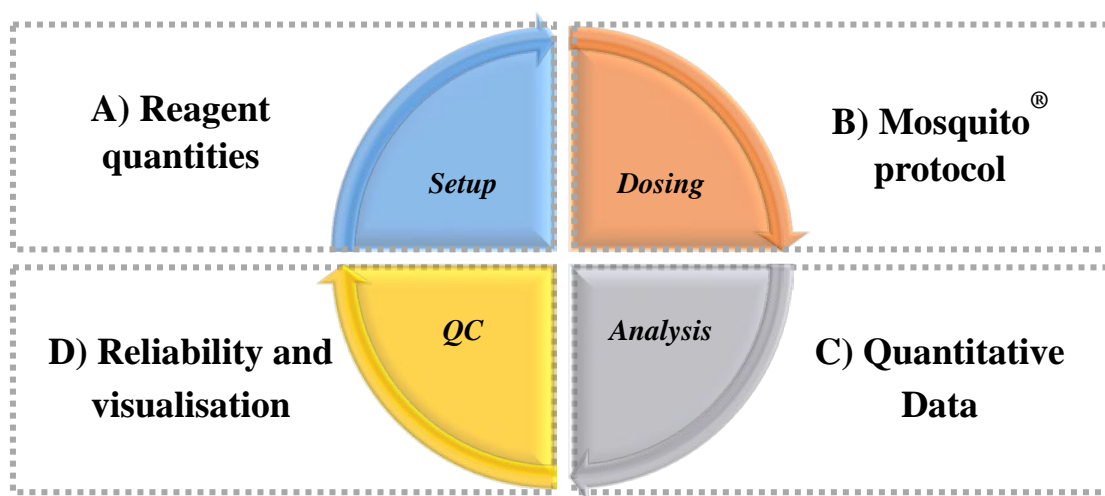


Figure 9: High-throughput optimisation protocol in four unique areas. 1) Reaction setup where reaction quantities need to be calculated; 2) Using the Mosquito® to dose a well plate with reagents for reaction optimisation; 3) Analysing all the reaction rapidly and quantitatively; 4) Assessing all the data using statistical modelling and heatmaps for rapid hit identification.

The setup process was key to the entire high-throughput process (Figure 9a). Excel-based spreadsheets were identified as the perfect ‘analytical suite’ to aid the calculation of reagent quantities and stock solution volumes. The designed spreadsheet could also be adapted to screen any desired component set. Once stock solutions were calculated, a ‘source plate’ needed to be prepared before the ‘reactor plate’ is dosed by the Mosquito®.

Prior to reactor plate dosing, the Mosquito® needed to be programmed to (Figure 9b). The Mosquito® aspirates preprogrammed aliquots of each component from the source plate and dispenses it into a desired location on the reactor plate. Key information such as stock solution or reaction mixing is also held within the protocol and it was important to understand how to tailor each protocol to the chosen reaction. Once the Mosquito® protocol has finished, the reactor plate needed to be sealed to minimise solvent evaporation.

The lynchpin to this project was the successful implementation of quantitative LCMS (QLCMS) for high-throughput analysis. (Figure 9c). Short analytical method run times were

paramount to the concept as well as understanding of mass spectrometry and its associated phenomena. The Mosquito[®] could be used to prepare analysis plates with small volumes of reaction mixture which needed to be quenched to prevent over reaction during analysis. Internal standards and calibration curves were key to quantification. Data capture from thousands of different reactions needed to be simple and automated as well. Furthermore, statistical tests needed to be introduced to assess all data and exclude potentially anomalous results (Figure 9d). These tests were incorporated into the same Excel-spreadsheet for reaction setup, completing the high-throughput method.

This entire high-throughput process employing the Mosquito[®] robot requires a shift from the conventional 20th-century techniques of mechanical stirring and individual manual reagent preparation. As alluded to earlier, reactor microtiter plates are used where all reactions occur in wells. A small, microscale well does not require mechanical stirring as microfluidic mixing phenomena dominate over diffusion limited mixing.¹⁷⁶ Furthermore, for large screening arrays, individual substrate weighing only needs to be completed once as the LHR combines small aliquots of each reagent. As a result, all components need to be solubilised in the reaction media prior to setup.

2.2. How the Mosquito[®] Works

The Mosquito[®] LHR, designed by TTP LabTech, has been primarily used for protein crystallisation and serial dilution experiments until MSD reported its potential for chemistry.¹⁶⁷ In essence, the Mosquito[®] automates the pipetting of nanolitres of solvent from a ‘source plate’ to a ‘reactor plate’. The two plates are loaded onto the deck in any of the five different positions starting from 1 on the far left to 5 on the far right (Figure 10). The deck moves in a left to right fashion with only a small up-down movement.

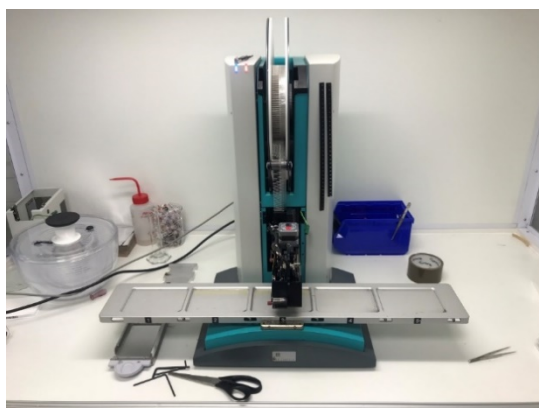


Figure 10: The Mosquito[®] liquid handling robot in the fume cupboard.

The solvent is transferred in small positive displacement pipettes (Figure 11) that are loaded onto the machine in large reels of over 30,000 pipettes and fed into the head by a set of motors.

A small clamp grips onto the pipettes to pull the metal syringe up to draw liquid up or push liquid out. The positive displacement nature of the pipettes means that highly accurate aliquot volumes can be measured and dosed (50 nL minimum volume) over conventional air displacement pipettes. There are two standard types of pipettes based on the distance between



the tips; 9.0 mm (compatible with 96- and 384-well plates) and 4.5 mm (compatible with 384- and 1536-well plates).

Figure 11: The pipettes the Mosquito[®] uses. Top = 9.0mm pitch needles for 96- or 384-well plates; Bottom = 4.5mm pipettes for 384- or 1536- well plates

The Mosquito[®] lowers the pipettes into the source plate and takes up a predetermined volume of liquid and subsequently doses this into the reactor plate. Each Mosquito[®] protocol can be simplified to the scenario presented in Figure 12. If three individual reagents (substrate, coupling partner and catalyst) were placed in different columns on the source plate and dosed to the same column on the reactor plate, four identical reactions will be prepared.

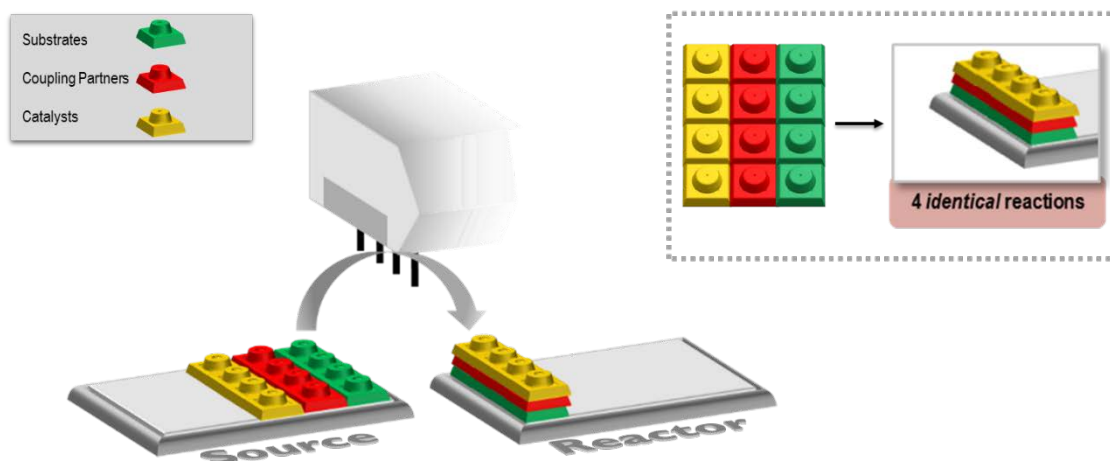


Figure 12: Simple Mosquito[®] liquid handling program. Simply compound all the columns on the source plate onto the reactor means 4 identical reactions are dosed.

Although this protocol is ideal for what the Mosquito[®] was designed for, it is otherwise limiting for synthetic purposes, in part due to the restrictions on the where the head can move and dose on the reactor plate. Therefore, to increase the number of reactions assessed in a single array a

more carefully designed source plate is needed with more complex patterns. For example, alternating the reagents can result in four different reactions in the reactor plate. Essentially, each row is compounded and added into one well on the reactor plate (Figure 13).

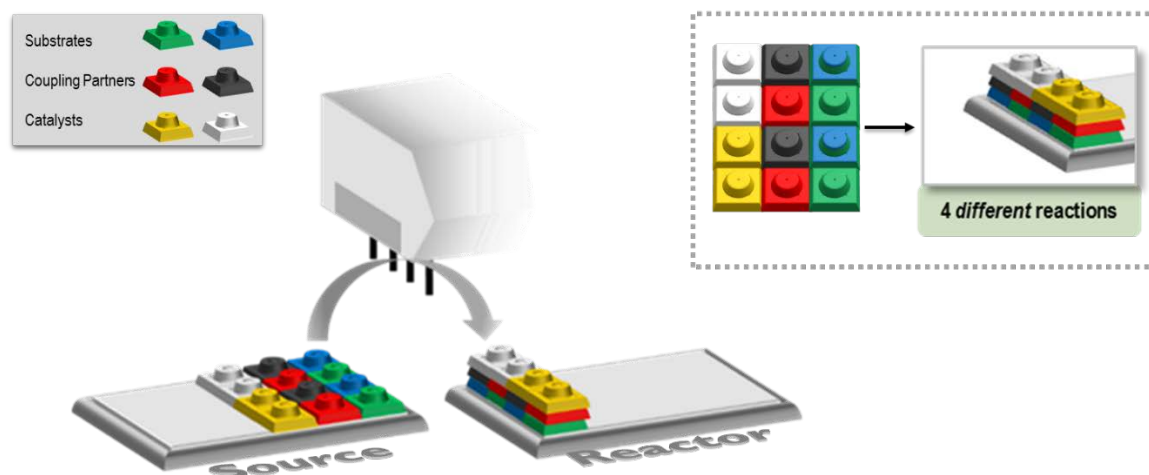


Figure 13: Increasing the number of substrates, coupling partners and catalysts from 1 to 2 and ordering them in a certain way on the source plate means we now have four individual and unique reaction conditions on the reactor plate.

2.3. Reaction Setup on Mosquito[®]

Before the Mosquito[®] LHR was used to prepare reactor plates, the source plate needed to be designed. Several factors needed to be considered such as the total number of reagents as well as the reaction scale and reagent equivalent loading. Reaction concentration and thus final reaction volume are also key to source plate preparation.

The simplest method to compute the total number of reagents that can be screened in a single array was by considering the dimensions of a 96-, 384- and 1536-well reactor plate (Figure 14). A 96-well plate is an array of 12 columns and 8 rows with an approximate working volume range of 40 to 500 μL (depending on the type of plate). The next step up is the 384-well plate with 24 columns and 16 rows with a total working volume range of 10 to 150 μL ; this array is twice the number of wells in each dimension, therefore, constituting a $2^2 = 4$ times increase. Lastly, the 1536-well plate is 48 columns by 32 rows with a total working volume range of 1 to 10 μL .

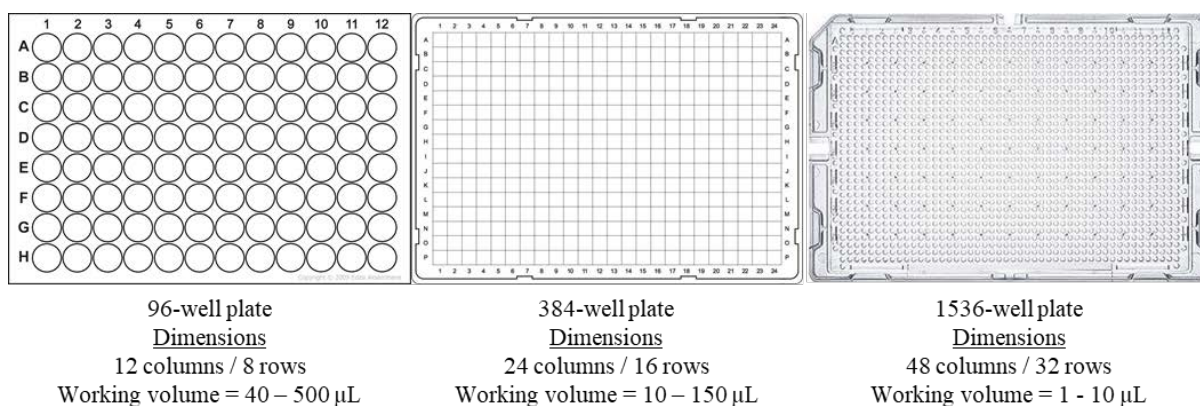


Figure 14: 96-, 384- and 1536-well plate used in high-throughput reaction screening.

To obtain the most information from a single high-throughput array, it is important to work out the total number of components assessed in a single screen and how to arrange these logically. In the simplest scenario for screening two variables, 12/24/48 different reagents can be organised on the x-axis of the plates and 8/16/32 different reagents on the y-axis on 96/384/1536-well plate respectively. Although multi-parallel screening of only two variables has previously been fruitful (as shown in Chapter 1), most synthetic reactions require more than two assessable components. Arranging three variables on a well plate, for example, requires each axis to be factored (Figure 15). Any number of different reagents can be screened and thus each axis can be cut multiple times corresponding to the number of variables.

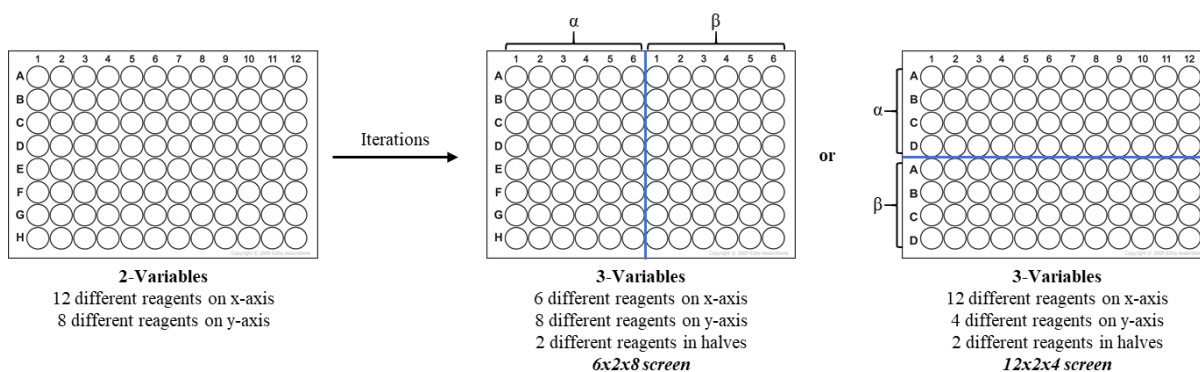


Figure 15: Increasing the number of variables screened from 2 to 3 requires a factoring of both axes, illustrated by a line.

Occasionally, integer numbers will only factor one of the dimensions, such as the number three. The y-axis of a 96/384/1536-well plate is 8/16/32 of a respectively and is not divisible by three. However, the x-axis is 12/24/48 which can be factored. Therefore, this restriction places a limit to the rule above such as the example presented in Figure 16. The x-axis of a 96-well plate can be easily cut into thirds to screen three different reagents, however, splitting the y-axis results in an unequal distribution of variables.

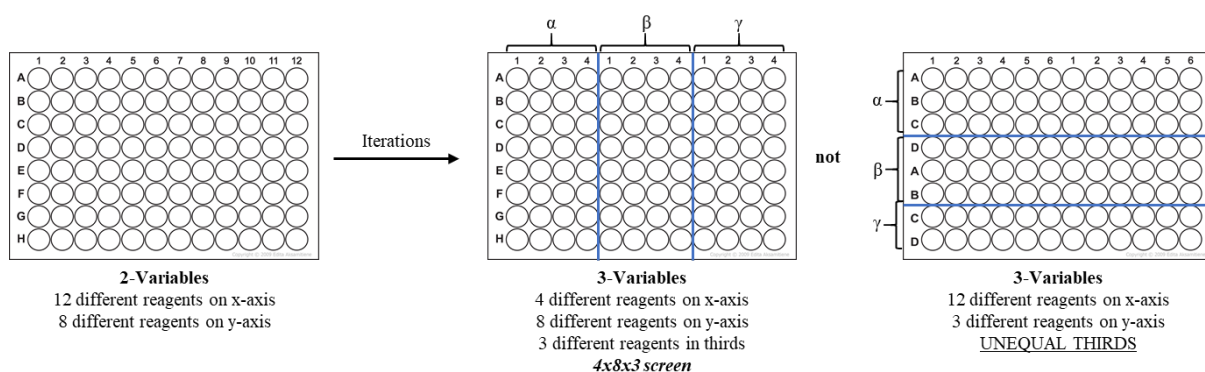


Figure 16: If there are three compounds within one variable screened then the reactor plate is limited to the x-axis. Splitting the y-axis into thirds leads to unequal division.

Adding a fourth variable adds another line to the 96-well plate either perpendicular to the current variables or within one of the previous factors, as shown in Figure 17.

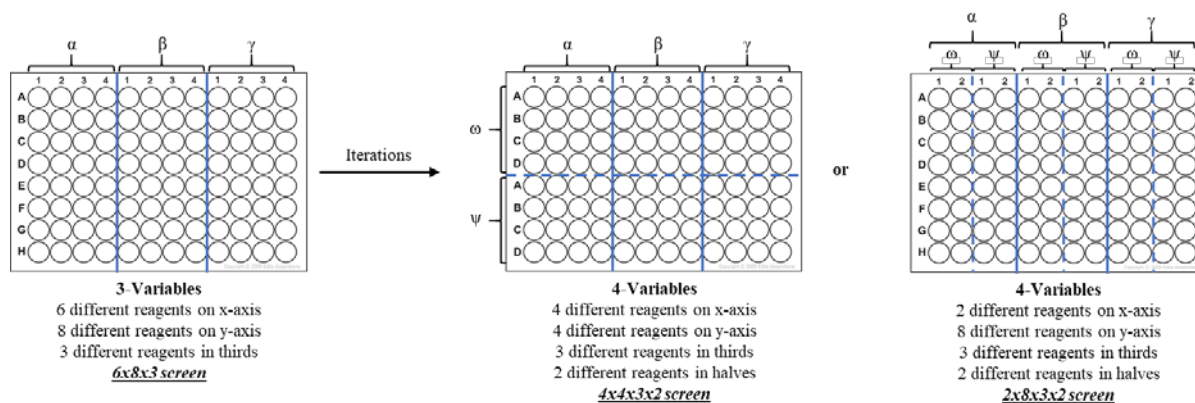


Figure 17: Increasing the total variables screened from three to four results in either a perpendicular factor or a split within one of the other factors.

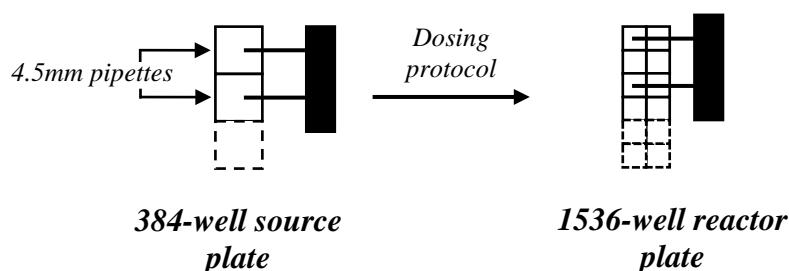
Throughout this process, patterns started to emerge when investigating different combinations in 96-well plates. A 96-well plate has prime factors of $2^5 \times 3$ that, when applied to each of the axes of the plate reveals a very simple way to calculate the variable that can be screened (Figure 18). The two-variable screen only has one set of combinations, 8×12 . Increasing to three variable screening reduces the total number of reagents assessed but allows greater chemical space to be explored. Colour-coding each axis allows easy identification of all combinations for both 3- and 4-variable reaction screening.



Figure 18: Example combinations for screening on a 96-well plate. Any permutation of these combinations can be used and are thus referred to as unique combinations.

Overall, this method identified 8 unique plate formats for 96-well plates, screening two-, three- or four variables on a single plate. Any permutations of these combinations are also allowed but these were noted as non-unique and therefore excluded. This process was also applied to 384-well plates ($2^7 \times 3$) to reveal nine unique reactor plate setups and 1536-well plates ($2^9 \times 3$) which returned only three unique reactor plate setups across two, three or four variable reactions. Limits of up to twelve different components within one variable were set to prevent potentially serendipitous reaction screening similar to the work of Hartwig¹⁵⁰ and MacMillan.¹⁵⁷ Therefore fewer unique combinations are possible. The unique reactor plate designs are shown in Appendix 4. To further simplify reactor plate design, a Python program was created to automatically generate all combinations for any reactor plate (Appendix 5).

With all potential reactor plate combinations in hand for the high-throughput reaction screening protocol, the corresponding source plates needed to be determined and designed. As alluded to earlier, different tape sizes are compatible with different plates (Figure 11). The tape fits into every source plate well but only into alternate wells on the reactor plate (Figure 19) and therefore, specific and unique reactor plates can also be designed based on the source plate



layout.

Figure 19: 4.5mm pipettes aspirating from a 384-well source plate to a 1536-well reactor plate. Dosing for every well on a 384-well plate means it dispenses every other well on a 1536-well plate thus one source plate well doses every other reactor plate well.

With all unique source plates and reactor plates designed, an Excel-spreadsheet was prepared to automate and facilitate reagent stock solution calculation (Figure 20). * Preparing the stock solutions can be daunting for a synthetic chemist so a simple and easy to use Excel spreadsheet was a key aim. Flexibility was also crucial for screening reaction conditions with different assessable components.

The top of the sheet specifies which reactor plate size is being used for future experimental reference. ‘# Reagents’, ‘Scale L.R.’ and ‘Final conc. Rxn (M)’ can also be input which subsequently calculates the ‘Stand. Aliq. (μL)’ (Equation 1) and ‘Reactor tot vol (μL)’, simply by multiplying ‘Stand. Aliq. (μL)’ by ‘# Reagents’.

$$\text{Standard aliquot volume} = \frac{\text{Scale L. R.}}{\left(\frac{\text{Final rxn concentration}}{\text{Reagent \#}}\right)} \quad \text{Equation 1*}$$

With the top row now populated, the white area can be filled out with ‘Compound’, ‘CAS’ and ‘FW (g mol⁻¹)’. The ‘Cat. No.’ column is purely there to aid chemical location in the laboratory inventory. The ‘Equiv’ column quickens the calculation of either stoichiometric or catalytic equivalents of reagent. The moles of each reagent per reaction, in micromole, is easily calculated by multiplying the scale of the reaction by the equivalent with Equation 2.

$$\text{Amount} = \text{Scale L. R.} * \text{Equiv.} \quad \text{Equation 2*}$$

‘mg per rxn’ is calculated using Equation 3. A simple logic function was applied to test whether data has been filled into the ‘Amount’ column; if a value is present the equation can be computed (green), if an error is found then a “N/A” is placed into the cell (red) alerting the user to a problem.

$$\text{mg per reaction} = \text{IFERROR}((\text{Amount} * 10^{-6} * \text{FW}), \text{"N/A"}) \quad \text{Equation 3*}$$

‘Solubility problems? Aliquot vol (μL)’ was added to allow seamless stock solution calculation for compounds that are sparingly soluble at the ‘Standard Aliq (μL)’ concentration. Boronic esters **S1–S8** are sparingly soluble at the standard aliquot volume and require a more dilute stock solution and an increased aliquot volume to ensure the correct volume was added to the reactor plate. Furthermore, boronic ester **S3**, **S6** and **S8** are less soluble than the others and require further dilution.

With the possibility of each reagent possessing different reagent aliquot additions, a complex logic equation had to be prepared to guarantee the ‘reactor tot vol’ was added to the reactor

* In collaboration with Dr Rachel Grainger

plate. Equation 4 shows the overall logic function to produce ‘Stock solution (mg/vial)’ that the user needs to weigh out. It initially tests whether all the aliquot volumes sum to the total reaction volume calculated at the top of the sheet. If true, the total mass of each reagent (green) is calculated. If the logic function fails, then “Aliq. ERR(red) is then displayed to notify the user that the aliquot volumes in ‘Solubility problems? Aliquot vol (µL)’ do not total the ‘Reactor tot vol (µL)’’. The last logic function, Equation 5, then assesses whether data is present or not.

Stock solution mg per vial

$$\begin{aligned}
 &= \left(IF \left(SUM(Aliquot R_n, Aliquot S_n, Aliquot B_n, Aliquot C_n, Aliquot L_n) \right. \right. \\
 &= Total\ reaction\ volume, \left. \left. \left(\frac{mg\ per\ reaction}{Aliquot\ volume} \right) \right. \right. \\
 &\left. \left. * Stock\ solution\ volume, Aliq.\ ERR. \right) \right) \quad \text{Equation 4}^*
 \end{aligned}$$

$$Stock\ solution\ per\ vial = IFERROR (number, "N/A") \quad \text{Equation 5}^*$$

PLATE 1536	# reagents 5	How much of plate? All	Input wells/column 32	Scale L.R. (umol) 0.25	Final conc. Rxn (M) 0.1	Stand. Alq. (ul) 0.5	Reactor tot vol (ul) 2.5	
constant? (constant)	Reagent	Compound	CAS	Cat No	FW (gMol-1)	Equiv.	mg per rxn	Solubility problems? Aliquot vol(ul)
(constant)	B1	4-phenylpiperidine	771-99-3	P.034	161.12	1	4.03E-02	0.38
	S1	PhBPin	24388-23-6	HTE	204.076	1	5.10E-02	1.00
	S2	4-OMeBPin	171364-79-7	HTE	234.102	1	5.85E-02	1.00
	S3	4-CF3BPin	214360-65-3	HTE	272.074	1	6.80E-02	1.25
	S4	4-IBPin	73852-88-7	HTE	329.972	1	8.25E-02	1.25
	S5	3-EOAcBPin	269410-00-6	HTE	276.139	1	6.90E-02	1.00
	S6	3-PyridineBPin	181219-01-2	HTE	205.064	1	5.13E-02	1.25
	S7	5-IndoleBPin	269410-24-4	HTE	243.113	1	6.08E-02	1.00
	S8	2-NapBPin	256652-04-7	HTE	254.136	1	6.35E-02	1.25
(k-constant, y-variable)	B1	No Base		0		0	0.00E+00	0.25
	B2	DBU	6674-22-2	D301	152.24	1	3.81E-02	0.25
	B3	Collidine	108-75-8	C31	121.18	1	3.03E-02	0.25
	B4	DABCO	280-57-9	D052	112.17	1	2.80E-02	0.25
	B5	Tetramethylurea	632-22-4	Dave	116.16	1	2.90E-02	0.25
	B6	Urea	57-13-6	U.002	60.06	1	1.50E-02	0.25
	B7	MTBD	84030-20-6	Dave	153.22	1	3.83E-02	0.25
	B8	BTMG	29166-72-1	B032	171.28	1	4.28E-02	0.25
(k-constant, y-variable)	C1	Cu(I)Cl	7758-89-6	cat.025	99.00	0.1	2.48E-03	0.13
	C2	Cu(I)Cl2		IC058	134.45	0.1	3.36E-03	0.13
	C3	Cu(I)(OTf)2	34946-82-2	cat.150	361.68	0.1	9.04E-03	0.13
	C4	Cu(I)(NO3)2.3H2O	10031-43-3	IC010	241.60	0.1	6.04E-03	0.13
	C5	Cu(I)(BF4)2.H2O	207121-39-9	IC014	237.16	0.1	5.93E-03	0.13
	C6	Cu(II)Br2	7789-45-9	IC022	223.35	0.1	5.58E-03	0.13
(k-variable, y-constant)	L1	1,10-phenantroline	66-71-7	P.228	180.21	0.1	4.51E-03	0.75
NORMAL DILUTION	L2	2,2-bipyridyl	366-18-7	B.462	156.18	0.1	3.90E-03	0.50
(k-variable, y-constant)	L1	1,10-phenantroline	66-71-7	P.228	180.21	0.1	4.51E-03	0.50
INCREASED DILUTION	L2	2,2-bipyridyl	366-18-7	B.462	156.18	0.1	3.90E-03	0.50

Stock solution (mg/vial)	Stock solution (solvent/vial)	Stock solution (min vol/vial)	Source (abs vol/vial)	Source (rec vol/vial)	Source plate loading (vol/well ul)	Liquid reagents (Vol/SS)	DMSO Top-up
107.4	1000	259	9	16	62.5	X	X
35.7	700	691	24	43			
41.0	700	691	24	43			
49.0	900	864	30	54	43.75	X	X
59.4	900	864	30	54			
48.3	700	691	24	43			
36.9	900	864	30	54			
42.5	700	691	24	43			
45.7	900	864	30	54			
0.0	100	0	0	0		X	X
15.2	100	0	6	11		13.7	86.3
12.1	100	0	6	11		13.3	86.7
11.2	100	0	6	11		X	X
11.6	100	0	6	11	50	12.0	88.0
6.0	100	0	6	11		X	X
15.3	100	0	6	11		14.4	85.6
17.1	100	0	6	11		20.2	79.8
7.9	400	14	1	1			
10.8	400	14	1	1	25	X	X
28.9	400	14	1	1			
19.3	400	14	1	1			
19.0	400	14	1	1			
17.9	400	14	1	1			
2.4	400	259	18	32	50.0	X	X
2.1	400	259	18	32			
3.6	400	173	12	22	50.0	X	X
3.1	400	173	12	22			

Figure 20: Excel Spreadsheet designed for source plate setup Spreadsheet shown split into two for clarification.*

The next three columns establish the total volume of stock solution that the end user needs to prepare to dose the reactor plate. Initially, the absolute source plate volume ‘Source (abs vol/well)’ is calculated by Equation 6; i.e. the minimum volume of stock solution required to dose the reactor plate. Multiplying the columns filled on a 1536-well plate by 2 is necessary as each source plate well on a 384-well plate is used to dose two rows on a 1536-well plate (Figure 19). For example, if one-quarter of a 1536-well plate has been filled then the number of columns filled is $48/4 = 12$ columns.

$$\begin{aligned} & \text{Source (Abs volume / well)} \\ & = (\text{Columns filled on 1536 w.p.* 2}) * \text{Aliquot volume} \quad \text{Equation 6*} \end{aligned}$$

Applying a safety factor of 1.8 to each of these absolute volumes gives the minimum required ‘Source rec (vol/well)’ which is there to guarantee enough stock solution is present in the source plate over the course of the dosing protocol. The required source plate volume is then converted into the stock solution volume by Equation 7. The source plate well-number is the total number of wells that the stock solution will be dosed into on each source plate well according to the source plate designed.

$$\begin{aligned} & \text{Stock solution (min vol/vial)} \\ & = \text{Source (rec per well)} * \text{Source plate well number} \quad \text{Equation 7*} \end{aligned}$$

The ‘source plate loading / (vol per well)’ column concerns the source plate loading volume given by Equation 8. Liquid reagents can also be tolerated by simply adding in the density of each reagent and subtracting that value from the stock solution volume shown with Equation 9 and Equation 10.

$$\begin{aligned} & \text{Source plate loading (vol per well)} \\ & = \frac{\text{Stock solution(vol per vial)}}{\text{Total number of source plate wells}} \quad \text{Equation 8*} \end{aligned}$$

$$\text{Liquid reagent vol per stock solution} = \frac{\text{Stock solution (mg per vial)}}{\text{Density}} \quad \text{Equation 9*}$$

$$\begin{aligned} & \text{DMSO top up} = \text{stock solution(vol per vial)} - \\ & \text{Liquid reagent vol per stock solution} \quad \text{Equation 10*} \end{aligned}$$

This Excel spreadsheet can be easily adapted to different high-throughput screens such as reaction optimisation (Chapter 3) and reaction discovery (Chapter 4) and is also being employed in current projects within the group (Chapter 5).

2.4. Dosing the reactor plate

Once all the stock solutions were prepared and the source plate has been dosed with stock solution, the Mosquito[®] needed to be programmed. Each of the unique reactor plates shown in the previous section comes with a unique dosing protocol and the method for preparing each of these will be discussed in this subsection.

The Mosquito[®] robot comes with dedicated software that is used to program each individual movement, aliquot volume as well as dispense location on the reactor plate. There are three main tabs on the Mosquito[®] software that will be discussed in detail. The first screen is known as the “Protocol” screen, where each protocol is designed (Figure 21a).

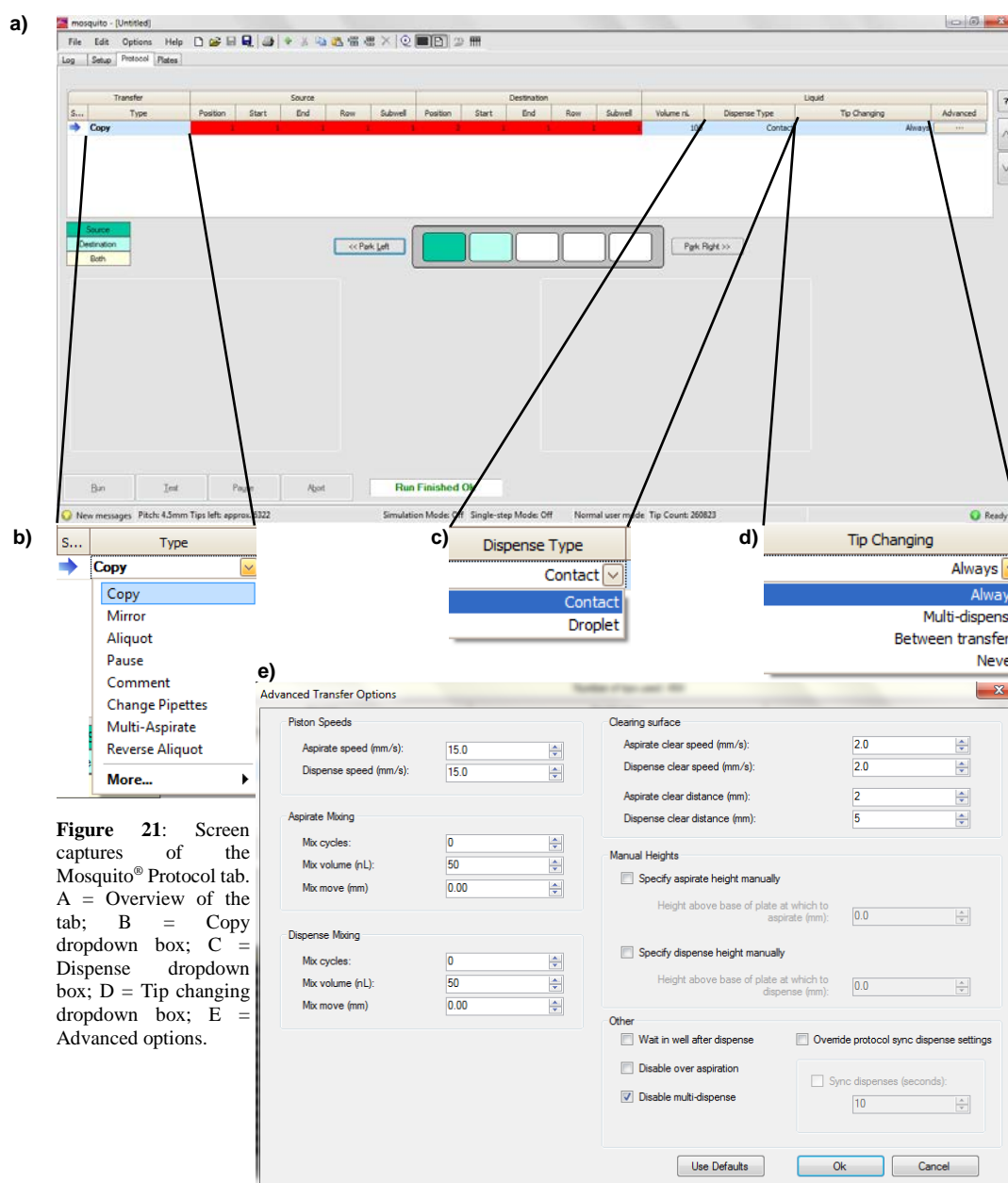


Figure 21: Screen captures of the Mosquito[®] Protocol tab. A = Overview of the tab; B = Copy dropdown box; C = Dispense dropdown box; D = Tip changing dropdown box; E = Advanced options.

The 'Type' drop-down box (Figure 21b) displays different types of aspirate commands such as 'Copy', 'Mirror' and 'Aliquot,' all of which can transfer a given amount of liquid from source to reactor. 'Copy' transfers the set of input wells to the same position on the reactor plate, 'Mirror' transfers the source plate layout to the reactor plate as a mirror image while 'Aliquot' allows more specific liquid dispensing across the plate. The 'Pause' function breaks the protocol for an allocated time, which is potentially useful for time-point studies. The 'Comment' feature allows the user to title the start of a new aspirate method which is useful for separating out different reagents. 'Change pipette' is a manual function that forces the machine to change pipettes. 'Multi-Aspirate' allows the machine to take up multiple different reagents in a single pipette tip and dose them all into one column on the source plate. Finally, the 'Reverse Aliquot' is used to reverse the order of addition i.e. from the right to left of the plate rather than left to right.

There are two methods of dispense type on the Mosquito, either contact or droplet (Figure 21c). 'Contact dispense' means the Mosquito[®] tip needs to contact the plate to dispense solvent which ensures all liquid dispensed is in the well. 'Droplet dispense' pushes the specified volume of reagent out of the tip, forming a droplet, before descending into the well plate. There are also four types of tip changing (Figure 21d): 'Always', 'Multi-dispense', 'Between transfers' and 'Never'. 'Always' means changing the tips after every dispense, 'Multi-dispense' optimises the Mosquito[®] to aspirate and dispense as many wells as possible in one transfer. 'Between transfers' changes the pipettes after performing all defined transfers in a row. 'Never' changing pipettes is self-evident.

Advanced Transfer Options (Figure 21e) allow protocol fine-tuning such as aspirate speeds (useful for variable liquid viscosity), aspirate or dispense mixing which are necessary for heterogeneous source plate reagents and for reactor plate mixing respectively. Clearing speed and distance are useful to tune if the user experiences "wicking" (*vide infra*) on the pipette tip; slower clearing distances can prevent material build up on the sides of the pipette tip. Manually defining aspirate and dispense height are very useful for trying new plates in a protocol if the user is finding that the pipettes are bending when aspirating from the source or reactor plate. There are three tick boxes that are key to some protocols; 'Wait in well after dispense', 'Disable over aspiration' and 'Disable multi-dispense.' 'Wait in well after dispense' can be useful if the compound dispensed is highly viscous and needs to flow off the pipette tip and into the well. To ensure all material is dispensed, the Mosquito[®] over aspirates by approximately 50 nL which can subsequently 'spray' over the Mosquito[®] when changed, contaminating source and reactor plates. Disabling this feature stops this from happening. Finally, 'Disable multi-dispense'

means each dispense will be done in a single transfer, i.e. the Mosquito[®] will not optimise and dispense multiple wells with one source plate aspiration.

The second tab is the ‘Setup’ tab where plates can be loaded into different positions on the Mosquito[®] (Figure 22). The key to this tab is ‘Initial Well Volumes’ indicated in the bottom left. Selecting ‘Don’t know volumes’ means the Mosquito[®] aspirates from the bottom of the well for each aspiration movement; this is standard if all the source plate wells have different volumes. “All wells empty” is normally selected for the reactor plate so the Mosquito[®] can optimise the dispense height in accordance with the plate parameters. If “All wells the same” is checked, the Mosquito[®] will optimise both aspirate and dispense height for all components.

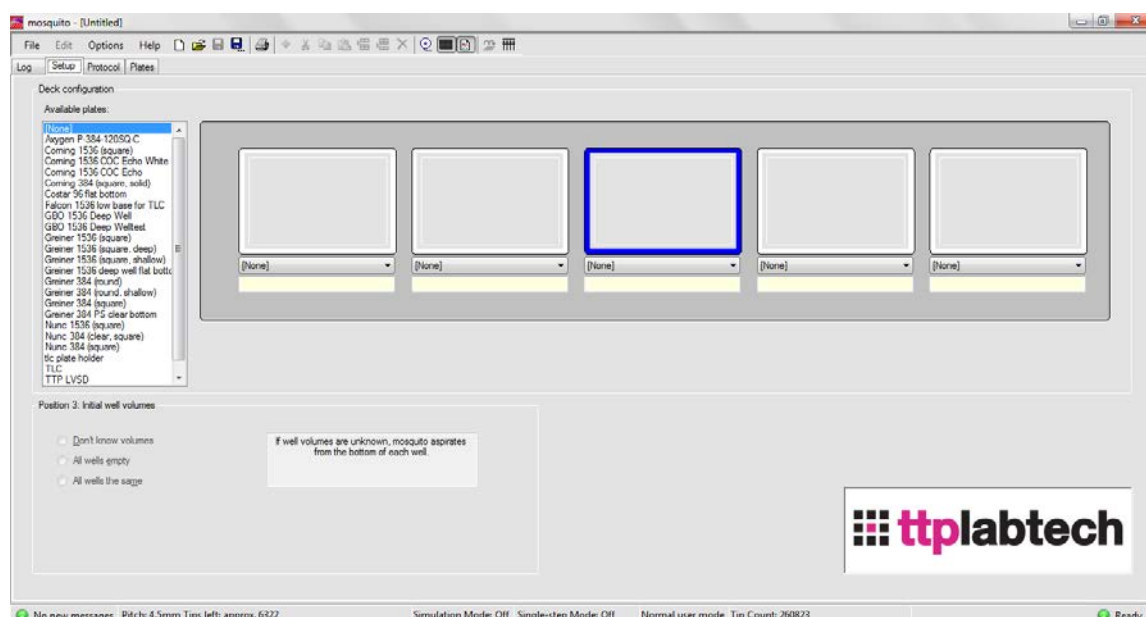


Figure 22: Setup tab on the 5-deck Mosquito.

The last important tab on the Mosquito[®] software governs the overall plate dimensions and technical information (Figure 23). Key to the overall reproducibility of the reactor plate is the XOffset and YOffset within the ‘Subwell’ category. Each manufactured plate will have slightly different dimensions which can cause the pipettes to touch the sides, resulting in cross-contamination. Therefore, it is important to adjust these values such that the pipette tips sit perfectly in the centre of each well.

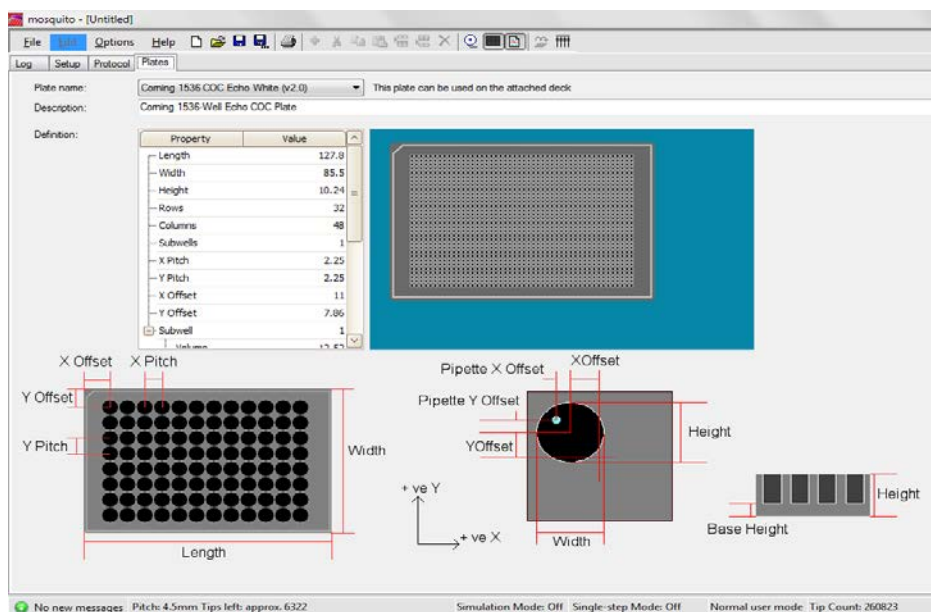


Figure 23: The plate design tab where technical information about each plate can be input.

2.5. High-Throughput Experimentation using Mosquito[®]

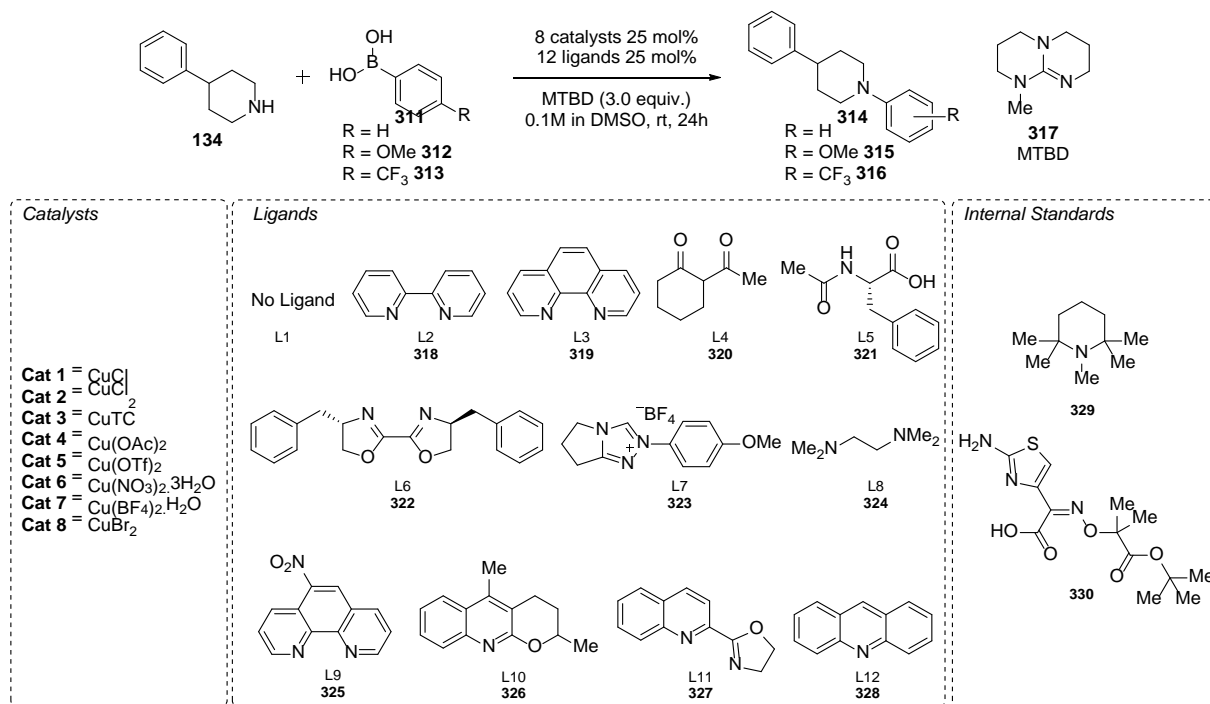
2.5.1. 384-Well Reactor Plates

To benchmark the high-throughput analysis optimisation, a series of standard Chan-Lam reactions were chosen to test the Excel spreadsheet and simultaneously optimise the Mosquito[®] dosing protocol and the Shimadzu LCMS 2020. Initially, work started with using 96-well plates as source plates and dosing into 384-well reactor plates.

An initial screen of the reaction of phenylpiperidine **134** with three different boronic acids (phenylboronic acid **311**, 4-methoxyphenylboronic acid **312** and 4-trifluoromethylphenylboronic acid **313**) was assessed in three different 384-well plates (Scheme 42). The three boronic acids chosen covered a range of electronics and assessed not only approximate performance of each boronic acid against different catalysts and ligands but also assessing their corresponding solubility in stock solutions. These three boronic acids were exposed to one base, twelve different ligands and eight different catalysts resulting in 96 unique reactions overall. To ensure reproducibility across the plate each reaction was screened in quadruplicate to minimise the error between wells and to increase precision and were also key to the quality control shown in section 2.8. A total reaction volume of 5.0 μL was dosed from two 96-well plates using Mosquito[®] dosing protocol 1 (Appendix 3). The reaction was sealed with tin foil (*vide infra*) and subsequently left to stand at room temperature for 24 hours.

The chosen base, MTBD, was screened at 3 equivalents with respect to the boronic acid and phenylpiperidine **134** as each turnover of the reaction produces 3 equivalents of acid. The ligands screened were commercially available, ten of which (**318-326**) were known to work well in combination with copper catalysis. They were phenanthrolines,¹⁷⁷ bipy,¹⁷⁸

acetylcyclohexanone,¹⁷⁹ box-ligand,¹⁸⁰ acetylphenylalanine,¹⁸¹ NHC,¹⁸² TMEDA,¹⁸³ 2-(4,5-dihydro-2-oxazolyl)quinoline¹⁸⁴ as well as two previously untested ligands, Li-quinoline and acridine which are mono-dentate variants of other heterocyclic ligands were also screened. Initially two internal standards (IS) were chosen, **329** and **330**, and their performance will be discussed in section 2.6.2.



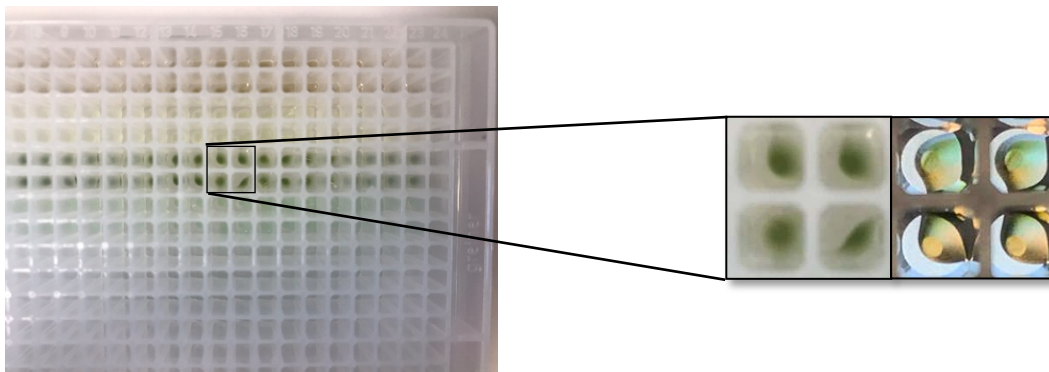
Scheme 42: Initial screening using two 96-well plate source plates and a 384-well reactor plate.

The initial Mosquito[®] protocol, although correct, produced some unexpected issues such as pipette bending, tape loading errors and pipette head errors which were resolved by adapting the plate definition (Figure 23c) shown in a previous section. With the 384-well plate dosed, the reactions were sealed and left to react at room temperature. Various sealing methods were assessed such as adhesive aluminium foil (VWR PN: 391-1275), catering aluminium foil and a control of no sealing. Each sealing method was placed over the plate and rolled on to form a tight seal. The adhesive seal and aluminium foil resulted in minimum evaporation across the plate whereas the ‘open air-no sealing’ method resulted in DMSO evaporation and concurrent reagent crystallisation.

Over time, it became obvious that the 384-well plates were not mixing correctly, with visual differences between repeat reactions. Investigating the mixing issue further revealed that only 5% of the well was occupied with reaction mixture in a 384-well plate (384-well plates have a total volume of 110 μ L and the reactions are only 5 μ L). Therefore, as shown in Figure 24 when

all the reagents were added to the reactor plate, optimal mixing was not achieved. The mix-dispense feature on the Mosquito[®] was not enough to resolve this issue.

Figure 24: 384-well reactor plate with two zoomed pictures on the same wells; Left hand zoom = Showing location



of catalyst in the well; Right hand zoom – Same wells against light box showing relative concentration of coloured copper complex.

Switching attention to different mixing methods, it was proposed that shaking the plates may ensure good mixing. At the time, plate centrifuges were unavailable, so other cruder methods were trialled. The vacuum pumps attached to the LCMS resonated at a high enough frequency that could sonicate the plate to homogenise the solution. However, this method was quickly eliminated as the vacuum pump dissipates heat resulting in faster solvent evaporation or a faster initial rate. A sand-bath was also prepared and floated in a large sonicator bath, but this returned similar outcomes to no mixing.

Across the initial plates throughout the optimisation, two ligands, L2 (**318**) and L3 (**319**), were assessed to be more broadly applicable across the three different boronic acids and were therefore used for the remainder of the screening process. As a consequence, ligands **318** and **319** were kept for the remainder of the screening so that more bases and catalysts could be evaluated.

2.5.2. 1536-Well Reactor Plates

With the observed mixing issues in 384-well plate reactors, 1536-well plates (Figure 25) were subsequently employed. The plate, Corning 3730 COC-copolymer plates with a total working volume of 6.0 μL , are 100% resistant to DMSO and strong, corrosive bases. The new plate also facilitated a reduction in reaction volume from 5.0 μL to 2.5 μL which was easily accommodated using Excel spreadsheet shown in Section 2.3. The new 1536-well plate required a new reactor plate design, source plate design and new Mosquito[®] protocol (Experimental 7.5).

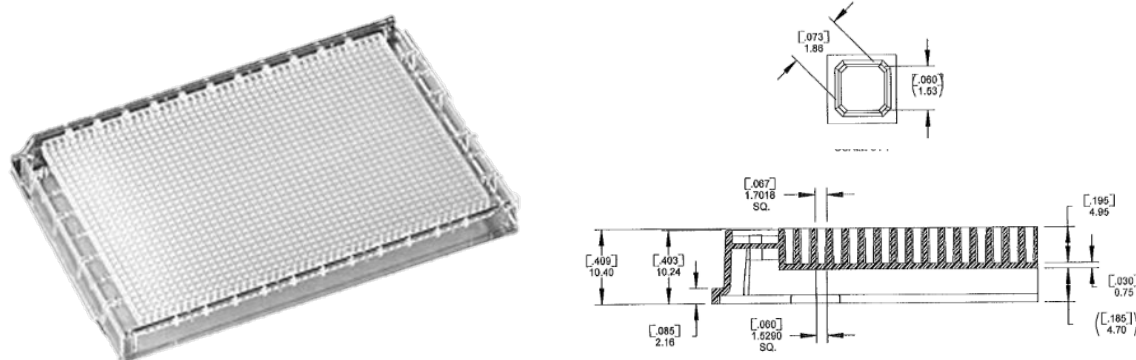
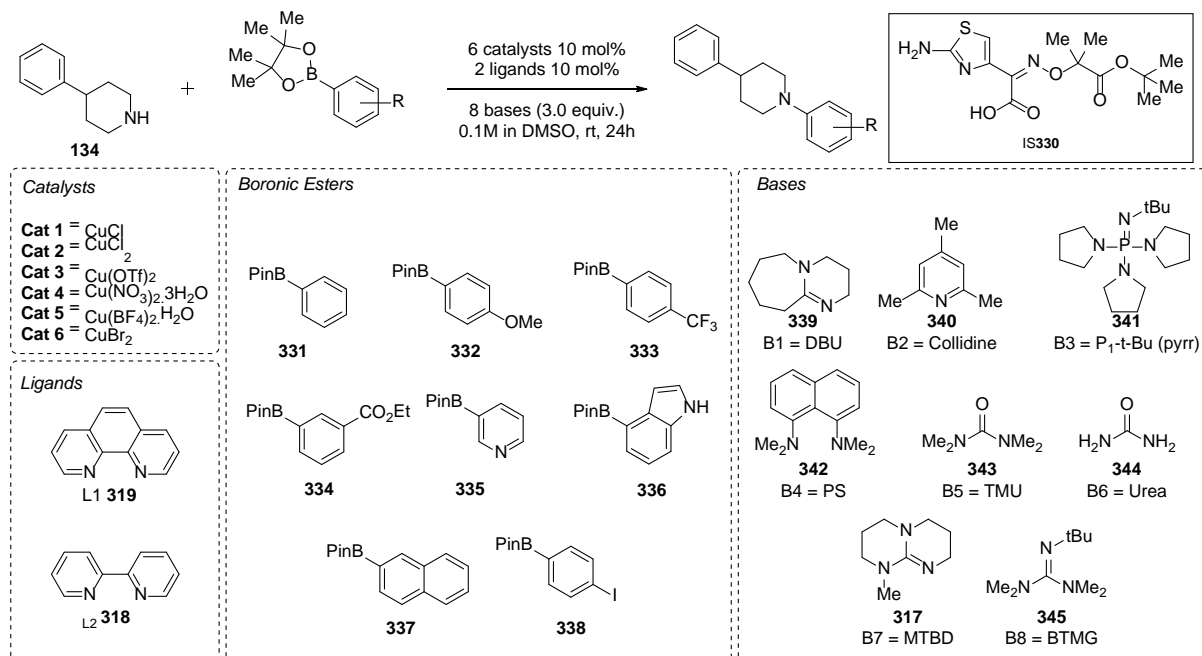


Figure 25: 1536-well plate with specification and size view of well size and dimensions

Using the new plate and a new plate dosing protocol, reaction optimisation was carried out using one amine, eight boronic esters, eight bases, six catalysts and two ligands, screened in two and a half 1536-well plates, totalling 3,072 reactions in quadruplicate, 768 unique reactions in total (Scheme 43). Each boronic ester screened in one-quarter of the plate. Independently to the high-throughput experiment, it was found that boronic esters performed better than boronic acids and were therefore used for the remaining screening (*vide infra*). Each reaction was performed, in quadruplicate and on a 0.25 micromole scale. The plates were then sealed with an assortment of different plate seals. Similar to the previous 384-well reactor plate, adhesive sealing and aluminium sealing were assessed as well as a control of no sealing to assess whether sealing was necessary.



Scheme 43: Initial screening using a 384-well source plate and a 1536-well reactor plate.

Adhesive seals were found to be intolerant to the reaction conditions on the new small-scale 1536-well plates. When peeled back for analysis plate preparation, solvent had obviously dissolved the adhesive and well-to-well contamination was apparent. Exposing the entire plate to air resulted in both DMSO evaporation and water absorption resulting in component

crystallisation. The best seal was aluminium foil rolled onto the top of the well and placed underneath a weighted thick-glass TLC-tank (Figure 26).

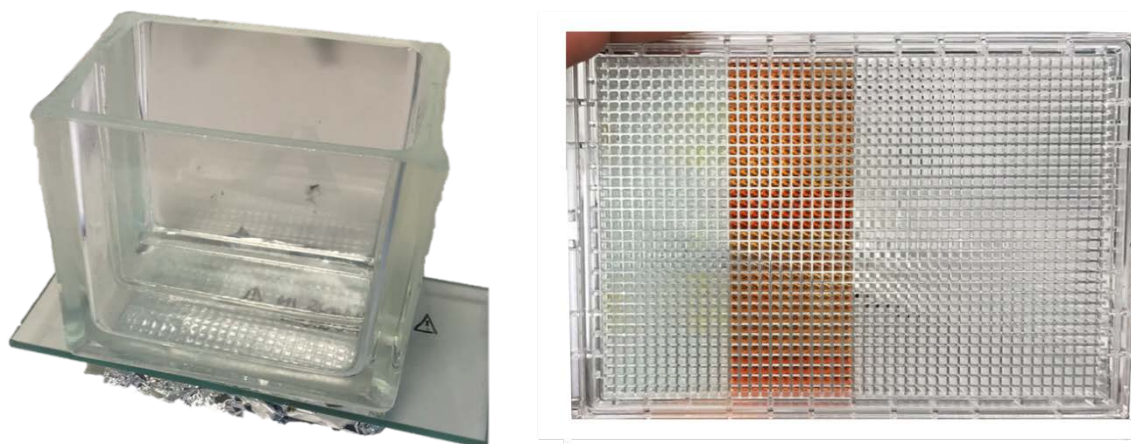


Figure 26: Left: Sealed 1536-well reactor plate under TLC-tank weight; Right: 1536-well plate with one quarter filled with reaction optimisation showing no compound crystallisation.

All reactions were prepared using Mosquito[®] dosing protocols 2-5 (Appendix 3) and sealed with aluminium foil and left to stand for 24 hours. Each reaction was dosed into an analysis plate prepared with a quenching mixture of internal standard and analysed by LCMS. The four-variable assessment of the Chan-Lam coupling was completed using eight boronic esters, eight bases, six catalysts and two ligands. The eight boronic esters chosen covered a range of different electron donating and withdrawing substituents as well as pharmaceutically relevant motifs. Bases were chosen with a broad distribution of pK_{as}^{185} to assess the effect of strong and weak on the reaction.

When the issues of mixing and plate sealing were resolved, attention turned to high-throughput quantitative analysis using the Shimadzu LCMS 2020.

2.6. High-Throughput Analysis by LCMS

Although there are many ways to analyse reactions in high-throughput (discussed in Chapter 1), a rapid, but also quantitative data analysis protocol using a LCMS from Shimadzu (Figure 27a) was unknown. The LCMS available in the Gaunt group is a relatively simple system, set up with an inline solvent degasser, two HPLC pumps, an autosampler, column oven, photodiode array (PDA) and mass spectrometer. The autosampler (Figure 27b) houses two sampling trays, an MTP rack (Figure 27c) that can house two 96-well or 384-well plates as well as a ‘controller rack’ capable of housing ten 1.5 mL vials. There are currently no examples of 1536-well autosamplers for LCMS.



Figure 27: LCMS 2020 by Shimadzu in the Gaunt group. A) The overall setup of the LCMS; B) Autosampler with MTP-tray on left and controller rack on right; 3) MTP-tray with 384-well plate in position.

A simplified scheme of how the LCMS works is shown in Figure 28. Initially, the sample is injected and chromatographically separated before being introduced to the mass spectrometer. The solvent is nebulised and ionised at the front of the machine either using ESI or APCI. The corona needle, which is highly charged, then fires the ions down the mass spectrometer. The solvent is subsequently evaporated by the desolation line and the ions are resonated by the quadrupoles. The ions can then be detected by an electron multiplier and a subsequent total ion count (TIC) can be measured and analysed on a computer.

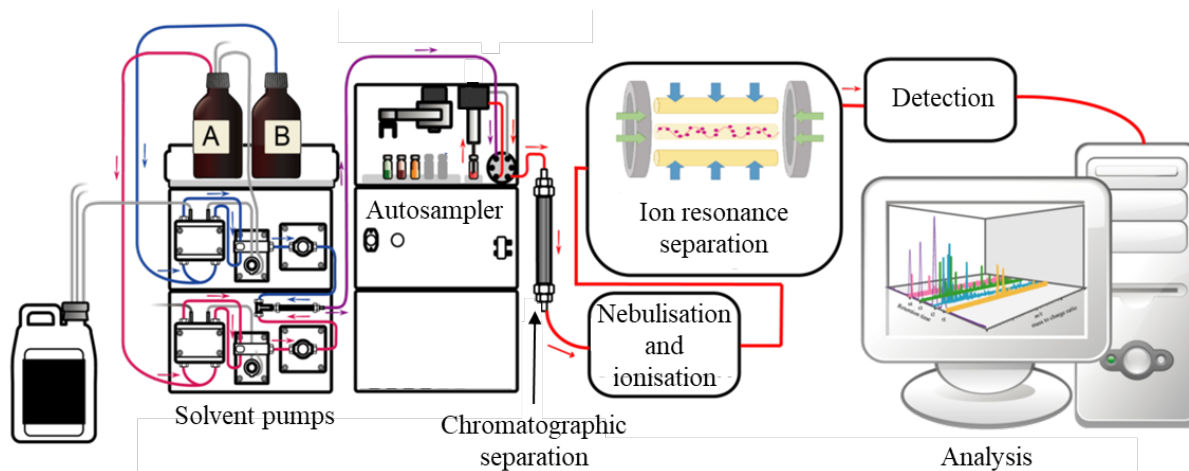


Figure 28: Standard-LCMS machine. Solvent A and B are pumped through the autosampler and chromatographic column. Once separation has occurred, the solvent is nebulised and ionised into the mass spectrometer. The ions are resonated and detected by the detector and visualised on a computer. Image adapted from original by YassineMrabet – all rights reserved.

There are many advantages to using LCMS for high-throughput analysis such as selectivity, speed and sensitivity over GCMS or HPLC. To achieve quantitative data, these complex instruments require an optimisation of many factors leading to a complex and co-dependent synergy of many parameters. Once all conditions are optimised, even then, other phenomena can cause issues for quantification such as matrix ion-suppression which will be covered in more detail later in the section.

The LCMS 2020 in the laboratory has 7 different variables that need to be optimised to achieve a quantitative high-throughput analysis protocol; 1) solvent, 2) pump flowrates, 3) pump gradient, 4) autosampler injection volume, 5) column type, 6) column oven temperature, 7) mass spectrum ionisation type.

The standard solvent system used for reverse phase liquid chromatography is a polar organic solvent such as methanol or acetonitrile normally modified with acid or base, and an aqueous mobile phase buffered with an acid/base mixture. The added acid/buffer mixture adjusts the interaction of the analyte with the stationary phase during chromatography which results in sharper peaks on UV/vis and MS. The solvent mixture prepared was A: water buffered with 0.01mM ammonium formate with 0.1% formic acid v/v and B: acetonitrile with 0.05% formic acid v/v. Formic acid/formate buffer was chosen over formic acid/acetate buffer as formate reduces baseline noise¹⁸⁶ as well as reducing the number of detectable ions in the MS.

The pumps attached to the LCMS are rated to up to 600 bar and have a recommended working pressure of 450 bar which constitutes a flow rate of approximately 1.0 ml min⁻¹. This was kept the same throughout, as this flow rate is compatible with the size of the tubing already installed in the machine, and results in good peak shape after chromatography. There is a “sweet spot” when applying LCMS to high-throughput analysis where you need to balance fast run times per sample while prioritising compound separation and peak shape.

The pump gradient, or method file, is the defining factor for chromatography. Separation of analytes within a short timeframe is of paramount importance to high-throughput reaction analysis, especially when trying to avoid ion-suppression.¹⁸⁷ When reaction optimisation is applied across a broad substrate scope, different products will have different associated polarities and, therefore, each new compound needs to be assessed and a bespoke method developed to ensure separation.

The column type is also a major contributor to reaction separation. Stationary phase particle size, internal column diameter and column length all affect analyte separation. The most readily available reverse phase LCMS columns are normally fitted with 3 µm silica particles derivatised with lipophilic compounds such as C18, phenyl-hexyl or perfluorinated chains and are usually 50-100 mm long. More recent UPLC machines with higher flow rates and pressures can have sub-two-micron stationary phase and shorter column lengths. It is also recommended to fit a guard column to increase the lifetime of the column. The oven housing each column can heat to allow for faster flow rates, decreasing the viscosity of the solvent but also results in increase stationary phase kinetics reducing analyte separation.

Lastly, the ionisation mode that the mass spectrometer can affect the size and shape of the peaks. The two standard types of ionisation are ESI or APCI.¹⁸⁸ Both come with their own advantages and disadvantages but, more recently, analytical companies have been developing a dual mode ESI/APCI ionisation mode, allowing for a “best-of-both-worlds” ionisation. There are also two different detection modes too; the first is a scan whereby the mass spectrometer looks for all compounds in a mass range parameter set on the machine; second is a selective ion mode, or SIM, which looks only for the masses determined by the user. The SIM method is preferred when completing high-throughput analysis, filtering out all the information that would otherwise make analysis complex, leaving only the mass spectrum peaks corresponding to your products and internal standard.

Not only does the LCMS machinery require optimisation, but the analysis plate preparation needs careful planning. Firstly, what plates are compatible with the LCMS autosampler will govern how many samples can be analysed per LCMS batch file. When the analysis plate is being prepared, the reaction mixture needs to be quenched to prevent overreaction during analysis, potentially resulting in false positives. Therefore, the analysis matrix must quench the reaction and give consistent product and internal standard ionisation throughout. The internal standard also needs to be broadly applicable across a wide range of product polarities during bespoke method file optimisation.

2.6.1. Early LCMS Optimisation for High-Throughput Analysis

Current LCMS autosamplers can only sample from 96- or 384-well plates which is in part due to the size of the autosampler needle meaning that it is simply too large to fit into the small 1536-well plate wells. Therefore, 384-well plates were used for high-throughput analysis to maximise overall analysis throughput. The LCMS autosampler MTP-rack, shown in Figure 27, can hold two 384-well plates, thus 768 reactions can be analysed in a single batch run. The controller rack, also shown in Figure 27, can house ten 1.5 mL vials, important for quantitative calibration sample housing.

Analysis of the first screen: 4-phenylpiperidine **134** and boronic acids **311**, **312** and **313**, against eight catalysts, twelve ligands and one base, would assess the overall applicability of the analysis across a range of different substrate polarities (Scheme 42). The reactor plate was prepared and incubated at room temperature for 24 hours. The analysis plate was then generated directly in the 384-well reactor plate by initially quenching the reaction with 50 μ L of 5% acetic acid in DMSO followed by 50 μ L of internal standard in DMSO.¹⁶⁷

Two internal standards, **IS329** and **IS330**, were chosen as candidates for the assay. **IS329** was identified as it contained similar structural motifs to the products (Scheme 42). However, it was found that to have the same mass ($[M+H]^+ = 156$ m/z) as a known DMSO dimer¹⁸⁹ in LCMS and was therefore excluded for the remainder of the optimisation. **IS330** was chosen as it is structurally distinct from our reaction components and does not have any fragments that match our products.

The initial three analysis screens can be summarised in three erratic and non-uniform chromatograms (Figure 29). Chromatogram A shows what is essentially a baseline signal suggesting that the LCMS has not sampled any analyte mixture; either because the needle cannot reach the solvent or that no product or internal standard is present in the well. Chromatogram B shows the presence of **IS330** but no presence of the product. Whereas Chromatogram C shows the presence of both **IS330** and products **314**, **315** and **316**. The variation of the peak intensities was also alarming (137,003 units in chromatogram C to 198,000 units in chromatogram B).

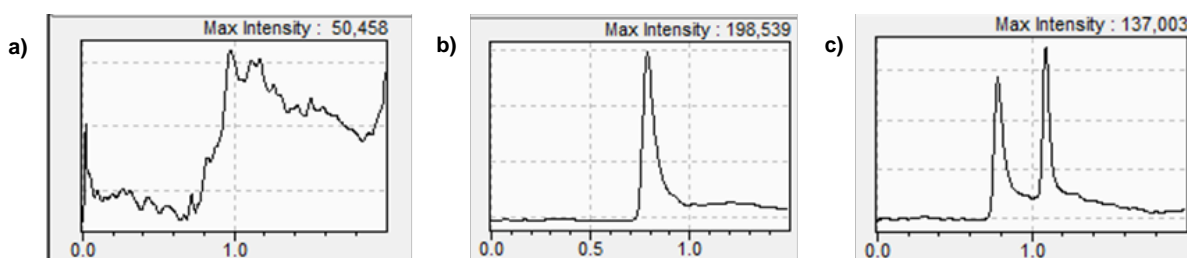


Figure 29: Three chromatograms summarising the initial screening on the LCMS 2020. A = Baseline trace is observed with no **IS330** or product present; B = Just **IS330** present; C = Both **IS330** and product were present.

Subsequent optimisation of the “needle stroke”, a feature in the LCMS method file that governs how far the needle drops into the sample well, guaranteed that all the sample was aspirated into the LCMS. Optimising the method gradient resulted in improved assaying (Figure 30): starting at 5% acetonitrile in water in chromatogram A to 50% in chromatogram D shifted the peaks from the end to the middle of the assay. The chromatogram shows a small peak at 0.7 minutes corresponding to **IS330** and the larger peak at 1.2 minutes corresponding to the product.

a)

b)

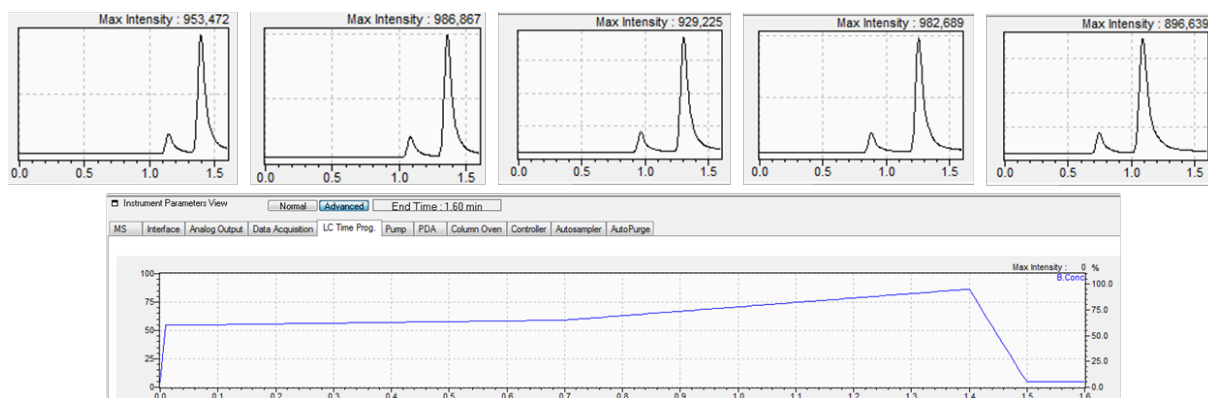
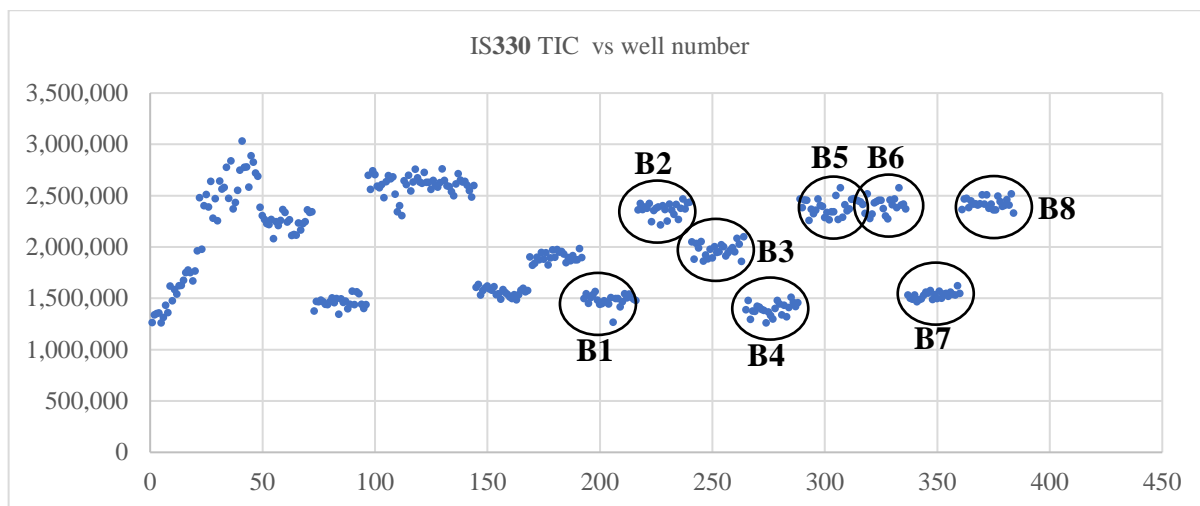


Figure 30: a) Progression of LCMS method file optimisation by increasing the initial starting point from 5% acetonitrile in water to 55% acetonitrile in water. b) The optimised gradient for product **314**.

2.6.2. Removal of Ion-Suppression

Using the improved analysis protocol, the original eight boronic esters were screened with amine **134**, two ligands, eight bases and six catalysts (Scheme 43) in eight 384-well plates. 384-well analysis plates were prepared with 1.2 μL of reaction mixture dosed to assess the overall viability of the analysis protocol and the applicability of **IS330** as the internal standard. The analysis was completed across eight overnight runs with 1.8 minutes assays per sample and totalling 120 hours of analysis time for 3,072 reactions.

Over the eight 384-well plates minimal variation was observed across quadruplicate reactions and greater than 90% of the samples showed both product and **IS330**. Closer inspection of the data revealed that ProtonSponge™ **342** generally outperformed all other bases. This result was scrutinised further and post-rationally hypothesised to be due to one of two reasons; the first being a genuine positive result that **342** is better than all other screened bases or, more critically, that the internal standard TIC was consistently lower for this base (seeing as we take a ratio of product TIC to internal standard TIC for quantification). Therefore, plotting a graph of **IS330** TIC against well-number revealed that different bases resulted in different **IS330** ionisation (Graph 1).



Graph 1: Internal standard total ion vs well-number showing ion-suppression of IS330 with different bases. B1 = DBU, B2 = Collidine, B3 = P1tBu, B4 = Proton Sponge, B5 = TMU, B6 = Urea, B7 = MTBD, B8= BTMG.

This phenomena, known as ion-suppression, is a well-documented and common occurrence in liquid chromatography-tandem mass spectrometry experiments, especially when investigating complex mixtures and trying to achieve quantification.^{187,190,191} It occurs when compounds coelute after chromatography and are ionised in the mass spectrometer at the same time resulting in unequal analyte ionisation and adduct formation. This phenomenon is lessened when using triple quadrupolar LCMS-MS which ionises and fragments the analyte a second time before being detected, breaking apart gas phase adducts. A comprehensive and critical review by Furey¹⁹² shows that ion-suppression is a consistent problem for “simple” single quadrupolar mass spectrometry but its effect can be ameliorated with careful sample preparation, good analyte separation and selective ionisation modes.

Ion-suppression of IS330 resulted in false positives for reactions containing Proton Sponge™ **342**, P1-t-Bu (pyrr) **341**, DBU **339** and MTBD **317** as these lipophilic and higher boiling point bases elute slowly from the column. **341** and **317** were used by MSD¹⁶⁷ when investigating the Buchwald-Hartwig coupling in high-throughput and were chosen for this screen to show complementarity. The strong bases employed by MSD are required to activate the palladium pre-catalysts¹⁹³ but as the copper catalysts screened in the Chan-Lam reactions do not require activation with strong bases, P1-t-Bu (pyrr) **341** and Proton Sponge™ **342**, the most lipophilic bases, were omitted for the remainder of the optimisation to prevent ion-suppression but DBU **339** and MTBD **317** were kept to maintain a broad pK_a screen.

To investigate the complexity of each high-throughput sample, the mass spectrometer was set to ‘scan’ mode to look at the overall profile of each run to assess where the internal standard and each component eluted (Figure 31). The first 0.25 minutes of low intensity is essentially a dead volume where analyte has not reached the mass spectrometer. Shortly after, in area **1**, the

most polar compounds eluted in one large peak. As IS330 eluted at 0.50 minutes, this was a reasonable explanation for the observed ion-suppression.

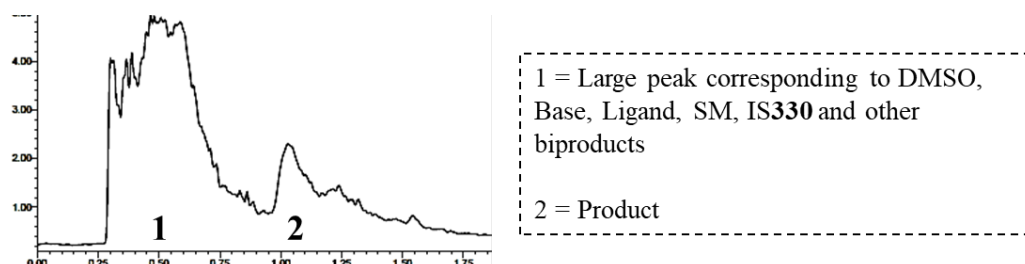


Figure 31: Scan of high-throughput LCMS assay showing a large peak (1) at the start of the chromatogram followed by a small peak of product at 1.0 minutes (2).

2.6.3. Selection of Internal Standard

The focus was immediately changed to finding an internal standard that didn't undergo ion-suppression. Furey¹⁹² suggested a fully deuterated or semi-deuterate version of the target substrate are generally the best internal standard as: 1) it will have the same retention time of the product; 2) the same ion-suppression effects as the product; 3) a different and distinguishable mass. However, deuterated internal standards were immediately ruled out as it would be prohibitively expensive to prepare multiple milligram quantities of each substrate. Furthermore, preparing deuterated standards for all products in a substrate scope would be tedious and expensive. A list of new internal standards was drawn up and assayed at different concentrations and using different method files (Figure 32). The perfect internal standard would not only be broadly applicable across a range of product polarities but also commercially available and cheap.

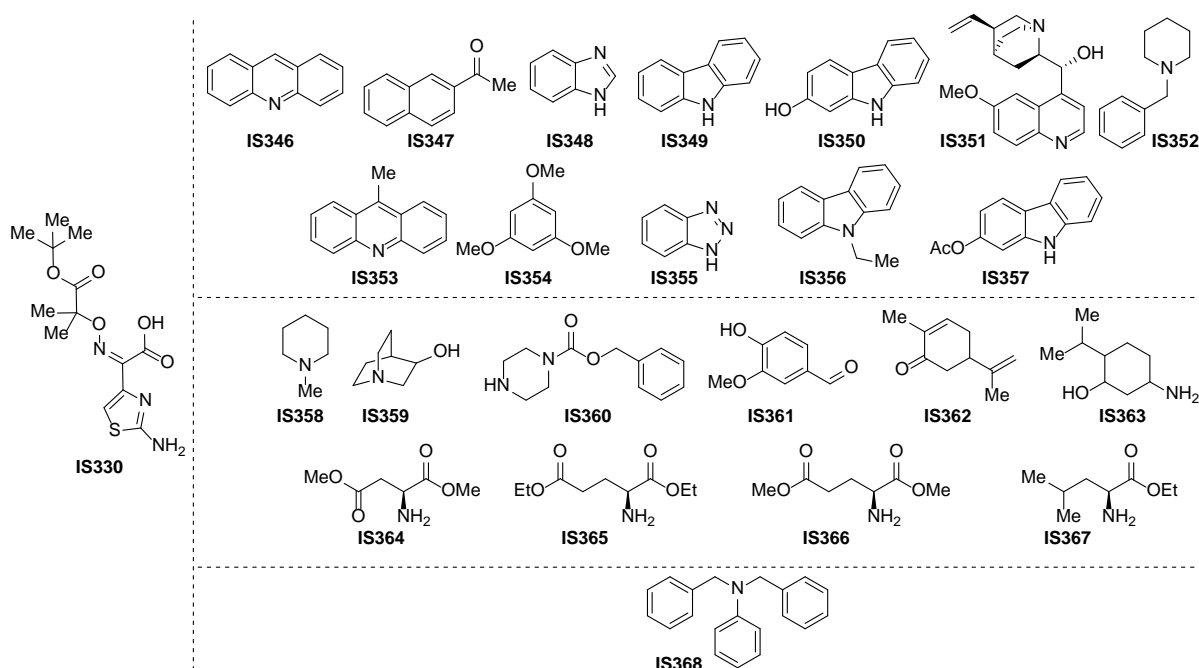


Figure 32: Internal standards screened for high-throughput quantification.

Aromatic internal standards IS346, IS348, IS351-353, IS346 and IS352 were too polar for the high-throughput assay (retention time 0.2-0.8 minutes) and coeluted with the reaction matrix leading to ion-suppression (Experimental 7.5). Internal standards IS347, IS349, IS350 and IS355 did not ionise in the LCMS assay. Aliphatic internal standards IS358-363 were too apolar or did not ionise. Amino acid-derived standards IS364-367 exhibited good ionisation but eluted at 0.6 minutes. Furthermore, the primary amine could potentially react with remaining boronic ester in the crude reaction mixture, potentially returning variable TIC responses. IS368, however, was found to be a suitable candidate as it ionised well in the mass spectrometer and had a retention time of 1.23 minutes (Figure 33). In addition, the fully substituted nitrogen means that it will not react with the crude reaction mixture.

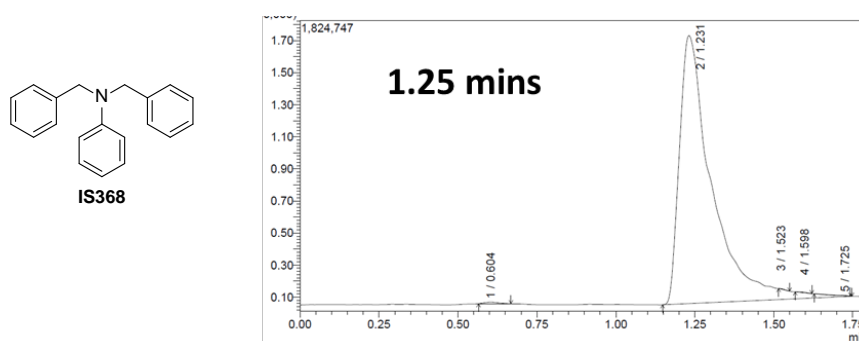
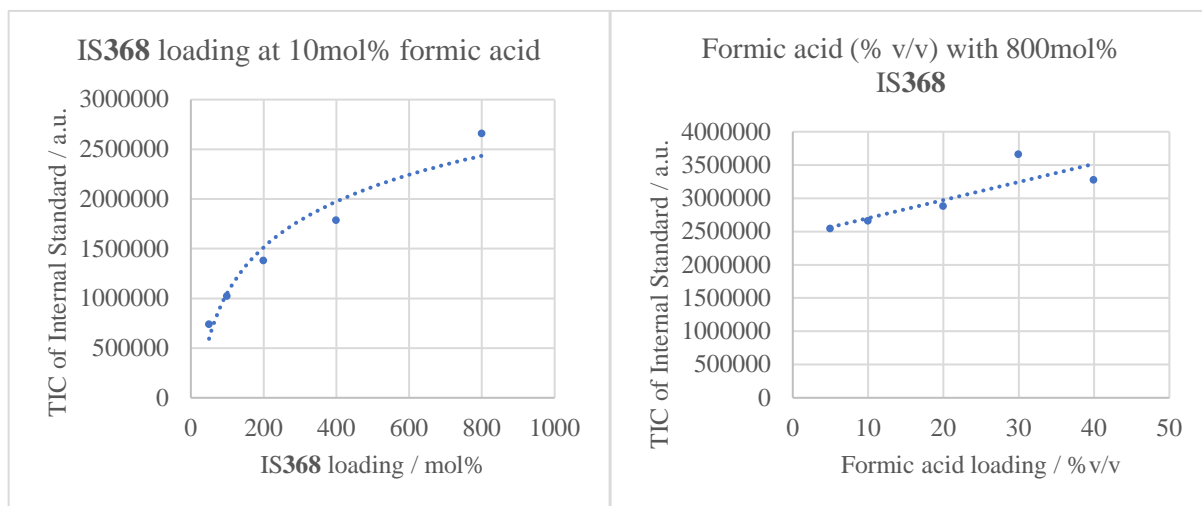


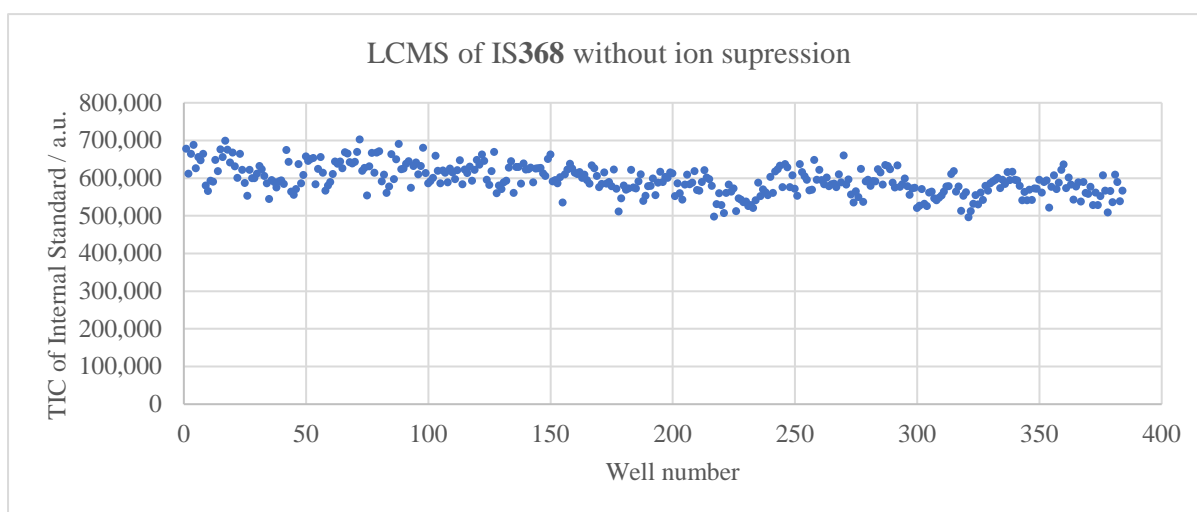
Figure 33: IS25 and the LCMS assay confirming the retention time and ionisation.

With IS368 chosen as the new internal standard, the loading per well was assessed to find an optimum concentration with the largest mass spectrometer detection. Screening 50 mol% loading to 800 mol% loading with respect to the initial amine, the latter gave the largest response on the LCMS and was therefore taken and screened against different acid loadings. Previously, acetic acid was the quench of choice similar to the conditions used by MSD,¹⁶⁷ but wanting to remove as many different ions from the matrix as possible, formic acid was screened at different loadings (Graph 2). It is also a slightly stronger acid (pK_a 3.75 vs pK_a 4.76) meaning reaction quenching would be faster and the equilibrium would lie further to amine protonation.



Graph 2: A) mol% of formic acid vs IS368 TIC showing a non-linear increase; B) v/v% of formic acid with 800 mol% of IS368.

To confirm whether this internal standard was experiencing ion-suppression with the bases in the screen, a further analysis plate was prepared and analysed. Testing the reaction conditions shown in Scheme 43 with boronic ester **331**, the resulting internal standard TIC vs well-number was plotted in Excel (Graph 3). Good consistency was observed across the 384-well plate with no ion-suppression occurring.



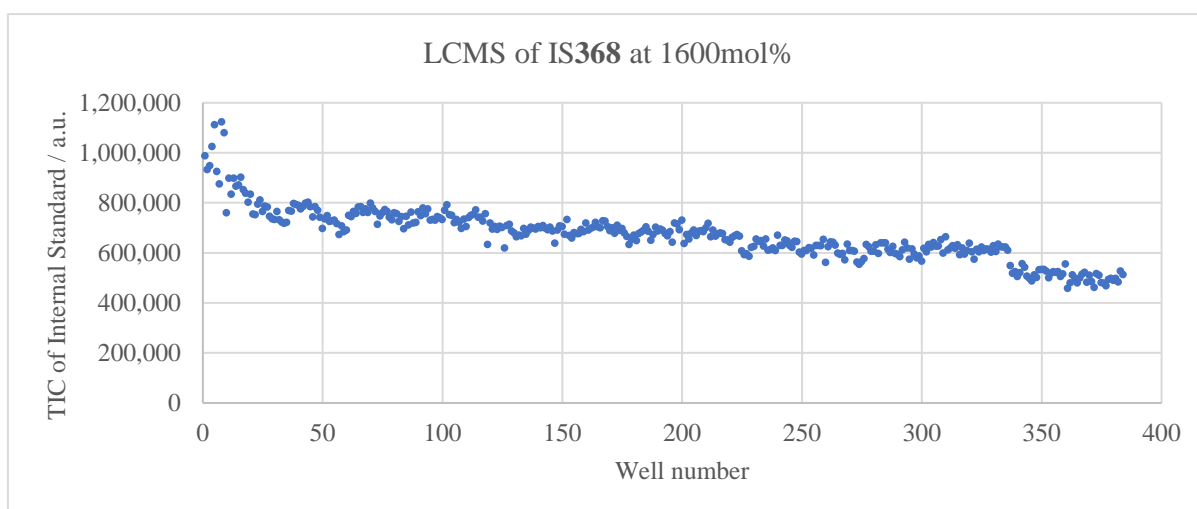
Graph 3: IS368 TIC vs well number showing that the new internal standard is no longer experiencing ion suppression.

To analyse these data, the coefficient of variance (CV) was chosen to express the distribution of the data,¹⁹⁴ calculated using Equation 11, as it expresses the overall precision of a repeat sample. As the same concentration of IS368 is used in every well, the overall distribution should be low. For Graph 3, the overall coefficient is 6.52%. Another semi-statistical measure of variance (Equation 12) uses the maximum range of the data divided by the mean which, in this case, gives a variance of 34.8%.

$$\% \text{ Coefficient of Variance} = \left(\frac{\text{Standard Deviation}}{\text{Mean average}} \right) * 100 \quad \text{Equation 11}$$

$$\% \text{ Variance of range} = \left(\frac{\text{Maximum range of data}}{\text{Mean average}} \right) * 100 \quad \text{Equation 12}$$

Although the coefficient of variance is low, the variance of the range is large suggesting the difference between the highest and lowest TIC values is 34% of the mean. If, for example, this occurred within a quadruplicate set of reactions, a 34% difference is considerable. A simple way to decrease the variance about the range is by increasing the total ion count of the internal standard. Therefore, doubling the concentration of the internal standard from 800 mol% to 1600 mol% was hypothesised to result in twice the IS368 TIC and therefore lower the variance in the range. However, this was not the case as doubling the concentration only resulted in an increase from 700,000 TIC to 900,000 TIC which only represents a 20% increase in ionisation (Graph 4).

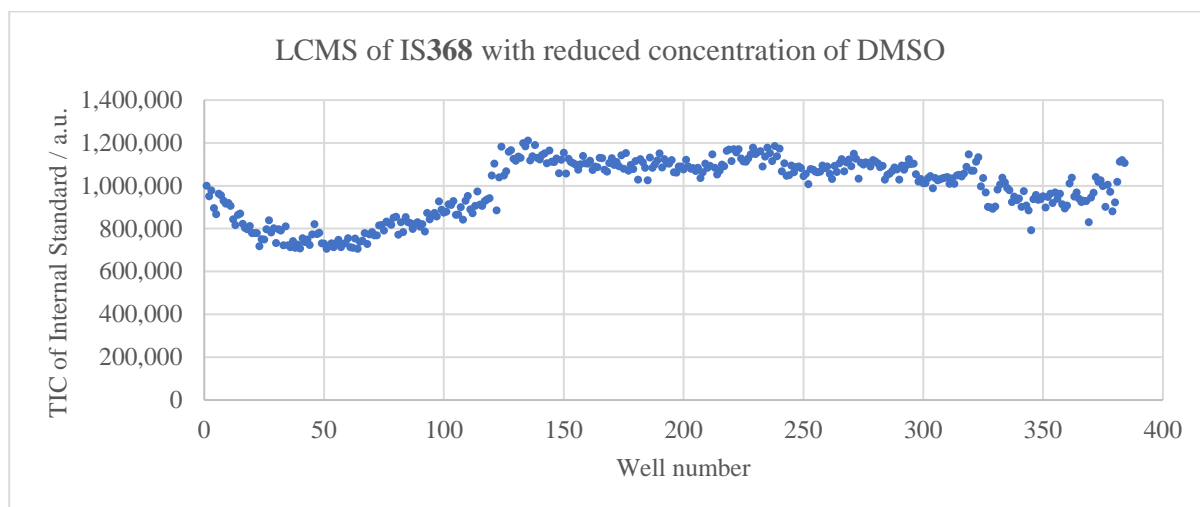


Graph 4: Doubling the IS368 concentration from 800mol% to 1600mol% resulted in an increase from 700,000 TIC to 900,000 TIC.

Puzzled by only a 20% increase in IS368 TIC as well as the reduction in LCMS sensitivity over the duration of analysis, the method for sample preparation was re-evaluated.¹⁹² To this point, over 90 μL of DMSO was used per well in the analysis samples and the autosampler injected 1.0 μL of the analysis mixture, meaning that at least 384 μL of DMSO was injected into the mass spectrometer for each plate. DMSO, although compatible with the Mosquito[®] and high-throughput reaction optimisation, is incompatible with mass spectrometry due its high boiling point (189 $^{\circ}\text{C}$) and a low vapour pressure (0.556 mbar @ 20 $^{\circ}\text{C}$). This means it coats the internal surfaces of the mass spectrometer reducing detector sensitivity. DMSO is well-documented to improve signal response for protein analysis when added as an additive to the solvent,^{195,196} but there is limited information for the DMSO and its effect on non-peptide quantitative mass spectrometry.

2.6.4. Effects of DMSO

With the new internal standard displaying no ion-suppression, it was important to remove as much DMSO as possible from the analysis plate preparation. Rather than topping each of the wells up with 40 μ L of DMSO, water was used instead which reduced DMSO content by over 40%. A plate containing 50 μ L of the internal standard stock solution in 50:50 formic acid:DMSO with 40 μ L of water was prepared and analysed using the same analysis method (Graph 5). The general trend for the TIC started with a steady decrease in detection until well 50, followed by a recovery period to approximately well 120. The TIC then plateaued until the end of the analysis.



Graph 5: IS368 TIC vs well-number shows an overall increase in the TIC but, more importantly, shows a recovery in TIC over the course of the analysis confirming that DMSO was reducing the overall signal.

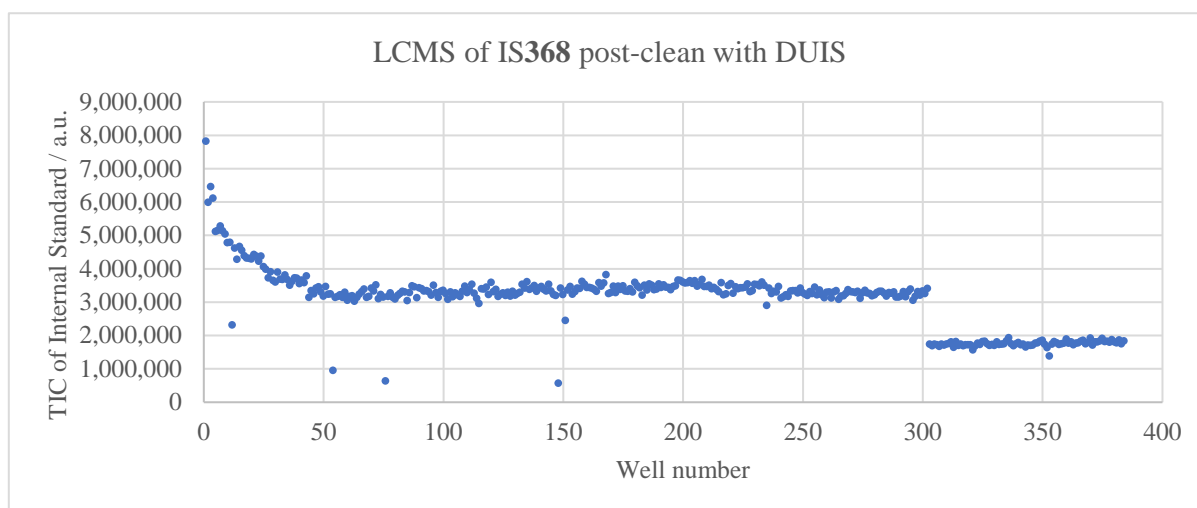
Using the same stock solution concentration as Graph 4 with a reduced volume of DMSO gave an increase in IS368 TIC (600,000 TIC to 1,100,000 TIC). It can be concluded that the mass spec has a direct response to the overall concentration of DMSO in the analyte sample. A high concentration of DMSO means the detector is saturated more easily, with the concurrent loss of sensitivity.

Having not observed the expected marked increase in TIC from doubling the IS368 concentration, it was suggested that previous overuse of DMSO had soiled the MS resulting in a dampening effect, reducing the number of ions observed by the detector. Cleaning was therefore required to remove as much DMSO from the mass spectrometer as possible. The three key parts to clean are shown in Figure 34. The corona needle, responsible for firing ions down the mass spectrometer, was coated in a film of brown oil which dampens the effective needle voltage. This can simply be removed without turning the machine off by unclipping the high-voltage cable. The pre-quad and the octopole are responsible for focussing the ions down the mass spectrometer for detection and a fine covering of these with DMSO can also dampen their influence on ion separation in the MS.



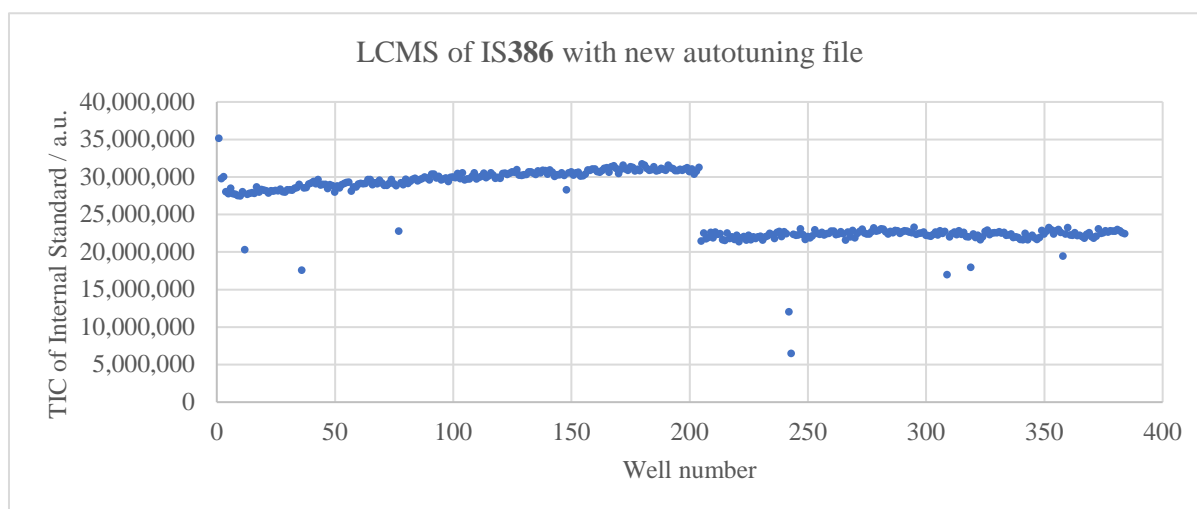
Figure 34: a) Corona Needle, Octopole, Skimmer and pre-quad assembly, b) disassembled pre-quad assembly.

Although many reports recommend using APCI as the ionisation mode to minimise ion-suppression,^{187,191,192} a combination of APCI and ESI (known as DUIS) was trailed in our analytical protocol. Not all compounds ionise well in APCI, so a mixture of ESI and APCI would ameliorate this issue. Although this mixed ionisation employs ESI, which is known to exhibit greater ion-suppression, the internal standard used is separated from the polar matrix, minimising this phenomenon and, therefore, will not be an issue (as shown earlier in Figure 33). A new analysis plate was completed using DUIS ionisation after the internal components were cleaned (Graph 6).



Graph 6: IS368 TIC vs well-number shows higher LCMS ionisation after cleaning the machine.

Intriguingly, the first 50 samples exhibit a decay to a plateau at 3,000,000 TIC and, after 300 samples, a drop from 3 million TIC to 1.8 million TIC was observed. Although these artefacts still need to be considered, the reduction in DMSO concentration has given improved consistency in ionisation over the course of the 384-well plate. It was recommended by Shimadzu to autotune the mass spectrometer with a known standard solution, so the ion beam can be focussed to hit the detector. All previous analyses were run using a tune file from 5 years prior. Autotuning the MS gave a 10-fold increase in the total ion count (Graph 7). Interestingly, the same drop in sensitivity as in Graph 6, was observed after 200 samples.



Graph 7: IS368 TIC vs well-number after autotuning the mass spectrometer. Autotuning the machine resulted in a huge increase in total ion count.

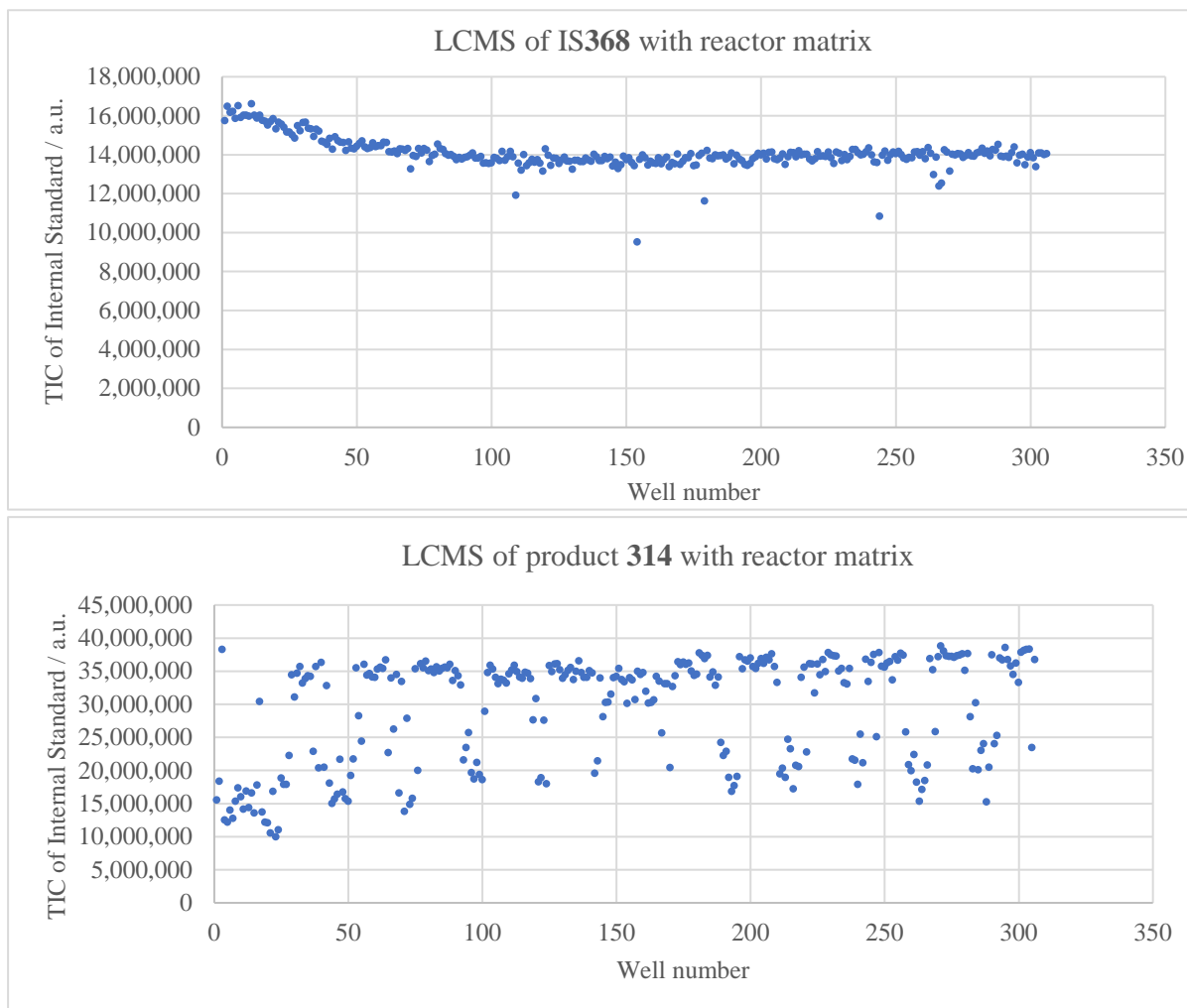
The TIC integral for the internal standard peak was over 44 million which is too high for the detector. Exposure at this high ionisation results in detector saturation and loss of sensitivity over the 15 hours analysis time, a possible reason for the sudden drop in TIC after 300 samples (Graph 6) and after 200 samples (Graph 7). Therefore, IS368 loading and analytical sample concentration needed to be reconsidered (Table 1). Entry 1 shows the original concentration of IS368 was too high, causing the detector to saturate at 44 million TIC. Reducing the concentration of the stock solution by a quarter dropped the TIC by over 30%. However, injection-to-injection error could be responsible for the difference between the two observed peaks. To confirm that this was not the case, the concentration was reduced by a factor of 10 and the autosampler injection volume was increased by 10 and a similar total ion count was observed (Entry 3). Although a strong ionisation signal was desirable for minimal CV and RV error, the conditions for Entry 3 were still potentially too high and could cause detector saturation during long analysis runs. Thus, reducing the concentration of IS368 to 0.139 mM and reducing the LCMS autosampler injection volume to 0.7 μL gave an overall TIC of 13 million which was deemed to be enough for quantitative analysis.

Entry	IS368 concentration / mM	Autosampler injection volume / μL	IS368 peak area TIC / a.u.
1	3.67	0.1	44,000,000
2	2.75	0.1	29,092,295
3	0.275	1.0	28,064,809
4	0.275	0.7	21,778,384
5	0.139	1.0	13,850,682
6	0.139	0.7	13,307,915

Table 1: Optimisation of IS368 stock solution.

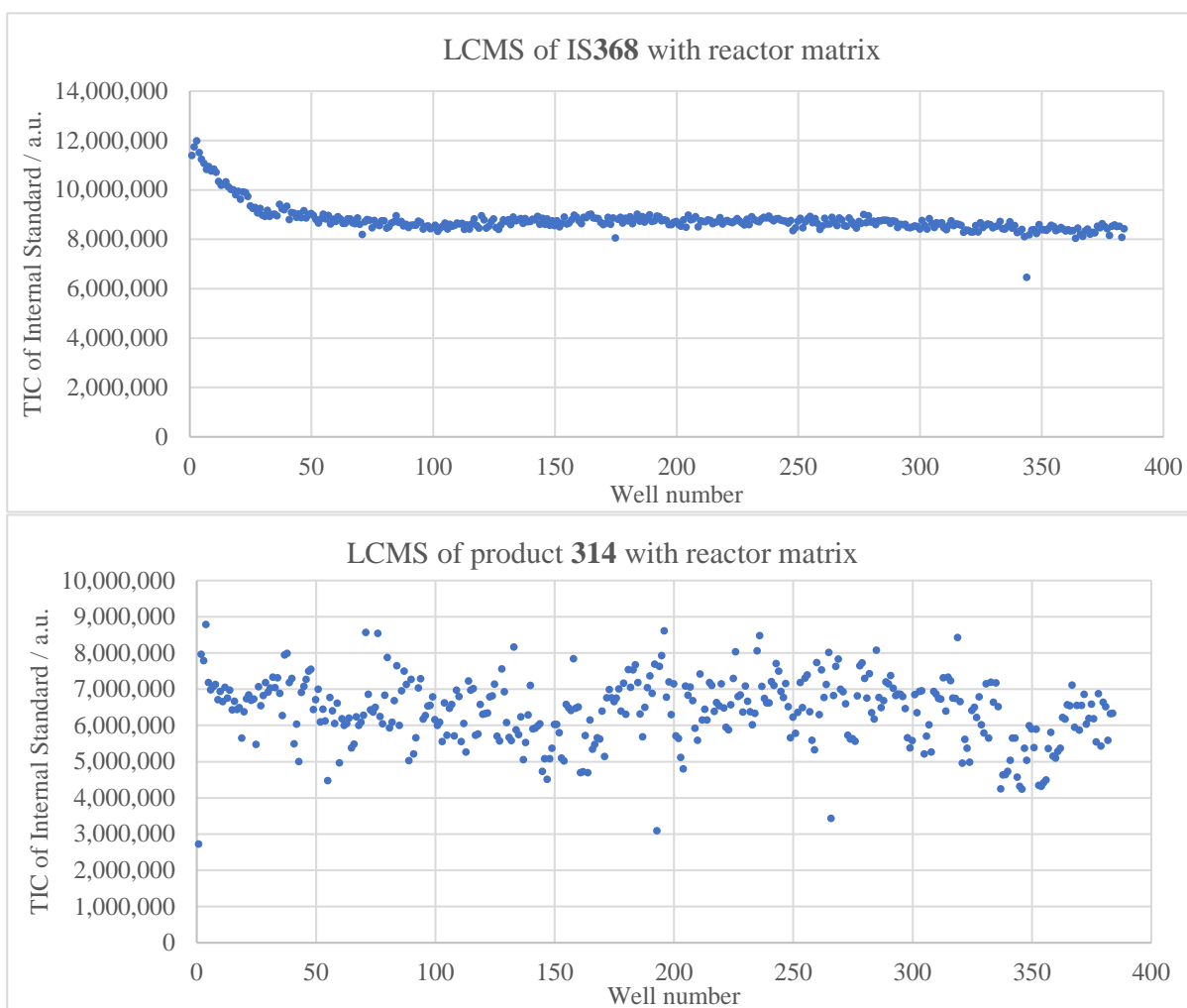
While the internal standard concentration optimisation was in progress, the high-throughput protocol adopted 1536-well reactor plates that resulted greater reaction consistency across quadruplicate reactions (discussed in Chapter 3). Using the 1536-well plate, a smaller and more controlled volume of reaction mixture could be added to the analysis mixture. Initially starting with 500 nL of reaction mixture, the sample preparation was changed to 50:50 water:formic acid containing 0.139 mM **IS368** stock solution (50 μ L) and additional water (40 μ L) to dilute the DMSO concentration to only 0.6%. This corresponds to injecting a total of 2.1 μ L of DMSO into the mass spectrometer per plate (181 times less than the first instance).

Screening the same conditions shown in Scheme 43 earlier in the section with boronic ester **331**, 500 nL of reaction mixture was added to the analysis plate and made up to 90.5 μ L with 50 μ L **IS368** quenching mixture and 40 μ L water. Unfortunately, the analysis run (Graph 8) was cut short by 80 samples due to an air bubble formed in one of the pumps. However, important learnings could still be taken from this run. The internal standard did not experience any ion-suppression from the bases which verifies the new internal standard. Secondly, the new DUIS ionisation mode performed well for both product and internal standard. Finally, the product concentration in the analysis mixtures is now too high, at 35 million TIC, thus nearing the detector's saturation level.



Graph 8: Top: IS368 TIC vs well-number shows almost consistent ionisation; Bottom: Product 314 TIC vs well-number shows there is now too much product in the analysis solution.

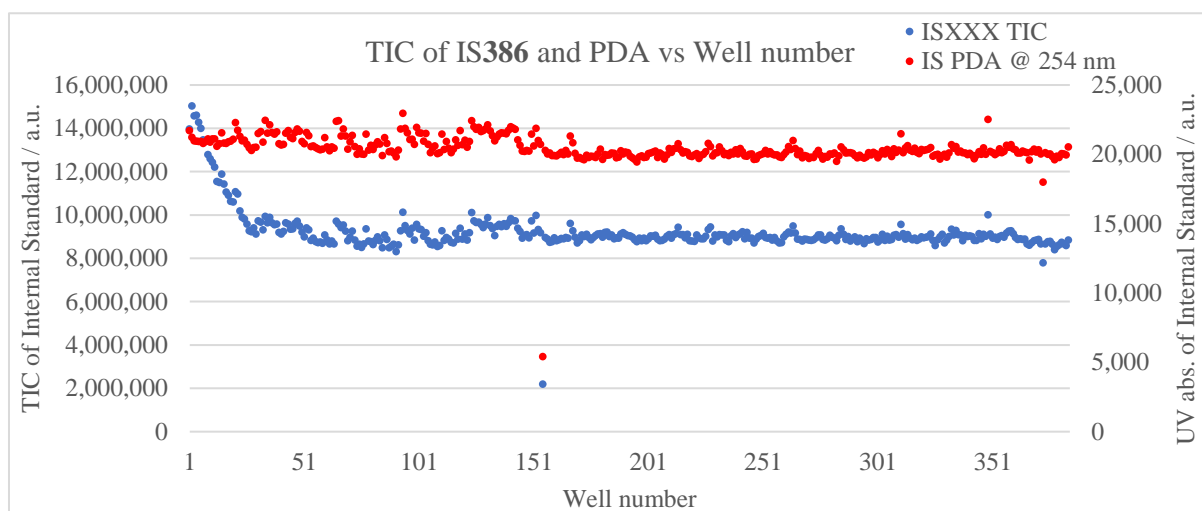
Reducing the volume of reaction mixture added to the analysis plate from 500 nL to 100 nL resulted in the expected reduction in the product TIC without affecting IS368 TIC (Graph 9). However, a reduction of 3,000,000 TIC for IS368 was observed over the first 25-50 samples. Mass spectrometer ‘conditioning’ was proposed as an explanation for this reduction over the first 50 samples. The LCMS used for this analysis is ‘open-access’ during the day and all analysis plates were run overnight after 10 hours of routine sample analysis. Therefore, a plethora of different solvents, metal ions, analytes and method files have been run through the machine. Therefore, it was hypothesised that the initial 50 samples are ‘conditioning’ the mass spectrometer and analytical column, with monolayers of material building up over the duration of analysis which standardises every subsequent sample.



Graph 9: Top: IS368 TIC vs well-number shows a steady decrease in ionisation over the first 50 samples then consistent ionisation after that; Bottom: Product 314 TIC shows that 100 nL of the crude reaction mixture in 90 μ L of solvent is enough for analysis.

2.6.5. LCMS Conditioning

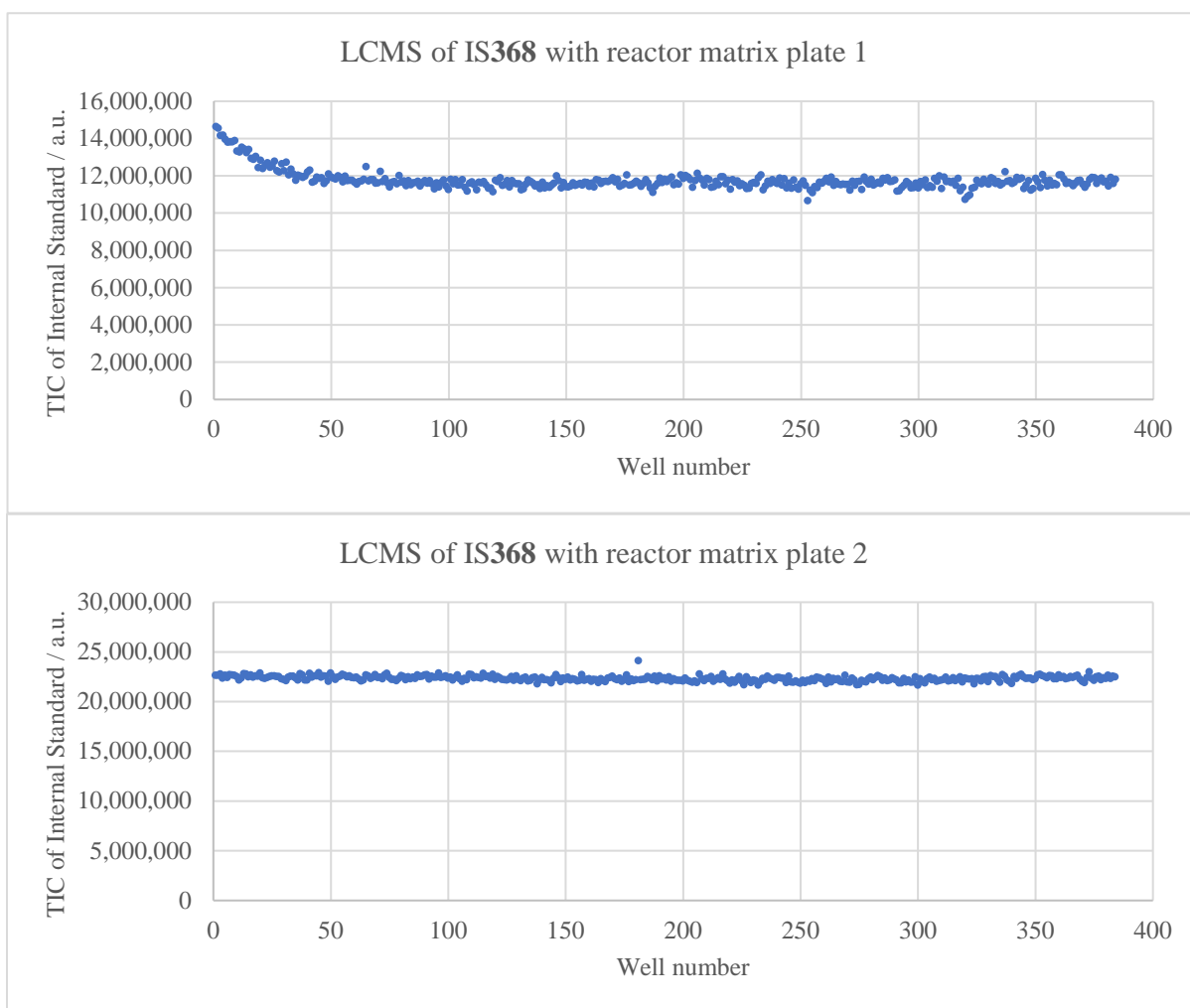
An optimisation plate was run with the PDA turned on assessed whether the column also required pre-equilibration or whether only the mass spectrometer required 'conditioning'. C18-columns are known to exhibit mass transfer effects that require conditioning with analyte before.¹⁹⁷ Over time, HPLC columns can deteriorate too which therefore means it imperative that columns are pre-dosed with the analyte matrix before analysis. Plotting the PDA peak area of the internal standard vs well-number as well as the TIC of the internal standard revealed that both the mass spectrometer and the column needed equilibrating (Graph 10).



Graph 10: Overlaid graphs of mass spectrometer TIC (Blue) and PDA absorption (Red).

The mass spectrometer TIC, in blue, shows that the first 25 samples have a steady decay in detection and then a consistent plateau after 150 samples. Meanwhile, the PDA chromatogram revealed that the column required equilibrating for the first 150 samples. After this time, a consistent PDA signal was observed for the remainder of the run. Therefore, both the mass spectrometer and the column needed conditioning before consistent data is obtained.

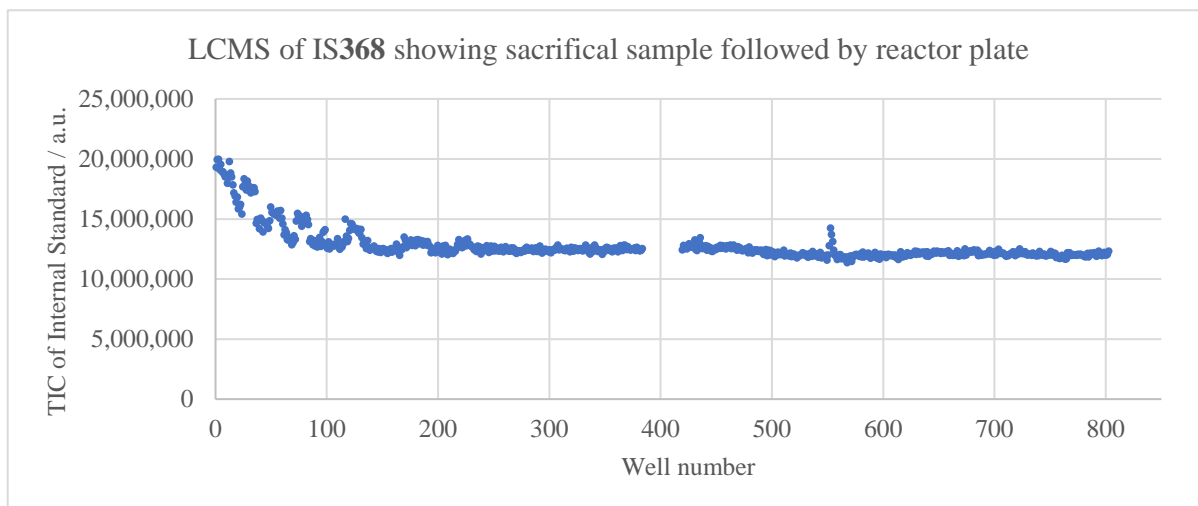
Therefore, as a proof of principle two plates were run in series after cleaning and autotuning the LCMS (Graph 11). It was hypothesised that the first plate would show a gradual decay in the internal standard TIC followed by a plateau and the second plate would show a consistent and flat ionisation across the plate. Gratifyingly, this hypothesis was confirmed, the first with 2-naphthylboronic acid pinacol ester **337** and the second with 4-trifluoromethylphenyl boronic acid pinacol ester **333** with the conditions shown in **Error! Reference source not found.** Two different IS**368** stock solutions were used for products **337** and **333** as they ionise very differently in the mass spectrometer. Graph 12 has approximately 12 million IS**368** TIC and the second with approximately 23 million IS**368** TIC. More importantly, it shows that, over the course of the analysis, the MS and column are equilibrating to the analytical conditions. The overall coefficient of variance for the second graph shown in Graph 11 was 0.91% with a range-based variance of only 11%.



Graph 11: Top: IS368 TIC vs well-number of the first plate shows that ionisation reduces across the first 50 samples and is then consistent; Bottom: IS368 TIC vs well-number of the second plate shows consistent ionisation.

This method required over 15 hours of analysis time before consistent IS368 ionisation was observed which is inherently limiting to the overall high-throughput optimisation protocol. Attempts at reducing the time taken to reach consistent ionisation were less fruitful. The only way to achieve quantitative analysis was by preparing a vial with a similar matrix as the analysis plate (DMSO, IS368 and product 314) at the same concentrations and running that sample 384 times before starting analysis of the plate (Graph 12).

This is referred to as the “sacrifice” or “sacrificial sample”. The initial 100 samples on the sacrificial run show both the conditioning of the mass spectrometer (gradual decay in sensitivity) and column (gathering of dots). After 250 samples, the LCMS is ready for quantitative analysis.

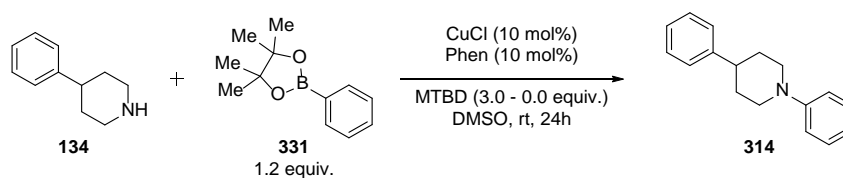


Graph 12: Sacrificial sample of product, IS368 and DMSO run for 384-samples followed by a reaction optimisation analysis plate. A gap here is shown between the two runs for clarity (in reality the two runs are run in series without a break).

2.7. Calibration Curves for Quantification of Yields

Equipment calibration is mandatory to standardise the response of any analytical instrument used for quantification. There are two types of standardisation, external and internal. External standardisation analyses authentic product outside of the target analyte mixture. An absolute dose response (for example TIC peak of chromatograph peak integral) is plotted against known concentration and therefore a calibration curve can be obtained for all results. The external method can experience considerable error due to subtle factors such as sample preparation and sample to sample fluctuation. Internal standardisation places a standard within the analytical mixture and a ratio between the standard and analyte is measured. The ratio can be plotted against known standard concentration curves. Both methods require isolation of authentic products. The internal standard is considered the best method for LCMS calibration as it accounts for sample to sample variation and lessens the impact of variable sample preparation.¹⁹⁸

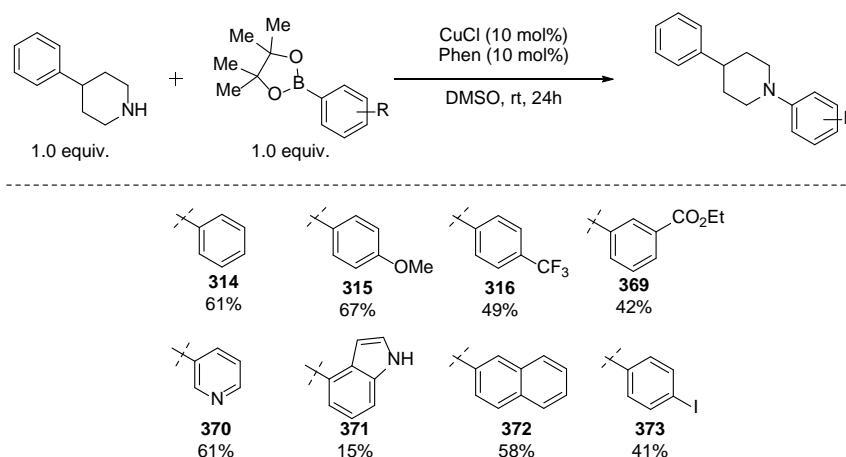
To generate authentic products of the boronic ester array (**Error! Reference source not found.**), batch scale optimisation was completed to verify the necessity of 3 equivalents of base in the reaction. When assessing the parameters for the Chan-Lam reaction it was thought that 3 equivalents of base were necessary to sequester the generated acid from the catalytic reaction, potentially protonating the starting amine. However, varying the amount of base added to each millimole scale reaction found that large excesses of base were detrimental to the reaction conditions (Table 2).



Entry	MTBD 317 / equiv.	NMR Yield of 314 / %	Isolated Yield of 314 / %
1	3.0	68	60
2	1.0	78	-
3	0.0	94	82

Table 2: Screening different equivalents of MTBD before isolating authentic products for high-throughput calibration.

Reducing the equivalents of the base resulted in a boost in yield: 68% to 94% NMR yield with and 60% to 82% isolated yield. The most likely explanation for this observed change is the amine is outcompeted for catalyst binding compared to the three-fold higher concentration of the base in Entry 1. Therefore, reducing the amount of base in the reaction results in a higher proportion of amine **134** coordinating to the catalyst (Entries 2-3) and more productive reactions can take place. In order to prepare the necessary products for calibration curves, Entry 3 conditions were used as the standard isolation protocol with stoichiometric quantities of amine and boronic ester. Boronic esters from **Error! Reference source not found.** were all reacted with standard amine **134** on 0.3 millimole scale with 10 mol% of copper(I) chloride and phenanthroline **319** to give their corresponding products in 15–67% isolated yield (Scheme 44).



Scheme 44: Preparation of Chan-Lam authentic products for calibration.

After isolation was completed and with the optimised analysis strategy in hand each compound was exposed to the high-throughput LCMS assay for method file, mass spectrometer optimisation and autosampler aliquot optimisation. Each assay was optimised using the “100% yield” calibration sample so that perfect compound separation could be achieved and with the product eluting after 1.0 minutes (or just before) so that no ion-suppression could occur. The mass spectrometer was optimised with the corresponding product ions and the mass spectrometry scan rate set to 15,000 a.u./s so smooth peaks could be obtained (Appendix 2).

Finally, autosampler aliquot volumes were optimised so detector saturation would not occur. For all eight compounds in Scheme 44, LCMS optimisation was completed, and the parameters summarised in Table 3.

Entry	Product	Autosampler aliquot volume / μL	IS stock solution / μL of 0.1M IS368 S.S. in 100 mL
1	314	0.5	135.0
2	315	0.3	225.0
3	316	1.0	62.5
4	369	0.3	225.0
5	370	0.3	225.0
6	371	0.3	225.0
7	372	0.2	337.5
8	373	0.2	337.5

Table 3: LCMS autosampler conditions and IS368 stock solution serial dilutions.

Each autosampler aliquot volume required a different IS stock solution. More electron-deficient products such as **316** required larger autosampler aliquot volumes due to the low nucleophilicity of the amine nitrogen and poor ionisation with DUIS. However, larger and more electron rich compounds ionise very well in DUIS and therefore could use a smaller autosampler aliquot volume so a more concentrated IS368 stock solution could be used.

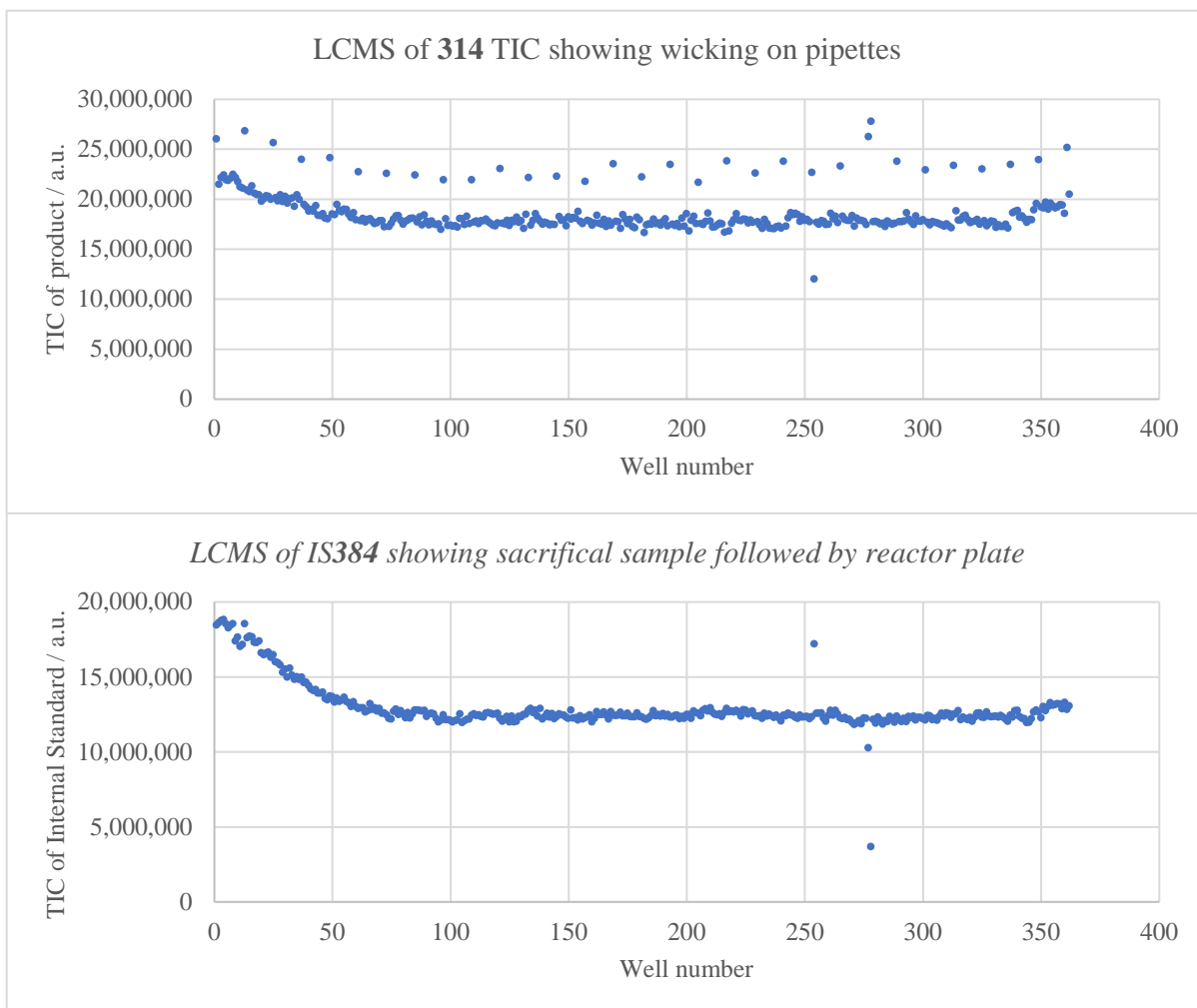
Calibration curves samples were prepared from a 2.5 mM stock solution of product in acetonitrile. Subsequent serial dilution of 500 μL into a 5 mL stock flask achieved the correct calibration curve concentration. LCMS vials were charged with 401 μL , 300 μL , 200 μL and 100 μL corresponding to 100%, 75%, 50% and 25% yield. It was assumed that 0% product would give 0 mass spectrometer detection and would give the origin as the intercept. For the 75% - 25% yield calibrations and an additional 101–301 μL of water was added to achieve the desired concentration. Each calibration sample was charged with 500 μL of the corresponding IS368 stock solution noted in Table 3. These samples were sealed with parafilm and run directly after the corresponding analysis plate to ensure the same LCMS conditions for analysis. Each sample was added into the “controller rack” indicated in Figure 27.

With the calibration samples in hand and the ratios of the product over internal standard from the LCMS analysis, each average ratio can be rendered quantitative with the gradient from the calibration curve. A quantitative heatmap can then be produced for simple and easy hit identification (Heatmap 1).

	No Base	DBU	DABCO	TMU	No Base	DBU	DABCO	TMU	No Base	DBU	DABCO	TMU	No Base	DBU	DABCO	TMU
CuCl	69.6	61.2	72.5	74.7	74.6	75.0	55.5	68.2	78.3	60.8	81.3	81.5	81.3	81.6	53.4	71.4
CuCl ₂	61.4	58.9	70.9	72.4	71.2	71.1	59.5	72.3	72.3	59.9	74.0	74.6	77.0	78.0	58.1	77.1
Cu(OTf) ₂	50.4	62.4	64.1	69.6	64.2	62.1	58.3	74.3	65.7	60.1	73.4	73.2	76.2	73.0	57.1	68.9
Cu(NO ₃) ₂	56.1	61.3	60.6	68.6	62.7	65.9	58.1	74.1	64.3	57.5	74.3	74.6	73.2	77.8	59.7	73.9
Cu(BF ₄) ₂	57.2	60.9	67.3	72.3	68.2	68.4	54.3	70.2	67.5	55.7	75.7	77.0	80.8	79.6	51.6	73.0
CuBr ₂	64.4	62.1	67.5	72.7	69.0	67.9	56.0	73.7	68.7	59.8	74.0	70.4	80.1	81.4	57.7	81.1
	Phenanthroline								Bipyridine							

Heatmap 1: Example heatmap using phenyl boronic acid pinacol ester 331.

To confirm whether the first quantitative high-throughput heatmap could be reported with confidence, the Mosquito[®] analysis plate protocol was tested with a known concentration of the product. The Mosquito[®] dosed 100 nL of 0.1M 314 stock solution into each well of a 384-well plate prepared in the same way as a conventional analysis plate (Graph 13). Using a non-quantitative overnight method without MS conditioning precautions, a steady decrease in IS368 TIC was observed as expected, but the product TIC spiked every 12 samples



Graph 13: A) Graph of IS368 TIC vs well-number showing a steady decrease in internal standard TIC as expected with an unconditioned LCMS; B) Graph of 314 TIC vs well-number showing spikes in product ionisation. These spikes occur every 12 wells.

The method used for analysis plate preparation was optimised in the Mosquito[®] dosing protocol to initially aspirate 1200 nL of 0.1M product **314** stock solution which added 100 nL to the first 12 columns (1-12). The Mosquito[®] then aspirated another 1200 nL of stock solution to add into the next 12 columns (13-24). The spike in product TIC is due to the product stock solution wicking to the sides of the pipette whereby more product stock solution is added to the analysis plate in column 1 and column 13 (Figure 35).

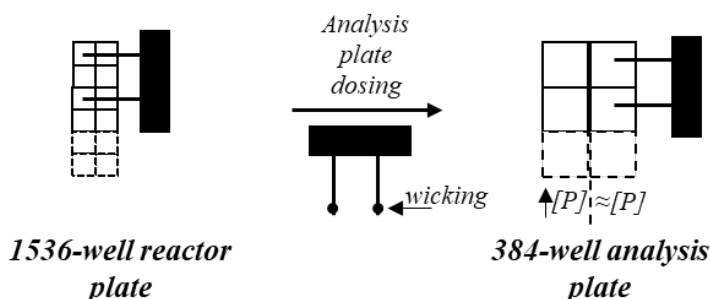


Figure 35: Wicking of the pipette when aspirating reaction mixtures from a reactor plate.

To resolve this issue, a needle washing protocol was prepared which initially aspirated 1100 nL of the crude reaction mixture (Figure 36). The Mosquito[®] then dosed 500 nL into a ‘wash’ plate filled with 85 μ L of DMSO. The washed tips then dispensed 100 nL of the crude reaction mixture into the analysis plate and the remaining 500 nL was dosed into the wash plate. This process utilised the “multi-dispense” feature in the Mosquito[®] software. Two columns were employed on the wash plate, one for columns 1-12 and the second 13-24 to ensure minimal product cross-contamination.

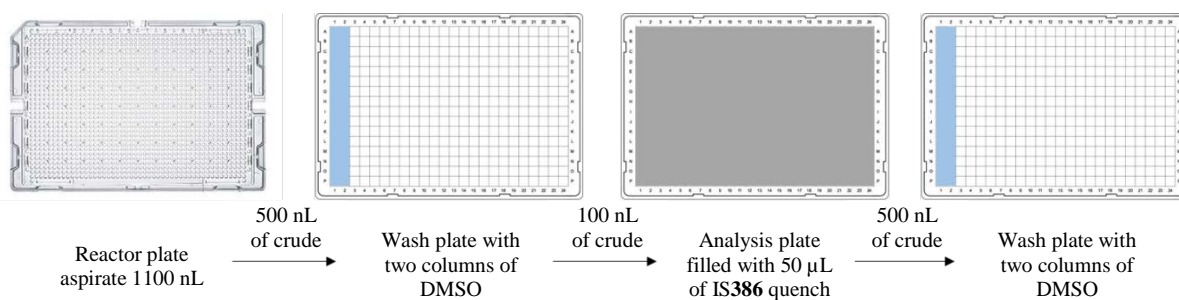


Figure 36: Analysis plate dosing protocol with pipette wash.

2.8. Quality Control, Data Visualisation and Validation

Quality control of thousands of data points is crucial for the end user to eliminate anomalous data and to test the robustness of the remaining generated data. Furthermore, a simple and easy way to visualise the data is imperative for rapid hit identification. Statistical analysis was therefore integrated into the Excel spreadsheet to automate data quality control and heatmap visualisation was used to complete the high-throughput optimisation protocol. Statistical analysis is the easiest way to assess large volumes of data and the equations they utilised are

easily transformed into the spreadsheet. There are many statistical methods that could be used but compared the standard deviation (SD) and median absolute deviation (MAD).

The reaction optimisation platform developed screens 96 different reaction conditions in quadruplicate. The quadruplicate reactions can be used to assess the overall deviation and can also be used to identify anomalous reactions. Standard deviation is a measure of the spread of data from the mean value given by Equation 13. Although one of the most utilised statistical methods, it can be easily skewed by anomalous results. The median absolute deviation (MAD) given by Equation 14, is less prevalent and uses the median value of the data that is less skewed by outlying results.

$$SD = \sqrt{\frac{\sum(x_n - \bar{x}_i)^2}{n - 1}} \quad \text{Equation 13}$$

$$MAD = k\bar{x}_n (|x_n - \bar{x}_i(x_i)|) \quad \text{Equation 14}$$

Often in small molecule high-throughput functional screening, the standard deviation is the primary statistical method of choice. Outliers and even strongly positive or negative data can skew the standard deviation dramatically and, therefore, having a plate specific statistical method can avoid undue influence from erroneous or outlying data.^{199,200} For data that follows a normal distribution, the 68-95-99.7 rule is commonly used to identify the distribution of data about the mean average (\bar{x}). With 68% of normally distributed data lying within one standard deviation (σ), 95% lying within 2σ and 99.7% lying within 3σ .²⁰¹ Accordingly, a test of 3 standard deviations about the mean ($\bar{x} \pm 3\sigma$) is commonly used as a test to identify good data, with anomalies assumed to fall outside of the 99.7%. More conservative estimations of 2.5σ and 2σ about the mean are also used.²⁰²

However, there has been criticism about using the mean and standard deviation about the mean, as a method for detecting outliers as the constants themselves can be skewed by anomalous data. Another method used for outlier detection is the median absolute deviation (MAD), as this is derived from the median, \bar{x} .²⁰³ Both approaches were tested to survey their suitability (Table 4).²⁰⁴

<i>Unprocessed Results</i>	<i>With 2.5 MAD or SD</i>	<i>With 2 MAD</i>	<i>With 2 SD</i>																																								
<table border="1"> <tr><td colspan="5">C1</td></tr> <tr><td>E1</td><td>0.7</td><td>0.7</td><td>0.6</td><td>1.2</td></tr> </table>	C1					E1	0.7	0.7	0.6	1.2	<table border="1"> <tr><td colspan="5">C1</td></tr> <tr><td>E1</td><td>0.7</td><td>0.7</td><td>0.6</td><td>1.2</td></tr> </table>	C1					E1	0.7	0.7	0.6	1.2	<table border="1"> <tr><td colspan="5">C1</td></tr> <tr><td>E1</td><td>0.7</td><td>0.7</td><td>0.6</td><td>BAD</td></tr> </table>	C1					E1	0.7	0.7	0.6	BAD	<table border="1"> <tr><td colspan="5">C1</td></tr> <tr><td>E1</td><td>BAD</td><td>BAD</td><td>BAD</td><td>1.2</td></tr> </table>	C1					E1	BAD	BAD	BAD	1.2
C1																																											
E1	0.7	0.7	0.6	1.2																																							
C1																																											
E1	0.7	0.7	0.6	1.2																																							
C1																																											
E1	0.7	0.7	0.6	BAD																																							
C1																																											
E1	BAD	BAD	BAD	1.2																																							
By inspection, the value of 1.2 is anomalous.	For this data set, no anomalies are found using a factor of 2.5 deviations for either the standard deviation or the median absolute deviation.	When a more conservative factor of two is used. The MAD clearly identifies the correct anomalous value (1.2).	As the SD is dependent on the Mean, it is very sensitive to outliers. Using a conservative estimation of: Mean \pm 2 SD The good values are discounted, and the anomalous result passes the statistical test.																																								

Table 4: Comparison between MAD and standard deviation.

The unprocessed, quadruplicate data in Table 4 has an obvious outlying ratio of 1.2 compared to the other three data points. When applying a deviation limit of 2.5σ or MAD units, no data are excluded from the quadruplicate data points. Reducing the parameter to 2.0 units, the MAD excludes the outlying data point from the quadruplicate. Whereas, 2.0 SD units remove the three “good” data points which are further from the mean value, showing that SD is skewed by large values.

A modified median absolute deviation was integrated into the Excel spreadsheet by simple four-part, iterative calculations. Initially, the median of the overall analysis plate and the median of each quadruplicate repeat were calculated; the median deviation was then derived using Equation 15. The scaled MAD can then be used to test the data. As shown in Figure 37 with ± 2.0 MAD, outlying data can be rapidly removed. Integrating this into the Excel spreadsheet using the logic function, shown in Equation 16, anomalous data can be immediately removed and replaced with “BAD”. The logic function (Equation 17) initially assesses whether the cell contains a MAD of greater than 2.0, if it does the phrase “BAD” is then given out as the true answer, if the MAD is less than 2.0 then the data is placed into the cell. The data was then

placed in a condensed heatmap and using the conditional formatting feature in Excel a gradient of the relative performance of the reaction from the worst (red) to the best (green) was added.

Absolute Deviation from Median

$$= |Well\ plate\ ratio - plate\ median| \quad \text{Equation 15}$$

$$Scaled\ MAD = 1.4826$$

$$* \frac{|(Well\ plate\ ratio - Quadruplicate\ Median)|}{Median\ Absolute\ Deviation\ from\ Median} \quad \text{Equation 16}$$

$$Data = IF((MAD > 2.0),BAD,Data) \quad \text{Equation 17}$$

Once all the data has been processed, a 384-well analysis plate was returned with all anomalous data removed and replaced with “BAD” (Figure 37). The processed data is averaged to produce an overall 96-well plate showing all unique reaction conditions screened. The data is only averaged if there are three or more data occupying a quadruplicate set of reactions otherwise “BAD” is placed in the cell. Once the statistical analysis is completed, the internal standard calibration curves obtained directly from the LCMS can be applied to the data to produce quantitative results.

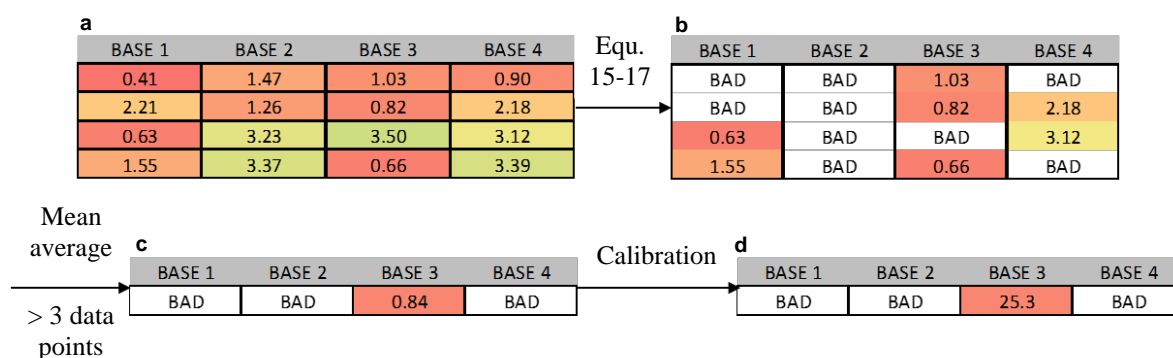


Figure 37: Example statistical analysis from high-throughput optimisation plate. a) unprocessed data, b) processed data by equations 15-17, c) Mean average of data if 3 or more data are present, d) Calibration of the plate with calibration curves.

To validate the quantitative assay, three different reactions (the best, worst and a median performing reactions) were assessed on a millimole scale (1200 times scale from nmol to mmol) The scale-up reactions are performed using the same principles of the Mosquito[®] i.e. preparing all reagents in stock solutions and dosing a reaction vial with aliquots of these stock solutions until a digital air displacement pipette. The reactions are then left to stir for the same reaction time as the plate and left and exposed to air to allow complete exchange of the reaction atmosphere.

2.9. Summary

Within this chapter, a quantitative high-throughput protocol has been described using simple, single quadrupolar LCMS. Excel spreadsheets have been prepared to facilitate the reagent weighing and stock solution preparation. Bespoke reactor plates and their associated source plates have also been designed to complement the Excel spreadsheet. Mosquito[®] software was used to program the dosing protocol using advanced settings to manually tune plate definitions for accurate reactor plate dispensing.

Once reactions were prepared, aluminium foil was found to be the best candidate for effective plate sealing over commercial adhesive seals. Once the reactor plate had been left for the allotted time, the Mosquito[®] was programmed to aspirate 100 nL of the crude reaction mixture into an optimised quenching mixture of 50:50 formic acid water. The analysis plate was topped up to a total of 90.1 μ L with 40 μ L of water. The analysis plate was then loaded into the LCMS where **IS368** was chosen and shown to not undergo deleterious ion-suppression. Prior to quantitative analysis, the key mass spectrometer parts (corona needle, octopole and pre-quad assembly) were meticulously cleaned by sonication. The parts were then returned to the machine which was subsequently autotuned using the Shimadzu standard sample. A simple sacrificial sample was prepared with a similar matrix to the analysis mixture, 0.11 mM of product **314**, 0.075 mM of **IS368** and in 0.1% DMSO in acetonitrile that was run 384 times before quantitative analysis was obtained.

Calibration curves of known product concentrations were prepared and loaded into the “controller” rack of the LCMS, adjacent to the analysis plates. These samples were run directly after the analysis plate to ensure similar LCMS conditions for quantification. MS peak area integrals were taken and uploaded to the Excel spreadsheet where a ratio of product TIC:internal standard TIC was calculated. The median absolute deviation was used to statistically assess the data and automatically remove anomalous data from the plate. The mean average of 3 or more data points within a quadruplicate reaction was completed and, when applied with the corresponding calibration curve, quantitative information was obtained.

Chapter 3: High-throughput experimentation of the Chan-Lam reaction to model reactivity

3.1. Introduction

The high-throughput protocol described in Chapter 2 allows quantitative data generation on a scale previously unprecedented in synthetic chemistry. This chapter discusses the application of the protocol for quantitative data generation and the development of a predictive modelling for the Chan-Lam reaction.

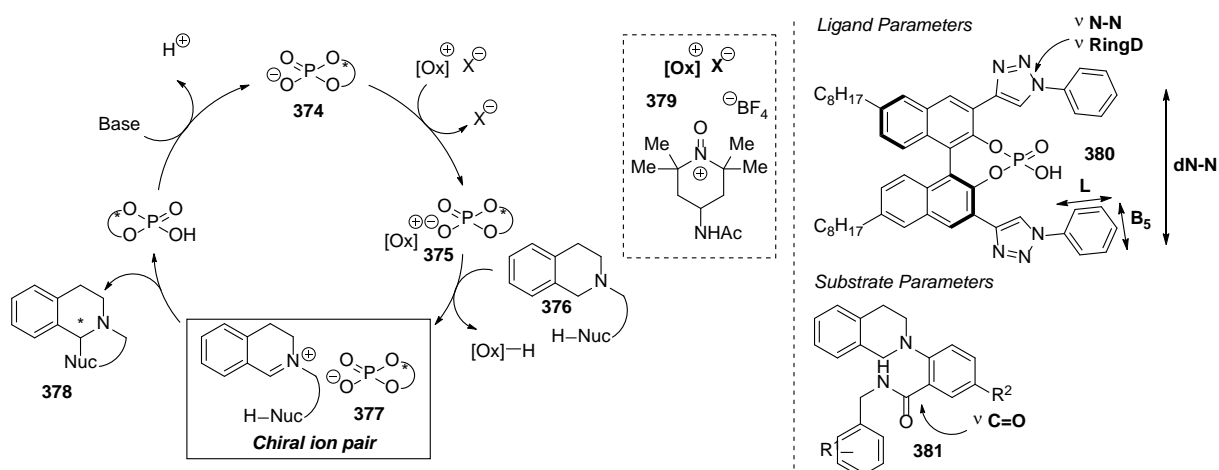
3.1.1. Application of Machine Learning in Synthetic Chemistry

Traditionally computational expertise has been used to model systems on a macroscale such as atmospheric systems²⁰⁵ and peptide tertiary and quaternary structures.²⁰⁶ Inorganic surface chemistry²⁰⁷ and theoretical particle interactions have also been modelled using computational methods.²⁰⁸ The advent of readily available computational software such as Gaussian and Avogadro has allowed synthetic chemists to investigate unisolable intermediates and high-energy transition state structures.²⁰⁹

Recently, the invention and application of, for example, statistical design-of-experiments (DoE)²¹⁰ has permitted industrial chemists to speed up batch and process scales optimisation.²¹¹ Principle-component analysis has also been used by Merck to ‘map chemical-space’ using chemoinformatics.²¹² The progression of computational chemistry over the last decade has been significant but modelling synthetic chemical reactions is currently in its infancy. Small data sets from iterative optimisations and reaction outcomes depending on highly non-linear functions are only handful of the difficulties associated with reaction modelling. The use of automated reaction setup procedures and high-throughput techniques has opened the possibility of reaction modelling. Large data sets of thousands of reactions are prepared simply and can include thorough component assessment.

Synthetic chemists are beginning to employ computational modelling to synthetic chemical outcomes to determine whether trends can be identified.²¹³ Toste and Sigman²¹⁴ employed a data-intensive approach to model an acid-catalysed amine-iminium cyclisation using a chiral ion pair to create an enantioselective environment (Scheme 45). Their initial studies focussed on a known chiral BINOL-phosphoric acid.²¹⁵ Through simple batch-scale screening BINOL-phosphoric acids, substituted with *N*-alkyl triazoles **380**, furnished enantiopure product **387** in 93% conversion and 45% e.e. Further assessment of four electronically diverse ligands and five different chiral *N*-alkyl triazole BINOL-phosphoric acid created a ‘training set’ for the model to correlate predicted reactivity and experimental outcome. Computational parameters such as

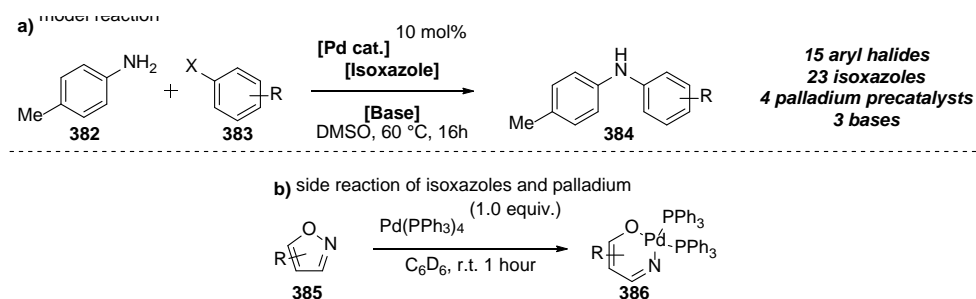
Sterimol (size, shape, geometry), Hammett (electronic) and vibrational frequencies were used to parameterise all substrates and *N*-alkyl triazole BINOL-phosphoric acids.



Scheme 45: Enantioselective addition of appended amide to in-situ generated iminium. a) Catalytic cycle to show Chiral Ion pair key to the computational model; b) computed parameters for the ligand and starting material.

As a result, computationally and experimentally determined Gibbs free energy relationships were correlated with a Pearson regression coefficient of 0.89. With the ‘training-set’ now complete, new ligand and substrate combinations were virtually assessed and validated experimentally. The model showed exemplary predictive power for enantioselectivities. The described data-intensive approach for reaction modelling, along with detailed mechanistic understanding, resulted in a model capable of correlating ligand and substrate structure to experimental enantioselectivity.

High-throughput protocols can be used to streamline data generation. Doyle, in collaboration with Merck, employed a Mosquito[®] high-throughput reaction optimisation protocol¹⁶⁷ to model the efficiency of the Buchwald-Hartwig amination in the presence of isoxazoles **385** (Scheme 46). High-throughput semi-quantitative UPLC data could be modelled using machine learning algorithms to predict whether the desired amination reaction would proceed over a known deleterious palladium-catalysed N–O oxidative insertion mechanism (Scheme 46b).²¹⁶



Scheme 46: Reaction modelled by Doyle and MSD. a) High-throughput screen for data gathering (total of 4,608 reactions); b) deleterious palladium-catalysed oxidative insertion of isoxazoles.

High-throughput screening assessed *p*-toluidine **382** against 15 different aromatic and heteroaromatic halides **383**, three organic bases and four different palladium-precatalysts. 23

different isoxazoles were also assessed to capture the electronic and structural factors important to the undesired side reaction. The high-throughput protocol assessed a total of 4,608 unique reaction conditions. Parameterisation of all reaction components by a combination of B3LYP and 6-31G* methods revealed isoxazole IR-stretching modes were key for predicting the reaction outcome (Figure 38a). Six machine learning algorithms (Figure 38b) were subsequently assessed for trend identification. Algorithms such as linear modeling and neural networks gave low Pearson's correlations between experimental and predicted yields ($\rho = 0.80 - 0.82$). Random-forests modeling gave exemplary correlation ($\rho = 0.96$) between the assay and observed yield (Figure 38b).

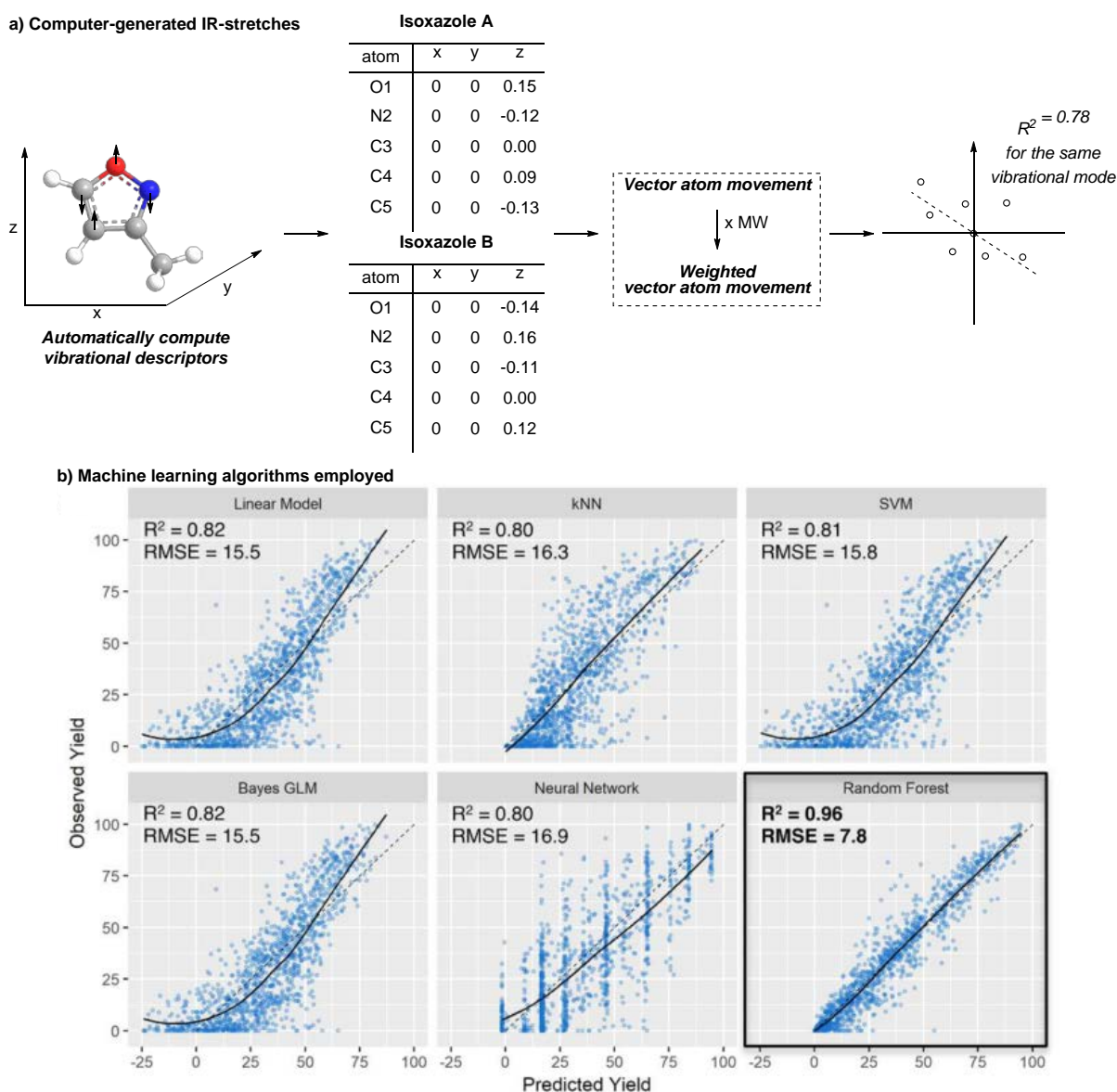


Figure 38: a) Computational method used for parameterising the effect of the isoxazole. Initial computation of common IR-stretching modes gives a vector matrix. Multiplying these vector matrices by the molecular weight of the isoxazole gives a weighted vector. Plotting and comparison between isoxazoles by Pearson correlation gives common computed IR-modes. B) Modelling methods used to model high-throughput data and their overall effectiveness towards prediction showing Random-Forest as the best.

With random-forests identified as the best method for predictive modelling, eight new and unassessed isoxazoles were virtually tested to assess the model's predictive power. Impressive correlations were found for five isoxazoles ($\rho > 0.90$) while the remaining three gave lower, but still impressive correlations of $0.86 < \rho < 0.90$. Attempts to predict the reaction performance between different aromatic halides were less fruitful with minimal correlation and, therefore, minimal predictive power.

The methods pioneered by Sigman, Toste, Doyle and Merck represent a significant contribution to synthetic chemical reaction prediction. The method described by Sigman and Toste, however, is hampered by lengthy synthesis and laborious quantification techniques. Conversely, Doyle and Merck used automated reaction setup and analysis to rapidly generate over 4000 unique data points. The random-forest method used returned exemplary correlations between experimental and predicted outcomes. Only semi-quantitative data was modelled however. The marriage of these two concepts, high-throughput automation and quantitative data accusation would be an important advancement for reaction prediction.

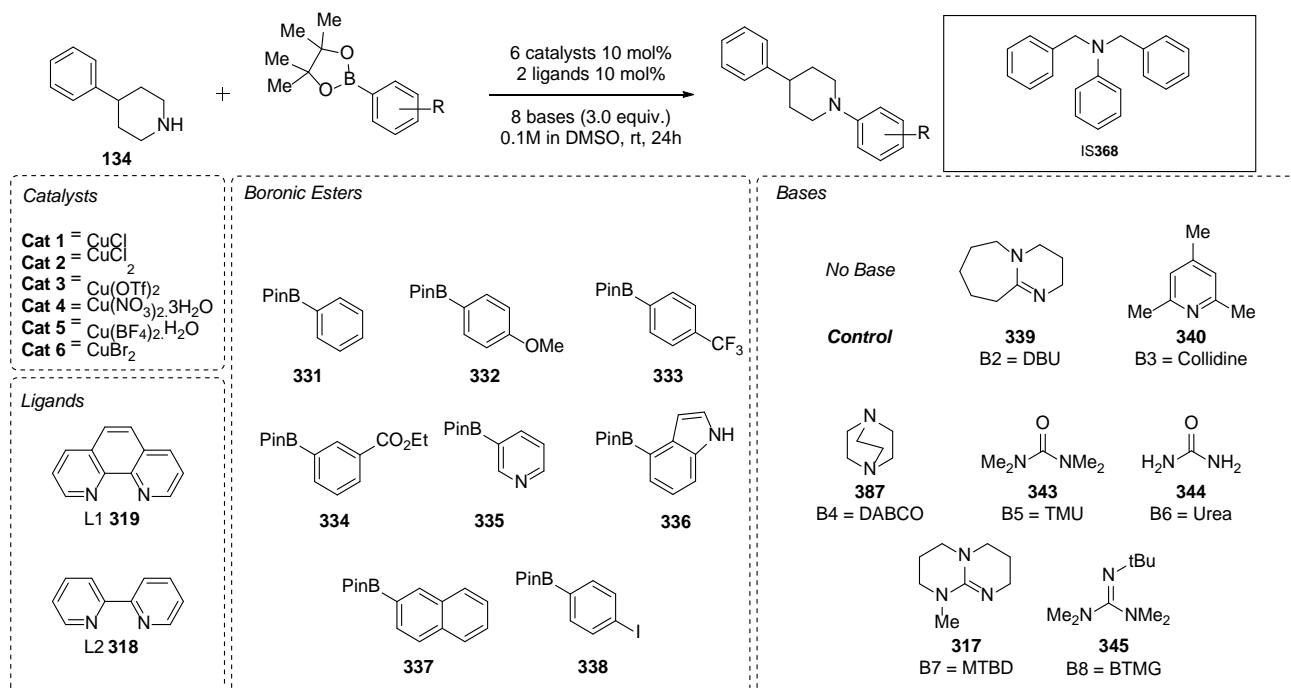
3.2. Parameter Screening of the Chan-Lam Reaction Using QLCMS

3.2.1. Initial Screening – 8 boronic esters

3.2.1.1. Optimisation Strategy

Eight simple boronic esters were chosen for initial high-throughput screening using the described protocol in Chapter 2. Boronic esters **331** – **338** were chosen to assess a range of electronics factors and important heterocyclic motifs. The initial eight substrates **331**–**338** were screened against 4-phenylpiperidine **134**, eight bases, two ligands and six catalysts (Scheme 47). The Mosquito[®] prepared the reactor plate according to Reactor Dosing Protocol 2-9 (Appendix 3). All arrays were sealed with tin foil and left at room temperature or 24 hours.

The analysis plate was prepared using dosing protocol 10-14 depending on the location on the reactor plate (Appendix 3). Each analysis plate was prepared using only 100 nL of reaction mixture. Before quantitative analysis was completed, the LCMS was cleaned (General Procedure 5) and conditioned using a “sacrificial sample” containing 0.11 mM of product **314**, 0.075 mM of **IS368** in water:formic acid:DMSO (1:0.28:0.001). The “sacrificial sample” was run 384 times at the same injection volume as the analysis plate to condition the column and mass spec to the correct DMSO concentration.

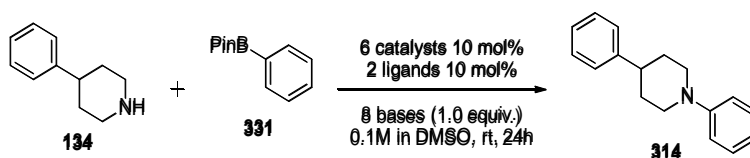


Scheme 47: Main 1 x 1 x 8 x 2 x 6 screening strategy for the Chan-Lam reaction.

Calibration curves for all compounds were prepared according to general procedure 4 using the corresponding IS368 stock solution used to prepare the analysis plate. The calibration samples were prepared to assess four yields: 100%, 75%, 50% and 25%. These were placed into the ‘controller rack’ and run directly after the corresponding high-throughput plate. If a substrate required a larger or smaller autosampler injection volume (better or worse substrate ionisation), 20-sacrificial samples were run to clean and pre-condition the column and mass spectrometer.

3.2.1.2. Optimisation Results

In this section all nanoscale reactions are quoted to 1 decimal place and colour coordinated such that the best yields are coloured green and the lowest yields are coloured red. Orange and yellow yields are in the middle of this range. Nanoscale assay yields were validated on a millimole scale, a scale-up factor of 1200 times. All reactions were validated within 15% error unless otherwise stated or discussed.

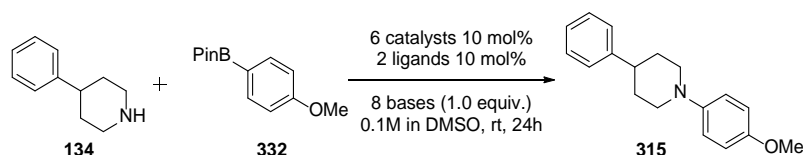


	No Base	DBU	Collidine	DABCO	TMU	Urea	MTBD	BTMG	No Base	DBU	Collidine	DABCO	TMU	Urea	MTBD	BTMG
CuCl	53.2	38.4	57.0	53.4	50.8	54.0	39.7	52.1	57.7	42.7	53.4	57.7	55.1	58.0	33.4²	49.3
CuCl ₂	49.8	36.3	52.6	57.2	51.1	52.6	42.5	53.2	52.4	42.9	56.9	60.0	56.4	50.5	38.6	53.7
Cu(OTf) ₂	49.5	39.3	51.5	47.5	46.8	49.7	39.1	58.7	57.6	44.1	56.9	60.3	58.4	52.1	33.2	50.3
Cu(NO ₃) ₂	45.2	40.2₂	45.6	48.0	43.7	46.0	38.0	60.0	55.5	41.1	57.1	59.1	52.8	52.2	35.3	53.9
Cu(BF ₄) ₂	48.0	36.7	53.9	54.2	46.7	53.6	29.0	57.2	60.9	40.3	62.1¹	60.4	55.7	56.2	27.9	46.3
CuBr ₂	44.0	37.6	52.5	51.4	42.6	52.4	BAD	58.9	55.0	39.9	57.8	53.4	53.9	50.7	29.3	50.0
Phenanthroline								Bipyridine								

Entry	Product	Nanoscale LCMS assay yield / %	Milliscale NMR assay yield / %
1		62	59
2	314	40	57
3		33	40

Array 1: Phenylpiperidine **134** screened with **331**. Each cell shown is an average of three or more data points. Each averaged reaction was calibrated using the corresponding calibration curve. Scale up reactions are highlighted in **bold**.

The first plate assessed the reaction of phenylboronic acid pinacol ester **331** with amine **134** and was prepared following the standard protocols outlined in section 7.7 (Array 1). One set of data points was eliminated because it failed the statistical test (labelled “BAD”). Reactions involving bases **339** and **317** gave a lower yield of product (as determined by the quantitative LCMS assay) compared with reactions using **340**, **387** and **344** as a base. When bipyridine **318** was used as the ligand, the reaction produced the highest yield of 61%, as determined by the Q-LCMS assay. A sampling of three reactions, which reflected good, average and poor outcomes, were further assessed on millimole scale and the yields of these reactions were found to correlate with the nanoscale cases (within 15% of the Q-LCMS yield, see table in Array 1).

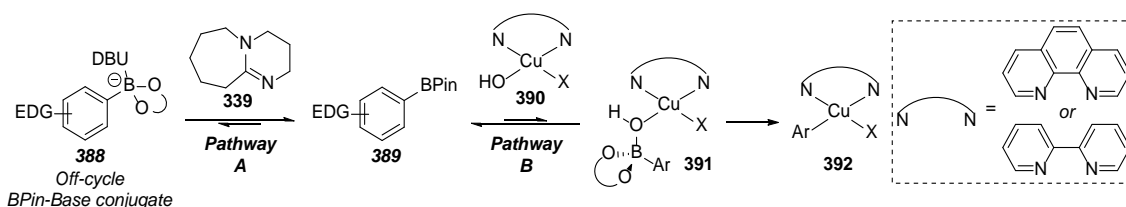


	No Base	DBU	Collidine	DABCO	TMU	Urea	MTBD	BTMG	No Base	DBU	Collidine	DABCO	TMU	Urea	MTBD	BTMG
CuCl	62.7	46.0	61.7	BAD	64.2	65.4	51.8	59.4	64.7	50.6	66.8¹	63.8	57.5	57.4	BAD	BAD
CuCl ₂	60.8	45.3	62.1	61.0	56.1	56.0	58.1	62.9	52.7	47.9	59.4	59.9	55.0	60.9	46.2	BAD
Cu(OTf) ₂	57.8	48.2	60.3	63.2	56.7	55.6	56.4	65.6	54.9	50.1	62.9	62.5	61.7	58.1	BAD	48.8
Cu(NO ₃) ₂	51.9	40.8	53.1	52.6²	48.6	52.1	54.4	63.8	56.9	48.5	59.4	64.6	56.5	53.9	44.1	BAD
Cu(BF ₄) ₂	53.4	30.7	62.0	56.8	53.1	59.4	46.1	57.1	59.0	39.7	59.3	58.1	51.7	51.6	28.2³	58.0
CuBr ₂	48.0	37.9	55.3	57.5	52.1	56.8	53.8	66.5	61.7	50.1	59.3	BAD	54.4	52.9	47.3	BAD
Phenanthroline								Bipyridine								

Entry	Product	Nanoscale LCMS assay yield / %	Milliscale NMR assay yield / %
1		67	80
2	315	53	75
3		28	51

Array 2: Phenylpiperidine **134** screened with **332**. Each cell shown is an average of three or more data points. Each averaged reaction was calibrated using the corresponding calibration curve. Scale up reactions are highlighted in **bold**.

4-Methoxyphenylboronic acid pinacol ester **332** was assessed in high-throughput screening with amine **134** (Array 2). The array returned the most reactions that failed the statistical test throughout the initial eight boronic esters (8 “BAD” reactions out of 96). While disappointing, 92% of the 96 reactions passed the statistical test. Reactions involving bases **339** and **317** gave the lowest assay yields but reactions using base **340** (a strong base with increased sterics) returned more product by Q-LCMS. When bipyridine **318** was used as the ligand, the highest assay yield was observed with 67% product. Three reactions were used to validate the assay. All reactions furnished more product by NMR assay on a milligram scale, with the lowest assay yield returning 22% more product on scale (see table in Array 2).

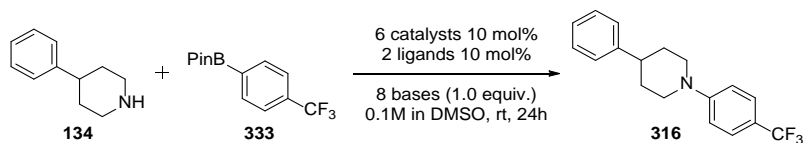


Scheme 48: Two suggested pathways for boronic esters with electron-deficient substituents on the aromatic moiety. If weak bases are employed, Pathway A dominates with greater transmetalation to give **391**. If nucleophilic bases are employed, off cycle complex **388** forms in line with previous literature.²¹⁷

We proposed that, following Watson’s mechanism (Scheme 40), two competing pathways would occur with different boronates (Scheme 48). Electron rich boronic esters would be less Lewis-acidic and, therefore, nucleophilic bases such as **317** and **339** would not coordinate to the empty p-orbital on the boron (Pathway A). This would give more boronic ester **389** in

— High-throughput experimentation of the Chan-Lam reaction to model reactivity —

solution. The decreased Lewis-acidity would also reduce the boronic esters ability to coordinate to copper(II) hydroxide species **390** resulting in lower concentrations of organocuprate **392**.

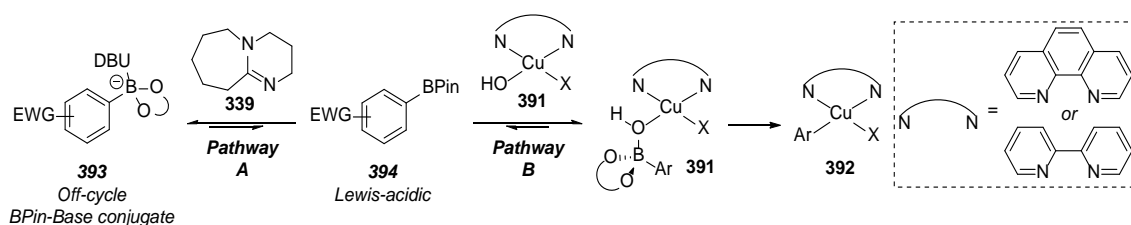


	No Base	DBU	Collidine	DABCO	TMU	Urea	MTBD	BTMG	No Base	DBU	Collidine	DABCO	TMU	Urea	MTBD	BTMG
CuCl	BAD	23.9	41.9	37.5	36.4	38.7	19.7	31.6	30.0²	20.7	20.5	39.3	22.5	16.1	14.5	27.5
CuCl₂	43.2	27.2	38.5	35.4	38.3	36.0	26.3	24.6	34.6	25.2	35.7	40.7	33.9	28.6	19.2	33.9
Cu(OTf)₂	47.4¹	24.9	42.4	39.2	40.7	39.5	22.2	37.8	19.8	19.8	20.0	39.4	23.4	16.2	13.7	23.1
Cu(NO₃)₂	44.5	26.3	41.6	39.3	39.4	37.5	22.8	36.3	26.2	22.7	18.6	37.0	20.0	16.1	12.1³	26.8
Cu(BF₄)₂	46.5	22.4	45.5	40.4	41.1	39.2	20.4	32.3	37.8	19.4	35.5	36.2	25.1	27.7	12.0	27.7
CuBr₂	43.4	27.8	40.1	41.0	40.3	36.1	24.0	46.8	42.0	24.1	39.6	43.5	27.5	35.5	17.9	35.0
	Phenanthroline								Bipyridine							

Entry	Product	Nanoscale LCMS assay yield / %	Milliscale NMR assay yield / %
1		48	44
2	316	30	55
3		12	30

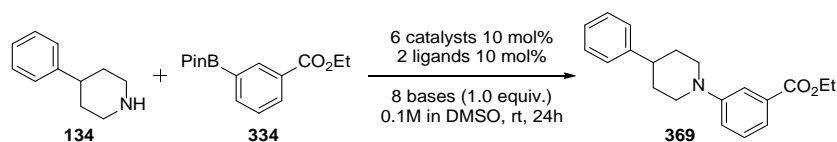
Array 3: Phenylpiperidine **134** screened with **333**. Each cell shown is an average of three or more data points. Each averaged reaction was calibrated using the corresponding calibration curve. Scale up reactions are highlighted in **bold**.

The next array assessed the reaction of 4-trifluoromethylphenylboronic ester **333** with amine **134** (Array 3). Reactions involving bases **339**, **317** and **345** gave a lower product yield by QLCMS assay compared with reactions using **340**, **387** and **344** as the base. When phenanthroline **319** was screened, more product was observed by Q-LCMS assay. The best conditions found employed copper(II) triflate with phenanthroline without any base, which furnished 47% product. Assay validation was completed on milliscale and, while the best yield was confirmed within 4% yield, the average and lowest assay yields gave 55% and 30% product respectively. These were outside of our targeted 15% difference (see table in Array 3).



Scheme 49: Two suggested pathways for boronic esters with electron-deficient substituents on the aromatic moiety. If weak bases are employed, Pathway B dominates with faster transmetalation to give **391**. If nucleophilic bases are employed, off cycle complex **393** forms in line with previous literature.²¹⁷

The increased Lewis-acidity of boronic ester **333** in combination with nucleophilic bases would lead to more off-cycle conjugate **393**, with the boron p-orbital occupied.²¹⁷ If less nucleophilic bases were used, pathway B would proceed. Copper-hydroxide complex **391** would chelate the Lewis-acidic boronic ester facilitating transmetalation. When boronic esters with electron withdrawing groups were assessed on scale, GCMS analysis showed that boronic ester homocoupling was the main by-product.



	No Base	DB U	Collidine	DABCO	TMU	Urea	MTBD	BTMG	No Base	DB U	Collidine	DABCO	TMU	Urea	MTBD	BTMG
CuCl	60.1	42.1	64.2	64.5	65.0	63.9	53.4	64.3	65.0	46.4	65.3	61.5	65.5	61.1	46.5	60.3
CuCl ₂	52.0	44.8	57.2	57.5	56.9	55.8 ₂	57.6	65.5	55.3	45.7	56.2	58.5	53.8	52.5	54.5	BAD
Cu(OTf) ₂	59.2	46.2	65.6	65.6	63.4	59.7	51.9	60.5	64.9	44.9	64.0	61.4	65.3	59.2	44.5	55.6
Cu(NO ₃) ₂	59.6	45.8	63.1	65.0	64.3	59.6	51.4	59.4	63.8	42.3	62.9	65.6	63.2	59.9	46.5	51.8
Cu(BF ₄) ₂	59.2	41.8	66.0 ¹	63.5	63.5	62.2	49.3	58.0	62.9	43.9	63.8	65.8	64.6	59.4	41.6 ²	51.0
CuBr ₂	60.3	44.7	60.0	60.0	57.0	58.0	53.0	64.7	60.1	46.1	58.0	61.4	56.6	57.9	51.8	62.1
Phenanthroline									Bipyridine							

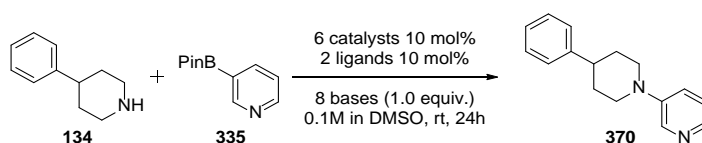
Entry	Product	Nanoscale LCMS assay yield / %	Milliscale NMR assay yield / %
1		66	36
2	369	51	31
3		31	51

Array 4: Phenylpiperidine **134** screened with **334**. Each cell shown is an average of three or more data points. Each averaged reaction was calibrated using the corresponding calibration curve. Scale up reactions are highlighted in **bold**.

To probe the effect of meta-substituted aromatics, boronic ester **344** was assessed with amine **134** (Array 4). Reaction using copper(II) chloride returned slightly lower yields by Q-LCMS assay compared to other catalysts. Both phenanthroline **319** and bipyridine **318** performed well across the array. Seven reaction conditions returned 66% assay yield (Heatmap shown in Array 4). Disappointingly, when three reactions assessed on scale, minimal correlation was observed. The maximum assay yield (66%) correlated to a 36% NMR assay yield, 30% lower than

— High-throughput experimentation of the Chan-Lam reaction to model reactivity —

expected. The median assay yield (51%) returned 20% less product by NMR assay while the lowest assay yield returned 20% more product.

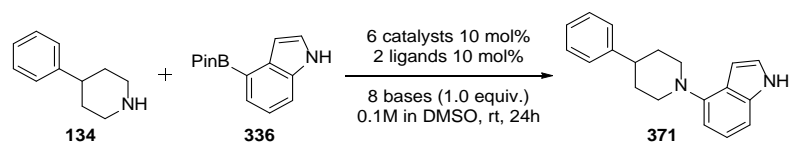


	No Base	DBU	Collidine	DABCO	TMU	Urea	MTBD	BTMG	No Base	DBU	Collidine	DABCO	TMU	Urea	MTBD	BTMG
CuCl	60.8	38.4	64.0	63.2	60.7	59.5	53.3	46.1	51.9	31.2	52.0	55.2	54.0	55.1	6.0	35.0
CuCl ₂	61.8	42.9	63.6	61.2	60.7	60.2	58.1	56.1	54.9	32.7	52.3	53.6	57.5	54.5	50.9	44.0 ²
Cu(OTf) ₂	51.7	37.0	60.2	64.4	58.7	58.9	50.8	50.4	62.7	28.8	54.4	60.9	57.6	54.9	42.4	37.0
Cu(NO ₃) ₂	54.2	42.5	62.7	67.0	57.1	63.0	58.8	52.5	59.5	31.1	58.6	60.9	53.5	56.5	42.0	37.9
Cu(BF ₄) ₂	54.5	35.2	61.8	62.8	57.4	54.8	48.2	48.1	60.1	27.2 ₃	60.8	59.0	55.6	59.8	38.4	38.1
CuBr ₂	57.2	41.3	65.3	68.2 ¹	56.6	57.7	51.6	53.8	63.8	28.6	61.7	61.9	59.5	56.2	33.6	39.2
Phenanthroline								Bipyridine								

Entry	Product	Nanoscale LCMS assay yield / %	Milliscale NMR assay yield / %
1		68	53
2	370	43	50
3		6	16

Array 5: Phenylpiperidine **134** screened with **335**. Each cell shown is an average of three or more data points. Each averaged reaction was calibrated using the corresponding calibration curve. Scale up reactions are highlighted in **bold**.

Heterocyclic boronic ester **335** was assessed with amine **134** and all Q-LCMS yields passed the statistical method (Array 5). While reactions involving bases **339** gave lower assay yields, reactions using **340** and **387** gave more product. When phenanthroline **319** was used as the ligand, the best yield of 68% was found by Q-LCMS. Three reactions, which reflected best, average and worst outcomes, were further assessed on millimole scale and the yields of these reactions were found to correlate with the nanoscale cases (see table in Array 5).



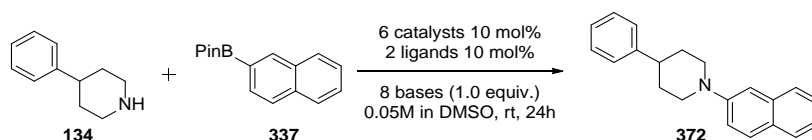
	No Base	DB U	Collidine	DABCO	TMU	Urea	MTBD	BTMG	No Base	DB U	Collidine	DABCO	TMU	Urea	MTBD	BTMG
CuCl	39.9	14.2	41.9	48.0	45.5	39.9	19.3	33.1	45.2	16.4	50.8	56.4¹	51.8	50.0	21.9	34.8
CuCl ₂	38.0	11.8	39.3	41.4	37.8	39.3	23.7	40.2	43.0	16.4	43.6	44.9	44.2	42.7	23.5	42.7
Cu(OTf) ₂	30.3	14.2	30.2	36.5	30.9	29.6	23.1	43.0	36.8	16.4	36.3	42.5	42.1	34.0	24.9	45.8
Cu(NO ₃) ₂	30.8	16.2	32.4	36.9	33.0₂	29.4	26.1	43.3	40.5	38.3	36.8	44.0	41.2	36.4	27.7	48.3
Cu(BF ₄) ₂	24.6	8.8³	27.9	33.5	27.8	26.9	17.8	32.8	34.9	21.7	34.2	45.5	34.8	33.5	20.4	41.6
CuBr ₂	41.1	16.6	40.7	43.1	39.8	41.9	27.1	45.1	46.4	BAD	46.3	51.9	48.4	45.3	29.3	45.4
Phenanthroline								Bipyridine								

Entry	Product	Nanoscale LCMS assay yield / %	Milliscale NMR assay yield / %
4		56	31
5	371	33	18
6		9	0

Array 6: Phenylpiperidine **134** screened with **336**. Each cell shown is an average of three or more data points. Each averaged reaction was calibrated using the corresponding calibration curve. Scale up reactions are highlighted in **bold**.

The final plate assessed at 0.1M tested indole-4-boronic ester **336** with amine **134** (Array 6). Only one reaction was excluded from the data set as it failed the statistical test (“BAD”). Bipyridine **318** showed improved reactivity over phenanthroline **319**, returning the best conditions by Q-LCMS assay. When copper(I) chloride or copper(II) bromide was screened, good yields were observed. Reactions involving bases **339** and **317** gave a lower yield of product (as determined by the quantitative LCMS assay) compared with reactions using **387** as the base. The best conditions found by Q-LCMS used copper(I) chloride in combination with DABCO **387** and bipyridine **318** (56%). The assay was validated on milligram scale with all reactions yielding less product compared to the nanoscale, but all were within the 15% difference target (see table in Array 6).

High-throughput experimentation of the Chan-Lam reaction to model reactivity

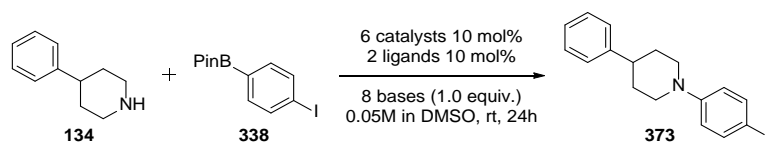


	No Base	DBU	Collidine	DABCO	TMU	Urea	MTBD	BTMG	No Base	DBU	Collidine	DABCO	TMU	Urea	MTBD	BTMG
CuCl	66.6	40.3	69.1	71.6	65.5	66.1	39.2	38.0	63.7	38.7	69.0	68.3	68.8	67.6	47.4	26.3
CuCl₂	69.7	41.9	72.7	71.5	66.4	67.6	48.8	45.4	65.1	40.6	71.3	66.9	64.4	62.3	64.2	34.7
Cu(OTf)₂	63.4	42.5	67.3	69.2	59.5	57.7	46.4	42.2	64.9	37.2	65.2	65.1	63.0	61.0	51.4²	29.1³
Cu(NO₃)₂	64.8	43.2	66.9	69.4	59.2	57.9	52.8	45.5	64.0	39.2	71.1	69.2	68.6	64.2	63.0	33.2
Cu(BF₄)₂	73.4¹	39.5	69.6	63.7	62.7	61.4	48.9	40.9	63.2	32.8	71.0	65.9	65.9	64.7	48.0	29.4
CuBr₂	69.6	43.0	67.9	63.7	60.1	62.9	50.4	42.8	62.3	38.7	67.9	66.4	64.7	68.8	62.0	39.3
	Phenanthroline								Bipyridine							

Entry	Product	Nanoscale LCMS assay yield / %	Milliscale NMR assay yield / %
1		73	78
2	372	51	48
3		29	14

Array 7: Phenylpiperidine **134** screened with **337**. Each cell shown is an average of three or more data points. Each averaged reaction was calibrated using the corresponding calibration curve. Scale up reactions are highlighted in **bold**.

The first substrate assessed at 0.05M concentration was boronic ester **337**. The product, **388**, crystallised in previous screens at 0.1M. The array was prepared using Spreadsheet 3 in section 7.7 with the same Mosquito[®] dosing protocols (Array 7). Reactions involving bases **339**, **317** and **345** gave a lower yield of product while reactions using **339**, **317** and **345** as base resulted in more product being observed by Q-LCMS. When phenanthroline **319** was used as the ligand, the reaction produced marginally more product. The assay was validated on millimole scale; all reactions yields correlated to the nanoscale yields with 15% (see table in Array 7).



	No Base	DB U	Collidine	DABCO	TM U	Urea	MTB D	BTM G	No Base	DB U	Collidine	DABCO	TM U	Urea	MTB D	BTM G
CuCl	BAD	30.8	60.2	64.0¹	56.9	BAD	39.0	37.5	BAD	30.3	58.6	26.8	59.9	BAD	41.3	22.2³
CuCl ₂	57.1	30.3	56.0	59.2	56.2	57.8	48.2	43.6	57.3	30.8	53.5	60.4	59.0	54.4	50.3	29.9
Cu(OTf) ₂	59.5	30.1	59.7	60.1	50.9	53.6	45.9	39.7	61.5	29.1	59.7	63.0	60.9	61.1	41.4	25.9
Cu(NO ₃) ₂	52.6	32.9	60.7	58.7	51.0	53.4	43.5²	42.6	63.3	32.9	58.4	62.0	59.5	62.9	48.2	29.2
Cu(BF ₄) ₂	59.5	30.4	57.2	55.3	51.3	53.6	35.6	35.2	55.0	23.7	58.3	60.9	55.3	54.4	44.0	23.5
CuBr ₂	55.5	31.7	56.4	54.8	51.6	54.1	45.2	43.3	58.9	31.0	57.8	61.5	58.5	60.5	55.4	33.7
Phenanthroline									Bipyridine							

Entry	Product	Nanoscale LCMS assay yield / %	Milliscale NMR assay yield / %
1		64	78
2	373	44	48
3		22	14

Array 8: Phenylpiperidine **134** screened with **338**. Each cell shown is an average of three or more data points. Each averaged reaction was calibrated using the corresponding calibration curve. Scale up reactions are highlighted in **bold**.

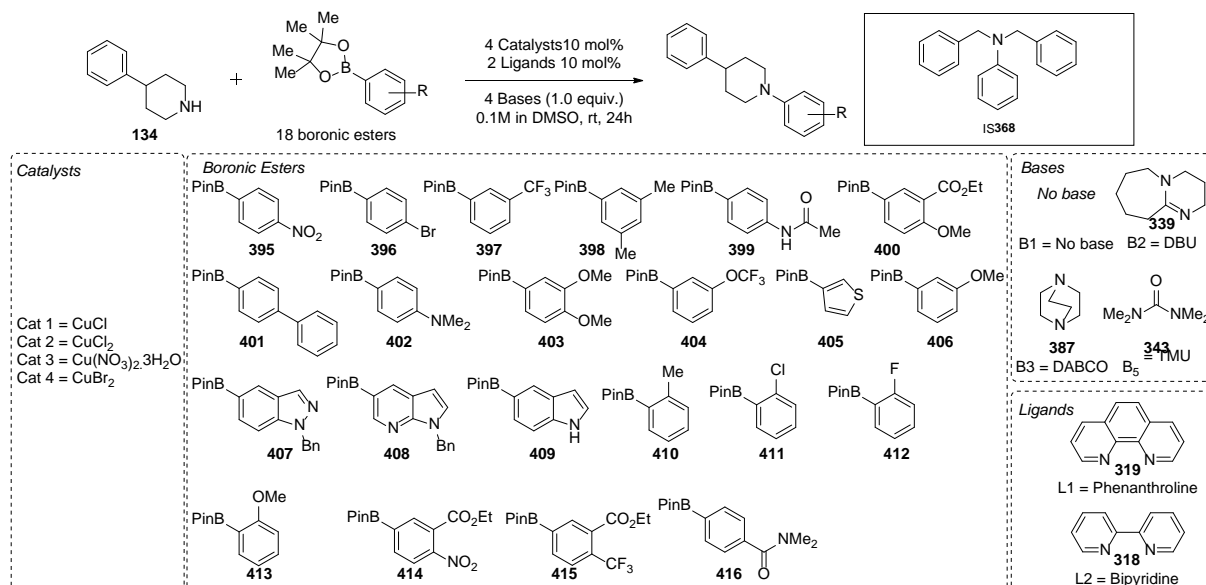
The last plate assessed at the lower reaction concentration was 4-iodophenylboronic ester. (Array 8). Four data points were eliminated because they failed the statistical test (labelled “BAD”). Reactions involving bases **339**, **317** and **345** gave a lower assay yields (as determined by the quantitative LCMS) compared with reactions using **340**, **387**, **343** and **344** as base. The best yield, however, used phenanthroline and copper(I) chloride with DABCO **387** (64%). Exemplary correlation between the nanoscale and milliscale reactions was discovered when three reactions were assessed (all reactions were within 15% of the assay yield, (see table in Array 8).

3.2.2. Substrate Scope Screening for Library Diversification

3.2.2.1. Optimisation Strategy

A new screening strategy was used to explore a more diverse set of boronic esters. The new library assessed different mono-substituted boronic esters with similar functional groups assessed in the first screen. More complex disubstituted boronic esters were also chosen to test the model's ability to correlate two mono-substituted compounds and their subsequent. Ortho-substituted boronic esters were also chosen to incorporate a steric parameter into the predictive model while heterocyclic compounds were assessed to investigate pharmaceutically relevant structures..

Each screen assessed 4-phenylpiperidine **134** against three boronic esters, four bases and four catalysts (Scheme 50). Phenanthroline and bipyridine were kept constant. Using this setup, a further 22 different boronic esters were screened.



Scheme 50: Substrate scope for high-throughput optimisation using a focused 1 x 3 x 4 x 2 x 4 strategy. The screen still maintained a range of base pKas and catalyst oxidation state and counter ions.

All products were isolated using the standard isolation conditions (Experimental 7.8). Prior to quantitative analysis, each new product was assessed by LCMS to optimise LCMS assay, autosampler injection volume and **IS368** stock solution (Experimental 7.8). Reactor plates were dosed using reactor dosing protocols 10-13 (Appendix 3) depending on the location with the source plate and analysis plates were dosed using analysis plate dosing protocols 5-8 (Appendix 3).

3.2.2.2. Optimisation Results

In this section all nanoscale reactions are quoted to 1 decimal place and colour coordinated such that the best yields are coloured green and the lowest yields are coloured red. Orange and yellow

— High-throughput experimentation of the Chan-Lam reaction to model reactivity —

yields are in the middle of this range. High-throughput reactions shown in grey were excluded from that screen and were repeated at a later stage. Nanoscale assay yields were validated on a millimole scale, a scale-up factor of 1200 times. All reactions were validated within 15% error unless otherwise stated or discussed.

	No Base	DBU	DABCO	TMU	No Base	DBU	DABCO	TMU		No Base	DBU	DABCO	TMU	No Base	DBU	DABCO	TMU	
CuCl	35.2	35.1	33.8	34.7	33.2	34.3	32.6	33.9	Boronic Ester 1	36.9	38.8	BAD	39.3	36.2	BAD	36.9	43.4	Cu(NO ₂) ₂
CuCl ₂	34.8	33.8	33.2	35.6	32.4	35.2	33.2	33.3		32.6	34.8	32.8	33.1	33.1	BAD	33.6	33.8	CuBr ₂
CuCl	69.8	48.9	75.9²	71.9	73.6	50.3	73.1	69.9	Boronic Ester 2	71.8	46.0	73.7	73.0	71.9	46.0²	71.7	67.1	Cu(NO ₂) ₂
CuCl ₂	64.3	48.9	66.9	64.0	66.3²	48.6	67.7	66.4		63.8	50.1	71.0	73.3	75.5	49.7	69.9	72.6	CuBr ₂
CuCl	48.3	33.4	51.1	47.4	47.0	32.6	53.0	42.9⁹	Boronic Ester 3	47.3	31.5	59.7⁴	47.7	42.7	27.8⁶	49.9	38.2	Cu(NO ₂) ₂
CuCl ₂	46.1	29.9	45.5	43.6	44.7	30.8	46.7	42.1		50.8	32.3	56.6	54.9	56.8	35.4	57.1	55.2	CuBr ₂
	Phenanthroline				Bipyridine					Phenanthroline				Bipyridine				

Entry	Product	Nanoscale LCMS assay yield / %	Milliscale NMR assay yield / %
1		76	73
2	418	66	65
3		46	33
4		60	61
5	419	43	51
6		28	17

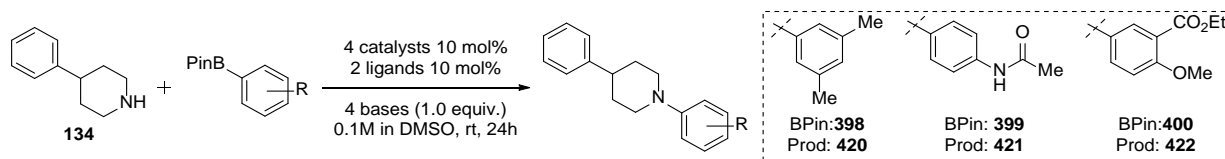
Array 9: Phenylpiperidine **134** screened with BE1: 4-nitrophenylboronic acid pinacol ester **390**, BE2: 4-bromophenylboronic acid pinacol ester **391**, BE3: 3-trifluoromethylphenylboronic acid pinacol ester **392**. Each cell shown is an average of three or more data points. Each averaged reaction was calibrated using the corresponding calibration curves. Scale up reactions are highlighted in **bold**.

The first plate assessed three electron-deficient boronic esters **395**, **396**, **397**. Boronic ester **395** was excluded from this screen (grey) as it was later found that the authentic product had decomposed before calibration. This was repeated later in Array 17.

The second boronic ester, 4-bromophenylboronic ester **396** was assessed with amine **134** following standard protocol outlined in section 7.8 (Array 9). Reactions conditions with base **339** returned lower assay yields, while bases **387** and **343** gave more product by Q-LCMS. Two reactions produced 76% assay yield. The first with copper(I) chloride and phenanthroline **319** with DABCO **387** and the second with just copper(II) bromide and bipyridine **318**. Exemplary correlations between the Q-LCMS assay and NMR assay were found for all three reactions.

When 3-trifluoromethylphenyl boronic ester **397** was investigated using high-throughput experimentation, base **339** was found to retard the reaction while DABCO **387** improved the

yield. While copper(II) bromide was generally active in combination with phenanthroline **319** or bipyridine **318**, the best conditions were employed copper(II) nitrate with phenanthroline in DABCO (60%). All reactions were validated within 15% yield.



	Phenanthroline				Bipyridine					Phenanthroline				Bipyridine				
	No Base	DBU	DABCO	TMU	No Base	DBU	DABCO	TMU		No Base	DBU	DABCO	TMU	No Base	DBU	DABCO	TMU	
CuCl	BAD	50.0	76.4	77.2	80.7	56.8	79.8	83.9¹	Boronic Ester 1	66.0	48.6	66.1	66.7	67.6	44.8	65.3	65.6	Cu(NO ₃) ₂
CuCl ₂	58.3	42.9	41.4	60.1	43.6	41.6	35.9²	46.8	Boronic Ester 1	62.6	51.4²	66.5	69.2	66.8	45.7	57.6	66.7	CuBr ₂
CuCl	85.4	57.6	85.2	83.9	86.9	67.7	83.9	89.4	Boronic Ester 2	79.2	58.1	74.7	75.9	76.4	52.2	74.1	78.4	Cu(NO ₃) ₂
CuCl ₂	65.3	52.6	52.4	56.7	47.7	49.2	45.7	48.5	Boronic Ester 2	71.1	58.7	70.4	71.2	71.6	54	63.7	70	CuBr ₂
CuCl	79.4	60.1	85.5	84.5	85.9	64.3	86.3	82.9	Boronic Ester 3	78.7	63.1	83.7	79.3	81.0	60.0	81.5	79.7	Cu(NO ₃) ₂
CuCl ₂	71.7	57.3³	75.4	76.1	74.1	61.0	71.2²	73.6	Boronic Ester 3	74.0	63.5	80.7	79.9	87.2²	61.5	81.2	80.8	CuBr ₂

Entry	Product	Nanoscale LCMS assay yield / %	Milliscale NMR assay yield / %
1		84	71
2	420	51	51
3		36	35
4		87	74
5	422	71	65
6		57	39

Array 10: Phenylpiperidine **134** screened with BE1: 3,5-dimethylphenylboronic acid pinacol ester **398**, BE2: 4-acetamidophenyl boronic acid pinacol ester **399**, BE3: Ethyl 2-methoxy-5-(4,4,5,5-tetramethyl-1,3,2-dioxaborolan-2-yl)benzoate **400**. Each cell shown is an average of three or more data points. Each averaged reaction was calibrated using the corresponding calibration curves. Scale up reactions are highlighted in **bold**.

The first substrate assessed was boronic ester **398**. One set of conditions were excluded after failing the statistical test (“BAD”). The heatmap showed that copper(II) chloride gave lower yields while copper(I) chloride gave the best Q-LCMS assay yields. Reactions assessed with bipyridine as the ligand gave more product with and were improved further when using DABCO **387** or TMU **343**. All reactions were validated with the assay yield assessed at 51% product returning the same milliscale NMR yield.

Boronic ester **399** was excluded from this screen as it underwent an undesired second arylation reaction on the acetamide,²¹⁸ that resulted in inseparable analysis mixture. The boronic ester was *N*-methylated and was reassessed in Array 16.

Boronic ester **400** with the same substituents of **332** and **369** on the same arene, was chosen to challenge the predictive model ability to relay two “known” substitution patterns to one molecule. When it was assessed using the quantitative assay, high-yielding conditions were

— High-throughput experimentation of the Chan-Lam reaction to model reactivity —

found when bases **387** or **343** was used. Even screening the reaction without a base returned 86% assay yield. Copper(I) chloride in combination with bipyridine **318** gave the good results by Q-LCMS but, copper(II) bromide and bipyridine without any base returned an assay yield of 87%. Two of the three sample reactions for validation were ratified on milligram quantities while the lowest assay yield returned 39% product by NMR assay (18% lower than expected).

BPIn: **401**
Prod: **423**

BPIn: **402**
Prod: **424**

BPIn: **403**
Prod: **425**

	No Base	DBU	DABCO	TMU	No Base	DBU	DABCO	TMU		No Base	DBU	DABCO	TMU	No Base	DBU	DABCO	TMU	
CuCl	11.7	BAD	12.0	10.5	BAD	9.0	7.5	8.5	Boronic Ester 1	5.6	9.7	5.9	6.5	12.3	24.0	10.5	10.2	Cu(NO ₃) ₂
CuCl ₂	3.9	10.2	4.3	3.7	BAD	BAD	BAD	23.6		13.9	14.8	12.4	12.3	30.7	16.5	BAD	12.8	CuBr ₂
CuCl	5.2	5.9	5.0³	7.7	32.5⁵	24.1	32.8	32.4	Boronic Ester 2	3.0	5.7	2.8	3.4	13.0	15.6²	15.4	15.3	Cu(NO ₃) ₂
CuCl ₂	0.3	4.0	0.4	0.5	27.7	25.3	25.7	25.7		4.1	5.6	4.6	5.2	23.5	21.5	21.6	23.5	CuBr ₂
CuCl	11.5	17.2	7.9	6.9	47.6	53.2⁴	53.4	53.4	Boronic Ester 3	10.2	15.3	8.5	9.5	35.8	47.0	43.5	41.9	Cu(NO ₃) ₂
CuCl ₂	3.0⁶	10.4	2.1	1.8	32.5	50.1	38.6⁵	37.8		11.7	15.1	10.2	9.8	44.5	48.8	47.5	44.7	CuBr ₂
	Phenanthroline				Bipyridine					Phenanthroline				Bipyridine				

Entry	Product	Nanoscale LCMS assay yield / %	Milliscale NMR assay yield / %
1		33	55
2	424	16	26
3		0	0
4		53	47
5	425	39	45
6		3	58

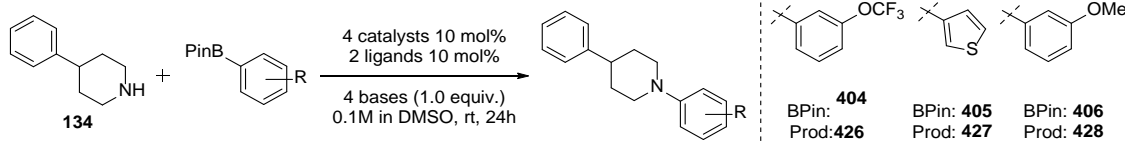
Array 11: Phenylpiperidine **134** screened with BE1: 4-biphenylboronic acid pinacol ester **401**, BE2: 4-diethylaminophenylboronic acid pinacol ester **402**, BE3: 3,4-dimethoxyphenylboronic acid pinacol ester **403**. Each cell shown is an average of three or more data points. Each averaged reaction was calibrated using the corresponding calibration curves. Scale up reactions are highlighted in **bold**.

Both 4-biphenylboronic ester **401** and its corresponding product **423** crystallised on the reactor plate when at 0.1M concentration resulting in erratic and low assay yields. This substrate was screened on Array 17 at 0.05M instead.

The third assay assessed two electron-rich boronic ester **402** and **403**. The effect of the ligand was immediately obvious from the heatmap. When phenanthroline **319** was used as the ligand very low assay yields were observed (>20%). Reactions which used bipyridine as the ligand gave superior reactivity. When boronic ester **402** was screened, the best conditions used copper(I) chloride as the catalysts with the best yields by Q-LCMS found without a base (33%) or with DABCO **387** (33%). However, when boronic ester **403** was evaluated, better yields were found when DBU **339** was used as the base. The best conditions used copper(I) chloride with bipyridine (53%).

— High-throughput experimentation of the Chan-Lam reaction to model reactivity —

For both substrates, three reactions were validated using milligram quantities of substrate. For boronic ester **402**, more product was observed on milliscale; the best assay yield furnished 22% more product while the other two reactions were validated within 15%. For boronic ester **403**, the best and average assay yields were validated with the target 15% difference while the lowest yield gave 55% more product.



	No Base	DBU	DABCO	TMU	No Base	DBU	DABCO	TMU		No Base	DBU	DABCO	TMU	No Base	DBU	DABCO	TMU	
CuCl	65.2	42.4	63.7	61.4	46.5	34.4	54.3	49.3²	Boronic Ester 1	48.4	36.4	56.9	51.5	41.3	29.5 ²	48.9	37.4	Cu(NO ₃) ₂
CuCl ₂	62.2	42.4	58.7	56.2	48.9	40.9	52.8	47.9		61.2	42.5	64.5	66.5²	55.5	38.8	58.9	55.4	CuBr ₂
CuCl	66.1	24.5	66.8	70.2	50.2	23.1	50.7	54.6	Boronic Ester 2	52.4	31.7	48.2	44.9	34.0	21.2	31.7	31.1	Cu(NO ₃) ₂
CuCl ₂	68.3	35.5	61.3	64.1	49.7	39.9	56.5	57.6		76.1	31.9	65.3	70.6	58.5	25.8	59.9	57.8	CuBr ₂
CuCl	80.1	61.3	78.8	80.8	78.0	66.1	79.1	79.4	Boronic Ester 3	66.5	63.8	73.1	61.7	71.3	63.6	78.9	71.1	Cu(NO ₃) ₂
CuCl ₂	76.7	62.1	76.2	73.1	72.5	67.0	78.1	76.4		75.1	64.1	74.8	72.9	75.4	67.6	78.8	69.7	CuBr ₂
Phenanthroline				Bipyridine					Phenanthroline				Bipyridine					

Entry	Product	Nanoscale LCMS assay yield / %	Milliscale NMR assay yield / %
1		67	53
2	426	49	51
3		30	28

Array 12: Phenylpiperidine **134** screened with BE1: 3-trifluoromethoxyphenylboronic acid pinacol ester, BE2: thiophen-3-boronic acid pinacol ester, BE3: 3-methoxyphenylboronic acid pinacol ester. Each cell shown is an average of three or more data points. Each averaged reaction was calibrated using the corresponding calibration curves. Scale up reactions are highlighted in **bold**.

Boronic ester **405** and **406** were excluded from the array and repeated later Array 17 and 16. Product **427** had decomposed prior to calibration. Product **428** undergoes strong non-linear ionisation in the mass spectrometer and was repeated with a smaller LCMS aliquot volume.

The only substrate which could be assessed in this array was boronic ester **404**. When DBU **339** was assessed lower yields were generally observed with the worst yields also employing bipyridine as the ligand (30-35%). Reactions that were screened with phenanthroline gave the best yields by Q-LCMS assay. Copper(I) chloride and phenanthroline without a base gave 65% yield while and copper(II) bromide with the same ligand and TMU **343** as the base returned 67% yield. The three reactions selected for validation confirmed the Q-LCMS assay within 15%.

	No Base	DBU	DABCO	TMU	No Base	DBU	DABCO	TMU		No Base	DBU	DABCO	TMU	No Base	DBU	DABCO	TMU	
CuCl	79.4	52.5	81.9	80.9	82.1	53.3	79.3	82.7¹	Boronic Ester 1	72.8	53.2	75.5	71.6	76.2	53.2	77.4	72.8	Cu(NO ₃) ₂
CuCl ₂	74.8	52.5³	74.2	75.2	74.4	52.8	67.8²	70.5		71.4	52.4	75.5	72.2	77.1	53.2	75.1	74.2	CuBr ₂
CuCl	82.5	58.0	84.6	85.1⁴	82.7	48.5	80.0	82.4	Boronic Ester 2	75.5	52.7⁶	78.2	77.5	75.8	46.2	73.1	69.1⁵	Cu(NO ₃) ₂
CuCl ₂	79.1	56.4	79.1	80.0	74.9	47.9	73.4	75.6		79.0	53.3	77.9	75.7	79.1	51.2	75.4	71.4	CuBr ₂
CuCl	54.8	14.3	65.6	61.5	62.5	14.1	68.8	64.2	Boronic Ester 3	33.5	15.2	40.4	34.9	48.0	15.6	52.9	51.1	Cu(NO ₃) ₂
CuCl ₂	44.6	11.6	51.2	44.5	40.9	12.6	51.4	45.1		45.8	14.8	51.4	48.9	54.1	16.1	60.3	56.4	CuBr ₂
Phenanthroline				Bipyridine					Phenanthroline				Bipyridine					

Entry	Product	Nanoscale LCMS assay yield / %	Milliscale NMR assay yield / %
1		83	78
2	429	75	42
3		53	20
4		73	71
5	430	65	74
6		51	48
7		69	23
8	431	40	12
9		14	0

Array 13: Phenylpiperidine **134** screened with BE1: 1-benzyl-5-(4,4,5,5-tetramethyl-1,3,2-dioxaborolan-2-yl)-1H-indazole **407**, BE2: 1-benzyl-5-(4,4,5,5-tetramethyl-1,3,2-dioxaborolan-2-yl)-1H-pyrrolo[2,3-b]pyridine **408**, BE3: 5-indole boronic acid pinacol ester **409**. Each cell shown is an average of three or more data points. Each averaged reaction was calibrated using the corresponding calibration curves. Scale up reactions are highlighted in **bold**.

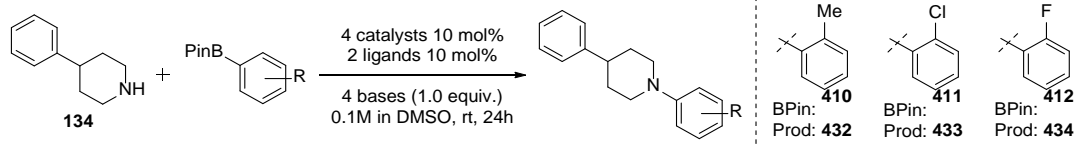
The fourth screen assessed three heterocyclic boronic esters. Boronic esters **407** and **08** needed to be benzyl-protected for reactivity to be observed.²¹⁹ For boronic ester **407**, the best condition used copper(I) chloride and bipyridine with TMU **343** as the base. When the assay was validated, the best yield was confirmed to be 5% lower by NMR assay, however, the remaining two reactions furnished 33% less product. While the scaled reactions were less than the predicted Q-LCMS yields, the trend in reactivity was validated.

The best conditions from the LCMS assay were copper(I) chloride and phenanthroline with TMU **343** as the base (85%) for boronic ester **408**. While the best reaction was not assessed on batch, a sampling of three reactions were used to validate the assay with all reactions being completed within the targeted 15% difference.

Q-LCMS assay found conditions that furnished 69% product for boronic ester **409** across the 32 reactions. However, when three reactions were scaled to validate the assay, a large difference

— High-throughput experimentation of the Chan-Lam reaction to model reactivity —

between the nanoscale and milliscale assay yields was observed. The best assay conditions returned only 23% product by NMR assay. The average performing reaction predicted 40% yield which correlated to only 14% product by NMR assay. The worse performing reaction gave only traces of product by NMR. Pleasingly, however, the overall reactivity trend was confirmed.



	No Base	DBU	DABCO	TMU	No Base	DBU	DABCO	TMU		No Base	DBU	DABCO	TMU	No Base	DBU	DABCO	TMU	
CuCl	11.7 ³	39.3	12.1	14.7	13.0	44.8	14.6	14.3	Boronic Ester 1	55.4	41.2	58.5	52.8	59.1	37.2	61.3	31.6	Cu(NO ₃) ₂
CuCl ₂	28.3	39.7	68.3	68.0	72.2	44.7	44.3	74.6¹		67.7	42.5	71.6	65.7	72.5	44.4²	51.4	55.0	CuBr ₂
CuCl	26.8	11.7	30.1	32.0	26.1	11.7	24.2	25.0	Boronic Ester 2	22.3	9.6	24.9	21.1	13.7	6.1⁶	14.8	14.1	Cu(NO ₃) ₂
CuCl ₂	33.9	12.7	28.5	30.3	27.7	13.6	26.8	26.3		36.4	11.9	36.9⁴	36.7	27.6	9.5	25.6	25.4	CuBr ₂
CuCl	16.7	5.7	14.9	16.6	13.8	6.4	13.2	14.1⁸	Boronic Ester 3	8.3	3.7	8.2	7.7	5.0	2.9⁹	4.6	5.0	Cu(NO ₃) ₂
CuCl ₂	17.8	7.0	16.7	17.7	14.6	9.2	14.8	16.9		19.5	6.0	20.7⁷	19.9	16.3	5.4	11.5	14.2	CuBr ₂
Phenanthroline				Bipyridine						Phenanthroline				Bipyridine				

Entry	Product	Nanoscale LCMS assay yield / %	Milliscale NMR assay yield / %
1	432	75	65
2		45	65
3		12	0
4	433	37	14
5		24	10
6		6	0
7	434	21	8
8		14	12
9		3	0

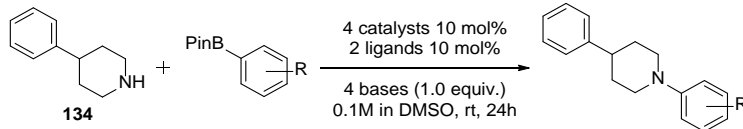
Array 14: Phenylpiperidine **134** screened with BE1: 2-methylphenylboronic acid pinacol ester **410**, BE2: 2-chlorophenylboronic acid pinacol ester **411**, BE3: 2-fluorophenylboronic acid pinacol ester **412**. Each cell shown is an average of three or more data points. Each averaged reaction was calibrated using the corresponding calibration curves. Scale up reactions are highlighted in **bold**.

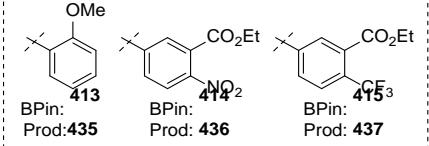
Four ortho-substituted boronic ester were assessed using the high-throughput protocol. The first three were assessed in Array 14. For boronic ester **410**, reactions involving copper(I) chloride gave significantly lower yield while copper(II) chloride or bromide gave more product by Q-LCMS. When DBU **339** was used as the base, lower yields were observed on the heatmap. The best condition was found when copper(II) chloride was used with bipyridine and TMU **343** (75%). Three reactions were selected for milliscale validation. The best and worst conditions were validated within 15% difference while the average yield gave 20% more product by NMR assay.

— High-throughput experimentation of the Chan-Lam reaction to model reactivity —

When boronic ester **411** was assessed using the automated protocol a strong bias for phenanthroline was found from the QLCMS assay. Reactions that used DBU **339** gave the lowest assay yields on the array. The best yield used copper(II) bromide with phenanthroline with DABCO **387** (37% assay yield). Across the three reactions chosen to validate the assay, lower yields were observed with the best conditions furnishing 14% product by NMR assay (23% lower than the assay). Pleasingly the general trend in the reactivity was conserved between the two scales.

Similar reactivity trends were observed when boronic ester **412** screened. A strong bias to phenanthroline **319** was obvious from the heatmap. The best conditions were the same as boronic ester **412**. However, when the assay was validated on milligram quantities of substrate, the reactivity trend was not supported by the NMR assay. The average yield returned 12% product, the best out of the three chosen reactions.





	No Base	DBU	DABCO	TMU	No Base	DBU	DABCO	TMU		No Base	DBU	DABCO	TMU	No Base	DBU	DABCO	TMU	
CuCl	66.7	28.1	64.0	67.4¹	62.5	25.6	58.0	64.4	Boronic Ester 1	52.0	28.2	55.5	53.6	50.1²	22.9 ²	46.8	46.8	Cu(NO ₃) ₂
CuCl ₂	66.8	33.9	65.2	65.1	61.8	32.7	60.7	60.1		65.9	33.2	65.9	66.1	65.1	27.8	62.5	62.5	CuBr ₂
CuCl	19.4	10.3	13.7	22.6	19.9	9.8⁵	22.6	18.2	Boronic Ester 2	13.6	10.5	20.4⁵	14.5	11.7	8.0	14.4	11.4	Cu(NO ₃) ₂
CuCl ₂	17.6	12.4	BAD	17.4	18.0	13.0	19.9	17.2		16.4	16.3	11.6	16.8	22.8⁴	11.6	15.0	18.6	CuBr ₂
CuCl	46.9	22.8	50.1	46.9	41.3	21.7	44.7	41.2	Boronic Ester 3	32.2	21.1	35.6	31.1	27.3	18.3³	31.9	27.5	Cu(NO ₃) ₂
CuCl ₂	41.8	22.0	43.6	41.6	36.0	25.3	40.2	36.2⁸		45.9	25.6	57.8⁷	49.8	46.7	24.6	50.6	44.0	CuBr ₂
	Phenanthroline				Bipyridine					Phenanthroline				Bipyridine				

Entry	Product	Nanoscale LCMS assay yield / %	Milliscale NMR assay yield / %
1		62	63
2	435	41	57
3		15	16
4		23	12
5	436	14	5
6		8	0
7		51	29
8	437	46	19
9		18	7

Array 15: Phenylpiperidine **134** screened with BE1: 2-methoxyphenylboronic acid pinacol ester **413**, BE2: Ethyl 2-nitro-5-(4-phenylpiperidin-1-yl)benzoate **414**, BE3: Ethyl 5-(4-phenylpiperidin-1-yl)-2-(trifluoromethyl)benzoate **415**. Each cell shown is an average of three or more data points. Each averaged reaction was calibrated using the corresponding calibration curves. Scale up reactions are highlighted in **bold**.

The last ortho-substituted boronic ester was 2-methoxyphenylboronic ester **413**. Reactions that were assessed with DBU **339** gave lower yields by QLCMS while weaker bases **387** and **333** gave improved results. When phenanthroline was assessed as the ligand, more product was observed by Q-LCMS. The best conditions used copper(I) chloride and phenanthroline without a base. The two out of the three reactions chosen to validate the assay correlated within 15%. The median yield gave 16% more product by NMR analysis.

When boronic ester **414** was assessed, one reaction was omitted from the heatmap after failing the statistical test. Reactions that contained DBU **339** returned significantly less product compared to when bases **387** and **343** were assessed. Two reactions returned 23% product by Q-LCMS both of which used bipyridine as the ligand. The first utilised copper(I) chloride and DABCO **387** while the second used copper(II) bromide without any base. When three reactions were chosen to validate the Q-LCMS assay, NMR assay gave generally less product. All reactions were within the targeted 15%.

Electron deficient boronic ester **415** generally gave better assay yields compared to **414**, with 51% product observed as the best conditions by Q-LCMS. Copper(II) bromide outperformed all other catalysts in the screen with a slight preference for phenanthroline over bipyridine. Similar outcomes to **414** were found for the three chosen scale-up reactions with lower yields being observed. The best assay conditions returned 22% less product while the average assay yield returned 27% less product compared to the predicted outcome.

Reaction scheme: Phenylpiperidine **134** + PinB-R → Product (R = H, Me, OMe) under conditions: 4 catalysts 10 mol%, 2 ligands 10 mol%, 4 bases (1.0 equiv.), 0.1M in DMSO, rt, 24h.

Inset structures and yields:

- BPin: **416** (R=H), Prod: **433**
- BPin: **439** (R=Me), Prod: **440**
- BPin: **406** (R=OMe), Prod: **428**

	No Base	DBU	DABCO	TMU	No Base	DBU	DABCO	TMU		No Base	DBU	DABCO	TMU	No Base	DBU	DABCO	TMU	
CuCl	71.0	42.9	75.7	75.0	77.4	45.5	79.0¹	78.0	Boronic Ester 1	65.1	43.8	70.0	67.6²	66.3	43.8	74.3	68.0	Cu(NO ₃) ₂
CuCl ₂	71.0	45.1	72.7	71.4	73.4	43.2³	73.9	72.5		70.4	45.2	70.2	69.3	72.7	47.6	77.0	74.6	CuBr ₂
CuCl	73.4	41.9	76.4	76.2	75.8	44.4	75.8	79.5⁴	Boronic Ester 2	65.5	42.4	66.7	62.4	64.2⁵	38.2⁶	68.3	59.8	Cu(NO ₃) ₂
CuCl ₂	68.2	42.8	68.2	65.8	69.5	43.6	70.7	67.4		74.5	46.2	67.7	67.9	66.6	39.8	63.8	66.0	CuBr ₂
CuCl	72.5	50.4	74.9	74.1⁷	78.8	58.0	80.4	82.5	Boronic Ester 3	60.7	57.4⁸	66.5	55.7	59.6	54.3	67.7	57.4	Cu(NO ₃) ₂
CuCl ₂	BAD	49.7	71.7	63.6	71.2⁸	55.8	79.5	78.0		70.7	56.2	79.0	67.5	74.4	54.7	69.8	71.8	CuBr ₂
	Phenanthroline				Bipyridine					Phenanthroline				Bipyridine				

Entry	Product	Nanoscale LCMS assay yield / %	Milliscale NMR assay yield / %
1		79	81
2	433	66	68
3		43	27
4		80	74
5	440	64	71
6		38	28
7		74	42
8	428	71	41
9		57	22

Array 16: Phenylpiperidine **134** screened with BE1: *N,N*-dimethyl-4-(4,4,5,5-tetramethyl-1,3,2-dioxaborolan-2-yl)benzamide **416**, BE2: *N*-methyl-*N*-(4-(4,4,5,5-tetramethyl-1,3,2-dioxaborolan-2-yl)phenyl)acetamide **439**, BE3: 3-methoxyphenylboronic acid pinacol ester **406**. Each cell shown is an average of three or more data points. Each averaged reaction was calibrated using the corresponding calibration curves. Scale up reactions are highlighted in **bold**.

Within this array, the final boronic ester of the scope **416** was assessed alongside two repeat substrates, *N*-methylacetamide **439** (a repeat of **399**) as well as 3-methoxyphenylboronic ester **406**.

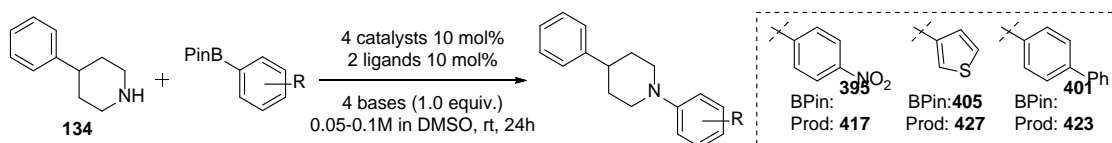
When boronic ester **416** was screened using the automated protocol, reactions using DBU **339** gave the lowest yields. Copper(I) chloride gave the most product while copper(II) catalysts performed less product by Q-LCMS. The best conditions utilised copper(I) chloride with bipyridine with DABCO **387** as the base (79%). Exemplary correlation was found when three reactions were assessed on millimole scale.

The first repeat boronic ester, *N*-methylacetamidephenylboronic ester **439**, was assessed using high-throughput experimentation. Reactions utilising copper(I) chloride gave more product by Q-LCMS assay compared to the other copper(II) catalysts. The best conditions employed

— High-throughput experimentation of the Chan-Lam reaction to model reactivity —

copper(I) chloride with bipyridine **318** and TMU **343** as the base (80%). Three reactions were chosen for validation and the Q-LCMS assay yields correlated to the milliscale NMR assay.

Boronic ester **406** was run with 0.2 μ L autosampler aliquot volume to attenuate the non-linear ionisation. When DBU **339** was assessed in the reaction lower yields were observed while bases and **387** and **343** gave more product. Reactions using bipyridine furnished more product but the reaction screening copper(II) bromide, DABCO **387** and phenanthroline **319** furnished 79% product. The best assessed conditions used copper(I) chloride, bipyridine **318** and TMU **343** (83%). Three reactions were assessed on milliscale and, although the reactivity trend was reflected, all reaction gave lower NMR yields. The best assay yield furnished 32% less product while the lowest assay yield gave 35% less product.



	Phenanthroline				Bipyridine					Phenanthroline				Bipyridine				
	No Base	DBU	DABCO	TMU	No Base	DBU	DABCO	TMU		No Base	DBU	DABCO	TMU	No Base	DBU	DABCO	TMU	
CuCl	73.9	48.8	64.2	67.8	65.6	39.0	61.5	42.2	Boronic Ester 1	55.4	45.8 ²	60.4	53.9	50.7	33.7	57.2	41.2 ²	Cu(NO ₂) ₂
CuCl ₂	74.1	49.5	61.7	55.2	60.6 ²	43.7	65.2	46.7		46.1	49.7	45.7	42.4	64.7	42.0	BAD	38.6	CuBr ₂
CuCl	43.2	11.9	43.5	42.7	40.7	12.0	36.8 ²	37.5	Boronic Ester 2	31.4	14.4	30.3	29.8	21.3	10.8 ²	20.4	21.2	Cu(NO ₂) ₂
CuCl ₂	43.0	13.2	42.6	43.0	31.8	15.6	38.6	33.3		48.3 ²	14.2	43.6	45.9	37.2	13.4	36.0	37.2	CuBr ₂
CuCl	15.0	38.6	16.6	16.1	19.3	36.2	25.0	22.2	Boronic Ester 3	24.7	37.8	24.9	46.5	23.3	32.8	18.5	11.9	Cu(NO ₂) ₂
CuCl ₂	16.0	46.3 ²	BAD	30.5	27.8	31.6	BAD	107.7 ²		35.1	42.9	26.5	BAD	BAD	33.3	14.4	11.9 ²	CuBr ₂

Entry	Product	Nanoscale LCMS assay yield / %	Milliscale NMR assay yield / %
1	417	60	22
2		46	11
3		42	30
4		48	33
5	427	37	31
6		11	21
7	423	108	78
8		46	25
9		12	80

Array 17: Phenylpiperidine **134** screened with BE1: 4-nitrophenylboronic acid pinacol ester **390**, BE2: Thiophene-3-boronic acid pinacol ester **400**, BE3: 4-biphenylboronic acid pinacol ester **396**. Each cell shown is an average of three or more data points. Each averaged reaction was calibrated using the corresponding calibration curves. Scale up reactions are highlighted in **bold**.

With pure product in hand, boronic esters **395** and **405** were reassessed. The LCMS assay gave results which were consistent with previous electron-deficient boronic esters. The best yields were discovered when copper(I) or copper(II) chloride and phenanthroline **319** were reacted without a base. Electron rich thiophene boronic ester **405** was also inhibited by DBU **339** while

——— *High-throughput experimentation of the Chan-Lam reaction to model reactivity* ——
weaker bases **387** and **343** improved the amount of product observed by LCMS assay. The heatmap revealed the best conditions used copper(II) bromide with phenanthroline without base. The high-throughput assay was validated on milliscale and, for boronic ester **395**, improved yields were observed for two of the three reactions. The best Q-LCMS assay returned 13% more product by NMR assay while the lowest returned 10% more product. The median yield, however, was confirmed within 2%.

Boronic ester **401** was screening using the high-throughput protocol at 0.05M. The LCMS assay returned four reactions that failed the statistical test. Intriguingly, DBU **339** improved the yield generally finishing 10-20% more product over other bases. The best conditions found used copper(II) chloride with bipyridine and TMU **343** as the base returned over 100% assay yield (108%). Two of the three reactions were not validated by the scale up protocol and NMR assay with the lowest assay yield returning 68% more product on milliscale.

3.2.3. Summary of High-Throughput Data

Over the 30 different boronic esters were screened using the standardised high-throughput procedure discussed in Chapter 2.

Initially, 4-phenylpiperidine **134** was screened against eight boronic esters, eight bases, six catalysts and two ligands totalling 768 unique reaction conditions run in quadruplicate (3,072 total reactions). Quantitative data was obtained for all 3,072 reactions. To validate the assay, 24 reactions covering the best, the worst and median assay yields were scaled from nanoscale to milliscale (1,200 times) only 7 out of the 24 reactions returning greater than 15% difference between the two scales.

A further 22 boronic esters were chosen and assessed using the high-throughput protocol with four bases, four catalysts and two ligands. 704 unique reaction conditions were assessed totalling 2,816 reactions were all of which were assessed using quantitative LCMS. 66 reaction conditions were chosen and assessed on a millimole scale to validate the assay. An average difference of only 13% was observed across the 66 scale up reactions only 18 out of the 66 reactions produced a difference greater than 15%.

Overall, this strategy enabled quantitative assessment of 5,888 reactions (1,472 unique reactions) within three weeks of LCMS run time. Across the 90 milliscale validation reactions performed, the average difference between assay yield and NMR yield was 13%. Only 26 out of 90 reactions returned a difference of greater than 15% between the two.

General trends were also observed across all the arrays. Nucleophilic bases inhibited the reaction, resulting in lower LCMS and NMR assay yields. This effect was more pronounced

—— *High-throughput experimentation of the Chan-Lam reaction to model reactivity* ——
with electron withdrawing substituents on the arene. Electron rich boronic esters were generally higher yielding than the electron poor substrates.

3.3. Computational Modelling of the Chan-Lam Reaction²

3.3.1. Reactant Parameterisation

Parameterisation of all reaction components is a key process before computational modelling can begin. Parameter selection can be difficult and if inappropriate descriptors or components are chosen the model can be biased to an incorrect prediction. The Chan-Lam reaction was rationally designed to assess reagent combinations would give product to give the model the best chance of predicting reactivity trends.

A list of 64 parameters was prepared which utilised computationally-derived descriptors (Experimental 7.8). This list incorporated simple parameters such as molecular weight and volume as well as more complex parameters such as reorganisation energy and molecular dipole moment. All these parameters were calculated using DFT. Three further experimentally determined parameters were collected to complement the computational factors to parameterise the boronic ester. We envisaged that both the ipso ¹³C–B and ¹¹B NMR shift would ratify the computationally determined partial charges and give an idea of Lewis-acidity or nucleophilicity. IR-spectra were also obtained to also compare with the computationally determined frequencies and intensities.

Computational modelling identified two key stretching modes in the IR-region (Figure 39).²²⁰ Although the C–B IR-stretch may be responsible for strength of the bond, it is also important to determine all other stretching modes as these can be important for electron density distribution during the modelling process.²¹⁶ IR-spectra were obtained for all boronic esters assessed in the high-throughput protocol and were provided to the computational collaborators. Two IR stretching intensities (Figure 39), termed I₂ and I₄, were important parameters with frequencies at ~1350 cm⁻¹ and 1550 cm⁻¹ respectively.

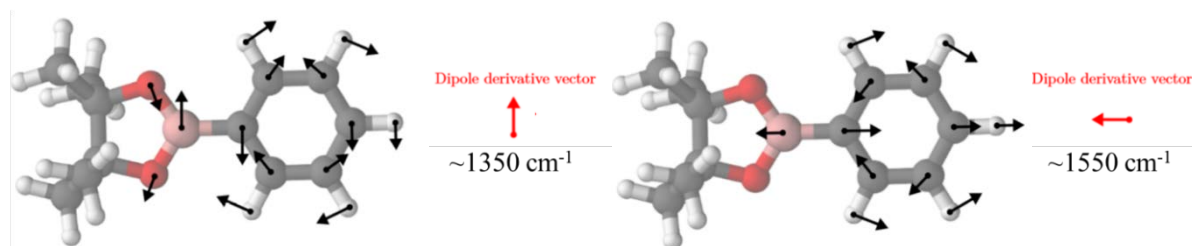


Figure 39: Key IR-stretches identified by the computational modelling.³ a) C-B stretch frequency (I₄); b) C-B bend stretch frequency (I₂).

² All computational work was completed in collaboration with Eric Zhao, Dr Carl Poelking and Dr Lucy Colwell

³ Figure prepared by Dr Carl Poelking.

A key part of the Chan-Lam mechanism proposed by Watson was the coordination of the Lewis-acidic boron to copper-hydroxide species **304** (Scheme 40). The complex facilitates smooth transmetalation aryl group to the copper catalyst by a lower energy transition state compared to coordination through a ligated acetate. Therefore, determining the relative electron density with ^{11}B NMR could serve as an important parameter for the model. Furthermore, the reaction conditions could be mimicked in the NMR studies by using DMSO- d_6 as the NMR solvent (Figure 40).²²¹ Generally, the boronic esters only showed subtle differences in NMR shifts however, electron-rich compound, 4-dimethylaminophenylboronic ester **402**, showed the largest downfield shift of all the boronic esters (35.0 ppm) which is surprising as this is one of the most electron rich boronic esters screened (Hammett = -0.83).²²¹

Ipsso- ^{13}C NMR of boronic acids and esters is extremely difficult due to the quadrupolar boron nuclei resulting in spin-spin coupling of the nuclei²²² extending the relaxation time of the ^{13}C nuclei. Rather than a conventional sharp peaks, small and often unresolved peaks are observed.²²³ Boroxines derived from boronic acids can be used for NMR studies, increasing the relative concentration of the ipso- ^{13}C but, in this case, would be an incorrect model to use.²²⁴ NMR machines with cryogenic probes attached reduce signal to noise ratios resulting in a more sensitive and resolved spectra. These cryoprobe-NMR machines are approximately four times more sensitive than non-cryocooled probes.²²⁵ Using the departmental NMR-cryoprobe, fully assigned ^{13}C -NMR was completed on all 30 boronic esters elucidating the ipso-shift ^{13}C (Figure 40).

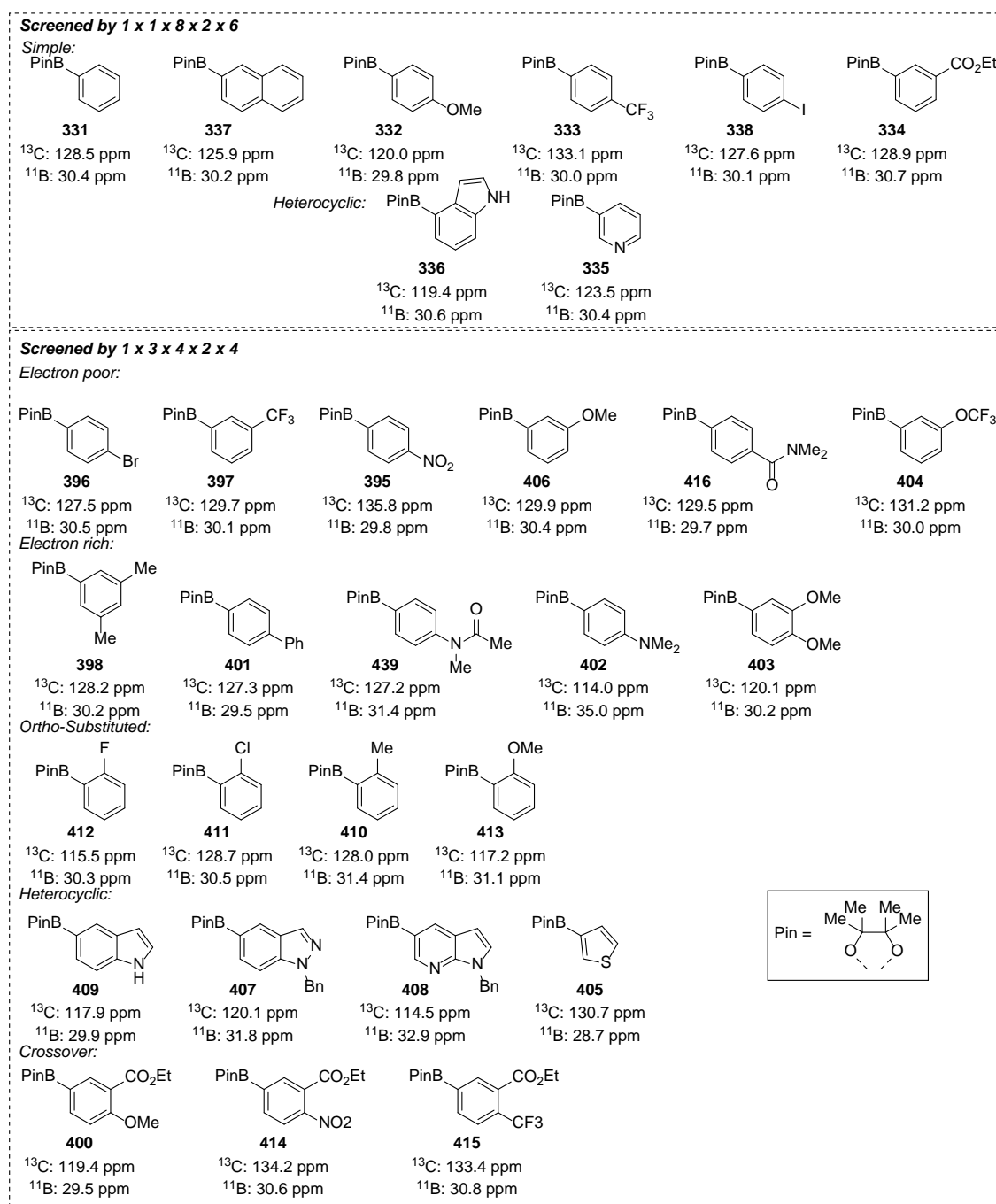


Figure 40: Ipso-¹³C and ¹¹B NMR of all boronic esters used in the quantitative high-throughput screen.

3.3.2. Construction of Computational Model

Initial effort focussed on the use of a single- (ϵ_1 and ϵ_{12}) and two-body terms (ϵ_2). The single-body terms incorporate Gibbs free energies of single reactants and the two-body terms involve interactions between component pairs (i.e. boronic ester and base). Graphical representation of these terms was produced show the distribution and dependence of these parameters (Figure 41). The first-order single-body term ϵ_1 and single-body ϵ_{12} for catalyst and ligand are narrow and precise meaning the distribution of these two reactants is based upon experimental error. Whereas the body terms for base and boronic ester are more spread suggesting these parameters impact the reaction outcome the most. When two body terms are used, a narrow distribution is

observed. The distribution, although narrow, is wider than the catalyst and ligand decomposition which suggests that two-body terms are present in the data.

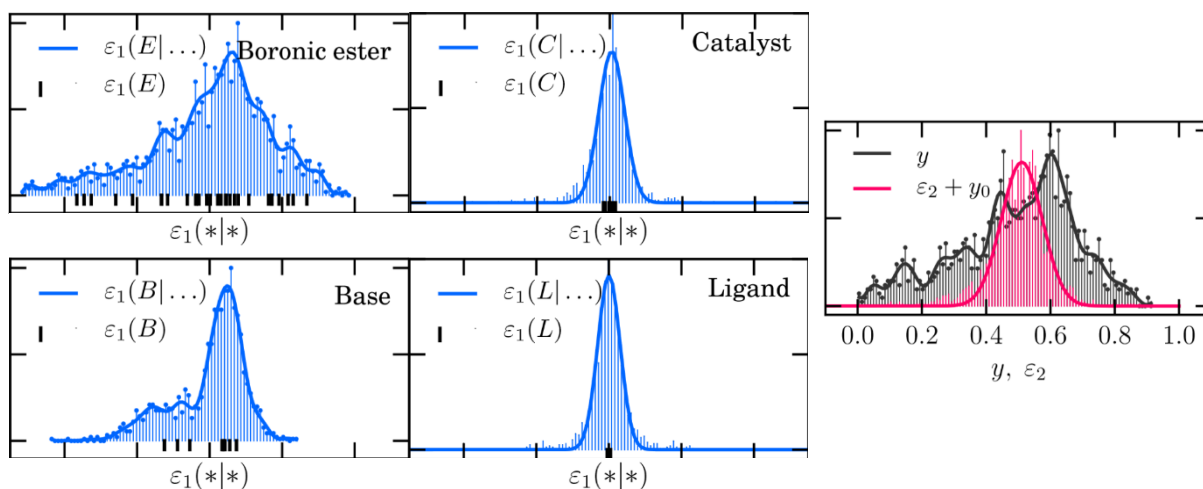


Figure 41: Body-term decomposition for the Chan-Lam reaction. Black ticks on x-axis are each individual component A) Single-body term for boronic ester; B) Single-body term for base; A) Single-body term for catalyst; A) Single-body term for ligand.³

With the knowledge that two-body terms are present, a nonlinear regression graph, known as a feature-graph regression, was used to model the data. The feature-graph generates output descriptors from the set of input descriptors through simple mathematical operations. As this process is iterative and computer processor intensive, a list of restrictions was incorporated to reduce the total number of possible operations; unary operators (+, -, x, / etc.) could only be completed on vector descriptors with matching dimensions while binary operators (log, exp, $\sqrt{\quad}$ etc.) were possible if the outcome was positive. The random forest modelling method employed by Doyle and Merck was also assessed for comparison.

Initially, a partial yield prediction based on one-body terms was produced using both random-forests (Figure 41) and the feature-graph regression (Figure 42) for both base and boronic ester. A standard leave-compound-out validation²²⁶ test was used whereby one compound is removed from the model and its outcome predicted based on the remaining data. All data shown in the graphs are the outcomes of the leave-compound-out test and each point incorporates all data from the associated high-throughput screen.

Two random forest methods were used to model the one-body parameters. The first, shown by red data, are part of a non-reduced neural network. The non-reduced algorithm gives equal weight to all decision trees but can take longer as each iteration covers all trees in the random-forest.²²⁷ The Pearson's correlation for base (0.51) and boronic ester (0.37) suggested only a slight correlation between the experimental single-body parameter and the predicted outcome. A reduced random-forest algorithm prioritises and weights each tree to reduce the total computing time as well as improve the accuracy.²²⁷ The new reduced model, shown by the blue

data, for base is improved to exhibit a Pearson's correlation of 0.67 while boronic ester is only marginally improve to 0.38.

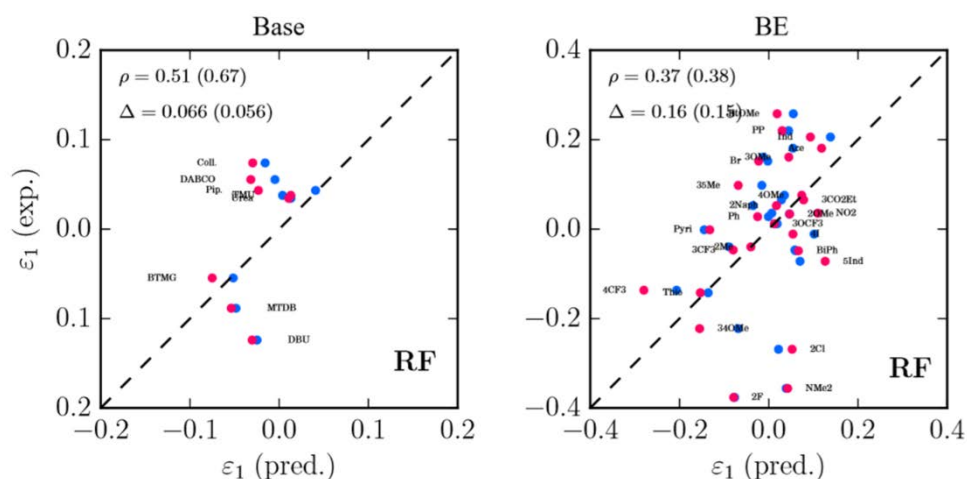


Figure 42: Partial yield prediction based on one-body terms using random-forests. Only test predictions are shown. Red dots represent complete parameter sets while blue dots represent reduced parameter sets. The two values given in panels represent Pearson's correlation (ρ) and RMSE (Δ). The value given in the bracket refer to the blue point cloud.³

In a similar manner, two feature graph methods were employed and tested. The first feature-graph used a single operation iteration, shown in blue. The Pearson's correlation of bases returned an exemplary correlation coefficient of 0.93 suggesting the algorithm is predicting the effect. Meanwhile, the boronic ester correlation of 0.61 is better than any of the random-forest methods used previously. When the data is exposed to a second iteration of the feature-graph algorithm, a 0.99 correlation coefficient is observed for the bases (shown in red). This is a truly remarkable correlation between predicted and experimental dependence of different bases. Furthermore, when the boronic esters are correlated through a second modelling iteration, an improved correlation of 0.73 is found.

As the feature-graph employs a combination of parameters that have undergone mathematical operations, a "best-fit" equation can be produced for each model to highlight what parameters were key for correlation. The equations that gave the best fits for the graphs shown in (Figure 42) were:

$$\text{Base } \varepsilon_1 = q_N^2 e^{(pKa)} + \sqrt{\mu_M} e^{(-\log P)} \quad \text{Equation 18}$$

$$\text{Boronic ester } \varepsilon_1 = \frac{\sqrt{I_4}}{S_{\pm}} + \frac{1}{\lambda_e I_2} \quad \text{Equation 19}$$

For the base, the key parameters in Equation 18 were: q_N (partial charge on nitrogen), pK_a (literature pK_a in water), μ_M (reduced mass of base), LogP (octanol:water partition coefficient). For the boronic ester, the key parameters in Equation 19 were: I_4 (intensity of IR C-B stretch in Figure 41a), S_{\pm} (total polar surface), λ_e (electron affinity), I_2 (intensity of IR C-B stretch in Figure 41b). These two equations incorporate specific physiochemical descriptors that were computationally calculated.

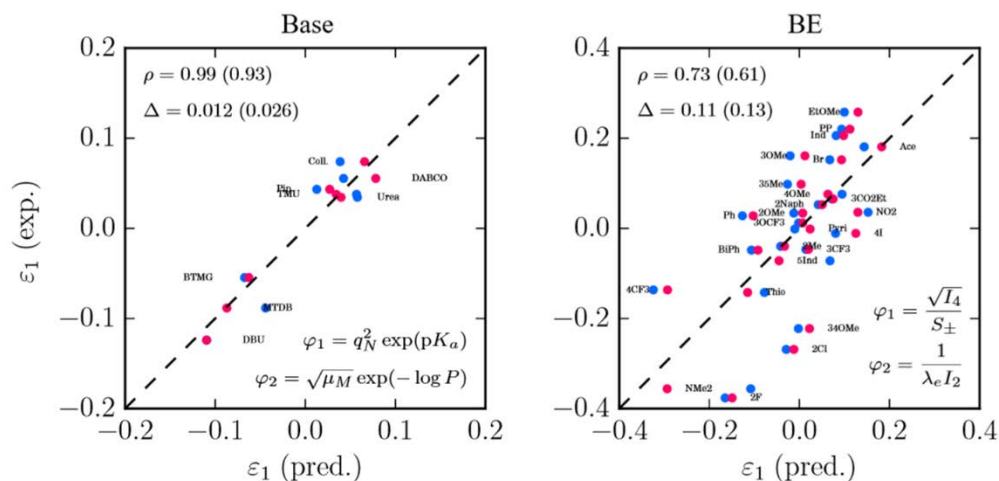


Figure 43: Partial yield prediction based on one-body terms using feature-graph regression. Only test predictions are shown. Red dots represent the first iteration ($\varepsilon_1 = c_1\phi_1$) while blue dots represent the second iteration ($\varepsilon_1 = c_1\phi_1 + c_2\phi_2$). The two values given in panels represent Pearson's correlation (ρ) and RMSE (Δ). The value given in the bracket refer to the blue point cloud.³

With the two tested modelling methods in hand, two predictive models were produced to correlate all experimental yields from the high-throughput assay to the predicted outcomes. Firstly, using the random-forest method, moderate correlation between experimental assay yield and predicted yield were found. The model captured the effect of the base with a correlation of 0.83 while the boronic ester experimental yields correlated poorly with a coefficient of 0.47. Leave-component-out-tests were also completed and coloured coded with the same test data in the same colour.

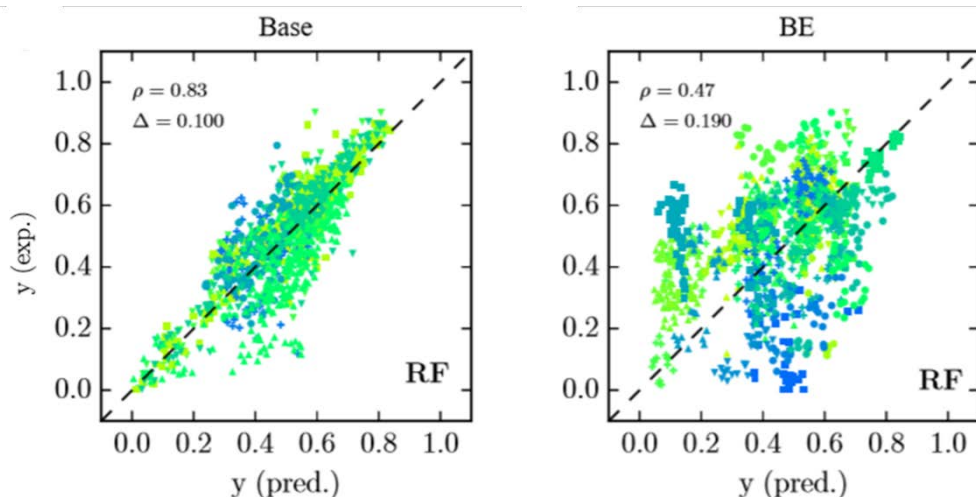


Figure 44: Total yield predictions for base and boronic ester using random-forests. Leave-compound-out cross-validation was performed, and only test predictions are shown. The two values given in panels represent Pearson's correlation (ρ) and RMSE (Δ). Between predicted yield and experimental yield.³

The novel feature-graph regression method improved the predictive capability of the model further. The effect of the base was improved over the random-forest method, with an observed correlation coefficient of 0.92. The model's ability to capture the boronic ester effect was also improved with an observed Pearson's coefficient of 0.66.

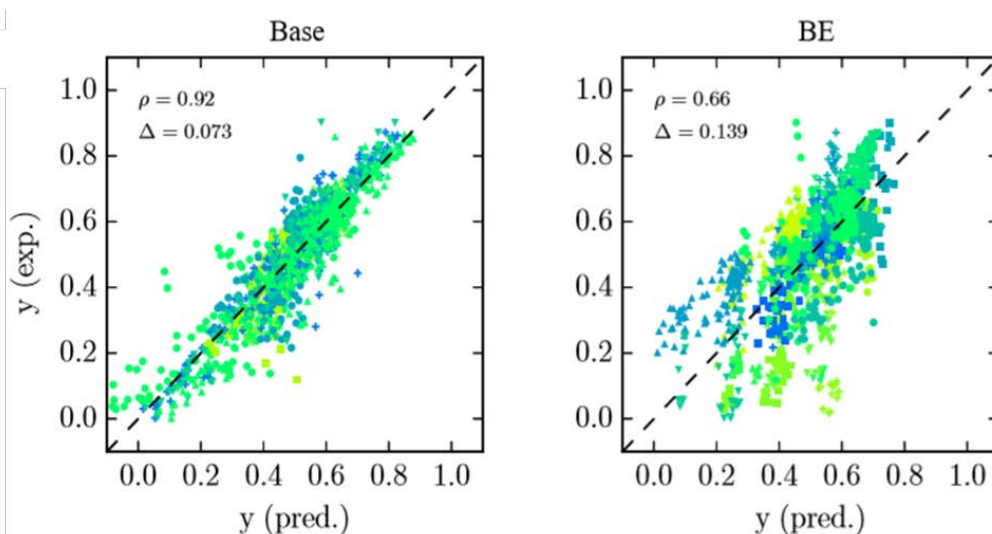


Figure 45: Total yield predictions for base and boronic ester using feature-graph regression. Leave-compound-out cross-validation was performed, and only test predictions are shown. The two values given in panels represent Pearson's correlation (ρ) and RMSE (Δ). Between predicted yield and experimental yield.³

3.4. Summary of Computational Model

Within this section, a working predictive computational model has been described for the Chan-Lam reaction.

Parameterisation of all reaction components using both computationally and experimentally determined parameters. All 30 boronic esters were parameterised using NMR to assess *ipso*-¹³C and ¹¹B nuclei shifts in DMSO-d₆ to mimic the reaction conditions. IR-spectra were also obtained and supplied.

A new feature-graph regression method was used to model the data along with the random-forests method. A histogram was prepared to correlate reaction yield to single-body terms which revealed the boronic ester had the largest influence on the reaction. Base had a marginal influence on the outcome. Two-body terms also showed interactions between components impacted the reaction as well. When partial yields were predicted based on these single-body terms using the two modelling methods, feature-graph regression improved the correlation over random-forests. Key correlations of the base pK_a and nitrogen dipole gave a 0.99 Pearson's correlation. Boronic ester IR-stretching mode I₄, and its computed intensity, were key to experimental and computed outcome correlation ($\rho = 0.73$).

Both random-forests and feature-graph regression were also used to model the reaction yields from the high-throughput assay. Random-forests returned moderate correlation between predicted yield and experimental yield (0.83 and 0.47 for base and boronic ester respectively). The feature-graph regression, on the other hand, correlated the predicted and experimental outcomes with a higher degree of correlation. The base correlated with a Pearson's correlation of 0.92 while the boronic ester was improved to 0.66. While a low correlation, this is a remarkable result from a small data set of 1,472 unique conditions. Work is still ongoing to improve the correlation between experimental yield and predicted yield.

Chapter 4: Reaction Discovery Using the High-Throughput Protocol

4.1. Introduction

Different analysis platforms can be used for reaction discovery and optimisation using either tagged materials (EIA, ELISA, MALDI) or non-functionalised material (GCMS, LCMS and LCMS-MS) (see Chapter 1). The often laborious and step-wise syntheses needed for the preparation of bespoke labelled substrates is one of the major draw-backs of the former analytical protocol. Conditions need to be compatible with the physical characterisation of the label which could be DNA or a protein. In contrast, GCMS and LCMS protocols are broad in their utility and require no substrate labelling, the complexity of a reaction chromatogram can be difficult and time-consuming to deconvolute however. Although significant steps have been made to improve the deconvolution process, it is still a laborious process.

A simple triaging approach to high-throughput reaction discovery would be ground breaking. Although the MISER technique can analyse 1536-reactions in 12 hours, spectrum simplification using SIM means that potentially interesting bond forming reactions are overlooked, in preference for a desired outcome. MALDI, on the other hand, has the greatest potential for reaction discovery in synthesis. The soft ionisation technique, coupled with post ionisation fragmentation, gives a snapshot of the reaction within seconds. The preparation of the MALDI target plate can be time consuming however.

One of the simplest reaction analysis techniques used in synthetic chemistry is thin-layer chromatography (TLC).²²⁸ Commonly, silica TLC-plates are manually prepared with reaction mixture and subsequently developed in a mobile phase. If there are any new or unexpected spots are found, then a new reaction has potentially been discovered. The challenges of associated with analysing thousands of reactions such as silica-plate size and preparation as well as plate visualisation and data capture needed to be addressed.

The compatibility of the standardised screening protocol (Chapter 2) and the liquid handling capabilities of the Mosquito[®] make this an attractive platform for TLC analysis. The Mosquito[®] has not been preceded for reaction discovery and, therefore, protocol invention and standardisation are required. There are currently no TLC-plate holders that fit onto the Mosquito[®] robot and therefore a suitable method needs to be produced.

4.2. Development of High-Throughput Thin Layer Chromatography for Reaction Triage

We initially used a Falcon 1536-well plate to house the TLC-plates. To prevent the plates from moving during the protocol, small plastic pipette tips (pegs) were cut and used to wedge the plate in place (Figure 46). Two pegs were placed along three of the sides and the TLC plate was pushed flush against the top of the holder. A second plate could then be aligned adjacent to the first, pegged into position using the same cut pipette tips. A 1cm gap was then measured from the left side of the TLC-plate to calculate the correct position to dose the reaction mixture (Column 7 for plate 1 and 27 for plate 2).



Figure 46: TLC-plates pegged onto 1536-well plate for HT-TLC assay.

A simple protocol was designed utilising both the ‘multi-dispense’ and ‘droplet-dispense’ features on the Mosquito[®] (Figure 47). Both features ensure a small TLC-spot with minimal cross-contamination. In this way, multiple reactions can be printed to a TLC plate in a short time (Figure 47). In a single run, 16 crude reaction mixtures could be spotted simultaneously. Overall, 128 crude reaction mixtures could be dosed onto 8 TLC plates within one minute. Once prepared, the TLC plates were run in the appropriate solvent system and visualised using UV/vis or TLC stains. Analysing 384 reactions takes approximately 30 minutes while a full 1536-well plate takes approximately two hours. Any hits could then be analysed by GC or LCMS.

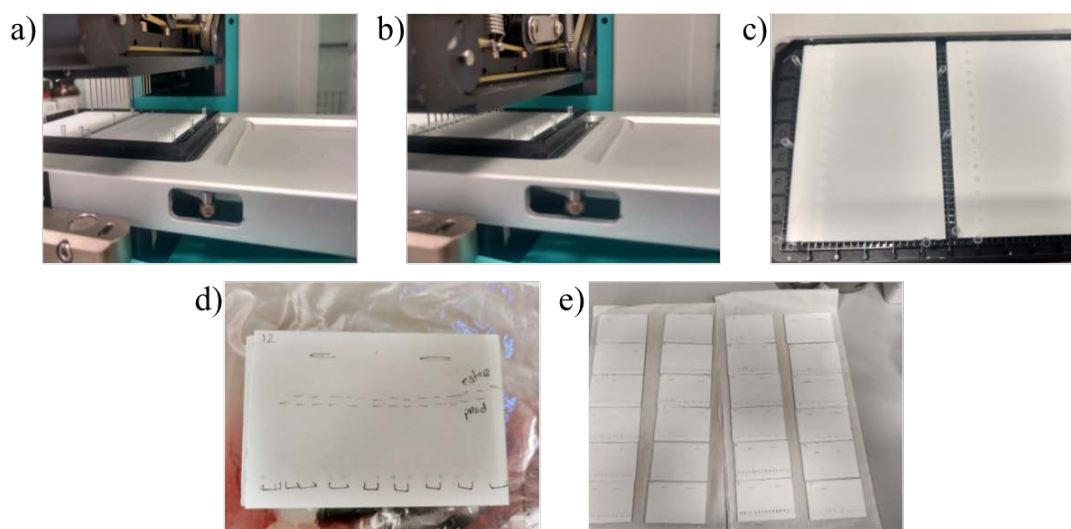


Figure 47: Mosquito® HT-TLC step-by-step method. A) Pegged TLC-Plates with Mosquito® pipette tips filled with 1 μ L of reaction mixture; B) Mosquito® creates 500 nL droplet which is touched onto TLC-plate; C) 32-crude reaction mixtures spotted within 30 seconds; D) TLC-plate after solvent run and UV visualisation; E) 384-reactions triaged and analysed with 30 minutes.

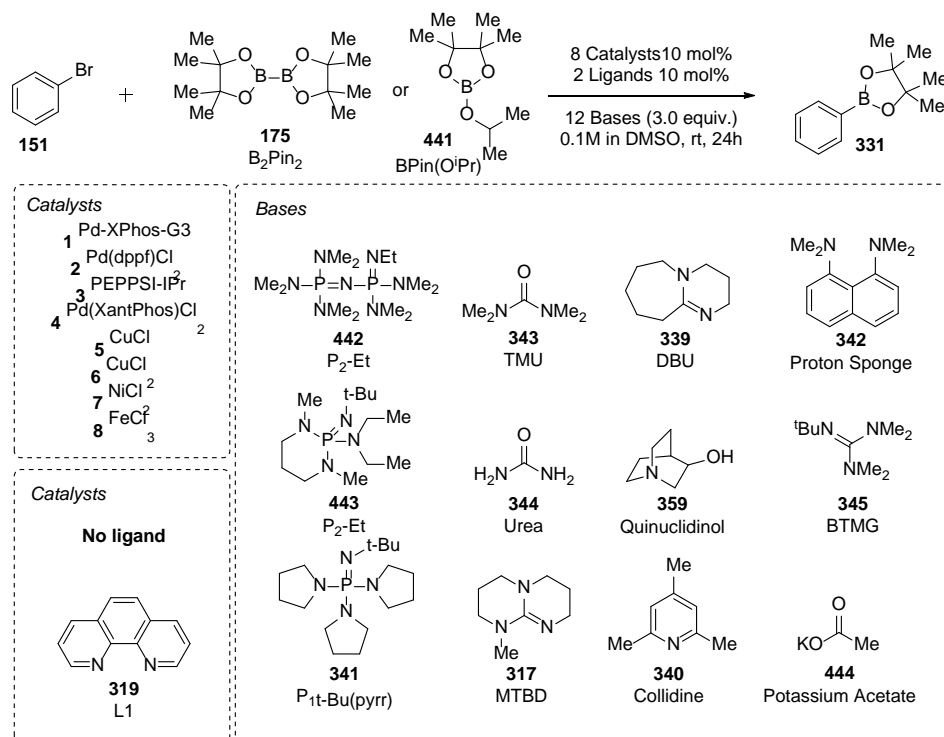
The high-throughput TLC (HT-TLC) method developed here represents a potentially powerful advance for accelerating reaction discovery. The automated preparation of TLC-plates potentially quickens the time taken to discover a new bond forming transformation. Furthermore, the deconvolution is simple as any new spot is a potential hit and can be rapidly identified for further analysis. Using the standardised quantitative protocol, 1536 analytical samples would take approximately 60 hours of LCMS time.

4.3. Reaction Discovery using HT-TLC

To validate the HT-TLC method, known reactions were chosen and adapted to use DMSO as the reaction media.

4.3.1. Palladium-Catalysed Miyaura borylation

Conventional synthesis of organoboron compounds requires stoichiometric metal reagents such as Grignards of alkyllithium reagents or hydroboration reactions.²²⁹ In the mid-1990s, Miyaura²³⁰ published the first borylation reaction using bis-alkoxydiboron reagents which has become a cornerstone reaction in industrial and academic synthesis utilising mild reactions conditions with low catalyst loadings.²³¹ The borylation reaction was chosen to give another synthetic route for the synthesis of boronate esters employed in the Chan-Lam reaction.



Scheme 51: Borylation reaction discovery focussing on palladium borylation and speculative first row transition metal catalysts. 384 reactions were screened in total.

HT-TLC was used to identify room temperature conditions for the borylation of aryl bromides with a focus on low catalyst loadings. Bromobenzene was used as the model substrate and was tested with two different boron reagents, B₂Pin₂ **175** and B(OⁱPr)Pin **441** (Scheme 51). Eight different catalytic metal sources (four palladium pre-catalyst sources, two copper, one nickel and one iron source) were assessed with or without phenanthroline. Eleven different organic bases were screened alongside heterogeneous potassium acetate, a common additive in borylation reactions.²²⁹ A total of 384 unique reaction conditions were assessed.

The HT-TLC triage found one new spot when Pd-XPhos-G3 was screened with BTMG **345**. GCMS analysis confirmed that biphenyl **445** was the outcome of the reaction (Figure 48). Although reductive homocoupling of aryl bromides with palladium is known,^{232,233} the reaction normally requires elevated temperatures or sacrificial alcoholic reductants to affect the transformation. It was proposed that desired borylation of bromobenzene **151**, but cross-coupling between **151** and **331** was prevalent. Batch scale reaction confirmed the borylated product by GCMS.

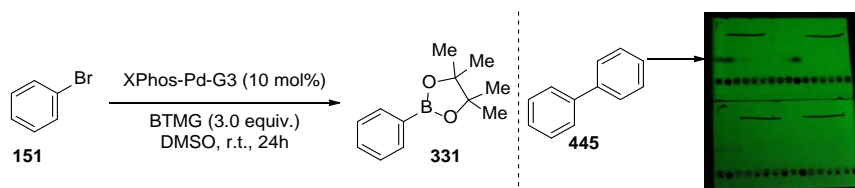
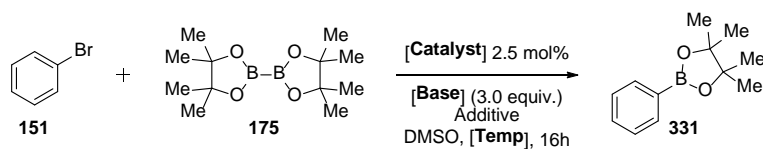


Figure 48: HT-TLC of palladium borylation reaction. Top spot is biphenyl confirmed using authentic commercial standard.

With the hit confirmed, conventional batch scale optimisation was completed. Using calibrated GC-FID, a small reaction component screen was undertaken to assess the potential of the discovered reaction conditions (Table 5). The catalyst loading was set to 2.5 mol% in order to optimise a borylation reaction with high-catalyst turnover. BTMG was found to be the best base for promoting the reaction, returning 17% yield at room temperature (Table 5, Entry 2) compared to 15% with MTBD (Table 5, Entry 2). Increasing the temperature to 50 °C also resulted in an increased yield to 25% GC-yield (Table 5, Entry 4). Water was found to be detrimental to the reaction returning only 14% yield (Table 5, Entry 5). While the addition of potassium acetate resulted in only 16% product by GCMS (Table 5, Entry 6), the addition of caesium fluoride increased the yield to 32% GC yield (Table 5, Entry 7). Using only 2.5 mol% of catalyst overall, this reaction demonstrates a turnover number of over 13 times.



Entry	Palladium source	Base	Additive	Temp. / °C	Yield of 331 / %
1	Pd-XPhos-G3	MTBD 317	-	25	14.8
2	Pd-XPhos-G3	BTMG 345	-	25	16.9
3	Pd-XPhos-G3	MTBD 317	-	50	23.8
4	Pd-XPhos-G3	BTMG 345	-	50	24.8
5	Pd-XPhos-G3	BTMG 345	5.0 eq. H ₂ O	50	13.7
6	Pd-XPhos-G3	BTMG 345	3.0 eq. KOAc	50	15.9
7	Pd-XPhos-G3	BTMG 345	3.0 eq. CsF	50	31.8

Table 5: Milliscale optimisation of borylation of **151** using calibrated GC-FID to yield assay.

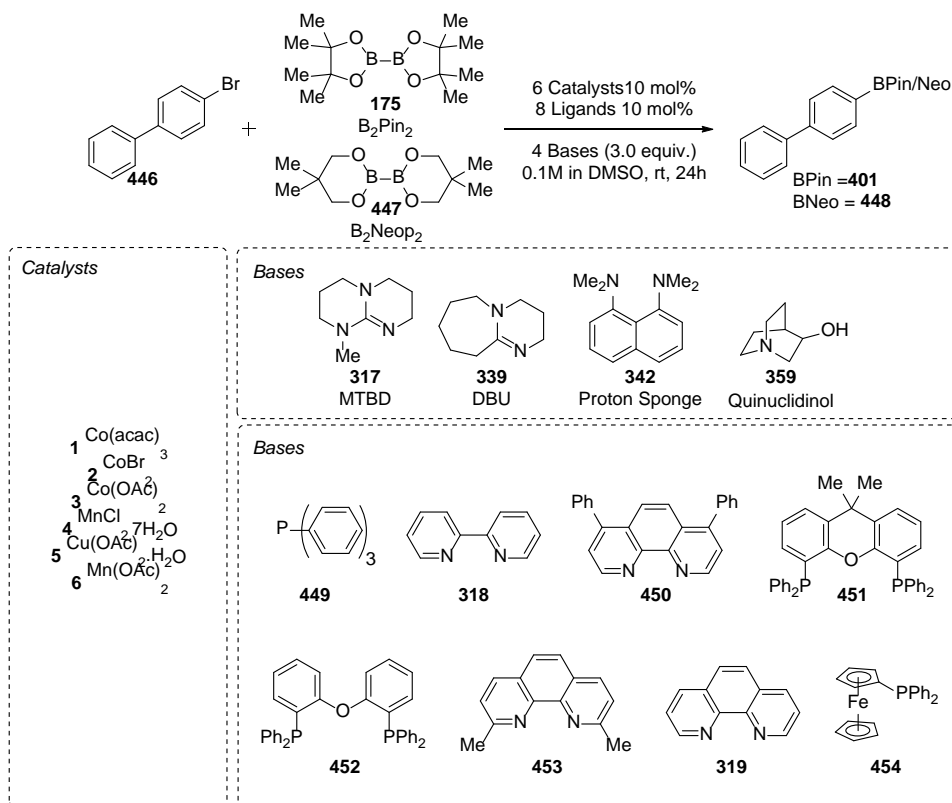
This reaction discovery delivers a proof-of-concept and validation that the high-throughput screening protocol and HT-TLC can be successfully utilised in reaction discovery. Similar conditions to those discovered have been reported recently by Ji using the same catalyst and borylating agent.²³⁴

4.3.2. Cobalt-Catalysed Borylation

With the validated protocol in hand, a more speculative screen was proposed to assess first row transition metal catalysts and their applicability for borylation. In the previous section, three first row transition metals (nickel, iron and copper) were tested for their reactivity but no hits were found. At the time, cobalt and manganese catalysis were being investigated in the group and therefore an appropriate screen was proposed using both these transition metals. These metals are known to catalyse borylation reactions,^{235,236} but under strongly reducing conditions

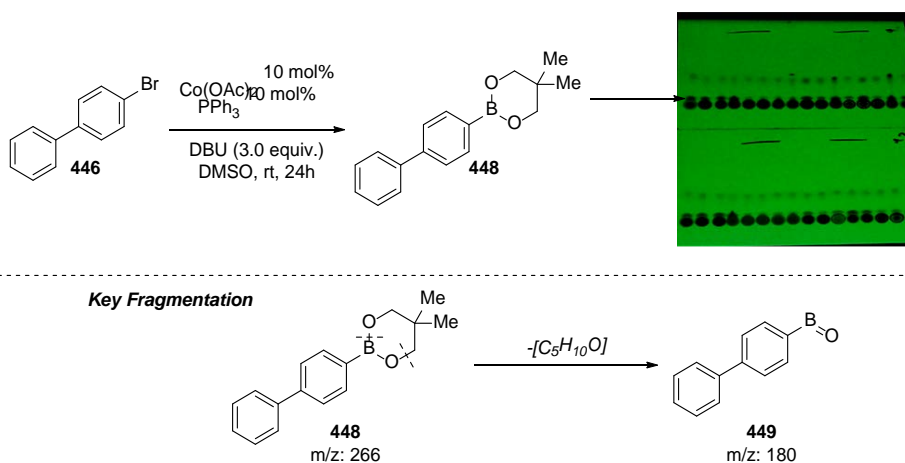
or at elevated temperatures. Thus, HT-TLC triage was used to assess whether cobalt and manganese borylation catalysis could proceed at room temperature in DMSO.

Bromobiphenyl **446** was used as the model substrate due its strong chomraphore. Two bis-boron reagents were chosen, previously used B_2Pin_2 **175** as well as less Lewis-acidic B_2Neo_2 **447**. Three cobalt sources were assessed with different counter ions and metal oxidation states alongside two manganese sources with different counterions. Copper(II) acetate was also assessed to investigate whether a similar copper-hydroxide-boronate intermediate could be accessed, similar to the proposed Chan-Lam mechanism by Watson.¹⁷² Four bases were screened to quench any generated acid as well as to investigate whether known boron-amine intermediates could be influential on the reaction.^{237,238} Eight diverse phosphine and nitrogen-based ligands were also included in the screen.



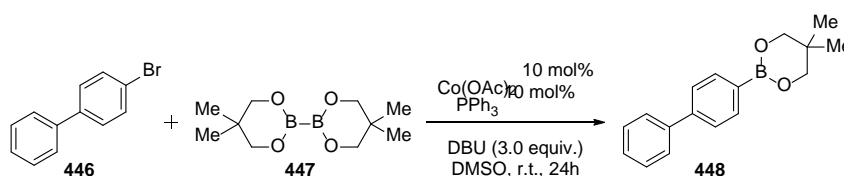
Scheme 52: First row transition metal catalysed borylation of bromobiphenyl. This screened strategy covered 384-different reaction conditions.

HT-TLC identified an initial hit when cobalt(II) acetate and triphenylphosphine were assessed with B_2Neo_2 and 3 equivalents of DBU. The hit was confirmed by GCMS with an authentic sample as well as a known boronic ester fragmentation pattern.²³⁹



Scheme 53: GCMS of well with product (10.4 minutes) and key fragmentation mode for boronic esters in GC-MS (ESI)²³⁹

With the hit identified and confirmed, batch-scale optimisation was undertaken on 0.1 mmol. All reactions were quantitated with calibrated GC-FID (Table 6). Millimole scale reaction of the discovered hit returned 8% of the borylated product (Table 6, Entry 1). Triphenylphosphine retarded the reaction and gave 15% of the borylation product (Table 6, Entry 2). Addition of caesium fluoride to the standard conditions returned and improved 16% of product (Table 6, Entry 3). Similar quantities of product were also found with caesium fluoride and without triphenylphosphine (Table 6, Entry 4). The loading of DBU was reduced to catalytic quantities but the reaction yield decreased to 9% (Table 6, Entry 5). Different solvents and bases didn't improve the reaction (Table 6, Entry 6-7). Changing the substrate to iodobiphenyl furnished 21% product at room temperature (Table 6, Entry 7), the best set of conditions found throughout the optimisation.



Entry	Variation from reaction discovery	GC-FID calibrated yield of 448 / %
1	None	7.7
2	No PPh ₃	14.5
3	With CsF (1.0 equiv.)	16.2
4	No PPh ₃ , with CsF (1.0 equiv.)	16.0
5	No PPh ₃ , 20 mol% DBU	8.4
6	No PPh ₃ , DMF rather than DMSO	8.3
7	No PPh ₃ , KOtBu rather than DBU	0.0
8	Iodobiphenyl rather than bromobiphenyl	21.0

Table 6: Summary of results from the small-scale optimisation of borylation of biphenylbromide **446** with B₂NeO₂ **447** using calibrated GC-FID.

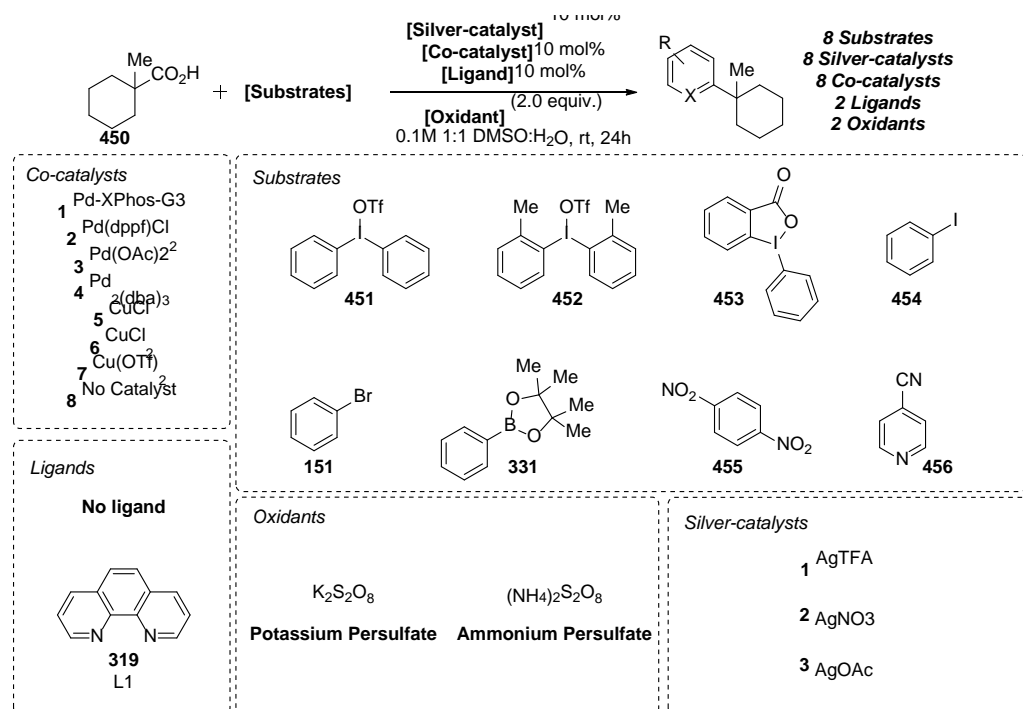
Disappointingly, the yield could not be improved beyond 20%. As more product was produced, more deleterious proto-dehalogenation or proto-deboronation was found which could not be ameliorated. Cobalt catalysts are known to be sensitive to aerobic conditions, especially prone to oxidation by molecular oxygen when solvated. Therefore, any low oxidation state catalyst available for oxidative insertion will be oxidised to catalytically inactive cobalt(II) or cobalt(III) species. When batch scale reactions were setup, a dramatic colour change was noted upon addition of DBU; purple to royal blue. Purple cobalt(II) acetate, a square planar complex, potentially undergoes a change in coordination geometry to a tetrahedral cobalt(II) complex a potentially key reaction intermediate.^{240,241} Attempts to isolate this complex were unfruitful.

While no further optimisation was completed, the reaction discovery protocol has been validated to discover a known transformation using a new metal catalyst in DMSO. This underpins the application of automated machinery for reaction discovery.

4.3.3. Silver-Decarboxylation Minisci-Coupling

As all reactions prepared by the Mosquito[®] liquid handling robot are conducted at room temperature, reactions employing reactive radical species were investigated. A radical sp^2 - sp^3 cross coupling reaction employing alkyl-carboxylic acids were assessed using HT-TLC. Strongly oxidising silver(II) salts are readily prepared *in situ* using silver(I) catalysts and inorganic salts.²⁴²

As the inorganic oxidants screened are not soluble in pure DMSO, a mixture 1:1 water:DMSO was employed as the matrix. 1-Methylcyclohexane-1-carboxylic acid **450** was chosen as the model substrate and was tested against a range of functionalised aryl coupling partners (Scheme 54). Seven metal co-catalysts (and a control) were screened in combination with three silver(I) salts, two inorganic oxidants and two ligands totalling 768 unique reaction conditions.



Scheme 54: Silver-catalysed decarboxylation of tertiary aliphatic carboxylic acids and radical addition to electron deficient substrates. A total of 768 reactions were screened.

No new spots were found when developing each plate in petroleum ether 40:60 and diethyl ether (8:2). When reaction assessed with polar substrate **456** were developed in dichloromethane and methanol (9:1), new spots were identified. The hit reaction conditions were analysed by GCMS and returned a product with mass consistent with the alkylated pyridine **457** (Figure 49). This reaction is currently being developed within the group for the late stage Minisci-alkylation of pharmaceutical drugs using primary and secondary carboxylic acids.

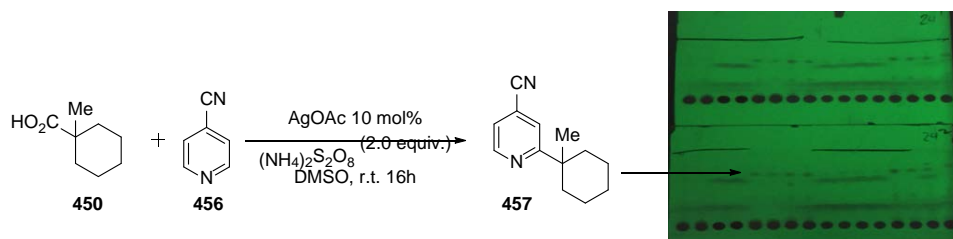


Figure 49: HT-TLC analysis of silver(II)-catalysed decarboxylation of aliphatic carboxylic acids. Hit identified by GCMS showing fragmentation modes similar to pyridinecarbonitrile with a cyclohexane substituent.

4.4. Summary

A new triaging analysis method for high-throughput reaction discovery has been developed. HT-TLC was developed by programming the Mosquito[®] to dose crude reaction mixtures onto the silica plates pegged onto 1536-well plates. This strategy could analyse over 1500 reactions in less than 2 hours.

The triaging method was validated when a palladium-catalysed borylation was discovered. When Pd-XPhos-G3 was screened as the catalyst, HT-TLC identified biphenyl as a new spot.

When confirmed by milliscale batch, only the borylate product was observed by GCMS. A small batch scale optimisation returned conditions that yielded 31% of the desired boronic ester product using only 2.5 mol% of the pre-catalyst.

Cobalt and manganese transition metal catalysts were screened for reactivity in the borylation reaction. HT-TLC identified a hit when cobalt(II) acetate was screened in combination with triphenylphosphine and DBU. The initial hit was confirmed by commercial authentic sample and a known boronic ester fragmentation pattern. Batch-scale optimisation was undertaken to assess component dependencies which gave 21% of the product when iodobiphenyl was employed. This ratifies the analysis method as a new first row transition metal catalyst was discovered for a borylation transformation.

A silver-catalysed alkylation of electron deficient substrates was investigated mixed 1:1 water DMSO matrix. When 4-pyridinecarbonitrile was assessed against the model tertiary carboxylic acid a hit set of conditions were discovered which gave the 2-alkylated pyridine exclusively. The hit was subsequently confirmed by GCMS fragmentation and this reaction is currently being investigated within the group.

Chapter 5: Conclusions and Future Work

A novel protocol for reaction optimisation and discovery has been developed using the Mosquito[®] LHR. Previously the Mosquito[®] was used only for biological applications; this project in close partnership with TTPLabTech has reinvented this machine for use in synthetic chemistry.

Microsoft Excel-based spreadsheets have been developed to plan the reaction screen, locate the chemicals in the lab and prepare the corresponding source plate. A simple Python program to produce all possible variable combinations as well as the total variables that can be screened in 96, 384 and 1536-well plates has also been developed for up to 8 variables in a single screen. Once data was generated, the same Excel spreadsheet was used for statistical assessment using median-absolute deviation. Then, by using complex logic functions, the data was automatically assessed, and anomalous data was excluded. Subsequent mean average of the data and heatmap visualisation, quickly identifies good reaction conditions. Not only does this protocol allow rapid generation of data using the LHR, but crucially the development of these Excel spreadsheets allows rapid planning before starting experimental work and rapid understanding once the data has been generated. This is imperative for high-throughput optimisation to be useful in real-time as huge amounts of data are generated.

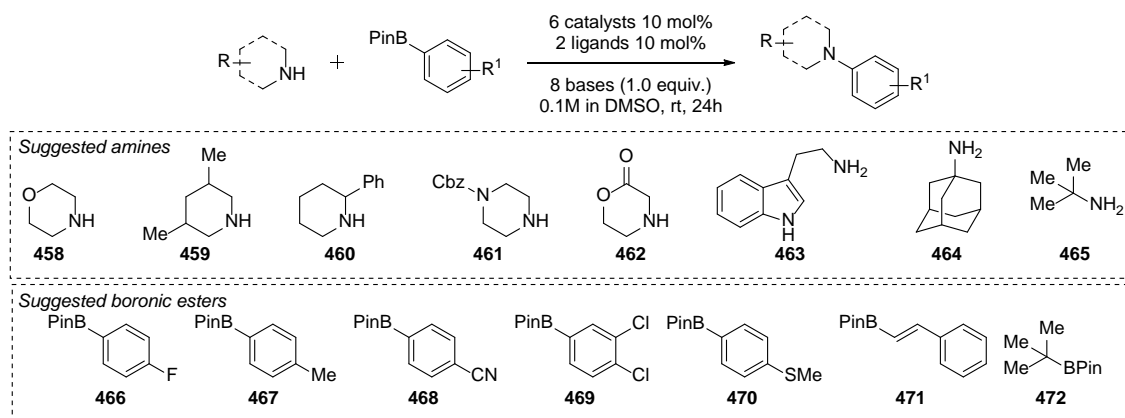
For high-throughput chemistry to be practical, an analytical method to quantitatively determine reaction performance is required that allows effective but timely analysis of large numbers of reactions. This work has utilised the laboratory LCMS, an inexpensive and accessible piece of equipment for all labs, for analysis of high-throughput reaction optimisation. Importantly, this protocol was made quantitative by comparing the data with calibration curves. In the beginning, ion suppression occurred with different bases, as the internal standard was too polar. Therefore, after screening over 20 different commercially available internal standards, *N,N*-dibenzylaniline was identified as the best, with wide applicability across a variety of different product polarities. Next, it was found that the analytical column and mass spectrometer underwent a conditioning of the internal surfaces resulting in a consistent reduction of sensitivity over the first 150-200 samples. Therefore, equilibrium with the plate conditions must be reached before quantitative analysis was possible. Overall, each well was analysed in 1.8 mins, i.e. one plate took 11.5 hours. Although run time could still be improved, the merits in this technique are obvious; no pre-functionalisation of substrate or product is required and so the method is applicable to a diverse range of chemistry, and no specialist equipment is necessary.

The optimised high-throughput protocol was used to investigate reaction conditions for the coupling of eight electronically and structurally different boronic esters with amine **134**. This reaction was screened against eight different bases, two ligands and six catalysts (totalling over 3000 reactions). Further assessment of 22 more electronically and structurally different boronic esters was carried out, in a focussed screened of four catalysts, tow ligands and four bases (totalling over 2800 reactions).

For each of the 30 boronic ester substrate scope, 3 scale up reactions were carried out to validate the quantitative assay; impressively, the majority of the reactions were found to scale from nanomole to millimole scale, a scale factor of 1200 times. Across the 90 milliscale validation reactions performed; the average difference between assay yield and NMR yield was 13%. Only 26 out of 90 reactions returned a difference of greater than 15% between the two.

Using the data generated from this validated quantitative high-throughput protocol, in collaboration with computational chemists, we have modelled the data to assess whether predictions can be made based on the trends observed in the data. Using experimentally obtained IR, ^{13}C and ^{11}B data alongside computationally-derived parameterisation, each boronic ester was modelled for its effect in the Chan-Lam reaction. A computational modelling using a feature-graph regression was prepared to model the 30 boronic esters screened in the Chan-Lam reaction.

We currently have a predictive model for a small subset of boronic esters with no understanding of the effect of various amines. The future goal of this work is to develop a full model capable of predicting reaction outcome and yield for the Chan-Lam reaction. We believe that an assortment of 50 simple amines and boronic esters would be enough to complete a fully predictive model (Scheme 55) Moreover, the lack of complex amines or boronic ester examples is also an area that warrants more investigation such as amines **458-465** and boronic esters **466-472**.



Scheme 55: Further screening of Chan-Lam reaction using the initial 1x4x8x2x6 screen. A) Suggesting amines for predictive model including secondary and primary amines; b) suggested boronic esters including simple substrates and more complex alkenyl and alkyl boronates.

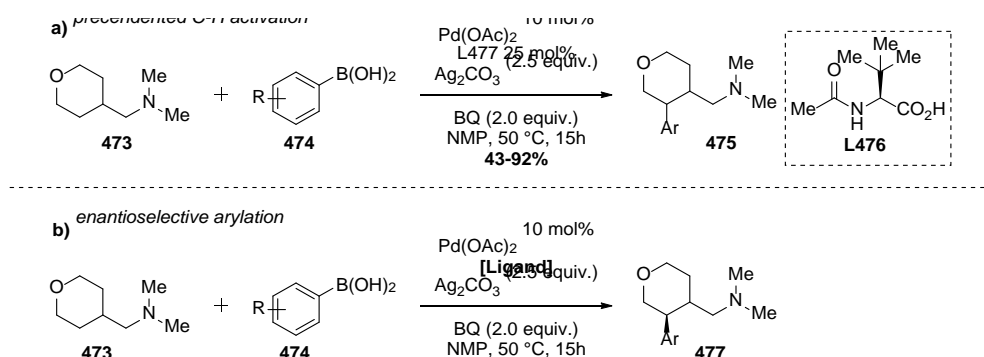
A second future goal of this work is to model other chemical reactions in a similar manner. At present, the Gaunt group are expanding the model to encompass the Buchwald-Hartwig amination, previously optimised and modelled by MSD. Although the MSD-Doyle example is pioneering for its advancement in computational modelling in synthetic chemistry, it does not predict reaction yield, only reaction outcome and whether the reaction would work in combination with different isoxazoles. The feature-graph regression used for the Chan-Lam model has since been applied to the reported data. Therefore, employing our quantitative assay and modelling approach we hope to model the Buchwald-Hartwig amination.

Modifying the high-throughput reaction optimisation protocol for reaction discovery, a triaging method (HT-TLC) has been developed to screen thousands of reactions conditions within hours. Further development of the Mosquito[®] LHR for use in chemistry, this novel technique employs the LHR to dose crude reaction mixtures onto silica gel TLC plates. As long as the retention times of the starting materials is known, any new spot is a potential new reaction which can be confirmed using GC or LCMS.

Using this triaging technique, three transformations were assessed. A Miyaura borylation reaction was assessed as a positive control and new conditions were found for the borylation of bromobenzene. The analysis technique was pushed further to assess the same borylation transformation but using first row transition metals. A new cobalt-catalysed transformation was found using HT-TLC ratifying this technique for reaction discovery. A Minisci-alkylation was also found using HT-TLC which is undergoing development within the Gaunt group.

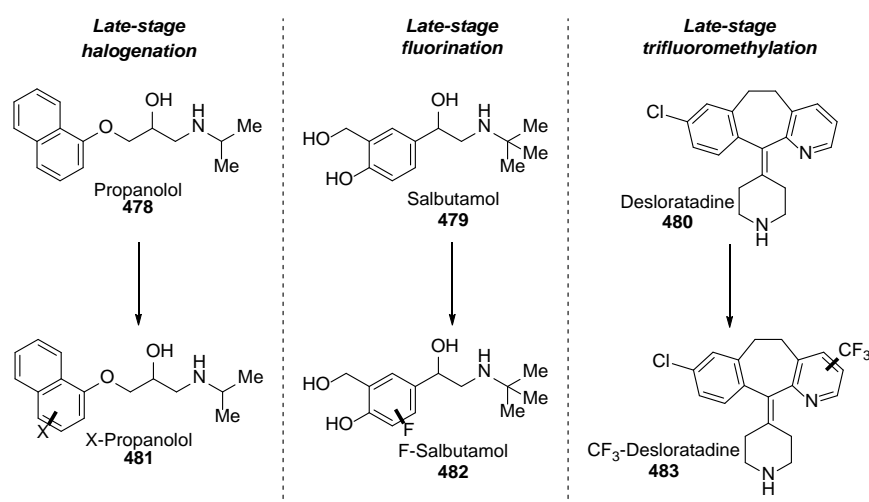
From the reaction discovery perspective, future work will follow in the Gaunt group's primary fields of palladium-catalysed C-H activation and biorthogonal reactions. Utilising HT-TLC, we can screen for new reaction modes and conditions capable of catalysing C-H activation at room temperature. Within the group, a relatively mild set of conditions for the C-H arylation

of tertiary amines in NMP has been discovered (Scheme 56). More intriguingly, a privileged example was found to selectively activate a six-membered ring. In combination with new technology from Shimadzu, we are interested in applying this C–H activation for high-throughput enantio-determination.



Scheme 56: C-H activation reaction discovered by Jesus Rodrialvarez. A) Precedented reactivity for further assessment by high-throughput screening; d) Potential for enantioselective methylene C(sp³)-H activation.

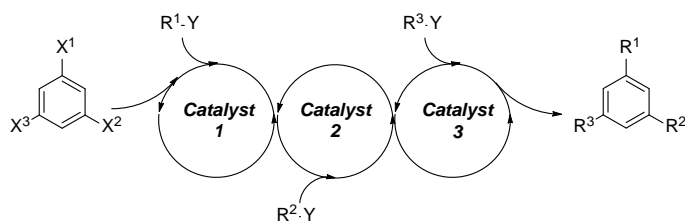
Industry are excited by applying high-throughput screening and reaction discovery to synthesise potential drug candidate otherwise inaccessible by conventional literature reaction conditions (Scheme 57). Therefore, collaborating with industry, we can take project leads which have failed key pharmaceutically relevant factors such as hERG, LogP and IC₅₀ amongst others.²⁴³ For example, fluorine and trifluoromethyl groups are important motifs that improve LogP, oral stability and persistence.²⁴⁴ Using the high-throughput reaction discovery platform to screen various nucleophilic and electrophilic fluorination and trifluoromethylation reactions, new and improve drug candidates can be prepared. In combination with computational modelling, computation of the HOMO/LUMO coefficients can also predict reaction regioselectivity thereby allowing for conditions to give selective reaction products.



Scheme 57: Example reactions on known blockbuster drugs. In reality, drug scaffolds from failed drug discovery projects could be assessed using high-throughput reaction discovery.

Miniaturising chemistry has been the focal point of this optimisation strategy. Using microtiter plates and only 2.5 microlitres of solvent means thousands of reactions can be performed using

only milligrams of material. As biochemical assays and high-throughput screening are more accurate and precise, they now only require micrograms of material to complete a full assignment. Relatable to microtiter reactor plate scales, we can envisage completing a small synthesis of drug targets within a well plate and directly screening the synthesised compound in a functional assay (Scheme 58). The nature of the screening arrays means explicit synthesis of thousands of drug targets can be completed, ameliorating difficult and time-consuming analysis associated with combinatorial library synthesis.



Scheme 58: Overview of multi-step catalysis for fine chemical synthesis.

Chapter 6: References

- (1) Fleming, A. *Bull. World Health Organ.* **2001**, 79 (8), 780–790.
- (2) Ligon, B. L. *Semin. Pediatr. Infect. Dis.* **2004**, 15 (1), 52–57.
- (3) Alharbi, S. A.; Wainwright, M.; Alahmadi, T. A.; Salleeh, H. Bin; Faden, A. A.; Chinnathambi, A. *Saudi J. Biol. Sci.* **2014**, 21 (4), 289–293.
- (4) Timmons, F. L. *Weed Sci.* **1970**, 18 (2), 294–307.
- (5) Carvalho, F. P. *Food Energy Secur.* **2017**, 6 (2), 48–60.
- (6) Sharma, K. K.; Singh, U. S.; Sharma, P.; Kumar, A.; Sharma, L. *J. Appl. Nat. Sci.* **2015**, 7 (1), 521–539.
- (7) Eneh, O. C. *J. Appl. Sci.* **2011**, 11, 2084–2091.
- (8) Dias, D. A.; Urban, S.; Roessner, U. *Metabolites* **2012**, 2 (2), 303–336.
- (9) Blakemore, D. C.; Castro, L.; Churcher, I.; Rees, D. C.; Thomas, A. W.; Wilson, D. M.; Wood, A. *Nat. Chem.* **2018**, 10 (4), 383–394.
- (10) Raymer, B.; Bhattacharya, S. K. *J. Med. Chem.* **2018**, acs.jmedchem.8b00407.
- (11) McMullen, J. P.; Jensen, K. F. *Annu. Rev. Anal. Chem.* **2010**, 3, 19–42.
- (12) Ab Rahman, A.; Abdul Hamid, U. Z.; Chin, T. *PERINTIS eJournal* **2017**, 7, 111–128.
- (13) Lee Howell. *Global Risks Report 2013 Eighth Edition*; Geneva, Sui, 2013.
- (14) Janzen, W. P. *Chem. Biol.* **2014**, 21 (9), 1162–1170.
- (15) Lander, E. S. et. al. *Nature* **2001**, 409 (6822), 860–921.
- (16) Kramer, R.; Cohen, D. *Nat. Rev. Drug Discov.* **2004**, 3 (11), 965–972.
- (17) Armbruster, D. A.; Overcash, D. R.; Reyes, J. *Clin Biochem Rev.* **2014**, 35 (3), 143–153.
- (18) Fytianos, K.; Vasilikiotis, G. S. *Chemosphere* **1983**, 12 (1), 83–91.
- (19) Eriksen, M.; Lebreton, L. C. M.; Carson, H. S.; Thiel, M.; Moore, C. J.; Borerro, J. C.; Galgani, F.; Ryan, P. G.; Reisser, J. *PLoS One* **2014**, 9 (12), 1–15.
- (20) Milo, A. *Isr. J. Chem.* **2018**, 58, 131–135.
- (21) Thompson, L. A.; Ellman, J. A. *Chem. Rev.* **1996**, 96 (1), 555–600.
- (22) Pei, T.; Tellers, D. M.; Streckfuss, E. C.; Chen, C.; Davies, I. W. *Tetrahedron* **2009**, 65 (16), 3285–3291.
- (23) Plutschack, M. B.; Pieber, B.; Gilmore, K.; Seeberger, P. H. *Chem. Rev.* **2017**, 117 (18), 11796–11893.
- (24) Jas, G.; Kirschning, A. *Chem. Eur. J.* **2003**, 9, 5708–5723.
- (25) Baumann, M.; Baxendale, I. R. *Beilstein J. Org. Chem.* **2015**, 11, 1194–1219.
- (26) Porta, R.; Benaglia, M.; Puglisi, A. *Org. Process Res. Dev.* **2016**, 20 (1), 2–25.
- (27) Adamo, A.; Beingsner, R. L.; Behnam, M.; Chen, J.; Jamison, T. F.; Jensen, K. F.; Monbaliu, J.-C. M.; Myerson, Allan, S.; Revalor, E. M.; Snead, D. R.; Stelzer, T.; Weeranoppanant, N.; Wong, S. Y.; Zhang, P. *Science (80-)*. **2016**, 352, 61–68.
- (28) Pastre, J. C.; Browne, D. L.; Ley, S. V. *Chem. Soc. Rev.* **2013**, 42 (23), 8849.
- (29) Ley, S. V.; Fitzpatrick, D. E.; Myers, R. M.; Battilocchio, C.; Ingham, R. J. *Angew. Chemie - Int. Ed.* **2015**, 54 (35), 10122–10136.
- (30) Ley, S. V.; Fitzpatrick, D. E.; Ingham, R. J.; Myers, R. M. *Angew. Chemie - Int. Ed.* **2015**, 54 (11), 3449–3464.
- (31) Murray, P. R. D.; Browne, D. L.; Pastre, J. C.; Butters, C.; Guthrie, D.; Ley, S. V. *Org. Process Res. Dev.* **2013**, 17 (9), 1192–1208.
- (32) Baxendale, I. R.; Deeley, J.; Griffiths-Jones, C. M.; Ley, S. V.; Saaby, S.; Tranmer, G. K. *Chem. Commun.* **2006**, 2566–2568.
- (33) Baxendale, I. R.; Ley, S. V.; Mansfield, A. C.; Smith, C. D. *Angew. Chemie - Int. Ed.* **2009**, 48 (22), 4017–4021.
- (34) Guetzoyan, L.; Nikbin, N.; Baxendale, I. R.; Ley, S. V. *Chem. Sci.* **2013**, 4 (2), 764–769.
- (35) Lau, S. H.; Galván, A.; Merchant, R. R.; Battilocchio, C.; Souto, J. A.; Berry, M. B.; Ley, S. V. *Org. Lett.* **2015**, 17 (13), 3218–3221.
- (36) Monfette, S.; Blacquiére, J. M.; Fogg, D. E. *Organometallics* **2011**, 30 (1), 36–42.
- (37) Perera, D.; Tucker, J. W.; Brahmabhatt, S.; Helal, C. J.; Chong, A.; Farrell, W.; Richardson, P.; Sach, N. W. *Science (80-)*. **2018**, 359, 429–434.
- (38) Pashkova, A.; Greiner, L. *Chemie Ing. Tech.* **2011**, 83, 1337–1342.
- (39) Merrifield, R. B. *J. Am. Chem. Soc.* **1963**, 85 (14), 2149.
- (40) Kodadek, T. *Chem. Commun.* **2011**, 47, 9757–9763.
- (41) Kennedy, J. P.; Williams, L.; Bridges, T. M.; Daniels, R. N.; Weaver, D.; Lindsley, C. W. *J. Comb. Chem.* **2008**, 10 (3), 345–354.
- (42) Cernak, T.; Gesmundo, N. J.; Dykstra, K.; Yu, Y.; Wu, Z.; Shi, Z. C.; Vachal, P.; Sperbeck, D.; He, S.; Murphy, B. A.; Sonatore, L.; Williams, S.; Madeira, M.; Verras, A.; Reiter, M.; Lee, C. H.; Cuff, J.; Sherer, E. C.; Kuethe, J.; Goble, S.; Perrotto, N.; Pinto, S.; Shen, D. M.; Nargund, R.; Balkovec, J.; DeVita, R. J.; Dreher, S. D. *J. Med. Chem.* **2017**, 60 (9), 3594–3605.
- (43) Burgess, K.; Lim, H. J.; Porte, A. M.; Sulikowski, G. A. *Angew. Chemie - Int. Ed.* **1996**, 35 (2), 220–222.
- (44) Gennari, C.; Ceccarelli, S.; Piarulli, U.; Montalbetti, C. A. G. N.; Jackson, R. F. W. *J. Org. Chem.* **1998**,

- 63 (16), 5312–5313.
- (45) Lack, O.; Weber, L. *Chimia (Aarau)*. **1996**, *50* (9), 445–447.
- (46) Taylor, S. J.; Morken, J. P. *Science (80-)*. **1998**, *280* (5361), 267–270.
- (47) Reetz, M. T.; Becker, M. H.; Kühling, K. M.; Holzwarth, A. *Angew. Chemie - Int. Ed.* **1998**, *37* (19), 2647–2650.
- (48) Reetz, M. T.; Kühling, K. M.; Deege, A.; Hinrichs, H.; Belder, D. *Angew. Chemie - Int. Ed.* **2000**, *39* (21), 3891–3893.
- (49) Fürstner, A.; Ackermann, L.; Gabor, B.; Goddard, R.; Lehmann, C. W.; Mynott, R.; Stelzer, F.; Thiel, O. R. *Chem. Eur. J.* **2001**, *7* (15), 3236–3253.
- (50) Friest, J. A.; Broussy, S.; Chung, W. J.; Berkowitz, D. B. *Angew. Chemie - Int. Ed.* **2011**, *50* (38), 8895–8899.
- (51) Ginotra, S. K.; Friest, J. A.; Berkowitz, D. B. *Org. Lett.* **2012**, *14* (4), 968–971.
- (52) Jung, E.; Kim, S.; Kim, Y.; Seo, S. H.; Lee, S. S.; Han, M. S.; Lee, S. *Angew. Chemie - Int. Ed.* **2011**, *50* (19), 4386–4389.
- (53) Kim, S.; Jung, E.; Kim, M. J.; Pyo, A.; Palani, T.; Eom, M. S.; Han, M. S.; Lee, S. *Chem. Commun.* **2012**, *48* (70), 8751.
- (54) Feigl, F. *Qualitative Analysis by Spot Tests*, 3rd ed.; Elsevier: New York, 1946.
- (55) Löber, O.; Kawatsura, M.; Hartwig, J. F. *J. Am. Chem. Soc.* **2001**, *123* (18), 4366–4367.
- (56) Sapan, C. V.; Lundblad, R. L.; Price, N. C. *Biotechnol. Appl. Biochem.* **1999**, *29*, 99–108.
- (57) Copeland, G. T.; Miller, S. J. *J. Am. Chem. Soc.* **1999**, *121* (17), 4306–4307.
- (58) Prasanna de Silva, A.; Nimal Gunaratne, H. Q.; Gunnlaugsson, T.; Huxley, A. J. M.; McCoy, Colin, P.; Rademacher, J. T.; Rice, T. E. *Chem. Rev.* **1997**, *97*, 1515–1566.
- (59) Scriven, B. E. F. V. *Chem. Soc. Rev.* **1983**, *12*, 129–161.
- (60) Shaughnessy, K. H.; Kim, P.; Hartwig, J. F. *J. Am. Chem. Soc.* **1999**, *121* (10), 2123–2132.
- (61) Bajar, B. T.; Wang, E. S.; Zhang, S.; Lin, M. Z.; Chu, J. *Sensors* **2016**, *16* (9), 1–24.
- (62) Stambuli, J. P.; Stauffer, S. R.; Shaughnessy, K. H.; Hartwig, J. F. *J. Am. Chem. Soc.* **2001**, *123* (11), 2677–2678.
- (63) Stauffer, S. R.; Beare, N. A.; Stambuli, J. P.; Hartwig, J. F. *J. Am. Chem. Soc.* **2001**, *123* (19), 4641–4642.
- (64) Stauffer, S. R.; Hartwig, J. F. *J. Am. Chem. Soc.* **2003**, *125* (23), 6977–6985.
- (65) Sashuk, V.; Schoeps, D.; Plenio, H. *Chem. Commun.* **2009**, *7*, 770–772.
- (66) Berkowitz, D. B.; Bose, M.; Choi, S. *Angew. Chemie - Int. Ed.* **2002**, *41* (9), 1603–1607.
- (67) Berkowitz, D. B.; Maiti, G. *Org. Lett.* **2004**, *6* (16), 2661–2664.
- (68) Dey, S.; Karukurichi, K. R.; Shen, W.; Berkowitz, D. B. *J. Am. Chem. Soc.* **2005**, *127* (24), 8610–8611.
- (69) Dey, S.; Powell, D. R.; Hu, C.; Berkowitz, D. B. *Angew. Chemie - Int. Ed.* **2007**, *46* (37), 7010–7014.
- (70) Taran, F.; Gauchet, C.; Mohar, B.; Meunier, S.; Valleix, A.; Renard, P. Y.; Créminon, C.; Grassi, J.; Wagner, A.; Mioskowski, C. *Angew. Chemie - Int. Ed.* **2002**, *41* (1), 124–127.
- (71) Engvall, E.; Perlmann, P. *Immunochemistry* **1971**, *8* (9), 871–874.
- (72) Van Weemen, B. K.; Schuur, A. H. W. M. *FEBS Lett.* **1971**, *15* (3), 232–236.
- (73) Brooks, K.; Autrey, T. *Energy Fuels* **2017**, *31*, 12603–12611.
- (74) Vicennati, P.; Bensel, N.; Wagner, A.; Créminon, C.; Taran, F. *Angew. Chemie - Int. Ed.* **2005**, *44* (42), 6863–6866.
- (75) Kolodych, S.; Rasolofonjatovo, E.; Chaumontet, M.; Nevers, M. C.; Créminon, C.; Taran, F. *Angew. Chemie - Int. Ed.* **2013**, *52* (46), 12056–12060.
- (76) Rostovtsev, V. V.; Green, L. G.; Fokin, V. V.; Sharpless, K. B. *Angew. Chemie - Int. Ed.* **2002**, *41* (14), 2596–2599.
- (77) Kuijpers, B. H. M.; Dijkmans, G. C. T.; Groothuys, S.; Quaedflieg, P. J. L. M.; Blaauw, R. H.; Van Delft, F. L.; Rutjes, F. P. J. T. *Synlett* **2005**, *20*, 3059–3062.
- (78) Shintani, R.; Fu, G. C. *J. Am. Chem. Soc.* **2003**, *125* (36), 10778–10779.
- (79) Kanan, M. W.; Rozenman, M. M.; Sakural, K.; Snyder, T. M.; Liu, D. R. *Nature* **2004**, *431* (7008), 545–549.
- (80) Diamandis, E. P.; Christopoulos, T. K. *Clin. Chem.* **1991**, *37* (5), 625–636.
- (81) Rozenman, M. M.; Kanan, M. W.; Liu, D. R. *J. Am. Chem. Soc.* **2007**, *129* (48), 14933–14938.
- (82) Liu, P.; Mara, B. W. O.; Warrack, B. M.; Wu, W.; Huang, Y.; Zhang, Y.; Zhao, R.; Lin, M.; Ackerman, M. S.; Hocknell, P. K.; Chen, G.; Tao, L.; Rieble, S.; Wang, J.; Wang-Iverson, D. B.; Tymiak, A. A.; Grace, M. J.; Russell, R. J. *J. Am. Soc. Mass Spectrom.* **2010**, *21* (5), 837–844.
- (83) Münzenberg, G. *Int. J. Mass Spectrom.* **2013**, *349–350*, 9–18.
- (84) Glish, G. L.; Vachet, R. W. *Nat. Rev. Drug Discov.* **2003**, *2* (2), 140–150.
- (85) Maher, S.; Jjunju, F. P. M.; Taylor, S. *Rev. Mod. Phys.* **2015**, *87* (1), 113–135.
- (86) Peer, C. J.; Shakleya, D. M.; Younis, I. R.; Kraner, J. C.; Callery, P. S. *J. Anal. Toxicol.* **2007**, *31*, 515–521.
- (87) Lebron-Aguilar, R.; Soria, A. C.; Quintanilla-Lopez, J. E. *Phil. Trans. R. Soc. A* **2016**, *374*, 1–14.
- (88) Markert, C.; Pfaltz, A. *Angew. Chemie - Int. Ed.* **2004**, *43* (19), 2498–2500.
- (89) Markert, C.; Rösel, P.; Pfaltz, A. *J. Am. Chem. Soc.* **2008**, *130* (11), 3234–3235.

- (90) Müller, C. A.; Pfaltz, A. *Angew. Chemie - Int. Ed.* **2008**, *47* (18), 3363–3366.
- (91) Teichert, A.; Pfaltz, A. *Angew. Chemie - Int. Ed.* **2008**, *47* (18), 3360–3362.
- (92) Fleischer, I.; Pfaltz, A. *Chem. Eur. J.* **2010**, *16* (1), 95–99.
- (93) Ebner, C.; Müller, C. A.; Markert, C.; Pfaltz, A. *J. Am. Chem. Soc.* **2011**, *133* (13), 4710–4713.
- (94) Montavon, T. J.; Li, J.; Cabrera-Pardo, J. R.; Mrksich, M.; Kozmin, S. A. *Nat. Chem.* **2012**, *4* (1), 45–51.
- (95) Mouradian, S.; Nelson, C. M.; Smith, L. M. *J. Am. Chem. Soc.* **1996**, *118* (36), 8639–8645.
- (96) Su, J.; Mrksich, M. *Angew. Chemie - Int. Ed.* **2002**, *41*, 4715–4718.
- (97) Cabrera-Pardo, J. R.; Chai, D. I.; Liu, S.; Mrksich, M.; Kozmin, S. A. *Nat. Chem.* **2013**, *5* (5), 423–427.
- (98) McCarley, T. D.; McCarley, R. L.; Limbach, P. A. *Anal. Chem.* **1998**, *70* (20), 4376–4379.
- (99) Macha, S. F.; McCarley, T. D.; Limbach, P. A. *Anal. Chim. Acta* **1999**, *397*, 235–245.
- (100) Lin, S.; Dikler, S.; Blincoe, W. D.; Ferguson, R. D.; Sheridan, R. P.; Peng, Z.; Conway, D. V.; Zawatzky, K.; Wang, H.; Cernak, T.; Davies, I. W.; DiRocco, D. A.; Sheng, H.; Welch, C. J.; Dreher, S. D. *Science (80-)*. **2018**, 10.1126/science.aar6236.
- (101) Weber, L.; Illgen, K.; Almstetter, M. *Synlett* **1999**, 1999 (3), 366–374.
- (102) Dreher, S. D.; Dormer, P. G.; Sandrock, D. L.; Molander, G. A. *J. Am. Chem. Soc.* **2008**, *130* (29), 9257–9259.
- (103) Molander, G. A.; Sandrock, D. L. *Curr. Opin. Drug Discov. Devel.* **2009**, *12* (6), 811–823.
- (104) Lu, X. *Top. Catal.* **2005**, *35*, 73–86.
- (105) Sandrock, D. L.; Jean-Gérard, L.; Chen, C. Y.; Dreher, S. D.; Molander, G. A. *J. Am. Chem. Soc.* **2010**, *132* (48), 17108–17110.
- (106) Molander, G. A.; Wisniewski, S. R. *J. Am. Chem. Soc.* **2012**, *134* (40), 16856–16868.
- (107) Ballini, R.; Petrini, M. *Adv. Synth. Catal.* **2015**, *357*, 2371–2402.
- (108) Wang, K.; Qian, X.; Cui, J. *Tetrahedron* **2009**, *65* (50), 10377–10382.
- (109) Orlandi, M.; Brenna, D.; Harms, R.; Jost, S.; Benaglia, M. *Org. Process Res. Dev.* **2016**, *22*, 430–445.
- (110) Marcé, P.; Lynch, J.; Blacker, A. J.; Williams, J. M. J. *Chem. Commun.* **2016**, *52* (5), 1013–1016.
- (111) Balasubramaniam, S.; Aidhen, I. S. *Synthesis (Stuttg.)*. **2008**, *23*, 3707–3738.
- (112) Obora, Y.; Ogawa, Y.; Imai, Y.; Kawamura, T.; Tsuji, Y. *J. Am. Chem. Soc.* **2001**, *123* (43), 10489–10493.
- (113) Schmink, J. R.; Krska, S. W. *J. Am. Chem. Soc.* **2011**, *133* (49), 19574–19577.
- (114) Preshlock, S. M.; Ghaffari, B.; Maligres, P. E.; Krska, S. W.; Maleczka, R. E.; Smith, M. R. *J. Am. Chem. Soc.* **2013**, *135* (20), 7572–7582.
- (115) Metz, A. E.; Berritt, S.; Dreher, S. D.; Kozlowski, M. C. *Org. Lett.* **2012**, *14* (3), 760–763.
- (116) Vangelder, K. F.; Wang, M.; Kozlowski, M. C. *J. Org. Chem.* **2015**, *80* (20), 10288–10293.
- (117) Zhang, J.; Stanciu, C.; Wang, B.; Hussain, M. M.; Da, C.-S.; Carroll, P. J.; Dreher, S. D.; Walsh, P. J. *J. Am. Chem. Soc.* **2011**, *133* (50), 20552–20560.
- (118) Zhang, J.; Bellomo, A.; Creamer, A. D.; Dreher, S. D.; Walsh, P. J. *J. Am. Chem. Soc.* **2012**, *134* (33), 13765–13772.
- (119) McGrew, G. I.; Temaismithi, J.; Carroll, P. J.; Walsh, P. J. *Angew. Chemie - Int. Ed.* **2010**, *49* (32), 5541–5544.
- (120) Jia, T.; Bellomo, A.; Baina, K. El; Dreher, S. D.; Walsh, P. J. *J. Am. Chem. Soc.* **2013**, *135* (10), 3740–3743.
- (121) Cheng, K.; Walsh, P. J. *Org. Lett.* **2013**, *15* (9), 2298–2301.
- (122) Molander, G. A.; Traister, K. M.; Barcellos, T. *J. Org. Chem.* **2013**, *78* (8), 4123–4131.
- (123) Amani, J.; Molander, G. A. *Org. Lett.* **2015**, *17* (14), 3624–3627.
- (124) Molander, G. A.; Amani, J.; Wisniewski, S. R. *Org. Lett.* **2014**, *16* (22), 6024–6027.
- (125) Molander, G. A.; Wisniewski, S. R.; Hosseini-Sarvaria, M. *Adv. Synth. Catal.* **2013**, *355*, 3037–3057.
- (126) Molander, G. A.; Argintaru, O. A.; Aron, I.; Dreher, S. D. *Org. Lett.* **2010**, *12* (24), 5783–5785.
- (127) Molander, G. A.; Traister, K. M.; O'Neill, B. T. *J. Org. Chem.* **2014**, *79* (12), 5771–5780.
- (128) Molander, G. A.; Wisniewski, S. R. *J. Org. Chem.* **2014**, *79* (17), 8339–8347.
- (129) Ryu, D.; Primer, D. N.; Tellis, J. C.; Molander, G. A. *Chem. Eur. J.* **2016**, *22* (1), 120–123.
- (130) Amani, J.; Alam, R.; Badir, S.; Molander, G. A. *Org. Lett.* **2017**, *19* (9), 2426–2429.
- (131) Phelan, J. P.; Wiles, R.; Lang, S. B.; Kelly, C. B.; Molander, G. A. *Chem. Sci.* **2018**, *9*, 3215–3220.
- (132) Amani, J.; Molander, G. A. *Org. Lett.* **2017**, *19* (13), 3612–3615.
- (133) Matsui, J. K.; Molander, G. A. *Org. Lett.* **2017**, *19* (3), 436–439.
- (134) Molander, G. A.; Trice, S. L. J.; Dreher, S. D. *J. Am. Chem. Soc.* **2010**, *132* (50), 17701–17703.
- (135) Molander, G. A.; Trice, S. L. J.; Kennedy, S. M.; Dreher, S. D.; Tudge, M. T. *J. Am. Chem. Soc.* **2012**, *134* (28), 11667–11673.
- (136) Molander, G. A.; Trice, S. L. J.; Kennedy, S. M. *J. Org. Chem.* **2012**, *77* (19), 8678–8688.
- (137) Molander, G. A.; Cavalcanti, L. N.; García-García, C. *J. Org. Chem.* **2013**, *78* (13), 6427–6439.
- (138) Amani, J.; Sodagar, E.; Molander, G. A. *Org. Lett.* **2016**, *18* (4), 732–735.
- (139) Fleury-Brégeot, N.; Raushel, J.; Sandrock, D. L.; Dreher, S. D.; Molander, G. A. *Chem. Eur. J.* **2012**, *18* (31), 9564–9570.
- (140) Tellis, J. C.; Primer, D. N.; Molander, G. A. *Science (80-)*. **2014**, *345* (6195), 433–436.
- (141) Zheng, S.; Primer, D. N.; Molander, G. A. *ACS Catal.* **2017**, *7* (11), 7957–7961.

- (142) Gao, X.; Kagan, H. B. *Chirality* **1998**, *124*, 120–124.
- (143) Saito, M. *J. Biosci. Bioeng.* **2013**, *115* (6), 590–599.
- (144) Nindakova, L. O.; Lebed', F. M.; Zamazei, a. Y.; Shainyan, B. a. *Russ. J. Org. Chem.* **2007**, *43* (9), 1322–1329.
- (145) Friedfeld, M. R.; Shevlin, M.; Hoyt, J. M.; Krska, S. W.; Tudge, M. T.; Chirik, P. J. *Science* **2013**, *342*, 1076–1080.
- (146) Shevlin, M.; Friedfeld, M. R.; Sheng, H.; Pierson, N. A.; Hoyt, J. M.; Campeau, L. C.; Chirik, P. J. *J. Am. Chem. Soc.* **2016**, *138* (10), 3562–3569.
- (147) McGrew, G. I.; Stanciu, C.; Zhang, J.; Carroll, P. J.; Dreher, S. D.; Walsh, P. J. *Angew. Chemie - Int. Ed.* **2012**, *51* (46), 11510–11513.
- (148) Imaduwaige, K. P.; Lakkub, J.; Go, E. P.; Desaire, H. *Sci. Rep.* **2017**, *7* (1), 1–10.
- (149) Roddy, T. P.; Horvath, C. R.; Stout, S. J.; Kenney, K. L.; Ho, P. I.; Zhang, J. H.; Vickers, C.; Kaushik, V.; Hubbard, B.; Karen Wang, Y. *Anal. Chem.* **2007**, *79* (21), 8207–8213.
- (150) Robbins, D. W.; Hartwig, J. F. *Science (80-.)*. **2011**, *333*, 1423–1427.
- (151) Nakao, Y.; Oda, S.; Hiyama, T. *J. Am. Chem. Soc.* **2004**, *126* (43), 13904–13905.
- (152) Lam, P. Y. S.; Clark, C. G.; Saubern, S.; Adams, J.; Winters, M. P.; Chan, D. M. T.; Combs, A. *Tetrahedron Lett.* **1998**, *39* (19), 2941–2944.
- (153) Hamid, M. H. S. A.; Allen, C. L.; Lamb, G. W.; Maxwell, A. C.; Maytum, H. C.; Watson, A. J. A.; Williams, J. M. J. *J. Am. Chem. Soc.* **2009**, *131*, 1766–1774.
- (154) Hayashi, T.; Inoue, K.; Taniguchi, N. **2001**, 9918–9919.
- (155) Xu, X.; Chen, J.; Gao, W.; Wu, H.; Ding, J.; Su, W. *Tetrahedron* **2010**, *66* (13), 2433–2438.
- (156) Troshin, K.; Hartwig, J. F. *Science (80-.)*. **2017**, *357* (6347), 175–181.
- (157) McNally, A.; Prier, C. K.; MacMillan, D. W. C. *Science (80-.)*. **2011**, *334*, 1114–1117.
- (158) Jäkel, C.; Paciello, R. *Chem. Rev.* **2006**, *106* (7), 2912–2942.
- (159) Zang, Q.; Javed, S.; Hill, D.; Ullah, F.; Bi, D.; Porubsky, P.; Neuenswander, B.; Lushington, G. H.; Santini, C.; Organ, M. G.; Hanson, P. R. *ACS Comb. Sci.* **2012**, *14* (8), 456–459.
- (160) Fenster, E.; Long, T. R.; Zang, Q.; Hill, D.; Neuenswander, B.; Lushington, G. H.; Zhou, A.; Santini, C.; Hanson, P. R. *ACS Comb. Sci.* **2011**, *13* (3), 244–250.
- (161) Stoll, N.; Allwardt, A.; Dingerdissen, U.; Thurow, K. *J. Autom. Methods Manag. Chem.* **2006**, *2006*, 1–9.
- (162) Porco, J. A. *Beilstein J. Org. Chem.* **2012**, *8*, 827–828.
- (163) DiRocco, D. A.; Dykstra, K.; Krska, S.; Vachal, P.; Conway, D. V.; Tudge, M. *Angew. Chemie - Int. Ed.* **2014**, *53* (19), 4802–4806.
- (164) Talele, T. T. *J. Med. Chem.* **2016**, *59* (19), 8712–8756.
- (165) Welch, C. J.; Gong, X.; Schafer, W.; Pratt, E. C.; Brkovic, T.; Pirzada, Z.; Cuff, J. F.; Kosjek, B. *Tetrahedron Asymmetry* **2010**, *21*, 1674–1681.
- (166) Bellomo, A.; Celebi-Olcum, N.; Bu, X.; Rivera, N.; Ruck, R. T.; Welch, C. J.; Houk, K. N.; Dreher, S. D. *Angew. Chemie - Int. Ed.* **2012**, *51* (28), 6912–6915.
- (167) Buitrago Santanilla, A.; Regalado, E. L.; Pereira, T.; Shevlin, M.; Bateman, K.; Campeau, L.-C.; Schneeweis, J.; Berritt, S.; Shi, Z.-C.; Nantermet, P.; Liu, Y.; Helmy, R.; Welch, C. J.; Vachal, P.; Davies, I. W.; Cernak, T.; Dreher, S. D. *Science (80-.)*. **2015**, *347* (6217), 49–53.
- (168) Chan, D. M. T.; Monaco, K. L.; Wang, R. P.; Winters, M. P. *Tetrahedron Lett.* **1998**, *39* (19), 2933–2936.
- (169) Lam, P. Y. S.; Vincent, G.; Bonne, D.; Clark, C. G. *Tetrahedron Lett.* **2003**, *44* (26), 4927–4931.
- (170) Chan, D. M. T.; Monaco, K. L.; Li, R.; Bonne, D.; Clark, C. G.; Lam, P. Y. S. *Tetrahedron Lett.* **2003**, *44* (19), 3863–3865.
- (171) King, A. E.; Brunold, T. C.; Stahl, S. S. *J. Am. Chem. Soc.* **2009**, *131* (14), 5044–5045.
- (172) Vantourout, J. C.; Miras, H. N.; Isidro-Llobet, A.; Sproules, S.; Watson, A. J. B. *J. Am. Chem. Soc.* **2017**, *139* (13), 4769–4779.
- (173) Chan, D. M. T.; Lam, P. Y. S. *Reactions* **2005**, 315–361.
- (174) Hall, D. G. *Structure, Properties, and Preparatio of Boronic Acid Derivatives. Overview of Their Reactions and Applications*, 2nd ed.; Wiley-VCH Verlag GmbH & Co. KGaA, Ed.; Wiley-VCH Verlag GmbH & Co. KGaA: Weinheim, 2011.
- (175) Boström, J.; Brown, D. G.; Young, R. J.; Keserü, G. M. *Nat. Drug Discov.* **2018**, 10.0.4.14/nrd.2018.116.
- (176) Atencia, J.; Beebe, D. J. *Nature* **2005**, *437* (7059), 648–655.
- (177) Pallenberg, A. J.; Koenig, K. S.; Barnhart, D. M. *Inorg. Chem.* **1995**, *34* (11), 2833–2840.
- (178) Crutchley, R. J.; Hynes, R.; Gabe, E. J. *Inorg. Chem.* **1990**, *29* (24), 4921–4928.
- (179) Sheremetev, A. B.; Palysaeva, N. V.; Struchkova, M. I.; Suponitsky, K. Y.; Antipin, M. Y. *Eur. J. Org. Chem.* **2012**, *11*, 2266–2272.
- (180) Desimoni, G.; Fàita, G.; Jørgensen, K. A. *Chem. Rev.* **2006**, *106* (9), 3561–3651.
- (181) Liu, M. Y.; Hong, S. Bin; Zhang, W.; Deng, W. *Chinese Chem. Lett.* **2015**, *26* (3), 373–376.
- (182) Zhou, Z. Z.; Liu, M.; Li, C. J. *ACS Catal.* **2017**, *7* (5), 3344–3348.
- (183) Kumaraswamy, G.; Rao, G. V.; Murthy, A. N.; Sridhar, B. *Synlett* **2009**, *7*, 1180–1184.
- (184) Kohout, J.; Kratsmar-Smogrovic, J. *Chem. Zvesti.* **1968**, *22*, 481–492.
- (185) Ishikawa, T. *Superbases for Organic Synthesis: Guanidines, Amidines, Phosphazenes and Related*

- Organocatalysts*, 1st ed.; Ishikawa, T., Ed.; John Wiley & Sons, Ltd: Chichester, 2009.
- (186) Trötz Müller, M.; Guo, X.; Fauland, A.; Köfeler, H.; Lankmayr, E. *J. Mass Spectrom.* **2011**, *46* (6), 553–560.
- (187) Annesley, T. M. *Clin. Chem.* **2003**, *49* (7), 1041–1044.
- (188) Awad, H.; Khamis, M. M.; El-Aneed, A. *Appl. Spectrosc. Rev.* **2015**, *50* (2), 158–175.
- (189) Keller, B. O.; Sui, J.; Young, A. B.; Whittal, R. M. *Anal. Chim. Acta* **2008**, *627* (1), 71–81.
- (190) King, R.; Bonfiglio, R.; Fernandez-Metzler, C.; Miller-Stein, C.; Olah, T. *J. Am. Soc. Mass Spectrom.* **2000**, *11* (11), 942–950.
- (191) Mallet, C. R.; Lu, Z.; Mazzeo, J. R. *Rapid Commun. Mass Spectrom.* **2004**, *18* (1), 49–58.
- (192) Furey, A.; Moriarty, M.; Bane, V.; Kinsella, B.; Lehane, M. *Talanta* **2013**, *115*, 104–122.
- (193) Biscoe, M. R.; Fors, B. P.; Buchwald, S. L. *J. Am. Chem. Soc.* **2008**, *130* (21), 6686–6687.
- (194) Reed, G. F.; Lynn, F.; Meade, B. D. *Clin. Diagn. Lab. Immunol.* **2002**, *9* (6), 1235–1239.
- (195) Hahne, H.; Pachl, F.; Ruprecht, B.; Maier, S. K.; Klaeger, S.; Helm, D.; Médard, G.; Wilm, M.; Lemeer, S.; Kuster, B. *Nat. Methods* **2013**, *10* (10), 989–991.
- (196) Strzelecka, D.; Holman, S. W.; Evers, C. E. *Int. J. Mass Spectrom.* **2015**, *391*, 157–160.
- (197) Gritti, F.; Guiochon, G. *J. Chromatogr. A* **2010**, *1217* (52), 8167–8180.
- (198) Muller, E. I.; Abad, F.; Dallarosa, J.; Adriano, C.; Cruz de Oliveira, E. *Quim. Nov.* **2010**, *33* (4), 984–987.
- (199) Zhang, X. D. Yang, X. C. Chung, N. Gates, A. Stec, E. Kunapuli, P. Holder, D. J. Ferrer, M. Espeseth, A. S. *Pharmacogenomics* **2006**, *7* (3), 299–309.
- (200) Chung, N.; Zhang, X. D.; Kreamer, A.; Locco, L.; Kuan, P. F.; Bartz, S.; Linsley, P. S.; Ferrer, M.; Strulovici, B. *J. Biomol. Screen.* **2008**, *13* (2), 149–158.
- (201) Pukelsheim, F. *Am. Stat.* **1992**, *48* (2), 88.
- (202) Miller, J. *Q. J. Exp. Psychol. A.* **1991**, *43* (3), 907–912.
- (203) Ley, C.; Klein, O.; Bernard, P.; Licata, L.; Leys, C. *Q. J. Exp. Psychol. A.* **2013**, *49*, 764.
- (204) Rousseeuw, P. J.; Croux, C. *J. Am. Stat. Assoc.* **1991**, 1273.
- (205) Ventura, O. N.; Kieninger, M. *Pure Appl. Chem.* **1998**, *70* (12), 2301–2307.
- (206) Kilburg, D.; Gallicchio, E. In *Insights into Enzyme Mechanisms and Functions from Experimental and Computational Methods*; Christov, C. Z., Ed.; Advances in Protein Chemistry and Structural Biology; Academic Press, 2016; Vol. 105, pp 27–57.
- (207) van Eldik, R.; Harvey, J. In *Theoretical and Computational Inorganic Chemistry*; van Eldik, R., Harvey, J., Eds.; Advances in Inorganic Chemistry; Academic Press, 2010; Vol. 62, pp xi–xii.
- (208) Darden, T. A.; Bartolotti, L.; Pedersen, L. G. *Environ. Health Perspect.* **1996**, *104*, 69–74.
- (209) Bachrach, S. M. *Computational organic chemistry / Steven M. Bachrach.*; 2007.
- (210) Weissman, S. A.; Anderson, N. G. *Org. Process Res. Dev.* **2015**, *19* (11), 1605–1633.
- (211) Murray, P. M.; Tyler, S. N. G.; Moseley, J. D. *Org. Process Res. Dev.* **2013**, *17* (1), 40–46.
- (212) Kutchukian, P. S.; Dropinski, J. F.; Dykstra, K. D.; Li, B.; DiRocco, D. A.; Streckfuss, E. C.; Campeau, L.-C.; Cernak, T.; Vachal, P.; Davies, I. W.; Krska, S. W.; Dreher, S. D. *Chem. Sci.* **2016**, *7* (4), 2604–2613.
- (213) Sigman, M. S.; Harper, K. C.; Bess, E. N.; Milo, A. *Acc. Chem. Res.* **2016**, *49* (6), 1292–1301.
- (214) Milo, A.; Neel, A. J.; Toste, F. D.; Sigman, M. S. *Science* (80-.). **2015**, *347* (6223), 737–743.
- (215) Neel, A. J.; Hilton, M. J.; Sigman, M. S.; Toste, F. D. *Nature* **2017**, *543* (7647), 637–646.
- (216) Ahneman, D. T.; Estrada, J. G.; Lin, S.; Dreher, S. D.; Doyle, A. G. *Science* (80-.). **2018**.
- (217) Bull, S. D.; Davidson, M. G.; Van Den Elsen, J. M. H.; Fossey, J. S.; Jenkins, A. T. A.; Jiang, Y.-B.; Kubo, Y.; Marken, F.; Sakurai, K.; Zhao, J.; James, T. D. *Acc. Chem. Res.* **2013**, *46* (2), 312–326.
- (218) He, C.; Chen, C.; Cheng, J.; Liu, C.; Liu, W.; Li, Q.; Lei, A. *Angew. Chemie - Int. Ed.* **2008**, *47* (37), 6414–6417.
- (219) Dufert, M. A.; Billingsley, K. L.; Buchwald, S. L. *J. Am. Chem. Soc.* **2013**, *135* (34), 12877–12885.
- (220) Smith, M. K.; Northrop, B. H. *Chem. Mater.* **2014**, *26* (12), 3781–3795.
- (221) Metola, P.; Chapin, B. M.; Anslyn, E. V. In *Boron: Sensing Synthesis and Supramolecular Self-Assembly*; The Royal Society of Chemistry, 2016; pp 44–60.
- (222) Harris, R. K.; Olivieri, A. C. *Prog. NMR Spectrosc.* **2000**, *24*, 435–456.
- (223) Oh, S.; Weiss, J. W. E.; Kerneghan, P. A.; Korobkov, I.; Maly, K. E.; Bryce, D. L. *Magn. Reson. Chem.* **2012**, *50*, 388–401.
- (224) Bruns, S.; Sinnwell, V.; Voss, J. *Magn. Reson. Chem.* **2003**, *41*, 269–272.
- (225) Colson, K. L. *Mod. Drug Discov.* **2003**, 47–49.
- (226) Little, M. A.; Varoquaux, G.; Saeb, S.; Lonini, L.; Jayaraman, A.; Mohr, D. C.; Kording, K. P. *Gigascience* **2017**, *6*, 1–6.
- (227) Mohsen, H.; Kurban, H.; Zimmer, K.; Jenne, M.; Dalkilic, M. M. Big Data Conference, **2015**, 118–125.
- (228) Hahn-Deinstrop, E. *Applied thin layer chromatography: best practice and avoidance of mistakes / Elke Hahn-Deinstrop; translated by R.G. Leach.*, 1st ed.; KGaA, W.-V. V. G. & C., Ed.; Wiley-VCH Verlag GmbH & Co. KGaA: Weinheim, 2000.
- (229) Miyaura, N.; Suzuki, A. *Chem. Rev.* **1995**, *95* (7), 2457–2483.
- (230) Ishiyama, T.; Murata, M.; Miyaura, N. *J. Org. Chem.* **1995**, *60* (23), 7508–7510.

- (231) Fyfe, J. W. B.; Watson, A. J. B. *Chem* **2017**, *3* (1), 31–55.
- (232) Hennings, D. D.; Iwama, T.; Rawal, V. H. *Org. Lett.* **1999**, *1* (8), 1205–1208.
- (233) Wang, L.; Zhang, Y.; Liu, L.; Wang, Y. *J. Org. Chem.* **2006**, *71* (3), 1284–1287.
- (234) Ji, H.; Wu, L. Y.; Cai, J. H.; Li, G. R.; Gan, N. N.; Wang, Z. H. *RSC Adv.* **2018**, *8* (25), 13643–13648.
- (235) Atack, T. C.; Cook, S. P. *J. Am. Chem. Soc.* **2016**, *138*, 6139–6142.
- (236) Yao, W.; Fang, H.; Peng, S.; Wen, H.; Zhang, L.; Hu, A.; Huang, Z. *Organometallics* **2016**, *35* (10), 1559–1564.
- (237) Lima, F.; Kabeshov, M. A.; Tran, D. N.; Battilocchio, C.; Sedelmeier, J.; Sedelmeier, G.; Schenkel, B.; Ley, S. V. *Angew. Chemie - Int. Ed.* **2016**, *55* (45), 14085–14089.
- (238) Lima, F.; Sharma, U. K.; Grunenber, L.; Saha, D.; Johannsen, S.; Sedelmeier, J.; Van der Eycken, E. V.; Ley, S. V. *Angew. Chemie - Int. Ed.* **2017**, *56* (47), 15136–15140.
- (239) Longstaff, C.; Rose, M. E. *Org. Mass Spectrom.* **1982**, *17* (10), 508–518.
- (240) Waizumi, K. *Inorganica Chim. Acta* **1995**, *238* (1–2), 121–127.
- (241) Musinu, A.; Paschina, G.; Piccaluga, G.; Magini, M. *J. Chem. Phys.* **1984**, *80* (6), 2772–2776.
- (242) Anderson, J. M.; Kochi, J. K. *J. Am. Chem. Soc.* **1970**, *92* (6), 1651–1659.
- (243) Hughes, J. P.; Rees, S.; Kalindjian, S. B.; Philpott, K. L. *Br. J. Pharmacol.* **2011**, *162*, 1239–1249.
- (244) Wang, J.; Sánchez-Roselló, M.; Aceña, J. L.; Del Pozo, C.; Sorochinsky, A. E.; Fustero, S.; Soloshonok, V. A.; Liu, H. *Chem. Rev.* **2014**, *114* (4), 2432–2506.
- (245) Armarego, W. L. F.; Chai, C. L. L. *Purification of Organic Chemicals*, 6th Ed.; Butterworth-Heinemann: Oxford, 2009.
- (246) Sargent, M.; Sage, A.; Wolff, C.; Mussell, C.; Neville, D.; Lord, G.; Saeed, M.; Lad, R.; Hird, S.; Varwick, V.; Godfrey, A. R. *Guide to achieving reliable quantitative LC-MS measurements*; RSC Analytical Methods Committee, Ed.; 2013.
- (247) Hitosugi, S.; Tanimoto, D.; Nakanishi, W.; Isobe, H. *Chem. Lett.* **2012**, *41* (9), 972–973.

Chapter 7: Chan-Lam Experimental

7.1. General Considerations

Nanoscale Reaction Optimisation

Nanoscale reactions (250-500 nmol) were run on Greiner® 1536-well plates (Cat No. 792870-906, Cyclic Olefin-Copolymer (COC) plastic, 16.0 µL-wells, flat bottom, clear) as reaction plates, and with Axygen® 384-well plates (Cat No. P-284-120SQ-C, Polypropylene, 120 µL, V-bottom, translucent) were used as the source plate for stock solution and for analytical plates on LCMS equipment. Dosing of mother plate components into 384- and 1536-well plates was achieved using a Mosquito® HTS liquid handling robot (Figure 10, TTP Labtech, 4.5mm pitch tip spool) with no special modifications. Upon dosing, the 1536-well plates were covered in tin-foil, flattened with a plate roller (Sigma Aldrich, Cat. No R1275) and placed under a glass sheet to minimise evaporation.

LCMS Crude Reaction Assay

Reactions were analysed using a Shimadzu LCMS; SIL-20AC XR autosampler, 2 × LC-20 AD XR pumps, CBM-20A communicator, SPD-M20A PDA, CTO-20AC column oven and LCMS-2020 mass spectroscopy unit. The 384-well analysis plate was placed into autosampler on a Shimadzu microtiter plate (MTP) rack. All samples were run on a Kinetex® 2.6 µm, 50 × 2.1 mm, 100 Å C18 column (PN: H16-189446) with mobile phase stock solutions: A = 2.5 L acetonitrile + 131 mL water + 1.25 mL and formic acid, B = 2.4 L water + 1.50 g ammonium formate + 2.4 mL formic acid. The autosampler was washed between each run with a 1:1 mixture of acetonitrile:water. The mass spectrum unit was set to dual mode atmospheric pressure chemical ionisation (APCI) and electrospray ionisation (ESI) mode termed DUIS in the positive mode and set for selective ion monitoring of [M+1] for product and internal standard (scan speed 15000u). Data analysis was undertaken using Shimadzu Lab Solutions software and exported into Microsoft Excel for further statistical tests. At the time of preparing this thesis, there are no LCMS autosamplers that are compatible with 1536 well plates.

Millimolar Scale Chemistry Experiments

Millimole reactions (0.3 mmol) were carried out in glass microwave vials (Kinesis, VMW20-C-50, 20 mL, round bottom) equipped with magnetic stirrer bars. Liquid handling was done using Viaflo II electronic pipettes (Integra, Cat. No. 4013 ,300 µL, single channel).

Compound Purification

Purification of millimolar scale reactions was completed using standard silica flash column chromatography (Fluka or Material Harvest silica gel (230–400 mesh)). Mobile phase solvents were distilled using traditional methods reported by Armarego.²⁴⁵

Compound Characterisation

Proton nuclear magnetic resonance (^1H NMR) spectra were recorded on a Bruker AM 400 (400 MHz) or an Avance 500 (500 MHz) spectrometer. Chemical shifts (δ) are reported in parts per million (ppm) and quoted to the nearest 0.01 ppm relative to the residual protons in CDCl_3 (7.26 ppm), C_6D_6 (7.16), $(\text{CD}_3)_2\text{SO}-d_6$ and coupling constants (J) are quoted in Hertz (Hz). Data are reported as follows; chemical shift (multiplicity, coupling constant, number of protons, assignment). Coupling constants were reported to the nearest 0.1 Hz and multiplicity reported according to the following convention: s = singlet, d = doublet, t = triplet, q = quartet, m = multiplet, br = broad and associated combinations e.g. dd = double of doublets. Where coincident coupling constants have been observed, the apparent (app) multiplicity of the proton resonance has been reported. Carbon nuclear magnetic resonance ($\{^1\text{H}\} \text{ }^{13}\text{C}$ NMR) spectra were a Bruker AM 400 (100 MHz) or an Avance 500 (125 MHz) spectrometer. Chemical shift (δ) was measured in ppm and quoted to the nearest 0.1 ppm relative to the residual solvent peaks in CDCl_3 (77.16), $(\text{CD}_3)_2\text{SO}-d_6$. Fluorine nuclear magnetic resonance (^{19}F NMR) were recorded on a Bruker AM 400 (376 MHz).

Infrared (IR) spectra were recorded on a Perkin Elmer Spectrum One FT-IR spectrometer as thin films deposited in chloroform or as solids. HRMS were measured at the EPSRC Mass Spectrometry Service at the University of Swansea. Melting points (m.p.) were recorded using a Gallenkamp melting point apparatus and are reported uncorrected.

Materials

Solvents

Dimethylsulfoxide was purchased from Alfa Aesar and used without anhydrous precautions. HPLC Acetonitrile and water was purchased from Fisher Scientific and used without anhydrous precautions.

Boronic esters

Boronic esters were purchased from Sigma Aldrich, Fluorochem, TCI, Acros or Alfa Aesar and used without further purification. Synthesised boronic esters were prepared from commercial substrates and according to literature conditions.

Copper salts

All copper sources were purchased from commercial sources and stored at room temperature in a desiccator. Copper (I) chloride was purified according to literature procedures.²⁴⁵ Copper (II) chloride and triflate were dried *in vacuo* at 100 °C for 12 hours before being stored in a desiccator without further purification. Copper (I) thiophene-2-carboxylate, copper (II) nitrate, tetrafluoroborate, bromide and acetate were stored in a desiccator and used without purification.

Bases

All bases were purchased from commercial sources. DBU was purchased from Sigma Aldrich and purified by Kugelrohr bulb-to-bulb distillation (50 °C @ 600 mbar) to give the corresponding bases as a colourless oil. Phosphazine bases were purchased from Sigma Aldrich and stored in 5 °C fridge.

Ligands

All ligands were purchased from commercial sources and stored at room temperature.

7.2. General Procedures

7.2.1. Nanoscale General Procedures

General Procedure 1: Source plate preparation

Stock solutions were prepared according to the corresponding high-throughput Excel spreadsheet. All reagents were freshly prepared in Eppendorf vials (StarLab TubeOne[®] Microcentrifuge tubes, 1.5 mL, natural PN: S1615-5500) and dissolved in DMSO. Liquid reagents were pipetted into the Eppendorf vial and made up to the correct stock solution volume with DMSO. Stock solutions were sonicated for 5 minutes and subsequently mixed by Vortex mixer to ensure homogeneity. Reagents that were not in solution were gently heated with a heat-gun, sonicated and left to cool to room temperature. Source plates were prepared according to source plate maps with the specified volumes in the high-throughput Excel spreadsheet.

General Procedure 2: Reactor plate dosing

Before each reactor plate was prepared, the 1536-well plate was optimised using the “Pipette XOffset” and “Pipette YOffset” functions to ensure the pipette dosed in the centre of each well. Each plate was prepared using the corresponding Mosquito protocol (Appendix 3). The reactions were then covered with aluminium foil and sealed with a plate-sealing roller. Sealed reactor arrays were placed under a heavy glass sheet and left to stand at room temperature for 24 hours.

General Procedure 3: Analysis plate preparation

A 384-well plate was prepared with 50 µL of 50:50 formic acid:water quench solution of a product-specific IS**368** concentration (Table 8, Table 9, or Table 10). A “wash plate” was also prepared with 85 µL of DMSO into columns equalling twice the number of substrates screened on the high-throughput array, i.e. 1 substrate = 2 columns, 3 substrates = 6 columns. The analysis plate was subsequently prepared with 100 nL of reaction mixture according to analysis plate protocols 1-4 for 1x1x8x2x6 screens or 5-6 for 1x3x4x2x4 screens. Once reaction mixture was added, the analysis plate was topped up with 40 µL of water and sealed using a 384-well plate seal (PN: 4ti-0516/384).

General Procedure 4: Calibration curve sample preparation

1x1x8x2x6

Four LCMS vials were prepared with 500 µL of the corresponding product-specific IS**386** concentration (Table 8 or Table 9). A 2.5 mM stock solution (**SS1**) of product was prepared and 500 µL (for 0.1M reactions) and 250 µL (for 0.05M reactions) was serial diluted into a 5 mL

volumetric flask (**SS2**). 401 μL of **SS2** was added into the first vial which denoted 100% yield. The remaining three LCMS vials were charged with 300, 200 and 100 μL of **SS2** and topped up with 101, 201, 301 μL of water to ensure the correct concentration. The vials were sealed with parafilm and placed into the controller rack of the LCMS.

1x3x4x2x4

Three LCMS vials were prepared with 500 μL of the corresponding product-specific IS386 concentration (Table 10). A 2.5 mM stock solution (**SS1**) of product was prepared and 500 μL (for 0.1M reactions) and 250 μL (for 0.05M reactions) was serial diluted into a 5 mL volumetric flask (**SS2**). 401 μL of **SS2** was added into the first vial which denoted 100% yield. The remaining two LCMS vials were charged with 250 and 100 μL of **SS2** and topped up with 251 and 301 μL of water respectively to ensure the correct concentration. The vials were sealed with parafilm and placed into the controller rack of the LCMS.

General Procedure 5: Mass spectrometer cleaning

Prior to each quantitative high-throughput analysis run, the LCMS was cleaned to ensure a stable internal standard ionisation. Firstly, the LCMS was shut down using the “Auto ShutDown” feature embedded in the software. Once, complete, the power to the entire machine was switched off, including the mass spectrometer. The APCI high-voltage cable was disconnected and the door to the corona needle opened to access the ionisation chamber. The corona needle was removed with a flathead screw driver and sonicated in methanol for 15 minutes. The inside of the chamber was inspected and any salt build-up removed using compressed air.

The top of the mass spectrometer was removed to access the octopole, prequads and skimmer. The octopole was removed initially, firstly removing the red wire and then the two black thumb screws and attached wires. The octopole was lifted out, immersed in methanol and sonicated for 15 minutes. The skimmer and prequads were subsequently removed. The three screws on the skimmer are removed to reveal two rubber seals (one on the prequads, one on the skimmer) which were set aside before sonication. Both the prequads and the skimmer were then sonicated for 15 minutes each.

All the cleaned parts were left to air dry and returned to the mass spectrometer. The mass spectrometer was turned on and vacuum pump started using the ‘autostartup’ feature embedded in the LCMS software. The vacuum was left to “settle” overnight to ensure a stable vacuum. Once stable, autotuning was completed using the recommended standard. The new tuning file was then used throughout the high-throughput run. **NB:** This tune file cannot be reused in

subsequent high-throughput analysis and, therefore, the entire process needs to be completed to before each high-throughput analysis.

General Procedure 6: Excel data capture

Once analysis was completed, the data was analysed using the “LCMS-browser” in the Shimadzu software. The mass spectrum parameters were changed in the “edit” mode of the mass spectrometer window (Figure 50) to the product analysed in the screen. “View” was then pressed to confirm the changes. Peak integration was automated in the “edit” mode again in the program button for both IS386 and product using the “Integration off” from 0.00, “Integration On” from the start of the peak, “Peak Top” at the middle of the peak and “Integration off” from the end of the peak. Once completed for both IS386 and product, the view button was pressed to confirm the changes.

The new settings were applied to the entire table by highlighting the “Area” column and, through the “Process” tab at the top of the page, the “Process Results by ID” was then used and the IS386 and product settings were applied. Data could then be copied to Notepad and transferred to the Excel spreadsheet. **NB:** Data is taken from the LCMS in chronological order and therefore needs to be reversed in the Excel spreadsheet.

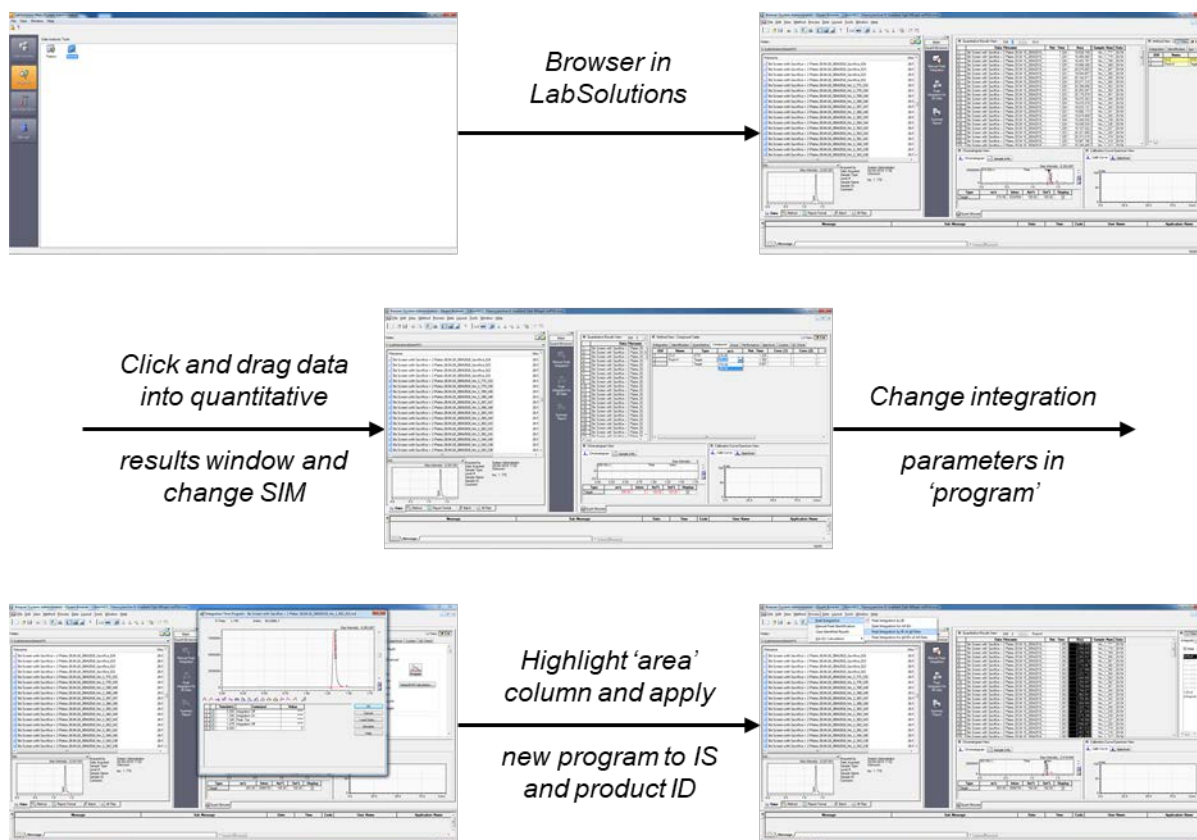


Figure 50: Quantitative data analysis using LabSolutions browser.

7.2.2. Milliscale General Procedures

General Procedure 7: Boronic acid esterification

An oven dried round bottom flask was charged with boronic ester (1.0 equiv.), pinacol (1.05 equiv.) and magnesium sulfate (5.0 equiv.) in dichloromethane (0.5 M). The resulting suspension was stirred for 6 hours and filtered. The filtrate was concentrated *in vacuo* and the resulting product purified by flash column chromatography.

General Procedure 8: Preparation of LCMS product standards

An oven dried microwave vial equipped with a magnetic stirrer bar was charged with following stock solutions: 4-phenylpiperidine (600 μL of 0.50 M), boronic ester (1200 μL of 0.25 M) and 1,10-phenanthroline (600 μL of 0.05 M). The corresponding solution was stirred for 3 minutes. The reaction was charged with the copper(I) chloride (600 μL of 0.05 M) stock solution and the resulting coloured solution was reacted, open to the air, for 24 hours. The corresponding reaction mixture was poured onto aqueous saturated ammonium chloride (27 mL) and extracted with ethyl acetate (3×20 mL). The combined organic extracts were dried (MgSO_4), filtered and concentrated *in vacuo*. The resulting crude material was purified by flash column chromatography to give the corresponding tertiary amine.

General Procedure 9: Millimole scale validation of nanomole scale high-throughput quantitative assay

An oven dried microwave vial equipped with a magnetic stirrer bar was charged with following stock solutions: 4-phenylpiperidine (600 μL of 0.50 M), boronic ester (1200 μL of 0.25 M), base (600 μL of 0.5 M) and ligand (300 μL of 0.1 M). The corresponding solution was stirred for 3 minutes. The reaction was finally charged with the catalyst (300 μL of 0.1 M) stock solution and the resulting coloured solution was reacted, open to the air, for 24 hours. The corresponding reaction mixture was poured onto aqueous saturated ammonium chloride (27 mL) and extracted with ethyl acetate (3×20 mL). The combined organic extracts were dried (MgSO_4), filtered and concentrated *in vacuo*. 1,1,2,2-tetrachloroethane (31.5 μL , 0.3 mmol) was added to the crude mixture and diluted with CDCl_3 (2.0 mL) and quantified by NMR.

7.3. Three Variable Optimisation of the Chan-Lam Reaction. 96 to 384-well plate

Stock solution preparation

Procedure for 384 nanomolar scale reactions (5.0 μL volume) in a 384-well plate. Stock solutions of each component were prepared according to general procedure 1: 4-phenylpiperidine **134** (1.0 M in DMSO), boronic acid (**311-313**, 0.33 M in DMSO), MTBD (**317**, 3M in DMSO), ligand (**318-328**, 0.025 M in DMSO), catalyst (C1-C8, 0.1 M in DMSO) using Spreadsheet 1. For the source plate layout, see Figure 52. For each 1536-well plate experiment, each well was charged with the amount of stock solution stated in 'Source plate loading' column, using a digital air displacement pipette, such that enough solution was present to dose the corresponding reactor plate.

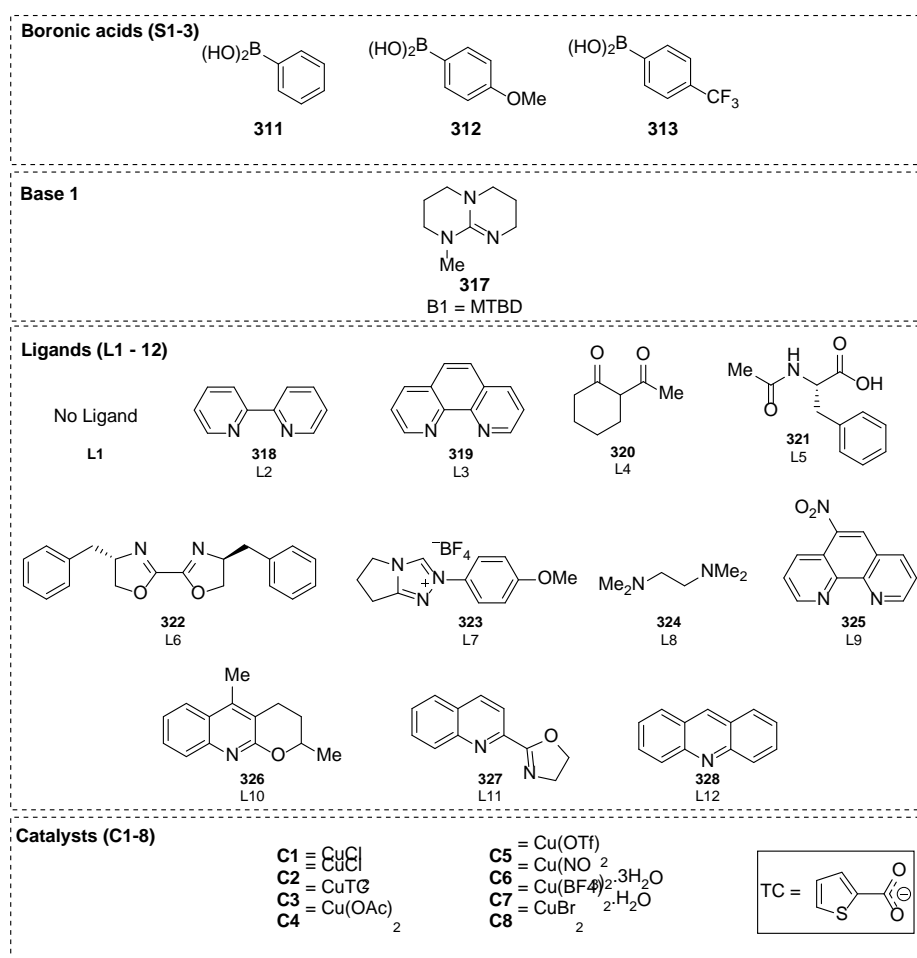


Figure 51: Reaction components assessed using 96-well source plates and 384-well reactor plates.

Reactor plate dosing

Reactor plates were prepared using Mosquito protocol 1. The Mosquito was used to dispense 1000 nL aliquots of each reagent stock solution from two 96-well source plates to one 384-well: 4-phenylpiperidine was added in 1000 nL, boronic acid **311-313** were added in 1000 nL, base (B1-8) was added in 1000 nL, Ligand (L1-2) was added in 1000 nL and catalyst (C1-8) were added in 1000 nL resulting in a total reaction volume of 5.0 μ L. The mosquito mixed the reaction mixture together three times using the mix-dispense feature.

96-well source plate layout

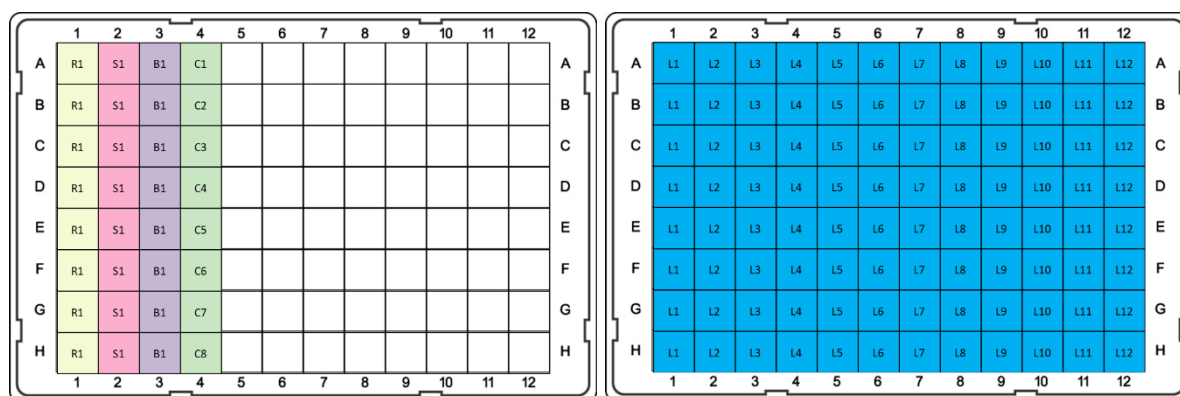


Figure 52: Two source plates used for reactor plate preparation.

Analysis plate preparation

The analysis was prepared in a similar manner to previous literature reports.¹⁶⁷ 100 μ L of 5% AcOH in DMSO was added to each well and the plate was sealed with an aluminium adhesive plate seal. Each plate was run overnight using a 1.8-minute run taking 15 hours to complete an entire 384-well plate. Once analysis was complete, peak integrals of both product and internal standard were taken and a ratio of product : internal standard was calculated. Heatmaps were created to show uncalibrated performance of each reaction.

PLATE 1536	# reagents 5	How much of plate? All	input wells/column 32	Scale L.R. (umol) 0.5	Final conc. Rxn (M) 0.1	Stand. Aliq. (uL) 1	Daughter tot vol (uL) 5	
Reaction parameters constant?	Reagent	Compound	CAS	Cat No	FW (gMol-1)	Amount (uMol)	mg per rxn	Solubility problems? Aliquot vol(uL)
(constant)	R1	4-phenylpiperidine	771-99-3	P 034	161.12	0.5	8.1E-02	1.00
(constant)	R2	PhenylBPin		THE	321.136	0.5	1.61E-01	1.00
(x-constant, y-variable)	B1	MTBD	84030-20-6	Dave	153.22	1.5	2.30E-01	1.00
(x-constant, y-variable)	C1	Cu(I)Cl	7758-89-6	cat 025	99.00	0.1	4.95E-03	1.00
	C2	Cu(II)Cl2		Dessi	134.45	0.1	6.72E-03	1.00
	C3	Cu(I)TC	68986-76-5	IC028	190.69	0.1	9.53E-03	1.00
	C4	Cu(II)OAc2	142-71-2	cat 188	181.63	0.1	9.08E-03	1.00
	C5	Cu(II)OTf2	34946-82-2	cat 150	361.68	0.1	1.81E-02	1.00
	C6	Cu(II)(NO3)2.3H2O	10031-43-3	IC010	241.60	0.1	1.21E-02	1.00
	C7	Cu(II)BF4.2.H2O	20721-39-9	IC014	237.16	0.1	1.19E-02	1.00
	C8	Cu(II)Br2	7789-45-9	IC022	223.35	0.1	1.12E-02	1.00
(x-variable, y-constant)	L1	no ligand	n/a			N/A	N/A	1.00
	L2	2,2-bipyridyl	366-18-7	B 462	156.19	0.1	7.81E-03	1.00
	L3	1,10-phenanthroline	66-71-7	P 228	180.21	0.1	9.01E-03	1.00
	L4	2-acetyl-cyclohexanone	874-23-7	FDG-A 025	140.18	0.1	7.01E-03	1.00
	L5	N-Acetyl-L-phenylalanine	2018-61-3	A044	207.23	0.1	1.04E-02	1.00
	L6	2,2-Bis((4S)-(-)-4-isopropylloxazoline)propane	131833-92-6	Box 004	266.38	0.1	1.39E-02	1.00
	L7	1,3-Bis(2,6-disisopropylphenyl)imidazolium chloride	250285-32-6	cat 078	425.05	0.1	2.13E-02	1.00
	L8	TMEDA	110-18-9	T 120	116.24	0.1	5.81E-03	1.00
	L9	5-Nitro-1,10-phenanthroline	4199-88-6	N 066	225.20	0.1	1.13E-02	1.00
	L10	Li-Quinoline	151657-37-3	Ben/Jaime	213.28	0.1	1.07E-02	1.00
	L11	2-(4,5-dihydro-2-oxazolyl)quinoline	202191-12-6	D 166	198.22	0.1	9.91E-03	1.00
	L12	acridine	260-94-6	A186	179.22	0.1	8.96E-03	1.00

Stock solution (mg/vial)	Stock solution (solvent/vial)	Stock solution (min vol/vial)	Mother (abs vol/well)	Mother (rec vol/well)	Source plate loading (vol/well uL)	Liquid reagents (Vol/SS)	DMSO Top-up
32.2	400	691	24	43	25	X	X
112.4	700	691	24	43	43.75	X	X
114.9	500	1382	48	86	31.25	112.9	387.1
2.0	400	173	48	86			
2.7	400	173	48	86			
3.8	400	173	48	86			
3.6	400	173	48	86			
7.2	400	173	48	86			
4.8	400	173	48	86			
4.7	400	173	48	86			
4.5	400	173	48	86			
N/A	400		3	7			
3.1	400	58	4	7			
3.6	400	58	4	7			
2.8	400	58	4	7			
4.1	400	58	4	7			
5.3	400	58	4	7			
8.5	400	58	4	7			
2.3	400	58	4	7			
4.5	400	58	4	7			
4.3	400	58	4	7			
4.0	400	58	4	7			
3.6	400	58	4	7			

Spreadsheet 1: High-throughput screen of Chan-Lam reaction (1 x 1 x 1 x 8 x 12 screen). All reagents were prepared and added to the source plate.

Phenylboronic acid, **311**

		L12		L11		L10		L9		L8		L7		L6		L5		L4		L3		L2		L1	
22.9	21.8	29.3	26.4	34.1	24.2	29.4	28.6	25.9	23.4	6.5	7.8	21.6	24.0	25.4	19.7	17.6	16.9	37.7	41.9	36.5	36.4	22.1	22.2		
21.0	21.5	33.3	36.7	26.5	25.5	28.0	30.7	24.6	24.1	6.8	7.1	17.0	19.7	24.3	27.2	18.9	16.2	39.5	49.0	42.2	43.8	20.2	31.6		
18.9	20.2	28.7	15.6	14.0	13.5	10.8	14.8	11.3	13.3	2.8	3.8	9.0	14.8	10.2	19.6	0.6	15.8	15.5	47.5	22.3	36.9	11.5	22.1		
26.5	13.5	31.5	14.6	22.8	12.8	17.3	12.7	19.5	10.9	5.0	3.1	19.5	0.0	14.6	11.2	0.4	0.0	16.5	16.9	23.2	23.1	15.2	13.7		
16.6	19.8	32.3	27.4	23.4	23.4	33.3	35.9	23.2	19.9	7.8	10.4	22.6	13.7	22.1	19.6	14.9	15.5	51.1	62.0	45.0	40.1	20.2	20.0		
17.7	18.0	27.8	31.7	19.8	22.9	30.1	29.6	21.3	18.4	7.5	7.9	16.8	17.4	17.3	22.9	16.1	11.4	46.3	43.1	35.9	38.2	20.5	20.8		
21.6	20.0	28.7	25.8	24.1	24.8	23.1	25.6	21.7	23.6	5.1	7.1	21.0	22.8	19.8	18.7	3.0	11.6	34.7	46.4	38.2	45.0	25.5	24.0		
22.1	21.2	27.6	30.4	25.3	25.9	24.3	24.5	22.3	22.8	6.4	5.6	20.8	20.5	20.9	20.2	3.5	3.2	32.6	38.3	38.3	28.4	19.4	23.9		
22.1	22.2	33.4	35.3	24.8	25.6	30.4	33.5	22.2	24.2	9.0	13.7	27.9	26.2	31.6	29.8	23.3	23.8	55.8	53.9	45.7	48.7	28.5	25.1		
23.9	25.0	38.2	48.0	28.6	33.9	43.2	37.1	25.1	23.5	11.9	12.9	27.8	27.6	24.7	29.4	24.9	25.5	56.1	53.9	47.5	42.5	27.0	26.2		
18.0	21.3	37.8	35.4	24.3	27.6	36.9	38.4	23.8	22.7	10.5	13.4	22.4	29.8	22.9	31.6	21.4	22.9	49.2	56.6	44.7	53.5	24.1	24.9		
26.6	27.7	34.0	35.0	22.9	24.1	37.4	37.1	26.8	27.1	14.3	15.7	25.3	25.9	26.3	27.7	18.0	23.1	50.7	56.8	51.4	47.3	22.7	24.2		
24.7	28.3	39.6	35.7	29.1	26.1	28.7	32.0	25.9	25.7	8.0	10.0	27.1	25.3	0.0	20.7	12.7	11.4	38.9	44.3	37.6	43.0	18.4	19.1		
26.3	21.4	38.3	41.0	30.3	31.6	29.7	31.6	24.6	27.8	9.2	7.1	24.2	22.7	18.8	22.1	12.7	11.5	44.7	42.3	39.3	41.5	20.3	24.9		
24.9	26.7	35.8	35.5	26.6	31.0	25.1	30.2	26.2	25.4	7.6	7.0	21.0	21.3	27.9	31.5	4.6	4.4	34.8	37.9	42.1	39.9	28.2	23.6		
20.5	26.8	36.6	38.6	24.3	32.9	27.2	20.7	25.1	28.3	6.3	6.7	24.5	24.2	28.6	26.0	5.9	4.6	35.0	37.2	38.8	34.4	29.1	27.5		

4-Methoxyphenylboronic acid, 312

L12		L11		L10		L9		L8		L7		L6		L5		L4		L3		L2		L1	
109.9	82.8	230.3	228.3	169.8	113.9	230.5	39.7	78.9	86.5	20.8	18.9	41.2	30.9	58.1	37.8	1.8	2.6	59.5	68.1	67.5	69.8	50.7	48.5
22.6	70.2	45.8	96.7	41.1	71.3	85.9	105.0	110.4	109.4	27.0	17.2	76.9	92.5	46.2	47.1	3.9	3.6	74.0	80.3	119.8	152.1	100.1	120.4
11.2	25.6	10.8	48.4	10.7	34.8	33.5	71.9	28.7	32.5	10.4	0.9	12.8	39.8	5.5	24.9	0.3	2.7	36.4	83.7	39.8	118.0	22.6	95.9
2.5	13.7	5.9	16.5	16.6	31.4	37.9	14.2	24.6	31.3	2.1	3.7	7.1	10.6	7.2	6.5	0.3	0.6	34.3	44.0	32.2	50.4	14.3	36.9
51.8	25.4	117.7	81.2	83.0	50.9	62.7	22.5	31.4	96.9	11.5	2.6	71.2	79.3	79.2	43.6	26.3	1.1	121.9	147.0	145.4	104.5	78.1	90.4
24.0	61.8	68.6	34.1	103.5	88.2	76.3	37.1	85.3	42.1	20.0	3.1	53.5	61.9	63.8	46.3	33.6	5.2	98.2	90.3	93.2	110.8	52.6	63.9
68.6	60.8	67.1	85.7	94.8	81.1	47.8	46.7	86.4	96.2	17.9	9.4	54.2	61.2	51.9	30.1	1.5	2.5	71.4	101.2	78.8	122.9	52.6	98.1
14.1	43.3	28.2	118.6	53.0	35.6	61.5	52.0	103.6	41.1	13.6	2.8	45.2	22.0	23.2	7.1	0.8	1.3	56.3	71.1	87.7	87.2	57.0	77.2
11.1	67.8	196.1	149.3	72.2	82.8	154.6	99.0	79.3	0.0	47.7	18.5	95.7	93.5	92.6	84.9	4.7	5.7	98.5	113.9	156.4	131.3	115.0	108.4
0.6	112.2	93.9	159.1	15.0	83.3	102.3	69.6	68.7	52.6	18.1	10.0	79.4	44.3	46.7	33.3	27.0	1.6	98.5	74.0	149.2	123.5	103.3	107.0
64.2	40.5	165.7	BAD	36.4	56.8	84.5	73.5	65.2	61.3	19.0	9.6	68.0	83.3	71.1	71.0	10.6	8.9	86.1	105.4	150.6	190.7	127.1	116.8
43.1	88.9	106.9	127.8	36.5	41.2	55.3	72.8	44.5	50.7	15.0	3.4	36.2	44.4	44.1	33.9	11.4	4.9	90.0	88.2	133.4	137.3	107.1	101.8
31.3	26.7	52.6	22.5	60.4	8.6	50.9	10.9	28.3	13.8	13.4	5.3	52.5	49.7	34.2	24.1	0.9	0.9	67.1	53.6	90.6	82.3	74.3	52.8
9.1	42.8	21.6	46.0	16.2	37.9	65.7	69.8	36.8	45.1	15.5	4.4	0.0	58.4	44.0	19.8	0.6	1.0	54.5	58.7	78.6	93.9	57.7	79.9
51.4	20.6	108.4	64.7	44.5	50.0	90.9	20.7	14.1	22.6	19.0	0.0	65.3	99.8	73.2	51.3	BAD	1.8	75.0	74.4	123.2	112.3	87.8	82.1
15.7	36.0	31.5	85.9	12.9	35.4	BAD	64.0	52.7	53.8	18.6	0.0	55.9	57.3	56.5	42.0	1.3	1.4	60.0	61.2	109.0	124.1	82.7	97.3

4-Trifluoromethylphenylboronic acid, **313**

		L1		L2		L3		L4		L5		L6		L7		L8		L9		L10		L11		L12	
1.0	1.4	0.0	2.8	0.8	2.5	3.7	3.3	0.5	0.3	1.1	1.0	1.6	1.5	0.4	0.7	1.2	1.4	1.3	1.1	1.5	1.4	1.1	1.0	1.4	1.0
		0.8	1.0	1.6	1.1	2.2	2.6	0.2	0.4	0.6	0.6	1.7	1.3	0.1	0.2	1.0	1.2	0.9	0.9	1.3	1.1	0.9	0.8	1.1	1.0
0.3	0.2	0.4	0.7	0.2	0.6	1.1	1.5	0.0	0.1	0.3	0.1	0.9	0.2	0.2	0.2	0.3	0.3	0.6	0.5	0.3	0.3	0.6	0.6	0.6	0.2
		0.3	0.2	0.3	0.3	1.2	1.1	0.0	0.0	0.1	0.1	0.2	0.2	0.1	0.1	0.1	0.2	0.2	0.3	0.2	0.2	0.3	0.2	0.2	0.2
0.5	0.4	0.4	0.3	0.5	1.0	1.1	1.3	0.1	0.1	0.3	0.4	0.5	0.5	0.4	0.2	0.4	0.5	0.6	0.6	0.5	0.4	0.5	0.4	0.4	0.4
		0.3	0.4	0.6	0.5	1.5	1.3	0.1	0.1	0.2	0.3	0.4	0.4	0.1	0.1	0.4	0.4	0.4	0.6	0.6	0.4	0.6	0.3	0.3	0.4
0.5	0.5	0.8	0.9	1.4	0.7	1.8	1.7	0.1	0.1	0.3	0.3	0.5	0.4	0.2	0.2	0.5	0.8	0.7	0.7	0.6	0.6	0.8	0.7	0.7	0.6
		1.1	0.7	0.8	0.9	1.8	1.5	0.1	0.1	0.2	0.2	0.5	0.6	0.2	0.2	0.4	0.7	0.7	0.4	0.8	0.8	0.8	0.8	0.8	0.8
1.2	0.9	1.3	0.8	1.4	1.5	1.8	2.3	0.2	0.2	0.9	0.6	0.8	0.9	0.2	0.2	1.0	1.0	0.8	1.0	1.1	1.2	1.1	1.2	1.2	1.2
		0.9	1.1	1.6	1.8	2.0	1.6	0.2	0.4	1.2	0.9	1.0	1.9	0.3	0.4	0.9	0.9	0.8	0.8	0.6	0.8	1.2	1.2	1.2	1.2
0.4	0.5	0.5	0.5	1.1	1.1	1.5	2.3	0.1	0.1	0.4	0.4	0.7	0.9	0.2	0.2	0.5	0.6	0.6	0.6	0.8	0.8	0.9	0.9	0.9	0.8
		0.6	0.7	0.9	1.6	1.6	1.2	0.3	0.3	0.4	0.4	0.8	0.7	0.5	0.5	0.6	0.5	0.5	0.7	0.7	0.7	1.2	1.1	1.1	1.1
0.9	1.1	1.6	0.8	1.8	1.4	2.3	1.6	0.3	0.3	0.8	0.9	1.3	0.9	0.2	0.2	1.5	1.5	1.3	1.9	1.4	1.4	1.6	1.6	1.6	1.6
		0.8	1.0	1.8	1.6	1.8	1.1	0.3	0.3	0.8	0.9	1.1	1.1	0.9	0.2	0.2	1.0	1.0	0.9	1.4	1.4	1.4	1.4	1.4	1.4
0.2	0.2	0.3	0.2	0.3	0.3	1.0	1.0	0.1	0.1	0.2	0.2	0.2	0.3	0.2	0.1	0.2	0.2	0.4	0.4	0.2	0.2	0.2	0.2	0.2	0.2
		0.2	0.3	0.3	0.3	1.0	1.0	0.1	0.1	0.2	0.2	0.2	0.2	0.3	0.2	0.1	0.2	0.2	0.4	0.4	0.2	0.2	0.2	0.2	0.2
0.2	0.3	0.2	0.5	0.4	0.8	0.9	0.7	0.1	0.1	0.2	0.1	0.2	0.2	0.2	0.1	0.2	0.2	0.3	0.3	0.2	0.2	0.2	0.2	0.2	0.2
		0.3	0.2	0.4	0.4	0.9	0.7	0.2	0.2	0.2	0.1	0.2	0.2	0.2	0.2	0.1	0.2	0.2	0.4	0.4	0.2	0.2	0.2	0.2	0.2

Average heatmaps of Boronic acids 311 - 313

Phenylboronic acid 311 semi-quantitative LCMS output

	CuCl	CuCl ₂	CuTC	Cu(OTf) ₂	Cu(OAc) ₂	Cu(NO ₃) ₂	Cu(BF ₄) ₂	CuBr ₂
L1	80.0	84.8	42.4	54.9	71.3	66.8	71.2	89.4
L2	102.3	107.4	60.1	83.1	113.5	101.4	94.2	115.6
L3	70.5	68.6	49.6	86.8	114.3	90.3	75.0	85.0
L4	3.0	2.6	1.0	7.1	16.6	10.7	1.5	3.1
L5	47.3	30.9	11.0	34.1	58.2	48.0	28.1	51.9
L6	60.4	55.5	17.6	42.1	66.5	57.7	45.6	64.1
L7	21.0	13.9	4.2	5.0	9.3	12.6	10.9	20.6
L8	96.3	70.2	29.3	46.1	63.9	77.5	81.8	56.0
L9	115.3	74.1	39.4	34.3	49.6	52.0	52.0	91.8
L10	99.0	39.5	23.4	45.5	81.4	91.9	66.1	60.9
L11	150.3	50.4	20.4	55.3	75.4	63.9	74.9	123.0
L12	71.4	32.4	13.3	23.4	40.7	53.8	46.7	34.1

4-Methoxyphenylboronic acid 312 semi-quantitative LCMS output

	CuCl	CuCl ₂	CuTC	Cu(OTf) ₂	Cu(OAc) ₂	Cu(NO ₃) ₂	Cu(BF ₄) ₂	CuBr ₂
L1	24.0	21.4	15.6	17.3	20.4	22.7	23.2	24.2
L2	39.7	36.3	26.4	32.9	39.8	39.3	37.5	40.3
L3	42.0	37.9	24.1	36.6	50.6	42.6	38.0	45.2
L4	17.4	12.9	4.2	7.7	14.5	10.5	5.3	13.5
L5	24.2	20.4	13.9	16.9	20.5	19.7	19.9	25.6
L6	20.6	15.1	10.8	14.0	17.6	19.5	21.3	23.9
L7	7.1	5.1	3.7	6.6	8.4	6.9	6.1	8.7
L8	24.5	18.3	13.8	18.4	20.7	21.3	22.6	22.9
L9	29.2	21.1	13.9	24.8	32.2	27.1	24.4	28.2
L10	27.6	19.9	15.8	20.6	22.4	22.9	25.0	25.4
L11	31.4	28.6	22.6	26.5	29.8	28.5	28.1	31.7
L12	21.8	20.4	19.8	19.1	18.0	19.3	21.2	21.9

3-Trifluoromethylphenylboronic acid **313** semi-quantitative LCMS output

	CuCl	CuCl ₂	CuTC	Cu(OTf) ₂	Cu(OAc) ₂	Cu(NO ₃) ₂	Cu(BF ₄) ₂	CuBr ₂
L1	1.3	0.8	0.4	0.3	0.4	0.6	0.7	0.8
L2	1.5	0.9	0.3	0.5	0.7	0.8	0.9	1.1
L3	2.9	1.8	1.2	1.2	1.3	1.6	1.7	1.9
L4	0.4	0.2	0.0	0.1	0.1	0.1	0.1	0.1
L5	0.8	0.4	0.2	0.2	0.3	0.2	0.3	0.5
L6	1.5	1.0	0.4	0.3	0.5	0.5	0.5	0.7
L7	0.4	0.2	0.1	0.1	0.1	0.1	0.2	0.2
L8	1.2	0.7	0.2	0.3	0.4	0.5	0.6	0.8
L9	1.0	0.7	0.4	0.4	0.5	0.6	0.6	0.7
L10	1.3	0.8	0.3	0.4	0.5	0.6	0.9	1.1
L11	1.0	0.8	0.4	0.3	0.4	0.4	0.8	1.2
L12	1.1	0.6	0.2	0.4	0.4	0.4	0.7	1.0

7.4. Four Variable Optimisation of the Chan-Lam Reaction. 384- to 1536-well plate

Procedure for 384 nanomolar scale reactions (2.5 μ L volume) in one quarter of a 1536-well plate. Stock solutions of each component were prepared according to general procedure 1: 4-phenylpiperidine **134** (1.0 M in DMSO), boronic ester (**331-338**, 0.33 M in DMSO), organic base (**339-345** and **317**, 3M in DMSO), ligand (**318** and **319**, 0.025 M in DMSO), catalyst (C1-C6, 0.1 M in DMSO) using Spreadsheet 2. For the source plate layout, see Figure 54. For each 1536-well plate experiment, each well was charged with the amount of stock solution stated in ‘Source plate loading’ column, using a digital air displacement pipette, such that enough solution was present to dose the corresponding reactor plate.

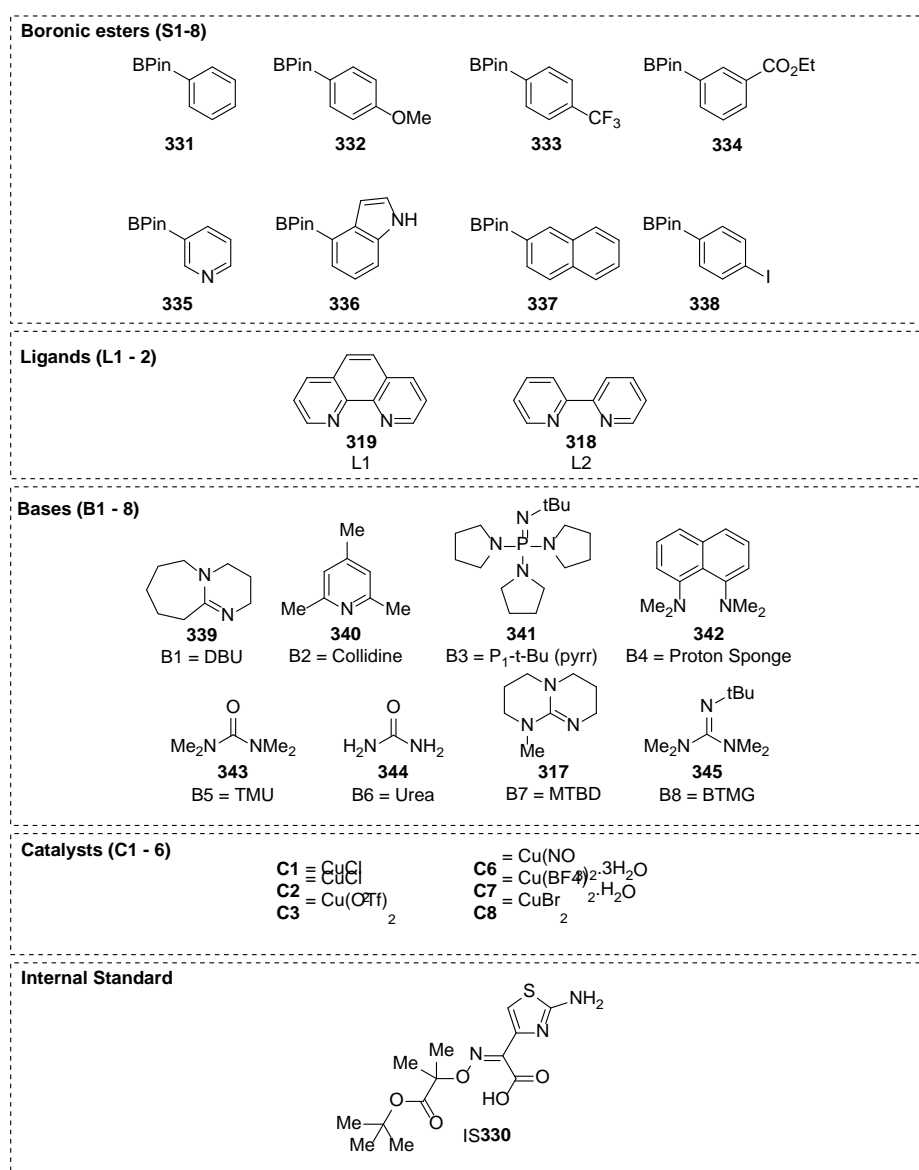


Figure 53: Components screened in 1536-well plates

The Mosquito was used to transfer variable volumes of stock solution from 384-well source plate to one quarter of a 1536-well reactor plate depending on the component added: 4-

phenylpiperidine was added in 375 nL, S1 was added in 750 nL, B1-8 was added in 250 nL, L1/2 was added in 750 nL and catalyst added in 125 nL resulting in a total reaction volume of 2.5 μ L. The mosquito mixed the reaction mixture together three times using the mix-dispense feature. The 1536-well reactor plate was then sealed with aluminium foil and placed under a heavy glass sheet for 24 hours.

Source Plate layout

	1	2	3	4	5	6	7	8	9	10	11	12	13	14	15	16	17	18	19	20	21	22	23	24	
A															C6	C5	C4	C3	C2	C1	L1	B1	S1	R1	A
B															C6	C5	C4	C3	C2	C1	L1	B2	S1	R1	B
C															C6	C5	C4	C3	C2	C1	L1	B3	S1	R1	C
D															C6	C5	C4	C3	C2	C1	L1	B4	S1	R1	D
E															C6	C5	C4	C3	C2	C1	L1	B5	S1	R1	E
F															C6	C5	C4	C3	C2	C1	L1	B6	S1	R1	F
G															C6	C5	C4	C3	C2	C1	L1	B7	S1	R1	G
H															C6	C5	C4	C3	C2	C1	L1	B8	S1	R1	H
I															C6	C5	C4	C3	C2	C1	L2	B1	S1	R1	I
J															C6	C5	C4	C3	C2	C1	L2	B2	S1	R1	J
K															C6	C5	C4	C3	C2	C1	L2	B3	S1	R1	K
L															C6	C5	C4	C3	C2	C1	L2	B4	S1	R1	L
M															C6	C5	C4	C3	C2	C1	L2	B5	S1	R1	M
N															C6	C5	C4	C3	C2	C1	L2	B6	S1	R1	N
O															C6	C5	C4	C3	C2	C1	L2	B7	S1	R1	O
P															C6	C5	C4	C3	C2	C1	L2	B8	S1	R1	P

Figure 54: Source plate layout for 1536-well reactor plate dosing.

Analysis plate preparation

The analysis was prepared in a similar manner to previous literature reports.¹⁶⁷ 100 μ L of 5% AcOH in DMSO was added to each well and the plate was sealed with an aluminium adhesive plate seal. Each plate was run overnight using a 1.8-minute run taking 15 hours to complete an entire 384-well plate. Once analysis was complete, peak integrals of both product and internal standard were taken and a ratio of product : internal standard was calculated. Heatmaps were created to show uncalibrated performance of each reaction.

PLATE	# reagents	How much of plate?	Input wells/column	Scale L.R. (umol)	Final conc. rxn (M)	Stand. Aliq. (ul)	Reactor tot vol (ul)	
1536	5	All	32	0.25	0.1	0.5	2.5	
constant?	Reagent	Compound	CAS	Cat No	FW (gMol-1)	Amount (uMol)	mg per rxn	Solubility problems?
(constant)	R1	4-phenylpiperidine	771-99-3	P 034	161.12	0.25	4.03E-02	0.38
(constant)	S1	PhBPin	24388-29-6	HTE	204.076	0.25	5.10E-02	1.00
	S2	4-OMeBPin	171364-79-7	HTE	234.102	0.25	5.85E-02	1.00
	S3	3-EOACBPin	269410-00-6	HTE	276.139	0.25	6.90E-02	1.00
	S4	5-IndoleBPin	269410-24-4	HTE	243.113	0.25	6.08E-02	1.00
	S5	4-CBPin	214360-65-3	HTE	272.074	0.25	6.80E-02	1.25
	S6	4-IBPin	7352-88-7	HTE	329.972	0.25	8.25E-02	1.25
	S7	3-PyridineBPin	181219-01-2	HTE	205.064	0.25	5.13E-02	1.25
	S8	2-NapBPin	256652-04-7	HTE	254.136	0.25	6.35E-02	1.25
(x-constant, y-variable)	B1	No Base				0	0.00E+00	0.25
	B2	DBU	6674-22-2	D301	152.24	0.25	3.81E-02	0.25
	B3	Collidine	108-75-8	C31	121.18	0.25	3.03E-02	0.25
	B4	DABCO	280-57-9	D052	112.17	0.25	2.80E-02	0.25
	B5	Tetramethylurea	632-22-4	Dave	116.16	0.25	2.90E-02	0.25
	B6	Urea	57-13-6	U002	60.06	0.25	1.50E-02	0.25
	B7	MTBD	84030-20-6	Dave	153.22	0.25	3.83E-02	0.25
	B8	BTMG	29166-72-1	B032	171.28	0.25	4.28E-02	0.25
(x-constant, y-variable)	C1	Cu(I)Cl	7758-89-6	cat 025	99.00	0.1	2.48E-03	0.13
	C2	CuCl2		IC058	134.45	0.1	3.36E-03	0.13
	C3	Cu(I)OTf2	34946-82-2	cat 150	361.68	0.1	9.04E-03	0.13
	C4	Cu(II)(NO3)2·3H2O	10031-43-3	IC010	241.60	0.1	6.04E-03	0.13
	C5	Cu(II)(Bz)2·H2O	207121-39-9	IC014	237.16	0.1	5.93E-03	0.13
	C6	Cu(II)Br2	7789-45-9	IC022	223.35	0.1	5.58E-03	0.13
(x-variable, y-constant)	L1	1,10-phenantroline	66-71-7	P 228	180.21	0.025	4.51E-03	0.75
NORMAL DILUTION	L2	2,2-bipyridyl	366-18-7	B 462	156.18	0.1	3.90E-03	0.50
(x-variable, y-constant)	L1	1,10-phenantroline	66-71-7	P 228	180.21	0.025	4.51E-03	0.50
INCREASED DILUTION	L2	2,2-bipyridyl	366-18-7	B 462	156.18	0.1	3.90E-03	0.50

Stock solution (mg/vial)	Stock solution (solvent/vial)	Stock solution (min vol/vial)	Source (abs vol/well)	Source (rec vol/well)	Source plate loading (vol/well ul)	Liquid reagents (Vol/SS)	DMSO Top-up
107.4	1000	259	9	16	62.5	X	X
35.7	700	691	24	43			
41.0	700	691	24	43			
48.3	700	691	24	43			
42.5	700	691	24	43			
49.0	900	864	30	54	43.75	X	X
59.4	900	864	30	54			
36.9	900	864	30	54			
45.7	900	864	30	54			
0.0	100	0	0	0		X	X
15.2	100	0	6	11		13.7	86.3
12.1	100	0	6	11		13.3	86.7
11.2	100	0	6	11		X	X
11.6	100	0	6	11		12.0	88.0
6.0	100	0	6	11		X	X
15.3	100	0	6	11		14.4	85.6
17.1	100	0	6	11		20.2	79.8
7.9	400	14	1	1			
10.8	400	14	1	1			
28.9	400	14	1	1	25	X	X
19.3	400	14	1	1			
19.0	400	14	1	1			
17.9	400	14	1	1			
2.4	400	259	18	32	50.0	X	X
2.1	400	259	18	32			
3.6	400	173	12	22	50.0	X	X
3.1	400	173	12	22			

Spreadsheet 2: High-throughput screen of Chan-Lam reaction (1 x 4 x 8 x 2 x 6 screen). Two different boronic ester stock solution concentrations were necessary. Boronic esters S1-S4 (**331, 332, 334, 336**) were prepared at 0.25M and was added into the reactor plate in 1.00 μ L. Boronic esters S5-S8 (**333, 338, 335, 337**) were prepared at 0.2M and was added into the reactor plate in 1.25 μ L. The ligand concentration was adjusted to allow for the more dilute boronic ester stock solution. For boronic esters S1-S4 (**331, 332, 334, 336**), ligand L1-2 (**319** and **318**) (0.033M) was added in 750 nL. For boronic esters S5-S8 (**333, 338, 335, 337**), ligand L1-2 (**319** and **318**) (0.05M) was added in 500 nL.

BE1: Phenylboronic acid pinacol ester, 331

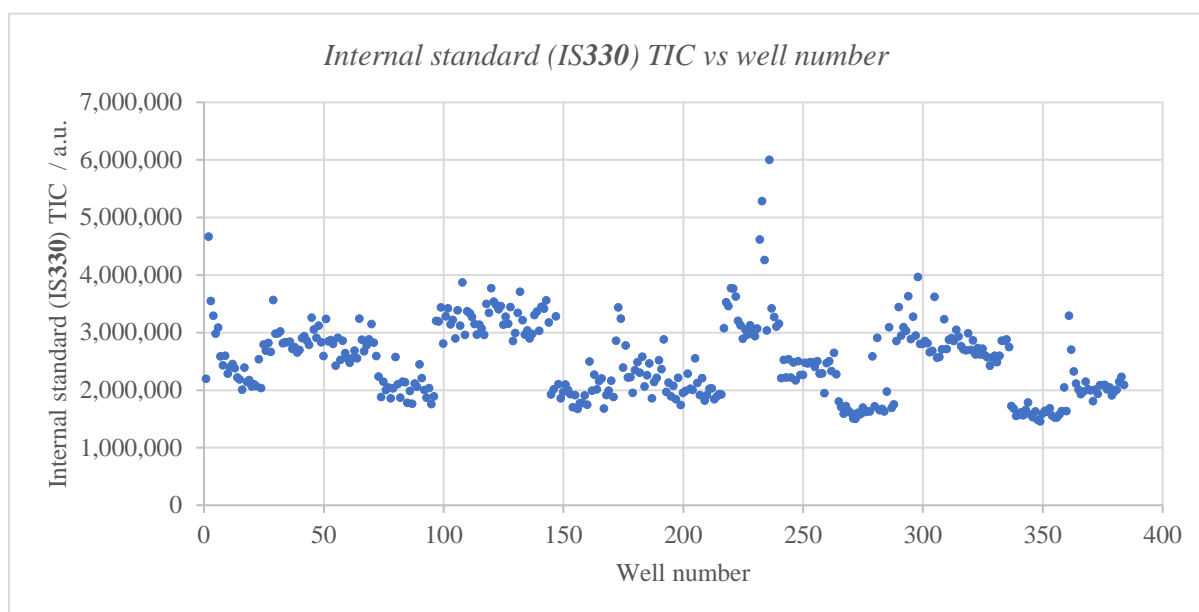
LCMS analysis post statistical test

		CuBr ₂			Cu(BF ₄) ₂			Cu(NO ₃) ₂			Cu(O Tf) ₂			CuCl ₂			CuCl								
2.37	BAD	2.31	2.30	1.32	1.32	1.28	1.43	1.11	1.89	1.66	1.86	BAD	1.20	1.13	1.34	1.23	1.63	1.38	1.22	BAD	BAD	0.58	0.70	0.71	DBU
1.75	2.02	1.86	1.55	1.00	1.00	0.79	0.85	0.82	1.37	1.86	1.66	1.56	BAD	1.52	1.62	1.76	1.67	1.66	1.79	BAD	BAD	1.26	1.43	1.17	Collidine
2.26	1.96	1.93	2.14	1.33	1.33	0.92	1.31	BAD	2.07	2.05	1.93	2.01	1.79	1.86	1.74	1.83	1.97	BAD	2.25	1.88	BAD	1.80	1.29	1.20	Pf1Bu
2.84	2.64	2.47	2.49	1.78	1.78	1.56	1.82	1.82	1.94	2.31	BAD	BAD	BAD	2.26	2.28	2.35	2.45	2.45	BAD	2.23	2.51	2.56	2.50	BAD	P.S.
1.75	1.79	1.88	2.05	0.74	0.81	1.23	0.92	0.92	1.34	1.54	1.21	1.56	1.29	1.59	1.26	1.60	1.63	1.66	1.55	1.61	BAD	1.81	BAD	1.11	TMU
1.53	1.47	1.49	1.47	1.39	1.22	1.24	1.28	1.28	1.47	1.19	1.28	1.20	1.17	1.28	1.41	1.54	1.26	1.55	1.38	1.53	1.59	1.59	1.02	0.96	Urea
1.75	BAD	1.48	1.68	1.64	1.34	1.57	1.21	2.20	2.20	1.97	2.04	1.98	1.90	1.73	1.91	1.63	1.73	1.76	1.74	BAD	1.59	BAD	1.52	1.38	MTBD
1.61	2.03	1.82	1.99	1.87	1.94	1.68	1.56	BAD	BAD	1.80	2.01	1.87	1.58	BAD	1.74	1.91	1.90	BAD	1.57	1.47	1.60	2.00	2.01	1.60	BTMG
1.69	1.64	1.74	1.85	1.47	1.33	1.54	1.50	1.77	1.92	1.92	1.78	BAD	1.39	1.54	1.32	1.57	1.91	2.17	BAD	1.85	1.76	1.86	1.47	1.59	DBU
1.47	1.46	1.31	1.33	0.61	BAD	0.82	0.68	0.81	0.81	1.14	1.27	1.01	1.25	1.24	1.22	1.29	1.31	1.31	1.13	1.08	1.19	1.30	1.31	1.50	Collidine
2.09	1.75	1.81	1.95	1.58	1.17	1.23	1.05	1.90	1.90	1.81	1.85	1.90	1.89	1.58	1.92	1.64	1.64	1.89	1.75	1.95	1.89	2.14	1.90	1.72	Pf1Bu
2.25	2.42	BAD	2.08	2.29	2.04	2.16	BAD	2.08	BAD	BAD	2.17	1.82	2.42	2.28	2.30	2.48	2.80	2.65	2.45	2.40	2.58	2.78	2.49	BAD	P.S.
1.60	1.59	1.23	1.44	1.35	BAD	1.41	0.86	1.42	1.42	1.56	1.38	1.39	1.32	1.42	BAD	1.36	1.39	1.51	1.17	1.47	1.48	1.64	1.48	1.58	TMU
1.60	1.51	1.56	1.63	1.43	1.42	1.31	1.29	1.44	1.44	1.34	1.21	1.05	1.39	1.44	1.38	1.37	1.38	1.35	1.44	1.52	1.61	1.57	1.38	1.66	Urea
1.60	1.25	1.59	1.77	1.60	1.81	1.64	1.58	1.94	1.94	2.15	2.10	2.13	1.81	1.76	1.74	1.75	1.96	1.95	2.01	1.99	2.06	2.05	1.82	1.63	MTBD
0.96	1.20	1.01	BAD	0.92	1.34	1.50	1.11	BAD	BAD	2.22	1.97	2.22	1.47	1.65	1.41	BAD	2.30	2.04	2.03	2.08	1.74	1.59	1.55	BAD	BTMG
Phenanthroline												Bipyridine													

Average heatmap output

	DBU	Collidine	P1tBu	P.S.	TMU	Urea	MTBD	BTMG	DBU	Collidine	P1tBu	P.S.	TMU	Urea	MTBD	BTMG
CuCl	0.70	1.30	1.40	2.50	BAD	1.30	1.50	1.80	1.70	1.30	1.90	2.60	1.50	1.60	1.90	1.60
CuCl ₂	1.40	1.70	2.00	2.40	1.60	1.40	1.70	1.60	2.00	1.20	1.80	2.60	1.40	1.40	2.00	2.10
Cu(OTf) ₂	1.20	1.60	1.80	2.30	1.40	1.40	1.80	1.70	1.50	1.20	1.80	2.40	1.40	1.40	1.80	1.50
Cu(NO ₃) ₂	1.80	1.60	2.00	BAD	1.40	1.30	2.00	1.90	1.80	1.10	1.90	2.00	1.40	1.30	2.10	2.10
Cu(BF ₄) ₂	1.30	0.90	1.20	1.70	0.90	1.30	1.40	1.80	1.50	0.70	1.30	2.20	1.20	1.40	1.70	1.20
CuBr ₂	2.30	1.80	2.10	2.60	1.90	1.50	1.60	1.90	1.70	1.40	1.90	2.30	1.50	1.60	1.50	1.10
	Phenanthroline								Bipyridine							

IS330 TIC vs well number



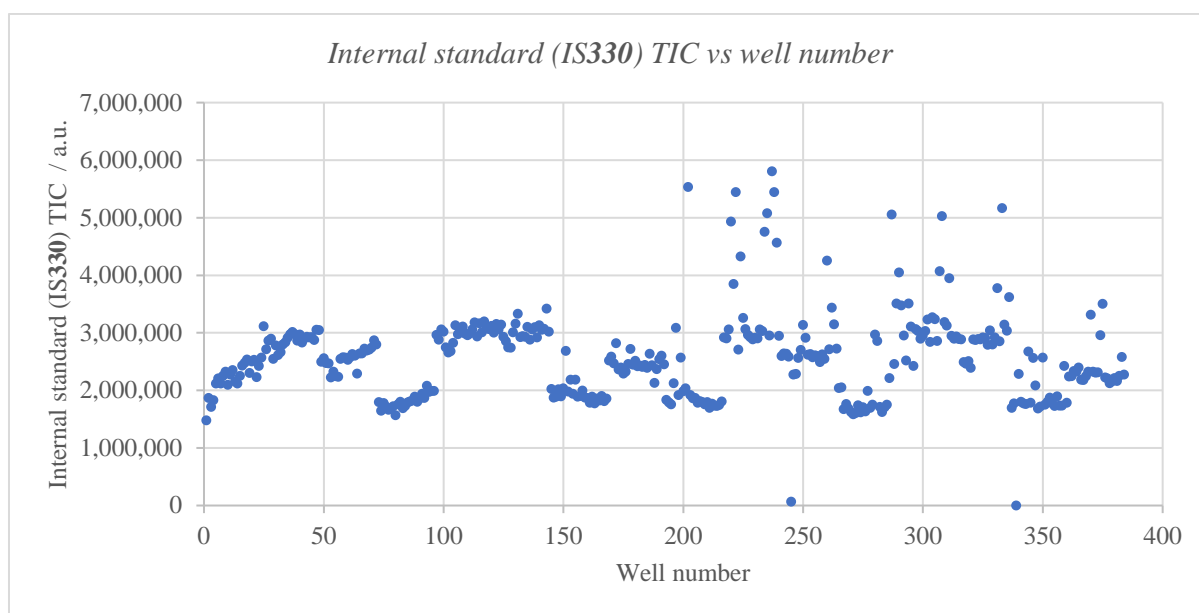
BE2: Naphthalene-2-boronic acid pinacol ester, 332
LCMS analysis post statistical test

CuBr ₂				Cu(BF ₄) ₂				Cu(NO ₃) ₂				Cu(OTf) ₂				CuCl ₂				CuCl			
2.60	1.97	3.11	2.50	1.96	2.03	1.93	1.94	2.49	2.93	2.81	2.84	2.41	2.39	2.50	2.42	1.81	2.02	1.85	2.00	3.35	3.35	3.01	3.12
1.71	1.47	2.86	2.58	2.84	2.62	BAD	2.66	2.71	3.15	2.92	2.92	2.71	2.86	2.94	3.10	0.50	0.41	0.52	0.61	3.67	3.58	3.75	3.18
3.10	2.63	3.64	3.60	3.26	3.16	3.31	3.23	4.08	3.81	3.76	3.70	3.22	3.22	3.68	3.64	0.59	0.87	0.84	0.91	3.97	3.97	4.01	4.08
4.89	4.62	4.66	4.41	4.44	4.01	4.71	4.59	4.55	4.77	4.74	4.71	5.31	5.31	4.55	4.99	1.24	1.00	1.12	1.32	5.63	5.61	5.75	5.00
3.59	3.59	3.67	3.39	3.21	2.93	3.11	2.89	3.10	3.38	3.15	3.20	3.18	3.18	3.29	3.04	0.54	0.48	0.60	0.95	3.50	3.58	3.50	3.29
3.40	3.03	3.51	3.45	3.14	3.29	3.07	3.00	3.29	3.15	3.22	3.18	2.96	2.96	3.23	3.30	0.78	0.92	0.79	0.77	3.63	3.70	3.41	3.56
3.85	3.93	3.98	4.12	3.88	3.95	3.68	3.75	3.97	3.80	3.67	3.74	3.40	3.40	3.55	3.33	3.14	2.29	2.93	3.19	3.80	3.72	3.74	3.20
4.46	4.09	4.32	4.58	4.63	3.94	3.82	4.03	4.69	4.68	4.53	4.41	4.30	4.30	3.88	4.20	2.61	2.58	2.38	2.51	3.99	4.02	4.37	3.99
3.88	3.84	3.86	3.94	3.53	3.44	3.52	3.30	4.25	4.05	4.13	3.85	3.70	3.70	BAD	3.40	2.82	2.15	2.69	1.72	3.76	4.15	4.10	4.04
BAD	2.21	1.89	1.70	3.06	1.75	1.92	2.98	3.44	3.48	3.49	2.90	3.07	3.07	3.15	3.08	0.12	0.28	0.11	0.20	BAD	3.52	3.74	3.60
3.77	3.31	3.00	3.75	BAD	3.51	3.33	3.50	3.96	4.13	4.08	4.05	3.27	3.27	3.35	3.67	0.37	0.42	0.45	BAD	4.19	3.95	3.83	4.06
3.63	BAD	4.00	BAD	4.91	4.85	4.94	4.94	BAD	5.47	5.31	4.67	5.14	5.14	5.52	5.30	0.40	0.39	0.43	0.48	5.95	5.97	4.79	4.98
3.30	2.51	3.22	3.16	1.76	2.07	BAD	2.58	2.74	3.26	2.82	3.06	3.17	3.17	2.88	2.91	0.18	0.15	0.16	0.24	3.65	3.00	2.65	2.87
2.21	2.82	2.71	1.94	3.06	2.26	2.89	3.00	2.78	3.34	3.10	3.08	3.31	3.31	3.15	3.22	0.29	0.26	0.24	0.28	3.63	3.82	3.54	3.68
3.80	BAD	3.65	3.79	3.36	3.50	3.41	3.20	3.90	3.77	BAD	3.97	2.88	2.88	2.47	3.69	BAD	3.49	3.31	3.48	2.94	BAD	3.48	3.68
3.23	3.45	3.98	3.74	3.77	3.61	BAD	3.55	3.89	BAD	BAD	4.28	3.94	3.94	BAD	4.02	1.57	1.54	1.61	1.77	4.12	3.31	3.40	3.82
Phenanthroline												Bipyridine											

Average heatmap output

	DBU	Collidine	P1tBu	P.S.	TMU	Urea	MTBD	BTMG	DBU	Collidine	P1tBu	P.S.	TMU	Urea	MTBD	BTMG
CuCl	3.20	3.50	4.10	5.50	3.50	3.60	3.60	4.10	4.00	3.60	4.00	5.40	3.00	3.70	3.40	3.70
CuCl ₂	1.90	0.50	0.80	1.20	0.60	0.80	2.90	2.50	2.30	0.20	0.40	0.40	0.20	0.30	3.40	1.60
Cu(OTf) ₂	2.40	2.90	3.40	4.90	3.20	3.20	3.50	4.10	3.60	3.20	3.50	5.30	3.00	3.20	3.10	3.80
Cu(NO ₃) ₂	2.80	2.90	3.80	4.70	3.20	3.20	3.80	4.60	4.10	3.30	4.10	5.10	3.00	3.10	3.90	BAD
Cu(BF ₄) ₂	2.00	2.70	3.20	4.40	3.00	3.10	3.80	4.10	3.40	2.40	3.40	4.90	2.10	2.80	3.40	3.60
CuBr ₂	2.50	2.20	3.20	4.60	3.60	3.30	4.00	4.40	3.90	1.90	3.50	BAD	3.00	2.40	3.70	3.60
	Phenanthroline								Bipyridine							

IS330 TIC vs well number



BE3: 4-Trifluoromethylphenylboronic acid pinacol ester, 333

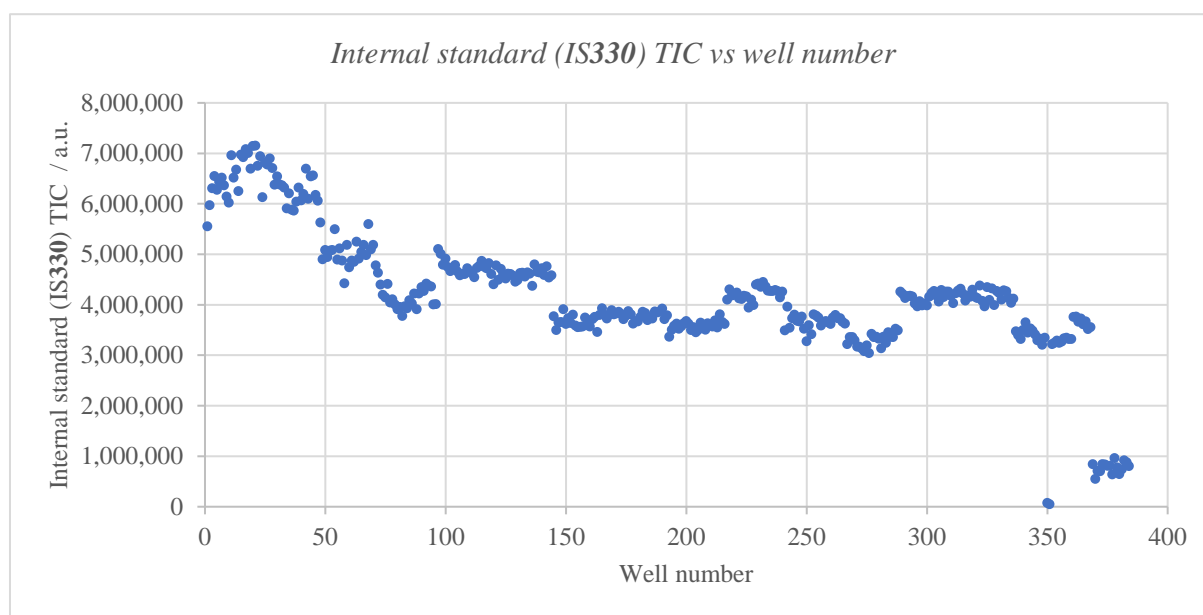
LCMS analysis post statistical test

CuBr ₂				Cu(BF ₄) ₂				Cu(NO ₃) ₂				Cu(OTf) ₂				CuCl ₂				CuCl								
0.29	0.07	0.08	0.07	0.06	0.05	0.10	0.06	0.18	0.27	0.36	0.27	0.26	0.28	0.52	0.18	0.42	0.42	0.42	0.42	0.45	0.27	0.32	0.32	0.24	0.32	0.27	0.27	DBU
BAD	0.34	0.32	0.27	0.37	0.39	0.43	0.34	1.18	0.92	0.66	0.92	1.07	1.21	1.15	1.18	0.87	0.74	0.85	0.84	0.74	0.85	0.48	0.75	0.68	0.48	0.59	0.59	Collidine
0.77	0.76	0.78	0.96	0.61	0.62	0.71	0.63	1.22	1.18	1.31	1.18	1.25	1.23	1.56	1.22	1.14	1.26	1.00	1.48	1.14	1.00	0.65	0.97	0.78	0.65	0.52	0.52	P1tBu
1.00	0.86	0.83	0.79	0.86	0.71	0.85	0.83	1.09	1.17	1.29	1.21	1.45	1.38	1.57	1.09	1.12	1.00	1.21	1.20	1.12	1.00	0.85	1.07	0.93	0.85	0.77	0.77	P.S.
1.02	0.91	0.87	0.85	0.84	0.81	0.94	1.08	1.07	1.11	1.09	1.18	1.22	1.16	1.38	1.07	0.91	0.87	0.91	1.03	1.07	1.07	BAD	1.04	1.04	BAD	0.65	0.65	TMU
0.64	0.71	0.67	0.98	0.90	0.92	0.95	0.89	1.04	1.03	0.98	0.85	1.28	1.06	1.34	1.04	0.65	0.77	0.69	1.06	1.21	1.12	0.92	1.12	1.12	0.92	BAD	BAD	Urea
0.34	0.37	0.37	0.56	0.43	0.47	0.58	0.40	0.56	0.60	0.69	0.55	0.53	0.39	0.64	0.56	0.49	0.50	0.52	0.89	0.45	0.42	0.17	0.45	0.42	0.17	0.12	0.12	MTBD
1.01	0.92	1.36	1.29	1.03	0.93	1.24	1.07	1.08	1.23	1.24	1.39	1.26	1.16	1.35	1.08	1.39	1.42	1.47	1.65	1.11	0.85	BAD	1.11	0.85	BAD	0.58	0.58	BTMG
0.48	0.36	0.36	0.41	0.39	0.28	0.46	0.32	0.23	0.71	0.69	0.44	0.41	0.29	0.45	0.23	0.49	0.43	0.44	0.52	0.52	0.35	0.11	0.52	0.35	0.11	0.23	0.23	DBU
0.87	0.81	0.96	0.85	1.27	1.01	1.02	0.98	1.09	1.19	1.09	1.06	0.96	1.03	0.99	1.09	0.63	0.57	0.66	0.57	0.91	0.81	0.33	0.91	0.81	0.33	BAD	BAD	Collidine
1.03	1.12	1.28	1.28	0.86	0.73	1.02	0.65	1.12	1.08	1.07	1.12	0.94	0.65	0.97	0.61	1.03	1.02	1.05	1.19	1.03	0.86	0.46	1.03	0.86	0.46	0.45	0.45	P1tBu
0.91	0.78	1.26	1.24	1.27	1.11	1.24	1.26	1.23	1.44	1.34	1.30	1.23	1.14	1.32	1.23	0.93	0.92	0.93	0.90	1.13	1.12	0.36	1.13	1.12	0.36	BAD	BAD	P.S.
0.77	0.89	1.01	0.89	1.23	0.98	0.97	0.98	0.95	1.14	1.08	1.01	0.94	0.88	0.99	0.95	0.77	0.70	0.75	0.71	0.95	0.85	BAD	0.95	0.85	BAD	0.61	0.61	TMU
1.08	0.55	0.85	0.86	0.95	0.96	0.97	0.80	0.88	0.99	0.89	0.89	0.88	0.92	1.02	0.88	0.58	0.59	0.60	0.71	0.78	0.81	0.40	0.78	0.81	0.40	0.23	0.23	Urea
0.10	0.12	0.12	0.13	0.12	0.10	0.11	0.12	0.10	0.18	BAD	0.18	0.11	0.08	0.11	0.10	0.12	0.14	0.10	0.17	0.12	0.10	0.05	0.12	0.10	0.05	0.04	0.04	MTBD
0.18	0.14	0.21	0.20	0.10	0.11	0.13	0.10	0.08	0.15	0.12	0.15	0.12	0.07	0.14	0.08	0.45	0.74	0.81	0.87	0.37	0.32	0.12	0.37	0.32	0.12	0.18	0.18	BTMG
Phenanthroline												Bipyridine																

Average heatmap output

	DBU	Collidine	P1tBu	P.S.	TMU	Urea	MTBD	BTMG	DBU	Collidine	P1tBu	P.S.	TMU	Urea	MTBD	BTMG
CuCl	0.30	0.60	0.70	0.90	0.90	1.10	0.30	0.80	0.30	0.70	0.70	0.90	0.80	0.60	0.10	0.20
CuCl ₂	0.40	0.80	1.20	1.10	0.90	0.80	0.60	1.50	0.50	0.60	1.10	0.90	0.70	0.60	0.10	0.70
Cu(OTf) ₂	0.30	1.20	1.30	1.40	1.20	1.20	0.50	1.20	0.30	1.00	0.80	1.20	0.90	0.90	0.10	0.10
Cu(NO ₃) ₂	0.20	0.60	1.00	1.20	1.10	1.00	0.60	1.30	0.60	1.10	1.10	1.30	1.00	1.00	BAD	0.10
Cu(BF ₄) ₂	0.10	0.40	0.60	0.80	0.90	0.90	0.50	1.10	0.40	1.10	0.80	1.20	1.00	0.90	0.10	0.10
CuBr ₂	0.10	0.30	0.80	0.90	0.90	0.70	0.40	1.10	0.40	0.90	1.20	1.00	0.90	0.80	0.10	0.20
	Phenanthroline								Bipyridine							

IS330 TIC vs well number



BE4: 4-Methoxyphenylboronic acid pinacol ester, 332

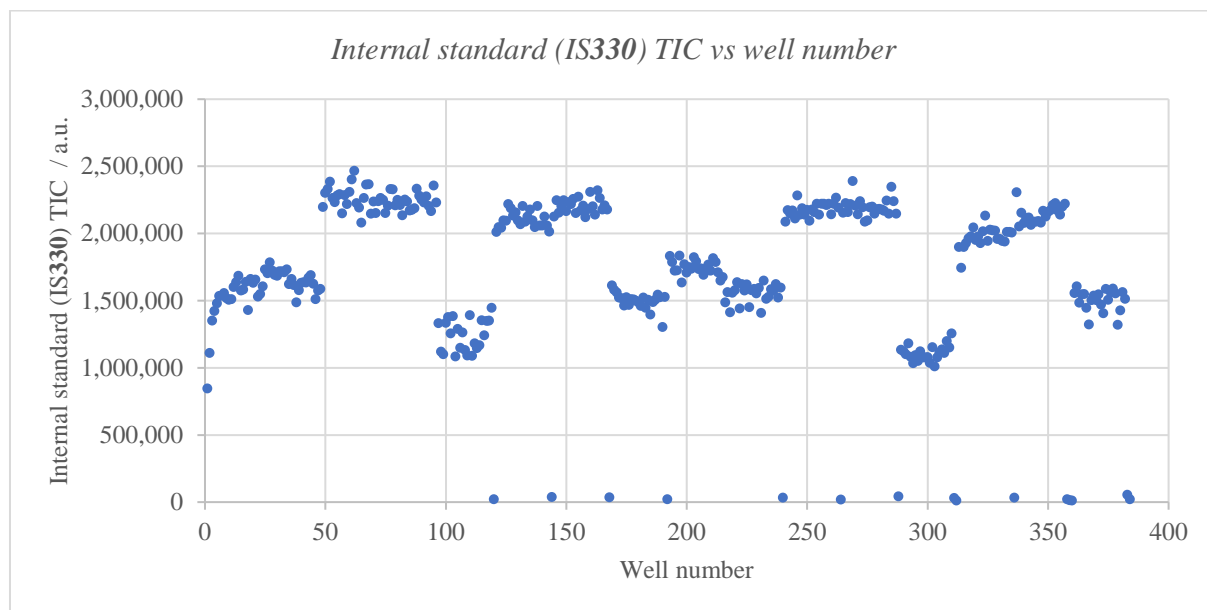
LCMS analysis post statistical test

CuBf ₄				Cu(BF ₄) ₂				Cu(NO ₃) ₂				Cu(OTf) ₂				CuCl ₂				CuCl			
2.24	3.31	2.39	2.95	3.35	4.21	4.97	4.81	4.03	4.24	3.20	4.16	4.29	3.58	4.37	3.39	4.31	3.46	3.33	2.93	3.69	3.79	4.80	DBU
2.90	2.98	3.24	3.06	3.25	3.32	3.44	3.49	3.06	2.96	2.78	3.54	3.69	3.30	3.01	2.70	2.74	2.66	2.76	3.27	3.07	3.30	3.21	Collidine
3.09	3.33	4.55	4.91	4.26	4.32	4.60	5.01	4.87	4.48	4.26	4.21	3.96	4.36	4.43	4.18	4.20	4.26	4.38	3.68	3.87	3.86	4.06	PtBu
5.07	4.59	4.37	5.00	4.97	5.20	5.11	4.97	4.74	5.02	5.44	4.93	4.85	5.05	4.96	4.86	5.13	4.54	4.91	4.49	5.08	4.55	4.33	P.S.
BAD	4.33	4.29	4.98	7.21	6.26	7.69	7.91	8.21	7.67	8.14	8.13	7.41	7.96	7.70	8.22	6.70	7.08	7.09	6.62	8.07	7.92	7.25	TMU
BAD	BAD	5.52	4.85	5.62	5.73	5.17	5.88	5.94	5.60	5.33	4.36	5.62	5.54	5.72	5.55	5.30	5.19	5.33	5.09	5.51	5.75	5.63	Urea
4.16	4.33	5.48	5.66	5.09	5.26	5.67	5.30	5.27	5.37	5.51	5.46	5.41	5.72	5.39	5.44	5.54	5.64	5.33	5.10	5.56	5.30	5.63	MTBD
BAD	5.99	6.77	6.66	6.39	6.06	6.58	7.01	6.08	5.70	6.27	6.20	6.50	6.83	6.21	5.93	5.94	6.15	6.35	6.86	6.90	6.81	6.61	BTMG
7.29	6.98	7.18	BAD	6.77	BAD	7.08	7.68	6.91	6.65	6.88	7.06	6.79	6.99	7.43	7.01	6.97	7.24	6.43	7.22	7.02	7.24	7.39	DBU
BAD	5.82	5.43	5.76	5.88	5.86	6.40	6.54	5.83	6.14	5.95	6.15	6.33	6.92	6.20	5.86	5.72	5.97	6.08	6.36	6.23	7.09	BAD	Collidine
BAD	4.66	5.43	4.39	5.76	5.44	5.42	5.73	4.96	5.11	5.13	5.36	5.07	5.30	5.20	4.88	5.19	5.16	5.33	5.49	5.52	5.52	5.40	PtBu
BAD	4.65	5.69	BAD	6.01	5.62	6.13	5.91	5.60	5.03	5.15	5.44	5.45	5.69	5.47	5.18	5.80	5.12	4.80	5.85	5.72	4.94	5.37	P.S.
BAD	BAD	8.29	8.96	8.34	8.81	9.20	9.50	9.10	8.78	9.52	8.46	8.58	9.13	8.25	8.65	9.01	8.85	9.20	8.20	9.23	8.29	9.04	TMU
3.60	4.24	BAD	3.96	6.11	6.12	6.42	6.62	6.17	BAD	6.39	5.85	6.20	5.79	6.21	5.64	6.12	5.95	5.98	5.65	BAD	4.60	6.17	Urea
17.8	18.1	BAD	BAD	5.73	5.83	6.00	5.85	5.42	5.29	5.81	5.33	5.54	5.48	5.29	5.54	5.97	5.60	5.75	6.07	5.52	5.51	BAD	MTBD
BAD	BAD	BAD	BAD	3.90	BAD	BAD	5.09	3.66	4.80	4.09	5.03	4.19	4.00	4.13	3.80	BAD	4.45	3.67	BAD	4.22	3.88	4.03	BTMG

Average heatmap output

	DBU	Collidine	P1tBu	P.S.	TMU	Urea	MTBD	BTMG	DBU	Collidine	P1tBu	P.S.	TMU	Urea	MTBD	BTMG
CuCl	3.80	3.20	3.90	4.60	7.50	5.50	5.40	6.80	7.20	6.60	5.50	5.50	8.70	5.50	5.70	4.00
CuCl ₂	3.60	2.70	4.30	4.90	7.30	5.30	5.50	6.10	6.90	5.90	5.10	5.20	8.90	5.90	5.70	4.00
Cu(OTf) ₂	4.10	3.40	4.20	4.90	7.80	5.30	5.50	6.40	7.10	6.40	5.20	5.50	8.60	6.00	5.40	4.30
Cu(NO ₃) ₂	3.80	3.10	4.50	5.10	7.80	5.60	5.50	6.00	6.90	6.00	5.00	5.40	9.00	6.30	5.60	3.80
Cu(BF ₄) ₂	4.30	3.40	4.50	5.10	7.30	5.60	5.30	6.50	7.20	6.20	5.60	5.90	9.00	6.30	5.90	BAD
CuBr ₂	2.70	3.00	4.00	4.80	4.50	BAD	4.90	6.50	7.10	5.70	4.80	BAD	BAD	3.90	BAD	BAD
	Phenanthroline								Bipyridine							

IS330 TIC vs well number



BE5: 3-Ethoxycarbonylphenylboronic acid pinacol ester, 334

LCMS analysis post statistical test

CuBf ₄				Cu(BF ₄) ₂				Cu(NO ₃) ₂				Cu(OTf) ₂				CuCl ₂				CuCl								
0.86	1.00	0.91	1.19	1.10	0.95	0.97	0.94	0.86	0.97	1.07	0.96	1.02	1.24	1.08	1.09	1.32	1.23	1.40	1.50	1.44	1.52	1.44	1.63	1.56	1.63	1.56	1.63	DBU
1.39	1.27	1.30	1.29	1.27	0.86	0.88	0.89	0.70	0.88	0.69	0.95	1.13	1.29	1.16	1.40	1.32	1.15	1.63	1.37	1.53	1.84	1.53	1.65	1.24	1.65	1.24	1.65	Collidine
1.75	1.86	1.67	1.94	1.35	1.46	1.06	1.36	0.79	1.06	1.45	0.74	1.57	1.48	1.49	1.49	1.42	1.52	1.55	1.63	1.97	2.06	1.97	1.95	1.82	1.95	1.82	1.82	PtBu
2.86	2.84	2.86	2.51	2.60	2.78	2.38	2.55	BAD	2.38	1.93	2.29	2.95	2.50	2.65	2.65	2.59	2.61	2.63	2.53	2.98	2.97	2.98	2.96	3.12	3.12	3.12	3.12	P.S.
1.82	1.75	1.77	1.77	1.42	1.61	1.13	1.67	1.05	1.13	0.93	0.94	1.62	1.57	1.49	1.57	1.45	1.52	1.62	1.54	1.68	1.76	1.68	1.86	1.65	1.65	1.65	1.65	TMU
1.75	1.95	1.76	1.78	1.71	1.74	1.57	1.68	1.52	1.57	1.38	1.49	1.79	1.73	1.68	1.71	1.67	1.68	1.51	1.64	1.89	1.88	1.89	1.74	1.83	1.83	1.83	1.83	Urea
2.29	2.41	2.27	2.40	2.19	2.10	1.89	2.11	2.03	1.89	1.96	1.87	2.19	2.18	2.14	2.08	2.13	2.11	2.04	2.17	2.26	2.22	2.26	2.01	1.91	1.91	1.91	1.91	MTBD
2.61	2.52	2.65	2.59	2.32	2.31	2.03	2.28	2.14	2.03	2.17	2.00	2.31	2.26	2.26	2.49	2.31	2.41	2.01	2.38	2.39	2.49	2.39	2.50	2.25	2.25	2.25	2.25	BTMG
2.39	2.35	2.33	2.36	1.84	1.83	1.67	1.96	1.77	1.67	2.02	1.70	1.91	2.00	1.98	2.12	2.03	2.00	1.91	1.89	2.18	2.24	2.18	2.08	1.97	1.97	1.97	1.97	DBU
1.70	1.71	1.68	1.65	1.18	1.23	0.81	1.16	0.97	0.81	0.56	0.79	1.30	1.34	1.27	1.19	0.93	1.04	0.89	0.95	1.72	1.75	1.72	1.66	1.62	1.62	1.62	1.62	Collidine
2.02	2.42	2.00	BAD	1.21	0.96	1.00	0.91	1.00	1.18	0.80	0.90	1.17	1.23	1.05	1.44	0.92	1.05	1.01	0.90	1.46	2.05	1.46	2.05	1.75	1.75	1.75	1.75	PtBu
2.64	2.69	2.70	2.35	1.67	1.91	1.44	1.52	1.48	1.44	1.56	1.67	2.02	2.25	2.18	2.04	1.61	1.60	1.51	1.42	2.80	2.74	2.80	2.47	2.55	2.55	2.55	2.55	P.S.
1.85	1.44	1.88	1.74	0.92	0.86	1.09	1.01	0.94	1.09	0.77	0.96	1.05	1.03	1.15	1.40	1.12	1.04	1.12	0.86	1.58	1.42	1.58	1.49	1.56	1.56	1.56	1.56	TMU
1.89	1.68	1.63	1.59	1.17	1.01	0.86	0.76	0.95	0.86	0.87	0.89	1.23	0.87	0.87	1.41	1.10	0.59	0.87	0.85	1.62	1.41	1.62	1.65	1.48	1.48	1.48	1.48	Urea
1.47	1.46	1.00	1.22	0.72	0.80	0.86	0.86	0.86	0.86	0.93	0.89	0.87	0.84	0.93	0.87	0.99	1.00	0.92	0.98	1.13	1.02	1.13	1.18	0.99	0.99	0.99	0.99	MTBD
1.91	1.69	1.56	1.39	0.72	0.78	0.92	BAD	0.92	0.73	0.30	0.69	0.18	0.76	0.30	1.08	1.00	0.67	0.68	0.68	1.59	1.35	1.59	1.70	BAD	BAD	BAD	BAD	BTMG

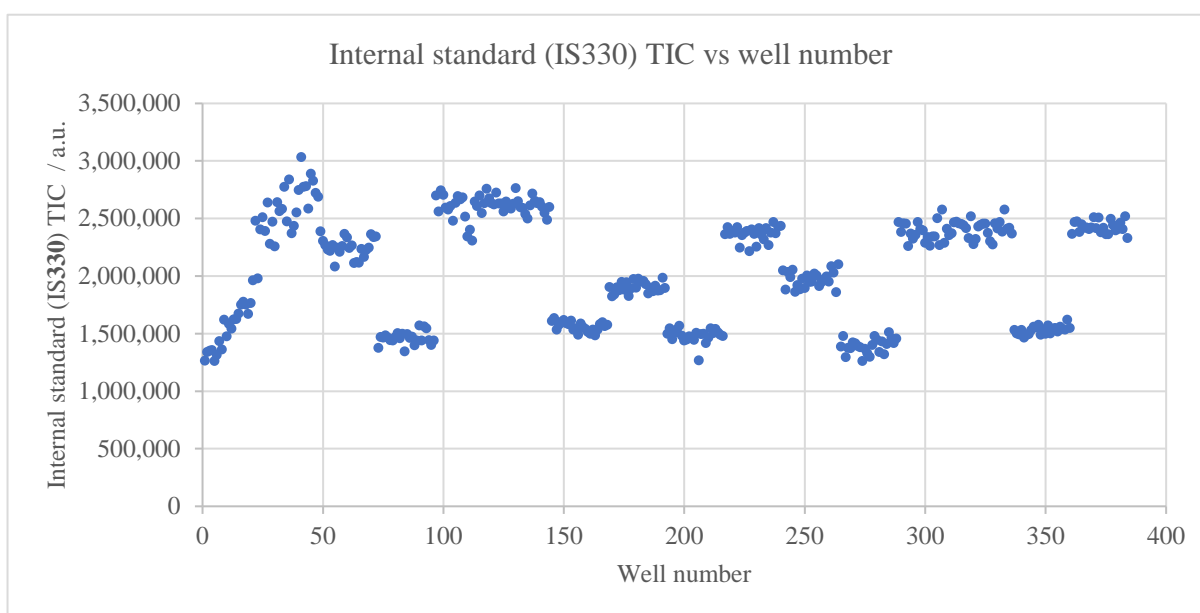
Phenanthroline

Bipyridine

Average heatmap output

	DBU	Collidine	P1tBu	P.S.	TMU	Urea	MTBD	BTMG	DBU	Collidine	P1tBu	P.S.	TMU	Urea	MTBD	BTMG
CuCl	1.50	1.60	2.00	3.00	1.70	1.80	2.10	2.40	2.10	1.70	1.80	2.60	1.50	1.50	1.10	1.50
CuCl ₂	1.40	1.40	1.50	2.60	1.50	1.60	2.10	2.30	2.00	1.00	1.00	1.50	1.00	0.90	1.00	0.80
Cu(OTf) ₂	1.10	1.20	1.50	2.70	1.60	1.70	2.20	2.30	2.00	1.30	1.20	2.10	1.20	1.10	0.90	0.60
Cu(NO ₃) ₂	1.00	0.80	1.00	2.20	1.00	1.50	1.90	2.10	1.80	0.80	1.00	1.50	0.90	0.90	0.90	0.70
Cu(BF ₄) ₂	1.00	1.10	1.40	2.60	1.60	1.70	2.10	2.30	1.90	1.20	1.00	1.70	1.00	1.00	0.80	0.90
CuBr ₂	1.00	1.30	1.80	2.80	1.80	1.80	2.30	2.60	2.40	1.70	2.10	2.60	1.70	1.70	1.30	1.60
	Phenanthroline								Bipyridine							

IS330 TIC vs well number



BE6: 4-Iodophenylboronic acid pinacol ester, 338

LCMS analysis post statistical test

CuBr ₂			Cu(BF ₄) ₂			Cu(NO ₃) ₂			Cu(OTf) ₂			CuCl ₂			CuCl							
1.73	1.68	1.95	1.20	BAD	2.31	1.75	2.03	2.35	2.51	1.70	1.44	BAD	1.72	2.29	2.21	2.28	2.23	BAD	1.33	1.58	2.12	DBU
2.69	1.98	2.08	2.30	BAD	2.45	2.32	BAD	2.92	2.83	1.97	2.53	3.09	2.65	2.21	2.36	1.87	1.92	2.19	2.57	2.13	1.98	Collidine
2.25	2.35	3.06	3.05	3.04	3.36	3.02	2.63	2.72	2.93	BAD	3.19	2.95	3.32	2.50	3.01	2.03	3.06	1.88	2.14	2.32	1.70	P1tBu
3.17	BAD	3.21	3.28	3.07	3.26	3.48	3.93	3.70	4.03	3.28	3.74	3.75	3.27	BAD	BAD	3.20	3.58	2.63	1.80	2.26	2.48	P.S.
1.74	2.40	2.35	1.62	2.18	2.60	2.94	2.22	2.60	BAD	2.97	2.51	2.46	2.82	1.73	2.41	2.30	2.72	2.25	2.19	1.73	1.79	TMU
2.74	3.01	2.30	1.88	2.61	2.54	2.88	3.05	3.11	2.78	BAD	3.25	2.69	3.38	2.28	2.59	1.87	2.15	1.86	BAD	1.67	2.32	Urea
2.74	2.90	2.71	2.88	2.48	2.61	2.57	BAD	3.81	3.51	2.87	3.73	3.43	3.20	3.28	2.76	2.61	3.09	2.38	2.81	2.00	1.73	MTBD
4.01	4.11	3.48	4.28	3.55	3.93	3.80	3.79	3.38	BAD	3.87	3.81	3.70	3.13	3.41	3.92	3.39	3.52	2.74	2.74	3.24	3.23	BTMG
2.11	2.89	2.60	3.01	2.98	2.43	2.36	3.04	3.12	2.99	3.31	2.79	2.62	2.96	2.42	2.48	2.36	3.01	2.70	2.08	1.84	2.49	DBU
2.83	1.89	1.81	2.46	2.28	2.52	2.72	2.96	3.10	3.56	2.91	2.47	2.79	2.75	1.00	1.26	1.18	1.46	2.31	BAD	2.40	2.09	Collidine
2.74	BAD	2.31	BAD	2.51	2.48	3.08	3.73	2.97	3.05	3.15	3.31	2.90	3.68	2.41	1.54	2.18	1.86	2.60	2.63	1.71	1.71	P1tBu
2.96	BAD	3.49	3.76	3.04	3.09	3.21	3.39	4.61	3.34	2.56	2.32	2.71	2.95	1.10	1.16	1.45	1.64	2.40	1.34	2.10	BAD	P.S.
2.39	BAD	2.08	2.46	1.86	1.95	2.70	2.41	3.11	2.77	2.66	2.82	3.15	3.25	1.16	1.69	1.62	1.55	2.52	2.36	2.91	2.55	TMU
1.43	1.45	1.88	BAD	2.07	2.65	1.78	3.13	2.35	3.23	2.00	BAD	2.66	2.93	0.79	1.40	1.21	1.46	1.95	2.36	2.05	2.08	Urea
2.13	BAD	2.71	2.55	1.83	1.17	1.41	1.27	1.50	2.26	1.20	1.42	0.84	1.76	1.23	1.66	1.83	1.79	1.05	0.65	1.08	1.35	MTBD
BAD	2.56	2.88	3.36	1.50	1.93	1.73	1.08	BAD	1.45	1.37	BAD	1.88	BAD	1.38	1.91	1.29	BAD	1.11	1.34	0.75	BAD	BTMG

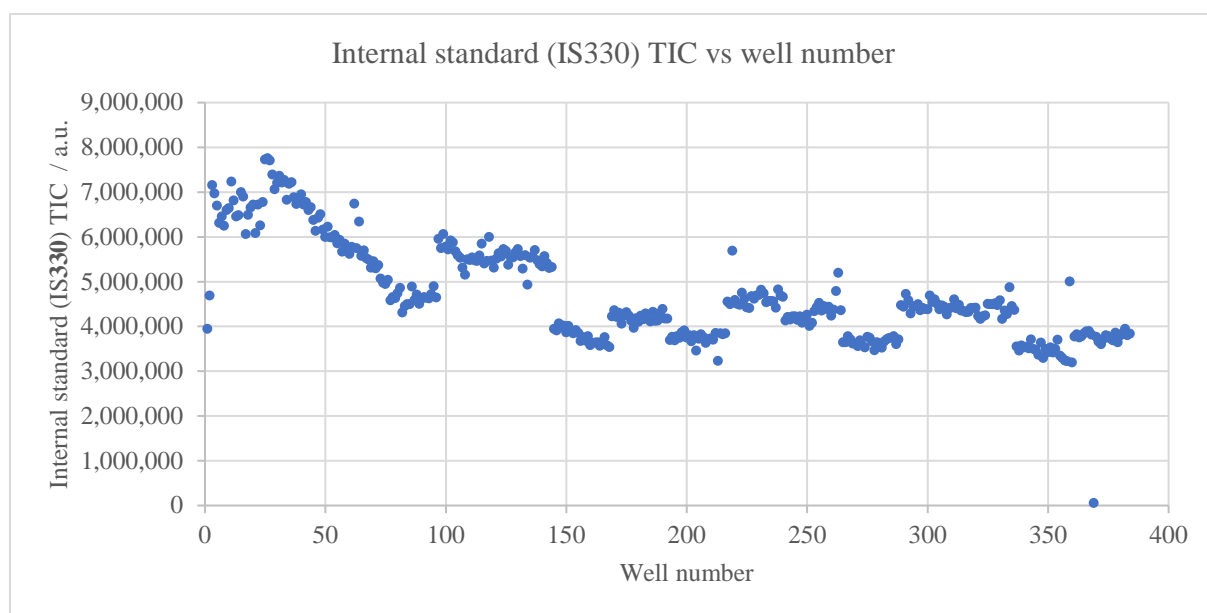
Phenanthroline

Bipyridine

Average heatmap output

	DBU	Collidine	P1tBu	P.S.	TMU	Urea	MTBD	BTMG	DBU	Collidine	P1tBu	P.S.	TMU	Urea	MTBD	BTMG
CuCl	1.70	2.20	2.00	2.30	2.00	1.90	2.20	3.00	2.30	2.30	2.20	1.90	2.60	2.10	1.00	1.10
CuCl ₂	2.30	2.10	2.70	BAD	2.30	2.20	2.90	3.60	2.60	1.20	2.00	1.30	1.50	1.20	1.60	1.50
Cu(OTf) ₂	1.60	2.60	3.20	3.50	2.70	3.10	3.30	3.60	2.90	2.70	3.30	2.60	3.00	2.50	1.30	BAD
Cu(NO ₃) ₂	2.20	2.70	2.80	3.90	2.50	3.00	3.40	3.80	3.10	3.00	3.10	4.00	2.80	2.80	1.80	BAD
Cu(BF ₄) ₂	BAD	2.40	3.00	3.20	2.50	2.50	2.60	3.80	2.60	2.60	2.80	3.00	2.20	2.10	1.40	1.70
CuBr ₂	1.60	2.30	2.70	3.20	2.00	2.50	2.80	4.00	2.70	2.20	BAD	3.40	2.30	1.60	2.50	2.90
	Phenanthroline								Bipyridine							

IS330 TIC vs well number



BE7: 4-Indoleboronic acid pinacol ester, 336
LCMS analysis post statistical test

CuBr ₂				Cu(BF ₄) ₂				Cu(NO ₃) ₂				Cu(OTf) ₂				CuCl ₂				CuCl				
8.5	7.9	8.8	8.6	4.7	4.6	5.3	4.8	10.8	12.8	12.8	16.9	15.0	16.4	16.9	18.1	15.8	14.4	14.4	14.6	20.3	20.6	20.3	21.6	22.6
BAD	15.3	16.7	17.9	9.6	9.0	11.8	8.0	22.2	21.8	21.6	22.2	23.6	20.1	20.7	22.4	20.8	18.1	20.4	18.3	27.7	26.8	27.7	28.1	27.6
25.1	BAD	27.8	23.6	9.6	9.9	4.2	11.3	22.2	21.5	16.0	21.9	21.5	18.9	22.0	12.7	13.3	7.7	12.1	14.9	19.9	21.6	19.9	27.3	23.5
37.0	36.1	33.4	BAD	17.9	17.3	20.8	22.0	38.0	37.1	36.6	35.1	38.5	BAD	43.0	40.4	30.1	32.1	27.5	29.0	49.7	55.7	49.7	47.1	50.6
27.7	27.5	30.9	27.6	6.6	3.8	4.7	5.1	21.2	22.8	21.1	23.6	21.5	22.1	19.7	21.1	15.2	15.1	14.8	16.0	26.5	27.8	26.5	27.6	26.1
26.2	28.7	26.5	26.9	5.2	5.0	4.5	5.4	21.9	21.7	21.7	20.4	21.4	22.2	18.7	21.8	14.1	10.4	18.5	10.8	30.3	27.8	30.3	28.9	27.4
25.2	24.7	24.9	22.9	24.4	21.4	23.0	21.2	25.0	25.5	28.2	25.8	22.8	25.7	20.7	24.2	21.6	21.9	20.5	23.2	24.4	23.0	24.4	26.2	24.0
33.8	34.1	32.0	32.2	24.1	25.2	24.2	28.4	37.2	34.5	35.1	33.4	29.3	29.4	32.2	29.1	26.1	28.5	25.6	24.6	33.7	31.2	33.7	34.1	34.1
15.7	13.3	16.7	14.2	8.7	6.0	7.7	7.0	17.5	16.2	15.8	16.8	11.4	14.2	11.9	13.2	10.9	10.5	12.2	11.2	17.8	20.3	17.8	18.7	21.7
26.3	31.2	25.2	25.4	17.0	16.7	11.5	11.9	27.5	23.8	24.5	26.1	25.0	21.6	22.8	24.4	16.9	16.8	18.8	20.2	33.3	32.6	33.3	34.3	31.3
26.0	25.5	30.8	24.1	9.0	9.0	9.1	13.5	28.5	27.4	24.5	29.5	25.1	22.7	18.9	21.8	14.5	21.2	21.3	17.8	32.2	31.6	32.2	32.1	33.6
52.1	46.9	40.1	46.6	29.9	32.5	21.0	27.8	39.6	48.4	48.4	47.1	50.0	41.0	49.9	41.4	37.2	BAD	44.7	36.2	68.0	59.6	68.0	58.9	BAD
30.3	33.6	27.1	29.7	17.4	17.0	11.2	11.6	24.4	26.8	27.8	27.6	21.5	23.2	26.1	21.2	13.8	19.2	13.0	16.8	34.2	33.3	34.2	33.9	32.6
24.6	32.0	23.5	31.7	16.4	19.0	16.4	17.5	26.5	27.6	25.1	25.1	26.6	22.6	26.0	26.0	24.0	20.7	20.7	16.7	31.5	30.4	31.5	32.7	32.9
25.1	24.4	20.0	25.9	9.2	14.2	14.9	15.5	26.3	26.3	25.7	28.4	17.9	14.9	20.0	24.0	12.0	16.1	10.8	13.4	25.2	23.8	25.2	23.8	25.5
44.6	44.0	42.6	49.1	BAD	27.0	17.0	26.2	47.2	42.3	46.3	46.9	44.3	40.7	42.8	42.5	27.9	30.0	25.6	24.4	43.2	43.3	43.2	45.4	43.8

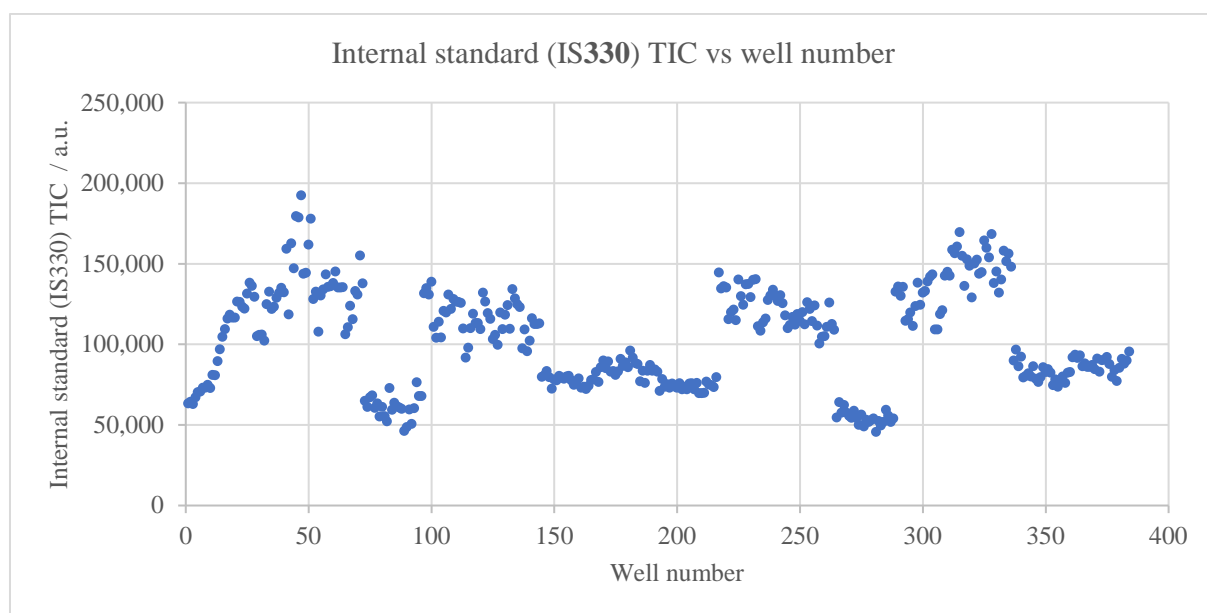
Phenanthroline

Bipyridine

Average heatmap output

	DBU	Collidine	P1tBu	P.S.	TMU	Urea	MTBD	BTMG	DBU	Collidine	P1tBu	P.S.	TMU	Urea	MTBD	BTMG
CuCl	21.3	27.5	23.1	50.8	27.0	28.6	24.4	33.3	19.6	32.9	32.4	62.2	33.5	31.9	24.6	43.9
CuCl ₂	15.1	19.4	12.0	29.7	15.3	13.4	21.8	26.2	11.2	18.2	18.7	39.4	15.7	20.5	13.1	27.0
Cu(OTf) ₂	16.6	21.7	18.8	40.6	21.1	21.0	23.3	30.0	12.7	23.5	22.1	45.6	23.0	25.3	19.2	42.6
Cu(NO ₃) ₂	13.3	21.9	20.4	36.7	22.2	21.5	26.1	35.0	16.6	25.4	27.5	45.9	26.6	26.1	26.7	45.7
Cu(BF ₄) ₂	4.8	9.6	8.7	19.5	5.0	5.0	22.5	25.5	7.3	14.3	10.1	27.8	14.3	17.3	13.4	23.4
CuBr ₂	8.4	16.6	25.5	35.5	28.4	27.1	24.4	33.0	15.0	27.0	26.6	46.4	30.2	28.0	23.9	45.1
	Phenanthroline								Bipyridine							

IS330 TIC vs well number



BE8: Pyridine-3-boronic acid pinacol ester, 335
LCMS analysis post statistical test

CuBr ₂				Cu(BF ₄) ₂				Cu(NO ₃) ₂				Cu(OTf) ₂				CuCl ₂				CuCl			
3.3	1.0	0.5	1.1	2.0	0.5	BAD	2.1	1.0	0.8	0.9	0.7	0.8	BAD	0.5	0.9	0.8	0.6	0.8	0.7	0.7	BAD	0.4	DBU
6.9	9.4	6.9	6.3	9.6	10.0	9.6	11.6	11.0	9.1	13.2	8.4	5.0	3.8	9.6	9.7	11.9	6.8	6.4	9.0	9.4	7.8	10.0	Collidine
11.1	7.5	8.7	6.9	BAD	6.5	2.9	9.0	10.7	10.0	8.8	7.4	7.7	5.7	5.5	4.2	5.3	6.8	3.6	BAD	2.9	3.6	5.2	PitBu
5.8	5.0	6.4	5.8	7.4	4.4	5.3	4.8	6.4	5.8	6.4	7.9	5.7	5.5	6.1	6.2	1.9	5.3	1.7	5.6	4.9	5.6	5.2	P.S.
13.8	8.7	9.0	9.9	10.5	10.2	9.9	8.8	12.2	11.8	15.2	9.1	10.8	11.3	12.8	8.4	6.2	8.7	8.9	9.6	11.0	7.6	10.5	TMU
BAD	10.7	11.2	9.5	BAD	10.6	8.0	11.2	15.0	12.9	16.2	12.1	13.5	BAD	12.2	12.1	9.0	7.7	9.0	9.4	12.6	9.3	10.2	Urea
0.5	1.7	2.5	1.5	BAD	0.7	1.4	0.6	0.4	2.2	2.2	BAD	1.4	0.7	1.1	2.1	1.5	1.2	0.9	0.8	BAD	BAD	MTBD	
10.8	8.2	9.7	5.8	5.4	3.2	3.6	7.2	8.2	5.2	6.3	2.9	5.0	2.6	2.6	6.5	4.7	3.8	6.2	4.8	2.7	2.3	2.7	BTMG
2.4	1.9	1.8	1.7	1.5	0.7	1.0	1.8	1.8	1.2	1.6	0.7	1.2	0.6	0.6	1.0	1.2	1.2	0.7	1.1	0.5	0.6	0.8	DBU
10.8	12.0	8.6	8.7	BAD	7.8	7.6	15.9	11.7	11.3	11.8	7.4	5.1	6.6	6.3	8.8	4.9	6.5	5.7	8.3	6.4	5.3	5.8	Collidine
BAD	6.0	8.4	7.1	5.5	6.6	4.4	10.7	10.7	9.6	8.5	4.1	5.4	2.2	5.9	6.9	6.8	5.5	5.6	6.0	2.8	4.5	0.7	PitBu
BAD	6.0	3.1	4.3	5.3	4.3	3.3	7.2	7.0	4.8	4.6	4.4	4.3	3.1	3.1	3.7	3.1	2.2	2.6	5.4	3.0	3.0	3.6	P.S.
15.7	14.5	10.0	11.8	8.1	8.3	5.6	14.9	11.7	11.9	11.3	7.3	6.4	3.3	4.8	BAD	5.4	4.9	5.1	8.9	6.6	4.9	6.7	TMU
15.6	15.4	11.4	9.9	7.7	7.0	3.7	BAD	13.3	11.2	10.1	8.7	4.1	3.0	5.1	5.9	8.1	5.0	5.7	5.9	6.2	5.3	4.4	Urea
0.5	0.3	0.4	0.3	BAD	BAD	BAD	0.4	0.3	BAD	0.2	BAD	BAD	BAD	BAD	BAD	BAD	BAD	BAD	BAD	BAD	BAD	BAD	MTBD
BAD	3.1	8.1	5.1	3.3	1.3	1.4	4.1	2.2	4.8	3.5	2.2	2.4	0.3	1.2	4.1	2.1	2.2	1.5	2.9	0.4	0.3	0.4	BTMG

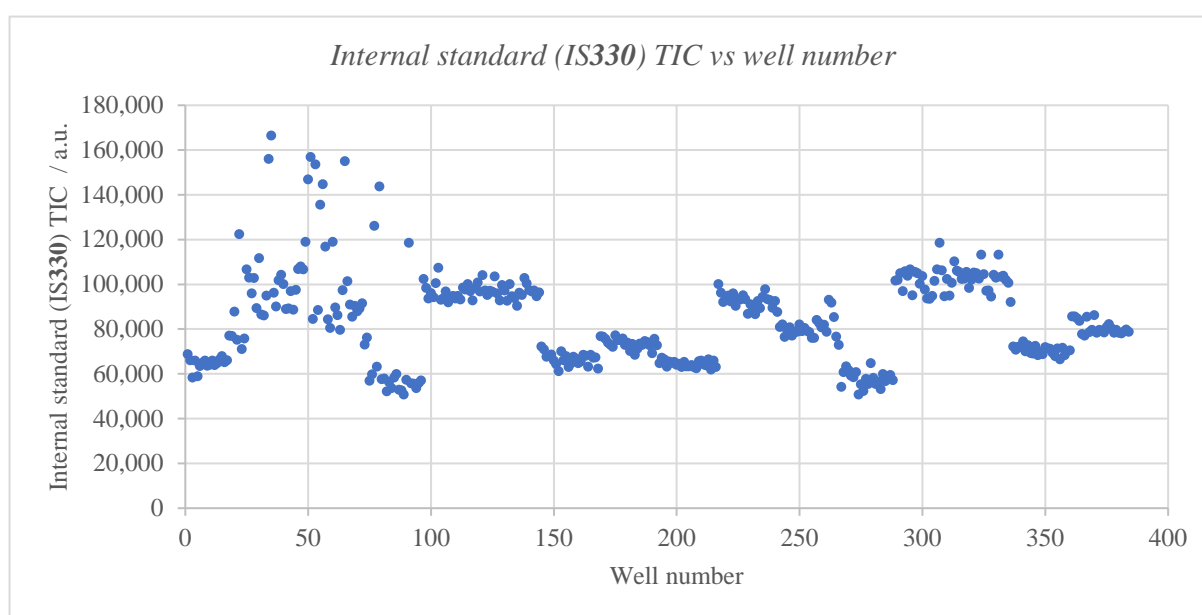
Phenanthroline

Bipyridine

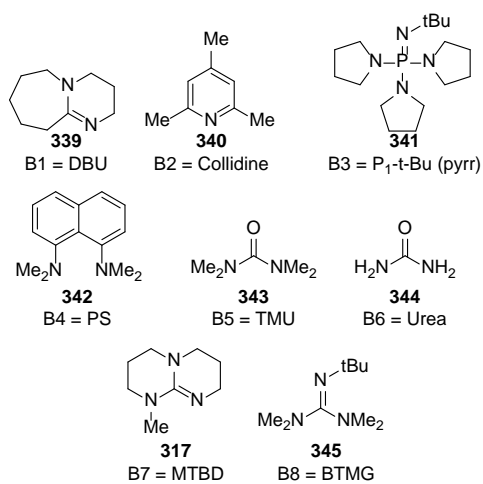
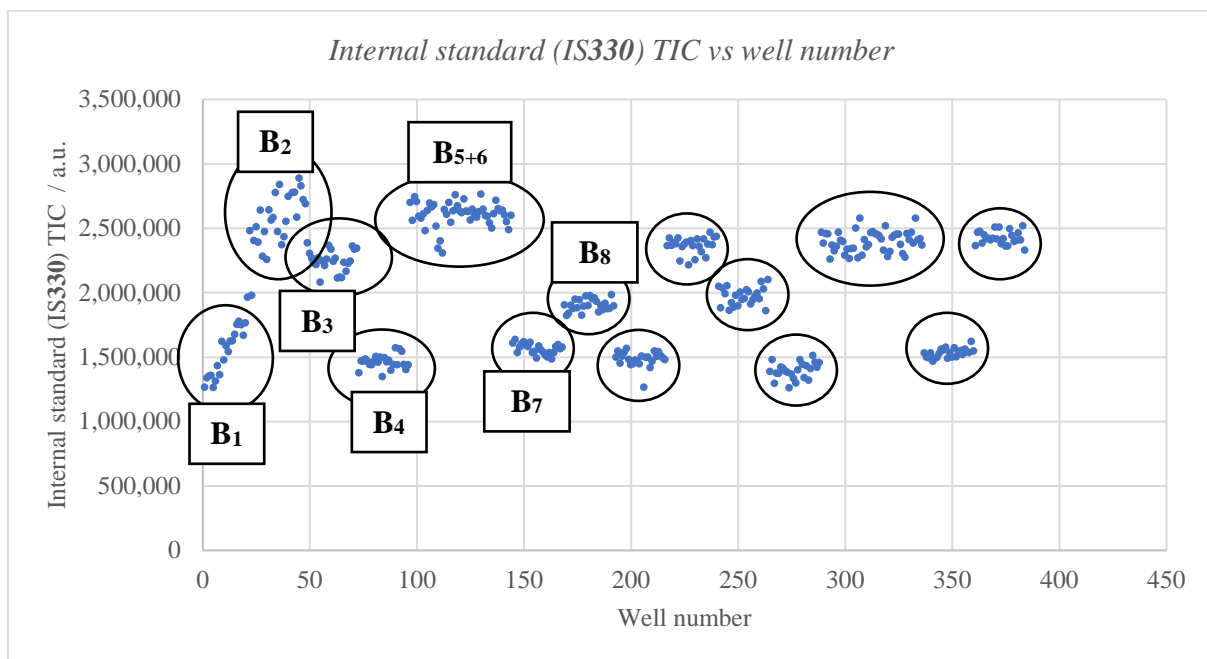
Average heatmap output

	DBU	Collidine	P1tBu	P.S.	TMU	Urea	MTBD	BTMG	DBU	Collidine	P1tBu	P.S.	TMU	Urea	MTBD	BTMG
CuCl	0.6	9.0	3.9	5.3	9.7	10.4	BAD	3.2	0.7	6.4	3.5	3.7	6.8	5.4	BAD	1.0
CuCl ₂	0.8	8.7	5.0	3.8	8.0	9.4	1.4	5.3	1.0	6.5	6.2	2.9	5.2	6.2	BAD	2.5
Cu(OTf) ₂	0.6	6.7	6.6	6.3	11.0	12.6	1.1	3.2	0.8	6.3	4.4	3.7	5.5	5.2	BAD	1.5
Cu(NO ₃) ₂	1.2	11.2	9.6	6.0	13.3	14.0	1.7	6.7	1.6	12.7	9.9	5.9	12.4	11.5	0.3	3.6
Cu(BF ₄) ₂	1.0	9.9	5.4	5.5	9.9	9.9	0.9	3.9	0.9	7.7	5.5	3.9	6.8	6.1	BAD	1.6
CuBr ₂	1.5	7.4	8.6	5.8	10.4	10.4	1.5	8.6	1.9	10.0	7.1	4.4	13.0	13.0	0.4	5.4
	Phenanthroline								Bipyridine							

IS330 TIC vs well number



Ion Suppression of IS330 by different bases



Validation of new internal standard

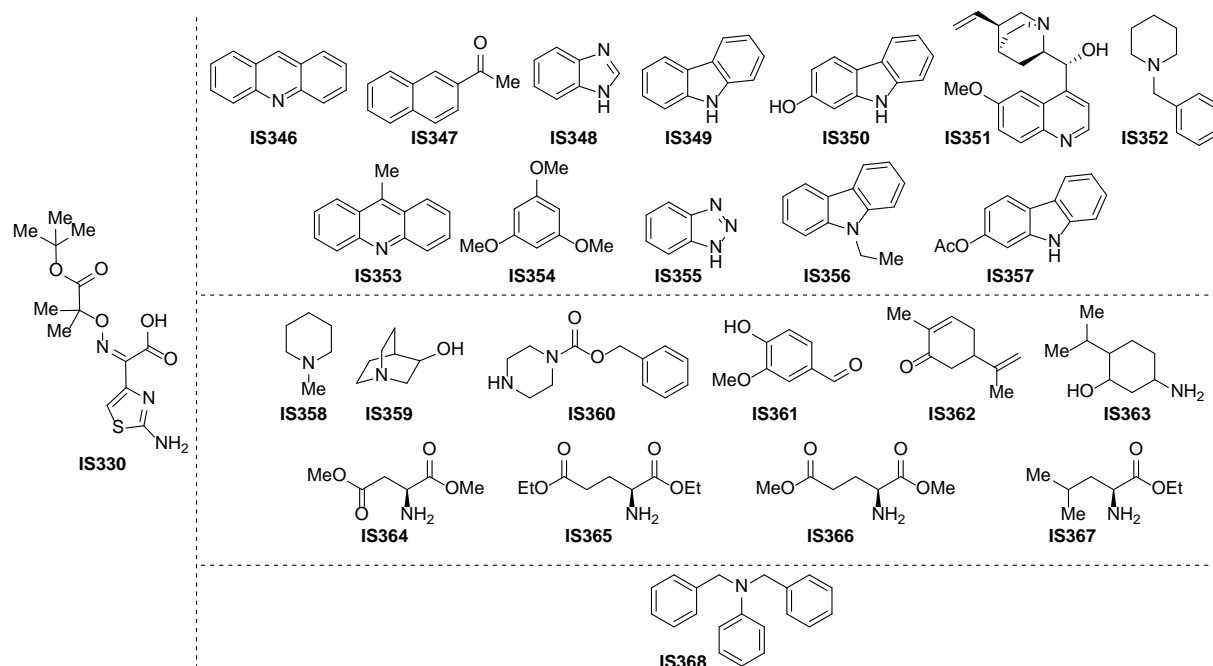


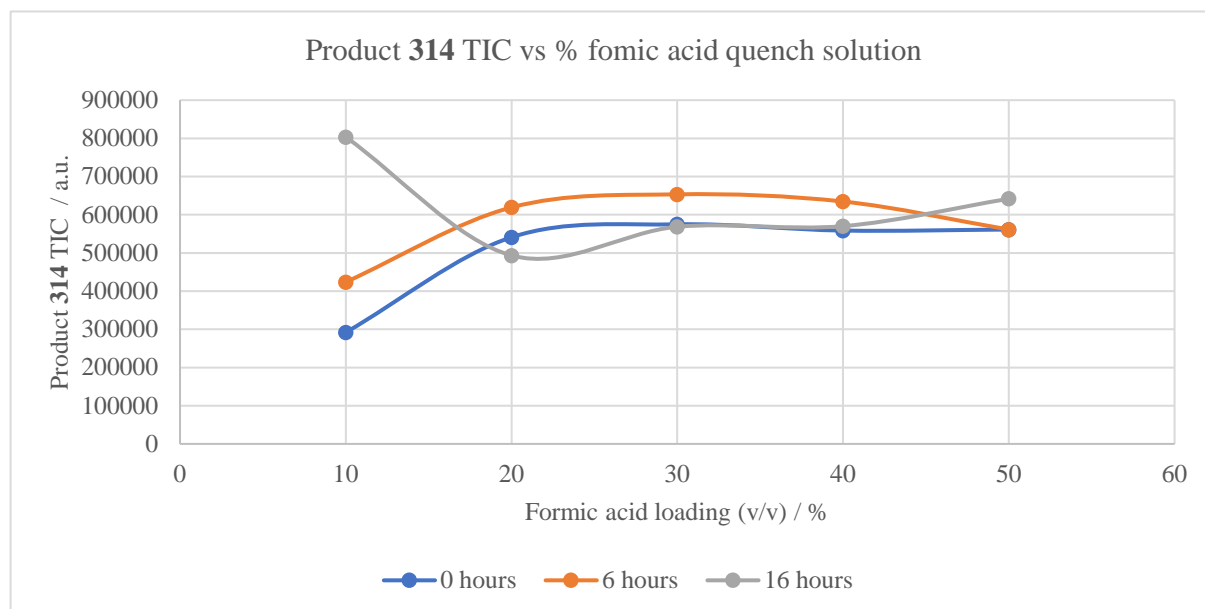
Figure 55: Compounds assessed as potential internal standards

Entry	Internal Standard	[M+H] ⁺	Retention time / mins	Comment
1	IS2	180	0.8	Too early.
2	IS3	171	-	Does not ionise.
3	IS4	119	0.3	Too early. Free N-H could react.
4	IS5	168	-	Does not ionise. Free N-H, could react.
5	IS6	184	-	Does not ionise. Free N-H could react.
6	IS7	325	0.60	Multiple ionisation modes
7	IS8	176	0.60	Too early. Free N-H could react.
8	IS9	194	0.60	Too early.
9	IS10	169	-	Does not ionise.
10	IS11	120	0.40	Too early. Free N-H could react.
11	IS12	196	-	Does not ionise. Free N-H could react.
12	IS13	226	0.70	Too early. Free N-H could react.
13	IS14	100	-	Too low molecular weight
14	IS15	128	-	Too low molecular weight
15	IS16	221	0.60	Too early. Free N-H could react.
16	IS17	153	-	Does not ionise
17	IS18	153	-	Does not ionise
18	IS19	158	-	Does not ionise
19	IS20	162	0.60	Too early. Primary amine could react.
20	IS21	204	0.60	Too early. Primary amine could react.
21	IS22	176	0.40	Too early. Primary amine could react.
22	IS23	146	-	Too early. Primary amine could react.
23	IS24	273	1.20	Tertiary amine and good retention time.

Table 7: Retention time of internal standards from Figure 55.

Optimisation of Formic acid quench

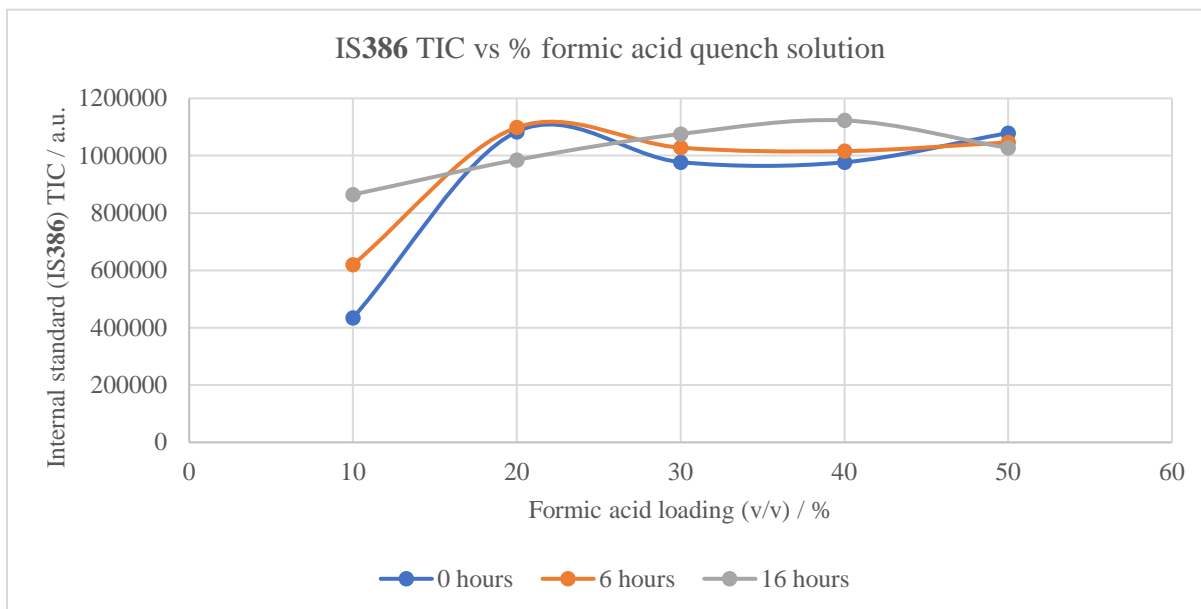
Miniature reactions were prepared in a 1 mL LCMS vial using the following procedure. Five LCMS vials equipped with a small magnetic stirrer bars were charged with the following DMSO stock solutions in the following order: 4-phenylpiperidine (100 μ L of 13.2 mM stock solution), phenylboronic acid pinacol ester (100 μ L of 13.2 mM stock solution), DBU (100 μ L of 39.5 mM stock solution), 1,10-phenanthroline (100 μ L of 1.3 mM stock solution), copper(I) chloride (100 μ L of 13.2 mM stock solution). The reaction was stirred at room temperature, open to the air, for 3 hours and subsequently quenched with 500 μ L IS368 quench stock solution (prepared by serial dilution of 135 μ L of 0.1M solution in acetonitrile into 100 mL prepared with 10–50% formic acid (v/v) in acetonitrile). The samples were sealed using parafilm and analysed by LCMS and ratios of the product : internal standard was taken. The quenched vials were subsequently analysed at 6 hours and 16 hours to assess whether the quenching mixture stopped the reaction.



Entry	Formic acid quench /%	t = 0 hours / a.u.	t = 6 hours / a.u.	t = 16 hours / a.u.
1	10	620110	864389	434629
2	20	1083564	1098429	985457
3	30	977637	1027976	1075748
4	40	977013	1015980	1122986
5	50	1079042	1046374	1026822

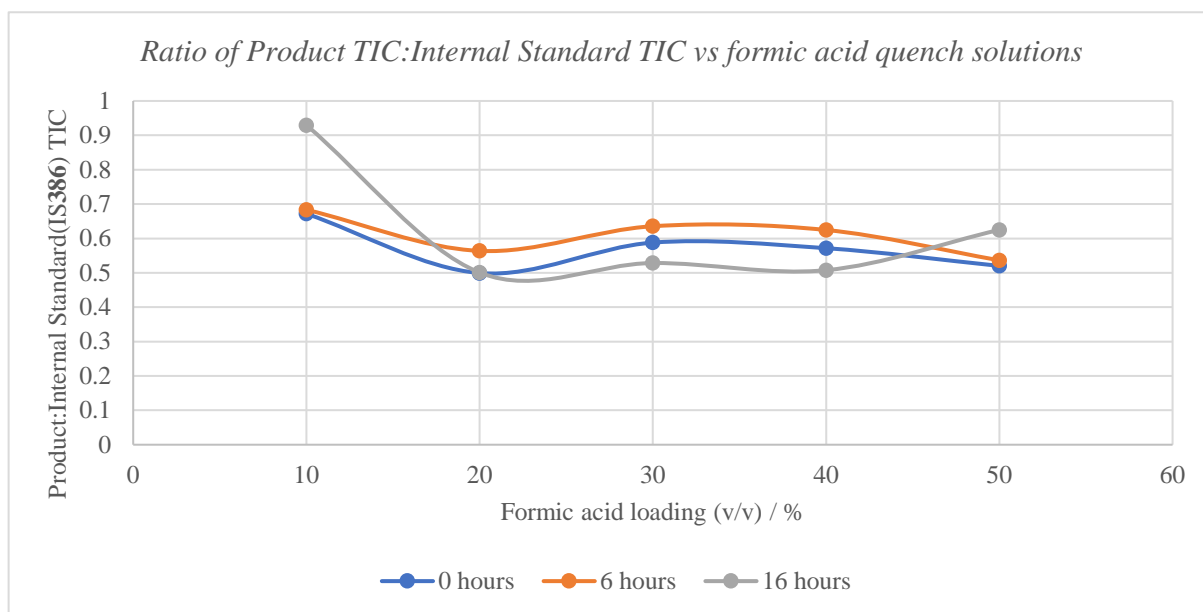
Graph 14: Product 314 TIC vs formic acid loading (v/v %) shows that 10% formic acid does not quench the reaction.

Entry	Formic acid quench /%	t = 0 hours / a.u.	t = 6 hours / a.u.	t = 16 hours / a.u.
1	10	291975	423829	803566
2	20	541112	619282	493434
3	30	574848	653397	568549
4	40	558542	634610	570138
5	50	561290	561285	641840



Graph 15: IS386 TIC vs formic acid loading (v/v %) shows 50% gives the most consistent IS368 TIC.

Entry	Formic acid quench /%	t = 0 hours / a.u.	t = 6 hours / a.u.	t = 16 hours / a.u.
1	10	1.463114	1.075691	1.488583
2	20	2.002476	1.773714	1.997140
3	30	1.700688	1.573279	1.892094
4	40	1.749220	1.600952	1.969674
5	50	1.922432	1.864247	1.599810



Graph 16: Ratio of IS386:Product TIC vs formic acid loading (v/v %) shows the most consistent reactions are at 50:50 formic acid:water.

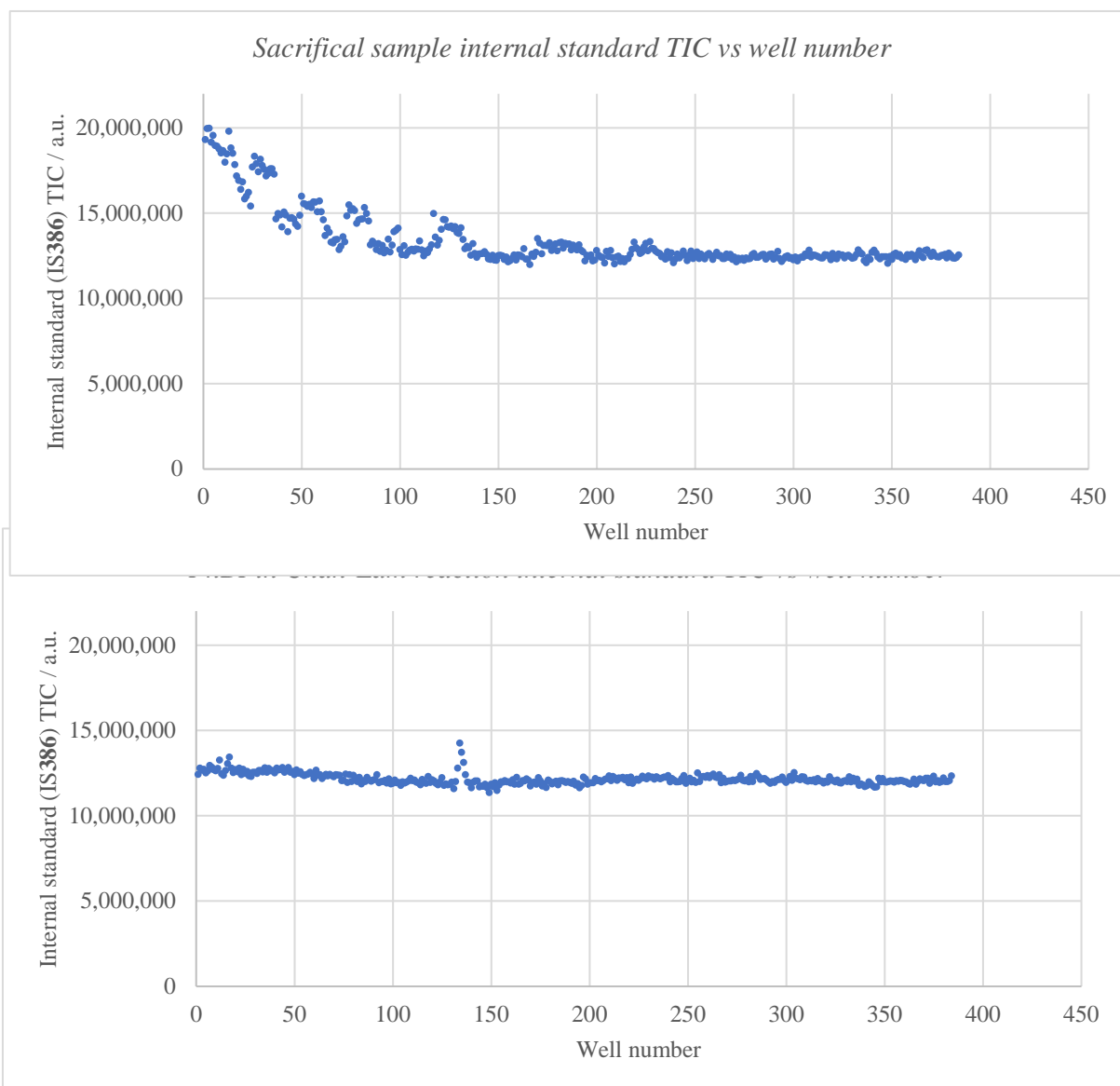
Optimisation of IS368 loading after mass spec cleaning and tuning

An LCMS vial was charged with 500 μL of IS386 stock solution with different concentrations (3.67 mM, 2.75 mM, 0.275 mM and 0.139 mM) in 50:50 formic acid:water and topped up with 401 μL of acetonitrile. Each sample was analysed by LCMS with different injection volumes (0.1, 0.7 and 1.0 μL) to assess the mass-spec detector response. IS368 peaks were integrated to obtain a total ion count (TIC).

Entry	IS386 concentration / mM	LCMS injection volume / μL	TIC / a.u.
1	3.67	0.1	44,000,000
2	2.75	0.1	29,092,295
3	0.275	1.0	28,064,809
4	0.275	0.7	21,778,384
5	0.139	1.0	13,850,682
6	0.139	0.7	13,307,915

Developing a Sacrificial method to achieve quantitative LCMS

An LCMS vial was charged with 1 mL of 0.135 M internal standard in 50:50 formic acid:water, 800 μ L of 0.0125 mM 1,4-diphenylpiperidine **313** stock solution in acetonitrile and 2.0 μ L of DMSO. The vial was sealed with parafilm and placed into the “controller vial” rack in a Shimadzu autosampler. The sample was run 384 times to condition the mass spectrometer and analytical column. Once conditioned, an analysis plate was prepared following analysis plate general procedure 3. The analysis plate was run directly after the sacrificial sample had completed.



7.5. High-Throughput Quantitative Analysis of Chan-Lam Reaction

Procedure for 384 nanomolar scale reactions (2.5 μ L volume) in one quarter of a 1536-well plate. Stock solutions of each component were prepared according to general procedure 1: 4-phenylpiperidine **134** (1.0 M in DMSO), boronic esters (**311-336**, 0.33 M in DMSO), organic base (**317**, **339**, **340**, **343-345**, **387**), 3M in DMSO), ligand (**319** and **318**, 0.025 M in DMSO), catalyst (C1-C8, 0.1 M in DMSO) using Spreadsheet 3. For the source plate layout, see Figure 57. For each 1536-well plate experiment, each well was charged with the amount of stock solution stated in ‘Source plate loading’ column, using a digital air displacement pipette, such that enough solution was present to dose the corresponding reactor plate.

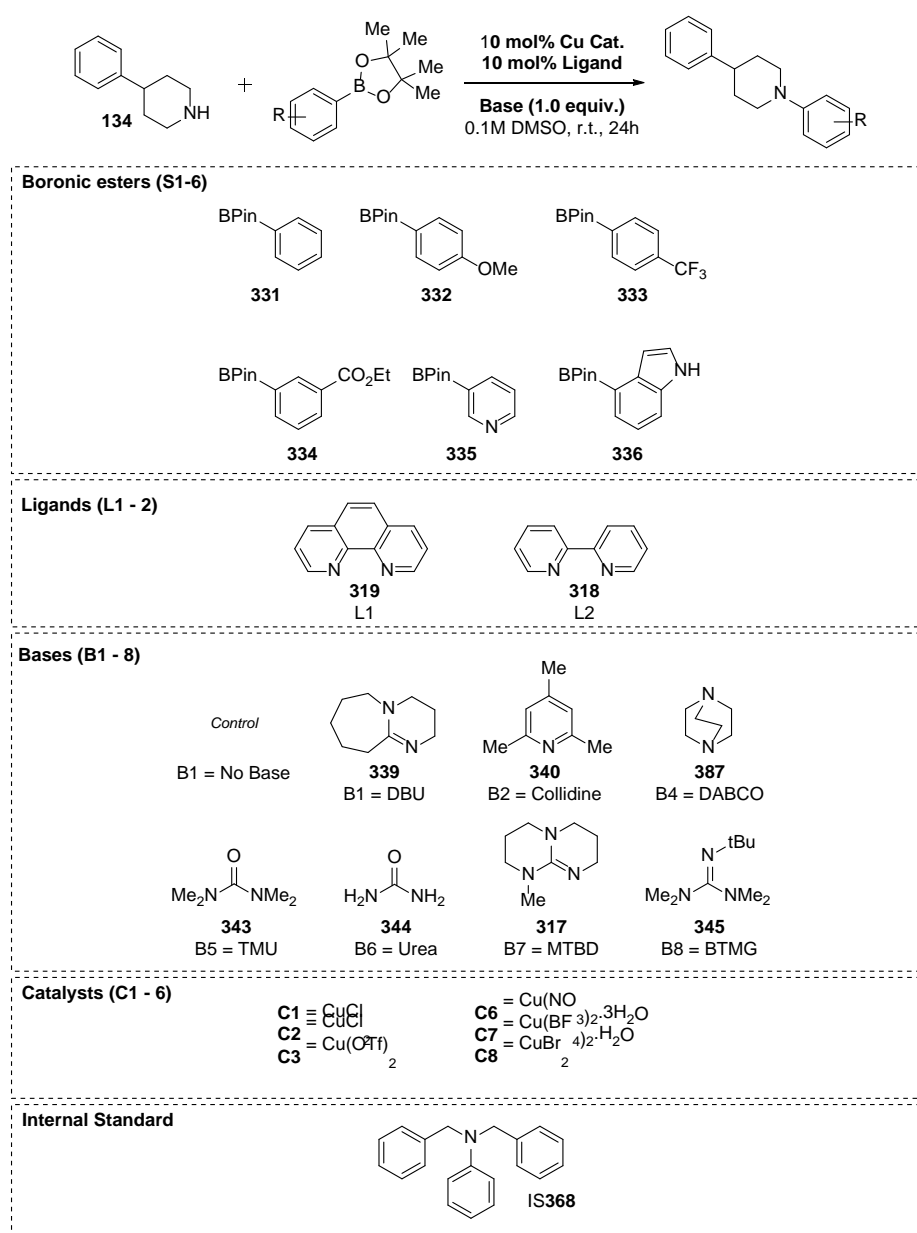


Figure 56: Components assessed in 1536-well reactor plate

The Mosquito was used to transfer aliquot volumes according to the “Solubility problems? Aliquotvol” column on the Excel Spreadsheet. Two different boronic ester stock solutions were

employed: **Mosquito aliquot protocol 1 for normal solubility**: R1 was added in 375 nL, S1 was added in 750 nL, B1-8 was added in 250 nL, L1/2 was added in 750 nL and catalyst added in 125 nL resulting in a total reaction volume of 2.5 μ L. **Mosquito aliquot protocol 1 for low solubility**: R1 was added in 250 nL, S1 was added in 1250 nL (2×625 nL), B1-8 was added in 250 nL, L1/2 was added in 500 nL and catalyst added in 250 nL resulting in a total reaction volume of 2.5 μ L. When the catalyst had been added, the Mosquito mixed the reaction mixture together three times using the mix-dispense feature. The 1536-well reactor plate was then sealed with aluminium foil and placed under a heavy glass sheet for 24 hours.

Source Plate Layout

	1	2	3	4	5	6	7	8	9	10	11	12	13	14	15	16	17	18	19	20	21	22	23	24
A															C6	C5	C4	C3	C2	C1	L1	B1	S1	R1
B															C6	C5	C4	C3	C2	C1	L1	B2	S1	R1
C															C6	C5	C4	C3	C2	C1	L1	B3	S1	R1
D															C6	C5	C4	C3	C2	C1	L1	B4	S1	R1
E															C6	C5	C4	C3	C2	C1	L1	B5	S1	R1
F															C6	C5	C4	C3	C2	C1	L1	B6	S1	R1
G															C6	C5	C4	C3	C2	C1	L1	B7	S1	R1
H															C6	C5	C4	C3	C2	C1	L1	B8	S1	R1
I															C6	C5	C4	C3	C2	C1	L2	B1	S1	R1
J															C6	C5	C4	C3	C2	C1	L2	B2	S1	R1
K															C6	C5	C4	C3	C2	C1	L2	B3	S1	R1
L															C6	C5	C4	C3	C2	C1	L2	B4	S1	R1
M															C6	C5	C4	C3	C2	C1	L2	B5	S1	R1
N															C6	C5	C4	C3	C2	C1	L2	B6	S1	R1
O															C6	C5	C4	C3	C2	C1	L2	B7	S1	R1
P															C6	C5	C4	C3	C2	C1	L2	B8	S1	R1

Figure 57: Source plate used to dose 1536-well reactor plate

Analysis plate preparation

Prior to quantitative analysis, the LCMS was cleaned using general procedure 5. Analysis plates were prepared according to general procedure 3 and Calibration curves were prepared using general procedure 4. If curves were found to undergo non-linear correlations, a quadratic formula was used to fit the data.²⁴⁶ Each substrate was run in using a bespoke LCMS assay method file (Appendix 2) with bespoke autosampler aliquot volume and IS368 stock solution shown in Table 8. Each assay was 1.8 minute and each plate analysed using General procedure 6.

Optimised LCMS assay conditions

Entry	Product	Autosampler aliquot volume / μL	IS stock solution / μL of 0.1M IS368 S.S. in 100 mL
1	314	0.5	135.0
2	315	0.3	225.0
3	316	1.0	62.5
4	369	0.3	225.0
5	370	0.3	225.0
6	371	0.3	225.0

PLATE	# reagents	How much of plate?	Input wells/column	Scale L.R. (μmol)	Final conc. Rxn (M)	Stand. Aliq. (μL)	Reactor tot vol (μL)	
1536	5	All	32	0.25	0.1	0.5	2.5	
constant?	Reagent	Compound	Reaction parameters					Solubility problems?
(constant)	R1	4-phenylpicridine	CAS	Cat No	FW (gMol-1)	Equiv.	Amount (μMol)	mg per rxn
(constant)	S1	PhBPin	771-99-3	P 034	161.12	1	0.25	4.03E-02
	S2	4-OMeBPin	24388-23-6	HTE	204.076	1	0.25	5.10E-02
	S3	3-EOACBPin	171364-79-7	HTE	234.102	1	0.25	5.85E-02
	S4	5-IndoleBPin	269410-00-6	HTE	276.139	1	0.25	6.90E-02
	S5	4-CFBPin	269410-24-4	HTE	243.113	1	0.25	6.08E-02
	S6	3-PyridineBPin	214360-65-3	HTE	272.074	1	0.25	6.80E-02
(k-constant, y-variable)	B1	No Base	181219-01-2	HTE	205.064	1	0.25	5.33E-02
	B2	DBU	6674-22-2	D301	152.24	1	0	0.00E+00
	B3	Collidine	108-75-8	C31	121.18	1	0.25	3.81E-02
	B4	DABCO	280-57-9	D052	112.17	1	0.25	3.03E-02
	B5	Tetramethylurea	632-22-4	Dave	116.16	1	0.25	2.80E-02
	B6	Urea	57-13-6	U 002	60.06	1	0.25	2.90E-02
	B7	MTBD	84030-20-6	Dave	153.22	1	0.25	1.90E-02
	B8	BTMG	29166-72-1	B032	171.28	1	0.25	3.83E-02
(k-constant, y-variable)	C1	Cu(I)Cl	7758-89-6	cat 025	99.00	0.1	0.025	2.48E-03
	C2	CuCl2	34946-82-2	IC058	134.45	0.1	0.025	3.36E-03
	C3	Cu(II)(OTf)2	10091-43-3	cat 150	361.68	0.1	0.025	9.04E-03
	C4	Cu(II)(NG3)2.3H2O	207121-39-9	IC010	241.60	0.1	0.025	6.04E-03
	C5	Cu(II)(BF4)2.H2O	7789-45-9	IC014	237.16	0.1	0.025	5.93E-03
	C6	Cu(II)Br2	7789-45-9	IC022	223.35	0.1	0.025	5.58E-03
(k-variable, y-constant)	L1	1,10-phenantroline	66-71-7	P 228	180.21	0.1	0.025	4.51E-03
NORMAL DILUTION	L2	2,2-bipyridyl	366-18-7	B 462	156.18	0.1	0.025	3.90E-03
(k-variable, y-constant)	L1	1,10-phenantroline	66-71-7	P 228	180.21	0.1	0.025	4.51E-03
INCREASED DILUTION	L2	2,2-bipyridyl	366-18-7	B 462	156.18	0.1	0.025	3.90E-03

Table 8: Autosampler and IS368 stock solution preparation for substrates

Stock solution (μmol/vial)	Stock solution (min vol/vial)	Source (abs vol/well)	Source (rec vol/well)	Source plate loading (vol/well μL)	Liquid reagents (vol/SS)	DMSO Top-up
1000	259	9	16	62.5	X	X
700	691	24	43			
700	691	24	43	43.75	X	X
700	691	24	43			
700	691	24	43			
900	864	30	54	56.25	X	X
900	864	30	54			
100	0	0	0		X	X
100	0	6	11		13.7	86.3
100	0	6	11		13.3	86.7
100	0	6	11	50	X	X
100	0	6	11		12.0	88.0
100	0	6	11		X	X
100	0	6	11		14.4	85.6
100	0	6	11		20.2	79.8
400	14	1	1			
400	14	1	1			
400	14	1	1	25	X	X
400	14	1	1			
400	14	1	1			
400	14	1	1			
400	14	1	1			
400	259	18	32	50.0	X	X
400	259	18	32			
400	173	12	22	50.0	X	X
400	173	12	22			

Spreadsheet 3: High-throughput screen of Chan-Lam reaction (1 x 4 x 8 x 2 x 6 screen). Two different boronic ester stock solution concentrations were necessary. Boronic esters S1-S4 (**331**, **332**, **334**, **336**) were prepared at 0.25M and was added into the reactor plate in 1.00 μL. Boronic esters S5-S6 (**333**, **335**) were prepared at 0.2M and was added into the reactor plate in 1.25 μL. The ligand concentration was adjusted to allow for the more dilute boronic ester stock solution. For boronic esters S1-S4 (**331**, **332**, **334**, **336**), ligand L1-2 (**319** and **318**) (0.033M) was added in 750 nL. For boronic esters S5-S6 (**333**, **335**), ligand L1-2 (**319** and **318**) (0.05M) was added in 500 nL.

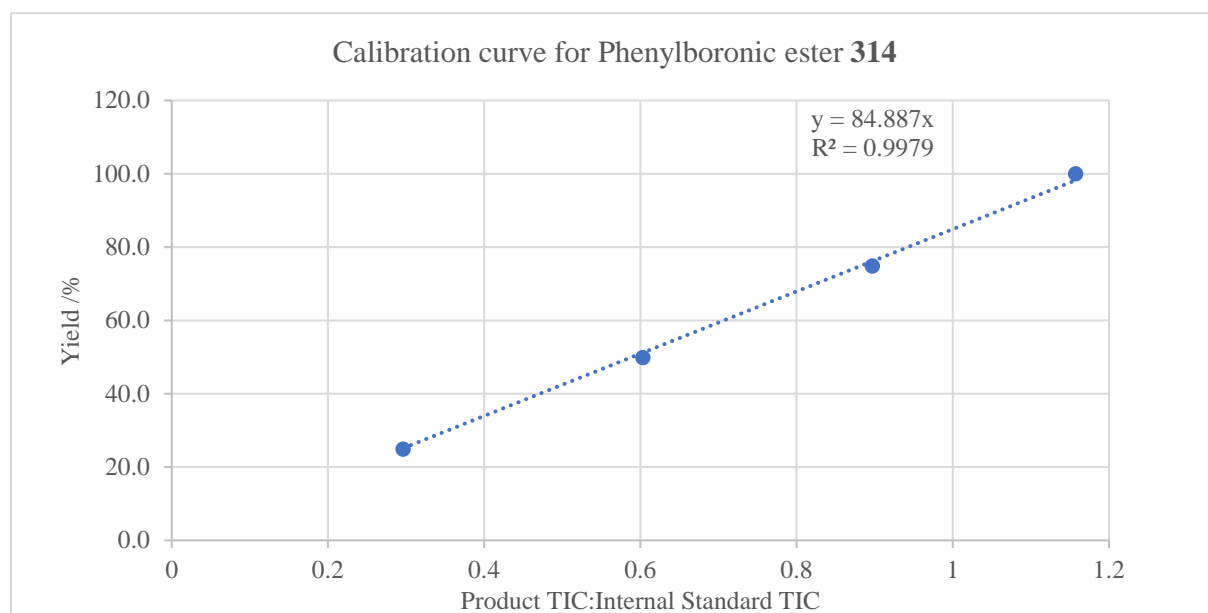
S1 = Phenylboronic acid pinacol ester, 331

		CuBr ₂				Cu(BF ₄) ₂				Cu(NO ₃) ₂				Cu(OTf) ₂				CuCl ₂				CuCl				
0.82	0.91	0.82	0.87	0.66	0.81	0.84	0.74	0.73	0.72	0.80	0.73	0.67	0.64	0.71	0.82	0.85	0.85	0.75	0.92	0.93	0.93	BAD	0.93	No Base		
0.78	0.84	0.80	0.88	0.78	0.79	0.84	0.82	0.80	0.80	0.84	0.78	0.84	0.80	0.79	0.81	0.79	0.78	0.75	0.80	0.84	0.82	0.82	0.79	DBU		
0.88	0.93	0.88	0.90	0.90	0.86	0.95	0.87	0.79	0.79	0.85	0.77	0.84	0.87	0.83	0.97	0.95	0.90	0.90	0.99	0.93	0.96	0.96	0.97	Collidine		
0.96	1.01	0.96	0.94	0.99	0.90	1.03	0.92	0.91	0.95	0.87	0.87	0.92	0.95	0.86	0.98	0.96	0.96	0.93	1.02	1.01	0.99	0.99	0.95	DABCO		
0.86	0.99	0.88	0.95	0.93	0.90	0.92	0.88	0.85	0.79	0.81	0.81	0.85	0.88	0.80	0.98	0.99	0.87	0.93	1.04	0.98	0.97	0.97	0.97	TMU		
0.86	0.93	0.91	0.90	0.91	0.88	0.89	0.96	0.90	0.83	0.83	0.83	0.87	0.81	0.79	0.97	0.94	0.99	0.87	1.03	1.01	0.96	0.96	0.98	Urea		
0.74	0.75	0.71	0.77	0.71	0.70	0.76	0.71	0.78	0.73	0.79	0.79	0.79	0.77	0.79	0.76	0.78	0.78	0.84	0.75	0.78	0.78	0.75	0.67	MTBD		
0.98	0.99	0.99	0.95	0.94	0.94	0.93	0.92	0.98	0.95	0.97	0.97	1.02	0.97	0.95	1.00	0.97	0.92	0.92	0.96	0.94	0.90	0.90	0.81	BTMG		
0.90	0.83	0.95	0.96	0.92	0.90	0.86	0.90	0.87	0.88	0.81	0.81	0.89	0.83	0.88	0.98	0.95	0.96	0.96	1.14	1.02	0.97	0.97	1.04	No Base		
0.78	0.79	0.79	0.81	0.73	0.75	0.74	0.74	0.75	0.77	0.75	0.75	0.87	0.82	0.76	0.78	0.89	0.78	0.74	0.83	0.83	0.80	0.80	0.76	DBU		
0.96	0.99	0.94	1.04	1.03	1.01	0.96	1.02	0.98	0.95	1.03	0.96	1.02	0.98	0.96	1.04	1.00	0.93	1.07	1.13	1.13	0.99	0.99	1.13	Collidine		
0.85	0.99	0.91	0.99	0.99	1.01	1.10	0.99	1.03	1.00	1.00	0.93	1.03	0.97	0.99	1.00	1.07	0.94	0.94	1.10	1.10	1.03	1.03	1.11	DABCO		
1.04	1.08	1.05	1.09	1.08	1.05	1.11	1.05	0.94	1.01	0.94	1.00	1.06	1.01	0.97	0.97	1.07	1.07	1.07	1.11	1.14	1.02	1.02	1.05	TMU		
1.10	1.07	1.06	1.10	1.05	1.06	1.02	1.10	0.97	1.05	1.01	1.10	0.99	0.95	0.97	1.07	1.04	0.98	1.10	1.11	1.11	1.02	1.10	1.10	Urea		
0.77	0.77	0.72	0.81	0.64	0.64	0.73	0.73	0.79	0.80	0.74	0.84	0.77	0.77	0.74	0.75	0.75	0.80	0.80	0.72	0.76	0.71	0.71	0.65	MTBD		
1.00	1.07	1.09	1.15	0.92	0.91	1.00	1.05	0.99	1.03	0.92	BAD	0.89	0.91	1.01	1.00	1.02	0.99	0.92	0.92	1.00	1.04	1.04	0.84	BTMG		
Phenanthroline												Bipyridine														

Average of data repeats from quantitative LCMS assay

	No Base	DBU	Collidine	DABCO	TMU	Urea	MTBD	BTMG	No Base	DBU	Collidine	DABCO	TMU	Urea	MTBD	BTMG
CuCl	0.63	0.45	0.67	0.63	0.60	0.64	0.47	0.61	0.68	0.50	0.63	0.68	0.65	0.68	0.39	0.58
CuCl ₂	0.59	0.43	0.62	0.67	0.60	0.62	0.50	0.63	0.62	0.51	0.67	0.71	0.66	0.59	0.45	0.63
Cu(OTf) ₂	0.58	0.46	0.61	0.56	0.55	0.59	0.46	0.69	0.68	0.52	0.67	0.71	0.69	0.61	0.39	0.59
Cu(NO ₃) ₂	0.53	0.47	0.54	0.57	0.51	0.54	0.45	0.71	0.65	0.48	0.67	0.70	0.62	0.62	0.42	0.64
Cu(BF ₄) ₂	0.57	0.43	0.63	0.64	0.55	0.63	0.34	0.67	0.72	0.47	0.73	0.71	0.66	0.66	0.33	0.55
CuBr ₂	0.52	0.44	0.62	0.61	0.50	0.62	BAD	0.69	0.65	0.47	0.68	0.63	0.63	0.60	0.34	0.59
Phenanthroline								Bipyridine								

Calibration curve post quantitative LCMS assay



Calibrated high-throughput optimisation of S1

	No Base	DBU	Collidine	DABCO	TMU	Urea	MTBD	BTMG	No Base	DBU	Collidine	DABCO	TMU	Urea	MTBD	BTMG
CuCl	53.2	38.4	57.0	53.4	50.8	54.0	39.7	52.1	57.7	42.7	53.4	57.7	55.1	58.0	33.4	49.3
CuCl ₂	49.8	36.3	52.6	57.2	51.1	52.6	42.5	53.2	52.4	42.9	56.9	60.0	56.4	50.5	38.6	53.7
Cu(OTf) ₂	49.5	39.3	51.5	47.5	46.8	49.7	39.1	58.7	57.6	44.1	56.9	60.3	58.4	52.1	33.2	50.3
Cu(NO ₃) ₂	45.2	40.2	45.6	48.0	43.7	46.0	38.0	60.0	55.5	41.1	57.1	59.1	52.8	52.2	35.3	53.9
Cu(BF ₄) ₂	48.0	36.7	53.9	54.2	46.7	53.6	29.0	57.2	60.9	40.3	62.1	60.4	55.7	56.2	27.9	46.3
CuBr ₂	44.0	37.6	52.5	51.4	42.6	52.4	#VALUE!	58.9	55.0	39.9	57.8	53.4	53.9	50.7	29.3	50.0
Phenanthroline								Bipyridine								

S2 = 4-Methoxyphenylboronic acid pinacol ester, 332

		CuBr ₂				Cu(BF ₄) ₂				Cu(NO ₃) ₂				Cu(OTf) ₂				CuCl ₂				CuCl						
1.27	1.27	1.28	1.31	1.41	1.34	1.32	1.44	1.35	1.39	1.36	1.32	1.46	1.57	1.43	1.48	1.53	1.54	1.47	1.49	1.48	1.57	1.48	1.53	1.57	1.53	1.60	No Base	
1.06	1.04	1.07	1.15	1.05	0.95	0.87	0.96	1.17	1.17	1.13	1.10	1.34	1.28	1.27	1.26	1.26	1.25	1.22	1.19	1.27	1.13	1.27	1.25	1.25	1.25	1.21	DBU	
1.39	1.43	1.39	1.44	1.54	1.53	1.56	1.50	1.43	1.36	1.39	1.31	1.53	1.47	1.53	1.48	1.56	1.51	1.54	1.53	1.69	1.56	1.69	1.55	1.55	1.46	1.46	Collidine	
BAD	1.48	1.44	1.45	1.52	1.46	1.42	1.36	1.32	1.41	1.39	1.35	1.56	1.57	1.56	1.51	1.52	1.49	1.53	1.51	BAD	1.65	1.65	1.71	1.53	1.53	1.53	DABCO	
1.30	1.40	1.32	1.41	1.41	1.35	1.38	1.36	1.30	1.32	1.26	1.28	1.39	1.52	1.45	1.39	1.40	1.47	1.44	1.41	1.53	1.42	1.53	1.58	1.42	1.60	1.60	TMU	
1.45	1.44	1.43	1.44	1.49	1.41	1.56	1.49	1.37	1.42	1.32	1.31	1.44	1.46	1.39	1.39	1.43	1.44	1.41	1.43	1.58	1.59	1.58	1.60	1.48	1.60	1.48	Urea	
1.41	1.44	1.38	1.32	1.26	1.23	1.23	1.26	1.46	1.35	1.45	1.33	1.42	1.46	1.37	1.48	1.58	1.50	1.44	1.46	1.35	1.33	1.35	1.37	1.33	1.24	1.24	MTBD	
1.59	1.62	1.63	1.58	1.42	1.43	1.47	1.46	1.56	1.56	1.55	1.58	1.59	1.60	1.57	1.61	BAD	1.56	1.52	1.56	1.47	1.47	1.47	1.57	1.44	1.44	1.44	BTMG	
1.45	1.52	1.55	1.57	1.45	1.48	1.51	1.48	1.42	1.47	1.58	1.44	1.39	1.35	1.46	1.43	1.40	1.31	1.40	1.36	1.44	1.61	1.44	1.56	1.56	1.56	1.56	No Base	
1.36	1.30	1.38	1.25	1.14	1.11	1.13	1.09	1.34	1.34	1.26	1.22	1.32	1.35	1.26	1.34	1.28	1.29	1.29	1.25	1.31	1.32	1.31	1.30	1.30	1.38	1.38	DBU	
1.45	1.54	BAD	1.46	1.48	1.51	1.50	1.46	1.53	1.45	1.53	1.43	1.52	1.53	1.62	1.51	1.52	1.45	1.52	1.46	1.68	1.57	1.68	1.65	1.54	1.54	1.54	Collidine	
BAD	BAD	BAD	BAD	BAD	1.49	1.47	1.42	1.58	1.62	1.60	1.50	1.51	1.53	1.58	1.54	1.49	1.47	1.54	1.49	1.60	1.61	1.60	1.53	1.50	1.50	1.50	DABCO	
1.40	1.38	1.41	1.41	1.39	1.49	1.30	1.36	1.46	1.43	1.49	1.36	1.45	1.55	1.56	1.53	1.42	1.44	1.36	1.41	1.61	1.57	1.61	1.41	1.39	1.39	1.39	TMU	
1.33	1.45	1.31	1.39	1.39	1.30	1.36	1.34	1.35	1.39	1.37	1.44	1.51	1.46	1.44	1.43	1.55	1.51	1.48	BAD	1.50	1.43	1.50	1.48	1.39	1.39	1.39	Urea	
BAD	1.25	1.28	1.28	0.87	0.81	0.91	BAD	BAD	1.18	1.21	1.23	BAD	1.14	1.14	BAD	1.26	1.23	1.25	BAD	BAD	BAD	BAD	BAD	BAD	BAD	BAD	BAD	MTBD
1.53	1.70	BAD	BAD	1.47	1.51	1.40	BAD	1.80	1.79	BAD	BAD	1.31	BAD	1.33	1.25	BAD	BAD	BAD	BAD	1.42	BAD	1.42	BAD	BAD	1.25	1.25	BTMG	

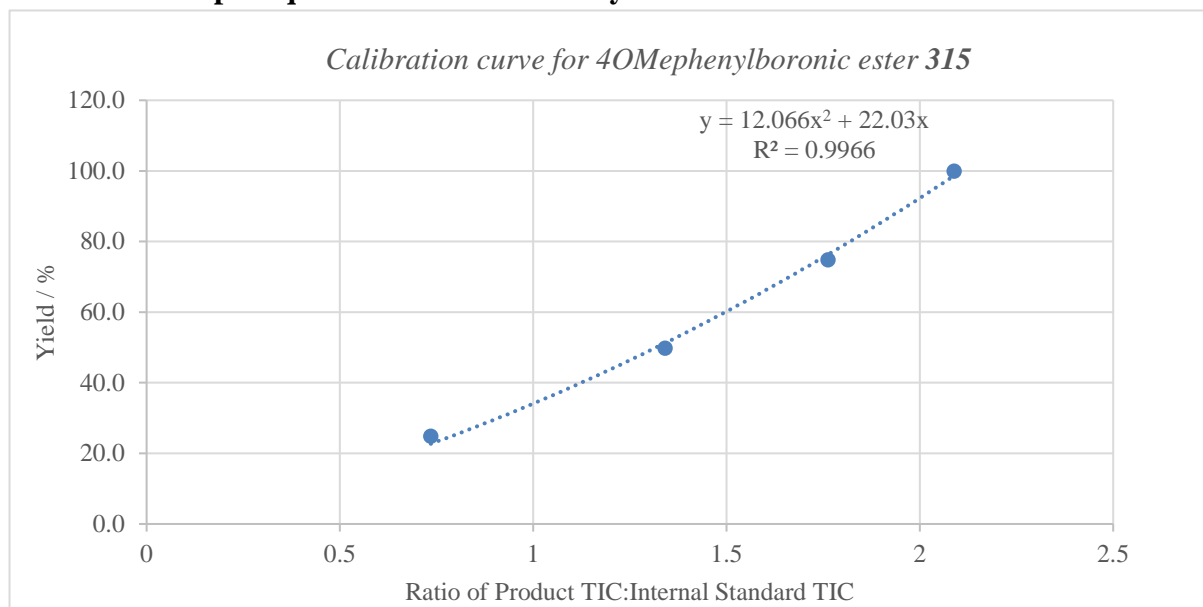
Phenanthroline

Bipyridine

Average of data repeats from quantitative LCMS assay

	No Base	DBU	Collidine	DABCO	TMU	Urea	MTBD	BTMG	No Base	DBU	Collidine	DABCO	TMU	Urea	MTBD	BTMG
CuCl	1.54	1.21	1.57	1.63	1.53	1.56	1.32	1.49	1.54	1.33	1.61	1.56	1.49	1.45	BAD	BAD
CuCl ₂	1.51	1.23	1.53	1.51	1.43	1.43	1.49	1.55	1.37	1.28	1.49	1.50	1.41	1.51	1.25	BAD
Cu(OTf) ₂	1.49	1.29	1.50	1.55	1.44	1.42	1.43	1.59	1.41	1.32	1.55	1.54	1.53	1.46	BAD	1.30
Cu(NO ₃) ₂	1.35	1.14	1.37	1.37	1.29	1.36	1.40	1.56	1.48	1.29	1.49	1.57	1.44	1.39	1.21	BAD
Cu(BF ₄) ₂	1.38	0.96	1.53	1.44	1.38	1.49	1.25	1.45	1.48	1.12	1.48	1.46	1.38	1.35	0.87	1.46
CuBr ₂	1.28	1.08	1.41	1.45	1.36	1.44	1.39	1.61	1.53	1.32	1.48	BAD	1.40	1.37	1.27	BAD
Phenanthroline								Bipyridine								

Calibration curve post quantitative LCMS assay



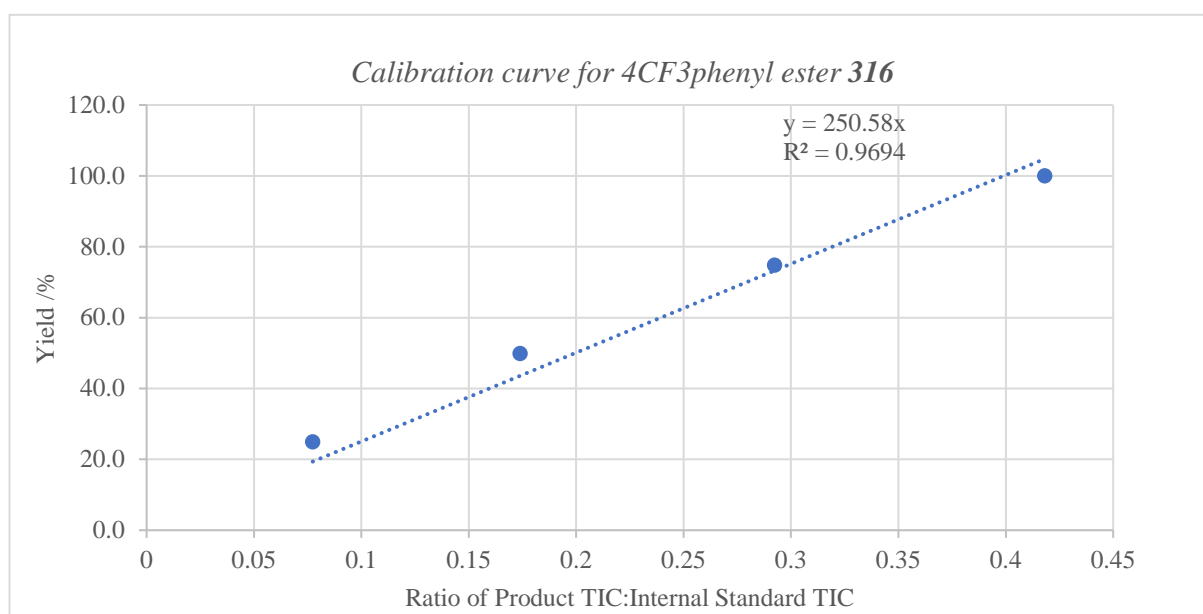
Calibrated high-throughput optimisation of S2

	No Base	DBU	Collidine	DABCO	TMU	Urea	MTBD	BTMG	No Base	DBU	Collidine	DABCO	TMU	Urea	MTBD	BTMG
CuCl	62.7	46.0	61.7	BAD	64.2	65.4	51.8	59.4	64.7	50.6	66.8	63.8	57.5	57.4	BAD	BAD
CuCl ₂	60.8	45.3	62.1	61.0	56.1	56.0	58.1	62.9	52.7	47.9	59.4	59.9	55.0	60.9	46.2	BAD
Cu(OTf) ₂	57.8	48.2	60.3	63.2	56.7	55.6	56.4	65.6	54.9	50.1	62.9	62.5	61.7	58.1	BAD	48.8
Cu(NO ₃) ₂	51.9	40.8	53.1	52.6	48.6	52.1	54.4	63.8	56.9	48.5	59.4	64.6	56.5	53.9	44.1	BAD
Cu(BF ₄) ₂	53.4	30.7	62.0	56.8	53.1	59.4	46.1	57.1	59.0	39.7	59.3	58.1	51.7	51.6	28.2	58.0
CuBr ₂	48.0	37.9	55.3	57.5	52.1	56.8	53.8	66.5	61.7	50.1	59.3	BAD	54.4	52.9	47.3	BAD
Phenanthroline								Bipyridine								

Average of data repeats from quantitative LCMS assay

	No Base	DBU	Collidine	DABCO	TMU	Urea	MTBD	BTMG	No Base	DBU	Collidine	DABCO	TMU	Urea	MTBD	BTMG
CuCl	BAD	0.10	0.17	0.15	0.15	0.15	0.08	0.13	0.12	0.08	0.08	0.16	0.09	0.06	0.06	0.11
CuCl ₂	0.17	0.11	0.15	0.14	0.15	0.14	0.11	0.10	0.14	0.10	0.14	0.16	0.14	0.11	0.08	0.14
Cu(OTf) ₂	0.19	0.10	0.17	0.16	0.16	0.16	0.09	0.15	0.08	0.08	0.08	0.16	0.09	0.06	0.05	0.09
Cu(NO ₃) ₂	0.18	0.10	0.17	0.16	0.16	0.15	0.09	0.14	0.10	0.09	0.07	0.15	0.08	0.06	0.05	0.11
Cu(BF ₄) ₂	0.19	0.09	0.18	0.16	0.16	0.16	0.08	0.13	0.15	0.08	0.14	0.14	0.10	0.11	0.05	0.11
CuBr ₂	0.17	0.11	0.16	0.16	0.16	0.14	0.10	0.19	0.17	0.10	0.16	0.17	0.11	0.14	0.07	0.14
Phenanthroline									Bipyridine							

Calibration curve post quantitative LCMS assay



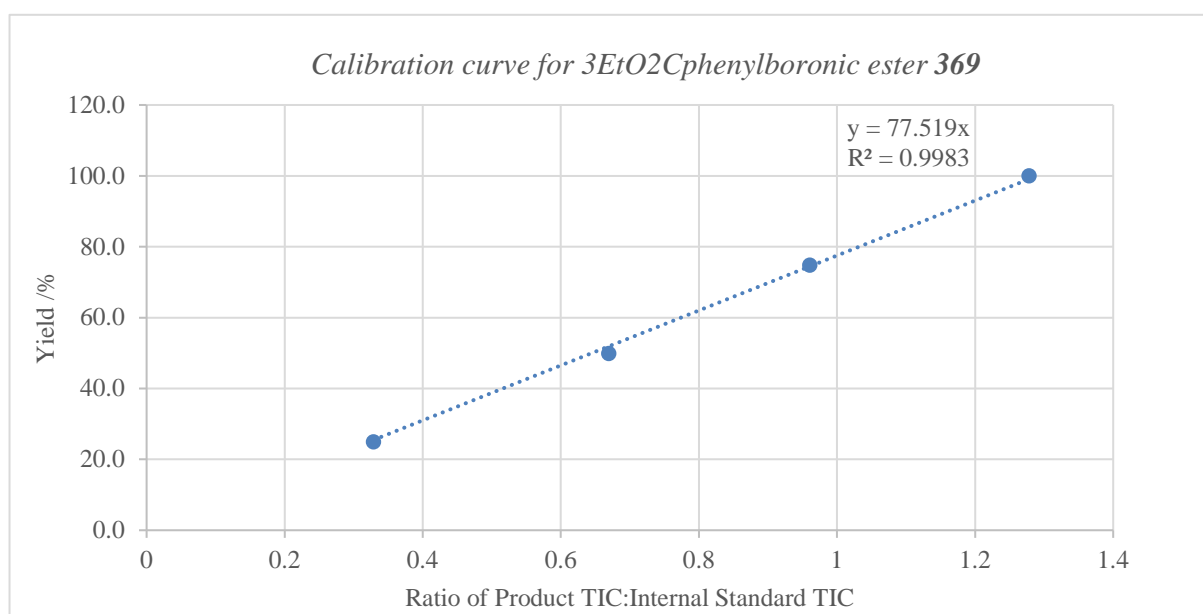
Calibrated high-throughput optimisation of S3

	No Base	DBU	Collidine	DABCO	TMU	Urea	MTBD	BTMG	No Base	DBU	Collidine	DABCO	TMU	Urea	MTBD	BTMG
CuCl	BAD	23.9	41.9	37.5	36.4	38.7	19.7	31.6	30.0	20.7	20.5	39.3	22.5	16.1	14.5	27.5
CuCl ₂	43.2	27.2	38.5	35.4	38.3	36.0	26.3	24.6	34.6	25.2	35.7	40.7	33.9	28.6	19.2	33.9
Cu(OTf) ₂	47.4	24.9	42.4	39.2	40.7	39.5	22.2	37.8	19.8	19.8	20.0	39.4	23.4	16.2	13.7	23.1
Cu(NO ₃) ₂	44.5	26.3	41.6	39.3	39.4	37.5	22.8	36.3	26.2	22.7	18.6	37.0	20.0	16.1	12.1	26.8
Cu(BF ₄) ₂	46.5	22.4	45.5	40.4	41.1	39.2	20.4	32.3	37.8	19.4	35.5	36.2	25.1	27.7	12.0	27.7
CuBr ₂	43.4	27.8	40.1	41.0	40.3	36.1	24.0	46.8	42.0	24.1	39.6	43.5	27.5	35.5	17.9	35.0
Phenanthroline									Bipyridine							

Average of data repeats from quantitative LCMS assay

	No Base	DBU	Collidine	DABCO	TMU	Urea	MTBD	BTMG	No Base	DBU	Collidine	DABCO	TMU	Urea	MTBD	BTMG
CuCl	0.78	0.54	0.83	0.83	0.84	0.82	0.69	0.83	0.84	0.60	0.84	0.79	0.84	0.79	0.60	0.78
CuCl ₂	0.67	0.58	0.74	0.74	0.73	0.72	0.74	0.84	0.71	0.59	0.72	0.75	0.69	0.68	0.70	BAD
Cu(OTf) ₂	0.76	0.60	0.85	0.85	0.82	0.77	0.67	0.78	0.84	0.58	0.83	0.79	0.84	0.76	0.57	0.72
Cu(NO ₃) ₂	0.77	0.59	0.81	0.84	0.83	0.77	0.66	0.77	0.82	0.55	0.81	0.85	0.82	0.77	0.60	0.67
Cu(BF ₄) ₂	0.76	0.54	0.85	0.82	0.82	0.80	0.64	0.75	0.81	0.57	0.82	0.85	0.83	0.77	0.54	0.66
CuBr ₂	0.78	0.58	0.77	0.77	0.73	0.75	0.68	0.83	0.78	0.59	0.75	0.79	0.73	0.75	0.67	0.80
	Phenanthroline								Bipyridine							

Calibration curve post quantitative LCMS assay



Calibrated high-throughput optimisation of S4

	No Base	DBU	Collidine	DABCO	TMU	Urea	MTBD	BTMG	No Base	DBU	Collidine	DABCO	TMU	Urea	MTBD	BTMG
CuCl	60.1	42.1	64.2	64.5	65.0	63.9	53.4	64.3	65.0	46.4	65.3	61.5	65.5	61.1	46.5	60.3
CuCl ₂	52.0	44.8	57.2	57.5	56.9	55.8	57.6	65.5	55.3	45.7	56.2	58.5	53.8	52.5	54.5	BAD
Cu(OTf) ₂	59.2	46.2	65.6	65.6	63.4	59.7	51.9	60.5	64.9	44.9	64.0	61.4	65.3	59.2	44.5	55.6
Cu(NO ₃) ₂	59.6	45.8	63.1	65.0	64.3	59.6	51.4	59.4	63.8	42.3	62.9	65.6	63.2	59.9	46.5	51.8
Cu(BF ₄) ₂	59.2	41.8	66.0	63.5	63.5	62.2	49.3	58.0	62.9	43.9	63.8	65.8	64.6	59.4	41.6	51.0
CuBr ₂	60.3	44.7	60.0	60.0	57.0	58.0	53.0	64.7	60.1	46.1	58.0	61.4	56.6	57.9	51.8	62.1
	Phenanthroline								Bipyridine							

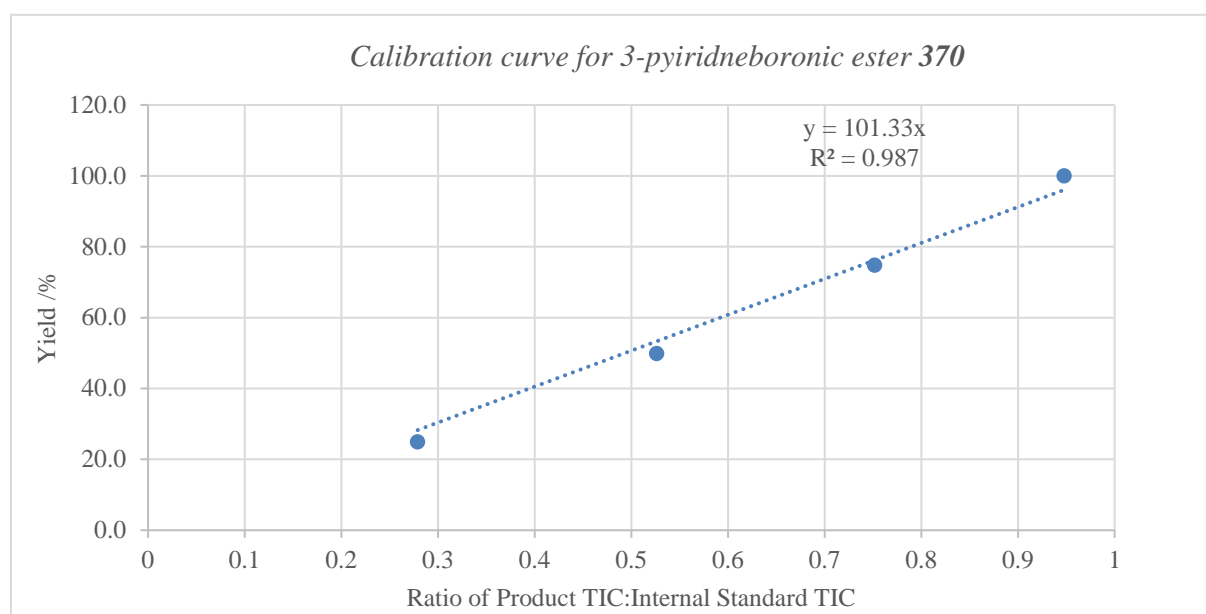
S5 = Pyridine-3-boronic acid pinacol ester, 335

				CuBr ₂				Cu(BF ₄) ₂				Cu(NO ₃) ₂				Cu(OTf) ₂				CuCl ₂				CuCl							
Phenanthroline		Bipyridine		0.58	0.37	0.53	0.62	0.60	0.52	0.50	0.53	0.56	0.48	0.61	0.50	0.54	0.49	0.50	0.59	0.64	0.62	0.58	0.62	0.54	0.61	0.62	0.54	0.64	No Base		
0.37	0.40	0.42	0.44	0.34	0.32	0.33	0.39	0.32	0.32	0.40	0.42	0.45	0.41	0.35	0.35	0.39	0.37	0.41	0.43	0.43	0.43	0.36	0.38	0.38	0.40	0.40	DBU				
0.59	0.67	0.64	0.68	0.58	0.58	0.62	0.66	0.62	0.62	0.62	0.60	0.61	0.64	0.57	0.60	0.60	0.59	BAD	0.63	0.61	0.65	0.61	0.59	0.68	0.64	0.64	Collidine				
0.66	0.65	0.67	0.72	0.60	0.61	0.62	0.64	0.63	0.62	0.63	0.68	0.65	0.68	BAD	BAD	0.62	0.67	0.62	0.56	0.66	0.65	0.57	0.63	0.68	BAD	DABCO					
0.58	0.57	0.57	0.52	0.55	0.60	0.58	0.54	0.55	0.58	0.55	0.60	0.60	0.51	0.56	0.60	0.58	0.58	0.59	0.56	0.66	0.58	0.61	0.61	0.58	0.59	TMU					
0.53	0.56	0.56	0.63	0.48	0.56	0.55	0.57	0.48	0.55	0.61	0.61	0.61	0.65	BAD	BAD	0.58	0.58	0.55	0.64	0.63	0.56	0.60	0.57	0.60	0.58	Urea					
0.49	0.50	0.54	0.54	0.46	0.47	0.45	0.52	0.46	0.47	0.49	0.47	0.55	0.60	0.50	0.50	0.53	0.54	0.55	0.60	0.55	0.55	0.54	0.51	0.55	0.50	MTBD					
0.50	0.54	0.57	0.52	0.43	0.47	0.49	0.51	0.43	0.47	0.49	0.51	0.51	0.55	0.52	0.52	0.45	0.50	0.53	0.53	0.55	0.61	0.46	0.45	0.45	0.45	BTMG					
0.63	0.60	0.61	0.67	0.55	0.61	0.61	0.60	0.60	0.61	0.60	0.57	0.54	0.65	0.60	0.60	0.64	0.62	0.61	0.53	0.55	0.55	0.55	0.57	0.48	0.45	No Base					
0.28	0.28	0.28	0.29	0.24	0.29	0.28	0.27	0.29	0.29	0.29	0.32	0.32	0.30	0.22	0.30	0.30	0.31	0.32	0.32	0.33	BAD	0.25	0.33	0.35	0.31	DBU					
0.60	0.60	0.62	0.61	0.57	0.62	0.62	0.59	0.55	0.55	0.55	0.59	0.58	0.59	0.53	0.53	0.54	0.55	0.53	0.49	0.53	0.50	BAD	0.55	0.51	0.48	Collidine					
0.58	0.58	0.62	0.66	0.56	0.59	0.57	0.61	0.57	0.57	0.57	0.56	0.65	0.62	0.57	0.61	0.60	0.61	0.54	0.50	0.50	0.53	0.53	BAD	0.58	0.52	DABCO					
0.54	0.53	0.64	0.64	0.52	0.52	0.57	0.58	0.50	0.52	0.57	0.53	0.54	0.53	BAD	0.57	0.59	0.54	0.59	0.56	0.55	0.58	0.56	0.49	0.49	0.49	TMU					
0.51	0.59	0.63	0.48	0.57	0.57	0.61	0.61	0.60	0.61	0.61	0.54	0.59	0.51	0.52	0.54	0.54	0.54	0.56	0.51	0.52	0.57	0.52	0.55	0.55	0.55	Urea					
0.31	0.27	0.38	0.37	BAD	0.35	0.38	0.41	0.44	0.44	0.44	0.41	0.43	0.39	0.39	0.39	0.47	0.37	0.45	0.51	0.50	0.49	0.37	0.41	0.47	0.37	MTBD					
0.39	0.36	0.40	0.41	0.37	0.37	BAD	0.38	0.37	0.37	0.38	0.38	0.36	0.37	0.36	0.38	0.34	0.38	0.38	0.41	0.48	0.39	0.33	0.39	0.32	0.34	BTMG					

Average of data repeats from quantitative LCMS assay

	No Base	DBU	Collidine	DABCO	TMU	Urea	MTBD	BTMG	No Base	DBU	Collidine	DABCO	TMU	Urea	MTBD	BTMG
CuCl	0.60	0.38	0.63	0.62	0.60	0.59	0.53	0.46	0.51	0.31	0.51	0.55	0.53	0.54	0.40	0.35
CuCl ₂	0.61	0.42	0.63	0.60	0.60	0.59	0.57	0.55	0.54	0.32	0.52	0.53	0.57	0.54	0.50	0.43
Cu(OTf) ₂	0.51	0.36	0.59	0.64	0.58	0.58	0.50	0.50	0.62	0.28	0.54	0.60	0.57	0.54	0.42	0.36
Cu(NO ₃) ₂	0.54	0.42	0.62	0.66	0.56	0.62	0.58	0.52	0.59	0.31	0.58	0.60	0.53	0.56	0.41	0.37
Cu(BF ₄) ₂	0.54	0.35	0.61	0.62	0.57	0.54	0.48	0.47	0.59	0.27	0.60	0.58	0.55	0.59	0.38	0.38
CuBr ₂	0.56	0.41	0.64	0.67	0.56	0.57	0.51	0.53	0.63	0.28	0.61	0.61	0.59	0.56	0.33	0.39
	Phenanthroline								Bipyridine							

Calibration curve post quantitative LCMS assay



Calibrated high-throughput optimisation of S5

	No Base	DBU	Collidine	DABCO	TMU	Urea	MTBD	BTMG	No Base	DBU	Collidine	DABCO	TMU	Urea	MTBD	BTMG
CuCl	62.8	38.4	64.0	BAD	60.7	59.5	53.3	46.1	54.1	33.3	52.0	55.2	52.1	55.1	38.7	35.0
CuCl ₂	61.8	42.9	63.6	61.2	58.6	60.2	58.1	54.2	54.9	32.7	52.3	53.6	57.5	54.5	50.9	44.0
Cu(OTf) ₂	51.7	37.0	60.2	64.4	58.7	58.9	52.7	50.4	62.7	30.9	54.4	60.9	57.6	54.9	42.4	37.0
Cu(NO ₃) ₂	51.8	42.5	62.7	67.0	59.0	63.0	58.8	52.5	57.4	31.1	58.6	60.9	53.5	56.5	42.0	37.9
Cu(BF ₄) ₂	52.5	35.2	60.0	62.8	57.4	56.8	48.2	48.1	60.1	27.2	60.8	59.0	55.6	59.8	38.4	38.1
CuBr ₂	55.3	41.3	67.3	68.2	56.6	55.7	51.6	53.8	63.8	28.6	61.7	61.9	59.5	BAD	35.6	39.2
	Phenanthroline								Bipyridine							

S6 = Indole-5-boronic acid pinacol ester, 336

	CuBr ₂				Cu(BF ₄) ₂				Cu(NO ₃) ₂				Cu(OTf) ₂				CuCl ₂				CuCl											
	0.61	0.60	0.61	0.65	0.35	0.36	0.38	0.39	0.48	0.43	0.45	0.49	0.47	0.48	0.49	0.38	0.59	0.59	0.57	0.54	0.67	0.60	0.60	0.54	0.67	0.60	0.60	0.58	0.54	0.58	0.54	0.54
	0.24	0.27	0.25	0.62	0.13	0.13	0.13	0.13	0.25	0.25	0.28	0.19	0.23	0.21	0.22	0.20	0.18	0.18	0.19	0.17	0.23	0.23	0.23	0.20	0.23	0.20	0.23	0.20	0.20	0.23	0.20	0.20
	0.65	0.62	0.56	0.62	0.49	0.41	0.40	0.38	0.52	0.47	0.51	0.44	0.47	0.45	0.47	0.43	0.57	0.62	0.60	0.58	0.56	0.68	0.67	0.62	0.56	0.68	0.67	0.62	0.62	0.67	0.62	0.62
	0.63	0.68	0.63	0.65	0.51	0.50	0.51	0.49	0.60	0.54	0.55	0.53	0.57	0.56	0.52	0.55	0.55	0.71	0.58	0.65	0.76	0.68	0.76	0.68	0.76	0.68	0.77	0.68	0.68	0.68	0.68	0.68
	0.62	0.61	0.62	0.55	0.38	0.43	0.42	0.43	0.48	0.52	0.49	0.49	0.50	0.46	0.48	0.41	0.60	0.53	0.60	0.55	0.67	0.72	0.67	0.64	0.67	0.72	0.69	0.64	0.64	0.69	0.64	0.64
	0.65	0.64	0.61	0.62	0.39	0.39	0.43	0.41	0.39	0.48	0.46	0.44	0.44	0.50	0.39	0.47	0.58	0.60	0.60	0.58	0.67	0.56	0.67	0.50	0.67	0.56	0.50	0.67	0.50	0.50	0.50	0.67
	0.44	0.40	0.41	0.38	0.27	0.24	0.30	0.25	0.40	0.44	0.38	0.35	0.37	0.35	0.35	0.33	0.41	0.35	0.35	0.32	0.29	0.31	0.29	0.31	0.29	0.31	0.29	0.27	0.32	0.29	0.32	0.27
	0.72	0.69	0.62	0.68	0.54	0.51	0.46	0.46	0.63	0.71	0.59	0.67	0.61	0.71	0.62	0.65	0.57	0.66	0.65	0.53	0.53	0.54	0.53	0.53	0.53	0.54	0.53	0.39	0.53	0.53	0.53	0.39
	0.72	0.67	0.67	0.73	0.54	0.54	0.50	0.52	0.60	0.61	0.64	0.59	0.63	0.57	0.55	0.47	0.66	0.66	0.66	0.62	0.64	0.60	0.64	0.60	0.64	0.60	0.64	0.74	0.62	0.73	0.62	0.74
	BAD	0.78	0.69	0.69	0.39	0.35	0.27	0.29	0.51	0.63	0.54	0.62	0.26	0.26	0.24	0.23	0.28	0.28	0.25	0.23	0.21	0.29	0.21	0.29	0.21	0.29	0.21	0.23	0.23	0.25	0.23	0.23
	0.70	0.70	0.69	0.70	0.59	0.44	0.56	0.47	0.59	0.52	0.57	0.52	0.56	0.54	0.62	0.47	0.70	0.66	0.65	0.61	0.79	0.74	0.79	0.74	0.79	0.74	0.79	0.74	0.79	0.79	0.74	0.74
	0.81	0.76	0.76	0.79	0.73	0.68	0.66	0.67	0.69	0.64	0.67	0.64	0.67	0.61	0.67	0.61	0.74	0.64	0.64	0.65	0.85	0.82	0.85	0.82	0.85	0.82	0.85	0.85	0.85	0.88	0.85	0.85
	0.74	0.84	0.63	0.71	0.47	0.55	0.54	0.53	0.60	0.71	0.60	0.57	0.62	0.64	0.61	0.66	0.63	0.66	0.68	0.68	0.83	0.70	0.83	0.70	0.83	0.70	0.82	0.78	0.82	0.82	0.82	0.78
	0.67	0.73	0.64	0.69	0.52	0.49	0.49	0.52	0.56	0.50	0.56	0.56	0.50	0.53	0.51	0.51	0.65	0.62	0.65	0.65	0.79	0.72	0.79	0.72	0.79	0.72	0.77	0.73	0.73	0.77	0.73	0.73
	0.45	0.46	0.49	0.37	0.32	0.28	0.31	0.32	0.44	0.44	0.43	0.36	0.36	0.42	0.35	0.37	0.39	0.35	0.37	0.31	0.35	0.36	0.35	0.36	0.35	0.36	0.35	0.35	0.35	0.26	0.35	0.35
	0.64	0.72	0.73	0.64	0.66	0.64	0.64	0.57	0.74	0.74	0.72	0.70	0.76	0.63	0.63	0.74	0.68	0.70	0.59	0.59	0.59	0.57	0.59	0.57	0.59	0.57	0.59	0.44	0.50	0.50	0.50	0.44

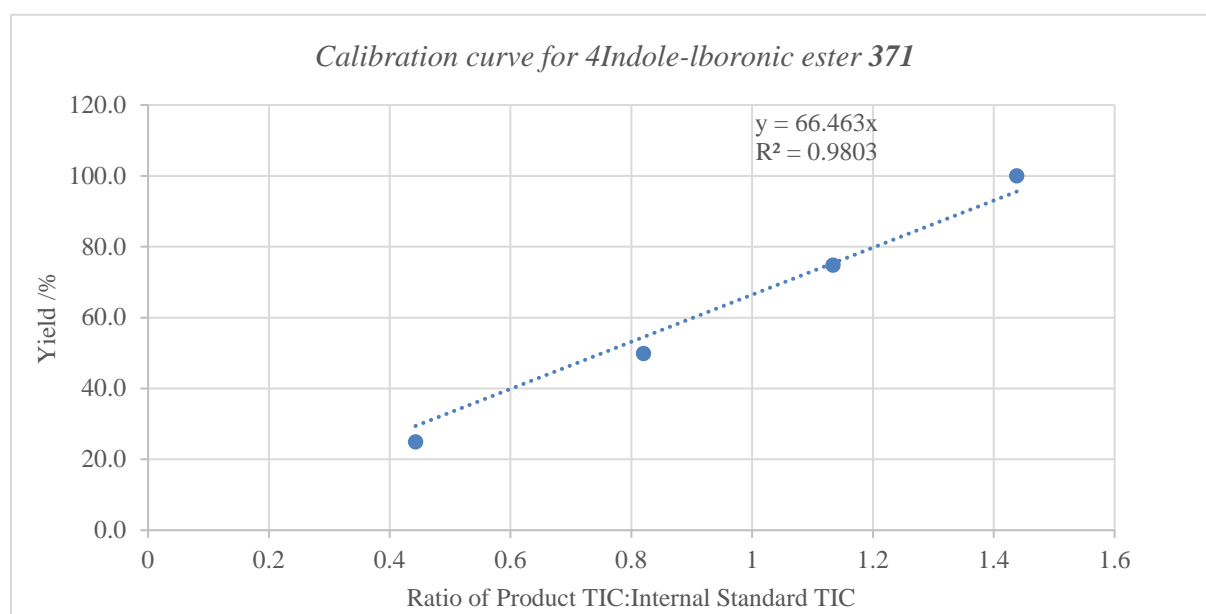
Phenanthroline

Bipyridine

Average of data repeats from quantitative LCMS assay

	No Base	DBU	Collidine	DABCO	TMU	Urea	MTBD	BTMG	No Base	DBU	Collidine	DABCO	TMU	Urea	MTBD	BTMG
CuCl	0.60	0.21	0.63	0.72	0.68	0.60	0.29	0.50	0.68	0.25	0.76	0.85	0.78	0.75	0.33	0.52
CuCl ₂	0.57	0.18	0.59	0.62	0.57	0.59	0.36	0.60	0.65	0.25	0.66	0.68	0.66	0.64	0.35	0.64
Cu(OTf) ₂	0.46	0.21	0.46	0.55	0.47	0.45	0.35	0.65	0.55	0.25	0.55	0.64	0.63	0.51	0.37	0.69
Cu(NO ₃) ₂	0.46	0.24	0.49	0.56	0.50	0.44	0.39	0.65	0.61	0.58	0.55	0.66	0.62	0.55	0.42	0.73
Cu(BF ₄) ₂	0.37	0.13	0.42	0.50	0.42	0.40	0.27	0.49	0.53	0.33	0.51	0.68	0.52	0.50	0.31	0.63
CuBr ₂	0.62	0.25	0.61	0.65	0.60	0.63	0.41	0.68	0.70	BAD	0.70	0.78	0.73	0.68	0.44	0.68
Phenanthroline									Bipyridine							

Calibration curve post quantitative LCMS assay



Calibrated high-throughput optimisation of S6

	No Base	DBU	Collidine	DABCO	TMU	Urea	MTBD	BTMG	No Base	DBU	Collidine	DABCO	TMU	Urea	MTBD	BTMG
CuCl	39.9	14.2	41.9	48.0	45.5	39.9	19.3	33.1	45.2	16.4	50.8	56.4	51.8	50.0	21.9	34.8
CuCl ₂	38.0	11.8	39.3	41.4	37.8	39.3	23.7	40.2	43.0	16.4	43.6	44.9	44.2	42.7	23.5	42.7
Cu(OTf) ₂	30.3	14.2	30.2	36.5	30.9	29.6	23.1	43.0	36.8	16.4	36.3	42.5	42.1	34.0	24.9	45.8
Cu(NO ₃) ₂	30.8	16.2	32.4	36.9	33.0	29.4	26.1	43.3	40.5	38.3	36.8	44.0	41.2	36.4	27.7	48.3
Cu(BF ₄) ₂	24.6	8.8	27.9	33.5	27.8	26.9	17.8	32.8	34.9	21.7	34.2	45.5	34.8	33.5	20.4	41.6
CuBr ₂	41.1	16.6	40.7	43.1	39.8	41.9	27.1	45.1	46.4	BAD	46.3	51.9	48.4	45.3	29.3	45.4
Phenanthroline									Bipyridine							

Low Concentration boronic esters

Procedure for 384 nanomolar scale reactions (2.5 μL volume) in one quarter of a 1536-well plate. Stock solutions of each component were prepared according to general procedure 1: 4-phenylpiperidine **134** (0.33 M in DMSO), boronic ester (**337** and **338**, 0.1 M in DMSO), organic base (**317**, **339**, **340**, **343-345**, **387**, 0.5M in DMSO), ligand (**319** and **318**, 0.025 M in DMSO), catalyst (C1-C8, 0.1 M in DMSO) using Spreadsheet 4. For the source plate layout, see Figure 58. For each 1536-well plate experiment, each well was charged with the amount of stock solution stated in ‘Source plate loading’ column, using a digital air displacement pipette, such that enough solution was present to dose the corresponding reactor plate.

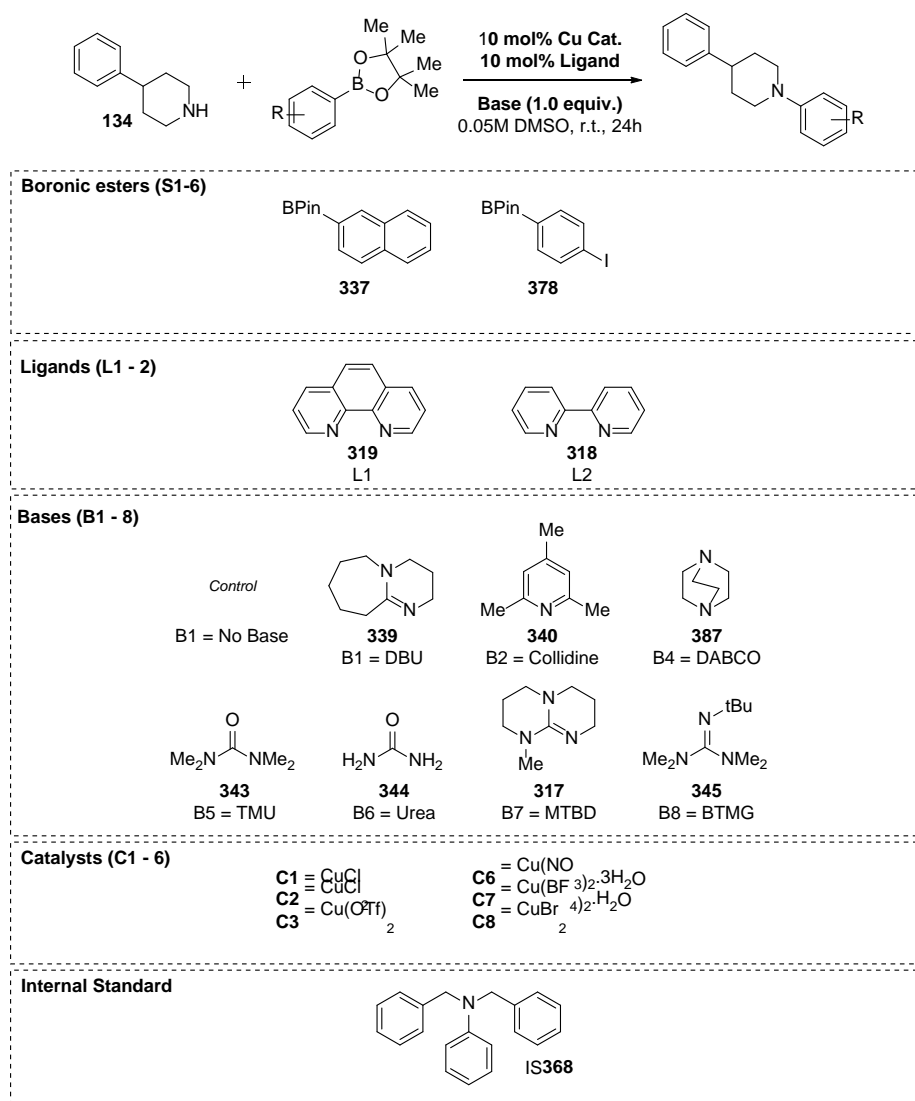


Figure 58: Components assessed on 1536-well plate at 0.05M.

The Mosquito was used to transfer aliquot volumes according to the ‘‘Solubility problems? Aliquotvol’’ column on the Excel Spreadsheet. The reactor plate was dosed using Mosquito aliquot protocol 2-4 for low solubility: R1 was added in 250 nL, S1 was added in 1250 nL (2×625 nL), B1-8 was added in 250 nL, L1/2 was added in 500 nL and catalyst added in 250 nL resulting in a total reaction volume of 2.5 μL . When the catalyst had been added, the Mosquito

mixed the reaction mixture together three times using the mix-dispense feature. The 1536-well reactor plate was then sealed with aluminium foil and placed under a heavy glass sheet for 24 hours.

Source Plate Layout

	1	2	3	4	5	6	7	8	9	10	11	12	13	14	15	16	17	18	19	20	21	22	23	24	
A															C6	C5	C4	C3	C2	C1	L1	B1	S1	R1	A
B															C6	C5	C4	C3	C2	C1	L1	B2	S1	R1	B
C															C6	C5	C4	C3	C2	C1	L1	B3	S1	R1	C
D															C6	C5	C4	C3	C2	C1	L1	B4	S1	R1	D
E															C6	C5	C4	C3	C2	C1	L1	B5	S1	R1	E
F															C6	C5	C4	C3	C2	C1	L1	B6	S1	R1	F
G															C6	C5	C4	C3	C2	C1	L1	B7	S1	R1	G
H															C6	C5	C4	C3	C2	C1	L1	B8	S1	R1	H
I															C6	C5	C4	C3	C2	C1	L2	B1	S1	R1	I
J															C6	C5	C4	C3	C2	C1	L2	B2	S1	R1	J
K															C6	C5	C4	C3	C2	C1	L2	B3	S1	R1	K
L															C6	C5	C4	C3	C2	C1	L2	B4	S1	R1	L
M															C6	C5	C4	C3	C2	C1	L2	B5	S1	R1	M
N															C6	C5	C4	C3	C2	C1	L2	B6	S1	R1	N
O															C6	C5	C4	C3	C2	C1	L2	B7	S1	R1	O
P															C6	C5	C4	C3	C2	C1	L2	B8	S1	R1	P

Analysis plate preparation

Prior to quantitative analysis, the LCMS was cleaned using General Procedure 5. Analysis plates were prepared according to General procedure 3 and Calibration curves were prepared using General procedure 4. If curves were found to undergo non-linear correlations, a quadratic formula was used to fit the data.²⁴⁶ Each substrate was run in using a bespoke LCMS assay method file (Appendix 2) with bespoke autosampler aliquot volume and IS368 stock solution shown in Table 9.

Optimised LCMS assay conditions

Entry	Product	Autosampler aliquot volume / μL	IS stock solution / μL of 0.1M IS368 S.S. in 100 mL S.S
1	372	0.2	337.5
2	373	0.2	337.5

Table 9: LCMS autosampler aliquot volumes and corresponding IS368 quench concentration

PLATE	# reagents	How much of plate?	input wells/column	Scale L.R. (umol)	Final conc. Rxn (M)	Stand. Alig. (ul)	Reactor tot vol (ul)	
1536	5	All	32	0.125	0.05	0.5	2.5	
constant?	Reagent	Compound	CAS	Cat No	FW (gMol-1)	Amount (uMol)	mg per rxn	Solubility problems?
(constant)	R1	4-phenylpiperidine	771-99-3	P 034	161.12	0.125	2.01E-02	0.38
(constant)	S6	4-IBPIn	73852-88-7	HTE	329.972	0.125	4.12E-02	1.25
(x-constant, y-variable)	S8	2-NaapBPin	256652-04-7	HTE	254.136	0.125	3.18E-02	1.25
	B1	No Base		0		0	0.00E+00	0.25
	B2	DBU	6674-22-2	D301	152.24	0.125	1.90E-02	0.25
	B3	Collidine	108-75-8	C31	121.18	0.125	1.51E-02	0.25
	B4	DABCO	280-57-9	D052	112.17	0.125	1.40E-02	0.25
	B5	Tetramethylurea	632-22-4	Dave	116.16	0.125	1.45E-02	0.25
	B6	Urea	57-13-6	U 002	60.06	0.125	7.51E-03	0.25
	B7	MTBD	84030-20-6	Dave	153.22	0.125	1.92E-02	0.25
	B8	BTMG	29166-72-1	B032	171.28	0.125	2.14E-02	0.25
(x-constant, y-variable)	C1	Cu(I)Cl	7758-89-6	cat 025	99.00	0.0125	1.24E-03	0.13
	C2	Cu(O)		iC058	134.45	0.0125	1.68E-03	0.13
	C3	Cu(I)(OTf)2	34946-82-2	cat 150	361.68	0.0125	4.52E-03	0.13
	C4	Cu(I)(NO3)2.3H2O	10031-43-3	iC010	241.60	0.0125	3.02E-03	0.13
	C5	Cu(I)(BF4)2.H2O	207121-39-9	iC014	237.16	0.0125	2.96E-03	0.13
	C6	Cu(I)Br2	7789-45-9	iC022	223.35	0.0125	2.79E-03	0.13
(x-variable, y-constant)	L1	1,10-phenantroline	66-71-7	P 228	180.21	0.0125	2.25E-03	0.50
	L2	2,2-bipyridyl	366-18-7	B 462	156.18	0.0125	1.95E-03	0.50

Stock solution (mg/vial)	Stock solution (solvent/vial)	Stock solution (min vol/vial)	Source (abs vol/vial)	Source (rec vol/well)	Source	Source plate loading (vol/well ul)	Liquid reagents (Vol/SS)	DMSO Top-up
21.5	400	259	9	16	16	25	X	X
29.7	900	864	30	54	54	56.25	X	X
22.9	900	864	30	54	54	56.25	X	X
0.0	100	0	0	0	0		X	X
7.6	100	0	6	11	11		6.9	93.1
6.1	100	0	6	11	11		6.7	93.3
5.6	100	0	6	11	11			X
5.8	100	0	6	11	11	50	6.0	94.0
3.0	100	0	6	11	11		X	X
7.7	100	0	6	11	11		7.2	92.8
8.6	100	0	6	11	11		10.1	89.9
4.0	400	14	1	1	1			
5.4	400	14	1	1	1			
14.5	400	14	1	1	1	25	X	X
9.7	400	14	1	1	1			
9.5	400	14	1	1	1			
8.9	400	14	1	1	1			
1.8	400	173	12	22	22	50.0	X	X
1.6	400	173	12	22	22	50.0	X	X

Spreadsheet 4: High-throughput screen of Chan-Lam reaction at 0.05M (1 x 4 x 8 x 2 x 6 screen).

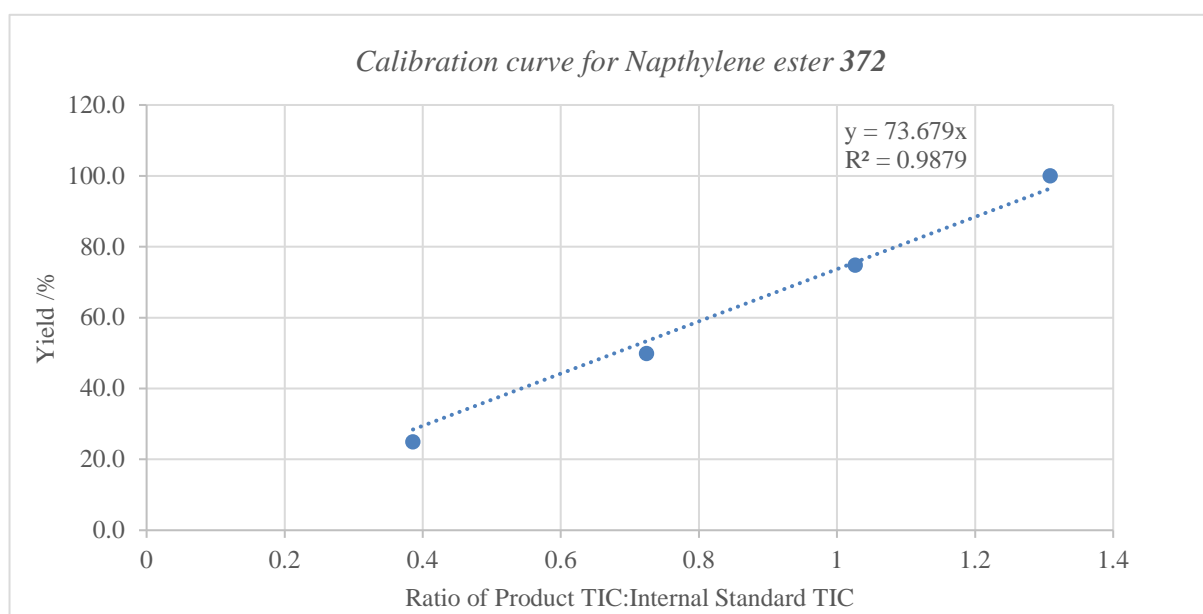
S7 = 2-Naphthyleneboronic acid pinacol ester, 337 @ 0.05M

CuBr ₂				Cu(BF ₄) ₂				Cu(NO ₃) ₂				Cu(OTf) ₂				CuCl ₂				CuCl											
0.96	0.90	0.58	0.61	1.05	0.99	1.03	0.91	0.85	0.91	0.88	0.87	0.84	0.94	0.83	0.84	0.97	0.93	0.96	0.93	0.90	0.88	0.90	0.93	0.90	0.88	0.90	0.94	0.94	0.90	0.58	No Base
0.61	0.60	0.60	0.54	0.56	0.51	0.53	0.54	0.54	0.60	0.61	0.60	0.60	0.55	0.64	0.60	0.62	0.56	0.57	0.53	0.55	0.55	0.50	0.58	0.58	0.55	0.50	DBU	0.58	0.50	0.58	DBU
0.95	0.84	0.95	0.94	0.95	0.95	BAD	0.93	0.90	0.89	0.93	0.91	0.88	0.95	0.88	0.95	1.00	0.99	0.99	0.96	0.94	0.94	0.89	BAD	0.98	0.94	0.89	Collidine	BAD	BAD	BAD	Collidine
0.87	0.89	0.78	0.92	0.77	0.86	0.95	0.88	0.95	BAD	0.93	0.95	0.98	0.98	0.91	0.97	0.97	0.94	0.98	0.98	0.98	1.00	0.98	0.93	0.98	1.00	0.98	DABCO	0.93	0.98	0.93	DABCO
0.82	0.85	0.83	0.76	0.86	0.86	0.87	0.81	0.77	0.82	0.86	0.77	0.82	0.82	0.79	0.77	0.85	0.90	0.95	0.91	0.92	0.84	0.95	0.91	0.92	0.84	0.95	TMU	0.85	0.95	0.85	TMU
0.80	0.88	0.85	0.89	0.78	0.83	0.86	0.86	0.75	0.84	0.84	0.71	0.73	0.73	0.70	0.85	0.90	0.94	0.90	0.93	0.95	0.92	0.83	0.93	0.95	0.92	0.83	Urea	BAD	BAD	BAD	Urea
0.68	0.65	0.72	0.69	0.63	BAD	0.67	0.69	0.74	0.71	BAD	0.69	0.69	0.69	0.55	0.62	0.69	0.64	0.62	0.70	0.58	0.54	0.48	0.53	0.58	0.54	0.48	MTBD	0.53	0.48	0.53	MTBD
0.60	0.58	0.62	0.52	0.53	0.56	0.58	0.55	0.62	0.63	0.68	0.54	0.64	0.64	0.52	0.59	0.56	0.66	0.66	0.59	0.56	0.54	0.47	0.49	0.56	0.54	0.47	BTMG	0.49	0.47	0.49	BTMG
0.77	0.82	0.92	0.87	0.89	0.83	0.80	0.90	0.83	0.91	0.90	0.84	0.84	0.93	0.88	0.88	0.84	0.90	0.91	0.88	0.86	0.91	BAD	0.83	0.86	0.91	BAD	No Base	0.83	0.83	0.83	No Base
0.54	0.52	0.52	0.52	0.43	0.47	0.47	0.41	0.59	0.54	0.52	0.48	0.57	0.52	0.46	0.48	0.52	0.54	0.59	0.51	0.50	0.54	0.58	0.48	0.50	0.54	0.58	DBU	0.48	0.48	0.48	DBU
0.84	0.93	0.97	0.94	0.97	0.94	0.99	0.96	0.93	1.00	1.00	0.94	0.92	0.92	0.87	0.88	0.93	0.93	1.01	1.00	0.90	1.00	0.93	0.92	0.90	1.00	0.93	Collidine	0.92	0.93	0.92	Collidine
0.90	0.89	0.91	0.90	0.92	0.92	0.86	0.87	1.00	0.92	0.89	0.95	0.91	0.91	0.90	0.84	BAD	0.92	0.91	0.90	0.94	1.01	0.90	0.85	0.94	1.01	0.90	DABCO	0.85	0.90	0.85	DABCO
0.83	0.91	0.95	0.81	0.90	0.80	0.99	0.89	0.93	0.92	0.94	0.93	0.80	0.80	0.83	0.88	0.90	0.83	0.87	0.90	0.99	0.96	0.88	0.91	0.99	0.96	0.88	TMU	0.91	0.88	0.91	TMU
0.85	0.97	0.98	0.93	0.92	0.84	BAD	0.88	0.90	0.88	0.83	0.87	0.87	0.87	0.90	0.74	0.87	0.89	0.81	0.82	0.94	0.89	0.86	0.99	0.94	0.89	0.86	Urea	0.99	0.86	0.99	Urea
0.82	0.87	0.85	0.83	0.65	0.64	0.70	0.62	0.84	0.84	0.82	0.91	0.68	0.75	0.65	0.71	0.86	0.96	0.80	0.87	0.66	0.63	0.64	BAD	0.66	0.63	0.64	MTBD	BAD	BAD	BAD	MTBD
0.52	0.56	0.50	0.56	0.43	0.42	0.35	0.40	0.43	0.40	0.50	0.48	0.42	0.40	0.39	0.37	0.50	0.47	0.44	0.44	0.40	0.39	0.31	0.33	0.40	0.39	0.31	BTMG	0.33	0.31	0.33	BTMG
Phenanthroline												Bipyridine																			

Average of data repeats from quantitative LCMS assay

	No Base	DBU	Collidine	DABCO	TMU	Urea	MTBD	BTMG	No Base	DBU	Collidine	DABCO	TMU	Urea	MTBD	BTMG
CuCl	0.90	0.55	0.94	0.97	0.89	0.90	0.53	0.52	0.86	0.52	0.94	0.93	0.93	0.92	0.64	0.36
CuCl ₂	0.95	0.57	0.99	0.97	0.90	0.92	0.66	0.62	0.88	0.55	0.97	0.91	0.87	0.85	0.87	0.47
Cu(OTf) ₂	0.86	0.58	0.91	0.94	0.81	0.78	0.63	0.57	0.88	0.50	0.89	0.88	0.85	0.83	0.70	0.39
Cu(NO ₃) ₂	0.88	0.59	0.91	0.94	0.80	0.79	0.72	0.62	0.87	0.53	0.96	0.94	0.93	0.87	0.85	0.45
Cu(BF ₄) ₂	1.00	0.54	0.94	0.86	0.85	0.83	0.66	0.55	0.86	0.44	0.96	0.89	0.89	0.88	0.65	0.40
CuBr ₂	0.94	0.58	0.92	0.86	0.82	0.85	0.68	0.58	0.85	0.53	0.92	0.90	0.88	0.93	0.84	0.53
	Phenanthroline								Bipyridine							

Calibration curve post quantitative LCMS assay



Calibrated high-throughput optimisation of S7

	No Base	DBU	Collidine	DABCO	TMU	Urea	MTBD	BTMG	No Base	DBU	Collidine	DABCO	TMU	Urea	MTBD	BTMG
CuCl	66.6	40.3	69.1	71.6	65.5	66.1	39.2	38.0	63.7	38.7	69.0	68.3	68.8	67.6	47.4	26.3
CuCl ₂	69.7	41.9	72.7	71.5	66.4	67.6	48.8	45.4	65.1	40.6	71.3	66.9	64.4	62.3	64.2	34.7
Cu(OTf) ₂	63.4	42.5	67.3	69.2	59.5	57.7	46.4	42.2	64.9	37.2	65.2	65.1	63.0	61.0	51.4	29.1
Cu(NO ₃) ₂	64.8	43.2	66.9	69.4	59.2	57.9	52.8	45.5	64.0	39.2	71.1	69.2	68.6	64.2	63.0	33.2
Cu(BF ₄) ₂	73.4	39.5	69.6	63.7	62.7	61.4	48.9	40.9	63.2	32.8	71.0	65.9	65.9	64.7	48.0	29.4
CuBr ₂	69.6	43.0	67.9	63.7	60.1	62.9	50.4	42.8	62.3	38.7	67.9	66.4	64.7	68.8	62.0	39.3
	Phenanthroline								Bipyridine							

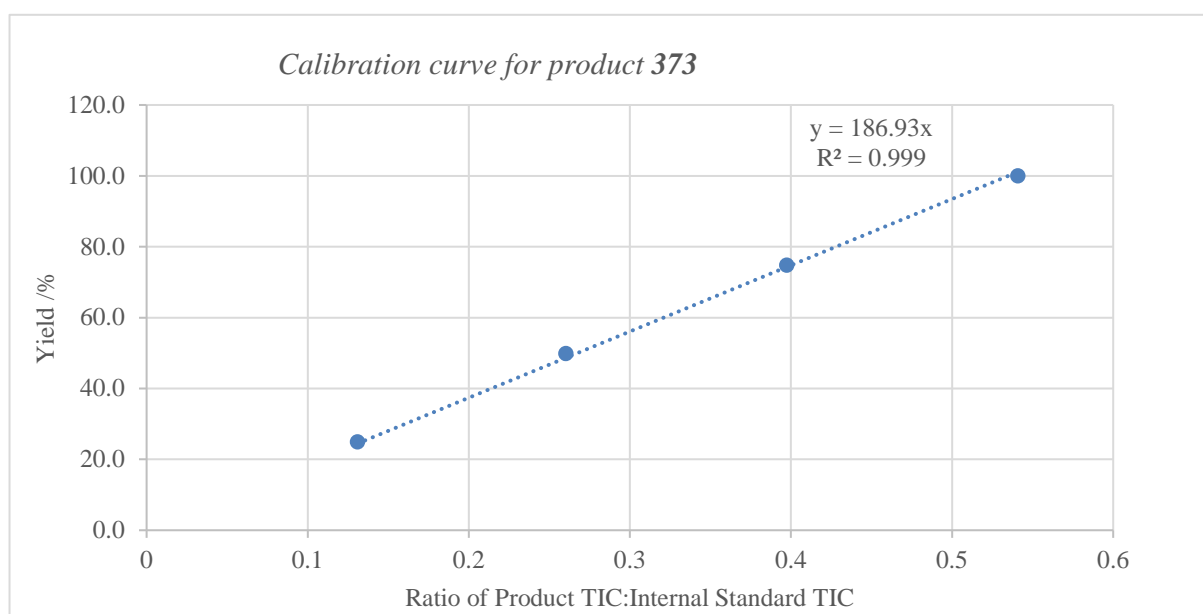
S8 = 4-Iodophenylboronic acid pinacol ester, 338 @ 0.05M

CuBr ₂				Cu(BF ₄) ₂				Cu(NO ₃) ₂				Cu(OTf) ₂				CuCl ₂				CuCl				
0.29	0.33	0.30	0.26	BAD	0.33	0.32	0.30	0.27	0.29	0.29	0.30	0.32	0.33	0.30	0.30	0.33	0.29	0.30	0.30	BAD	BAD	BAD	BAD	No Base
0.18	0.15	0.17	0.18	0.15	0.16	0.19	0.15	0.18	0.18	0.18	0.18	0.18	0.14	0.14	0.14	0.16	0.16	0.15	0.15	0.16	0.17	0.17	0.16	DBU
0.29	0.31	0.30	0.30	0.32	0.31	0.31	0.28	0.33	0.33	0.32	0.33	0.32	0.32	0.33	BAD	0.31	0.30	0.33	0.28	0.31	0.33	0.33	0.30	Collidine
0.28	BAD	0.31	0.29	0.31	0.28	0.30	0.30	0.30	0.31	0.33	0.33	0.34	0.34	0.32	0.32	0.31	0.31	0.32	0.32	0.36	0.35	0.34	0.33	DABCO
0.27	0.27	0.29	0.28	0.27	0.27	0.29	0.24	0.28	0.27	0.28	0.28	0.29	0.27	0.24	0.24	0.31	0.30	0.29	0.28	0.29	0.31	0.31	0.30	TMU
0.29	0.29	0.30	0.28	0.28	0.30	0.27	0.29	0.29	0.29	0.29	0.28	0.29	0.29	0.28	0.28	0.31	0.31	0.31	0.31	BAD	BAD	BAD	BAD	Urea
0.23	0.25	0.23	0.25	0.21	0.18	0.18	0.19	0.22	0.22	0.21	0.23	0.26	0.26	0.26	0.26	0.26	0.25	0.20	0.26	0.20	0.22	0.21	0.21	MTBD
BAD	0.24	0.24	0.22	0.19	0.19	0.18	0.19	0.23	0.23	0.22	0.19	0.22	0.21	0.19	0.25	0.24	0.23	0.21	0.21	0.21	0.20	0.21	0.21	BTMG
0.31	0.32	BAD	0.32	0.31	0.28	0.32	0.27	0.33	0.35	0.34	0.33	0.34	0.33	0.33	0.32	0.29	0.31	0.30	0.30	BAD	BAD	BAD	BAD	No Base
0.15	0.16	0.16	0.19	0.13	0.13	0.13	0.12	0.18	0.17	0.17	0.16	0.15	0.15	0.16	0.17	0.17	0.16	0.16	0.16	0.16	0.17	0.16	0.16	DBU
0.30	BAD	0.32	0.31	0.30	0.33	0.31	0.31	0.32	0.33	0.31	0.32	0.32	0.32	0.32	0.26	0.30	0.29	0.29	0.29	BAD	0.32	0.32	0.30	Collidine
0.33	0.32	0.31	0.35	0.30	0.34	0.32	0.34	0.34	0.35	0.34	0.31	0.34	0.36	0.31	0.34	0.30	0.32	0.33	0.33	0.14	0.16	0.13	BAD	DABCO
0.32	0.32	0.30	0.31	0.29	0.30	0.33	0.31	0.29	0.33	0.32	0.32	0.34	0.32	0.32	0.33	BAD	0.31	0.31	0.31	BAD	0.33	0.32	0.31	TMU
0.30	0.32	0.33	0.35	0.27	0.29	0.35	0.30	0.35	0.31	0.32	0.33	0.32	0.34	0.33	0.30	0.29	0.27	0.30	0.30	BAD	BAD	BAD	BAD	Urea
0.31	0.29	0.29	0.30	0.24	0.24	0.22	0.25	0.25	0.26	0.22	0.22	0.22	0.24	0.22	0.27	0.27	0.26	0.27	0.27	0.23	0.23	0.23	0.23	MTBD
0.16	0.19	0.19	0.18	0.13	0.13	0.12	0.12	0.17	0.15	0.15	0.13	0.14	0.14	0.13	0.18	0.15	0.16	0.15	0.15	0.13	0.13	0.13	0.13	BTMG
Phenanthroline												Bipyridine												

Average of data repeats from quantitative LCMS assay

	No Base	DBU	Collidine	DABCO	TMU	Urea	MTBD	BTMG	No Base	DBU	Collidine	DABCO	TMU	Urea	MTBD	BTMG
CuCl	BAD	0.16	0.32	0.34	0.30	BAD	0.21	0.20	BAD	0.16	0.31	0.14	0.32	BAD	0.22	0.12
CuCl ₂	0.31	0.16	0.30	0.32	0.30	0.31	0.26	0.23	0.31	0.16	0.29	0.32	0.32	0.29	0.27	0.16
Cu(OTf) ₂	0.32	0.16	0.32	0.32	0.27	0.29	0.25	0.21	0.33	0.16	0.32	0.34	0.33	0.33	0.22	0.14
Cu(NO ₃) ₂	0.28	0.18	0.32	0.31	0.27	0.29	0.23	0.23	0.34	0.18	0.31	0.33	0.32	0.34	0.26	0.16
Cu(BF ₄) ₂	0.32	0.16	0.31	0.30	0.27	0.29	0.19	0.19	0.29	0.13	0.31	0.33	0.30	0.29	0.24	0.13
CuBr ₂	0.30	0.17	0.30	0.29	0.28	0.29	0.24	0.23	0.31	0.17	0.31	0.33	0.31	0.32	0.30	0.18
Phenanthroline									Bipyridine							

Calibration curve post quantitative LCMS assay



Calibrated high-throughput optimisation of S8

	No Base	DBU	Collidine	DABCO	TMU	Urea	MTBD	BTMG	No Base	DBU	Collidine	DABCO	TMU	Urea	MTBD	BTMG
CuCl	BAD	30.8	60.2	64.0	56.9	BAD	39.0	37.5	BAD	30.3	58.6	26.8	59.9	BAD	41.3	22.2
CuCl ₂	57.1	30.3	56.0	59.2	56.2	57.8	48.2	43.6	57.3	30.8	53.5	60.4	59.0	54.4	50.3	29.9
Cu(OTf) ₂	59.5	30.1	59.7	60.1	50.9	53.6	45.9	39.7	61.5	29.1	59.7	63.0	60.9	61.1	41.4	25.9
Cu(NO ₃) ₂	52.6	32.9	60.7	58.7	51.0	53.4	43.5	42.6	63.3	32.9	58.4	62.0	59.5	62.9	48.2	29.2
Cu(BF ₄) ₂	59.5	30.4	57.2	55.3	51.3	53.6	35.6	35.2	55.0	23.7	58.3	60.9	55.3	54.4	44.0	23.5
CuBr ₂	55.5	31.7	56.4	54.8	51.6	54.1	45.2	43.3	58.9	31.0	57.8	61.5	58.5	60.5	55.4	33.7
Phenanthroline									Bipyridine							

Validation of Quantitative Assay**Milliscale validation of quantitative assay**

All reactions were performed according to general procedure 9 with the titled boronic ester and reaction components detailed in the tables.

4,4,5,5-Tetramethyl-2-phenyl-1,3,2-dioxaborolane, 331

Entry	Base	Ligand	Catalyst	Nanoscale yield of 314 / %	Millimole yield of 314 / %
1	Collidine	Bipy	Cu(BF ₄) ₂	62	59
2	DBU	Phen	Cu(NO ₃) ₂	40	57
3	MTBD	Bipy	CuCl	33	40

2-(4-Methoxyphenyl)-4,4,5,5-tetramethyl-1,3,2-dioxaborolane, 332

Entry	Base	Ligand	Catalyst	Nanoscale yield of 315 / %	Millimole yield of 315 / %
1	Collidine	Bipy	CuCl	67	80
2	DABCO	Phen	Cu(NO ₃) ₂	53	75
3	MTBD	Bipy	Cu(BF ₄) ₂	28	51

4,4,5,5-tetramethyl-2-(4-(trifluoromethyl)phenyl)-1,3,2-dioxaborolane, 333

Entry	Base	Ligand	Catalyst	Nanoscale yield of 316 / %	Millimole yield of 316 / %
1	No Base	Phen	Cu(OTf) ₂	48	44
2	No Base	Bipy	CuCl	30	55
3	MTBD	Bipy	Cu(NO ₃) ₂	12	30

Ethyl 3-(4,4,5,5-tetramethyl-1,3,2-dioxaborolan-2-yl)benzoate, 334

Entry	Base	Ligand	Catalyst	Nanoscale yield of 369 / %	Millimole yield of 369 / %
1	Collidine	Phen	Cu(BF ₄) ₂	66	36
2	Urea	Phen	CuCl ₂	51	31
3	MTBD	Bipy	Cu(BF ₄) ₂	31	51

3-(4,4,5,5-tetramethyl-1,3,2-dioxaborolan-2-yl)pyridine, 335

Entry	Base	Ligand	Catalyst	Nanoscale yield of 370 / %	Millimole yield of 370 / %
1	DABCO	Phen	CuBr ₂	68	53
2	BTMG	Bipy	CuCl ₂	43	50
3	DBU	Bipy	Cu(BF ₄) ₂	6	16

4-(4,4,5,5-Tetramethyl-1,3,2-dioxaborolan-2-yl)-1H-indole, 336

Entry	Base	Ligand	Catalyst	Nanoscale yield of 371 / %	Millimole yield of 371 / %
1	DABCO	Bipy	CuCl	56	30
2	TMU	Phen	Cu(NO ₃) ₂	33	18
3	DBU	Phen	Cu(BF ₄) ₂	9	0

4,4,5,5-Tetramethyl-2-(naphthalen-2-yl)-1,3,2-dioxaborolane, 337

Entry	Base	Ligand	Catalyst	Nanoscale yield of 372 / %	Millimole yield of 372 / %
1	No Base	Phen	Cu(BF ₄) ₂	73	78
2	MTBD	Bipy	Cu(OTf) ₂	51	48
3	BTMG	Bipy	Cu(OTf) ₂	29	14

2-(4-Iodophenyl)-4,4,5,5-tetramethyl-1,3,2-dioxaborolane, 338

Entry	Base	Ligand	Catalyst	Nanoscale yield of 373 / %	Millimole yield of 373 / %
1	DABCO	Phen	CuCl	64	78
2	MTBD	Phen	Cu(NO ₃) ₂	44	48
3	BTMG	Bipy	CuCl	24	14

7.6. High-Throughput Substrate Scope

Procedure for 384 nanomolar scale reactions (2.5 μL volume) in one quarter of a 1536-well plate. Stock solutions of each component were prepared according to general procedure 1:4-phenylpiperidine **134** (0.67 M in DMSO), boronic ester (**395-416** and **439**, 0.2 M in DMSO), organic base (**339**, **387**, **343**; 1M in DMSO), ligand (**319** and **318**, 0.05 M in DMSO), catalyst (C1-C8, 0.2 M in DMSO). For the source plate layout, see Figure 59. For each 1536-well plate experiment, each well was charged with the amount noted in the “Source plate loading” column on the Excel spreadsheet, using a digital air displacement pipette, such that enough solution was present to dose the corresponding reactor plate.

The Mosquito was used to transfer aliquot volumes according to the “Solubility problems? Aliquotvol” column on the Excel Spreadsheet: amine was added in 375 nL, boronic ester was added in 1250 nL (2×625 nL), base was added in 250 nL, ligand was added in 500 nL and catalyst added in 125 nL resulting in a total reaction volume of 2.5 μL . When the catalyst had been added, the Mosquito mixed the reaction mixture together three times using the mix-dispense feature. The 1536-well reactor plate was then sealed with aluminium foil and placed under a heavy glass sheet for 24 hours.

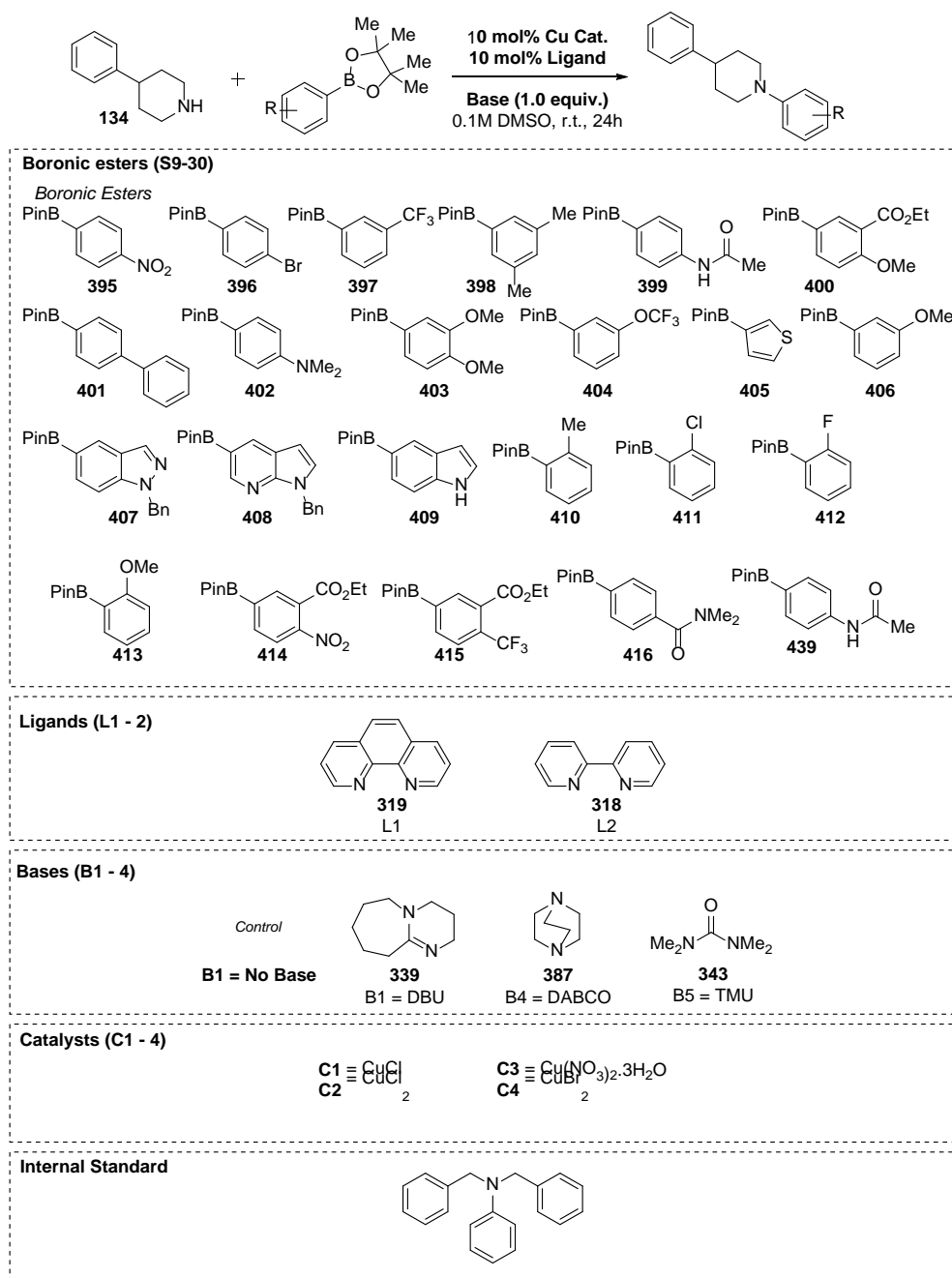


Figure S9: Components screened in 1536-well plate at 0.1M.

PLATE 1536	# reagents 5	How much of plate? All	input wells/column 32	Scale L.R. (umol) 0.25	Final conc. Rcn (M) 0.1	Stand. Aliq. (uL) 0.5	Daughter tot vol (uL) 2.5		
Reaction parameters (constant)	Reagent	Compound	CAS	Cat No	RW (g/mol)	Equiv.	Amount (uMol)	mg per rxn	Solubility problems? Aliquot vol(uL)
	R1	4-phenylpiperidine	771-99-3	P-034	161.12	1	0.25	4.0E-02	0.38
	S1	4-NO2BPIn	171364-83-3	HTE	249.07	1	0.25	6.2E-02	1.25
	S2	3,4-OMeBPIn	365564-10-9	HTE	264.13	1	0.25	6.9E-02	1.25
	S3	4-BromoBPIn	68716-49-4	HTE	282.97	1	0.25	7.1E-02	1.25
	S4	4-CONMe2BPIn	40072757-3	HTE	275.16	1	0.25	6.9E-02	1.25
	S5	EtOMeBPIn	N/A	HTE	306.17	1	0.25	7.7E-02	1.25
	S6	3-CF3BPIn	325142-82-3	HTE	272.07	1	0.25	6.8E-02	1.25
	S7	3-OCF3BPIn	262376-21-8	HTE	288.07	1	0.25	7.2E-02	1.25
	S8	3OMeBPIn	325142-84-5	HTE	234.10	1	0.25	5.9E-02	1.25
	S9	4-NMe2BPIn	171364-78-6	HTE	247.15	1	0.25	6.2E-02	1.25
	S10	3,5-MeBPIn	325142-93-6	HTE	232.13	1	0.25	5.8E-02	1.25
	S11	4-NMeAcetoBPIn	1056456-21-3	HTE	275.16	1	0.25	6.9E-02	1.25
	S12	5-IndoleBPIn	269410-24-4	HTE	243.11	1	0.25	6.1E-02	1.25
	S13	BnPyroloPyridineBPIn	n/a	HTE	334.23	1	0.25	8.4E-02	1.25
	S14	BnIndazBPIn	n/a	HTE	334.23	1	0.25	8.4E-02	1.25
	S15	2NMeBPIn	196062-59-0	HTE	218.10	1	0.25	5.5E-02	1.25
	S16	2ClBPIn	870195-94-1	HTE	238.52	1	0.25	6.0E-02	1.25
	S17	2FBPIn	876002-39-4	HTE	222.07	1	0.25	5.0E-02	1.25
	S18	2OMeBPIn	190788-60-4	HTE	234.10	1	0.25	5.9E-02	1.25
	S19	EtNO2BPIn	n/a	HTE	321.14	1	0.25	8.0E-02	1.25
	S20	EtCF3BPIn	n/a	HTE	344.14	1	0.25	8.6E-02	1.25
	S21	3-ThioBPIn	214360-70-0	HTE	210.10	1	0.25	5.3E-02	1.25
(x-constant, y-variable)	B1	No Base			152.24	1	0.25	3.8E-02	0.25
	B2	DBU	6674-22-2	D301	112.17	1	0.25	2.8E-02	0.25
	B3	DABCO	280-57-9	D052	116.16	1	0.25	2.9E-02	0.25
	B4	Tetramethylurea	632-32-4	D056	99.00	0.1	0.025	2.5E-03	0.13
(k-constant, y-variable)	C1	Cu(I)Cl	7756-86-6	cat025	134.45	0.1	0.025	3.4E-03	0.13
	C2	CuCl2		IC058	241.60	0.1	0.025	5.6E-03	0.13
	C3	Cu(II)NO32.3H2O	10031-43-3	IC010	223.35	0.1	0.025	5.6E-03	0.13
	C4	Cu(I)Br2	7789-45-9	IC022	180.21	0.1	0.025	4.5E-03	0.50
(k-variable, y-constant)	L1	1,10-phenantroline	66-71-7	P-228	156.18	0.1	0.025	3.9E-03	0.50
	L2	2,2-bipyridyl	366-18-7	B-462					

Stock solution (mg/vial)	Stock solution (solvent/vial)	Stock solution (pin vol/vial)	Mother (abs vol/well)	Mother (rec vol/well)	Source plate loading (vol/well uL)	Liquid reagents (vol/25)	DMSO Top-up
483.0	400	259	9	16	25	X	X
19.9	400	288	10	18			X
21.1	400	288	10	18			X
22.6	400	288	10	18			X
22.0	400	288	10	18			X
24.5	400	288	10	18			X
21.8	400	288	10	18			X
23.0	400	288	10	18			X
18.7	400	288	10	18			X
19.8	400	288	10	18			X
18.6	400	288	10	18			X
22.0	400	288	10	18	25	X	X
19.4	400	288	10	18			X
26.7	400	288	10	18			X
26.7	400	288	10	18			X
17.4	400	288	10	18			X
19.1	400	288	10	18			X
17.8	400	288	10	18			X
18.7	400	288	10	18			X
25.7	400	288	10	18			X
27.5	400	288	10	18			X
16.8	400	288	10	18			X
15.2	100	43	6	11			X
15.2	100	43	6	11	25	X	X
11.2	100	43	6	11			X
11.6	100	43	6	11			X
7.9	400	43	3	5			X
10.8	400	43	3	5	50	X	X
19.3	400	43	3	5			X
17.2	400	43	3	5			X
3.6	600	173	12	22	50.0	X	X
3.1	600	173	12	22			X

Boronic ester **401** and its corresponding product **423** crystallised at 0.1M and were

Spreadsheet 5: High-throughput screen of Chan-Lam reaction (1 x 12 x 4 x 2 x 4 screen).

screened at 0.1M (Figure 60). This substrate was also assessed at 0.05M concentration using Spreadsheet 6.

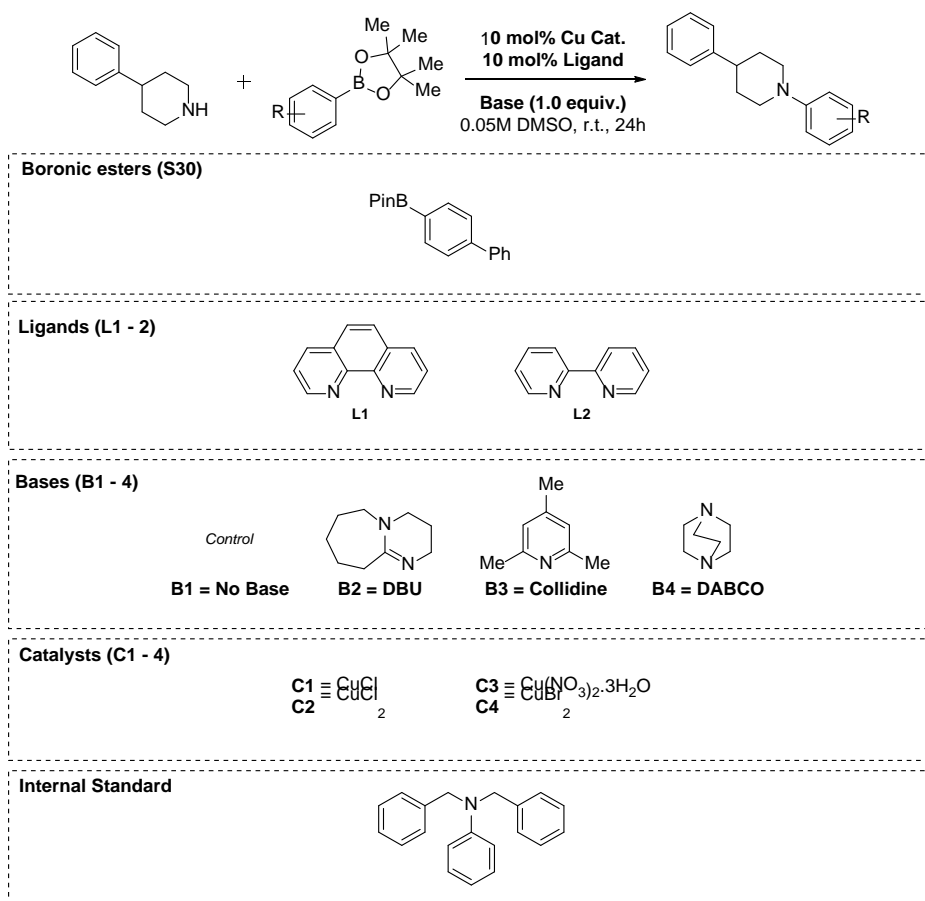


Figure 60: Components screened in 1536-well plate at 0.05M concentration.

PLATE	# reagents	How much of plate?	input wells/column	Scale L.R. (umol)	Final conc. Rxn (M)	Stand. Aliq. (ul)	Daughter tot vol (ul)	
.1536	5	All	32	0.125	0.05	0.5	2.5	
Reaction parameters constant?	Reagent	Compound	CAS	Cat No	FW (gMol-1)	Amount (uMol)	mg per rxn	Solubility problems? Aliquot vol(ul)
(constant)	R1	4-phenylpiperidine	771-99-3	P.034	161.12	0.125	2.0E-02	0.38
(x-constant, y-variable)	S1	4-biphenylBPin	144432-80-4	HTE	280.17	0.125	3.5E-02	1.25
	B1	No Base				0.125	1.9E-02	0.25
	B2	DBU	6674-22-2	D301	152.24	0.125	1.9E-02	0.25
	B3	DABCO	280-57-9	D052	112.17	0.125	1.4E-02	0.25
	B4	Tetramethylurea	632-22-4	Dave	116.16	0.125	1.5E-02	0.25
(x-constant, y-variable)	C1	Cu(I)Cl	7758-89-6	cat 025	99.00	0.0125	1.2E-03	0.13
	C2	CuCl2		IC058	134.45	0.0125	1.7E-03	0.13
	C3	Cu(II)(NO3)2.3H2O	10031-43-3	IC010	241.60	0.0125	3.0E-03	0.13
	C4	Cu(II)Br2	7789-45-9	IC022	223.35	0.0125	2.8E-03	0.13
(x-variable, y-constant)	L1	1,10-phenanthroline	66-71-7	P.228	180.21	0.0125	2.3E-03	0.50
	L2	2,2-bipyridyl	366-18-7	B.462	156.18	0.0125	2.0E-03	0.50

Stock solution (mg/vial)	Stock solution (solvent/vial)	Stock solution (min vol/vial)	Mother (abs vol/well)	Mother (rec vol/well)	Source plate loading (vol/well ul)	Liquid reagents (Vo/SS)	DMSO Top-up
21.5	400	259	9	16	25	X	X
11.2	400	288	10	18	25	X	X
7.6	100	43	6	11	25	X	X
7.6	100	43	6	11	25	6.9	93.1
5.6	100	43	6	11	25	X	X
5.8	100	43	6	11	25	6.0	94.0
4.0	400	43	3	5	50	X	X
5.4	400	43	3	5	50	X	X
9.7	400	43	3	5	50	X	X
8.9	400	43	3	5	50.0	X	X
1.8	400	173	12	22	50.0	X	X
1.6	400	173	12	22	50.0	X	X

Spreadsheet 6: High-throughput screen of Chan-Lam reaction (1 x 12 x 4 x 2 x 4 screen).

Source Plate Layout

	1	2	3	4	5	6	7	8	9	10	11	12	13	14	15	16	17	18	19	20	21	22	23	24	
A																	C3	C1	L1	B1	S2	S2	S1	R1	A
B																	C3	C1	L1	B2	S2	S2	S1	R1	B
C																	C3	C1	L1	B3	S2	S2	S1	R1	C
D																	C3	C1	L1	B4	S2	S2	S1	R1	D
E																	C3	C1	L2	B1	S2	S2	S1	R1	E
F																	C3	C1	L2	B2	S2	S2	S1	R1	F
G																	C3	C1	L2	B3	S2	S2	S1	R1	G
H																	C3	C1	L2	B4	S2	S2	S1	R1	H
I																	C4	C2	L1	B1	S2	S2	S1	R1	I
J																	C4	C2	L1	B2	S2	S2	S1	R1	J
K																	C4	C2	L1	B3	S2	S2	S1	R1	K
L																	C4	C2	L1	B4	S2	S2	S1	R1	L
M																	C4	C2	L2	B1	S2	S2	S1	R1	M
N																	C4	C2	L2	B2	S2	S2	S1	R1	N
O																	C4	C2	L2	B3	S2	S2	S1	R1	O
P																	C4	C2	L2	B4	S2	S2	S1	R1	P
	1	2	3	4	5	6	7	8	9	10	11	12	13	14	15	16	17	18	19	20	21	22	23	24	

Analysis plate preparation

Prior to quantitative analysis, the LCMS was cleaned using general procedure 5. Analysis plates were prepared according to general procedure 3 and Calibration curves were prepared using general procedure 4. If curves were found to undergo non-linear correlations, a quadratic formula was used to fit the data.²⁴⁶ Each substrate was run in using a bespoke LCMS assay method file (Appendix 2) with bespoke autosampler aliquot volume and IS368 stock solution shown in Table 10. Each assay was 1.8 minute and each plate analysed using General procedure 6.

Optimised LCMS assay conditions

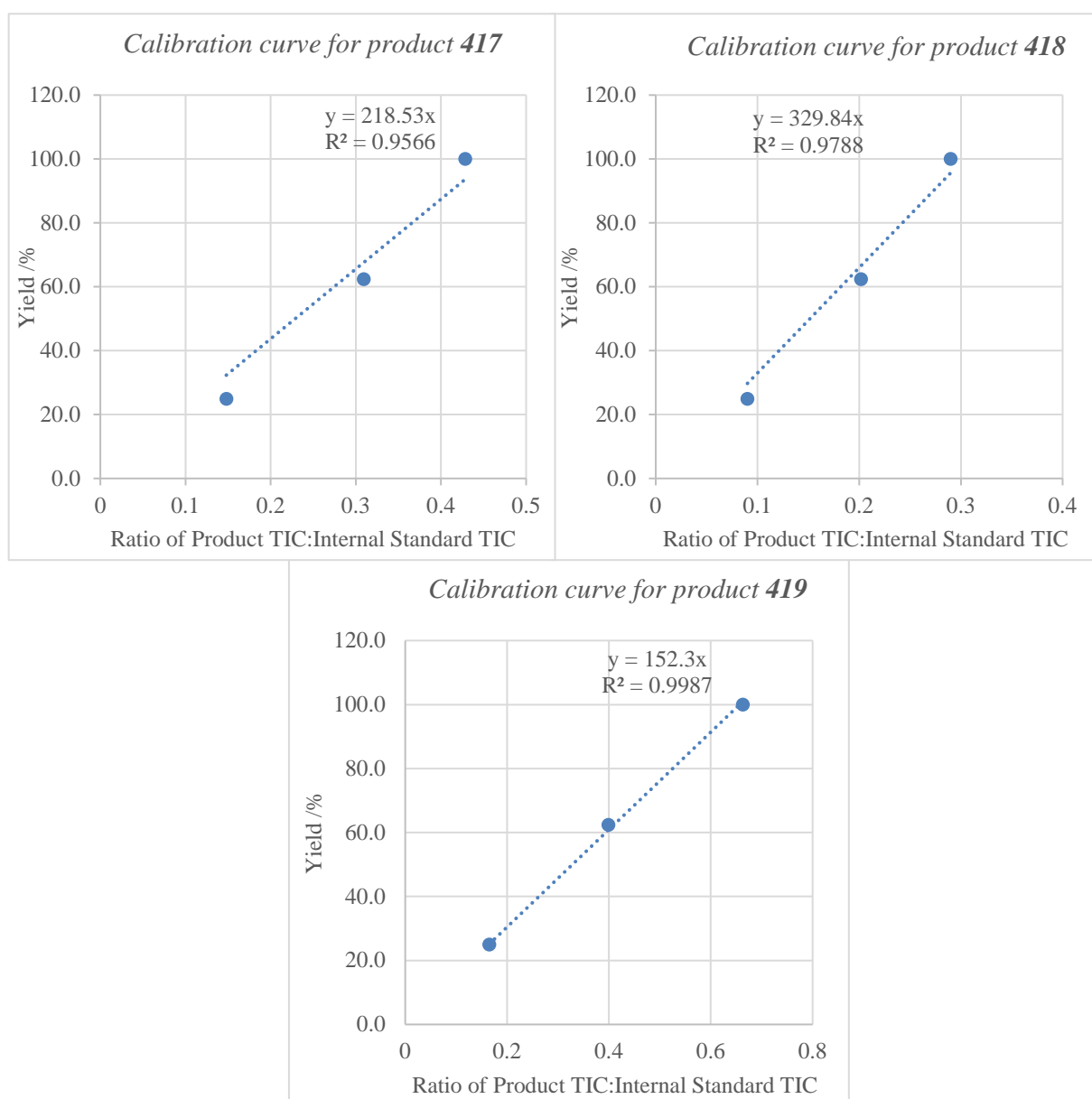
Entry	Product	Autosampler injection volume / μL	IS stock solution / μL of 0.1M IS368 S.S in 100 mL S.S.
1	417	1.0	67.5
2	418	1.0	67.5
3	419	1.0	67.5
4	420	0.2	337.5
5	422	0.2	337.5
6	423	0.2	337.5
7	424	0.2	337.5
8	425	0.2	337.5
9	426	0.5	135.0
10	427	0.5	135.0
11	428	0.2	67.5
12	429	0.3	225.0
13	430	0.2	337.5
14	431	0.2	337.5
15	432	0.2	337.5
16	433	1.0	67.5
17	434	1.0	67.5
18	435	0.2	337.5
19	436	1.0	67.5
20	437	1.0	67.5
21	438	0.2	337.
22	440	0.2	337.5

Table 10: Autosampler and IS368 stock solution preparation for substrates

Average of data repeats from quantitative LCMS assay

	No Base	DBU	DABCO	TMU	No Base	DBU	DABCO	TMU		No Base	DBU	DABCO	TMU	No Base	DBU	DABCO	TMU	
CuCl	0.16	0.16	0.15	0.16	0.15	0.16	0.15	0.16	BE1	0.17	0.18	BAD	0.18	0.17	BAD	0.17	0.20	Cu(NO ₃) ₂
CuCl ₂	0.16	0.15	0.15	0.16	0.15	0.16	0.15	0.15		0.15	0.16	0.15	0.15	0.15	0.15	BAD	0.15	0.15
CuCl	0.21	0.15	0.23	0.22	0.22	0.15	0.22	0.21	BE2	0.22	0.14	0.22	0.22	0.22	0.14	0.22	0.20	Cu(NO ₃) ₂
CuCl ₂	0.19	0.15	0.20	0.19	0.20	0.15	0.21	0.20		0.19	0.15	0.22	0.22	0.23	0.15	0.21	0.22	CuBr ₂
CuCl	0.32	0.22	0.34	0.31	0.31	0.21	0.35	0.28	BE3	0.31	0.21	0.39	0.31	0.28	0.18	0.33	0.25	Cu(NO ₃) ₂
CuCl ₂	0.30	0.20	0.30	0.29	0.29	0.20	0.31	0.28		0.33	0.21	0.37	0.36	0.37	0.23	0.38	0.36	CuBr ₂
	Phenanthroline				Bipyridine					Phenanthroline				Bipyridine				

Calibration curve post quantitative LCMS assay



Calibrated high-throughput optimisation of 395, 396 and 397

	No Base	DBU	DABCO	TMU	No Base	DBU	DABCO	TMU		No Base	DBU	DABCO	TMU	No Base	DBU	DABCO	TMU	
CuCl	35.2	35.1	33.8	34.7	33.2	34.3	32.6	33.9	BE1	36.9	38.8	BAD	39.3	36.2	BAD	36.9	43.4	Cu(NO₃)₂
CuCl₂	34.8	33.8	33.2	35.6	32.4	35.2	33.2	33.3		32.6	34.8	32.8	33.1	33.1	BAD	33.6	33.8	CuBr₂
CuCl	69.8	48.9	75.9	71.9	73.6	50.3	73.1	69.9	BE2	71.8	46.0	73.7	73.0	71.9	46.0	71.7	67.1	Cu(NO₃)₂
CuCl₂	64.3	48.9	66.9	64.0	66.3	48.6	67.7	66.4		63.8	50.1	71.0	73.3	75.5	49.7	69.9	72.6	CuBr₂
CuCl	48.3	33.4	51.1	47.4	47.0	32.6	53.0	42.9	BE3	47.3	31.5	59.7	47.7	42.7	27.8	49.9	38.2	Cu(NO₃)₂
CuCl₂	46.1	29.9	45.5	43.6	44.7	30.8	46.7	42.1		50.8	32.3	56.6	54.9	56.8	35.4	57.1	55.2	CuBr₂
	Phenanthroline				Bipyridine					Phenanthroline				Bipyridine				

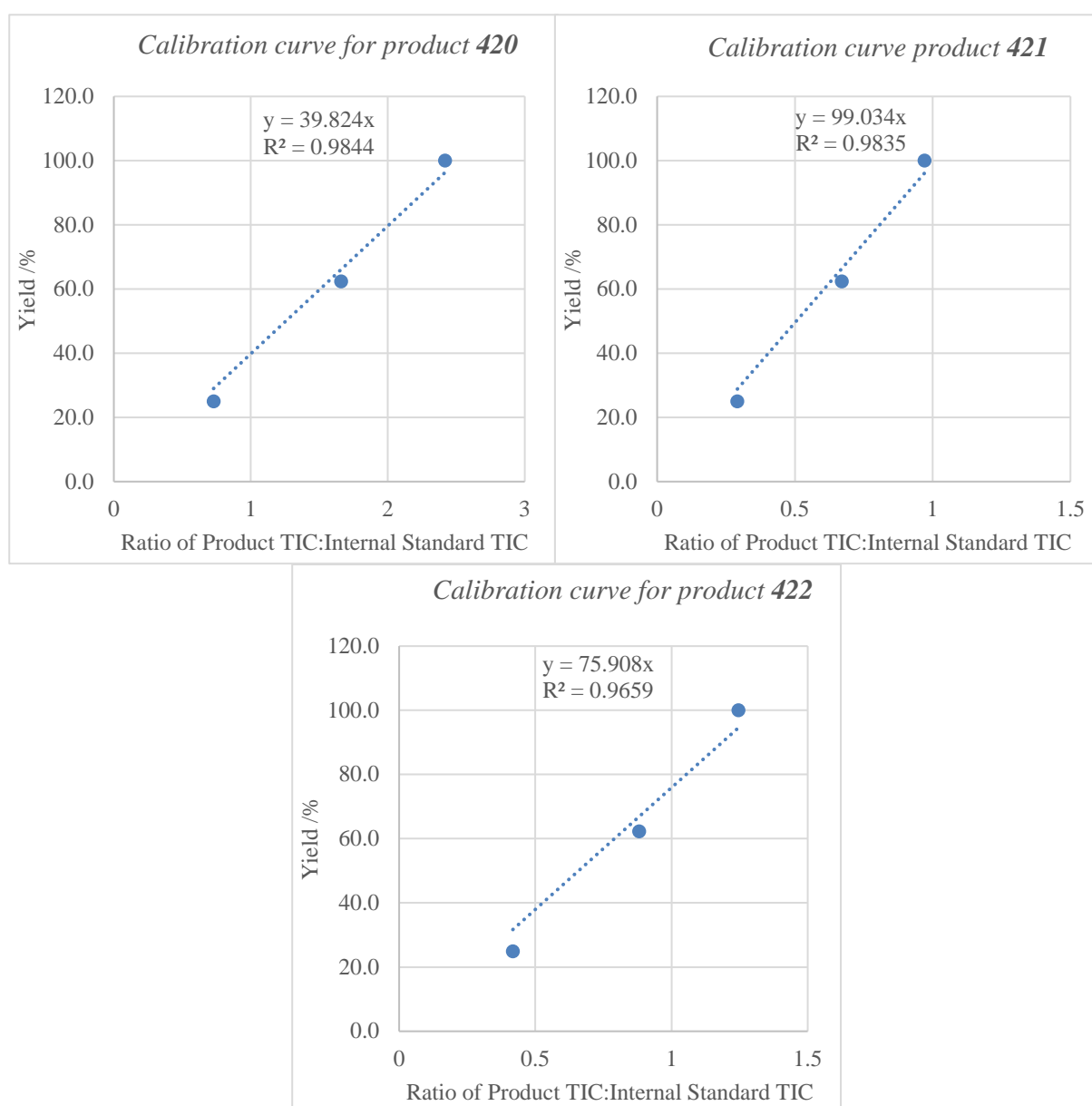
Boronic Ester scope Plate 2: 4-Phenylpiperidine **134** was assessed with BE1: 3,5-dimethylphenylboronic acid pinacol ester **398**, BE2: 4-acetamidophenylboronic acid pinacol ester **399**, BE3: Ethyl 2-methoxy-5-(4,4,5,5-tetramethyl-1,3,2-dioxaborolan-2-yl)benzoate **400**.

		CuCl ₂				CuCl				CuCl ₂				CuCl				CuCl ₂				CuCl											
		No Base	DBU	DABCO	TMU	No Base	DBU	DABCO	TMU	No Base	DBU	DABCO	TMU	No Base	DBU	DABCO	TMU	No Base	DBU	DABCO	TMU	No Base	DBU	DABCO	TMU	No Base	DBU	DABCO	TMU				
Phenanthroline		0.99	0.95	0.91	0.94	1.09	1.00	1.00	1.09	0.63	0.68	0.67	0.66	0.87	0.79	0.87	0.92	1.45	1.58	1.45	1.38	BAD	BAD	BAD	BAD	1.28	1.27	1.26	1.26	1.94	1.93	1.91	1.95
		0.72	0.77	0.76	1.00	0.80	0.78	0.54	0.52	0.63	0.51	0.54	0.52	0.63	0.58	0.59	0.54	1.06	1.11	1.14	1.00	1.14	1.14	1.01	1.07	1.14	1.11	1.11	1.07	1.01	1.01	1.01	1.01
Bipyridine		1.00	1.02	0.96	1.00	1.13	1.07	0.52	0.55	0.85	0.54	0.51	0.55	0.86	0.86	0.86	0.87	1.16	0.95	1.16	1.01	1.39	1.57	1.43	1.64	1.06	1.11	1.11	1.07	1.06	1.11	1.06	1.06
		1.00	1.02	1.00	0.98	1.12	1.10	0.57	0.56	BAD	0.57	0.59	0.56	0.82	0.82	0.84	0.88	1.06	1.04	1.04	1.02	1.04	1.00	1.12	1.02	1.04	1.00	1.12	1.02	0.97	0.83	0.86	0.86
Phenanthroline		0.95	0.95	0.98	0.99	1.08	1.11	0.47	0.47	0.87	0.47	0.51	0.47	0.87	0.92	0.90	0.92	1.24	1.03	1.30	1.14	1.24	1.03	1.30	1.14	1.24	1.03	1.30	1.14	2.04	2.04	2.04	2.08
		0.94	0.95	0.93	0.93	1.13	1.09	0.48	0.40	0.85	0.49	0.47	0.40	0.85	0.81	0.88	0.86	0.97	0.83	0.95	0.86	0.97	0.83	0.95	0.86	0.97	0.83	0.95	0.86	2.04	2.04	2.04	2.08
Bipyridine		0.95	0.95	0.98	0.99	1.08	1.11	0.51	0.47	0.87	0.51	0.51	0.47	0.87	0.92	0.90	0.92	1.24	1.03	1.30	1.14	1.24	1.03	1.30	1.14	1.24	1.03	1.30	1.14	2.04	2.04	2.04	2.08
		0.94	0.95	0.93	0.93	1.13	1.09	0.48	0.40	0.85	0.49	0.47	0.40	0.85	0.81	0.88	0.86	0.97	0.83	0.95	0.86	0.97	0.83	0.95	0.86	0.97	0.83	0.95	0.86	2.04	2.04	2.04	2.08
		Boronic Ester 1																															
Phenanthroline		0.96	0.99	0.95	0.99	1.04	1.03	1.03	1.05	0.72	0.73	0.73	0.69	0.76	0.80	0.79	0.84	1.59	1.53	1.72	1.45	1.53	1.34	1.25	1.21	1.66	1.66	1.66	1.66	1.66	1.66	1.66	1.66
		0.82	0.83	0.82	0.87	0.81	0.85	0.85	0.84	0.66	0.57	0.54	0.60	0.60	0.60	0.59	0.56	1.36	1.34	1.25	1.21	1.36	1.34	1.25	1.21	1.66	1.66	1.66	1.66	1.66	1.66	1.66	1.66
Bipyridine		1.05	1.06	1.06	1.08	1.16	1.07	1.04	1.11	0.72	0.73	0.70	0.70	0.71	0.73	0.76	0.81	1.60	1.68	1.74	1.66	1.60	1.68	1.74	1.66	1.67	1.67	1.67	1.67	1.60	1.63	1.65	1.79
		1.05	1.06	1.05	1.06	1.07	1.04	1.04	1.03	0.72	0.72	0.70	0.74	0.76	0.80	0.77	0.75	1.69	1.67	1.74	1.85	1.69	1.67	1.74	1.85	1.67	1.63	1.65	1.79	1.60	1.63	1.65	1.79
		Boronic Ester 2																															
Phenanthroline		1.06	1.07	1.08	1.04	1.04	1.07	1.04	1.03	0.75	0.72	0.70	0.74	0.77	0.79	0.78	0.75	1.61	1.66	1.76	1.68	1.61	1.66	1.76	1.68	1.61	1.66	1.76	1.68	1.61	1.66	1.76	1.68
		0.80	0.81	0.82	0.81	0.78	0.78	0.78	0.79	0.56	0.52	0.57	0.54	0.56	0.57	0.50	0.47	1.13	1.16	1.18	1.13	1.13	1.16	1.18	1.13	1.13	1.16	1.18	1.13	1.05	1.05	1.05	1.10
Bipyridine		1.04	1.08	1.07	1.05	1.05	1.09	0.72	0.79	0.72	0.67	0.61	0.57	0.81	0.75	0.70	0.74	1.44	1.41	1.49	1.45	1.44	1.41	1.49	1.45	1.65	1.62	1.62	1.65	1.62	1.62	1.62	1.65
		1.04	1.08	1.07	1.05	1.05	1.09	0.72	0.79	0.72	0.67	0.61	0.57	0.81	0.75	0.70	0.74	1.44	1.41	1.49	1.45	1.44	1.41	1.49	1.45	1.65	1.62	1.62	1.65	1.62	1.62	1.62	1.65
		Boronic Ester 3																															
Phenanthroline		1.06	1.07	1.08	1.04	1.04	1.07	1.04	1.03	0.75	0.72	0.70	0.74	0.77	0.79	0.78	0.75	1.61	1.66	1.76	1.68	1.61	1.66	1.76	1.68	1.61	1.66	1.76	1.68	1.61	1.66	1.76	1.68
		0.80	0.81	0.82	0.81	0.78	0.78	0.78	0.79	0.56	0.52	0.57	0.54	0.56	0.57	0.50	0.47	1.13	1.16	1.18	1.13	1.13	1.16	1.18	1.13	1.13	1.16	1.18	1.13	1.05	1.05	1.05	1.10
Bipyridine		1.04	1.08	1.07	1.05	1.05	1.09	0.72	0.79	0.72	0.67	0.61	0.57	0.81	0.75	0.70	0.74	1.44	1.41	1.49	1.45	1.44	1.41	1.49	1.45	1.65	1.62	1.62	1.65	1.62	1.62	1.62	1.65
		1.04	1.08	1.07	1.05	1.05	1.09	0.72	0.79	0.72	0.67	0.61	0.57	0.81	0.75	0.70	0.74	1.44	1.41	1.49	1.45	1.44	1.41	1.49	1.45	1.65	1.62	1.62	1.65	1.62	1.62	1.62	1.65

Average of data repeats from quantitative LCMS assay

	No Base	DBU	DABCO	TMU	No Base	DBU	DABCO	TMU		No Base	DBU	DABCO	TMU	No Base	DBU	DABCO	TMU	
CuCl	BAD	1.26	1.92	1.94	2.03	1.43	2.00	2.11	BE1	1.66	1.22	1.66	1.67	1.70	1.13	1.64	1.65	Cu(NO₃)₂
CuCl₂	1.47	1.08	1.04	1.51	1.10	1.04	0.90	1.17		1.57	1.29	1.67	1.74	1.68	1.15	1.45	1.67	CuBr₂
CuCl	0.86	0.58	0.86	0.85	0.88	0.68	0.85	0.90	BE2	0.80	0.59	0.75	0.77	0.77	0.53	0.75	0.79	Cu(NO₃)₂
CuCl₂	0.66	0.53	0.53	0.57	0.48	0.50	0.46	0.49		0.72	0.59	0.71	0.72	0.72	0.54	0.64	0.71	CuBr₂
CuCl	1.05	0.79	1.13	1.11	1.13	0.85	1.14	1.09	BE3	1.04	0.83	1.10	1.04	1.07	0.79	1.07	1.05	Cu(NO₃)₂
CuCl₂	0.94	0.75	0.99	1.00	0.98	0.80	0.94	0.97		0.98	0.84	1.06	1.05	1.15	0.81	1.07	1.06	CuBr₂
	Phenanthroline				Bipyridine					Phenanthroline				Bipyridine				

Calibration curve post quantitative LCMS assay



Calibrated high-throughput optimisation of 398, 399 and 400

	No Base	DBU	DABCO	TMU	No Base	DBU	DABCO	TMU		No Base	DBU	DABCO	TMU	No Base	DBU	DABCO	TMU	
CuCl	BAD	50.0	76.4	77.2	80.7	56.8	79.8	83.9	BE1	66.0	48.6	66.1	66.7	67.6	44.8	65.3	65.6	Cu(NO₃)₂
CuCl₂	58.3	42.9	41.4	60.1	43.6	41.6	35.9	46.8		62.6	51.4	66.5	69.2	66.8	45.7	57.6	66.7	CuBr₂
CuCl	85.4	57.6	85.2	83.9	86.9	67.7	83.9	89.4	BE2	79.2	58.1	74.7	75.9	76.4	52.2	74.1	78.4	Cu(NO₃)₂
CuCl₂	65.3	52.6	52.4	56.7	47.7	49.2	45.7	48.5		71.1	58.7	70.4	71.2	71.6	54.0	63.7	70.0	CuBr₂
CuCl	79.4	60.1	85.5	84.5	85.9	64.3	86.3	82.9	BE3	78.7	63.1	83.7	79.3	81.0	60.0	81.5	79.7	Cu(NO₃)₂
CuCl₂	71.7	57.3	75.4	76.1	74.1	61.0	71.2	73.6		74.0	63.5	80.7	79.9	87.2	61.5	81.2	80.8	CuBr₂
	Phenanthroline				Bipyridine					Phenanthroline				Bipyridine				

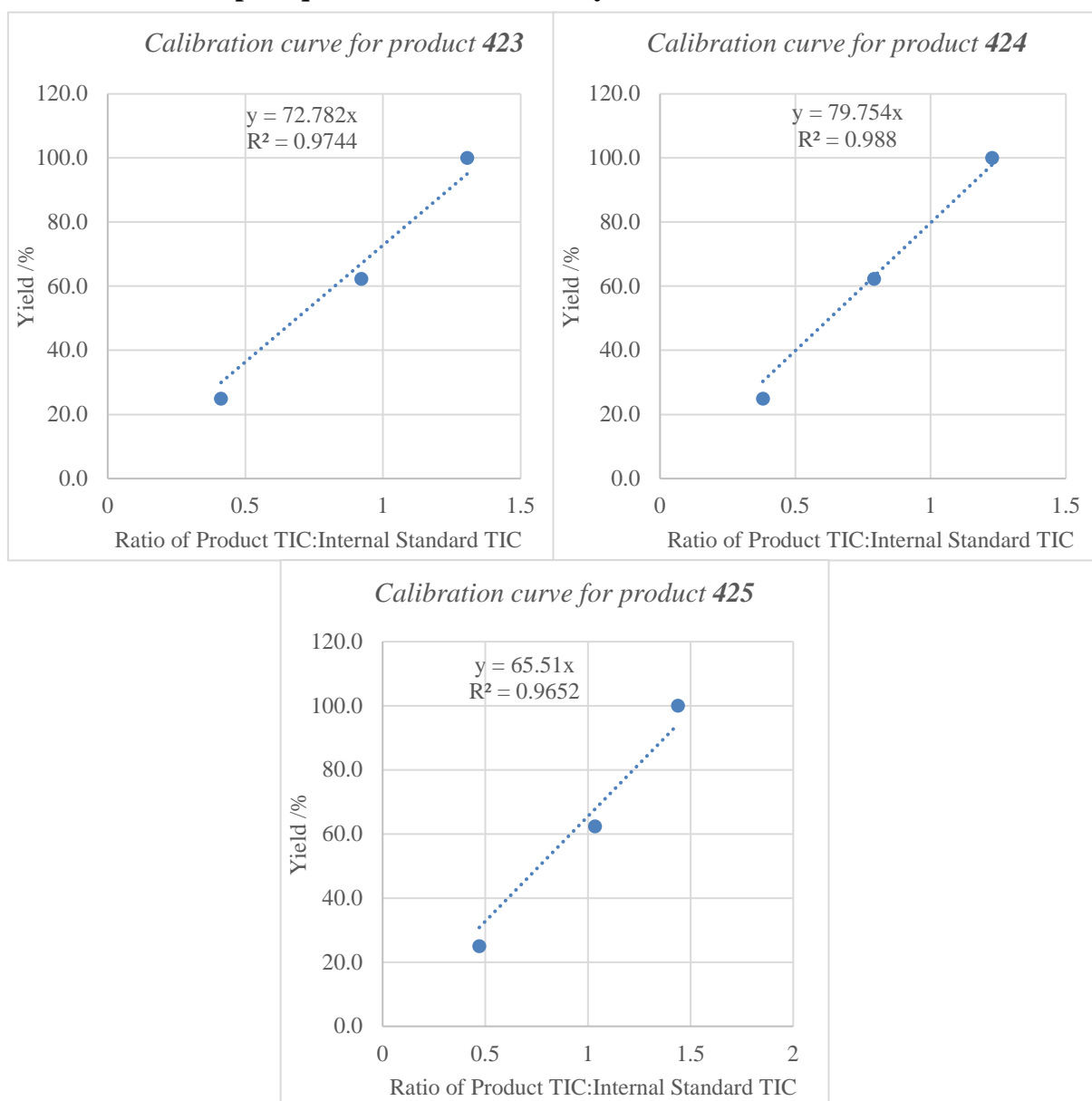
Boronic Ester scope Plate 3: 4-Phenylpiperidine **134** was assessed with BE1: 4-biphenylboronic acid pinacol ester **401**, BE2: 4-dimethylphenylboronic acid pinacol ester **402**, BE3: 3,4-dimethoxyphenylboronic acid pinacol ester **403**.

	CuCl ₂				CuCl				CuCl ₂				CuCl				CuCl ₂				CuCl				CuCl ₂							
	No Base	DBU	DABCO	TMU	No Base	DBU	DABCO	TMU	No Base	DBU	DABCO	TMU	No Base	DBU	DABCO	TMU	No Base	DBU	DABCO	TMU	No Base	DBU	DABCO	TMU	No Base	DBU	DABCO	TMU				
Phenanthroline	0.04	0.05	0.03	0.03	0.14	0.27	0.13	0.10	0.04	0.16	0.15	0.16	0.05	0.07	0.18	0.17	0.04	0.16	0.15	0.14	0.05	0.07	0.18	0.17	0.04	0.16	0.15	0.14	0.05	0.07	0.18	0.17
	0.16	0.16	0.15	0.16	0.27	0.24	0.10	0.09	0.16	0.14	0.15	0.14	0.11	0.11	0.14	0.14	0.16	0.14	0.15	0.14	0.14	0.11	0.14	0.14	0.16	0.14	0.15	0.14	0.14	0.11	0.14	0.14
	0.04	0.03	0.03	0.03	0.13	0.13	0.13	0.10	0.06	0.06	0.06	0.06	0.06	0.06	0.06	0.06	0.06	0.06	0.06	0.06	0.06	0.06	0.06	0.06	0.06	0.06	0.06	0.06	0.06	0.06	0.06	0.06
	0.03	0.03	0.03	0.03	0.10	0.10	0.10	0.10	0.07	0.07	0.07	0.07	0.07	0.07	0.07	0.07	0.07	0.07	0.07	0.07	0.07	0.07	0.07	0.07	0.07	0.07	0.07	0.07	0.07	0.07	0.07	0.07
Bipyridine	0.48	0.50	0.47	0.53	0.74	0.71	0.74	0.74	0.35	0.36	0.34	0.36	0.41	0.41	0.41	0.41	0.35	0.36	0.34	0.36	0.41	0.41	0.41	0.41	0.35	0.36	0.34	0.36	0.41	0.41	0.41	0.41
	0.76	0.76	0.75	0.79	0.79	0.78	0.79	0.79	0.32	0.32	0.32	0.32	0.32	0.32	0.32	0.32	0.32	0.32	0.32	0.32	0.32	0.32	0.32	0.32	0.32	0.32	0.32	0.32	0.32	0.32	0.32	0.32
	0.56	0.63	0.59	0.59	0.87	0.77	0.87	0.87	0.46	0.46	0.46	0.46	0.46	0.46	0.46	0.46	0.46	0.46	0.46	0.46	0.46	0.46	0.46	0.46	0.46	0.46	0.46	0.46	0.46	0.46	0.46	0.46
	0.55	0.55	0.59	0.62	0.88	0.81	0.88	0.88	0.41	0.41	0.41	0.41	0.41	0.41	0.41	0.41	0.41	0.41	0.41	0.41	0.41	0.41	0.41	0.41	0.41	0.41	0.41	0.41	0.41	0.41	0.41	0.41
Phenanthroline	0.17	0.17	0.24	0.20	0.13	0.19	0.11	0.18	0.04	0.04	0.04	0.04	0.04	0.04	0.04	0.04	0.04	0.04	0.04	0.04	0.04	0.04	0.04	0.04	0.04	0.04	0.04	0.04	0.04	0.04	0.04	0.04
	0.22	0.22	0.24	0.23	0.24	0.24	0.24	0.24	0.07	0.07	0.07	0.07	0.07	0.07	0.07	0.07	0.07	0.07	0.07	0.07	0.07	0.07	0.07	0.07	0.07	0.07	0.07	0.07	0.07	0.07	0.07	0.07
	0.12	0.19	0.17	0.15	0.18	0.11	0.12	0.18	0.04	0.04	0.04	0.04	0.04	0.04	0.04	0.04	0.04	0.04	0.04	0.04	0.04	0.04	0.04	0.04	0.04	0.04	0.04	0.04	0.04	0.04	0.04	0.04
	0.13	0.11	0.18	0.18	0.15	0.18	0.15	0.18	0.04	0.04	0.04	0.04	0.04	0.04	0.04	0.04	0.04	0.04	0.04	0.04	0.04	0.04	0.04	0.04	0.04	0.04	0.04	0.04	0.04	0.04	0.04	0.04
Bipyridine	0.70	0.68	0.66	0.68	0.56	0.55	0.54	0.54	0.24	0.24	0.24	0.24	0.32	0.32	0.32	0.32	0.32	0.32	0.32	0.32	0.32	0.32	0.32	0.32	0.32	0.32	0.32	0.32	0.32	0.32	0.32	0.32
	0.72	0.78	0.73	0.75	0.75	0.69	0.71	0.73	0.27	0.27	0.27	0.27	0.27	0.27	0.27	0.27	0.27	0.27	0.27	0.27	0.27	0.27	0.27	0.27	0.27	0.27	0.27	0.27	0.27	0.27	0.27	0.27
	0.68	0.74	0.74	0.74	0.61	0.67	0.66	0.70	0.31	0.31	0.31	0.31	0.31	0.31	0.31	0.31	0.31	0.31	0.31	0.31	0.31	0.31	0.31	0.31	0.31	0.31	0.31	0.31	0.31	0.31	0.31	0.31
	0.64	0.66	0.70	0.72	0.64	0.66	0.62	0.64	0.28	0.28	0.28	0.28	0.28	0.28	0.28	0.28	0.28	0.28	0.28	0.28	0.28	0.28	0.28	0.28	0.28	0.28	0.28	0.28	0.28	0.28	0.28	0.28

Average of data repeats from quantitative LCMS assay

	Phenanthroline				Bipyridine					Phenanthroline				Bipyridine				
	No Base	DBU	DABCO	TMU	No Base	DBU	DABCO	TMU		No Base	DBU	DABCO	TMU	No Base	DBU	DABCO	TMU	
CuCl	0.16	BAD	0.16	0.14	BAD	0.12	0.10	0.12	BE1	0.08	0.13	0.08	0.09	0.17	0.33	0.14	0.14	Cu(NO ₃) ₂
CuCl ₂	0.05	0.14	0.06	0.05	BAD	BAD	BAD	0.32		0.19	0.20	0.17	0.17	0.42	0.23	BAD	0.18	CuBr ₂
CuCl	0.06	0.07	0.06	0.10	0.41	0.30	0.41	0.41	BE2	0.04	0.07	0.03	0.04	0.16	0.20	0.19	0.19	Cu(NO ₃) ₂
CuCl ₂	0.00	0.05	0.00	0.01	0.35	0.32	0.32	0.32		0.05	0.07	0.06	0.06	0.30	0.27	0.27	0.29	CuBr ₂
CuCl	0.18	0.26	0.12	0.11	0.73	0.81	0.82	0.82	BE3	0.16	0.23	0.13	0.15	0.55	0.72	0.66	0.64	Cu(NO ₃) ₂
CuCl ₂	0.05	0.16	0.03	0.03	0.50	0.76	0.59	0.58		0.18	0.23	0.16	0.15	0.68	0.75	0.72	0.68	CuBr ₂

Calibration curve post quantitative LCMS assay



Calibrated high-throughput optimisation of 401, 402 and 403

	No Base	DBU	DABCO	TMU	No Base	DBU	DABCO	TMU		No Base	DBU	DABCO	TMU	No Base	DBU	DABCO	TMU	
CuCl	11.7	BAD	12.0	10.5	BAD	9.0	7.5	8.5	BE1	5.6	9.7	5.9	6.5	12.3	24.0	10.5	10.2	Cu(NO₃)₂
CuCl₂	3.9	10.2	4.3	3.7	BAD	BAD	BAD	23.6		13.9	14.8	12.4	12.3	30.7	16.5	BAD	12.8	CuBr₂
CuCl	5.2	5.9	5.0	7.7	32.5	24.1	32.8	32.4	BE2	3.0	5.7	2.8	3.4	13.0	15.6	15.4	15.3	Cu(NO₃)₂
CuCl₂	0.3	4.0	0.4	0.5	27.7	25.3	25.7	25.7		4.1	5.6	4.6	5.2	23.5	21.5	21.6	23.5	CuBr₂
CuCl	11.5	17.2	7.9	6.9	47.6	53.2	53.4	53.4	BE3	10.2	15.3	8.5	9.5	35.8	47.0	43.5	41.9	Cu(NO₃)₂
CuCl₂	3.0	10.4	2.1	1.8	32.5	50.1	38.6	37.8		11.7	15.1	10.2	9.8	44.5	48.8	47.5	44.7	CuBr₂
	Phenanthroline				Bipyridine					Phenanthroline				Bipyridine				

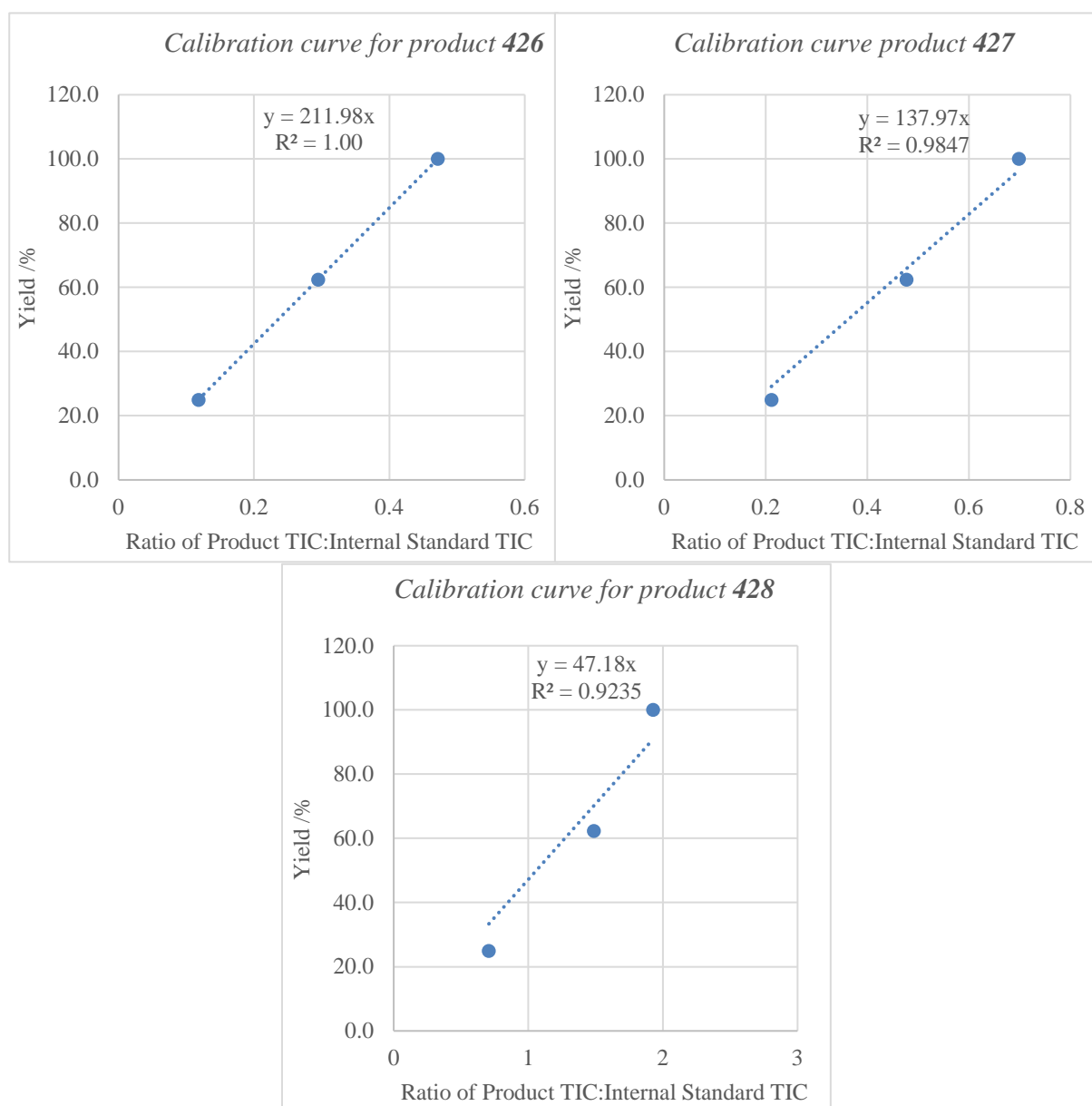
Boronic Ester scope Plate 4: BE1: 3-trifluoromethoxyphenylboronic acid pinacol ester **404**, BE2: thiophen-3-boronic acid pinacol ester **405**, BE3: 3-methoxyphenylboronic acid pinacol ester **406**.

		CuCl ₂				CuCl				CuCl ₂				CuCl				CuCl ₂				CuCl				
		Phenanthroline		Bipyridine		Phenanthroline		Bipyridine		Phenanthroline		Bipyridine		Phenanthroline		Bipyridine		Phenanthroline		Bipyridine		Phenanthroline		Bipyridine		
		No Base	DBU	DABCO	TMU	No Base	DBU	DABCO	TMU	No Base	DBU	DABCO	TMU	No Base	DBU	DABCO	TMU	No Base	DBU	DABCO	TMU	No Base	DBU	DABCO	TMU	
Boronic Ester 1																										
1.62	1.63	1.66	1.60	1.65	1.72	1.70	1.71	0.54	0.47	0.48	0.48	0.44	0.45	0.54	0.49	0.29	0.28	0.30	0.30	0.29	0.29	0.30	0.32	0.32	0.30	0.29
1.32	1.33	1.34	1.28	1.30	1.31	1.32	1.27	0.27	0.25	0.25	0.18	0.18	0.19	0.16	0.18	0.20	0.20	0.20	0.20	0.20	0.20	0.20	0.20	0.20	0.20	0.20
BAD	1.60	1.60	1.64	1.67	1.65	1.72	1.65	0.45	0.40	0.48	0.50	0.49	0.47	0.49	0.28	0.28	0.27	0.28	0.28	0.31	0.29	0.29	0.30	0.29	0.29	
1.56	1.49	1.57	1.58	1.66	1.74	1.71	1.74	0.46	0.45	0.46	0.49	0.49	0.53	0.52	0.49	0.27	0.26	0.25	0.28	0.28	0.28	0.30	0.29	0.29	0.30	
1.45	1.51	1.56	1.63	1.68	1.65	1.63	1.67	0.36	0.38	0.36	0.37	0.37	0.38	0.34	0.37	0.23	0.24	0.22	0.23	0.22	0.22	0.22	0.22	0.22	0.22	
1.44	1.45	BAD	1.37	1.39	1.47	1.37	1.39	0.31	0.29	0.26	0.15	0.19	0.16	0.17	0.21	0.19	0.19	0.18	0.18	0.15	0.17	0.16	0.17	0.16	0.16	
1.66	1.59	1.69	1.68	1.68	1.63	1.73	1.66	0.40	0.40	0.43	0.37	0.37	0.38	0.35	0.23	0.26	0.25	0.25	0.26	0.26	0.26	0.26	0.25	0.25	0.26	
1.63	1.59	1.61	1.65	1.64	1.72	1.65	1.73	0.37	0.40	0.47	0.37	0.37	0.39	0.38	0.24	0.21	0.22	0.22	0.23	0.23	0.23	0.23	0.23	0.23	0.24	
Boronic Ester 2																										
1.56	1.40	1.61	1.55	BAD	1.62	1.49	1.54	0.47	0.48	0.49	0.34	0.34	0.33	0.36	0.29	0.28	0.29	0.30	0.31	0.29	0.27	0.25	0.25	0.21	0.22	
1.38	1.40	1.29	1.37	1.36	1.35	1.28	1.42	0.23	0.23	0.24	0.24	0.24	0.23	0.23	0.22	0.19	0.19	0.19	0.20	0.22	0.17	0.18	0.18	0.18	0.18	
1.60	1.61	1.55	BAD	BAD	1.62	1.49	1.54	0.47	0.48	0.49	0.34	0.34	0.33	0.36	0.29	0.28	0.29	0.30	0.31	0.29	0.27	0.25	0.25	0.21	0.22	
1.52	1.56	1.57	1.53	1.28	BAD	1.32	1.32	0.48	0.52	0.53	0.30	0.30	0.32	0.32	BAD	0.32	0.31	0.31	0.31	0.22	0.22	0.24	0.23	0.23	0.24	
1.63	1.59	1.54	1.63	1.50	1.46	1.54	1.55	0.42	0.42	0.43	0.24	0.24	0.24	0.24	0.25	0.27	0.26	0.27	0.19	0.19	0.19	0.20	0.19	0.19	0.20	
1.45	1.44	1.40	1.44	1.40	1.38	1.30	1.32	0.19	0.17	0.19	0.14	0.16	0.15	0.16	0.18	0.18	0.18	0.18	0.18	0.14	0.14	0.14	0.14	0.14	0.14	
1.67	BAD	1.68	1.66	BAD	1.68	1.68	1.65	0.44	0.44	0.39	0.21	0.21	0.25	0.24	0.26	0.28	0.28	0.29	0.22	0.22	0.22	0.23	0.23	0.23	0.24	
1.47	1.47	1.45	1.53	1.50	1.48	BAD	1.54	0.44	0.37	0.43	0.24	0.24	0.22	0.22	0.28	0.26	0.26	0.25	0.25	0.18	0.18	0.16	0.16	0.16	0.19	
Boronic Ester 3																										
1.56	1.56	1.61	1.64	1.43	1.36	1.43	1.42	BAD	0.55	0.56	0.38	0.38	0.38	0.40	0.36	0.29	0.28	0.29	0.30	0.25	0.25	0.24	0.24	0.24	0.24	
1.38	1.40	1.29	1.37	1.36	1.35	1.28	1.42	0.23	0.23	0.24	0.24	0.24	0.23	0.23	0.22	0.19	0.19	0.19	0.20	0.17	0.17	0.18	0.18	0.18	0.18	
1.60	1.61	1.55	BAD	BAD	1.62	1.49	1.54	0.47	0.48	0.49	0.34	0.34	0.33	0.36	0.29	0.28	0.29	0.30	0.31	0.27	0.25	0.24	0.24	0.24	0.24	
1.52	1.56	1.57	1.53	1.28	BAD	1.32	1.32	0.48	0.52	0.53	0.30	0.30	0.32	0.32	BAD	0.32	0.31	0.31	0.31	0.22	0.22	0.24	0.23	0.23	0.24	
1.63	1.59	1.54	1.63	1.50	1.46	1.54	1.55	0.42	0.42	0.43	0.24	0.24	0.24	0.24	0.25	0.27	0.26	0.27	0.19	0.19	0.19	0.20	0.19	0.19	0.20	
1.45	1.44	1.40	1.44	1.40	1.38	1.30	1.32	0.19	0.17	0.19	0.14	0.16	0.15	0.16	0.18	0.18	0.18	0.18	0.14	0.14	0.14	0.14	0.14	0.14	0.14	
1.67	BAD	1.68	1.66	BAD	1.68	1.68	1.65	0.44	0.44	0.39	0.21	0.21	0.25	0.24	0.26	0.28	0.28	0.29	0.22	0.22	0.22	0.23	0.23	0.23	0.24	
1.47	1.47	1.45	1.53	1.50	1.48	BAD	1.54	0.44	0.37	0.43	0.24	0.24	0.22	0.22	0.28	0.26	0.26	0.25	0.25	0.18	0.18	0.16	0.16	0.16	0.19	

Average of data repeats from quantitative LCMS assay

	No Base	DBU	DABCO	TMU	No Base	DBU	DABCO	TMU		No Base	DBU	DABCO	TMU	No Base	DBU	DABCO	TMU	
CuCl	0.31	0.20	0.30	0.29	0.22	0.16	0.26	0.23	BE1	0.23	0.17	0.27	0.24	0.19	0.14	0.23	0.18	Cu(NO ₃) ₂
CuCl ₂	0.29	0.20	0.28	0.27	0.23	0.19	0.25	0.23		0.29	0.20	0.30	0.31	0.26	0.18	0.28	0.26	CuBr ₂
CuCl	0.48	0.18	0.48	0.51	0.36	0.17	0.37	0.40	BE2	0.38	0.23	0.35	0.33	0.25	0.15	0.23	0.23	Cu(NO ₃) ₂
CuCl ₂	0.50	0.26	0.44	0.46	0.36	0.29	0.41	0.42		0.55	0.23	0.47	0.51	0.42	0.19	0.43	0.42	CuBr ₂
CuCl	1.70	1.30	1.67	1.71	1.65	1.40	1.68	1.68	BE3	1.41	1.35	1.55	1.31	1.51	1.35	1.67	1.51	Cu(NO ₃) ₂
CuCl ₂	1.63	1.32	1.61	1.55	1.54	1.42	1.65	1.62		1.59	1.36	1.58	1.54	1.60	1.43	1.67	1.48	CuBr ₂
	Phenanthroline				Bipyridine					Phenanthroline				Bipyridine				

Calibration curve post quantitative LCMS assay



Calibrated high-throughput optimisation of 404, 405 and 406

	No Base	DBU	DABCO	TMU	No Base	DBU	DABCO	TMU		No Base	DBU	DABCO	TMU	No Base	DBU	DABCO	TMU	
CuCl	65.2	42.4	63.7	61.4	46.5	34.4	54.3	49.3	BE1	48.4	36.4	56.9	51.5	41.3	29.5	48.9	37.4	Cu(NO ₃) ₂
CuCl ₂	62.2	42.4	58.7	56.2	48.9	40.9	52.8	47.9		61.2	42.5	64.5	66.5	55.5	38.8	58.9	55.4	CuBr ₂
CuCl	66.1	24.5	66.8	70.2	50.2	23.1	50.7	54.6	BE2	52.4	31.7	48.2	44.9	34.0	21.2	31.7	31.1	Cu(NO ₃) ₂
CuCl ₂	68.3	35.5	61.3	64.1	49.7	39.9	56.5	57.6		76.1	31.9	65.3	70.6	58.5	25.8	59.9	57.8	CuBr ₂
CuCl	80.1	61.3	78.8	80.8	78.0	66.1	79.1	79.4	BE3	66.5	63.8	73.1	61.7	71.3	63.6	78.9	71.1	Cu(NO ₃) ₂
CuCl ₂	76.7	62.1	76.2	73.1	72.5	67.0	78.1	76.4		75.1	64.1	74.8	72.9	75.4	67.6	78.8	69.7	CuBr ₂
	Phenanthroline				Bipyridine					Phenanthroline				Bipyridine				

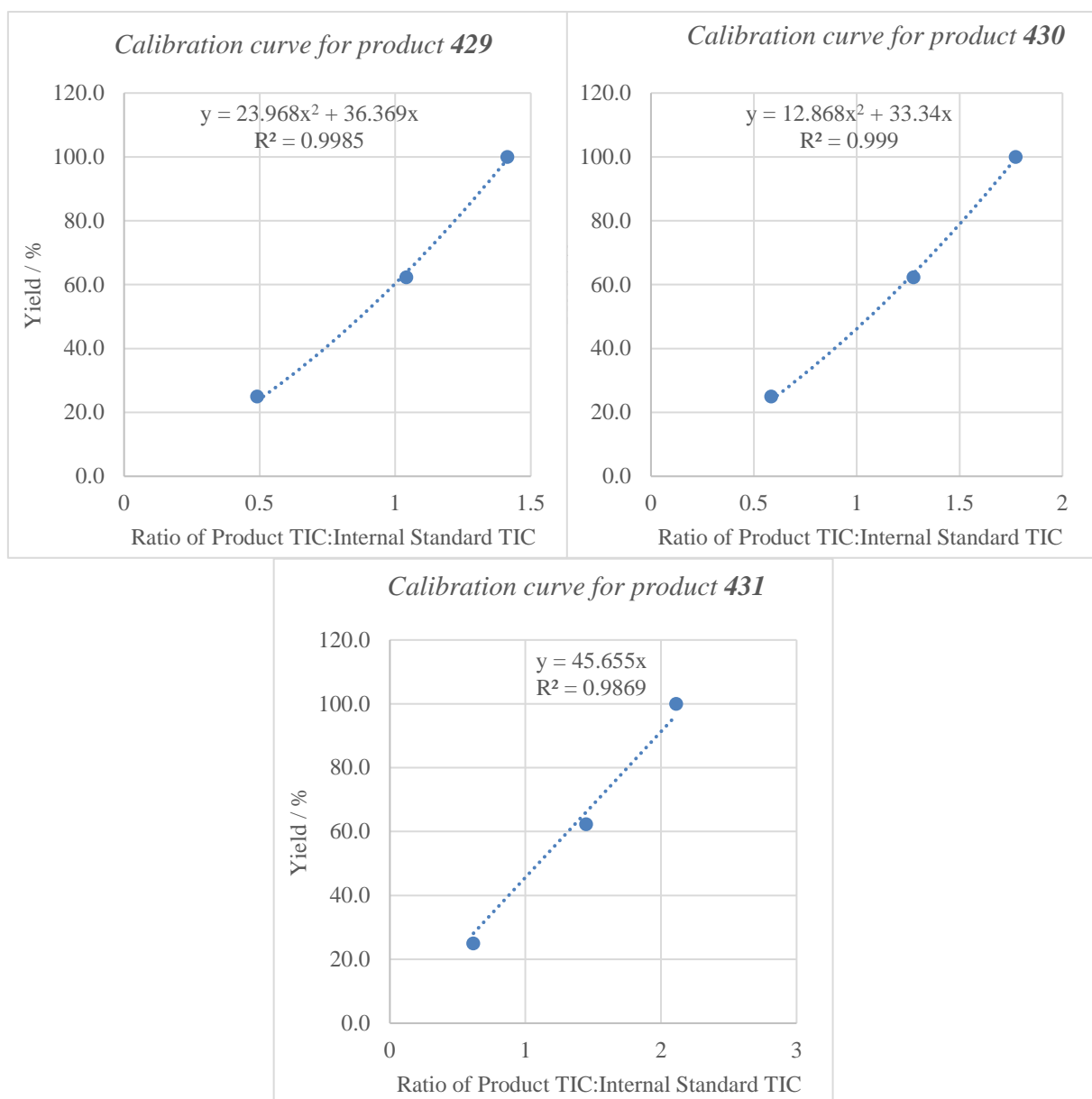
Boronic Ester scope Plate 5: BE1: 1-benzyl-5-(4,4,5,5-tetramethyl-1,3,2-dioxaborolan-2-yl)-1*H*-indazole **407**, BE2: 1-benzyl-5-(4,4,5,5-tetramethyl-1,3,2-dioxaborolan-2-yl)-1*H*-pyrrolo[2,3-*b*]pyridine **408**, BE3: 5-indole boronic acid pinacol ester **409**.

		CuCl ₂				CuCl				CuCl ₂				CuCl				CuCl ₂				CuCl									
		No Base	DBU	DABCO	TMU	No Base	DBU	DABCO	TMU	No Base	DBU	DABCO	TMU	No Base	DBU	DABCO	TMU	No Base	DBU	DABCO	TMU	No Base	DBU	DABCO	TMU	No Base	DBU	DABCO	TMU		
Phenanthroline	CuCl ₂	0.96	0.97	0.98	1.01	1.17	1.22	1.19	1.22	1.22	1.54	1.49	1.48	1.46	1.57	1.52	1.54	1.58	1.11	1.11	1.11	1.10	1.13	1.16	1.16	1.25	1.22	1.22	1.18	1.18	
		0.25	0.23	0.28	0.26	0.32	0.30	0.34	0.29	0.29	1.06	1.07	1.04	1.07	1.08	1.06	1.13	1.10	0.85	0.78	0.78	0.85	0.79	0.79	0.84	0.78	0.78	0.79	0.78	0.78	
		1.15	1.09	1.18	1.06	1.42	1.42	1.44	1.48	1.51	1.48	1.48	1.49	1.49	1.55	1.59	1.62	1.61	1.12	1.13	1.16	1.12	1.13	1.16	1.12	1.25	1.19	1.19	1.25	1.25	
		0.96	0.97	0.93	1.03	1.35	1.37	1.21	1.45	1.51	1.50	1.49	1.52	1.52	1.59	1.57	1.62	1.63	1.22	1.06	1.18	1.22	1.23	1.22	1.22	1.23	1.24	1.23	1.22	1.22	
Bipyridine	CuCl ₂	0.86	0.87	0.85	1.00	1.34	1.36	1.40	1.38	1.40	1.42	1.43	1.39	1.39	1.54	1.56	1.56	1.57	1.15	1.12	1.15	1.15	1.12	1.15	1.15	1.21	1.28	1.28	1.23	1.23	
		0.29	0.23	0.30	0.29	0.29	0.31	0.29	0.35	0.95	0.92	0.84	0.91	0.95	0.95	0.90	0.95	0.85	0.84	0.80	0.78	0.80	0.84	0.84	0.82	0.79	0.81	0.82	0.82	0.82	
		1.17	0.97	1.25	1.11	1.58	1.37	1.50	1.59	1.40	1.38	1.41	1.34	1.34	1.52	1.50	1.50	1.51	1.04	1.02	1.04	1.04	BAD	1.04	1.04	1.22	1.21	1.22	1.22	1.18	1.18
		1.01	0.87	1.03	1.04	1.37	1.32	1.39	1.54	1.40	1.43	1.46	1.41	1.41	1.41	1.55	1.53	1.57	BAD	1.05	1.03	1.09	1.11	1.09	1.09	1.28	1.26	1.27	1.22	1.22	
		Boronic Ester 3				Boronic Ester 2				Boronic Ester 1																					
Phenanthroline	CuBr ₂	0.93	0.98	1.06	1.05	0.71	0.72	0.73	0.77	1.52	1.49	1.48	1.45	1.48	1.48	1.44	1.42	1.35	1.09	1.07	1.09	1.10	1.07	1.09	1.09	1.09	1.11	1.13	1.11	1.11	
		0.35	0.33	0.33	0.30	0.36	0.31	0.33	0.34	0.97	1.05	0.98	1.02	1.00	1.00	1.01	0.96	0.79	0.82	0.78	0.80	0.79	0.80	0.79	0.83	0.83	0.83	0.78	0.78	0.78	0.78
		1.11	1.11	1.15	1.13	0.90	0.90	0.91	0.83	1.46	1.43	1.51	1.47	1.47	1.47	1.45	1.48	1.48	1.17	1.12	1.14	1.17	1.14	1.14	1.15	1.12	1.18	1.18	1.14	1.14	1.14
		1.05	1.10	1.07	1.07	0.74	0.78	0.76	0.77	1.42	1.41	1.40	1.47	1.50	1.43	1.47	1.43	1.43	1.43	1.10	1.09	1.07	1.14	1.07	1.14	1.14	1.05	1.03	1.13	1.13	1.13
Bipyridine	CuBr ₂	1.24	1.18	1.17	1.15	1.09	1.07	1.06	0.99	1.47	1.51	1.44	1.54	1.41	1.43	1.45	1.42	1.42	1.22	1.13	1.14	1.22	1.14	1.14	1.19	1.15	1.13	1.17	1.17	1.17	
		0.34	0.38	0.36	0.33	0.36	0.37	0.32	0.32	0.99	0.94	0.97	0.96	0.87	0.91	0.88	0.82	0.82	0.80	0.82	0.80	0.80	0.80	0.81	0.82	0.83	0.83	0.78	0.78	0.78	0.78
		1.35	1.34	1.31	1.28	1.18	1.15	1.16	1.14	1.39	1.42	1.41	1.46	1.37	1.41	1.41	1.41	1.32	1.12	1.14	1.16	1.14	1.16	1.16	1.18	1.17	1.21	1.15	1.15	1.15	1.15
		1.22	1.23	1.25	1.24	1.14	1.16	1.08	1.10	1.29	1.29	1.39	1.41	1.41	1.31	1.28	1.30	1.31	1.31	1.14	BAD	1.14	1.10	1.14	1.10	1.13	1.12	1.12	1.12	1.05	1.05
		Cu(NO ₃) ₂				Cu(NO ₃) ₂				Cu(NO ₃) ₂				Cu(NO ₃) ₂				Cu(NO ₃) ₂													

Average of data repeats from quantitative LCMS assay

	No Base	DBU	DABCO	TMU	No Base	DBU	DABCO	TMU		No Base	DBU	DABCO	TMU	No Base	DBU	DABCO	TMU	
CuCl	1.21	0.80	1.25	1.23	1.25	0.81	1.21	1.26	BE1	1.11	0.81	1.15	1.09	1.16	0.81	1.18	1.11	Cu(NO₃)₂
CuCl₂	1.14	0.80	1.13	1.14	1.13	0.80	1.03	1.07		1.09	0.80	1.15	1.10	1.17	0.81	1.14	1.13	CuBr₂
CuCl	1.55	1.09	1.59	1.60	1.56	0.91	1.51	1.55	BE2	1.42	0.99	1.47	1.46	1.43	0.87	1.38	1.30	Cu(NO₃)₂
CuCl₂	1.49	1.06	1.49	1.51	1.41	0.90	1.38	1.42		1.49	1.00	1.47	1.43	1.49	0.96	1.42	1.34	CuBr₂
CuCl	1.20	0.31	1.44	1.35	1.37	0.31	1.51	1.41	BE3	0.73	0.33	0.88	0.76	1.05	0.34	1.16	1.12	Cu(NO₃)₂
CuCl₂	0.98	0.25	1.12	0.98	0.90	0.28	1.13	0.99		1.00	0.32	1.12	1.07	1.18	0.35	1.32	1.23	CuBr₂
	Phenanthroline				Bipyridine					Phenanthroline				Bipyridine				

Calibration curve post quantitative LCMS assay



Calibrated high-throughput optimisation of 407, 408 and 409

	No Base	DBU	DABCO	TMU	No Base	DBU	DABCO	TMU		No Base	DBU	DABCO	TMU	No Base	DBU	DABCO	TMU	
CuCl	78.8	44.3	82.5	81.0	82.8	45.2	78.7	83.7	BE1	69.6	45.1	73.4	68.1	74.3	45.2	76.0	71.4	Cu(NO₃)₂
CuCl₂	72.5	44.4	71.5	75.5	71.9	44.7	63.0	66.5		67.8	44.2	73.3	68.8	75.6	45.1	72.8	71.5	CuBr₂
CuCl	82.8	51.8	85.9	86.5	83.2	41.2	79.5	82.8	BE2	73.5	45.8	77.0	76.1	73.9	38.8	70.2	65.2	Cu(NO₃)₂
CuCl₂	78.2	50.0	78.2	79.4	72.6	40.5	70.6	73.6		78.1	46.4	76.6	73.7	78.2	44.1	73.3	68.1	CuBr₂
CuCl	54.8	14.3	65.6	61.5	62.5	14.1	68.8	64.2	BE3	33.5	15.2	40.4	34.9	48.0	15.6	52.9	51.1	Cu(NO₃)₂
CuCl₂	44.6	11.6	51.2	44.5	40.9	12.6	51.4	45.1		45.8	14.8	51.4	48.9	54.1	16.1	60.3	56.4	CuBr₂
	Phenanthroline				Bipyridine					Phenanthroline				Bipyridine				

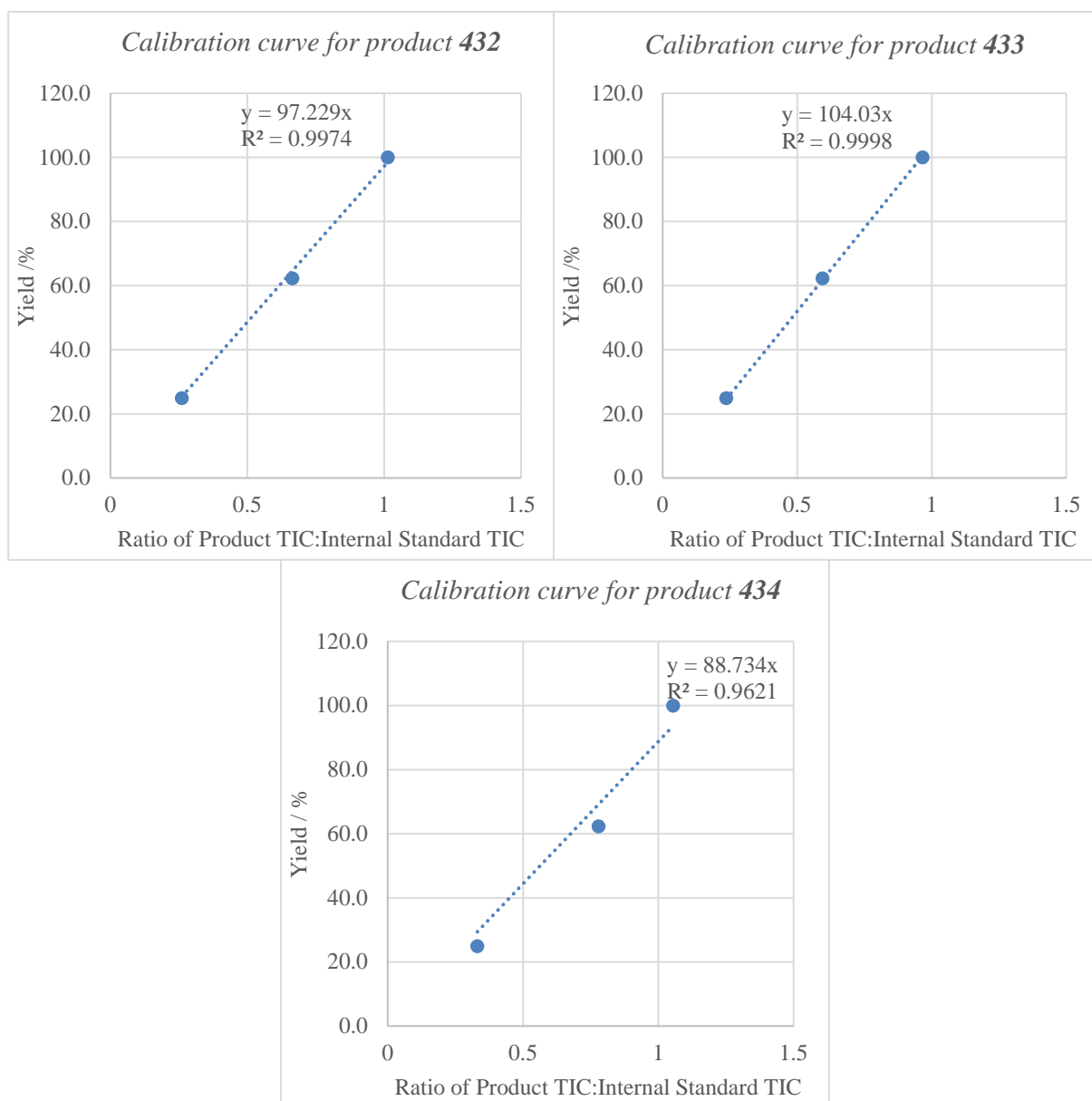
Boronic Ester scope Plate 6: BE1: 2-methylphenylboronic acid pinacol ester **410**, BE2: 2-chlorophenylboronic acid pinacol ester **411**, BE3: 2-fluorophenylboronic acid pinacol ester **412**.

		CuCl ₂				CuCl				CuCl ₂				CuCl				CuCl							
		No Base	DBU	DABCO	TMU	No Base	DBU	DABCO	TMU	No Base	DBU	DABCO	TMU	No Base	DBU	DABCO	TMU	No Base	DBU	DABCO	TMU				
Phenanthroline	Boronic Ester 1	0.20	0.19	0.20	0.21	0.17	0.20	0.18	0.20	0.32	0.33	0.34	0.31	0.29	0.26	0.22	0.26	0.64	BAD	0.13	0.10	0.14	BAD	0.11	0.11
		0.08	0.07	0.08	0.08	0.06	0.07	0.07	0.06	0.12	0.12	0.12	0.12	0.11	0.11	0.11	0.11	0.40	0.41	0.39	0.44	0.42	0.41	0.41	0.38
		0.17	0.20	0.20	0.19	0.16	0.17	0.17	0.17	0.28	0.28	0.26	0.27	BAD	BAD	0.70	0.71	0.70	0.70	0.12	0.12	0.12	BAD	0.13	0.12
		0.19	0.20	0.20	0.21	0.18	0.19	0.20	0.18	0.27	0.28	0.29	0.32	0.30	0.30	0.32	0.30	0.69	BAD	0.72	0.70	0.11	0.12	0.10	0.28
	Bipyridine	0.16	0.16	0.17	0.17	0.16	0.15	0.15	0.16	0.26	0.26	0.29	0.26	0.26	0.22	0.27	0.22	0.74	0.69	0.77	0.78	0.14	BAD	0.13	0.13
		0.10	0.10	0.11	0.10	0.07	0.08	0.07	0.07	0.13	0.13	0.13	0.13	0.13	0.10	0.10	0.11	0.48	0.43	0.48	0.45	0.47	0.47	0.45	0.45
		0.15	0.16	0.17	0.18	0.14	0.14	0.16	0.16	0.26	0.26	0.22	0.29	0.23	0.21	0.21	0.27	0.18	0.75	0.19	0.70	0.16	0.15	0.14	BAD
		0.18	0.19	0.20	0.20	0.16	0.16	0.17	0.15	0.26	0.25	0.25	0.26	0.25	0.27	0.22	0.23	0.73	0.88	0.70	BAD	0.13	0.14	0.15	0.16
Phenanthroline	Boronic Ester 2	0.19	0.21	0.21	0.22	0.09	0.10	0.10	0.09	0.35	0.36	0.35	0.34	0.22	0.19	0.25	0.19	0.70	0.65	0.73	0.71	0.56	0.58	0.55	0.59
		0.06	0.07	0.08	0.08	0.04	0.05	0.04	0.04	0.11	0.12	0.13	0.10	0.09	0.08	0.10	0.09	0.43	0.46	0.44	0.42	0.40	0.45	0.43	0.41
		0.19	0.20	0.20	0.28	0.10	0.10	0.08	0.09	0.34	0.36	0.33	0.38	0.22	0.24	BAD	0.26	BAD	0.72	0.77	0.72	0.62	0.60	BAD	0.58
		0.20	0.21	0.21	0.23	0.09	0.08	0.09	0.09	0.35	0.30	0.35	0.41	0.17	0.24	0.19	0.21	0.66	BAD	0.69	0.68	0.54	0.57	0.54	0.53
	Bipyridine	0.17	0.19	0.20	0.17	0.05	0.05	0.06	0.05	0.28	0.23	0.25	0.30	0.13	0.16	0.10	0.13	0.72	BAD	0.76	0.75	0.60	0.64	0.58	0.61
		0.06	0.06	0.06	0.06	0.03	0.03	0.04	0.03	0.09	0.09	0.09	0.09	0.06	0.06	0.06	0.06	0.45	0.47	0.45	0.47	0.41	0.40	0.39	0.33
		0.12	0.13	0.12	0.14	0.05	0.05	0.05	0.05	0.26	0.20	0.27	0.26	0.12	0.16	0.13	0.15	0.71	0.67	0.21	BAD	0.63	0.64	0.61	BAD
		0.14	0.16	0.17	0.17	0.06	0.06	0.04	0.06	0.22	0.27	0.25	0.24	0.15	0.13	0.13	0.13	0.24	0.72	BAD	0.73	0.59	0.58	0.06	0.07
Phenanthroline	Boronic Ester 3	0.19	0.21	0.22	0.26	0.09	0.10	0.10	0.09	0.35	0.36	0.35	0.34	0.22	0.19	0.25	0.19	0.70	0.65	0.73	0.71	0.56	0.58	0.55	0.59
		0.06	0.07	0.06	0.08	0.04	0.05	0.04	0.04	0.11	0.12	0.13	0.10	0.09	0.08	0.10	0.09	0.43	0.46	0.44	0.42	0.40	0.45	0.43	0.41
		0.19	0.20	0.27	0.28	0.10	0.10	0.08	0.09	0.34	0.36	0.33	0.38	0.22	0.24	BAD	0.26	BAD	0.72	0.77	0.72	0.62	0.60	BAD	0.58
		0.20	0.21	0.25	0.23	0.09	0.08	0.09	0.09	0.35	0.30	0.35	0.41	0.17	0.24	0.19	0.21	0.66	BAD	0.69	0.68	0.54	0.57	0.54	0.53
	Bipyridine	0.17	0.19	0.20	0.17	0.05	0.05	0.06	0.05	0.28	0.23	0.25	0.30	0.13	0.16	0.10	0.13	0.72	BAD	0.76	0.75	0.60	0.64	0.58	0.61
		0.06	0.06	0.06	0.06	0.03	0.03	0.04	0.03	0.09	0.09	0.09	0.09	0.06	0.06	0.06	0.06	0.45	0.47	0.45	0.47	0.41	0.40	0.39	0.33
		0.12	0.13	0.12	0.14	0.05	0.05	0.05	0.05	0.26	0.20	0.27	0.26	0.12	0.16	0.13	0.15	0.71	0.67	0.21	BAD	0.63	0.64	0.61	BAD
		0.14	0.16	0.17	0.17	0.06	0.06	0.04	0.06	0.22	0.27	0.25	0.24	0.15	0.13	0.13	0.13	0.24	0.72	BAD	0.73	0.59	0.58	0.06	0.07
		CuBr ₂				Cu(NO ₃) ₂				CuBr ₂				Cu(NO ₃) ₂				Cu(NO ₃) ₂							

Average of data repeats from quantitative LCMS assay

	No Base	DBU	DABCO	TMU	No Base	DBU	DABCO	TMU		No Base	DBU	DABCO	TMU	No Base	DBU	DABCO	TMU
CuCl	0.12	0.40	0.12	0.15	0.13	0.46	0.15	0.15	Boronic Ester 1	0.57	0.42	0.60	0.54	0.61	0.38	0.63	0.32
CuCl ₂	0.29	0.41	0.70	0.70	0.74	0.46	0.46	0.77	Boronic Ester 2	0.70	0.44	0.74	0.68	0.75	0.46	0.53	0.57
CuCl	0.26	0.11	0.29	0.31	0.25	0.11	0.23	0.24	Boronic Ester 3	0.21	0.09	0.24	0.20	0.13	0.06	0.14	0.14
CuCl ₂	0.33	0.12	0.27	0.29	0.27	0.13	0.26	0.25	Boronic Ester 3	0.35	0.11	0.35	0.35	0.27	0.09	0.25	0.24
CuCl	0.19	0.06	0.17	0.19	0.16	0.07	0.15	0.16	Boronic Ester 3	0.09	0.04	0.09	0.09	0.06	0.03	0.05	0.06
CuCl ₂	0.20	0.08	0.19	0.20	0.16	0.10	0.17	0.19	Boronic Ester 3	0.22	0.07	0.23	0.22	0.18	0.06	0.13	0.16
	Phenanthroline				Bipyridine					Phenanthroline				Bipyridine			

Calibration curve post quantitative LCMS assay



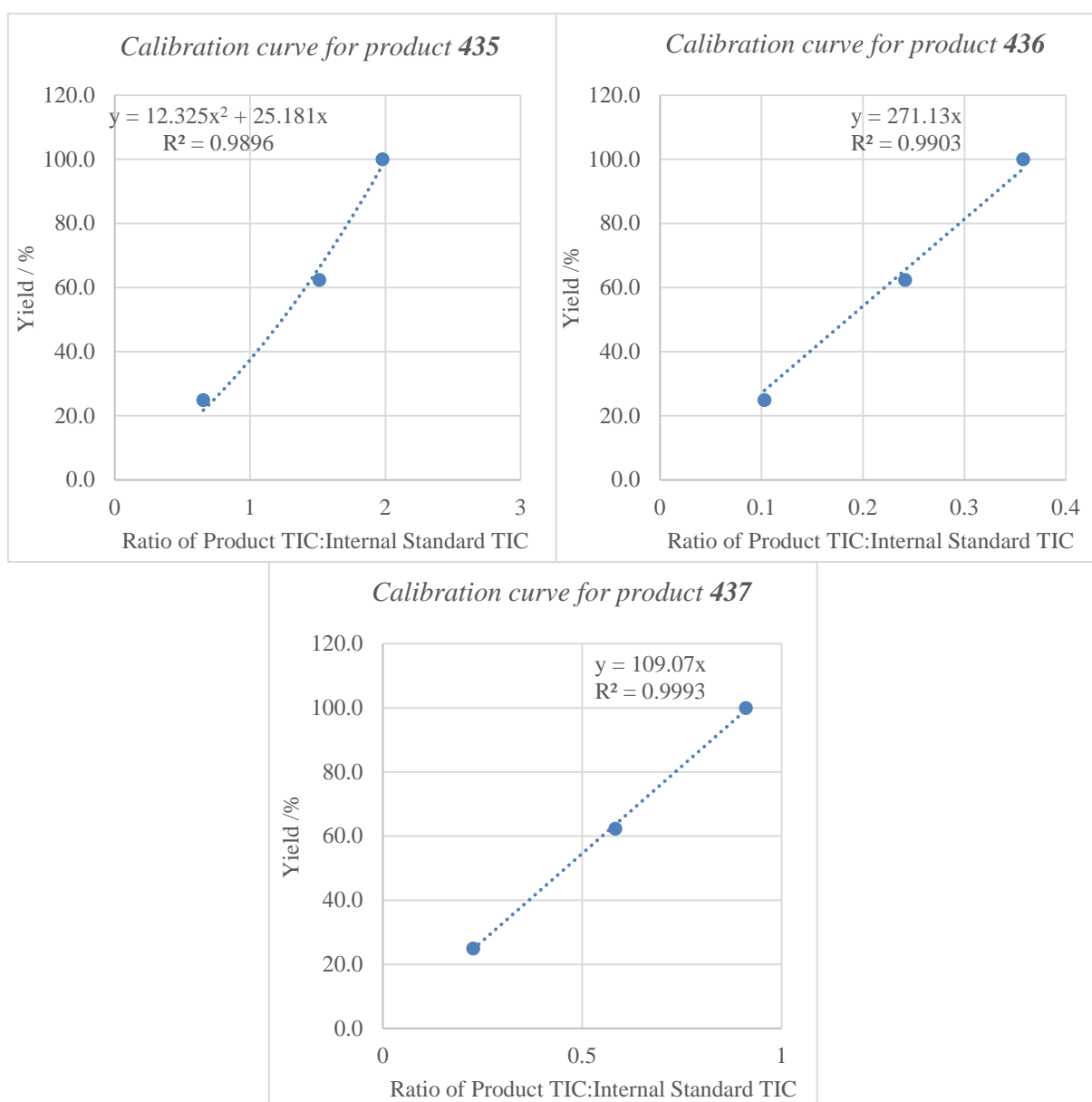
Calibrated high-throughput optimisation of 410, 411 and 412

	No Base	DBU	DABCO	TMU	No Base	DBU	DABCO	TMU		No Base	DBU	DABCO	TMU	No Base	DBU	DABCO	TMU	
CuCl	11.7	39.3	12.1	14.7	13.0	44.8	14.6	14.3	Boronic Ester 1	55.4	41.2	58.5	52.8	59.1	37.2	61.3	BAD	Cu(NO ₃) ₂
CuCl ₂	BAD	39.7	68.3	68.0	72.2	44.7	BAD	74.6		67.7	42.5	71.6	65.7	72.5	44.4	BAD	BAD	CuBr ₂
CuCl	26.8	11.7	30.1	32.0	26.1	11.7	24.2	25.0	Boronic Ester 2	22.3	9.6	24.9	21.1	13.7	6.1	14.8	14.1	Cu(NO ₃) ₂
CuCl ₂	33.9	12.7	28.5	30.3	27.7	13.6	26.8	26.3		36.4	11.9	36.9	36.7	27.6	9.5	25.6	25.4	CuBr ₂
CuCl	16.7	5.7	14.9	16.6	13.8	6.4	13.2	14.1	Boronic Ester 3	8.3	3.7	8.2	7.7	5.0	2.9	4.6	5.0	Cu(NO ₃) ₂
CuCl ₂	17.8	7.0	16.7	17.7	14.6	9.2	14.8	16.9		19.5	6.0	20.7	19.9	16.3	5.4	11.5	14.2	CuBr ₂
	Phenanthroline				Bipyridine					Phenanthroline				Bipyridine				

Average of data repeats from quantitative LCMS assay

	No Base	DBU	DABCO	TMU	No Base	DBU	DABCO	TMU		No Base	DBU	DABCO	TMU	No Base	DBU	DABCO	TMU	
CuCl	1.43	0.60	1.38	1.45	1.34	0.55	1.25	1.38	Boronic Ester 1	1.12	0.61	1.19	1.15	1.08	0.49	1.01	1.00	Cu(NO ₃) ₂
CuCl ₂	1.44	0.73	1.40	1.40	1.33	0.70	1.30	1.29		1.42	0.71	1.42	1.42	1.40	0.60	1.34	1.34	CuBr ₂
CuCl	0.07	0.04	0.05	0.08	0.07	0.04	0.08	0.07	Boronic Ester 2	0.05	0.04	0.08	0.05	0.04	0.03	0.05	0.04	Cu(NO ₃) ₂
CuCl ₂	0.06	0.05	BAD	0.06	0.07	0.05	0.07	0.06		0.06	0.06	0.04	0.06	0.08	0.04	0.06	0.07	CuBr ₂
CuCl	0.43	0.21	0.46	0.43	0.38	0.20	0.41	0.38	Boronic Ester 3	0.30	0.19	0.33	0.29	0.25	0.17	0.29	0.25	Cu(NO ₃) ₂
CuCl ₂	0.38	0.20	0.40	0.38	0.33	0.23	0.37	0.33		0.42	0.23	0.53	0.46	0.43	0.23	0.46	0.40	CuBr ₂
	Phenanthroline				Bipyridine					Phenanthroline				Bipyridine				

Calibration curve post quantitative LCMS assay



Average of data repeats from quantitative LCMS assay

	No Base	DBU	DABCO	TMU	No Base	DBU	DABCO	TMU		No Base	DBU	DABCO	TMU	No Base	DBU	DABCO	TMU	
CuCl	61.4	19.7	58.0	62.3	56.1	17.6	50.5	58.4	Boronic Ester 1	45.9	19.8	47.5	45.4	41.4	15.4	40.2	37.7	Cu(NO₃)₂
CuCl₂	61.5	24.9	59.5	59.3	55.2	23.8	53.8	53.1		60.3	24.2	60.3	60.7	59.3	19.5	56.0	56.1	CuBr₂
CuCl	19.4	10.3	13.7	22.6	19.9	9.8	22.6	18.2	Boronic Ester 2	13.6	10.5	20.4	14.5	11.7	8.0	14.4	11.4	Cu(NO₃)₂
CuCl₂	17.6	12.4	BAD	17.4	18.0	13.0	19.9	17.2		16.4	16.3	11.6	16.8	22.8	11.6	15.0	18.6	CuBr₂
CuCl	46.9	22.8	50.1	46.9	41.3	21.7	44.7	41.2	Boronic Ester 3	32.2	21.1	35.6	31.1	27.3	18.3	31.9	27.5	Cu(NO₃)₂
CuCl₂	41.8	22.0	43.6	41.6	36.0	25.3	40.2	36.2		45.9	25.6	57.8	49.8	46.7	24.6	50.6	44.0	CuBr₂
	Phenanthroline				Bipyridine					Phenanthroline				Bipyridine				

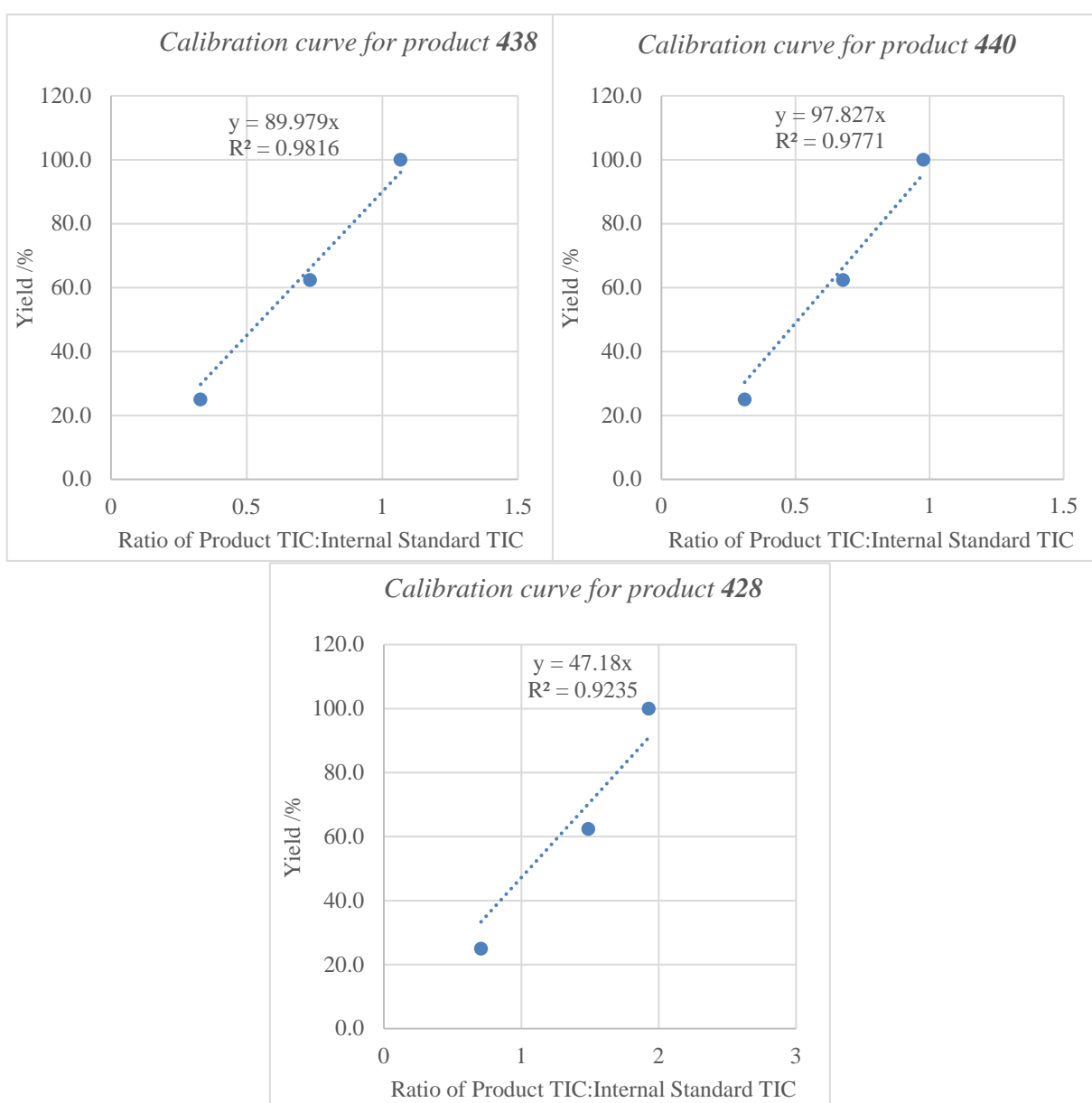
Boronic Ester scope Plate 8: BE1: *N,N*-dimethyl-4-(4,4,5,5-tetramethyl-1,3,2-dioxaborolan-2-yl)benzamide **416**, BE2: *N*-methyl-*N*-(4-(4,4,5,5-tetramethyl-1,3,2-dioxaborolan-2-yl)phenyl)acetamide **439**, BE3: 3-methoxyphenylboronic acid pinacol ester **406**.

		CuCl ₂				CuCl				CuCl ₂				CuCl							
		CuCl ₂		CuCl		CuCl ₂		CuCl		CuCl ₂		CuCl		CuCl ₂		CuCl					
		No Base	DBU	DABCO	TMU	No Base	DBU	DABCO	TMU	No Base	DBU	DABCO	TMU	No Base	DBU	DABCO	TMU				
Phenanthroline		1.29	1.27	BAD	BAD	1.26	1.26	BAD	BAD	0.69	0.71	0.69	0.72	0.78	0.72	0.72	0.76	0.81	0.76	0.82	0.76
Bipyridine		1.08	1.11	1.06	1.05	1.09	1.12	1.04	1.04	0.43	0.45	0.42	0.42	0.53	0.39	0.41	0.46	0.51	0.47	0.48	0.46
Phenanthroline		1.30	1.28	1.25	1.30	1.28	1.32	1.29	1.30	0.66	0.70	0.71	0.72	0.79	0.82	0.82	0.76	0.85	0.85	0.85	0.82
Bipyridine		1.22	1.16	1.19	1.25	1.30	1.31	1.31	1.25	0.67	0.67	0.66	0.66	0.78	0.81	0.80	0.75	0.83	0.82	0.84	0.84
Phenanthroline		1.26	1.21	1.28	1.34	1.34	1.33	1.31	1.34	0.69	0.72	0.72	0.72	0.82	0.76	0.78	0.73	0.87	0.85	0.85	0.86
Bipyridine		1.16	1.12	1.13	1.17	1.15	1.12	1.17	1.15	0.45	0.46	0.43	0.43	0.46	BAD	0.45	0.43	0.51	0.51	0.51	0.50
Phenanthroline		1.31	1.34	1.35	1.36	1.28	BAD	1.39	1.36	0.74	0.70	0.73	0.74	0.81	0.76	0.79	0.76	0.87	0.88	0.86	0.91
Bipyridine		1.31	1.32	1.35	1.37	1.36	1.36	1.35	1.37	0.70	0.71	0.68	0.66	0.81	0.79	0.81	0.84	0.86	0.88	0.88	0.86
Boronic Ester 1																					
Phenanthroline		1.21	1.24	1.13	1.14	1.15	1.19	1.18	1.17	0.76	0.74	BAD	0.70	0.63	0.65	0.63	0.63	0.74	0.72	0.74	0.70
Bipyridine		1.14	1.13	1.10	1.14	BAD	1.15	1.13	1.14	0.48	0.47	BAD	0.46	0.42	0.43	0.42	0.42	0.51	0.48	0.48	0.48
Phenanthroline		1.33	1.35	1.30	1.23	1.23	1.22	1.23	1.22	0.72	0.69	0.67	0.71	0.68	0.68	0.66	0.66	0.80	0.78	0.80	0.75
Bipyridine		1.27	1.26	1.18	1.22	1.07	1.14	1.17	BAD	0.72	0.68	0.68	0.64	0.62	0.65	0.64	0.64	0.77	0.75	0.77	0.73
Phenanthroline		1.29	1.29	1.30	1.21	1.21	1.11	1.13	1.20	0.69	0.69	0.64	0.66	0.64	0.67	0.65	0.65	0.76	0.76	0.73	0.70
Bipyridine		1.12	1.10	BAD	1.12	1.08	1.14	1.10	1.12	0.41	0.40	0.39	BAD	0.40	0.40	0.37	0.54	0.52	0.52	0.48	0.43
Phenanthroline		1.21	1.29	1.22	1.24	1.23	1.24	1.24	1.24	0.61	0.63	0.68	0.67	0.71	0.72	0.70	0.85	0.85	0.83	0.84	0.79
Bipyridine		1.27	1.27	1.28	1.18	1.17	1.07	1.18	BAD	0.65	0.64	0.70	0.65	0.58	0.61	BAD	0.84	0.84	0.76	0.77	0.72
Boronic Ester 2																					
Phenanthroline		1.21	1.24	1.13	1.14	1.15	1.19	1.18	1.17	0.76	0.74	BAD	0.70	0.63	0.65	0.63	0.63	0.74	0.72	0.74	0.70
Bipyridine		1.14	1.13	1.10	1.14	BAD	1.15	1.13	1.14	0.48	0.47	BAD	0.46	0.42	0.43	0.42	0.42	0.51	0.48	0.48	0.48
Phenanthroline		1.33	1.35	1.30	1.23	1.23	1.22	1.23	1.22	0.72	0.69	0.67	0.71	0.68	0.68	0.66	0.66	0.80	0.78	0.80	0.75
Bipyridine		1.27	1.26	1.18	1.22	1.07	1.14	1.17	BAD	0.72	0.68	0.68	0.64	0.62	0.65	0.64	0.64	0.77	0.75	0.77	0.73
Phenanthroline		1.29	1.29	1.30	1.21	1.21	1.11	1.13	1.20	0.69	0.69	0.64	0.66	0.64	0.67	0.65	0.65	0.76	0.76	0.73	0.70
Bipyridine		1.12	1.10	BAD	1.12	1.08	1.14	1.10	1.12	0.41	0.40	0.39	BAD	0.40	0.40	0.37	0.54	0.52	0.52	0.48	0.43
Phenanthroline		1.21	1.29	1.22	1.24	1.23	1.24	1.24	1.24	0.61	0.63	0.68	0.67	0.71	0.72	0.70	0.85	0.85	0.83	0.84	0.79
Bipyridine		1.27	1.27	1.28	1.18	1.17	1.07	1.18	BAD	0.65	0.64	0.70	0.65	0.58	0.61	BAD	0.84	0.84	0.76	0.77	0.72
Boronic Ester 3																					
Phenanthroline		1.21	1.24	1.13	1.14	1.15	1.19	1.18	1.17	0.76	0.74	BAD	0.70	0.63	0.65	0.63	0.63	0.74	0.72	0.74	0.70
Bipyridine		1.14	1.13	1.10	1.14	BAD	1.15	1.13	1.14	0.48	0.47	BAD	0.46	0.42	0.43	0.42	0.42	0.51	0.48	0.48	0.48
Phenanthroline		1.33	1.35	1.30	1.23	1.23	1.22	1.23	1.22	0.72	0.69	0.67	0.71	0.68	0.68	0.66	0.66	0.80	0.78	0.80	0.75
Bipyridine		1.27	1.26	1.18	1.22	1.07	1.14	1.17	BAD	0.72	0.68	0.68	0.64	0.62	0.65	0.64	0.64	0.77	0.75	0.77	0.73
Phenanthroline		1.29	1.29	1.30	1.21	1.21	1.11	1.13	1.20	0.69	0.69	0.64	0.66	0.64	0.67	0.65	0.65	0.76	0.76	0.73	0.70
Bipyridine		1.12	1.10	BAD	1.12	1.08	1.14	1.10	1.12	0.41	0.40	0.39	BAD	0.40	0.40	0.37	0.54	0.52	0.52	0.48	0.43
Phenanthroline		1.21	1.29	1.22	1.24	1.23	1.24	1.24	1.24	0.61	0.63	0.68	0.67	0.71	0.72	0.70	0.85	0.85	0.83	0.84	0.79
Bipyridine		1.27	1.27	1.28	1.18	1.17	1.07	1.18	BAD	0.65	0.64	0.70	0.65	0.58	0.61	BAD	0.84	0.84	0.76	0.77	0.72

Average of data repeats from quantitative LCMS assay

	No Base	DBU	DABCO	TMU	No Base	DBU	DABCO	TMU		No Base	DBU	DABCO	TMU	No Base	DBU	DABCO	TMU	
CuCl	0.79	0.48	0.84	0.83	0.86	0.51	0.88	0.87	Boronic Ester 1	0.72	0.49	0.78	0.75	0.74	0.49	0.83	0.76	Cu(NO ₃) ₂
CuCl ₂	0.79	0.50	0.81	0.79	0.82	0.48	0.82	0.81		0.78	0.50	0.78	0.77	0.81	0.53	0.86	0.83	CuBr ₂
CuCl	0.75	0.43	0.78	0.78	0.77	0.45	0.78	0.81	Boronic Ester 2	0.67	0.43	0.68	0.64	0.66	0.39	0.70	0.61	Cu(NO ₃) ₂
CuCl ₂	0.70	0.44	0.70	0.67	0.71	0.45	0.72	0.69		0.76	0.47	0.69	0.69	0.68	0.41	0.65	0.68	CuBr ₂
CuCl	1.28	1.07	1.30	1.29	1.33	1.15	1.34	1.36	Boronic Ester 3	1.17	1.14	1.23	1.13	1.16	1.11	1.24	1.14	Cu(NO ₃) ₂
CuCl ₂	BAD	1.06	1.27	1.20	1.27	1.13	1.34	1.32		1.26	1.13	1.33	1.23	1.29	1.12	1.25	1.27	CuBr ₂
	Phenanthroline				Bipyridine					Phenanthroline				Bipyridine				

Calibration curve post quantitative LCMS assay



Average of data repeats from quantitative LCMS assay

	No Base	DBU	DABCO	TMU	No Base	DBU	DABCO	TMU		No Base	DBU	DABCO	TMU	No Base	DBU	DABCO	TMU	
CuCl	71.0	42.9	75.7	75.0	77.4	45.5	79.0	78.0	Boronic Ester 1	65.1	43.8	70.0	67.6	66.3	45.5	74.3	68.0	Cu(NO₃)₂
CuCl₂	BAD	45.1	72.7	71.4	73.4	43.2	73.9	72.5		70.4	45.2	70.2	70.9	72.7	47.6	77.0	74.6	CuBr₂
CuCl	73.4	41.9	76.4	76.2	75.8	44.4	75.8	79.5	Boronic Ester 2	65.5	42.4	66.7	62.4	64.2	38.2	68.3	59.8	Cu(NO₃)₂
CuCl₂	68.2	42.8	68.2	65.8	69.5	43.6	70.7	67.4		74.5	46.2	67.7	67.9	66.6	39.8	63.8	66.0	CuBr₂
CuCl	72.5	50.4	74.9	74.1	78.8	58.0	80.4	82.5	Boronic Ester 3	60.7	57.4	66.5	55.7	59.6	54.3	67.7	57.4	Cu(NO₃)₂
CuCl₂	BAD	49.7	71.7	63.6	71.2	55.8	79.5	78.0		70.7	56.2	79.0	67.5	74.4	54.7	69.8	71.8	CuBr₂
	Phenanthroline				Bipyridine					Phenanthroline				Bipyridine				

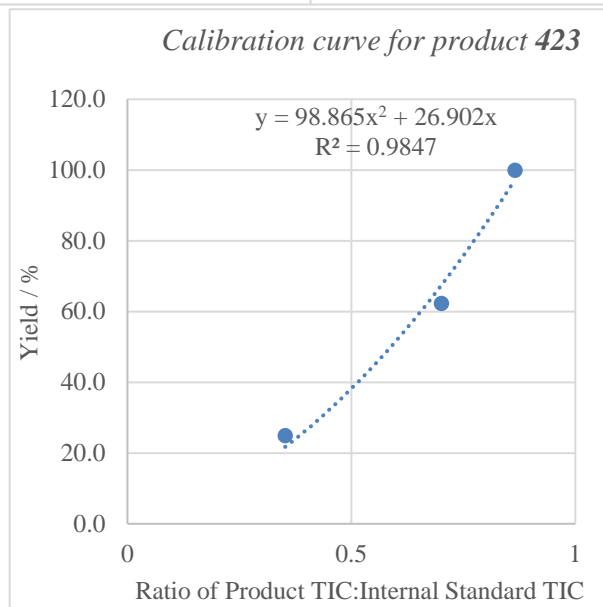
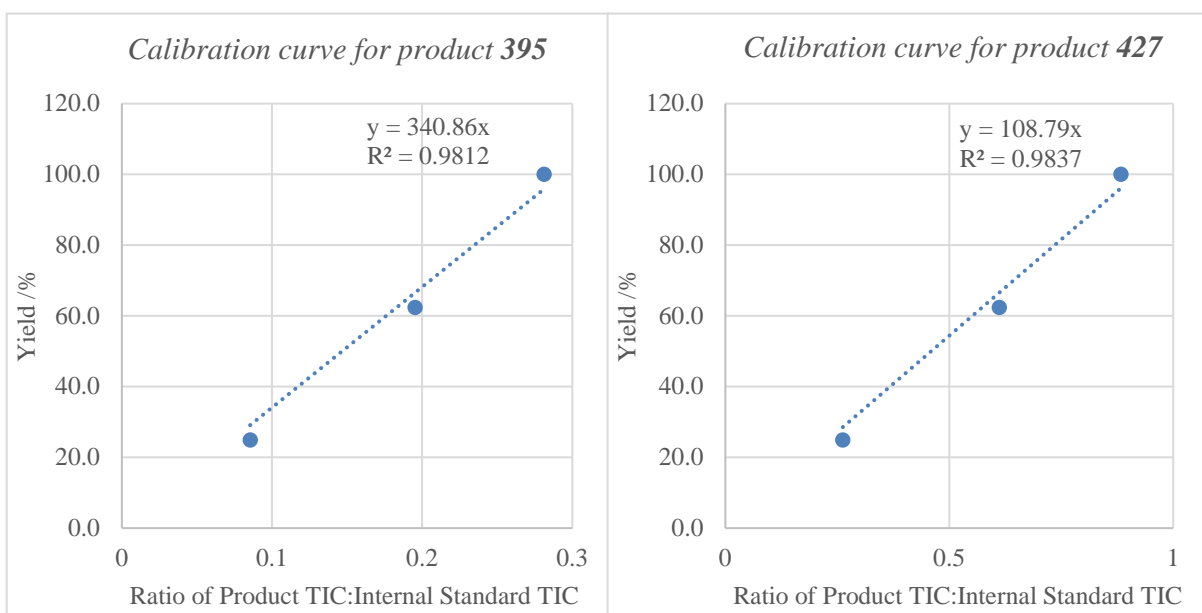
Boronic Ester scope Plate 9: BE1: 4-nitrophenylboronic acid pinacol ester **395**, BE2: Thiophene-3-boronic acid pinacol ester **405**, BE3: 4-biphenylboronic acid pinacol ester **401**.

		Phenanthroline				Bipyridine				Phenanthroline				Bipyridine					
		CuCl ₂		CuCl		CuCl ₂		CuCl		CuCl ₂		CuCl		CuCl ₂		CuCl			
		No Base	DBU	DABCO	TMU	No Base	DBU	DABCO	TMU	No Base	DBU	DABCO	TMU	No Base	DBU	DABCO	TMU		
Average of data repeats from quantitative LCMS assay	Boronic Ester 3	CuBr ₂	0.29	0.55	BAD	BAD	0.49	BAD	BAD	BAD	0.54	0.55	0.38	BAD	BAD	0.50	0.22	0.17	
			0.24	0.57	BAD	BAD	0.39	0.87	0.90	0.82	0.87	0.69	BAD	BAD	BAD	BAD	0.20	0.19	0.13
		0.36	0.54	0.33	0.45	0.50	0.41	0.45	0.50	0.43	0.57	0.55	0.36	0.63	0.40	0.43	0.30	0.16	0.10
		0.26	0.59	0.49	0.47	0.35	0.43	0.47	0.38	0.43	0.41	0.51	0.46	0.45	0.45	0.47	0.18	0.19	0.14
	Boronic Ester 2	Cu(NO ₃) ₂	0.20	0.49	0.28	0.24	0.29	0.50	0.40	0.40	0.49	0.18	0.15	0.43	0.23	0.13	0.12	0.11	0.17
			0.28	0.53	0.32	0.30	0.29	0.45	0.40	0.40	0.42	0.18	0.15	0.38	0.23	0.12	0.10	0.11	0.13
		0.46	0.14	0.46	0.47	0.35	0.18	0.38	0.38	0.42	0.49	0.43	0.43	0.33	0.23	0.12	0.12	0.11	0.16
		0.41	0.15	0.42	0.41	0.32	0.17	0.40	0.40	0.37	0.48	0.16	0.45	0.46	0.42	0.20	0.12	0.18	0.17
	Boronic Ester 1	Cu(NO ₃) ₂	0.47	0.15	0.45	0.45	0.33	0.16	0.42	0.42	0.34	0.16	0.39	0.36	0.23	0.12	0.12	0.10	0.16
			0.43	0.16	0.41	0.43	0.34	0.19	0.40	0.42	0.49	0.15	0.39	0.39	0.24	0.12	0.10	0.16	0.14
		0.49	0.14	0.43	0.43	0.42	0.14	0.37	0.42	0.41	0.34	0.17	0.33	0.33	0.24	0.13	0.17	0.18	0.17
		0.45	0.14	0.44	0.45	0.40	0.14	0.40	0.40	0.41	0.33	0.15	0.34	0.32	0.24	0.12	0.10	0.18	0.14
Boronic Ester 3	Cu(NO ₃) ₂	0.37	0.54	0.29	0.35	0.38	0.51	0.34	0.34	0.39	0.51	0.43	0.60	0.40	0.48	0.31	0.24	0.14	
		0.26	0.46	0.30	0.26	0.35	0.48	0.40	0.40	0.41	0.50	0.37	0.37	0.32	0.32	0.23	0.23	0.11	
	0.33	0.49	0.32	0.30	0.28	0.45	0.40	0.40	0.36	0.48	0.48	0.48	0.48	0.38	0.38	0.32	0.27	0.16	
	0.49	0.14	0.44	0.44	0.42	0.14	0.37	0.42	0.41	0.37	0.15	0.43	0.48	0.35	0.15	0.15	0.16	0.16	

Average of data repeats from quantitative LCMS assay

	No Base	DBU	DABCO	TMU	No Base	DBU	DABCO	TMU		No Base	DBU	DABCO	TMU	No Base	DBU	DABCO	TMU	
CuCl	0.22	0.14	0.19	0.20	0.19	0.11	0.18	0.12	Boronic Ester 1	0.16	0.13	0.18	0.16	0.15	0.10	0.17	0.12	Cu(NO ₃) ₂
CuCl ₂	0.22	0.15	0.18	0.16	0.18	0.13	0.19	0.14		0.14	0.15	0.13	0.12	0.19	0.12	BAD	0.11	CuBr ₂
CuCl	0.44	0.14	0.44	0.44	0.42	0.14	0.38	0.39	Boronic Ester 2	0.33	0.16	0.32	0.32	0.24	0.12	0.23	0.23	Cu(NO ₃) ₂
CuCl ₂	0.44	0.15	0.44	0.44	0.34	0.18	0.40	0.35		0.49	0.16	0.45	0.47	0.39	0.15	0.38	0.39	CuBr ₂
CuCl	0.28	0.50	0.30	0.29	0.33	0.48	0.39	0.36	Boronic Ester 3	0.38	0.50	0.38	0.56	0.37	0.46	0.32	0.24	Cu(NO ₃) ₂
CuCl ₂	0.29	0.56	BAD	0.44	0.41	0.45	BAD	0.92		0.47	0.54	0.40	BAD	BAD	0.46	0.27	0.24	CuBr ₂
	Phenanthroline				Bipyridine					Phenanthroline				Bipyridine				

Calibration curve post quantitative LCMS assay



Average of data repeats from quantitative LCMS assay

	No Base	DBU	DABCO	TMU	No Base	DBU	DABCO	TMU		No Base	DBU	DABCO	TMU	No Base	DBU	DABCO	TMU	
CuCl	73.9	48.8	64.2	67.8	65.6	39.0	61.5	42.2	Boronic Ester 1	55.4	45.8	60.4	53.9	50.7	33.7	57.2	41.2	Cu(NO₃)₂
CuCl₂	74.1	49.5	61.7	55.2	60.6	43.7	65.2	46.7		46.1	49.7	45.7	42.4	64.7	42.0	BAD	38.6	CuBr₂
CuCl	43.2	11.9	43.5	42.7	40.7	12.0	36.8	37.5	Boronic Ester 2	31.4	14.4	30.3	29.8	21.3	10.8	20.4	21.2	Cu(NO₃)₂
CuCl₂	43.0	13.2	42.6	43.0	31.8	15.6	38.6	33.3		48.3	14.2	43.6	45.9	37.2	13.4	36.0	37.2	CuBr₂
CuCl	15.0	38.6	16.6	16.1	19.3	36.2	25.0	22.2	Boronic Ester 3	24.7	37.8	24.9	46.5	23.3	32.8	18.5	11.9	Cu(NO₃)₂
CuCl₂	16.0	46.3	BAD	30.5	27.8	31.6	BAD	107.7		35.1	42.9	26.5	BAD	BAD	33.3	14.4	11.9	CuBr₂
Phenanthroline				Bipyridine				Phenanthroline				Bipyridine						

Milliscale validation of quantitative assay

All reactions were performed according to general procedure 9 with the titled boronic ester and reaction components detailed in the tables.

4,4,5,5-Tetramethyl-2-(4-nitrophenyl)-1,3,2-dioxaborolane, 395

Entry	Base	Ligand	Catalyst	Nanoscale yield of 417 /%	Millimole yield of 417 /%
1	No Base	Bipy	CuCl ₂	56	22
2	DBU	Phen	Cu(NO ₃) ₂	40	11
3	TMU	Bipy	Cu(NO ₃) ₂	36	30

2-(4-Bromophenyl)-4,4,5,5-tetramethyl-1,3,2-dioxaborolane, 396

Entry	Base	Ligand	Catalyst	Nanoscale yield of 418 /%	Millimole yield of 418 /%
1	DABCO	Phen	CuCl	76	73
2	No Base	Bipy	Cu(NO ₃) ₂	66	65
3	DBU	Phen	CuCl ₂	46	33

4,4,5,5-Tetramethyl-2-(3-(trifluoromethyl)phenyl)-1,3,2-dioxaborolane, 397

Entry	Base	Ligand	Catalyst	Nanoscale yield of 419 /%	Millimole yield of 419 /%
1	DABCO	Phen	Cu(NO ₃) ₂	60	61
2	TMU	Bipy	CuCl	43	51
3	DBU	Bipy	Cu(NO ₃) ₂	28	17

2-(3,5-Dimethylphenyl)-4,4,5,5-tetramethyl-1,3,2-dioxaborolane, 398

Entry	Base	Ligand	Catalyst	Nanoscale yield of 420 /%	Millimole yield of 420 /%
1	TMU	Bipy	CuCl	84	71
2	DBU	Phen	CuBr ₂	51	51
3	DABCO	Bipy	CuCl ₂	36	35

Ethyl 2-methoxy-5-(4,4,5,5-tetramethyl-1,3,2-dioxaborolan-2-yl)benzoate, **400**

Entry	Base	Ligand	Catalyst	Nanoscale yield of 422 /%	Millimole yield of 422 /%
1	No Base	Bipy	CuBr ₂	87	74
2	DABCO	Bipy	CuCl ₂	71	65
3	DBU	Phen	CuCl ₂	57	39

2-([1,1'-Biphenyl]-4-yl)-4,4,5,5-tetramethyl-1,3,2-dioxaborolane, **401**

Entry	Base	Ligand	Catalyst	Nanoscale yield of 423 /%	Millimole yield of 423 /%
1	TMU	Bipy	CuCl ₂	108	78
2	DBU	Phen	CuCl ₂	46	25
3	TMU	Bipy	CuBr ₂	12	80

N,N-dimethyl-4-(4,4,5,5-tetramethyl-1,3,2-dioxaborolan-2-yl)aniline, **402**

Entry	Base	Ligand	Catalyst	Nanoscale yield of 424 /%	Millimole yield of 424 /%
1	No Base	Bipy	CuCl	33	55
2	DBU	Bipy	Cu(NO ₃) ₂	16	26
3	DABCO	Phen	CuCl ₂	0	0

2-(3,4-Dimethoxyphenyl)-4,4,5,5-tetramethyl-1,3,2-dioxaborolane, **403**

Entry	Base	Ligand	Catalyst	Nanoscale yield of 425 /%	Millimole yield of 425 /%
1	DBU	Bipy	CuCl	53	47
2	DABCO	Bipy	CuCl ₂	39	45
3	No Base	Phen	CuCl ₂	3	58

4,4,5,5-Tetramethyl-2-(3-(trifluoromethoxy)phenyl)-1,3,2-dioxaborolane, **404**

Entry	Base	Ligand	Catalyst	Nanoscale yield of 426 /%	Millimole yield of 426 /%
1	TMU	Phen	CuBr ₂	67	53
2	TMU	Bipy	CuCl	49	51
3	DBU	Bipy	Cu(NO ₃) ₂	30	28

4,4,5,5-Tetramethyl-2-(thiophen-3-yl)-1,3,2-dioxaborolane, **405**

Entry	Base	Ligand	Catalyst	Nanoscale yield of 427 /%	Millimole yield of 427 /%
1	No Base	Phen	CuBr ₂	48	33
2	DABCO	Bipy	CuCl	37	31
3	DBU	Bipy	Cu(NO ₃) ₂	11	21

2-(3-Methoxyphenyl)-4,4,5,5-tetramethyl-1,3,2-dioxaborolane, **406**

Entry	Base	Ligand	Catalyst	Nanoscale yield of 428 /%	Millimole yield of 428 /%
1	TMU	Phen	CuCl	74	42
2	No Base	Bipy	CuCl ₂	71	41
3	DBU	Phen	Cu(NO ₃) ₂	57	22

1-Benzyl-5-(4,4,5,5-tetramethyl-1,3,2-dioxaborolan-2-yl)-1*H*-indazole, **407**

Entry	Base	Ligand	Catalyst	Nanoscale yield of 429 /%	Millimole yield of 429 /%
1	TMU	Bipy	CuCl	83	78
2	DABCO	Bipy	CuCl ₂	75	42
3	DBU	Phen	CuCl ₂	53	20

1-Benzyl-5-(4,4,5,5-tetramethyl-1,3,2-dioxaborolan-2-yl)-1*H*-pyrrolo[2,3-*b*]pyridine, **408**

Entry	Base	Ligand	Catalyst	Nanoscale yield of 430 /%	Millimole yield of 430 /%
1	TMU	Phen	CuCl	73	71
2	TMU	Bipy	Cu(NO ₃) ₂	65	74
3	DBU	Bipy	Cu(NO ₃) ₂	51	48

5-(4,4,5,5-Tetramethyl-1,3,2-dioxaborolan-2-yl)-1*H*-indole, **409**

Entry	Base	Ligand	Catalyst	Nanoscale yield of 431 /%	Millimole yield of 431 /%
1	DABCO	Bipy	CuCl	69	23
2	DABCO	Phen	Cu(NO ₃) ₂	40	12
3	DBU	Phen	CuCl ₂	14	0

4,4,5,5-Tetramethyl-2-(*o*-tolyl)-1,3,2-dioxaborolane, **410**

Entry	Base	Ligand	Catalyst	Nanoscale yield of 432 /%	Millimole yield of 432 /%
1	TMU	Bipy	CuCl ₂	75	65
2	DBU	Bipy	CuBr ₂	45	65
3	No base	Phen	CuCl	12	0

2-(2-Chlorophenyl)-4,4,5,5-tetramethyl-1,3,2-dioxaborolane, **411**

Entry	Base	Ligand	Catalyst	Nanoscale yield of 433 /%	Millimole yield of 433 /%
1	DABCO	Phen	CuBr ₂	37	14
2	DABCO	Bipy	CuCl	24	10
3	DBU	Bipy	Cu(NO ₃) ₂	6	0

2-(2-Fluorophenyl)-4,4,5,5-tetramethyl-1,3,2-dioxaborolane, **412**

Entry	Base	Ligand	Catalyst	Nanoscale yield of 434 /%	Millimole yield of 434 /%
1	DABCO	Phen	CuBr ₂	21	8
2	TMU	Bipy	CuCl	14	12
3	DBU	Bipy	Cu(NO ₃) ₂	3	0

2-(2-Methoxyphenyl)-4,4,5,5-tetramethyl-1,3,2-dioxaborolane, **413**

Entry	Base	Ligand	Catalyst	Nanoscale yield of 435 /%	Millimole yield of 435 /%
1	TMU	Phen	CuCl	62	63
2	No Base	Bipy	Cu(NO ₃) ₂	41	57
3	DBU	Bipy	Cu(NO ₃) ₂	15	16

Ethyl 2-nitro-5-(4,4,5,5-tetramethyl-1,3,2-dioxaborolan-2-yl)benzoate, **414**

Entry	Base	Ligand	Catalyst	Nanoscale yield of 436 /%	Millimole yield of 436 /%
1	No Base	Bipy	CuBr ₂	23	12
2	DABCO	Phen	Cu(NO ₃) ₂	14	5
3	DBU	Bipy	CuCl	8	0

Ethyl 5-(4,4,5,5-Tetramethyl-1,3,2-dioxaborolan-2-yl)-2-(trifluoromethyl)benzoate, **415**

Entry	Base	Ligand	Catalyst	Nanoscale yield of 437 /%	Millimole yield of 437 /%
1	DABCO	Phen	CuBr ₂	51	29
2	TMU	Bipy	CuCl ₂	46	19
3	DBU	Bipy	Cu(NO ₃) ₂	18	7

N,N-dimethyl-4-(4,4,5,5-tetramethyl-1,3,2-dioxaborolan-2-yl)benzamide, **416**

Entry	Base	Ligand	Catalyst	Nanoscale yield of 438 /%	Millimole yield of 438 /%
1	DABCO	Bipy	CuCl	79	81
2	TMU	Phen	Cu(NO ₃) ₂	66	68
3	DBU	Bipy	CuCl ₂	43	27

N-methyl-*N*-(4-(4,4,5,5-tetramethyl-1,3,2-dioxaborolan-2-yl)phenyl)acetamide, **439**

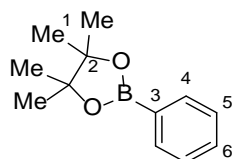
Entry	Base	Ligand	Catalyst	Nanoscale yield of 440 /%	Millimole yield of 440 /%
1	TMU	Bipy	CuCl	80	74
2	No base	Bipy	Cu(NO ₃) ₂	64	71
3	DBU	Bipy	Cu(NO ₃) ₂	38	28

Computational parameters used for modelling the Chan-Lam reaction

Boronic ester	Base	Catalyst	Ligand
total polar surface area	dissociation constant	partial charge on Cu	Boolean
molecular weight	Three Sterimol parameters	dipole moment magnitude	-
partition coefficient	total polar surface area	total charge	-
molecular volume	molecular weight	binding energy	-
surface area	partition coefficient	vdW volume	-
substituent volume	molecular volume	reoxidation energy	-
substituent surface area	surface area	-	-
Three dimensions along principal axes of inertia tensor	Three dimensions along principal axes of inertia tensor	-	-
Eight partial charges on main atoms	molecular dipole magnitude	-	-
electron affinity	partial charge on nitrogen	-	-
Two reorganisation energies	electron affinity	-	-
ionization energy	reorganization energy, anion/neutral	-	-
hardness	Ionization energy	-	-
HOMO/LUMO gap	Two reorganisation energies	-	-
5 computed IR stretching modes	hardness	-	-
5 computed IR stretching intensities	HOMO-LUMO gap	-	-

7.7. Commercial Boronic Ester Experimental Parameterisation

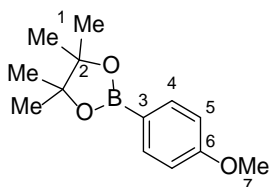
4,4,5,5-Tetramethyl-2-phenyl-1,3,2-dioxaborolane, 331



4,4,5,5-Tetramethyl-2-phenyl-1,3,2-dioxaborolane was purchased from Fluorochem and ^{13}C NMR was taken in $\text{DMSO-}d_6$ on a Bruker 500 MHz machine equipped with a cryoprobe.

^{13}C NMR (125 MHz, $\text{DMSO-}d_6$) δ_{C} : 134.4 (C_4), 131.4 (C_6), 128.5 (C_3), 127.8 (C_5), 83.6 (C_2), 24.6 (C_1); ^{11}B NMR (128 MHz, $\text{DMSO-}d_6$) δ_{B} : 30.4; IR (ν_{max} solid) / cm^{-1} : 2979, 1603, 1437, 1372, 1355, 1328, 1268, 1166, 1139, 1091, 1025, 962, 857.

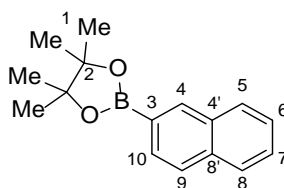
2-(4-Methoxyphenyl)-4,4,5,5-tetramethyl-1,3,2-dioxaborolane, 332



2-(4-Methoxyphenyl)-4,4,5,5-tetramethyl-1,3,2-dioxaborolane was purchased from TCI and ^{13}C NMR was taken in $\text{DMSO-}d_6$ on a Bruker 500 MHz machine equipped with a cryoprobe.

^{13}C NMR (125 MHz, $\text{DMSO-}d_6$) δ_{C} : 161.9 (C_6), 136.2 (C_4), 120.0 (C_3), 113.5 (C_5), 83.3 (C_2), 55.0 (C_7), 24.7 (C_1); ^{11}B NMR (128 MHz, $\text{DMSO-}d_6$) δ_{B} : 29.8; IR (ν_{max} solid) / cm^{-1} : 2979, 1603, 1396, 1354, 1244, 1141, 1090, 1029, 963, 859, 829, 653.

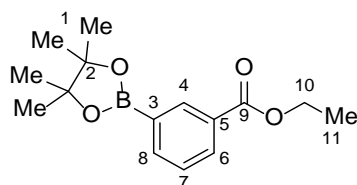
4,4,5,5-Tetramethyl-2-(naphthalen-2-yl)-1,3,2-dioxaborolane, 337



4,4,5,5-tetramethyl-2-(naphthalen-2-yl)-1,3,2-dioxaborolane was purchased from TCI and ^{13}C NMR was taken in $\text{DMSO-}d_6$ on a Bruker 500 MHz machine equipped with a cryoprobe.

^{13}C NMR (125 MHz, $\text{DMSO-}d_6$) δ_{C} : 135.9 (C_{10}), 134.5 (C_4), 132.4 ($\text{C}_{8'}$), 130.0 (C_5), 128.5 (C_9), 127.6 (C_8), 127.3 (C_4), 127.0 (C_7), 126.1 (C_6), 125.9 (C_3), 83.8 (C_2), 24.7 (C_1); ^{11}B NMR (128 MHz, $\text{DMSO-}d_6$) δ_{B} : 30.2; IR (ν_{max} solid) / cm^{-1} : 2971, 1629, 1478, 1384, 1371, 1351, 1298, 1142, 1130, 1079, 963, 850, 824, 751, 687.

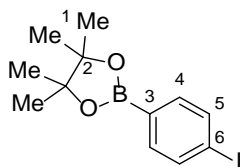
Ethyl 3-(4,4,5,5-tetramethyl-1,3,2-dioxaborolan-2-yl)benzoate, 334



Ethyl 3-(4,4,5,5-tetramethyl-1,3,2-dioxaborolan-2-yl)benzoate was purchased from Fluorochem and NMR was taken in DMSO- d_6 on a Bruker 500 MHz machine equipped with a cryoprobe.

^{13}C NMR (125 MHz, DMSO- d_6) δ_{C} : 165.6 (C₉), 138.9 (C₄), 134.8 (C₈), 132.0 (C₅), 129.4 (C₆), 128.9 (C₃), 128.4 (C₇), 84.0 (C₂), 60.8 (C₁₀), 24.6 (C₁), 14.2 (C₁₁); ^{11}B NMR (128 MHz, DMSO- d_6) δ_{B} : 30.7; IR (ν_{max} solid) / cm^{-1} : 2978, 1713, 1607, 1368, 1353, 1277, 1255, 1142, 1026, 1025, 962, 902, 853, 751, 678, 652.

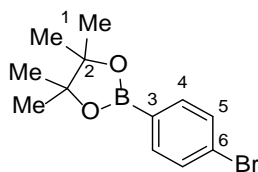
2-(4-Iodophenyl)-4,4,5,5-tetramethyl-1,3,2-dioxaborolane, 338



2-(4-Iodophenyl)-4,4,5,5-tetramethyl-1,3,2-dioxaborolane was purchased from Sigma Aldrich and NMR was taken in DMSO- d_6 on a Bruker 500 MHz machine equipped with a cryoprobe.

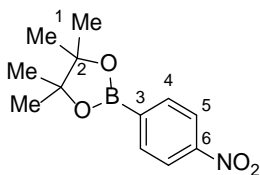
^{13}C NMR (125 MHz, DMSO- d_6) δ_{C} : 136.8 (C₅), 136.2 (C₄), 127.6 (C₃), 99.5 (C₆), 83.0 (C₂); 24.6 (C₁); ^{11}B NMR (128 MHz, DMSO- d_6) δ_{B} : 30.1; IR (ν_{max} solid) / cm^{-1} : 2976, 1583, 1385, 1362, 1325, 1139, 1085, 1005, 856, 818, 721, 663.

2-(4-Bromophenyl)-4,4,5,5-tetramethyl-1,3,2-dioxaborolane, 396



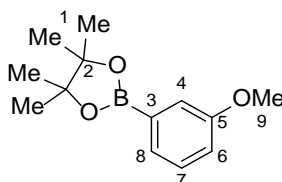
2-(4-Bromophenyl)-4,4,5,5-tetramethyl-1,3,2-dioxaborolane was purchased from Fluorochem and NMR was taken in DMSO- d_6 on a Bruker 500 MHz machine equipped with a cryoprobe.

^{13}C NMR (125 MHz, DMSO- d_6) δ_{C} : 136.3 (C₄), 131.0 (C₅), 127.5 (C₃), 125.5 (C₆), 83.9 (C₂), 24.6 (C₁); ^{11}B NMR (128 MHz, DMSO- d_6) δ_{B} : 30.5; IR (ν_{max} solid) / cm^{-1} : 2998, 1586, 1388, 1354, 1326, 1140, 1085, 1009, 857, 821, 723, 665.

4,4,5,5-Tetramethyl-2-(4-nitrophenyl)-1,3,2-dioxaborolane, 395

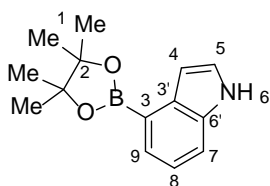
4,4,5,5-Tetramethyl-2-(4-nitrophenyl)-1,3,2-dioxaborolane was purchased from Fluorochem and NMR was taken in DMSO- d_6 on a Bruker 500 MHz machine equipped with a cryoprobe.

^{13}C NMR (125 MHz, DMSO- d_6) δ_{C} : 149.4 (C₆), 135.8 (C₃), 135.6 (C₄), 122.6 (C₅), 84.5 (C₂); 24.6 (C₁); ^{11}B NMR (128 MHz, DMSO- d_6) δ_{B} : 29.8; IR (ν_{max} solid) / cm^{-1} : 2976, 1598, 1515, 1397, 1362, 1349, 1334, 1305, 1145, 1085, 962, 876, 811, 695.

2-(3-Methoxyphenyl)-4,4,5,5-tetramethyl-1,3,2-dioxaborolane, 406

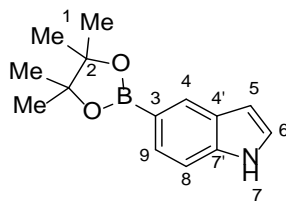
2-(3-Methoxyphenyl)-4,4,5,5-tetramethyl-1,3,2-dioxaborolane was purchased from Fluorochem and NMR was taken in DMSO- d_6 on a Bruker 500 MHz machine equipped with a cryoprobe.

^{13}C NMR (125 MHz, DMSO- d_6) δ_{C} : 158.7 (C₅), 129.9 (C₃), 129.1 (C₇), 126.8 (C₈), 118.5 (C₈), 117.6 (C₄), 83.7 (C₂), 54.9 (C₉), 24.6 (C₁); ^{11}B NMR (128 MHz, DMSO- d_6) δ_{B} : 30.4 IR (ν_{max} film) / cm^{-1} : 2978, 1576, 1420, 1350, 1311, 1142, 1043, 963, 850, 704.

4-(4,4,5,5-Tetramethyl-1,3,2-dioxaborolan-2-yl)-1H-indole, 336

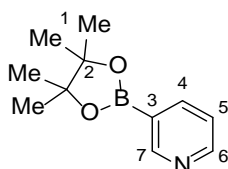
4-(4,4,5,5-Tetramethyl-1,3,2-dioxaborolan-2-yl)-1H-indole was purchased from Apollo Scientific and recrystallised from methanol. The resulting white powder was filtered and dried *in vacuo* to give the corresponding boronic ester. NMR analysis was taken in DMSO- d_6 on a Bruker 500 MHz machine equipped with a cryoprobe.

^{13}C NMR (125 MHz, DMSO- d_6) δ_{C} : 135.2 (C_{6'}), 132.3 (C_{3'}), 126.8 (C₅), 125.6 (C₈), 120.2 (C₉), 119.4 (C₃), 114.5 (C₇), 102.9 (C₄), 83.0 (C₂), 24.8 (C₁); ^{11}B NMR (128 MHz, DMSO- d_6) δ_{B} : 30.6; IR (ν_{max} solid) / cm^{-1} : 3333, 2979, 1609, 1508, 1373, 1337, 1182, 1132, 969, 853, 764, 668.

5-(4,4,5,5-Tetramethyl-1,3,2-dioxaborolan-2-yl)-1H-indole, 409

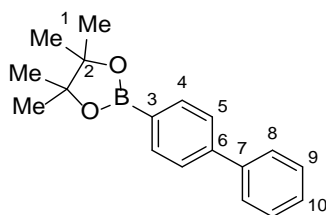
5-(4,4,5,5-Tetramethyl-1,3,2-dioxaborolan-2-yl)-1H-indole was purchased from Apollo Scientific and recrystallised from methanol. The resulting white powder was filtered and dried *in vacuo* to give the corresponding boronic ester. NMR analysis was taken in DMSO-*d*₆ on a Bruker 500 MHz machine equipped with a cryoprobe.

¹³C NMR (125 MHz, DMSO-*d*₆) δ_C: 137.9 (C_{7'}), 127.9 (C₈), 127.4 (C_{4'}), 126.8 (C₉), 125.5 (C₄), 117.9 (C₃), 110.8 (C₈), 101.8 (C₅), 83.0 (C₂), 24.7 (C₁); ¹¹B NMR (128 MHz, DMSO-*d*₆) δ_B: 29.9; IR (ν_{max} solid) / cm⁻¹: 3426, 3325, 2981, 1613, 1518, 1349, 1320, 1140, 1128, 1068, 963, 853, 737, 684.

3-(4,4,5,5-tetramethyl-1,3,2-dioxaborolan-2-yl)pyridine, 335

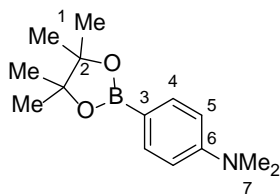
3-(4,4,5,5-tetramethyl-1,3,2-dioxaborolan-2-yl)pyridine was purchased from Fluorochem and NMR was taken in DMSO-*d*₆ on a Bruker 500 MHz machine equipped with a cryoprobe.

¹³C NMR (125 MHz, DMSO-*d*₆) δ_C: 154.5 (C₇), 152.1 (C₆), 141.9 (C₄), 123.5 (C₃₊₅), 84.1 (C₂), 24.6 (C₁); ¹¹B NMR (128 MHz, DMSO-*d*₆) δ_B: 30.4; IR (ν_{max} solid) / cm⁻¹: 2993, 2969, 1609, 1408, 1360, 1209, 1172, 1152, 1098, 1012, 953, 798, 704.

2-([1,1'-Biphenyl]-4-yl)-4,4,5,5-tetramethyl-1,3,2-dioxaborolane, 401

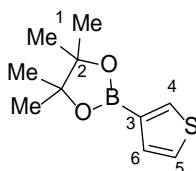
2-([1,1'-Biphenyl]-4-yl)-4,4,5,5-tetramethyl-1,3,2-dioxaborolane was purchased from TCI and NMR was taken in DMSO-*d*₆ on a Bruker 500 MHz machine equipped with a cryoprobe.

¹³C NMR (125 MHz, DMSO-*d*₆) δ_C: 142.9 (C₇), 139.7 (C₆), 135.1 (C₄), 129.0 (C₉), 127.9 (C₅), 127.3 (C₃), 126.7 (C₈), 126.1 (C₁₀), 83.7 (C₂), 24.7 (C₁); ¹¹B NMR (128 MHz, DMSO-*d*₆) δ_B: 29.5; IR (ν_{max} solid) / cm⁻¹: 2976, 1610, 1397, 1354, 1324, 1139, 1091, 860, 767, 732, 702.

***N,N*-dimethyl-4-(4,4,5,5-tetramethyl-1,3,2-dioxaborolan-2-yl)aniline, 402**

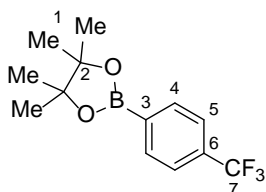
N,N-dimethyl-4-(4,4,5,5-tetramethyl-1,3,2-dioxaborolan-2-yl)aniline was purchased from Fluorochem and NMR was taken in DMSO-*d*₆ on a Bruker 500 MHz machine equipped with a cryoprobe.

¹³C NMR (125 MHz, DMSO-*d*₆) δ_C: 152.3 (C₆), 135.8 (C₄), 114.0 (C₃), 111.0 (C₅), 82.8 (C₂), 39.6 (C₇), 24.7 (C₁); ¹¹B NMR (128 MHz, DMSO-*d*₆) δ_B: 35.0; IR (ν_{max} solid) / cm⁻¹: 2978, 1603, 1349, 1138, 1089, 961, 859, 817.

4,4,5,5-Tetramethyl-2-(thiophen-3-yl)-1,3,2-dioxaborolane, 405

4,4,5,5-Tetramethyl-2-(thiophen-3-yl)-1,3,2-dioxaborolane was purchased from Fluorochem and NMR was taken in DMSO-*d*₆ on a Bruker 500 MHz machine equipped with a cryoprobe.

¹³C NMR (125 MHz, DMSO-*d*₆) δ_C: 137.0 (C₆), 131.7 (C₄), 130.7 (C₃), 126.3 (C₅), 83.4 (C₂), 24.6 (C₁); ¹¹B NMR (128 MHz, DMSO-*d*₆) δ_B: 28.7; IR (ν_{max} solid) / cm⁻¹: 2980, 1519, 1410, 1372, 1302, 1136, 1089, 964, 859, 811, 671.

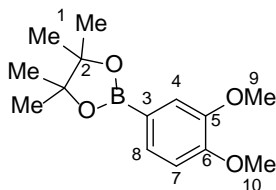
7.8. Synthesised Boronic Esters and Parameterisation**4-Trifluoromethylphenyl boronic acid pinacol ester, 333**

Prepared according to General Procedure 7 using (4-(trifluoromethyl)phenyl)boronic acid (2.00 g, 10.5 mmol), pinacol (1.26 g, 10.6 mmol), magnesium sulfate (2.84 g, 23.6 mmol) in dichloromethane (21.0 mL). The crude material was purified using flash column chromatography (0-5% diethyl ether in petroleum ether 40-60) to give the corresponding boronic ester **333** as a white solid (2.80 g, 10.3 mmol, 98%).

¹H NMR (500 MHz, DMSO-*d*₆) δ_H: 7.87 (d, *J* = 7.7, 2H, H₄), 7.72 (d, *J* = 7.7, 2H, H₅), 1.31 (s, 12H, H₁). ¹³C NMR (125 MHz, DMSO-*d*₆) δ_C: 135.1 (C₄), 133.1 (C₃), 131.4 (q, *J* = 31.5, C₆), 124.4 (q, *J* = 3.8, C₅), 124.1 (q, *J* = 272.4, C₇), 84.2 (C₂), 24.6 (C₁). ¹⁹F NMR (376 MHz,

DMSO- d_6) δ_F : -61.6; ^{11}B NMR (128 MHz, DMSO- d_6) δ_B : 30.0; HRMS (ASAP) found $[\text{M}+\text{H}]^+ = 273.1275$, $\text{C}_{13}\text{H}_{17}\text{BF}_3\text{O}$ requires 273.1274; IR (ν_{max} solid) / cm^{-1} : 2981, 1522, 1403, 1371, 1362, 1321, 1158, 1140, 1119, 1093, 842, 654..

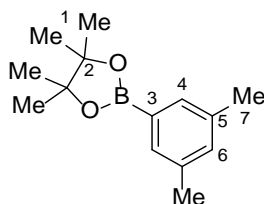
2-(3,4-Dimethoxyphenyl)-4,4,5,5-tetramethyl-1,3,2-dioxaborolane, 403



Prepared according to General Procedure 7 using (3,4-dimethoxyphenyl)boronic acid (2.00 g, 10.9 mmol), pinacol (1.36 g, 11.5 mmol), magnesium sulfate (6.57 g, 54.6 mmol) in dichloromethane (21.8 mL). The crude material was purified using flash column chromatography (2% diethyl ether in petroleum ether 40-60) to give the corresponding boronic ester **403** as a white solid (2.85 g, 10.8 mmol, 99%).

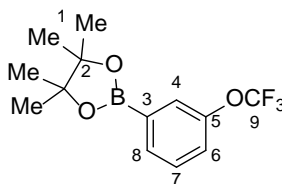
^1H NMR (500 MHz, DMSO- d_6) δ_H : 7.27 (d, $J = 7.6$, 1H, H₈), 7.13 (s, 1H, H₄), 6.96 (d, $J = 7.6$, 1H, H₇), 3.77 (s, 3H, H₁₀), 3.75 (s, 3H, H₉), 1.28 (s, 12H, H₁). ^{13}C NMR (125 MHz, DMSO- d_6) δ_C : 151.6 (C₉), 148.2 (C₁₀), 128.2 (C₈), 120.1 (C₃), 116.5 (C₄), 111.2 (C₇), 83.4 (C₂), 55.3 (C₉₊₁₀), 24.7 (C₁); ^{11}B NMR (128 MHz, DMSO- d_6) δ_B : 30.2; HRMS (ASAP) found $[\text{M}+\text{H}]^+ = 265.1612$, $\text{C}_{14}\text{H}_{22}\text{BO}_4$ requires 265.1611; IR (ν_{max} solid) / cm^{-1} : 2978, 1599, 1352, 1220, 1139, 1027, 968, 855, 755, 682.

2-(3,5-Dimethylphenyl)-4,4,5,5-tetramethyl-1,3,2-dioxaborolane, 398



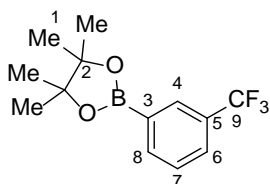
Prepared according to General Procedure 7 using (3,5-dimethylphenyl)boronic acid (2.00 g, 13.3 mmol), pinacol (1.65 g, 14.0 mmol), magnesium sulfate (8.03 g, 66.7 mmol) in dichloromethane (26.6 mL). The crude material was purified using flash column chromatography (0-2% diethyl ether in petroleum ether 40-60) to give the corresponding boronic ester **398** as a white solid (3.03 g, 13.0 mmol, 98%).

^1H NMR (500 MHz, DMSO- d_6) δ_H : 7.28 (s, 2H, H₄), 7.11 (s, 1H, H₁), 2.60 (s, 6H, H₇), 1.27 (s, 12H, H₁). ^{13}C NMR (125 MHz, DMSO- d_6) δ_C : 136.7 (C₅), 132.7 (C₆), 132.2 (C₄), 128.2 (C₃), 83.4 (C₂), 24.7 (C₁), 20.7 (C₇). ^{11}B NMR (128 MHz, DMSO- d_6) δ_B : 30.2; HRMS (ASAP) found $[\text{M}+\text{H}]^+ = 233.1715$, $\text{C}_{14}\text{H}_{22}\text{BO}_2$ requires 233.1713; IR (ν_{max} solid) / cm^{-1} : 2977, 1600, 1356, 1240, 1138, 1115, 964, 849, 711.

4,4,5,5-Tetramethyl-2-(3-(trifluoromethoxy)phenyl)-1,3,2-dioxaborolane, 404

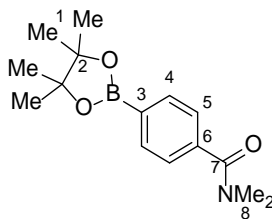
Prepared according to General Procedure 7 using (3-(trifluoromethoxy)phenyl)boronic acid (2.00 g, 9.71 mmol), pinacol (1.21 g, 10.2 mmol), magnesium sulfate (5.85 g, 48.6 mmol) in dichloromethane (19.4 mL). The crude material was purified using flash column chromatography (0-2% diethyl ether in petroleum ether 40-60) to give the corresponding boronic ester **404** as a white solid (2.55 g, 8.84 mmol, 91%).

¹H NMR (500 MHz, DMSO-*d*₆) δ_{H} : 7.68 (d, $J = 7.2$, 1H, H₈), 7.53 (td, $J = 7.7$, 0.8, 1H, H₇), 7.46–7.51 (m, 2H, H₄₊₆), 1.29 (s, 12H, H₁). **¹³C NMR** (125 MHz, DMSO-*d*₆) δ_{C} : 148.2 (C₅), 133.3 (C₈), 131.2 (C₃), 130.3 (C₇), 125.7 (C₆), 124.1 (C₄), 120.2 (q, $J = 192.1$, C₉), 84.2 (C₂), 24.6 (C₁); **¹⁹F NMR** (376 MHz, DMSO-*d*₆) δ_{F} : -57.8; **¹¹B NMR** (128 MHz, DMSO-*d*₆) δ_{B} : 30.0; **HRMS** (ASAP) found $[\text{M}+\text{H}]^+ = 289.1222$, C₁₃H₁₇BF₃O₃ requires 289.1223; **IR** (ν_{max} solid) / cm⁻¹: 2983, 1578, 1491, 1428, 1355, 1248, 1140, 1070, 966, 864, 702.

4,4,5,5-Tetramethyl-2-(3-(trifluoromethyl)phenyl)-1,3,2-dioxaborolane, 397

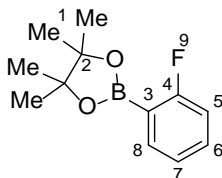
Prepared according to General Procedure 7 using (3-(trifluoromethyl)phenyl)boronic acid (2.00 g, 10.5 mmol), pinacol (1.31 g, 11.1 mmol), magnesium sulfate (6.34g, 52.7 mmol) in dichloromethane (21.0 mL). The crude material was purified using flash column chromatography (0-5% diethyl ether in petroleum ether 40-60) to give the corresponding boronic ester **397** as a white solid (2.57 g, 9.45 mmol, 90%).

¹H NMR (500 MHz, DMSO-*d*₆) δ_{H} : 7.94 (d, $J = 7.8$, 1H, H₈), 7.89 (s, 1H H₄), 7.85 (d, $J = 8.9$, 1H, H₆), 7.62 (t, $J = 7.8$, 1H, H₇), 1.30 (s, 12H, H₁); **¹³C NMR** (125 MHz, DMSO-*d*₆) δ_{C} : 138.2 (C₈), 130.2 (d, $J = 3.5$, C₄), 129.7 (C₃), 129.0 (C₇), 128.7 (q, $J = 29.3$, C₅), 127.9 (d, $J = 3.5$, C₆), 124.2 (q, $J = 272.2$, C₉), 84.2 (C₂), 24.6 (C₁); **¹⁹F NMR** (376 MHz, DMSO-*d*₆) δ_{F} : -61.4; **¹¹B NMR** (128 MHz, DMSO-*d*₆) δ_{B} : 30.1; **HRMS** (ASAP) found $[\text{M}+\text{H}]^+ = 273.1270$, C₁₃H₁₇BF₃O₂ requires 273.1274; **IR** (ν_{max} solid) / cm⁻¹: 2985, 1613, 1364, 1302, 1165, 1115, 1070, 962, 862, 815, 703, 681.

***N,N*-dimethyl-4-(4,4,5,5-tetramethyl-1,3,2-dioxaborolan-2-yl)benzamide, 416**

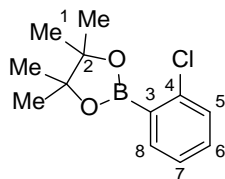
Prepared according to General Procedure 7 using (4-(dimethylcarbamoyl)phenyl)boronic acid (2.00 g, 10.4 mmol), pinacol (1.29 g, 10.9 mmol), magnesium sulfate (62.3 g, 51.8 mmol) in dichloromethane (20.8 mL). The crude material was purified using flash column chromatography (0-25% ethyl acetate in dichloromethane) to give the corresponding boronic ester **416** as a white solid (2.78 g, 10.1 mmol, 97%).

¹H NMR (500 MHz, DMSO-*d*₆) δ_{H} : 7.72 (d, $J = 8.1$, 2H, H₄), 7.39 (d, $J = 8.1$, 2H, H₅), 2.98 (s, 3H, H_{8a}), 2.87 (s, 3H, H_{8b}), 1.30 (s, 12H, H₁); **¹³C NMR** (125 MHz, DMSO-*d*₆) δ_{C} : 169.8 (C₇), 139.3 (C₆), 134.3 (C₄), 129.5 (C₃), 126.3 (C₅), 83.9 (C₂), 24.7 (C₁); **¹¹B NMR** (128 MHz, DMSO-*d*₆) δ_{B} : 29.7; **HRMS** (ASAP) found $[\text{M}+\text{H}]^+ = 276.1766$, C₁₅H₂₃BNO₃ requires 276.1771; **IR** (ν_{max} solid) / cm⁻¹: 2978, 1628, 1610, 1356, 1319, 1142, 1392, 1017, 961, 857, 658.

2-(2-Fluorophenyl)-4,4,5,5-tetramethyl-1,3,2-dioxaborolane, 412

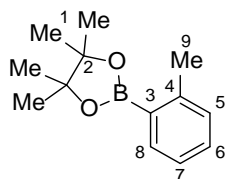
Prepared according to General Procedure 7 using (2-fluorophenyl)boronic acid (2.00 g, 14.3 mmol), pinacol (1.77 g, 15.0 mmol), magnesium sulfate (8.61 g, 71.5 mmol) in dichloromethane (28.6 mL). The crude material was purified using flash column chromatography (1% diethyl ether in petroleum ether 40-60) to give the corresponding boronic ester **412** as a white solid (2.48 g, 11.2 mmol, 78%).

¹H NMR (500 MHz, DMSO-*d*₆) δ_{H} : 7.65 (m, 1H, H₈), 7.54 (m, 1H, H₆), 7.20 (t, $J = 7.3$, 1H, H₅), 7.14 (t, $J = 9.0$, 1H, H₇), 1.29 (s, 12H, H₁); **¹³C NMR** (125 MHz, DMSO-*d*₆) δ_{C} : 166.4 (d, $J = 249.6$, C₄), 136.6 (d, $J = 8.0$, C₈), 133.9 (d, $J = 8.7$, C₆), 124.1 (d, $J = 3.3$, C₇), 115.5 (d, $J = 23.4$, C₅), 83.7 (C₂), 24.6 (C₁); **¹⁹F NMR** (376 MHz, DMSO-*d*₆) δ_{F} : -102.2; **¹¹B NMR** (128 MHz, DMSO-*d*₆) δ_{B} : 30.3; **HRMS** (ASAP) found $[\text{M}+\text{H}]^+ = 223.1307$, C₁₂H₁₇BFO₂ requires 223.1306; **IR** (ν_{max} film) / cm⁻¹: 2980, 1616, 1445, 1352, 1142, 1073, 860, 839, 761, 653.

2-(2-Chlorophenyl)-4,4,5,5-tetramethyl-1,3,2-dioxaborolane, 411

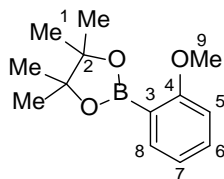
Prepared according to General Procedure 7 using (2-fluorophenyl)boronic acid (2.00 g, 12.8 mmol), pinacol (1.58 g, 13.4 mmol), magnesium sulfate (7.70 g, 64.0 mmol) in dichloromethane (25.6 mL). The crude material was purified using flash column chromatography (5% diethyl ether in petroleum ether 40-60) to give the corresponding boronic ester **411** as a white solid (1.89 g, 7.94 mmol, 62%).

¹H NMR (500 MHz, DMSO-*d*₆) δ_{H} : 7.63 (dd, $J = 7.2, 1.7$, 1H, H₈), 7.46 (ddd, $J = 8.0, 7.2, 1.7$, 1H, H₅), 7.41 (dd, $J = 8.0, 1.2$, 1H, H₆), 7.32 (td, $J = 11.0, 1.2$, 1H, H₇), 1.30 (s, 12H, H₁); **¹³C NMR** (125 MHz, DMSO-*d*₆) δ_{C} : 138.3 (C₈), 136.4 (C₄), 132.5 (C₆), 129.3 (C₅), 128.7 (C₃), 126.3 (C₇), 83.9 (C₂), 24.5 (C₁); **¹¹B NMR** (128 MHz, DMSO-*d*₆) δ_{B} : .30.5; **HRMS** (ASAP) found $[M+H]^+ = 239.1010$, C₁₂H₁₇BClO₂ requires 239.1010; **IR** (ν_{max} film) / cm⁻¹: 2980, 1593, 1428, 1348, 1316, 1142, 1104, 1038, 857, 756, 653.

4,4,5,5-Tetramethyl-2-(o-tolyl)-1,3,2-dioxaborolane, 410

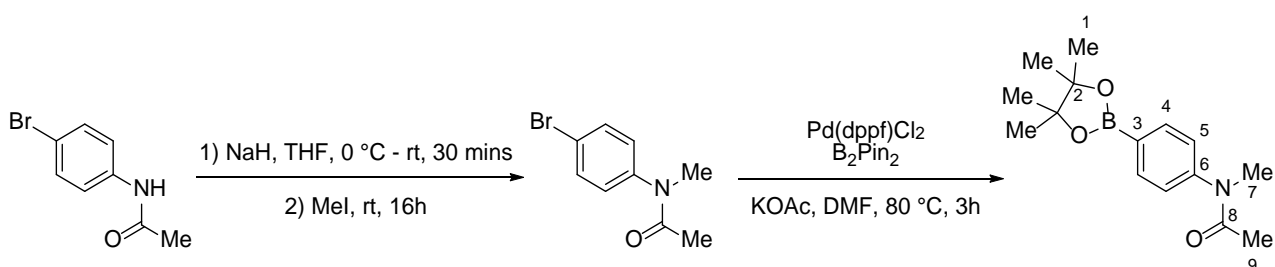
Prepared according to General Procedure 7 using o-tolylboronic acid (2.00 g, 14.7 mmol), pinacol (1.82 g, 15.4 mmol), magnesium sulfate (8.86 g, 73.6 mmol) in dichloromethane (29.4 mL). The crude material was purified using flash column chromatography (0-2% diethyl ether in petroleum ether 40-60) to give the corresponding boronic ester **410** as a white solid (3.02 g, 13.9 mmol, 90%).

¹H NMR (500 MHz, DMSO-*d*₆) δ_{H} : 7.63 (td, $J = 7.5, 1.1$, 1H, H₈), 7.33 (dt, $J = 7.5, 1.1$, 1H, H₆), 7.14 (t, $J = 7.5$, 2H, H₅₊₇), 2.46 (s, 3H, H₉), 1.28 (s, 12H, H₁); **¹³C NMR** (125 MHz, DMSO-*d*₆) δ_{C} : 144.0 (C₄), 135.5 (C₈), 130.9 (C₅), 129.7 (C₆), 128.0 (C₃), 124.7 (C₇), 83.2 (C₂), 24.6 (C₁), 21.8 (C₉); **¹¹B NMR** (128 MHz, DMSO-*d*₆) δ_{B} : .31.4; **HRMS** (ASAP) found $[M+H]^+ = 219.1560$, C₁₃H₂₀BO₂ requires 219.1556; **IR** (ν_{max} film) / cm⁻¹: 2978, 1602, 1343, 1310, 1143, 1071, 963, 861, 728, 658.

2-(2-Methoxyphenyl)-4,4,5,5-tetramethyl-1,3,2-dioxaborolane, 413

Prepared according to General Procedure 7 using (2-fluorophenyl)boronic acid (2.00 g, 13.2 mmol), pinacol (1.63 g, 13.8 mmol), magnesium sulfate (7.92 g, 65.8 mmol) in dichloromethane (26.4 mL). The crude material was purified using flash column chromatography (0-15% diethyl ether in petroleum ether 40-60) to give the corresponding boronic ester **413** as a white solid (2.97 g, 12.7 mmol, 96%).

¹H NMR (500 MHz, DMSO-*d*₆) δ_H: 7.53 (dd, *J* = 7.3, 1.8, 1H, H₈), 7.40–7.45 (m, 1H, H₆), 6.95 (d, *J* = 8.4, 1H, H₅), 6.91 (t, *J* = 7.3, 1H, H₇), 3.73 (s, 3H, H₉), 1.26 (s, 12H, H₁); **¹³C NMR** (125 MHz, DMSO-*d*₆) δ_C: 163.8 (C₄), 136.3 (C₈), 132.8 (C₆), 119.9 (C₇), 117.2 (C₃), 110.7 (C₅), 83.0 (C₂), 55.3 (C₉), 24.6 (C₁); **¹¹B NMR** (128 MHz, DMSO-*d*₆) δ_B: 31.1; **HRMS** (ASAP) found [M+H]⁺ = 235.1500, C₁₃H₁₉BO₃ requires 235.1506; **IR** (ν_{max} solid) / cm⁻¹: 2976, 1599, 1487, 14292, 1350, 1245, 1141, 1068, 1024, 862, 773, 656.

***N*-methyl-*N*-(4-(4,4,5,5-tetramethyl-1,3,2-dioxaborolan-2-yl)phenyl)acetamide, 439**

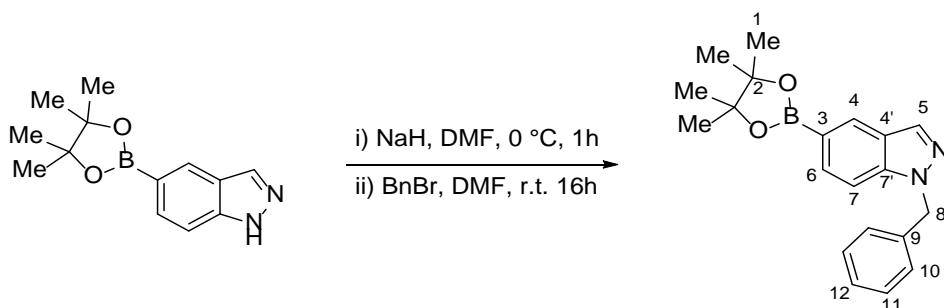
Step1: An oven dried round bottom flask equipped with a stirrer bar was charged with *N*-(4-bromophenyl)acetamide (5.0g, 23.4 mmol) and THF (78 mL) and the solution was cooled to 0 °C. NaH (1.68 g, 70.2 mmol) was carefully added portion-wise to the solution over 10 minutes. The resulting suspension was warmed to room temperature stirred for a further 10 minutes. Methyl iodide (2.91 mL, 46.8 mmol) was added dropwise over 5 minutes and the resulting suspension was stirred for 16 hours after which the reaction was cooled to 0 °C and water (10 mL) was added dropwise. The corresponding solution was diluted with ethyl acetate (10 mL) and the phases separated. The aqueous layer was extracted with ethyl acetate (2 × 20 mL) and the organic extracts combined, dried (MgSO₄), filtered and concentrated in vacuo to give *N*-(4-bromophenyl)-*N*-methylacetamide as a white solid which was used without further purification.

¹H NMR (400 MHz, (CDCl₃) δ_H: 7.48 (d, *J* = 9.2, 2H), 7.03 (d, *J* = 9.2, 2H), 3.18 (s, 3H), 1.81 (s, 3H); **¹³C NMR** (100 MHz, DMSO-*d*₆) δ_C: 170.0, 143.6, 132.7, 128.6, 121.2, 36.9, 22.2.

Step 2: An oven dried round bottom flask equipped with a magnetic stirrer bar was charged with *N*-(4-bromophenyl)-*N*-methylacetamide from step 1 (5.2g, 22.8 mmol) in *N,N*-dimethylformamide (76 mL) and subsequently sparged with N₂ for 15 minutes. Pd(dppf)Cl₂ (1.67 g, 2.28 mmol), bispinacolotodiboron (8.68 g, 34.2 mmol) and potassium acetate (6.71 g, 68.4 mol) were added to the sparged solution and the resulting reaction mixture was placed in a preheated oil bath at 80 °C and stirred for 3 hours. The resulting solution was cooled to room temperature, diluted with ethyl acetate (50 mL) and subsequently poured onto water (500 mL). The phases were separated and the aqueous layer was extracted with ethyl acetate (2 × 100 mL). The combined organic extracts were washed with brine (50 mL), dried (MgSO₄), filtered and concentrated *in vacuo*. The resulting crude oil was purified by flash column chromatography (0-25% ethyl acetate in petroleum ether 40-60) to yield the titled boronic ester as a white solid (4.64 g, 16.9 mmol, 74%).

¹H NMR (500 MHz, DMSO-*d*₆) δ_H: 7.72 (d, *J* = 8.0, 2H, H₄), 7.33 (d, *J* = 8.0, 2H, H₃), 3.16 (s, 3H, H₉), 1.81 (br. s, 3H, H₇), 1.29 (s, 12H, H₁); ¹³C NMR (125 MHz, DMSO-*d*₆) δ_C: 168.9 (C₈), 147.0 (C₄), 135.5 (C₅), 127.2 (C₃), 126.3 (C₆), 83.8 (C₂), 36.5 (C₇), 24.6 (C₁), 22.2 (C₉); ¹¹B NMR (128 MHz, DMSO-*d*₆) δ_B: 31.4; HRMS (ASAP) found [M+H]⁺ = 276.1772, C₁₅H₂₃BNO₃ requires 276.1771; IR (ν_{max} film) / cm⁻¹: 2979, 1651, 1604, 1361, 1322, 1139, 1092, 855, 842, 655.

1-Benzyl-5-(4,4,5,5-tetramethyl-1,3,2-dioxaborolan-2-yl)-1*H*-indazole, 407

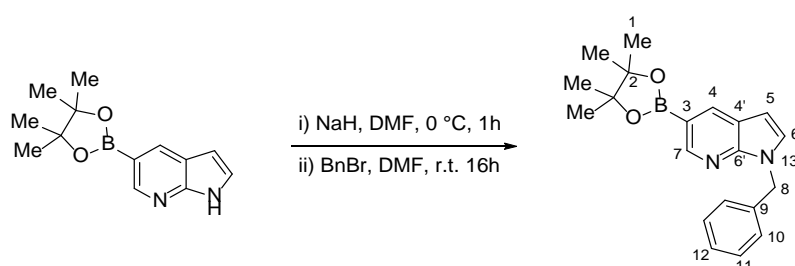


An oven dried round bottom flask equipped with a stirrer bar was charged with 5-(4,4,5,5-tetramethyl-1,3,2-dioxaborolan-2-yl)-1*H*-indazole (500 mg, 2.05 mmol) and *N,N*-dimethylformamide (10.2 mL) under nitrogen. The resulting solution was cooled to 0 °C and sodium hydride (147 mg, 6.15 mmol) was added portion wise over 30 minutes. The corresponding reaction mixture was stirred at 0 °C for a further 30 minutes. Benzyl bromide (292 μL, 2.46 mmol) was added dropwise to the reaction mixture at 0 °C over 20 minutes and the resulting reaction mixture was slowly allowed to warm to room temperature and stirred for 16 hours. The reaction was quenched with water (5 mL) and the aqueous mixture was extracted with ethyl acetate (15 mL₃) and the combined organic extracts were washed with water (10 mL), brine (10 mL × 2), dried (MgSO₄), filtered and concentrated *in vacuo*. The crude reaction

mixture was purified by flash column chromatography (0-50% diethyl ether in petroleum ether 40-60) to give the title compound as a white solid (349 mg, 1.05 mmol, 51%).

¹H NMR (500 MHz, DMSO-*d*₆) δ_{H} : 8.15–8.18 (m, 2H, H_{4,5}), 7.68 (d, *J* = 8.5, 1H, H₆), 7.62 (dd, *J* = 8.5, 0.9, 1H, H₇), 7.22–7.31 (m, 3H, H₁₁₊₁₂), 7.15–7.21 (m, 2H, H₁₀), 5.67 (s, 2H, H₈), 1.30 (s, 12H, H₁); **¹³C NMR** (125 MHz, DMSO-*d*₆) δ_{C} : 140.8 (C_{7'}), 137.5 (C_{4'}), 134.0 (C₅), 131.3 (C₇), 129.0 (C₄), 128.5 (C₁₁), 127.5 (C₁₂), 127.2 (C₁₀), 123.7 (C₉), 120.1 (C₃), 109.3 (C₆), 83.5 (C₂), 51.7 (C₈), 24.7 (C₁). **¹¹B NMR** (128 MHz, DMSO-*d*₆) δ_{B} : 31.8; **HRMS** (ASAP) found $[\text{M}+\text{H}]^+ = 335.1938$, C₂₀H₂₄BN₂O₂ requires 335.1931; **m.p.** 110 °C; **IR** (ν_{max} solid) / cm⁻¹: 3005, 2980, 2930, 1617, 1446, 1389, 13344, 1313, 1142, 1071, 964, 858, 723, 679.

1-Benzyl-5-(4,4,5,5-tetramethyl-1,3,2-dioxaborolan-2-yl)-1*H*-pyrrolo[2,3-*b*]pyridine, 408

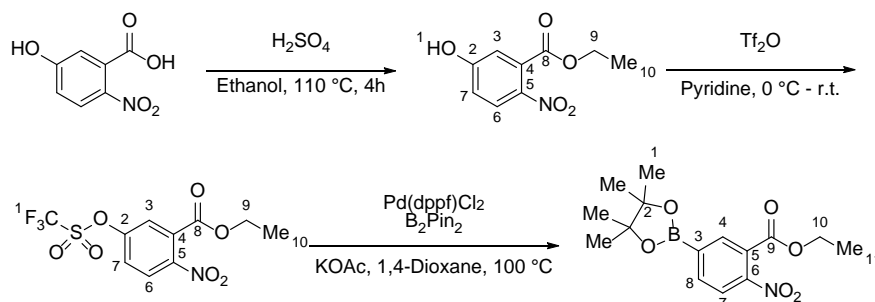


An oven dried round bottom flask equipped with a stirrer bar was charged with 5-(4,4,5,5-tetramethyl-1,3,2-dioxaborolan-2-yl)-1*H*-indazole (500 mg, 2.05 mmol) and *N,N*-dimethylformamide (10.2 mL) under nitrogen. The resulting solution was cooled to 0 °C and sodium hydride (147 mg, 6.15 mmol) was carefully added portion wise over 30 minutes. The corresponding reaction mixture was stirred at 0 °C for a further 30 minutes. Benzyl bromide (292 μ L, 2.46 mmol) was added dropwise to the reaction mixture at 0 °C over 20 minutes and the resulting reaction mixture was slowly allowed to warm to room temperature and stirred for 16 hours. The reaction was quenched with water (5 mL) and the aqueous mixture was extracted with ethyl acetate (15 mL \times 3) and the combined organic extracts were washed with water (10 mL), brine (10 mL \times 2), dried (MgSO₄), filtered and concentrated *in vacuo*. The crude reaction mixture was purified by flash column chromatography (0-40% diethyl ether in petroleum ether 40-60) to give the title compound as a white solid (472.8 mg, 1.41 mmol, 69%).

¹H NMR (500 MHz, DMSO-*d*₆) δ_{H} : 8.50 (d, *J* = 1.3, 1H, H₇), 8.26 (d, *J* = 1.3, 1H, H₄), 7.62 (d, *J* = 3.6, 1H, H₆), 7.29 (m, 2H, H₁₁), 7.24 (m, 1H, H₁₂), 7.19 (m, 2H, H₁₀), 6.55 (d, *J* = 3.6, 1H, H₅), 5.50 (s, 2H, H₈), 1.31 (s, 12H, H₁); **¹³C NMR** (125 MHz, DMSO-*d*₆) δ_{C} : 148.6 (C_{6'}), 148.2 (C₇), 138.3 (C_{4'}), 135.4 (C₄), 129.5 (C₆), 128.5 (C₁₁), 127.3 (C₁₂), 127.1 (C₁₀), 119.7 (C₉), 114.5 (C₃), 100.3 (C₅), 83.6 (C₂), 47.1 (C₈), 24.7 (C₁); **¹¹B NMR** (128 MHz, DMSO-*d*₆) δ_{B} : 32.9; **HRMS** (ASAP) found $[\text{M}+\text{H}]^+ = 335.1938$, C₂₀H₂₄BN₂O₂ requires 335.1931; **m.p.**: 123–

124 °C; IR (ν_{\max} solid) / cm^{-1} : 2973, 1596, 1560, 1511, 1371, 1345, 1323, 1138, 1115, 968, 854, 735.

Ethyl 2-nitro-5-(4,4,5,5-tetramethyl-1,3,2-dioxaborolan-2-yl)benzoate, 414



Step 1: An oven dried round bottom flask equipped with a stirrer bar was charged with 5-hydroxy-2-nitrobenzoic acid (5.0 g, 27.3 mmol) and ethanol (100 mL). Concentrated sulfuric acid (728 μL , 13.7 mmol) was added dropwise at room temperature and the resulting reaction mixture was placed in a preheated oil bath at 110 °C for 16 hours. The resulting solution was cooled to room temperature and poured onto saturated aqueous sodium hydrogen carbonate (100 mL) and the pH adjusted to >pH 10. The aqueous suspension was extracted with ethyl acetate (3 \times 50 mL) and the combined organic extracts were dried (MgSO_4), filtered and concentrated *in vacuo* giving the title compound as an off-white solid (5.65 g, 26.8 mmol, 98%) which was used without further purification.

$^1\text{H NMR}$ (500 MHz, $\text{DMSO}-d_6$) δ_{H} : 11.3 (br. s, 1H, H_1), 8.04 (d, $J = 9.2$, 1H, H_6), 7.03 (dd, $J = 9.2$, 2.8, 1H, H_7), 6.99 (d, $J = 2.8$, 1H, H_3), 4.30 (q, $J = 7.2$, 2H, H_9), 1.26 (t, $J = 7.2$, 3H, H_{10}). $^{13}\text{C NMR}$ (125 MHz, $\text{DMSO}-d_6$) δ_{C} : 165.5 (C_8), 162.8 (C_2), 137.9 (C_5), 131.2 (C_4), 127.3 (C_6), 117.3 (C_7), 115.2 (C_3), 61.9 (C_9), 13.7 (C_{10}).

Step 2: An oven dried round bottom flask equipped with a stirrer bar was charged with ethyl 5-hydroxy-2-nitrobenzoate from step 1 (5.65 g, 26.8 mmol) from step 1 and pyridine (60 mL) and subsequently cooled to 0 °C. Triflic anhydride (5.59 mL, 40.2 mol) was added dropwise to the reaction mixture and stirred for 30 minutes. The resulting solution was warmed to room temperature and stirred for a further 12 hours. The reaction mixture was diluted with diethyl ether (20 mL) and the organic solution washed with 1M copper (II) sulfate solution (5 \times 100 mL), water (3 \times 50 mL) and brine (50 mL). The organic phase was dried (MgSO_4) and concentrated *in vacuo*. The crude material was purified by flash column chromatography (0-12% diethyl ether in petroleum ether 40-60) to give the title compound as a colourless oil (8.74 g, 25.5 mmol, 95%).

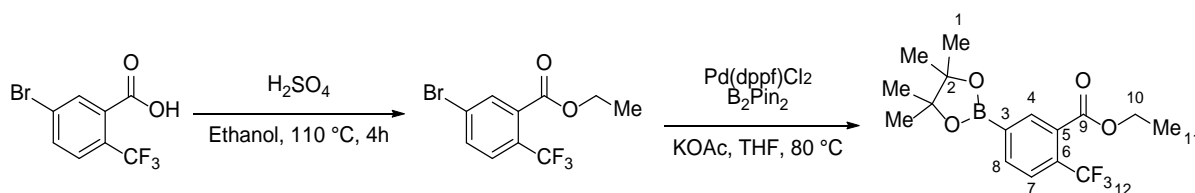
$^1\text{H NMR}$ (500 MHz, $\text{DMSO}-d_6$) δ_{H} : 8.02 (d, $J = 8.9$, 1H, H_6), 7.66 (d, $J = 2.6$, 1H, H_3), 7.55 (dd, $J = 8.9$, 2.6, 1H, H_7), 4.42 (q, $J = 7.2$, 2H, H_9), 1.37 (t, $J = 7.2$, 3H, H_{10}); $^{13}\text{C NMR}$ (125

MHz, DMSO-*d*₆) δ_{C} : 163.2 (C₈), 151.1 (C₂), 147.2 (C₅), 130.3 (C₄), 126.3 (C₆), 124.6 (C₃), 123.2 (C₇), 118.6 (q, $J = 321.0$, C₁), 63.3 (C₉), 13.7 (C₁₀); **¹⁹F NMR** (376 MHz, DMSO-*d*₆) δ_{F} : -73.4.

Step 3: An oven dried round bottom flask equipped with a stirrer bar was charged with ethyl 2-nitro-5-(((trifluoromethyl)sulfonyl)oxy)benzoate from step 2 (3.0 g, 8.74 mmol), Pd(dppf)Cl₂ (637 mg, 0.87 mmol), bispinacolotodiboron (3.33 g, 13.1 mmol) and potassium acetate (2.57 mg, 26.2 mmol) in 1,4-dioxane (43.7 mL). The flask was purged with nitrogen three times and the reaction mixture sparged with nitrogen for 5 minutes. The resulting purged suspension was placed in a preheated oil bath at 105 °C and stirred for 14 hours. The reaction was cooled to room temperature and filtered through a pad of Celite® and the mother liquors concentrated *in vacuo*. The crude material was purified by flash column chromatography (0–5% methanol in chloroform) collecting the fractions that contained product as visualised by TLC staining with anisaldehyde. The crude fractions were concentrated *in vacuo* and the resulting brown solids recrystallised from methanol to give the titled compound as a off-white crystalline powder (954 mg, 2.97 mmol, 34%).

¹H NMR (500 MHz, DMSO-*d*₆) δ_{H} : 8.03 (m, 3H, H_{3,6,7}), 4.32 (q, $J = 7.1$, 2H, H₉), 1.32 (s, 12H, H₁), 1.28 (t, $J = 7.1$, 3H, H₁₁); **¹³C NMR** (125 MHz, DMSO-*d*₆) δ_{C} : 164.3 (C₉), 149.9 (C₆), 138.5 (C₄), 135.2 (C₇), 134.2 (C₃), 125.4 (C₄), 123.5 (C₆), 84.8 (C₂), 62.2 (C₉), 24.6 (C₁), 13.7 (C₁₁); **HRMS**: (ASAP) found [M+H]⁺: 322.1472, C₁₅H₂₁BO₆N requires 322.1462; **¹¹B NMR** (128 MHz, DMSO-*d*₆) δ_{B} : 30.7; **m.p.**: 86–87 °C; **IR** (ν_{max} solid) / cm⁻¹: 2995, 1731, 1526, 1347, 1140, 1100, 1018, 964, 851, 845, 703.

Preparation of ethyl 5-(4,4,5,5-tetramethyl-1,3,2-dioxaborolan-2-yl)-2-(trifluoromethyl)benzoate, 415



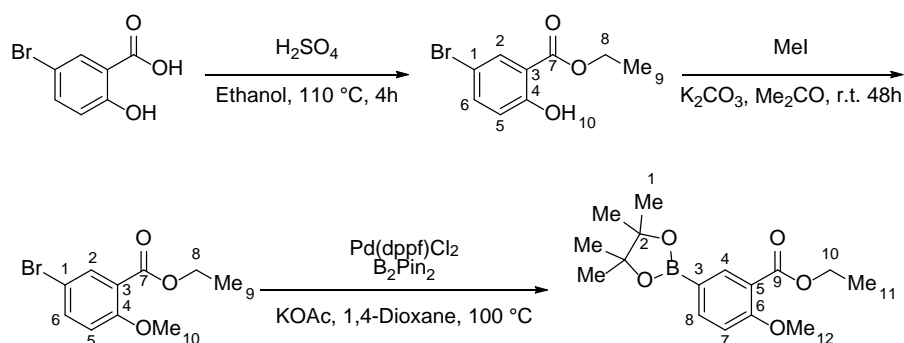
Step 1: An oven dried round bottom flask equipped with a stirrer bar was charged with 5-bromo-2-(trifluoromethyl)benzoic acid (1.0 g, 3.72 mmol) and ethanol (50 mL). Concentrated sulfuric acid (100 μ L, 1.86 mmol) was added dropwise at room temperature and the resulting reaction mixture was placed in a preheated oil bath at 110 °C for 16 hours. The resulting solution was cooled to room temperature and poured onto saturated aqueous sodium hydrogen carbonate (50 mL) and the pH adjusted to >pH 10. The aqueous suspension was extracted with ethyl acetate (3 \times 20 mL) and the combined organic extracts were dried (MgSO₄), filtered and concentrated

in vacuo giving the title compound as an off white solid (1.04 g, 3.50 mmol, 94%) which was used directly in the next step without further purification.

Step 2: An oven dried round bottom flask equipped with a stirrer bar was charged with ethyl 5-bromo-2-(trifluoromethyl)benzoate from step 1 (1.04 g, 3.50 mmol), Pd(dppf)Cl₂ (256 mg, 0.35 mmol), bispinacolatodiboron (1.33 g, 5.25 mmol) and potassium acetate (1.03 g, 10.5 mmol) in 1,4-dioxane (17.5 mL). The flask was purged with nitrogen three times and the reaction mixture sparged with nitrogen for 5 minutes. The resulting purged suspension was placed in a preheated oil bath at 80 °C and stirred for 14 hours. The reaction was cooled to room temperature and filtered through a pad of Celite[®] and the mother liquors concentrated *in vacuo*. The crude material was purified by flash column chromatography with boron doped silica²⁴⁷ (0–1% diethyl ether in petroleum ether 40–60) to give the titled compound as a colourless oil (746.8 mg, 2.17 mmol, 62%).

¹H NMR (500 MHz, DMSO-*d*₆) δ_H: 8.00 (m, 2H, H_{4,8}), 7.89 (d, *J* = 7.8, 1H, H₇), 4.34 (q, *J* = 7.1, 2H, H₁₀), 1.31 (m, 15H, H_{1,11}); ¹³C NMR (125 MHz, DMSO-*d*₆) δ_C: 166.0 (C₉), 137.4 (C₄), 135.1 (C₈), 133.4 (C₃), 130.4 (q, *J* = 2.0, C₅), 129.0 (q, *J* = 31.9, C₆), 126.2 (q, *J* = 7.8, C₇), 123.3 (q, *J* = 273.6, C₁₂), 84.6 (C₂), 61.9 (C₁₀), 24.6 (C₁), 13.8 (C₁₁); ¹⁹F NMR (376 MHz, DMSO-*d*₆) δ_F: -58.5; ¹¹B NMR (128 MHz, DMSO-*d*₆) δ_B: 30.8; HRMS: (ASAP) found [M]⁺: 344.1405, C₁₆H₂₀BF₃O₄ requires 344.1407; m.p.: 40–41 °C IR (ν_{max} solid) / cm⁻¹: 2983, 1732, 1371, 1309, 1128, 1099, 1038, 964, 850, 789.

Preparation of **Ethyl 2-methoxy-5-(4,4,5,5-tetramethyl-1,3,2-dioxaborolan-2-yl)benzoate**, 400



Step 1: An oven dried round bottom flask equipped with a stirrer bar was charged with 5-bromo-2-hydroxybenzoic acid (5.0 g, 23.0 mmol) and ethanol (100 mL). Concentrated sulfuric acid (614 μL, 11.5 mmol) was added dropwise at room temperature and the resulting reaction mixture was placed in a preheated oil bath at 110 °C for 16 hours. The resulting solution was cooled to room temperature and poured onto saturated aqueous sodium hydrogen carbonate (50 mL) and the pH adjusted to >pH 10. The aqueous suspension was extracted with ethyl acetate (3 × 20 mL) and the combined organic extracts were dried (MgSO₄), filtered and concentrated

in vacuo giving the title compound as an off white solid (5.07 g, 20.7 mmol, 90%) which was used without further purification.

¹H NMR (400 MHz, (CDCl₃) δ_H: 10.79 (s, 1H, H₁₀), 7.95 (d, *J* = 2.4, 1H, H₂), 7.53 (dd, *J* = 8.7, 2.4, 1H, H₆), 6.88 (d, *J* = 8.7, 1H, H₅), 4.42 (q, *J* = 7.1, 2H, H₈), 1.42 (t, *J* = 7.1, 3H, H₉); **¹³C NMR** (100 MHz, (CDCl₃) δ_C: 169.1 (C₇), 160.7 (C₁₀), 138.3 (C₆), 132.2 (C₂), 119.5 (C₅), 114.1 (C₃), 110.7 (C₁), 61.9 (C₈), 14.1 (C₉).

Step 2: An oven dried round bottom flask equipped with a stirrer bar was charged with ethyl 5-bromo-2-hydroxybenzoate from step 1 (5.07 g, 20.7 mmol) and potassium carbonate (8.58 g, 62.1 mmol) in acetone (41 mL). Methyl iodide (2.58 mL, 41.4 mmol) was added dropwise to the reaction mixture over 20 minutes and the resulting suspension stirred for 16 hours. The resulting suspension was filtered, the filtrate was washed with ethyl acetate (50 mL) and the resulting mother liquors were concentrated *in vacuo* to give the titled compound as a off white solid (3.75 g, 14.5 mmol, 70%). This material was used without further purification.

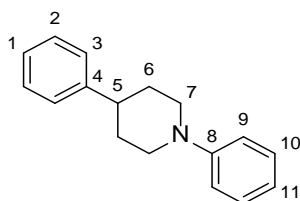
¹H NMR (400 MHz, (CDCl₃) δ_H: 7.88 (d, *J* = 2.5, 1H, H₂), 7.54 (dd, *J* = 8.9, 2.5, 1H, H₆), 6.85 (d, *J* = 8.9, 1H, H₅), 4.34 (q, *J* = 7.1, 2H, H₈), 3.88 (s, 3H, H₁₀), 1.37 (t, *J* = 7.1, 3H, H₉); **¹³C NMR** (100 MHz, (CDCl₃) δ_C: 164.7 (C₇), 158.2 (C₄), 135.9 (C₆), 134.0 (C₂), 122.0 (C₅), 113.8 (C₃), 112.1 (C₁), 61.2 (C₈), 56.2 (C₁₀), 14.2 (C₉).

Step 3: An oven dried round bottom flask equipped with a stirrer bar was charged with ethyl 5-bromo-2-methoxybenzoate from step 2 (3.75 g, 14.5 mmol), Pd(dppf)Cl₂ (1.06 g, 1.45 mmol), bispinacolatodiboron (5.54 g, 21.8 mmol) and potassium acetate (4.27 g, 43.5 mmol) in 1,4-dioxane (73 mL). The flask was purge with nitrogen three times and the reaction mixture sparged with nitrogen for 5 minutes. The resulting purged suspension was placed in a preheated oil bath at 105 °C and stirred for 14 hours. The reaction was cooled to room temperature and filtered through a pad of Celite® and the mother liquors concentrated *in vacuo*. The crude material was purified by flash column chromatography (0-20% ethyl acetate in petroleum ether 40–60) to give the titled compound as a light brown solid (5.16 g, 16.9 mmol, 86%).

¹H NMR (500 MHz, DMSO-*d*₆) δ_H: 7.92 (d, *J* = 1.7, 1H, H₄), 7.80 (dd, *J* = 8.4, 1.8, 1H, H₈), 7.15 (d, *J* = 8.4, 1H, H₇), 4.25 (q, *J* = 7.1, 2H, H₁₀), 3.84 (s, 3H, H₁₂), 1.28 (s, 12H, H₁) overlapped with 1.28 (t, *J* = 7.1, 3H, H₁₁); **¹³C NMR** (100 MHz, (CDCl₃) δ_C: 165.4 (C₉), 160.7 (C₆), 139.7 (C₄), 136.9 (C₈), 120.0 (C₇), 119.4 (C₃), 83.7 (C₂), 60.4 (C₁₀), 55.8 (C₁₂), 24.6 (C₁), 14.2 (C₁₁); **¹¹B NMR** (128 MHz, DMSO-*d*₆) δ_B: 29.5; **HRMS** (ASAP) found [M+H]⁺ = 307.1721, C₁₆H₂₄BO₅ requires 307.1717; **m.p.**: 85–86 °C; IR 2975, 1725, 1603, 1570, 1353, 1255, 1228, 1106, 1076, 1023, 965, 853, 826, 663.

7.9. Chan-Lam Product Characterisation

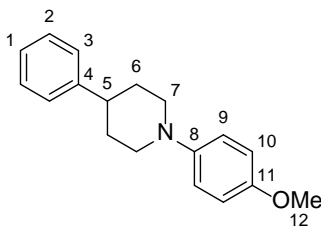
1,4-Diphenylpiperidine, 314



Prepared according to General Procedure 2. The crude mixture was purified by flash column chromatography (0% diethyl ether in petroleum ether to 3% diethyl ether in petroleum ether) to give the titled compound as a colourless crystalline powder (43.4 mg, 0.18 mmol, 61%).

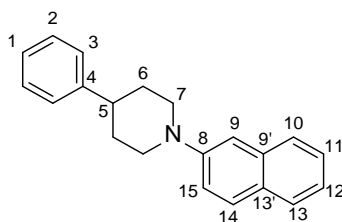
¹H NMR (400 MHz, (CDCl₃) δ_H: 7.37–7.21 (m, 7H, H₁₋₃₊₁₀), 7.02 (d, 8.0 Hz, 2H, H₉), 6.88 (t, 7.3 Hz, 1H, H₁₁), 3.84 (d, 12.4 Hz, H_{7a}), 2.84 (td, 12.4 Hz, 3.0 Hz, 2H, H_{7b}), 2.67 (m, 1H, H₅), 1.96 (m, 4H, H₆); **¹³C NMR** (100 MHz, (CDCl₃) δ_C: 151.9 (C₈), 146.1 (C₄), 129.1 (C₁₀), 128.5 (C₂), 126.9 (C₃), 126.3 (C₁), 119.5 (C₁₁), 116.7 (C₉), 50.6 (C₇), 42.5 (C₅), 33.4 (C₆); **m.p.** 86–87 °C; **HRMS** (NSI) found [M+H]⁺ = 238.1592, C₁₇H₁₉N requires 238.1590.

1-(4-Methoxyphenyl)-4-phenylpiperidine, 315



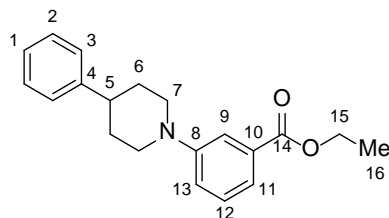
Prepared according to General Procedure 8. The crude mixture was purified by flash column chromatography (0% ethyl acetate in petroleum ether to 5% ethyl acetate in petroleum ether) to give the titled compound as a colourless powder (53.7 mg, 0.20 mmol, 67%).

¹H NMR (400 MHz, (CDCl₃) δ_H: 7.33 (t, *J* = 7.5, 2H, H₃), 7.25–7.30 (m, 2H, H₂), 7.23 (t, *J* = 7.5, 1H, H₁), 6.98 (d, *J* = 9.0, 2H, H₉), 6.86 (d, *J* = 9.0, 2H, H₈), 3.79 (s, 3H, H₁₂), 3.65 (d, *J* = 11.8, 2H, H_{7a}), 2.71–2.81 (m, 2H, H_{7b}), 2.58–2.66 (m, 1H, H₅), 1.90–2.00 (m, 4H, H₆); **¹³C NMR** (400 MHz, (CDCl₃) δ_C: 153.7 (C₇), 146.4 (C₁₁), 146.2 (C₄), 128.5 (C₃), 126.9 (C₂), 126.2 (C₁), 118.8 (C₈), 114.4 (C₉), 55.6 (C₁₂), 52.1 (C₇), 42.4 (C₅), 33.6 (C₆); **m.p.** 131–132 °C; **HRMS** (NSI) found [M+H]⁺ = 268.1698, C₁₈H₁₉F₃N requires 268.1696; **IR** (ν_{max} solid) / cm⁻¹: 2978, 1509, 1319, 1290, 1177, 1069, 1013, 918, 833, 793, 764, 702.

1-(Naphthalen-2-yl)-4-phenylpiperidine, 372

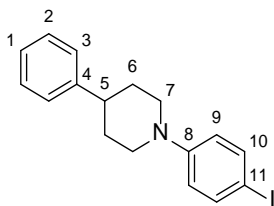
Prepared according to General Procedure 8. The crude mixture was purified by flash column chromatography (0% ethyl acetate in petroleum ether to 1% ethyl acetate in petroleum ether) to give the titled compound as a colourless powder (50.0 mg, 0.17 mmol, 58%).

¹H NMR (400 MHz, (CDCl₃) δ_H: 7.69–7.77 (m, 3H, H_{10,13,14}), 7.18–7.44 (m, 9H overlapped with CDCl₃ residual signal, H_{1-3,9,11,12,15}), 3.95 (d, *J* = 12.3, 2H, H_{7a}), 2.92 (td, *J* = 11.0, 3.5, 2H, H_{7b}), 2.72 (dt, *J* = 11.0, 3.5, 1H, H₅), 1.92–2.07 (m, 4H, H₆); **¹³C NMR** (125 MHz, (CDCl₃) δ_C: 149.6 (C₈), 146.0 (C₄), 134.7 (C_{9'}), 128.6 (C₁₄), 128.5 (C₃), 128.4 (C_{13'}), 127.4 (C₁₃), 126.9 (C₂), 126.7 (C₁₀), 126.3 (C₁), 126.2 (C₁₁), 123.2 (C₁₂), 120.1 (C₁₅), 110.6 (C₉), 50.8 (C₇), 42.6 (C₅), 33.3 (C₆); **HRMS** (NSI) found [M+H]⁺ = 288.1748, C₂₁H₂₁N requires 288.1747; **m.p.** 128–129 °C; **IR** (ν_{max} solid) / cm⁻¹: 2921, 1626, 1595, 1384, 1210, 1189, 1066, 955, 841, 756, 747, 698.

Ethyl 3-(4-phenylpiperidin-1-yl)benzoate, 369

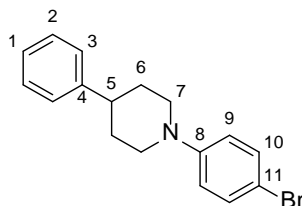
Prepared according to General Procedure 8. The crude mixture was purified by flash column chromatography (0% ethyl acetate in petroleum ether to 6% ethyl acetate in petroleum ether) to give the titled compound as a yellow oil (40.0 mg, 0.13 mmol, 42%).

¹H NMR (400 MHz, (CDCl₃) δ_H: 7.68 (app. t, *J* = 1.8, 1H, H₉), 7.54 (d, *J* = 7.6, 1H, H₁₂), 7.34 (m, 3H, H₂₊₁₁), 7.23 (m, 4H, H₁₊₃₊₁₃), 4.39 (d, *J* = 7.1, 2H, H₁₅), 3.88 (d, *J* = 12.4, 2H, H_{7a}), 2.87 (td, 18.2, *J* = 2.6, 2H, H_{7b}), 2.67 (tt, *J* = 17.6, 3.9, 1H, H₅), 1.94 (m, 4H, H₆), 1.41 (t, *J* = 7.14, 3H, H₁₆); **¹³C NMR** (125 MHz, (CDCl₃) δ_H: 166.9 (C₁₄), 151.6 (C₈), 145.8 (C₄), 131.3 (C₁₀), 129.0 (C₁₂), 128.5 (C₂), 126.9 (C₃), 126.4 (C₁), 120.9 (C₁₁), 120.4 (C₁₃), 117.2 (C₉), 60.9 (C₁₅), 50.3 (C₇), 42.4 (C₅), 33.2 (C₆), 14.4 (C₁₆); **HRMS** (NSI) found [M+H]⁺ = 310.1800, C₂₀H₂₄NO₂ requires 310.1807; **m.p.** 88 °C; **IR** (ν_{max} solid) / cm⁻¹: 2982, 1703, 1599, 1450, 1384, 1295, 1250, 1067, 992, 955, 874, 756, 700.

1-(4-Iodophenyl)-4-phenylpiperidine, 373

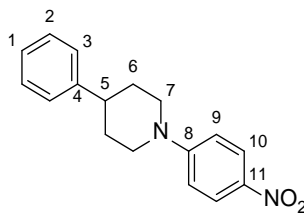
Prepared according to General Procedure 8. The crude mixture was purified by flash column chromatography (0% diethyl ether in petroleum ether to 5% diethyl ether in petroleum ether) to give the titled compound as an off white solid (44.7 mg, 0.12 mmol, 41%).

¹H NMR (400 MHz, (CDCl₃) δ_H: 7.52 (dt, *J* = 10.1, 2.6, 2H, H₁₀), 7.33 (t, 2H, H₂), 7.20–7.26 (m, 3H overlapped with CDCl₃ residual signal, H₁₊₃), 6.75 (dt, *J* = 10.1, 2.6, 2H, H₉), 3.78 (d, *J* = 12.3, 2H, H_{7a}), 2.83 (td, 12.3, 2.8, 2H, H_{7b}), 2.66 (tt, 17.8, 4.0, 1H, H₅), 1.81–2.00 (m, 4H, H₆). **¹³C NMR** (125 MHz, (CDCl₃) δ_C: 151.2 (C₈), 145.8 (C₄), 137.7 (C₁₀), 128.5 (C₂), 126.8 (C₃), 126.3 (C₁), 118.5 (C₉), 80.9 (C₁₁), 50.0 (C₇), 42.4 (C₅), 33.0 (C₆); **HRMS** (ASAP) found [M+H]⁺ = 364.0558, C₁₇H₁₉IN requires 364.0562; **m.p.** 127–128 °C; **IR** (ν_{max} solid) / cm⁻¹: 2972, 1579, 1484, 1380, 1212, 1066, 1011, 822, 756, 699.

1-(4-bromophenyl)-4-phenylpiperidine, 418

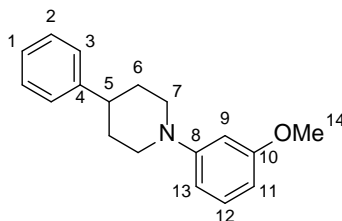
Prepared according to General Procedure 8. The crude mixture was purified by flash column chromatography (0–3% ethyl acetate in petroleum ether 40–60) to give the titled compound as an off white solid (74.8 mg, 0.24 mmol, 39%).

¹H NMR (400 MHz, (CDCl₃) δ_H: 7.30–7.38 (m, 4H, H₂₊₁₀), 7.20–7.28 (m, 3H overlapped with residual CDCl₃, H₁₊₃), 6.85 (d, *J* = 8.9, 2H, H₉), 3.77 (d, *J* = 12.3, 2H, H_{7a}), 2.82 (td, 12.3, 2.7, 2H, H_{7b}), 2.64 (tt, *J* = 17.6, 4.0, 1H, H₅), 1.82–2.01 (m, 4H, H₆); **¹³C NMR** (100 MHz, (CDCl₃) δ_C: 150.7 (C₈), 145.8 (C₄), 131.8 (C₁₀), 128.5 (C₂), 126.8 (C₃), 126.3 (C₁), 118.1 (C₉), 111.5 (C₁₁), 50.3 (C₇), 42.3 (C₅), 33.1 (C₆); **HRMS** (NSI) found [M+H]⁺: 316.0699, C₁₇H₁₉NBr requires 316.0695; **m.p.**: 130–131 °C; **IR** (ν_{max} solid) / cm⁻¹: 2937, 2813, 1584, 1489, 1385, 1215, 810, 757, 700.

1-(4-Nitrophenyl)-4-phenylpiperidine, 417

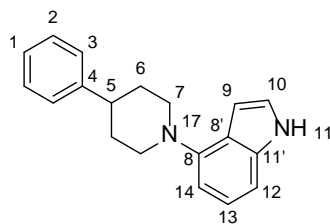
Prepared according to General Procedure 8. The crude mixture was purified by flash column chromatography (0-2% diethyl ether in hexanes) to give the titled compound as an off-white solid (20.2 mg, 0.07 mmol, 12%).

¹H NMR (500 MHz, (CDCl₃) δ_H: 8.13 (d, *J* = 9.3, 2H, H₁₀), 7.33 (t, *J* = 7.6, 2H, H₂), 7.21–7.25 (m, 3H, H_{1,3}), 6.87 (d, *J* = 9.3, 2H, H₉), 4.10 (d, *J* = 12.8, 2H, H_{7a}), 3.09 (td, *J* = 12.8, 2.3, 2H, H_{7b}), 2.79 (tt, *J* = 18.1, 3.6, 1H, H₅), 2.00 (d, *J* = 13.6, 2H, H_{6a}), 1.82 (dq, *J* = 12.8, 3.6, 2H, H_{6b}); **¹³C NMR** (125 MHz, (CDCl₃) δ_C: 154.7 (C₈), 145.0 (C₄), 137.9 (C₁₁), 128.6 (C₂), 126.7 (C₃), 126.6 (C₁), 126.1 (C₁₀), 112.6 (C₉), 48.2 (C₇), 42.4 (C₅), 32.7 (C₆); **HRMS** (NSI) found [M+H]⁺: 283.1442, C₁₇H₁₉N₂O₂ requires 283.1441; **m.p.**: 141–142 °C; **IR** (ν_{max} solid) / cm⁻¹: 2920, 2840, 1594, 1491, 1477, 1313, 1220, 1098, 828, 753, 692.

1-(3-Methoxyphenyl)-4-phenylpiperidine, 428

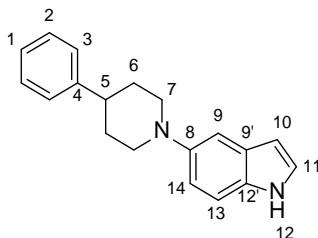
Prepared according to General Procedure 8. The crude mixture was purified by flash column chromatography (0-4% ethyl acetate in petroleum ether 40-60) to give the titled compound as an off white solid (101.4 mg, 0.38 mmol, 63%).

¹H NMR (400 MHz, (CDCl₃) δ_H: 7.34 (t, *J* = 7.7, 2H, H₂), 7.24–7.29 (m, 3H overlapped with residual CDCl₃, H₁₊₃), 7.20 (t, *J* = 8.2, 1H, H₁₂), 6.62 (dd, *J* = 8.2, 2.2, 1H, H₁₁), 6.55 (t, *J* = 2.2, 1H, H₉), 6.43 (dd, *J* = 8.2, 2.2, 1H, H₁₃), 3.79–3.87 (m, 5H, H_{7a+14}), 2.84 (td, *J* = 12.0, 3.1, 2H, H_{7b}), 2.62–2.72 (m, 1H, H₅), 1.85–2.01 (m, 4H, H₆); **¹³C NMR** (100 MHz, (CDCl₃) δ_C: 160.6 (C₁₀), 156.1 (C₈), 146.0 (C₄), 129.7 (C₁₂), 128.5 (C₂), 126.8 (C₃), 126.2 (C₁), 109.4 (C₁₁), 104.2 (C₁₃), 102.9 (C₉), 55.1 (C₁₄), 50.4 (C₇), 42.5 (C₅), 33.2 (C₆); **HRMS** (NSI) found [M+H]⁺: 268.1697, C₁₈H₂₂NO requires 268.1696; **m.p.**: 54–55 °C; **IR** (ν_{max} solid) / cm⁻¹: 2946, 2833, 2815, 1608, 1573, 1492, 1437, 1381, 1255, 1199, 1168, 1098, 1050, 825, 819, 752, 698, 682.

4-(4-Phenylpiperidin-1-yl)-1H-indole, 371

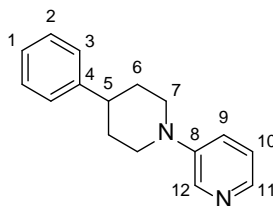
Prepared according to General Procedure 8. The crude mixture was purified by flash column chromatography (0% methanol in ethyl acetate to 10% methanol in ethyl acetate) to give the titled compound as an off white solid (12.4 mg, 0.05 mmol, 15%).

¹H NMR (500 MHz, (CDCl₃) δ_H: 8.15 (br. s, 1H, H₁₁), 7.30–7.39 (m, 4H, H_{2,3}), 7.22–7.26 (m, 1H, H₁), 7.15–7.18 (m, 1H, H₁₀), 7.13 (d, *J* = 7.7, 1H, H₁₃), 7.07 (d, *J* = 8.1, 1H, H₁₂), 6.65 (d, *J* = 7.3, 1H, H₁₄), 6.6 (t, *J* = 2.2, 1H, H₉), 3.87 (d, *J* = 12.1, 2H, H_{7a}), 2.88 (td, *J* = 12.1, 1.8, 2H, H_{7b}), 2.71 (tt, *J* = 17.8, 3.9, 1H, H₅), 1.98–2.14 (m, 4H, H₆); **¹³C NMR** (500 MHz, (CDCl₃) δ_C: 146.5 (C₅), 146.5 (C₈), 137.0 (C₁₁), 128.5 (C₂), 126.9 (C₃), 126.2 (C₁), 122.7 (C₁₃), 122.5 (C₁₀), 121.5 (C_{8'}), 106.8 (C₁₄), 105.5 (C₁₂), 101.4 (C₉), 52.5 (C₇), 43.0 (C₅), 33.9 (C₆); **m.p.**: 195 °C; **HRMS** (NSI) found [M+H]⁺: 277.1693, C₁₉H₂₁N₂ requires 277.1699; **IR** (ν_{max} solid) / cm⁻¹: 3392, 2928, 2804, 1602, 1577, 1499, 1380, 1222, 1087, 1062, 1031, 995, 898, 754, 727, 703.

5-(4-phenylpiperidin-1-yl)-1H-indole, 431

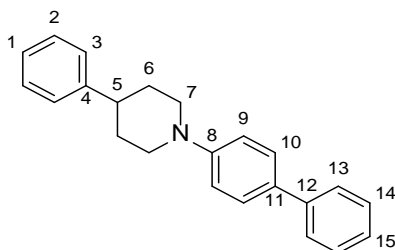
Prepared according to General Procedure 8. The crude mixture was purified by flash column chromatography (0-10% diethyl ether in 10% dichloromethane in petroleum ether 40-60) to give the titled compound as an off white solid (31.7 mg, 0.11 mmol, 19%).

¹H NMR (500 MHz, (CDCl₃) δ_H: 8.08 (br. s, 1H, H₁₂), 7.26–7.37 (m, 6H, H_{2,3,13,14}), 7.21–7.26 (m, 1H, H₁), 7.17 (t, *J* = 2.7, 1H, H₁₁), 7.07 (d, *J* = 8.3, 1H, H₉), 6.49 (s, 1H, H₁₀), 3.71 (d, *J* = 12.0, 2H, H_{7a}), 2.85 (d, *J* = 12.0, 2H, H_{7b}), 2.61, 2.71 (m, 1H, H₅), 1.95–2.11 (m, 4H, H₆); **¹³C NMR** (125 MHz, (CDCl₃) δ_C: 146.3 (C_{4,8}), 131.5 (C_{12'}), 128.4 (C₂), 128.3 (C_{9'}), 126.9 (C₃), 126.2 (C₁), 124.6 (C₁₁), 116.5 (C₉), 111.4 (C₁₃), 108.3 (C₁₄), 102.4 (C₁₀), 53.4 (C₇), 42.5 (C₅), 33.7 (C₆); **HRMS** (NSI) found [M+H]⁺: 277.1709, C₁₉H₂₁N₂ requires 277.1705; **m.p.**: 154 °C **IR** (ν_{max} solid) / cm⁻¹: 3372, 2920, 1600, 1572, 1473, 1382, 1215, 1137, 1016, 954, 858, 759, 723, 700.

3-(4-Phenylpiperidin-1-yl)pyridine, 370

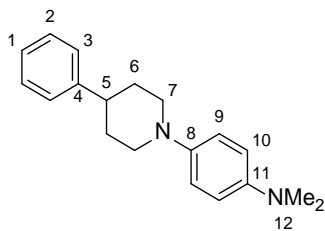
Prepared according to General Procedure 8. The crude mixture was purified by flash column chromatography (0% methanol in ethyl acetate to 10% methanol in ethyl acetate) to give the titled compound as an off white solid (43.7 mg, 0.18 mmol, 61%).

¹H NMR (400 MHz, (CDCl₃) δ_H: 8.37 (d, *J* = 2.2, 1H, H₁₁), 8.10 (d, *J* = 4.3, 1H, H₁₂), 7.33 (t, *J* = 7.5, 2H, H₂), 7.20–7.28 (m, 4H overlapped with residual CDCl₃ signal, 3H, H_{1,3,9}), 7.17 (dd, *J* = 8.4, 4.3, 1H, H₁₀), 3.83 (d, *J* = 12.2, 2H, H_{7a}), 2.88 (td, *J* = 12.2, 2.7, 2H, H_{7b}), 2.67 (tt, *J* = 17.9, 3.9, 1H, H₅), 1.83–2.02 (m, 4H, H₆); **¹³C NMR** (125 MHz, (CDCl₃) δ_C: 147.3 (C₈), 145.7 (C₄), 140.4 (C₁₁), 139.1 (C₁₂), 128.5 (C₂), 126.8 (C₃), 126.4 (C₁), 123.4 (C₁₀), 122.8 (C₉), 49.8 (C₇), 42.2 (C₅), 32.9 (C₆); **HRMS** (ASAP) found [M+H]⁺ = 239.1544, C₁₆H₁₉N₂ requires 239.1548; **m.p.** 79–80 °C; **IR** (ν_{max} solid) / cm⁻¹: 2943, 1580, 1485, 1420, 1215, 1144, 1069, 1012, 918, 799, 745, 698.

1-([1,1'-Biphenyl]-4-yl)-4-phenylpiperidine, 423

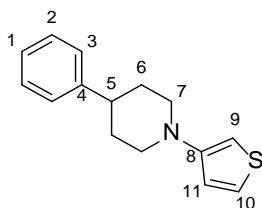
Prepared according to General Procedure 8. The crude mixture was purified by flash column chromatography (0-5% ethyl acetate in petroleum ether 40-60) to give the titled compound as an off white solid (51.1 mg, 0.16 mmol, 27%).

¹H NMR (400 MHz, (CDCl₃) δ_H: 7.58 (d, *J* = 7.5, 2H, H₁₃), 7.54 (d, *J* = 8.6, 2H, H₁₀), 7.41 (t, *J* = 7.5, 2H, H₁₄), 7.20–7.38 (m, 6H overlapped with residual CDCl₃, H₁₊₃₊₁₄₊₁₅), 7.06 (d, *J* = 8.6, 2H, H₉), 3.89 (d, *J* = 12.2, 2H, H_{7a}), 2.88 (td, *J* = 12.2, 2.7, 2H, H_{7b}), 2.64–2.75 (m, 1H, H₅), 1.86–2.05 (m, 4H, H₆); **¹³C NMR** (100 MHz, (CDCl₃) δ_C: 151.0 (C₈), 146.0 (C₅), 141.0 (C₁₂), 132.0 (C₁₁), 128.7 (C₁₄), 128.5 (C₂), 127.7 (C₁₀), 126.8 (C₃), 126.5 (C₁₃), 126.3 (C₁), 126.3 (C₁₅), 116.6 (C₉), 50.3 (C₇), 42.5 (C₅), 33.2 (C₆); **HRMS** (NSI) found [M+H]⁺: 314.1905, C₂₃H₂₄N requires 314.1903; **m.p.**: 156–157 °C; **IR** (ν_{max} solid) / cm⁻¹: 2935, 2918, 2832, 1603, 1494, 1447, 1388, 1306, 1119, 1073, 990, 938, 792, 762, 696.

***N,N*-dimethyl-4-(4-phenylpiperidin-1-yl)aniline, 424**

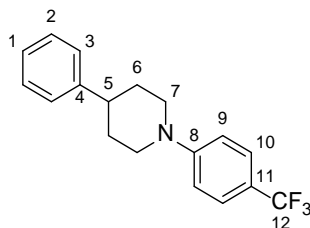
Prepared according to General Procedure 8. The crude mixture was purified by flash column chromatography (0% methanol in ethyl acetate to 10% methanol in ethyl acetate) to give the titled compound as an off white solid (22.0 mg, 0.08 mmol, 13%).

¹H NMR (500 MHz, (CDCl₃) δ_H: 7.32 (t, *J* = 7.7, 2H, H₂), 7.26–7.29 (m, 2H, H₃), 7.20–7.24 (m, 1H, H₁), 6.98 (br.s, 2H, H₉), 6.77 (br.s, 2H, H₁₀), 3.61 (br. s, 2H, H_{7a}), 2.89 (br. s, 6H, H₁₂), 2.74 (br. s, 2H, H_{7b}), 2.61 (pent, *J* = 7.8, 1H, H₁), 1.98 (br. s, 4H, H₆); **¹³C NMR** (125 MHz, (CDCl₃) δ_C: 146.3 (C₁), 145.6 (C₁₁), 144.0 (C₈), 128.4 (C₂), 126.9 (C₃), 126.2 (C₁), 119.0 (C₉), 114.4 (C₁₀), 52.4 (C₇), 42.5 (C₅), 41.5 (C₁₂), 33.7 (C₆); **HRMS** (NSI) found [M+H]⁺: 281.2012, C₁₉H₂₅N₂ requires 281.2012; **m.p.**: 123–124 °C; **IR** (ν_{max} solid) / cm⁻¹: 2938, 294, 22794, 1516, 1212, 808, 756, 696.

4-phenyl-1-(thiophen-3-yl)piperidine, 427

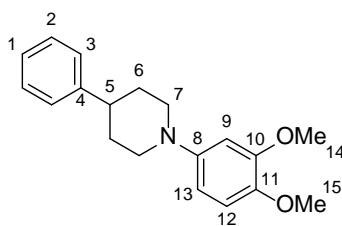
Prepared according to General Procedure 8. The crude mixture was purified by flash column chromatography (0% methanol in ethyl acetate to 10% methanol in ethyl acetate) to give the titled compound as an off white solid (20.2 mg, 0.08 mmol, 28%).

¹H NMR (500 MHz, (CDCl₃) δ_H: 7.33 (t, *J* = 7.5, 2H, H₂), 7.20–7.29 (m, 4H overlapped with residual CDCl₃ signal, H_{1,3,9}), 6.93 (dd, *J* = 5.2, 1.4, 1H, H₁₀), 6.23 (q, *J* = 1.4, 1H, H₁₁), 3.70 (d, *J* = 12.0, 2H, H_{7a}), 2.73–2.82 (m, 2H, H_{7b}), 2.59–2.68 (m, 1H, H₅), 1.87–2.00 (m, 4H, H₆); **¹³C NMR** (125 MHz, (CDCl₃) δ_C: 152.8 (C₈), 146.0 (C₄), 128.5 (C₂), 126.8 (C₃), 126.3 (C₁), 125.2 (C₉), 120.5 (C₁₀), 100.4 (C₁₁), 51.6 (C₇), 42.2 (C₅), 33.1 (C₆); **HRMS** (NSI) found [M+H]⁺: 244.1156, C₁₅H₁₈SN requires 244.1154; **m.p.**: 89–90 °C; **IR** (ν_{max} solid) / cm⁻¹: 2932, 2809, 1529, 1382, 960, 759, 699.

4-Phenyl-1-(4-(trifluoromethyl)phenyl)piperidine, 316

Prepared according to General Procedure 8. The crude mixture was purified by flash column chromatography (0% ethyl acetate in petroleum ether to 10% ethyl acetate in petroleum ether) to give the titled compound as a colourless powder (44.9 mg, 0.15 mmol, 49%).

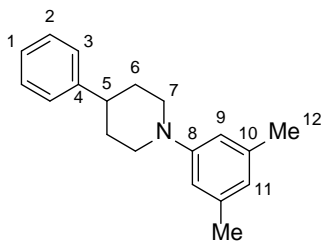
^1H NMR (400 MHz, CDCl_3) δ_{H} : 7.50 (d, 8.8 Hz, 2H, H_{10}), 7.34 (m, 2H, H_2), 7.24 (m, 3H, $\text{H}_{1,3}$), 6.99 (d, 8.8 Hz, 2H, H_9), 3.94 (app. dt, 12.6 Hz, 2.2 Hz, 2H, H_{7a}), 2.94 (td, 12.6 Hz, 2.2 Hz, H_{7b}), 2.73 (tt, 12.2 Hz, 3.9 Hz, 1H, H_5), 1.92 (m, 4H, H_6); **^{13}C NMR** (100 MHz, CDCl_3) δ_{C} : 153.6 (C_8), 145.8 (C_4), 128.7 (C_2), 126.9 (C_3), 126.5 (m, C_{3+10}), 120.1 (q, $J_{\text{C-F}} = 32.6$ Hz, C_{12}), 115.0 (C_9), 49.3 (C_7), 42.6 (C_5), 33.1 (C_6); **^{19}F NMR** (376 MHz, CDCl_3) δ_{F} : -64.0; **m.p.** 114–115 °C; **HRMS** (ASAP) found $[\text{M}+\text{H}]^+ = 306.1467$, $\text{C}_{18}\text{H}_{19}\text{F}_3\text{N}$ requires 306.1470; **IR** (ν_{max} solid) / cm^{-1} : 2978, 1612, 1521, 1453, 1388, 1323, 1140, 1096, 1011, 920, 825, 759, 701.

1-(3,4-Dimethoxyphenyl)-4-phenylpiperidine, 425

Prepared according to General Procedure 8. The crude mixture was purified by flash column chromatography (0–20% diethyl ether in petroleum ether 40–60) to give the titled compound as an off white solid (66.0 mg, 0.22 mmol, 37%).

^1H NMR (500 MHz, CDCl_3) δ_{H} : 7.33 (t, $J = 7.5$, 2H, H_2), 7.28 (d, $J = 7.5$, 2H, H_3), 7.23 (t, $J = 7.5$, 1H, H_1), 6.81 (d, $J = 8.7$, 1H, H_{12}), 6.65 (d, $J = 2.4$, 1H, H_9), 6.53 (dd, $J = 8.7$, 2.4, 1H, H_{13}), 3.89 (s, 3H, H_{15}), 3.85 (s, 3H, H_{14}), 3.66 (d, $J = 12.1$, 2H, H_{7a}), 2.77 (td, $J = 12.1$, 3.3, 2H, H_{7b}), 2.59–2.67 (m, 1H, H_5), 1.90–2.01 (m, 4H, H_6); **^{13}C NMR** (125 MHz, CDCl_3) δ_{C} : 149.4 (C_{10}), 147.0 (C_8), 146.1 (C_5), 143.5 (C_{11}), 128.5 (C_2), 126.8 (C_3), 126.3 (C_1), 111.9 (C_{12}), 108.4 (C_{13}), 103.6 (C_9), 56.3 (C_{14}), 55.8 (C_{15}), 52.2 (C_7), 42.4 (C_5), 33.6 (C_6); **m.p.**: 114–115 °C; **HRMS** (NSI) found $[\text{M}+\text{H}]^+ = 298.1798$, $\text{C}_{19}\text{H}_{24}\text{NO}_2$ requires 298.1802; **IR** (ν_{max} solid) / cm^{-1} : 2939, 2841, 2822, 1603, 1584, 1518, 1445, 1231, 1200, 1147, 1023, 963, 814, 753, 700.

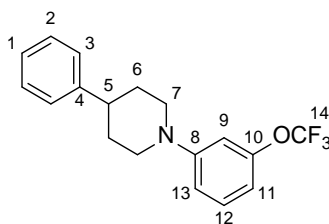
1-(3,5-Dimethylphenyl)-4-phenylpiperidine, 420



Prepared according to General Procedure 8. The crude mixture was purified by flash column chromatography (0-2% diethyl ether in petroleum ether 40-60) to give the titled compound as an off white solid (61.1 mg, 0.23 mmol, 38%).

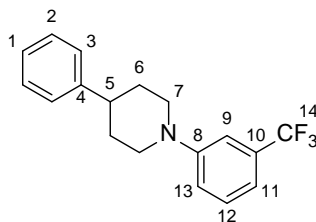
¹H NMR (400 MHz, (CDCl₃) δ_H: 7.33 (t, *J* = 7.3, 2H, H₂), 7.26–7.29 (m, 2H, H₃), 7.22 (t, *J* = 7.3, 1H, H₁), 6.64 (s, 2H, H₉), 6.54 (s, 1H, H₁₁), 3.80 (d, *J* = 12.0, 2H, H_{7a}), 2.80 (td, *J* = 12.0, 3.2, 2H, H_{7b}), 2.59–2.70 (m, 1H, H₅), 2.30 (s, 3H, H₁₂), 1.84–2.00 (m, 4H, H₆); **¹³C NMR** (100 MHz, (CDCl₃) δ_C: 152.0 (C₈), 146.2 (C₄), 138.5 (C₁₀), 128.5 (C₂), 126.9 (C₃), 126.2 (C₁), 121.5 (C₁₁), 114.7 (C₉), 50.7 (C₇), 42.6 (C₅), 33.4 (C₆), 21.7 (C₁₂); **HRMS** (NSI) found [M+H]⁺: 266.1906, C₁₉H₂₄N requires 266.1903; **m.p.**: 159–160 °C; **IR** (ν_{max} solid) / cm⁻¹: 2929, 2908, 2814, 1594, 1590, 1384, 1196, 994, 829, 758, 701.

4-phenyl-1-(3-(trifluoromethoxy)phenyl)piperidine, 426



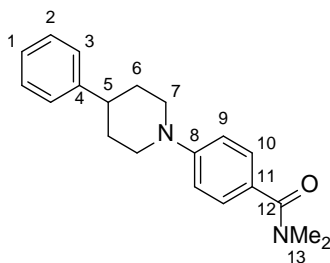
Prepared according to General Procedure 8. The crude mixture was purified by flash column chromatography (0-2% diethyl ether in petroleum ether 40-60) to give the titled compound as an off white solid (77.1 mg, 0.24 mmol, 40%).

¹H NMR (400 MHz, (CDCl₃) δ_H: 7.33 (t, *J* = 7.4, 2H, H₂), 7.21–7.28 (m, 3H overlapped with residual CDCl₃, H₁₊₃₊₁₂), 6.88 (dd, *J* = 8.4, 2.4, 1H, H₁₃), 6.78 (s, 1H, H₉), 6.68 (d, *J* = 8.4, 1H, H₁₁), 3.83 (dt, *J* = 12.3, 1.9, 2H, H_{7a}), 2.87 (td, *J* = 12.3, 2.7, 2H, H_{7b}), 2.67 (tt, *J* = 17.9, 3.8, 1H, H₅), 1.82–2.02 (m, 4H, H₆); **¹³C NMR** (100 MHz, (CDCl₃) δ_C: 152.9 (C₈), 150.3 (C₁₀), 145.7 (C₅), 129.9 (C₁₂), 128.5 (C₂), 126.8 (C₃), 126.4 (C₁), 120.5 (q, *J* = 256.6, C₁₄), 114.2 (C₁₃), 110.8 (C₁₁), 108.7 (C₉), 49.9 (C₇), 42.4 (C₅), 33.0 (C₆); **¹⁹F NMR** (376 MHz, (CDCl₃) δ_F: -58.5; **HRMS** (NSI) found [M+H]⁺: 322.1417, C₁₈H₁₉NOF₃ requires 322.1419; **m.p.**: 33–34 °C; **IR** (ν_{max} solid) / cm⁻¹: 2939, 2922, 2820, 1608, 1493, 1249, 1210, 1141, 993, 760, 700.

4-Phenyl-1-(3-(trifluoromethyl)phenyl)piperidine, 419

Prepared according to General Procedure 8. The crude mixture was purified by flash column chromatography (0% methanol in ethyl acetate to 10% methanol in ethyl acetate) to give the titled compound as an off white solid (55.8 mg, 0.18 mmol, 30%).

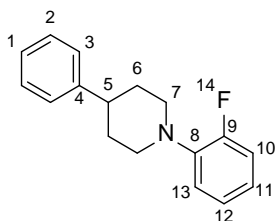
¹H NMR (400 MHz, (CDCl₃) δ_H: 7.31–7.38 (m, 3H, H₂₊₁₂), 7.25–7.29 (m, 2H overlapped with CDCl₃ residual signal, H₃), 7.21–7.25 (m, 1H, H₁), 7.18 (s, 1H, H₉), 7.13 (dd, *J* = 8.3, 2.0, 1H, H₁₃), 7.07 (d, *J* = 8.3, 1H, H₁₁), 3.86 (d, *J* = 12.3, 2H, H_{7a}), 2.89 (td, *J* = 12.3, 2.6, 2H, H_{7b}), 2.68 (tt, *J* = 18.0, 3.9, 1H, H₅), 1.83–2.04 (m, 4H, H₆); **¹³C NMR** (100 MHz, (CDCl₃) δ_C: 157.8 (C₈), 145.7 (C₄), 131.4 (q, *J* = 31.9, C₁₀), 129.5 (C₁₂), 128.5 (C₂), 126.8 (C₃), 126.4 (C₁), 124.4 (q, *J* = 272.5, C₁₄), 119.3 (q, *J* = 1.4, C₁₃), 115.5 (q, *J* = 3.8, C₁₁), 112.6 (q, *J* = 3.8, C₉), 50.0 (C₇), 42.3 (C₅), 33.1 (C₆); **¹⁹F NMR** (376 MHz, (CDCl₃) δ_F: -63.7; **HRMS** (NSI) found [M+H]⁺: 306.1464, C₁₈H₁₉F₃N requires 306.1464; **m.p.**: 75–76 °C; **IR** (ν_{max} solid) / cm⁻¹: 2936, 2831, 1603, 1494, 1446, 1306, 1163, 1152, 1119, 1098, 1073, 938, 792, 762, 696.

***N,N*-dimethyl-4-(4-phenylpiperidin-1-yl)benzamide, 438**

Prepared according to General Procedure 8. The crude mixture was purified by flash column chromatography (0-20% diethyl ether in dichloromethane) to give the titled compound as an off white solid (93.5 mg, 0.30 mmol, 51%).

¹H NMR (400 MHz, (CDCl₃) δ_H: 7.39 (d, *J* = 8.7, 2H, H₁₀), 7.32 (t, *J* = 7.5, 2H, H₂), 7.20–7.27 (m, 3H overlapped with CDCl₃ residual signal, H₁₊₃), 6.94 (d, *J* = 8.7, 2H, H₉), 3.90 (d, *J* = 12.5, 2H, H_{7a}), 3.07 (s, 6H, H₁₃), 2.89 (td, *J* = 12.5, 2.7, 2H, H_{7b}), 2.68 (tt, *J* = 18.0, 3.9, 1H, H₅), 1.81–2.01 (m, 4H, H₆); **¹³C NMR** (100 MHz, (CDCl₃) δ_C: 171.8 (C₁₂), 152.3 (C₈), 145.8 (C₄), 129.0 (C₁₀), 128.5 (C₂), 126.8 (C₃), 126.3 (C₁), 125.9 (C₁₁), 114.9 (C₉), 49.5 (C₇), 42.5 (C₅), 32.9 (C₆); **HRMS** (NSI) found [M+H]⁺: 309.1960, C₂₀H₂₅ON₂ requires 309.1961; **m.p.**: 112–113 °C; **IR** (ν_{max} solid) / cm⁻¹: 2923, 2822, 1608, 1836, 1086, 760, 701.

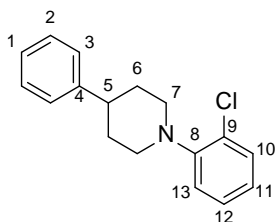
1-(2-Fluorophenyl)-4-phenylpiperidine, 434



Prepared according to General Procedure 8. The crude mixture was purified by flash column chromatography (0% methanol in ethyl acetate to 10% methanol in ethyl acetate) to give the titled compound as a colourless oil (9.6 mg, 0.04 mmol, 13%).

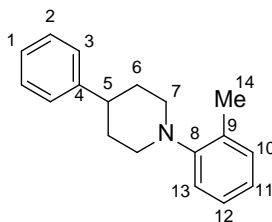
¹H NMR (500 MHz, (CDCl₃) δ_H: 7.21–7.35 (m, 5H overlapped with CDCl₃ residual signal, H₁₋₃), 6.99–7.10 (m, 3H, H_{10,12,13}), 6.91–6.97 (m, 1H, H₁₁), 3.58 (d, *J* = 11.8, 2H, H_{7a}), 2.79 (td, *J* = 17.2, 3.2, 2H, H_{7b}), 2.61–2.69 (m, 1H, H₅), 1.92–2.07 (m, 4H, H₆); **¹³C NMR** (125 MHz, (CDCl₃) δ_C: 155.9 (d, *J* = 245.8, C₉), 146.1 (C₄), 140.9 (d, *J* = 8.7, C₈), 128.5 (C₃), 126.9 (C₂), 126.4 (C₁), 124.4 (d, *J* = 3.7, C₁₀), 122.3 (d, *J* = 8.7, C₁₁), 119.3 (d, *J* = 3.7, C₁₂), 116.1 (d, *J* = 20.5, C₁₃), 51.9 (d, *J* = 3.7, C₇), 42.5 (C₅), 33.6 (C₆); **¹⁹F NMR** (376 MHz, (CDCl₃) δ_F: –122.7; **HRMS** (NSI) found [M+H]⁺: 256.1509, C₁₇H₁₉NF requires 256.1502; **IR** (ν_{max} solid) / cm⁻¹: 2930, 1498, 1453, 1217, 1144, 1102, 921, 751, 700.

1-(2-chlorophenyl)-4-phenylpiperidine, 433



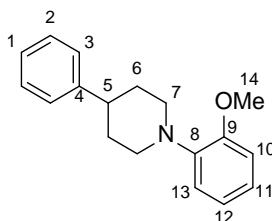
Prepared according to General Procedure 8. The crude mixture was purified by flash column chromatography (0% methanol in ethyl acetate to 10% methanol in ethyl acetate) to give the titled compound as a colourless oil (9.2 mg, 0.03 mmol, 11%).

¹H NMR (400 MHz, (CDCl₃) δ_H: 7.38 (dd, *J* = 7.9, 1.5, 1H, H₁₀), 7.29–7.36 (m, 4H, H₂₊₃), 7.20–7.25 (m, 2H, H₁₊₁₂), 7.11 (s, 1H, H₁₁), 6.97 (t, *J* = 7.6, 1H, H₁₃), 3.52 (d, *J* = 11.9, 2H, H_{7a}), 2.79 (s, 2H, H_{7b}), 2.65 (tt, *J* = 17.9, 4.0, 1H, H₅), 1.91–2.11 (m, 4H, H₆); **¹³C NMR** (125 MHz, (CDCl₃) δ_C: 150.2 (C₈), 146.2 (C₄), 130.6 (C₁₀), 128.9 (C₉), 128.5 (C₂), 127.5 (C₁₂), 126.9 (C₃), 126.2 (C₁), 123.4 (C₁₁), 120.6 (C₁₃), 52.6 (C₇), 42.5 (C₅), 33.7 (C₆); **HRMS** (NSI) found [M+H]⁺: 272.1204, C₁₇H₁₉NCl requires 272.1206; **IR** (ν_{max} solid) / cm⁻¹: 2932, 1586, 1478, 1398, 1274, 1172, 1061, 1012, 921, 886, 805, 758, 702, 689.

4-phenyl-1-(o-tolyl)piperidine, 432

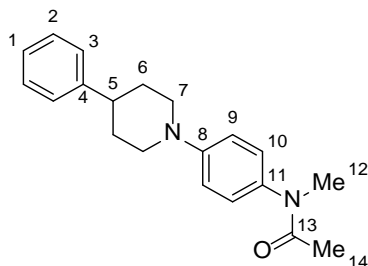
Prepared according to General Procedure 8. The crude mixture was purified by flash column chromatography (0% methanol in ethyl acetate to 10% methanol in ethyl acetate) to give the titled compound as an off white solid (55.4 mg, 0.22 mmol, 73%).

¹H NMR (400 MHz, (CDCl₃) δ_H: 7.28–7.39 (m, 4H, H_{2,3}), 7.16–7.26 (m, 3H overlapped with residual CDCl₃ signal, H_{1,10,12}), 7.07 (d, *J* = 7.6, 1H, H₁₃), 6.99 (t, *J* = 7.6, 1H, H₁₁), 3.25 (d, *J* = 11.5, 2H, H_{7a}), 2.73–2.85 (m, 2H, H_{7b}), 2.61–2.72 (m, 1H, H₅), 2.36 (s, 3H, H₁₄), 1.90–2.02 (m, 4H, H₆); **¹³C NMR** (100 MHz, (CDCl₃) δ_C: 152.4 (C₈), 146.5 (C₄), 132.7 (C₉), 131.0 (C₁₂), 128.4 (C₂), 126.9 (C₃), 126.4 (C₁), 126.1 (C₁₀), 122.8 (C₁₁), 119.0 (C₁₃), 53.0 (C₇), 42.6 (C₅), 34.1 (C₆), 17.9 (C₁₄); **HRMS** (NSI) found [M+H]⁺: 252.1747, C₁₈H₂₂N requires 252.1747; **m.p.**: 133–134 °C; **IR** (ν_{max} solid) / cm⁻¹: 2925, 1597, 1490, 1450, 1318, 1260, 1209, 1104, 1014, 923, 907.

1-(2-methoxyphenyl)-4-phenylpiperidine, 435

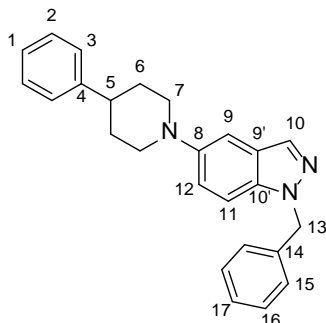
Prepared according to General Procedure 8. The crude mixture was purified by flash column chromatography (0% methanol in ethyl acetate to 10% methanol in ethyl acetate) to give the titled compound as an off white solid (70.5 mg, 0.26 mmol, 88%).

¹H NMR (500 MHz, (CDCl₃) δ_H: 7.29–7.38 (m, 4H, H₂₊₃), 7.20–7.27 (m, 1H, H₁), 6.87–7.06 (m, 4H, H₁₀₋₁₃), 3.9 (s, 3H, H₁₄), 3.63 (d, *J* = 11.6, 2H, H_{7a}), 2.61–2.77 (m, 3H, H_{5+7b}), 1.91–2.16 (m, 4H, H₆); **¹³C NMR** (125 MHz, (CDCl₃) δ_C: 152.3 (C₈), 146.5 (C₄), 142.3 (C₉), 128.4 (C₃), 126.9 (C₂), 126.1 (C₁), 122.7 (C₁₁), 120.9 (C₁₃), 118.4 (C₁₂), 111.0 (C₁₀), 55.3 (C₁₄), 52.0 (C₇), 42.7 (C₅), 33.8 (C₆); **HRMS** (ASAP) found [M+H]⁺: 268.1705, C₁₈H₂₂NO requires 268.1701; **m.p.**: 136–137 °C; **IR** (ν_{max} solid) / cm⁻¹: 2946, 1593, 1581, 1497, 1450, 1239, 1119, 1028, 1014, 921, 752, 703.

N-methyl-N-(4-(4-phenylpiperidin-1-yl)phenyl)acetamide, 421

Prepared according to General Procedure 8. The crude mixture was purified by flash column chromatography (0% methanol in ethyl acetate to 10% methanol in ethyl acetate) to give the titled compound as an off white solid (67.5 mg, 0.22 mmol, 73%).

¹H NMR (400 MHz, (CDCl₃) δ_H: 7.33 (t, *J* = 7.46, 2H, H₂), 7.20–7.28 (m, 3H, H₁₊₃), 7.06 (d, *J* = 8.8, 2H, H₁₀), 6.97 (d, *J* = 8.8, 2H, H₉), 3.84 (d, *J* = 12.3, 2H, H_{7a}), 3.23 (s, 3H, H₁₂), 2.86 (dt, *J* = 12.3, 3.8, 2H, H_{7b}), 2.66 (tt, *J* = 17.8, 3.8, 1H, H₅), 1.83–2.03 (m, 7H, H₆₊₁₄); **¹³C NMR** (100 MHz, (CDCl₃) δ_C: 171.1 (C₁₃), 150.8 (C₈), 145.7 (C₄), 135.9 (C₁₁), 128.5 (C₂), 127.6 (C₁₀), 126.8 (C₃), 126.3 (C₁), 116.8 (C₉), 50.1 (C₇), 42.3 (C₅), 37.2 (C₁₂), 33.1 (C₆), 22.3 (C₁₄); **HRMS** (ASAP) found [M+H]⁺: 309.1966, C₂₀H₂₄N₂O requires 309.1967; **m.p.**: 210 °C (decomp) **IR** (ν_{max} solid) / cm⁻¹: 2945, 1652, 1508, **1387**, 1210, 1146, 918, 839, 753, 704.

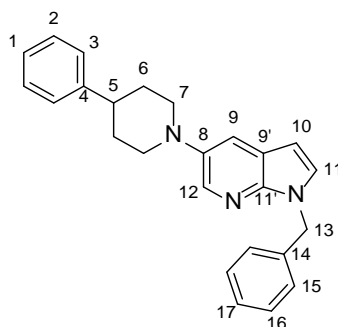
1-Benzyl-5-(4-phenylpiperidin-1-yl)-1*H*-indazole, 429

Prepared according to General Procedure 8. The crude mixture was purified by flash column chromatography (0-10% ethyl acetate in petroleum ether 40-60) to give the titled compound as an off white solid (154.3 mg, 0.42 mmol, 70%).

¹H NMR (400 MHz, (CDCl₃) δ_H: 7.94 (s, 1H, H₁₀), 7.26–7.37 (m, 8H, H_{2,3,11,16,17}), 7.17–7.26 (m, 5H, H_{1,9,12,15}), 5.57 (s, 2H, H₁₃), 3.70 (d, *J* = 12.0, 2H, H_{7a}), 2.76–2.86 (m, 2H, H_{7b}), 2.60–2.70 (m, 1H, H₅), 1.91–2.04 (m, 4H, H₆); **¹³C NMR** (100 MHz, (CDCl₃) δ_C: 147.1 (C₈), 146.1 (C₄), 137.1 (C₁₄), 135.7 (C_{10'}), 132.7 (C₁₀), 128.7 (C₁₆), 128.5 (C₂), 127.7 (C₁₇), 127.1 (C₁₅), 126.9 (C₃), 126.3 (C₁), 124.9 (C_{9'}), 122.0 (C₁₂), 109.8 (C₁₁), 106.2 (C₉), 53.1 (C₁₃), 52.7 (C₇), 42.4 (C₅), 33.7 (C₆); **HRMS** (NSI) found [M+H]⁺: 368.2117, C₂₅H₂₆N₃ requires 368.2121;

m.p.: 174–175 °C; **IR** (ν_{max} solid) / cm^{-1} : 2945, 2806, 1504, 1494, 1453, 1244, 1207, 1156, 854, 804, 758, 727, 697.

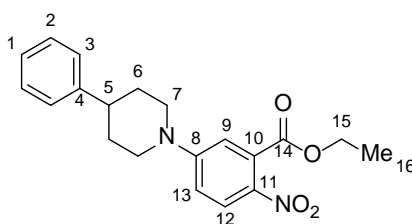
1-Benzyl-5-(4-phenylpiperidin-1-yl)-1*H*-pyrrolo[2,3-*b*]pyridine, 430



Prepared according to General Procedure 8. The crude mixture was purified by flash column chromatography (0% methanol in ethyl acetate to 10% methanol in ethyl acetate) to give the titled compound as an off white solid (132.3. mg, 0.36 mmol, 60%).

^1H NMR (400 MHz, CDCl_3) δ_{H} : 8.25 (d, $J = 2.4$, 1H, H_{11}), 7.56 (d, $J = 2.4$, 1H, H_{10}), 7.26–7.37 (m, 7H, $\text{H}_{2-3,15-17}$), 7.18–7.25 (m, 3H, H_{1+9+11}), 7.14 (d, $J = 3.5$, 1H, H_{12}), 6.40 (d, $J = 3.5$, 1H, H_9), 5.47 (s, 2H, H_{13}), 3.67 (d, $J = 11.8$, 2H, H_{7a}), 2.80 (m, 2H, H_{7b}), 2.59–2.71 (m, 1H, H_5), 1.95–2.10 (m, 4H, H_6); **^{13}C NMR** (100 MHz, CDCl_3) δ_{C} : 146.1 (C_4), 143.8 ($\text{C}_{11'}$), 143.5 (C_8), 138.0 (C_{14}), 137.8 (C_{11}), 128.6 (C_{16}), 128.5 (C_2), 128.2 (C_{12}), 127.5 (C_{17}), 127.4 (C_{15}), 126.9 (C_3), 126.3 (C_1), 120.3 ($\text{C}_{9'}$), 117.3 (C_{10}), 99.4 (C_9), 53.3 (C_7), 47.9 (C_{13}), 42.3 (C_5), 33.7 (C_6); **HRMS** (NSI) found $[\text{M}+\text{H}]^+$: 368.2118, $\text{C}_{25}\text{H}_{26}\text{N}_3$ requires 368.2121; **m.p.:** 106–107 °C; **IR** (ν_{max} solid) / cm^{-1} : 2933, 2802, 1490, 1449, 1222, 861, 737, 700.

Ethyl 2-nitro-5-(4-phenylpiperidin-1-yl)benzoate, 436

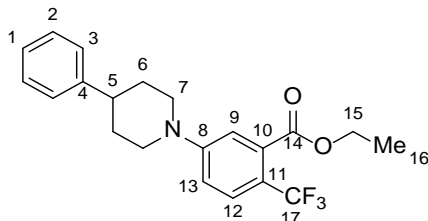


Prepared according to General Procedure 8. The crude mixture was purified by flash column chromatography (0% methanol in ethyl acetate to 10% methanol in ethyl acetate) to give the titled compound as an off white solid (8.5 mg, 0.02 mmol, 8%).

^1H NMR (500 MHz, CDCl_3) δ_{H} : 8.04 (d, $J = 9.7$, 2H, H_{12}), 7.33 (t, $J = 7.4$, 2H, H_2), 7.19–7.26 (m, 3H, $\text{H}_{1,3}$), 6.86–6.90 (m, 2H, $\text{H}_{9,13}$), 4.41 (q, $J = 7.1$, 2H, H_{15}), 4.09 (d, $J = 13.1$, 2H, H_{7a}), 3.10 (dt, $J = 13.1$, 2.6, 2H, H_{7b}), 2.79 (tt, $J = 18.3$, 3.7, 1H, H_5), 2.00 (d, $J = 13.1$, 2H, H_{6a}), 1.80 (dq, $J = 13.1$, 3.7, 2H, H_{6b}), 1.37 (t, $J = 7.1$, 3H, H_{16}); **^{13}C NMR** (125 MHz, CDCl_3) δ_{C} : 167.6 (C_{14}), 153.7 (C_8), 144.8 (C_4), 135.2 (C_{11}), 132.5 (C_{10}), 128.6 (C_2), 127.1 (C_{12}), 126.7

(C₃), 126.7 (C₁), 113.3 (C₉), 112.2 (C₁₃), 62.4 (C₁₅), 48.1 (C₇), 42.4 (C₆), 32.6 (C₆), 13.9 (C₁₆); **HRMS** (ASAP) found [M+H]⁺: 355.1658, C₂₀H₂₃N₂O₄ requires 355.1658; **IR** (ν_{max} solid) / cm⁻¹: 2920, 1731, 1600, 1579, 1480, 1318, 1218, 1137, 1006, 997, 814, 798, 752, 699.

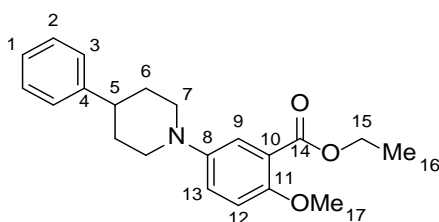
Ethyl 5-(4-phenylpiperidin-1-yl)-2-(trifluoromethyl)benzoate, 437



Prepared according to General Procedure 8. The crude mixture was purified by flash column chromatography (0% methanol in ethyl acetate to 10% methanol in ethyl acetate) to give the titled compound as an off white solid (19.2 mg, 0.05 mmol, 17%).

¹H NMR (500 MHz, (CDCl₃) δ_H: 7.56 (d, *J* = 8.8, 1H, H₁₂), 7.33 (t, *J* = 7.5, 2H, H₂), 7.20 (m, 4H, H_{1,3,9}), 7.00 (dd, *J* = 8.8, 2.6, 1H, H₁₃), 4.39 (q, *J* = 7.1, 2H, H₁₅), 3.97 (d, *J* = 12.8, 2H, H_{7a}), 2.97 (dt, *J* = 12.8, 2.4, 2H, H_{7b}), 2.72 (tt, *J* = 18.2, 3.7, 1H, H₅), 1.97 (d, *J* = 13.1, 2H, H_{6a}), 1.83 (dq, *J* = 13.0, 3.6, 2H, H_{6b}), 1.39 (t, *J* = 7.1, 3H, H₁₆); **¹³C NMR** (125 MHz, (CDCl₃) δ_C: 167.7 (C₁₄), 152.7 (C₈), 145.4 (C₄), 132.6 (q, *J* = 2.0, C₁₀), 128.6 (C₂), 128.1 (q, *J* = 5.4, C₁₂), 126.7 (C₃), 126.5 (C₁), 124.1 (q, *J* = 271.3, C₁₇), 117.2 (q, *J* = 32.7, C₁₁), 115.8 (C₉), 115.8 (C₁₃), 61.9 (C₁₅), 48.7 (C₇), 42.4 (C₅), 32.7 (C₆), 13.9 (C₁₆); **¹⁹F NMR** (376 MHz, (CDCl₃) δ_F: -58.8; **HRMS** (NSI) found [M+H]⁺: 387.1686, C₂₁H₂₃NO₂F₃ requires 387.1681; **IR** (ν_{max} solid) / cm⁻¹: 2931, 1727, 1606, 1313, 1100, 1032, 1010, 956, 817, 753, 698.

Ethyl 2-methoxy-5-(4-phenylpiperidin-1-yl)benzoate, 400



Prepared according to General Procedure 8. The crude mixture was purified by flash column chromatography (0-10% diethyl ether in petroleum ether 40-60) to give the titled compound as an off white solid (122.6 mg, 0.36 mmol, 60%).

¹H NMR (500 MHz, (CDCl₃) δ_H: 7.44 (d, *J* = 3.0, 2H, H₁₃), 7.33 (t, *J* = 7.2, 2H, H₂), 7.26–7.29 (m, 2H, H₃), 7.22 (t, *J* = 7.2, 1H, H₁), 7.13 (dd, *J* = 9.0, 3.0, 1H, H₁₃), 6.93 (d, *J* = 9.0, 1H, H₁₂), 4.37 (q, *J* = 7.1, 2H, H₁₅), 3.67 (d, *J* = 12.0, 2H, H_{7a}), 2.78 (td, *J* = 12.0, 3.2, 2H, H_{7b}), 2.57–2.67 (m, 1H, H₅), 1.86–2.02 (m, 4H, H₆), 1.39 (t, *J* = 7.1, 3H, H₁₆); **¹³C NMR** (125 MHz, (CDCl₃) δ_C: 166.5 (C₁₄), 153.2 (C₁₁), 146.0 (C₅), 145.7 (C₈), 128.5 (C₂), 126.8 (C₃), 126.3

(C₁), 122.6 (C₉), 120.8 (C₁₀), 120.3 (C₁₃), 113.5 (C₁₂), 60.8 (C₁₅), 56.6 (C₁₇), 51.7 (C₇), 42.3 (C₅), 33.4 (C₆), 14.3 (C₁₆); **HRMS** (NSI) found [M+H]⁺: 340.1909, C₂₁H₂₆NO₃ requires 340.1907; **m.p.**: 86–87 °C; **IR** (ν_{max} solid) / cm⁻¹: 2955, 2802, 1728, 1577, 1494, 1235, 1205, 1076, 1014, 813, 766, 704.

Chapter 8: Reaction Discovery Experimental

General Considerations

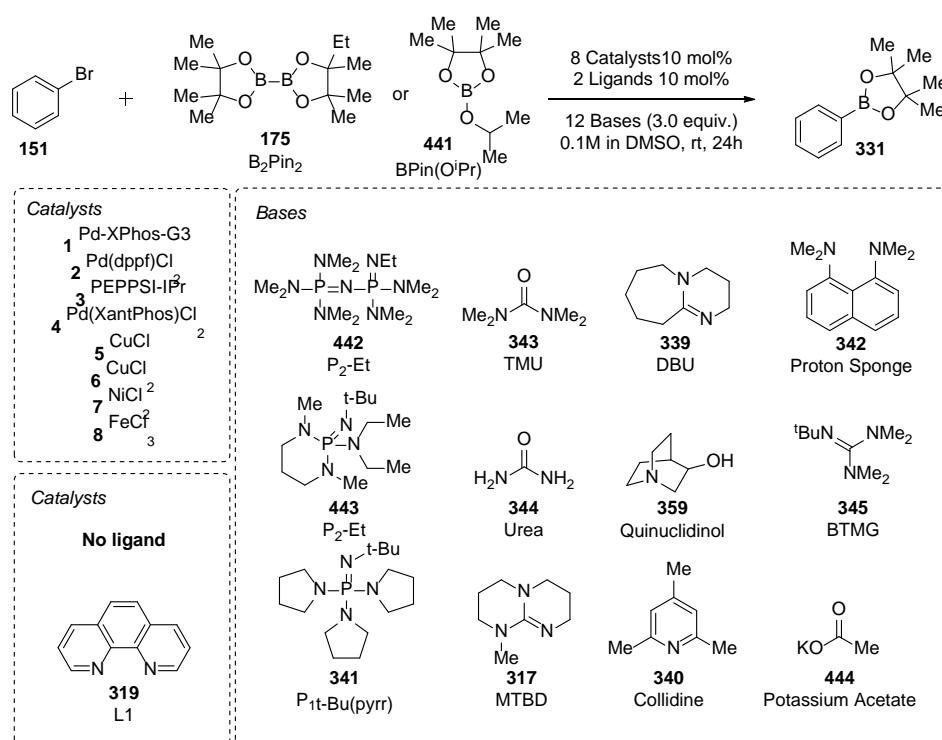
All general considerations are the same as those stated in Section 7.1.

HT-TLC assay

Reactions were analysed using the Mosquito[®] liquid handling robot and HT-TLC protocols 24-35. TLC-plates (silica gel 60 F254 pre-coated glass backed plates) were cut to specific dimensions (70mm x 140mm) and placed onto Falcon black low-base 1536-well plate (Cat No. 11927051). Two TLC-plates fitted onto one 1536-well plate and were secured using plastic pegs (prepared from 125 μ L pipette tips for the 125 μ L Viaflo pipette). The Mosquito dosed 1.0 μ L of reaction mixture onto the TLC-plates. Prepared TLC-plates were run in the corresponding mobile phase and visualised using ultraviolet radiation (254 nm) and/or an appropriate stain. Once new spots were identified, the associated reaction was located on the 1536-well reactor plate, the remaining mixture was aspirated using a Viaflo digital pipette (Integra, Cat. No. 4013, 125 μ L, multi-channel) and added into a low volume LCMS vial (PN: QMX V0054) topped up with acetonitrile. All samples were analysed on a Shimadzu GCMS.

8.1. Palladium Borylation

Procedure for 384 nanomolar scale reactions (2.5 μL volume) in one quarter of a 1536-well plate. Stock solutions of each component were prepared according to general procedure 1: **151** (0.2 M in DMSO), borylation reagent (**174** and **441**, 0.038 M in DMSO), organic base (**442**, **434**, **339**, **342**, **443**, **344**, **341**, **317**, **340**, **444**; 0.067M in DMSO), ligand (**319**, 0.005 M in DMSO), catalyst (C1-C8, 0.005 M in DMSO) using Spreadsheet 7. For each 1536-well plate experiment, each well was charged with the amount of stock solution stated in ‘Source plate loading’ column, using a digital air displacement pipette, such that enough solution was present to dose the corresponding reactor plate (Figure 61).



Scheme 59: Borylation reaction screening assessing 2 boronates, 8 catalysts, 2 ligands and 12 bases totalling 384 unique reaction conditions.

The Mosquito was used to transfer the following aliquot volumes: **151** was added in 250 nL, borylation reagent was added in 2000 nL (2×1000 nL), base was added in 750 nL, ligand was added in 1000 nL and catalyst added in 1000 nL resulting in a total reaction volume of 5.0 μL (Mosquito Protocol 22). When the catalyst had been added, the Mosquito mixed the reaction mixture together three times using the mix-dispense feature. The 1536-well reactor plate was then sealed with aluminium foil and placed under a heavy glass sheet for 24 hours.

Source plate layout

	1	2	3	4	5	6	7	8	9	10	11	12	13	14	15	16	17	18	19	20	21	22	23	24
A								L1	C2	C1	B12	B11	B10	B9	B8	B7	B6	B5	B4	B3	B2	B1	S1	R1
B								L1	C4	C3	B12	B11	B10	B9	B8	B7	B6	B5	B4	B3	B2	B1	S1	R1
C								L1	C6	C5	B12	B11	B10	B9	B8	B7	B6	B5	B4	B3	B2	B1	S1	R1
D								L1	C8	C7	B12	B11	B10	B9	B8	B7	B6	B5	B4	B3	B2	B1	S1	R1
E								L2	C2	C1	B12	B11	B10	B9	B8	B7	B6	B5	B4	B3	B2	B1	S1	R1
F								L2	C4	C3	B12	B11	B10	B9	B8	B7	B6	B5	B4	B3	B2	B1	S1	R1
G								L2	C6	C5	B12	B11	B10	B9	B8	B7	B6	B5	B4	B3	B2	B1	S1	R1
H								L2	C8	C7	B12	B11	B10	B9	B8	B7	B6	B5	B4	B3	B2	B1	S1	R1
I								L1	C2	C1	B12	B11	B10	B9	B8	B7	B6	B5	B4	B3	B2	B1	S2	R1
J								L1	C4	C3	B12	B11	B10	B9	B8	B7	B6	B5	B4	B3	B2	B1	S2	R1
K								L1	C6	C5	B12	B11	B10	B9	B8	B7	B6	B5	B4	B3	B2	B1	S2	R1
L								L1	C8	C7	B12	B11	B10	B9	B8	B7	B6	B5	B4	B3	B2	B1	S2	R1
M								L2	C2	C1	B12	B11	B10	B9	B8	B7	B6	B5	B4	B3	B2	B1	S2	R1
N								L2	C4	C3	B12	B11	B10	B9	B8	B7	B6	B5	B4	B3	B2	B1	S2	R1
O								L2	C6	C5	B12	B11	B10	B9	B8	B7	B6	B5	B4	B3	B2	B1	S2	R1
P								L2	C8	C7	B12	B11	B10	B9	B8	B7	B6	B5	B4	B3	B2	B1	S2	R1

Figure 61: Source plate for Palladium-catalysed borylation.

HT-TLC analysis

HT-TLC analysis was performed using Mosquito[®] protocol 24-35 spotting 1 μL of crude reaction mixture onto TLC plates, pegged into Falcon 1536-well plate using small, cut pipette tips. The TLC plates were developed using petroleum ether 40:60 and diethyl ether 8:2 mixture and visualised using a UV-vis lamp. Photos were taken using an iPhone camera.

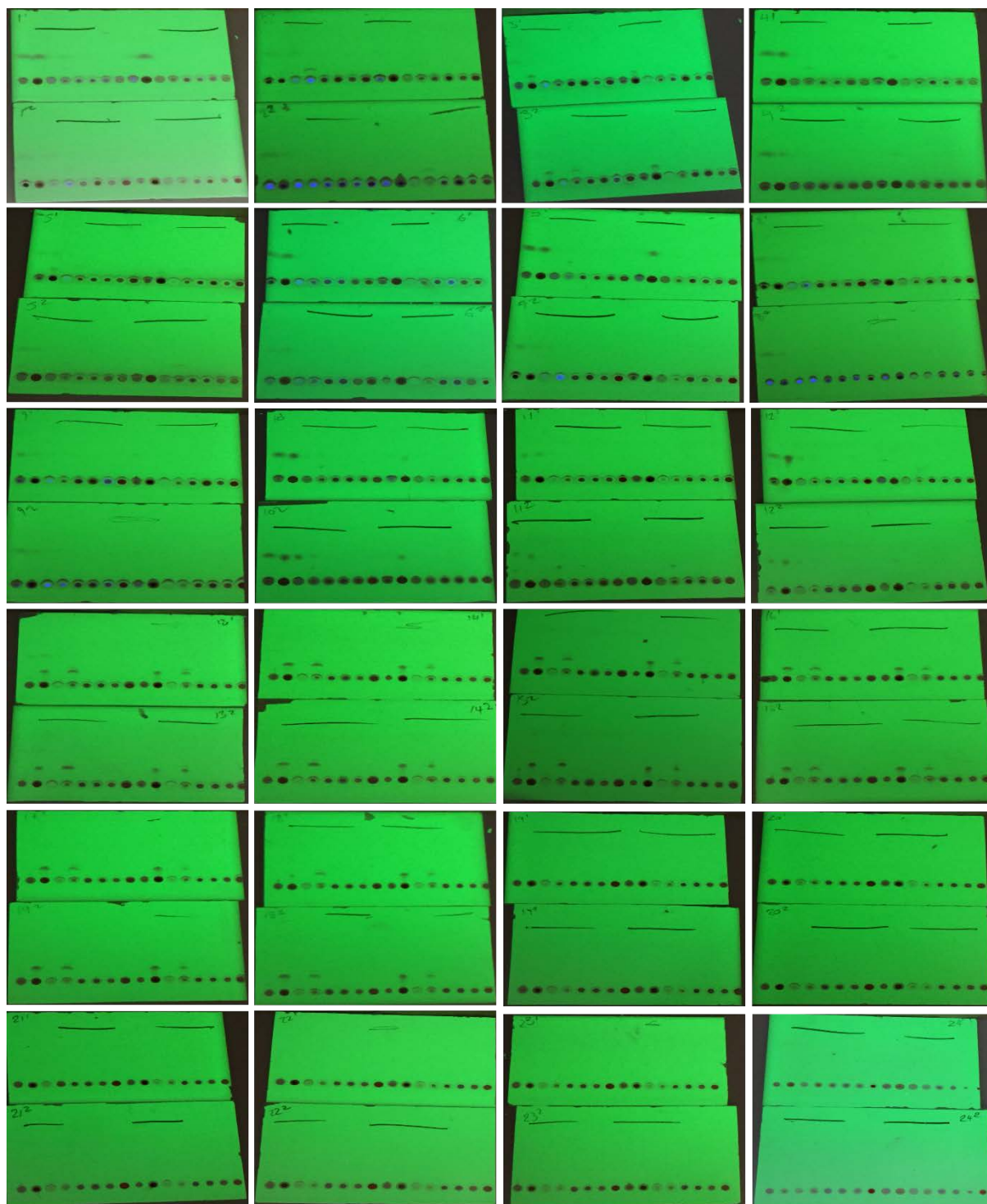
Any new spots identified from HT-TLC were subsequently aspirated from the 1536-well plate using an Integra multi-channel pipette and dosed into a microlitre analysis vial containing 300 μL of acetonitrile and analysed using GCMS.

PLATE 1536	# reagents 5	How much of plate? All	Input wells (column) 32	Scale L.R. (umol) 0.5	Final conc. Rwn (M) 0.1	Stand. Aliq. (uL) 1	Reaction parameters					Reactor tot vol (uL) 5
							Reagent	Compound	CAS	Cat No	FW (g/mol)	
constant?	R1	Iodobenzene	591-50-4	I137	204.01	1	0.5	1.02E-01		2.00		
(constant)	S1	B2pin2	73183-34-3	FDG-B-013	253.94	1.5	0.75	1.90E-01		2.00		
(constant)	S2	Bi(OiPr)3pin	61676-62-8	FDG-B-011	186.06	1.5	0.75	1.40E-01		2.00		
[k-constant, y-variable]	C1	Pc-Xphos-G3	1445085-55-1	Dave	846.45	0.1	0.05	4.23E-02		1.00		
	C2	Pd(ppf)Cl2	72287-26-4	Cat 085	731.70	0.1	0.05	3.66E-02		1.00		
	C3	PEPPSI-IPr	905459-27-0	Jaime	679.46	0.1	0.05	3.40E-02		1.00		
	C4	Pd(Xantphos)Cl2	05319-10-4	Aaron	755.94	0.1	0.05	3.78E-02		1.00		
	C5	CuCl	7758-89-6	Dessicator	99.00	0.1	0.05	4.95E-03		1.00		
	C6	CuCl2	7447-39-4	Dessicator	134.45	0.1	0.05	6.72E-03		1.00		
	C7	NiCl2	7718-54-9	IN 013	129.60	0.1	0.05	6.48E-03		1.00		
	C8	FeCl3	7705-08-0	il021	162.20	0.1	0.05	8.11E-03		1.00		
[k-constant, y-variable]	B1	P2Et	165535-45-5	Fridge	339.4	1	0.5	1.70E-01		0.75		
	B2	BEMP	98015-45-3	Fridge	274.39	1	0.5	1.37E-01		0.75		
	B3	PtBu(Pyrr)	161118-67-8	Fridge	312.43	1	0.5	1.56E-01		0.75		
	B4	TMU	652-22-4	Dave	116.16	1	0.5	5.81E-02		0.75		
	B5	Urea	57-13-6	Dave	60.06	1	0.5	3.00E-02		0.75		
	B6	MTBD	84030-20-6	Dave	153.22	1	0.5	7.66E-02		0.75		
	B7	DBU	6674-22-2	Dave	152.24	1	0.5	7.61E-02		0.75		
	B8	Quinuclidinol	1619-34-7	Dave	127.18	1	0.5	6.36E-02		0.75		
	B9	Collidine	108-75-8	C087	121.18	1	0.5	6.06E-02		0.75		
	B10	proton sponge	20734-58-1	Dave	214.31	1	0.5	1.07E-01		0.75		
	B11	BTMG	29166-72-1	Fridge	171.28	1	0.5	8.56E-02		0.75		
	B12	KOAc	127-08-2	iP037	98.14	1	0.5	4.91E-02		0.75		
Ligand	L1	DMSO	66-71-7	P228	180.21	0.1	0.05	0.00E+00		1.00		
	L2	Phen				0.1	0.05	9.01E-03		1.00		

Stock solution (mg/vial)	Stock solution (solvent/vial)	Stock solution (min vial)	Source (abs vol/well)	Source (rec vol/well)	Source (vol/well uL)	Liquid reagents (Vol/SS)	DMSO Top-up
163.2	400	346	12	22	25	89.5	310.5
133.3	1400	1382	96	173	87.5	X	1292.9
97.7	1400	1382	96	173			
8.5	200	173	48	86			
7.3	200	173	48	86			
6.8	200	173	48	86			
7.6	200	173	48	86			
1.0	200	173	48	86	100		X
1.3	200	173	48	86			
1.3	200	173	48	86			
1.6	200	173	48	86			
90.5	400	86	3	5		88.7	311.3
73.2	400	86	3	5		77.2	322.8
83.3	400	86	3	5		81.5	318.5
31.0	400	86	3	5		32.0	368.0
16.0	400	86	3	5		X	X
40.9	400	86	3	5		X	361.5
40.6	400	86	3	5	25.0	39.9	360.1
33.9	400	86	3	5		X	X
32.3	400	86	3	5		X	364.8
57.1	400	86	3	5		X	X
45.7	400	86	3	5		53.7	346.3
0.0	300	216	24	43	60	X	X
3.6	400	346	24	43	50	X	X

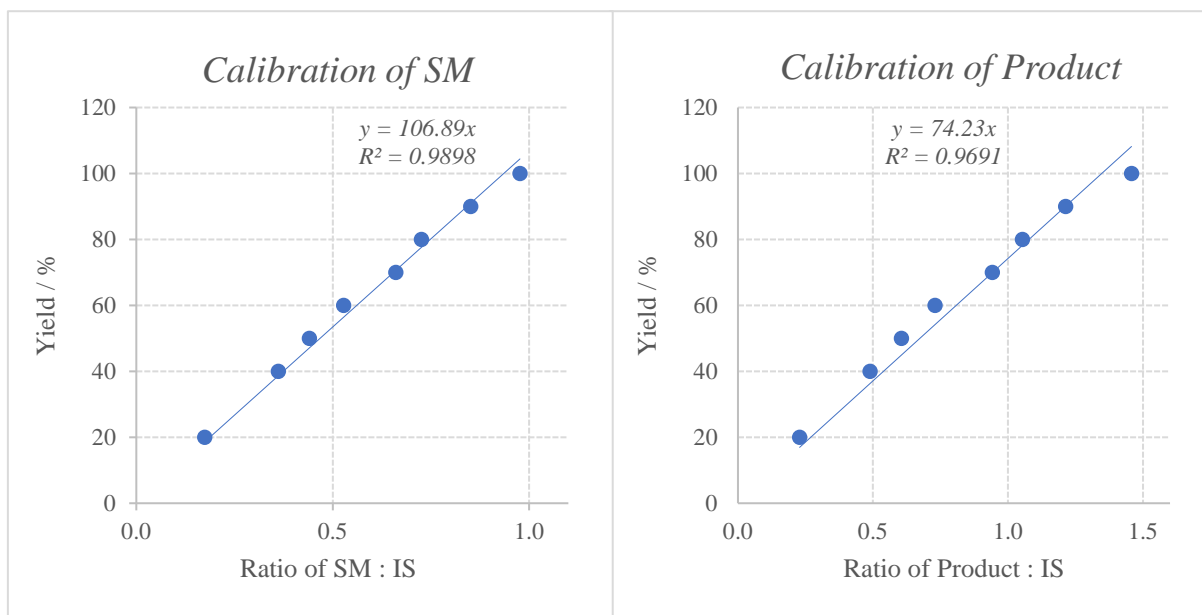
Spreadsheet 7: Excels spreadsheet used to prepare the reactor plate for the borylation of bromobenzene.

HT-TLC outcomes



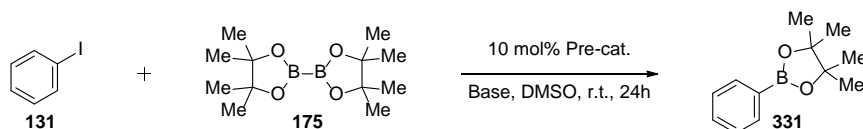
GC-MS calibration

Calibration was completed using dodecane as an internal standard. An GCMS vial was charged with 500 μL of 0.02M product **314** stock solution in ethyl acetate and 500 μL of 0.01M dodecane stock solution. The remaining 7 GCMS vials were charged with product stock solution in increments of 50 μL down to 100 μL . Each vial was charged with 500 μL of 0.01M dodecane stock solution and topped with the corresponding volume of ethyl acetate to achieve the correct concentration.



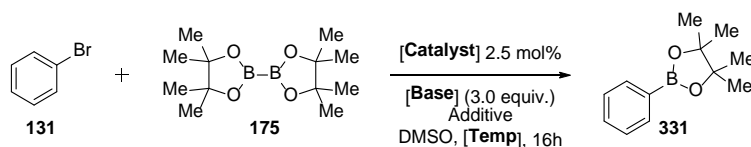
Entry	Yield / %	Dodecane TIC / a.u.	131 TIC / a.u.	331 TIC / a.u.	Ratio IS:SM	Ratio IS/Product
1	100	244023.6	238357.3	355620.4	1.0	1.5
2	90	248061.9	211168.7	300902.7	0.9	1.2
3	80	260849.6	189351.3	274668.0	0.7	1.1
4	70	251920.2	166511.9	237087.2	0.7	0.9
5	60	283666.1	149868.6	206854.8	0.5	0.7
6	50	284285.1	125396.3	171843.4	0.4	0.6
7	40	238573.7	86267.7	116569.0	0.4	0.5
8	20	286620.4	49939.1	65426.8	0.2	0.2

Batch scale optimisation



An oven-dried microwave vial equipped with a stir-bar was charged with borylating agent (0.45 mmol, 1.5 equiv.) and DMSO (600 μ L). In separate dram vials, solutions of iodobenzene, base, ligand and catalyst were prepared in DMSO and charged into the reaction flask in the following order: iodobenzene (0.3 mmol, 1.0 equiv. in 600 μ L DMSO), base (0.9 mmol, 3.0 equiv. in 600 μ L DMSO), ligand (0.03 mmol, 0.1 equiv. in 600 μ L DMSO) and catalyst (0.03 mmol, 0.1 equiv. in 600 μ L DMSO). The reaction mixture was sealed with a septum and stirred at the noted temperature for 24 hours. A GCMS vial charged with 100 μ L of crude reaction mixture, 500 μ L dodecane (0.01M in ethyl acetate) and topped up with 400 μ L of ethyl acetate. Each reaction was analysed using calibrated GC-FID.

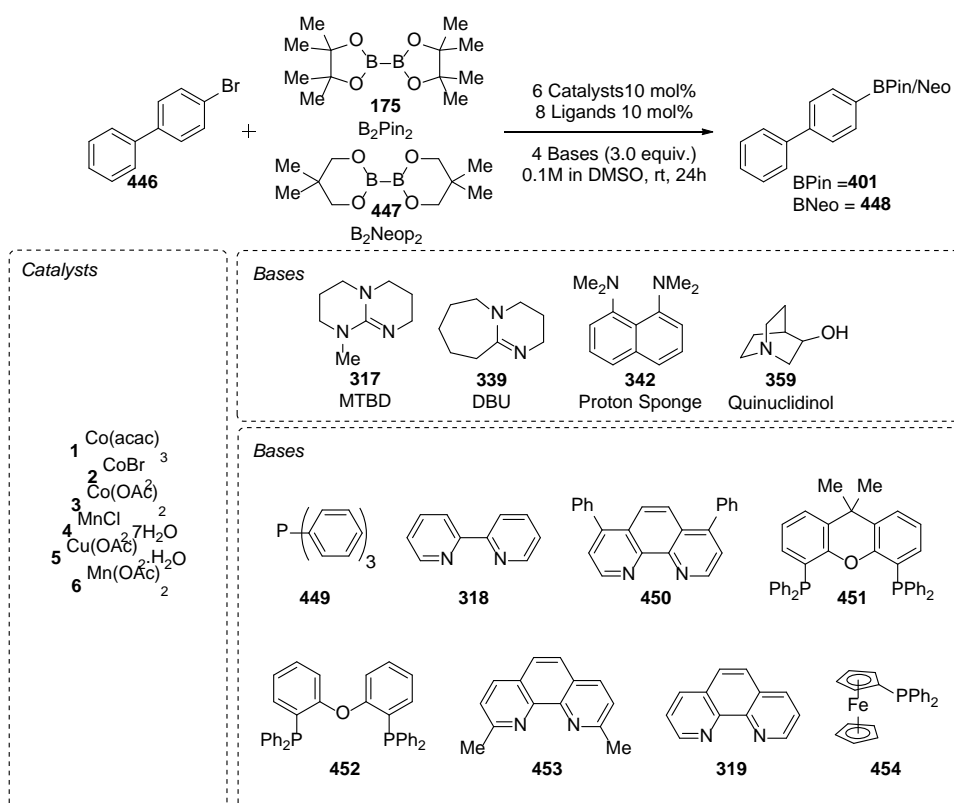
Selected Palladium-catalysed borylation results



Entry	Palladium source	Base	Additive	Temp. / °C	Yield of 131 / %
1	Pd-XPhos-G3	MTBD	-	25	14.8
2	Pd-XPhos-G3	BTMG	-	25	16.9
3	Pd-XPhos-G3	MTBD	-	50	23.8
4	Pd-XPhos-G3	BTMG	-	50	24.8
5	Pd-XPhos-G3	BTMG	5.0 eq. H ₂ O	50	13.7
6	Pd-XPhos-G3	BTMG	3.0 eq. KOAc	50	15.9
7	Pd-XPhos-G3	BTMG	3.0 eq. CsF	50	31.8

8.2. Cobalt Borylation

Procedure for 384 nanomolar scale reactions (5.0 μL volume) in one quarter of a 1536-well plate. Stock solutions of each component were prepared according to general procedure 1: **446** (0.2 M in DMSO), borylation reagent (**175** and **447**, 0.038 M in DMSO), organic base (**317**, **339**, **342**, **359**; 0.2M in DMSO), ligands (**449**, **318**, **450**, **451**, **452**, **453**, **319**, **454**; 0.0033M in DMSO), catalyst (C1-C6, 0.01 M in DMSO) using Spreadsheet 8. For each 1536-well plate experiment, each well was charged with the amount of stock solution stated in 'Source plate loading' column, using a digital air displacement pipette, such that enough solution was present to dose the corresponding reactor plate (Figure 62).



Scheme 60: Borylation reaction discovery using first row transition metals

The Mosquito was used to transfer the following aliquot volumes: **446** was added in 250 nL, borylation reagent was added in 2000 nL (2 × 1000 nL), base was added in 750 nL, ligand was added in 1500 nL (2 x 750 nL) and catalyst added in 500 nL resulting in a total reaction volume of 5.0 μL (Mosquito Protocol 23). When the catalyst had been added, the Mosquito mixed the reaction mixture together three times using the mix-dispense feature. The 1536-well reactor plate was then sealed with aluminium foil and placed under a heavy glass sheet for 24 hours.

Source Plate

	1	2	3	4	5	6	7	8	9	10	11	12	13	14	15	16	17	18	19	20	21	22	23	24
A													C6	C5	C4	C3	C2	C1	L2	L1	B1	S2	S1	R1
B													C6	C5	C4	C3	C2	C1	L4	L3	B1	S2	S1	R1
C													C6	C5	C4	C3	C2	C1	L6	L4	B1	S2	S1	R1
D													C6	C5	C4	C3	C2	C1	L8	L7	B1	S2	S1	R1
E													C6	C5	C4	C3	C2	C1	L2	L1	B2	S2	S1	R1
F													C6	C5	C4	C3	C2	C1	L4	L3	B2	S2	S1	R1
G													C6	C5	C4	C3	C2	C1	L6	L4	B2	S2	S1	R1
H													C6	C5	C4	C3	C2	C1	L8	L7	B2	S2	S1	R1
I													C6	C5	C4	C3	C2	C1	L2	L1	B3	S2	S1	R1
J													C6	C5	C4	C3	C2	C1	L4	L3	B3	S2	S1	R1
K													C6	C5	C4	C3	C2	C1	L6	L4	B3	S2	S1	R1
L													C6	C5	C4	C3	C2	C1	L8	L7	B3	S2	S1	R1
M													C6	C5	C4	C3	C2	C1	L2	L1	B4	S2	S1	R1
N													C6	C5	C4	C3	C2	C1	L4	L3	B4	S2	S1	R1
O													C6	C5	C4	C3	C2	C1	L6	L4	B4	S2	S1	R1
P													C6	C5	C4	C3	C2	C1	L8	L7	B4	S2	S1	R1

Figure 62: Source plate used to dose the 1536-well reactor plate.

HT-TLC analysis

HT-TLC analysis was performed using Mosquito[®] protocol 24-35 spotting 1 μ L of crude reaction mixture onto TLC plates, pegged into Falcon 1536-well plate using small, cut pipette tips. The TLC plates were developed using petroleum ether 40:60 and diethyl ether 8:2 mixture and visualised using a UV-vis lamp. Photos were taken using an iPhone camera.

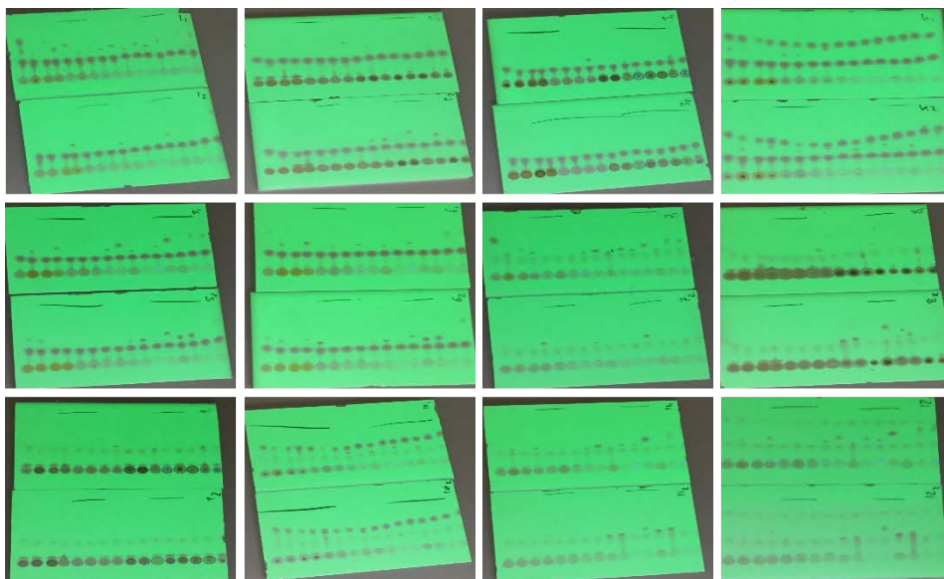
Any new spots identified from HT-TLC were subsequently aspirated from the 1536-well plate using an Integra multi-channel pipette and dosed into a microlitre analysis vial containing 300 μ L of acetonitrile and analysed using GCMS.

PLATE 1536	# reagents 5	How much of plate? All	input wells/column 32	Scale L.R. (umol) 0.5	Final conc. Rxn (M) 0.1	Stand. Aliq. (ul) 1	Reactor tot vol (ul) 5
constant? (constant)	Reagent	Compound	CAS	Cat No	FW (gMol-1)	Amount (ul/well)	mg per rxn
(constant)	R1	Biphenylbromide	92-66-0	Lev	233.10	0.5	1.17E-01
(constant)	S1	B2pin2	73183-34-3	B017	253.94	0.75	1.90E-01
Additive	S2	B2neop2	201733-56-4	FDG-N012	225.89	1.5	1.69E-01
	B1	MTBD	84030-20-6	M310	153.22	3	2.30E-01
	B2	proton sponge	20734-58-1	Jamie	214.31	1.5	3.21E-01
	B3	DBU	6674-22-2	D330	152.24	3	2.28E-01
	B4	quinuclidinol	1619-34-7	Lev	127.18	3	1.91E-01
(x-constant, y-variable)	C1	col(acac)3	21679-46-9	Ali	356.26	0.1	1.78E-02
	C2	CoBr2	7789-43-7	Ca1040	218.74	0.1	1.09E-02
	C3	Co(Oac)2	71-48-7	Ali	0.05	0.05	8.85E-03
	C4	MnCl2.7H2O	13446-34-9	IM017	197.91	0.1	9.90E-03
	C5	Cu(Oac)2.H2O	6046-93-1	IC001	199.65	0.1	9.98E-03
	C6	Mn(Oac)2	638-38-0	Ali	245.09	0.1	1.23E-02
(x-constant, y-variable)	L1	PPH3	603-35-0	T149	262.29	0.1	1.31E-02
	L2	bipy	366-18-7	HTE B462	156.18	0.1	7.81E-03
	L3	bathophen.	1662-01-7	David	332.40	0.1	1.66E-02
	L4	xantphos	161265-03-8	Cat phos033	578.62	0.1	2.89E-02
	L5	DPEphos	166330-10-5	cat phos030	538.55	0.1	2.69E-02
	L6	neocuproine	484-11-7	N006	208.26	0.1	1.04E-02
	L7	phenanthroline	66-71-7	P228	180.21	0.1	9.01E-03
	L8	dppf	12150-46-8	Phos 014	554.38	0.1	2.77E-02
							Solubility problems? Aliquot vol(ul)
							0.25 2.00 2.00 0.75 0.75 0.75 0.50 0.50 0.50 0.50 0.50 1.50 1.50 1.50 1.50 1.50 1.50 1.50

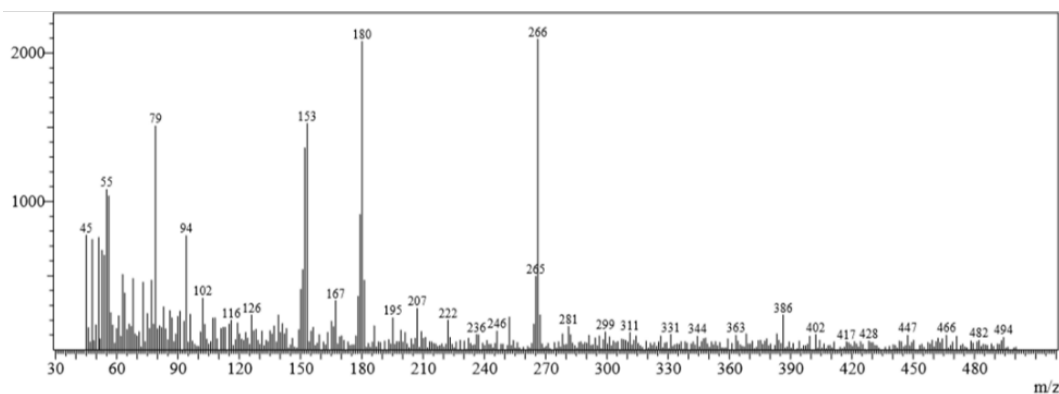
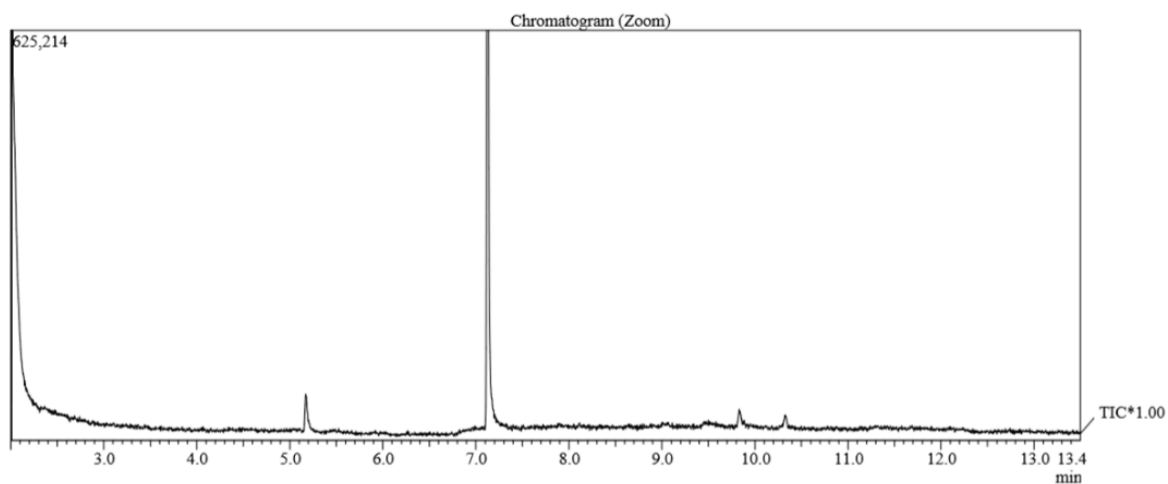
Stock solution (mg/vial)	Stock solution (solvent/vial)	Stock solution (min vol/vial)	Source (abs vol/well)	Source (rec vol/well)	Source plate loading (vol/well ul)	Liquid reagents (Vol/SS)	DMSO Top-up
186.5	400	173	6	11	25	X	X
66.7	700	691	24	43	43.75	X	X
59.3	700	691	24	43			
61.3	200	130	18	32	50	57.4	142.6
85.7	200	130	18	32		X	X
60.9	200	130	18	32		59.8	140.2
50.9	200	130	18	32		X	X
10.7	300	58	2	4			
6.6	300	58	2	4			
5.3	300	58	2	4	18.75	X	X
5.9	300	58	2	4			
6.0	300	58	2	4			
7.4	300	58	2	4			
3.5	400	130	18	32			
2.1	400	130	18	32			
4.4	400	130	18	32			
7.7	400	130	18	32	100.0		
7.2	400	130	18	32			
2.8	400	130	18	32			
2.4	400	130	18	32			
7.4	400	130	18	32			

Spreadsheet 8: Excels spreadsheet used to prepare the reactor plate for the borylation of bromobiphenyl.

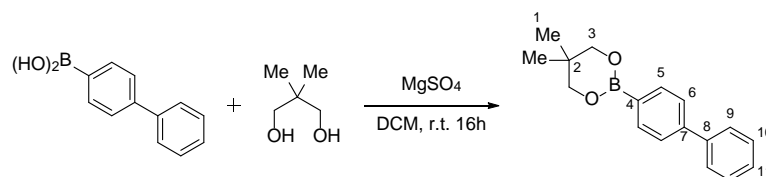
HT-TLC outcomes



Mass spectra of key peak



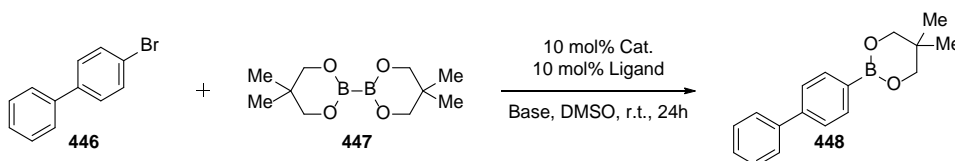
Preparation of biphenyl boronic ester standard



An oven dried round bottom flask equipped with a stirrer bar was charged with 4-biphenylboronic acid (3.00 g, 15.1 mmol), 2,2-dimethyl-1,3-propanediol (15.9 mmol, 1.05 equiv.) and magnesium sulfate (9.09g, 75.5 mmol) and dichloromethane (30.0 mL). The suspension was stirred for 16 hours and subsequently filtered. The mother liquors were concentrated *in vacuo* to give the titled compound as a white solid (3.33g, 12.5 mmol, 83%).

$^1\text{H NMR}$ (400 MHz, CDCl_3) δ_{H} : 7.95 (d, $J = 8.2$, 2H, H_5), 7.63–7.70 (m, 4H, H_{6+9}), 7.47–7.52 (m, 2H, H_{10}), 7.36–7.42 (m, 1H, H_{11}), 3.83 (s, 4H, H_3), 1.08 (s, 6H, H_1); $^{13}\text{C NMR}$ (100 MHz, CDCl_3) δ_{C} : 143.2 (C_8), 141.2 (C_7), 134.3 (C_5), 128.7 (C_{10}), 127.3 (C_6), 127.2 (C_9), 126.3 (C_{11}), 72.3 (C_3), 31.8 (C_2), 21.8 (C_1).

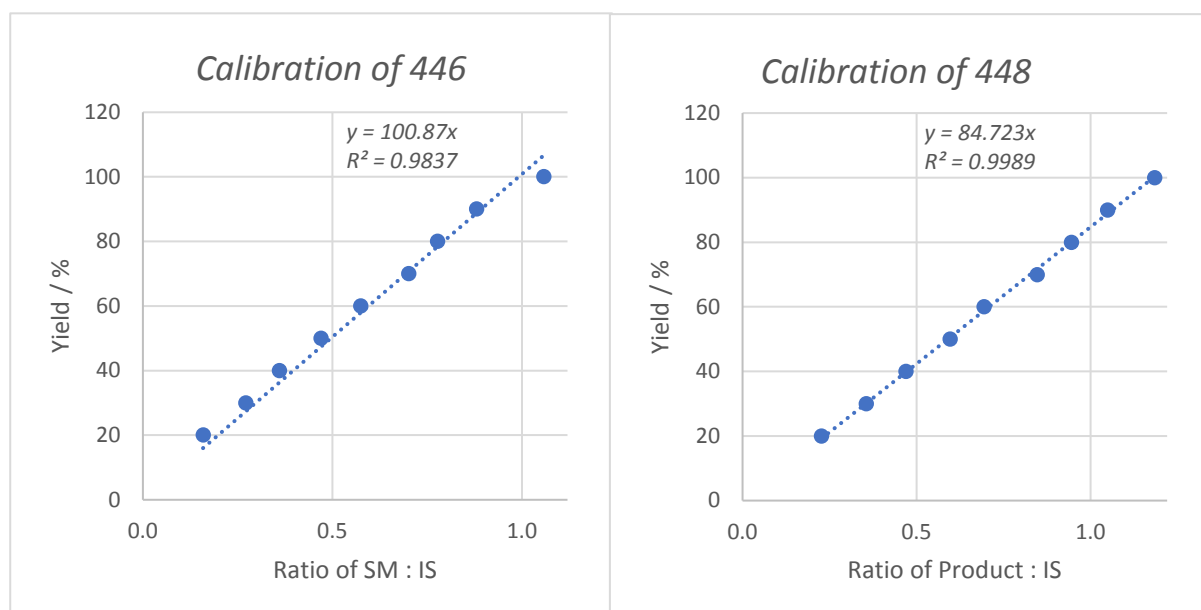
Batch scale optimisation



An oven-dried microwave vial equipped with a stir-bar was charged with borylating agent (0.45 mmol, 1.5 equiv.) and DMSO (600 μL). In separate dram vials, solutions of the bromobiphenyl, base, ligand and catalyst were prepared in DMSO and charged into the reaction flask in the following order: bromobiphenyl (0.3 mmol, 1.0 equiv. in 600 μL DMSO), base (0.9 mmol, 3.0 equiv. in 600 μL DMSO), ligand (0.03 mmol, 0.1 equiv. in 600 μL DMSO) and catalyst (0.03 mmol, 0.1 equiv. in 600 μL DMSO). The reaction mixture was sealed with a septum and stirred at room temperature for 24 hours. A GCMS vial charged with 100 μL of crude reaction mixture, 500 μL dodecane (0.01M in ethyl acetate) and topped up with 400 μL was analysed using calibrated GC-FID.

GC-MS calibration

Entry	Yield / %	Dodecane TIC / a.u.	446 TIC / a.u.	448 TIC / a.u.	Ratio Dodecane:446	Ratio Dodecane:448
1	100	238614.4	252271.3	282563.6	1.1	1.2
2	90	237921.4	209285.2	249659.7	0.9	1.0
3	80	251659.3	195502.1	237779.8	0.8	0.9
4	70	237921.5	166827.2	201456.0	0.7	0.8
5	60	246826.3	141829.4	171243.6	0.6	0.7
6	50	246362.9	115653.0	146895.9	0.5	0.6
7	40	238062.2	85551.7	111840.0	0.4	0.5
8	30	243492.8	65917.0	86634.8	0.3	0.4
9	20	251694.5	39903.5	57132.4	0.2	0.2

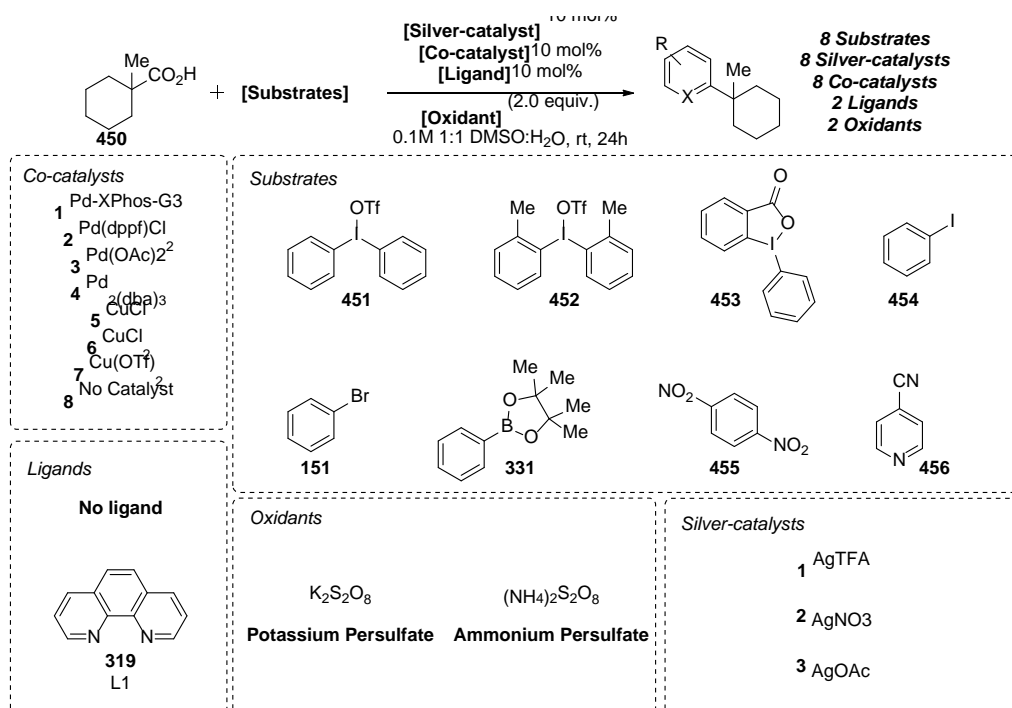


Selected Cobalt-catalysed borylation results

Entry	Variation from reaction discovery	GC-FID calibrated yield of 446 / %	GC-FID calibrated yield of 448 / %
1	None	73.4	7.7
2	No PPh ₃	52.1	14.5
3	With CsF (1.0 equiv.)	50.6	16.2
4	No PPh ₃ , with CsF (1.0 equiv.)	50.6	16.0
5	No PPh ₃ , 20 mol% DBU	60.5	8.4
6	No PPh ₃ , DMF rather than DMSO	63.7	8.3
7	No PPh ₃ , KOtBu rather than DBU	90.1	0.0
8	Iodobiphenyl rather than bromobiphenyl	-	21.0

8.3. Silver-Decarboxylation Minisci-Coupling

Procedure for 768 nanomolar scale reactions (3.0 μL volume) in one quarter of a 1536-well plate. Stock solutions of each component were prepared according to general procedure 1: **450** (0.12 M in DMSO), sp^2 coupling partner (**451**, **452**, **453**, **454**, **151**, **331**, **455**, **456**; 0.06 M in DMSO), silver-catalyst (Ag1-3, 0.006M in DMSO), inorganic oxidant (Ox1 and Ox2; 0.06M in DMSO), co-catalyst (C1-8, 0.006m in DMSO), ligand (**319**, 0.012M in DMSO) using Spreadsheet 9. For each 1536-well plate experiment, each well was charged with the amount of stock solution stated in ‘Source plate loading’ column, using a digital air displacement pipette, such that enough solution was present to dose the corresponding reactor plate (Figure 63).



Scheme 61: Silver-catalysed decarboxylation reaction discovery screening.

The Mosquito was used to transfer the following aliquot volumes: **450** was added in 250 nL, sp^2 coupling partner was added in 500 nL, silver catalyst was added in 500 nL, inorganic oxidant was added in 1000 nL, co-catalyst was added in 500 nL and ligand added in 250 nL resulting in a total reaction volume of 3.0 μL (Mosquito Protocol 24). When the catalyst had been added, the Mosquito mixed the reaction mixture together three times using the mix-dispense feature. The 1536-well reactor plate was then sealed with aluminium foil and placed under a heavy glass sheet for 24 hours.

Source plate

	1	2	3	4	5	6	7	8	9	10	11	12	13	14	15	16	17	18	19	20	21	22	23	24
A									Ox1	L1	Ag3	Ag2	Ag1	C2	C1	S8	S7	S6	S5	S4	S3	S2	S1	R1
B									Ox1	L1	Ag3	Ag2	Ag1	C4	C3	S8	S7	S6	S5	S4	S3	S2	S1	R1
C									Ox1	L1	Ag3	Ag2	Ag1	C6	C5	S8	S7	S6	S5	S4	S3	S2	S1	R1
D									Ox1	L1	Ag3	Ag2	Ag1	C8	C7	S8	S7	S6	S5	S4	S3	S2	S1	R1
E									Ox2	L1	Ag3	Ag2	Ag1	C2	C1	S8	S7	S6	S5	S4	S3	S2	S1	R1
F									Ox2	L1	Ag3	Ag2	Ag1	C4	C3	S8	S7	S6	S5	S4	S3	S2	S1	R1
G									Ox2	L1	Ag3	Ag2	Ag1	C6	C5	S8	S7	S6	S5	S4	S3	S2	S1	R1
H									Ox2	L1	Ag3	Ag2	Ag1	C8	C7	S8	S7	S6	S5	S4	S3	S2	S1	R1
I									Ox1	L2	Ag3	Ag2	Ag1	C2	C1	S8	S7	S6	S5	S4	S3	S2	S1	R1
J									Ox1	L2	Ag3	Ag2	Ag1	C4	C3	S8	S7	S6	S5	S4	S3	S2	S1	R1
K									Ox1	L2	Ag3	Ag2	Ag1	C6	C5	S8	S7	S6	S5	S4	S3	S2	S1	R1
L									Ox1	L2	Ag3	Ag2	Ag1	C8	C7	S8	S7	S6	S5	S4	S3	S2	S1	R1
M									Ox2	L2	Ag3	Ag2	Ag1	C2	C1	S8	S7	S6	S5	S4	S3	S2	S1	R1
N									Ox2	L2	Ag3	Ag2	Ag1	C4	C3	S8	S7	S6	S5	S4	S3	S2	S1	R1
O									Ox2	L2	Ag3	Ag2	Ag1	C6	C5	S8	S7	S6	S5	S4	S3	S2	S1	R1
P									Ox2	L2	Ag3	Ag2	Ag1	C8	C7	S8	S7	S6	S5	S4	S3	S2	S1	R1

Figure 63: Source plate used to prepare the 1536-well reactor plate.

HT-TLC analysis

HT-TLC analysis was performed using Mosquito[®] protocol 24-35 spotting 1 μ L of crude reaction mixture onto TLC plates, pegged into Falcon 1536-well plate using small, cut pipette tips. The TLC plates were developed using petroleum ether 40:60 and diethyl ether 8:2 mixture and visualised using a UV-vis lamp. Photos were taken using an iPhone camera.

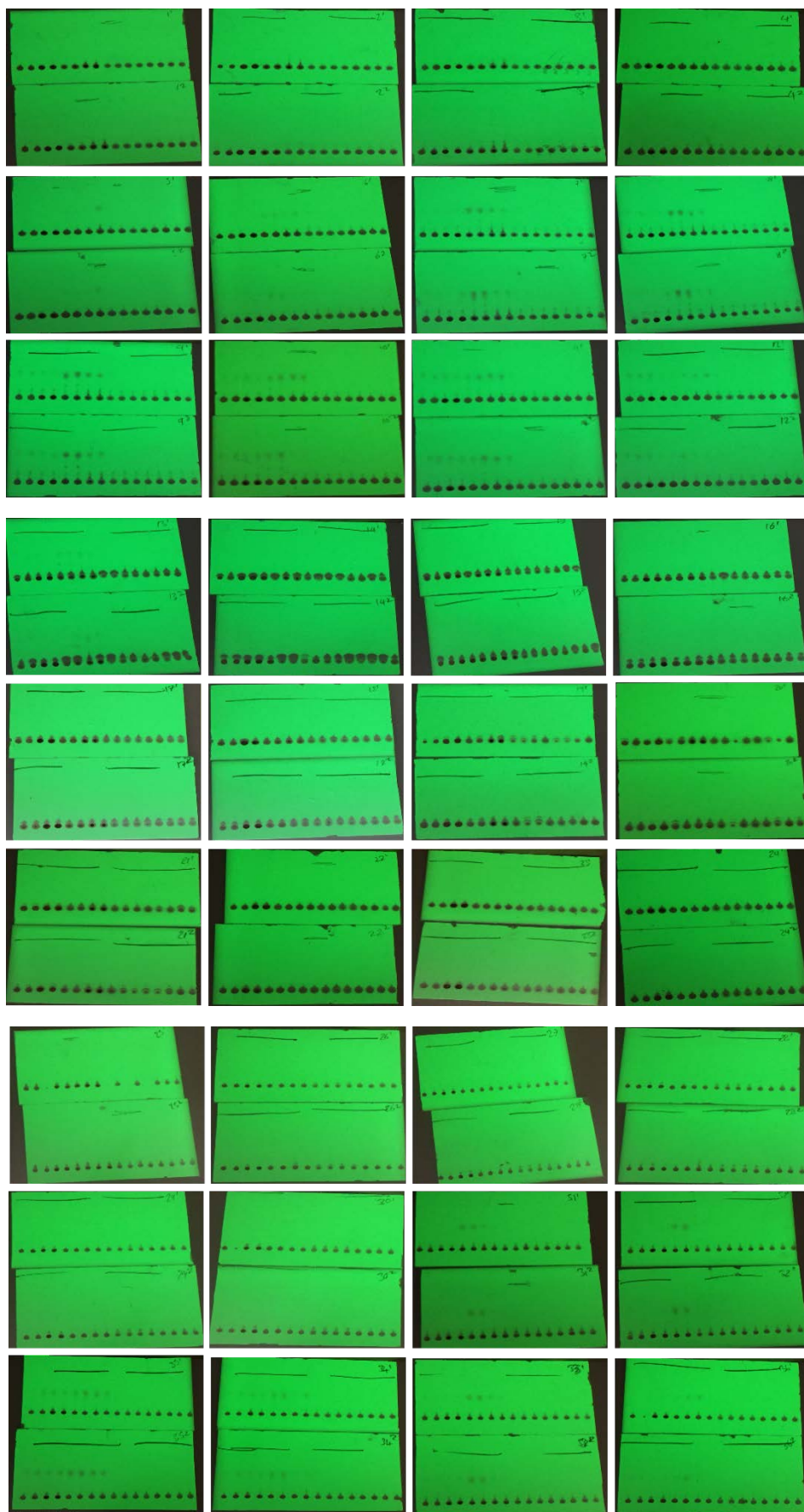
Any new spots identified from HT-TLC were subsequently aspirated from the 1536-well plate using an Integra multi-channel pipette and dosed into a microlitre analysis vial containing 300 μ L of acetonitrile and analysed using GCMS.

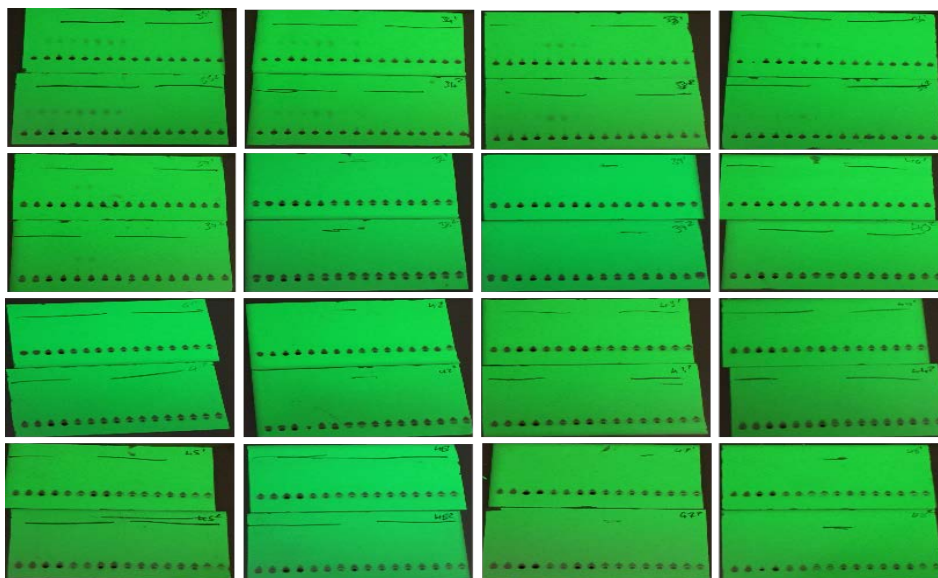
PLATE 1536	# reagents 6	How much of plate? All	input wells/column 32	Scale L.R. (umol) 0.3	Final conc. Rxn (M) 0.1	Stand. Aliq. (ul) 0.5	Daughter tot vol (ul) 3		
constant? (constant)	Reagent	Compound	CAS	Cat No	FW (gMol-1)	Equiv.	Amount (uMol)	mg per rxn	Solubility problems? Aliquot vol(ul)
	R1	1-methylcyclohexane-1-carboxylic acid	1123-25-7	All	142.198	1	0.3	4.27E-02	0.25
	S1	Diaryliodonium Triflate	66003-76-7	Dave	430.18	1	0.3	1.29E-01	0.50
	S2	Ditolyliodonium tetrafluoroborate	-	Daniel	395.974	1	0.3	1.19E-01	0.50
	S3	Cyclic iodonium salt	-	Dave	324.117	1	0.3	9.72E-02	0.50
	S4	Iodobenzene	591-50-4	I137	204.01	1	0.3	6.12E-02	0.50
	S5	Bromobenzene	108-86-1	B108	157.01	1	0.3	4.71E-02	0.50
	S6	Phenylboronic acid pinacol ester	24388-23-6	P009	204.07	1	0.3	6.12E-02	0.50
	S7	1,4-dinitrobenzene	100-25-4	Rachel	168.11	1	0.3	5.04E-02	0.50
	S8	4-cyanopyridine	100-48-1	C250	104.11	1	0.3	3.12E-02	0.50
(k-constant, y-variable)	Ag1	AgTFA	2966-50-9	IS 029	220.88	0.1	0.03	6.63E-03	0.50
	Ag2	AgNO3	7761-88-8	IS 019	169.87	0.1	0.03	5.10E-03	0.50
	Ag3	AgOAc	563-63-3	IS 087	166.91	0.1	0.03	5.01E-03	0.50
(k-variable, y-constant)	OX1	Potassium persulfate	7727-21-1	IP 029	270.32	2	0.6	1.62E-01	1.00
	OX2	Ammonium persulfate	7727-54-0	IA 009	228.2	2	0.6	1.37E-01	1.00
Catalysts	C1	Pd-Xphos-G3	1445085-55-1	dave	846.45	0.1	0.03	2.54E-02	0.50
	C2	Pd(dppf)Cl2	95464-05-4	cat 084	816.64	0.1	0.03	2.45E-02	0.50
	C3	Pd(OAc)2	3375-31-3	cat 001	224.15	0.1	0.03	6.72E-03	0.50
	C4	Pd2dba3	32005-36-0	cat 028	575.00	0.1	0.03	1.73E-02	0.50
	C5	CuCl	7758-89-6	Dessicator	99.00	0.1	0.03	2.97E-03	0.50
	C6	CuCl2	7447-39-4	Dessicator	134.45	0.1	0.03	4.03E-03	0.50
	C7	Cu(Otf)2	34946-82-2	Dessicator	361.68	0.1	0.03	1.09E-02	0.50
	C8	BLANK	-	-	-	0.1	0.03	-	0.50
Ligand	L1	dmso	66-71-7	P228	180.21	0.1	0.03	5.41E-03	0.25
	L2	Phen	-	-	-	0.1	0.03	-	0.25

Stock solution (mg/vial)	Stock solution (solvent/vial)	Stock solution (min vol/vial)	Source (abs vol/well)	Source (rec vol/well)	Source plate loading (vol/well ul)	Liquid reagents (Vol/SS)	DMSO Top-up
163.2	400	346	12	22	25	89.5	310.5
133.3	1400	1382	96	173	87.5	107.1	1292.9
97.7	1400	1382	96	173	87.5	107.1	1292.9
8.5	200	173	48	86			
7.3	200	173	48	86			
6.8	200	173	48	86			
7.6	200	173	48	86	100	X	X
1.0	200	173	48	86			
1.3	200	173	48	86			
1.3	200	173	48	86			
1.6	200	173	48	86			
90.5	400	86	3	5		88.7	311.3
73.2	400	86	3	5		77.2	322.8
83.3	400	86	3	5		81.5	318.5
31.0	400	86	3	5		32.0	368.0
16.0	400	86	3	5		X	X
40.9	400	86	3	5	25.0	38.5	361.5
40.6	400	86	3	5		39.9	360.1
33.9	400	86	3	5		X	X
32.3	400	86	3	5		35.2	364.8
57.1	400	86	3	5		X	X
45.7	400	86	3	5		53.7	346.3
26.2	400	86	3	5		X	X
0.0	300	216	24	43	60		
2.4	100	86	24	43	50		
2.6	200	173	24	43	50	X	X
3.6	400	346	24	43	50		
4.3	400	346	24	43	50		

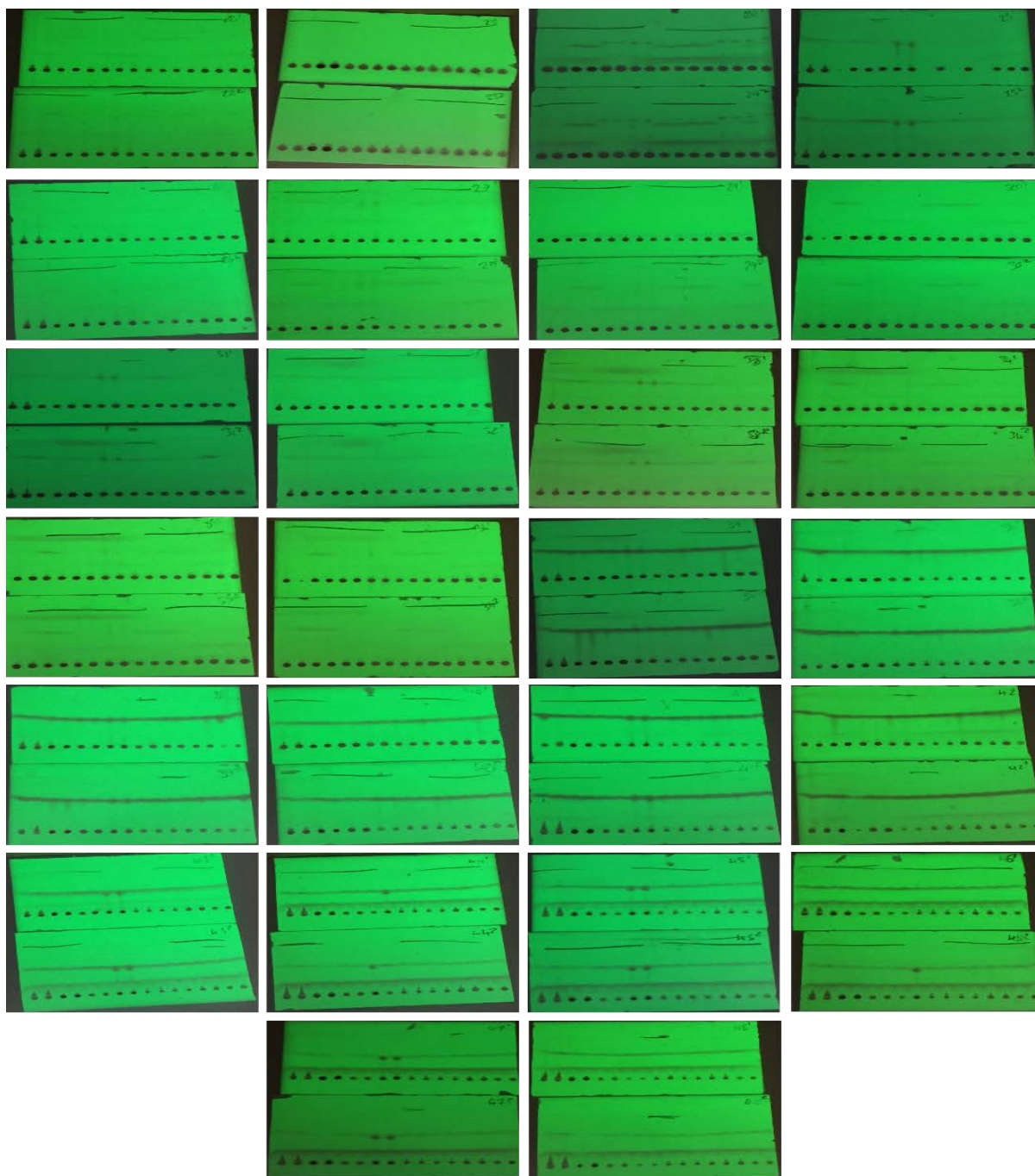
Spreadsheet 9: Excel spreadsheet used to prepare the reactor plate for the alkylation of various sp² substrates.

HT-TLC outcomes – Plate runs using 10% ethyl acetate in petroleum ether 40:60.

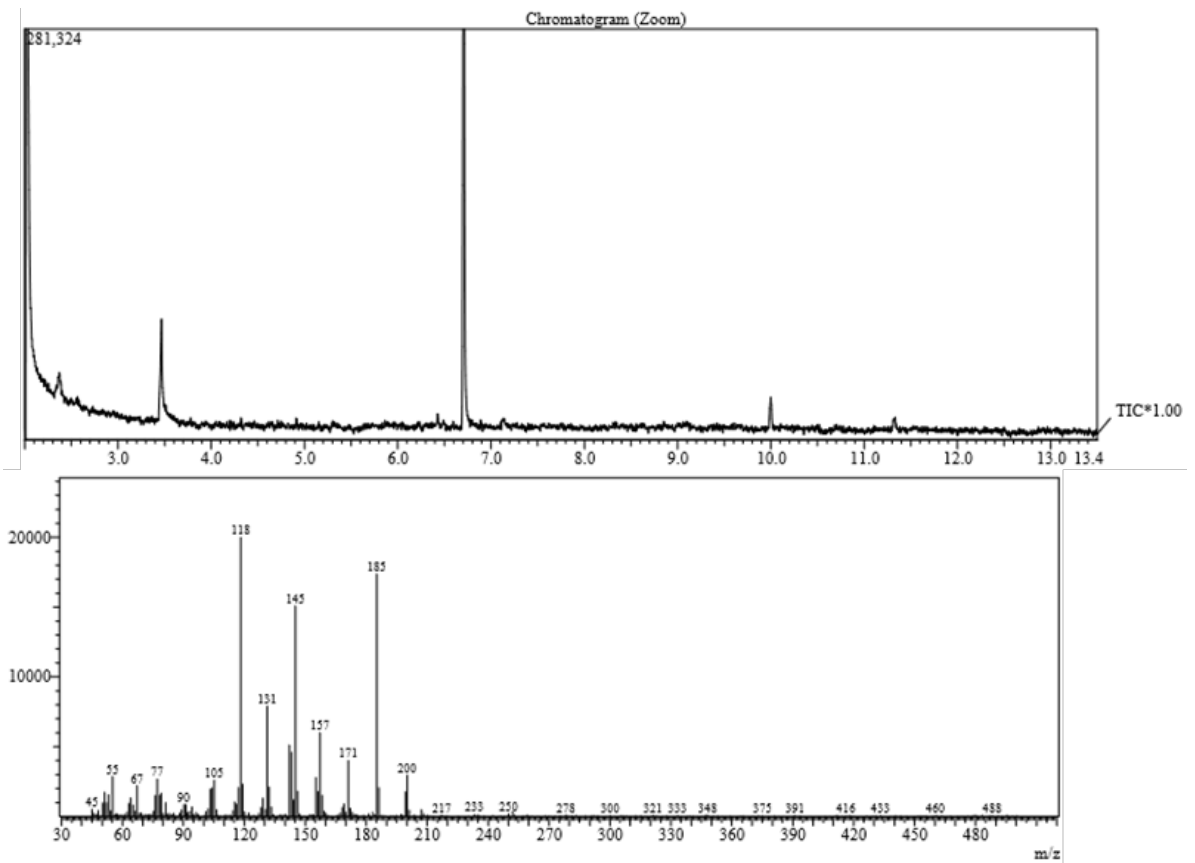




HT-TLC outcomes – Polar substrates runs using 10% methanol in dichloromethane.

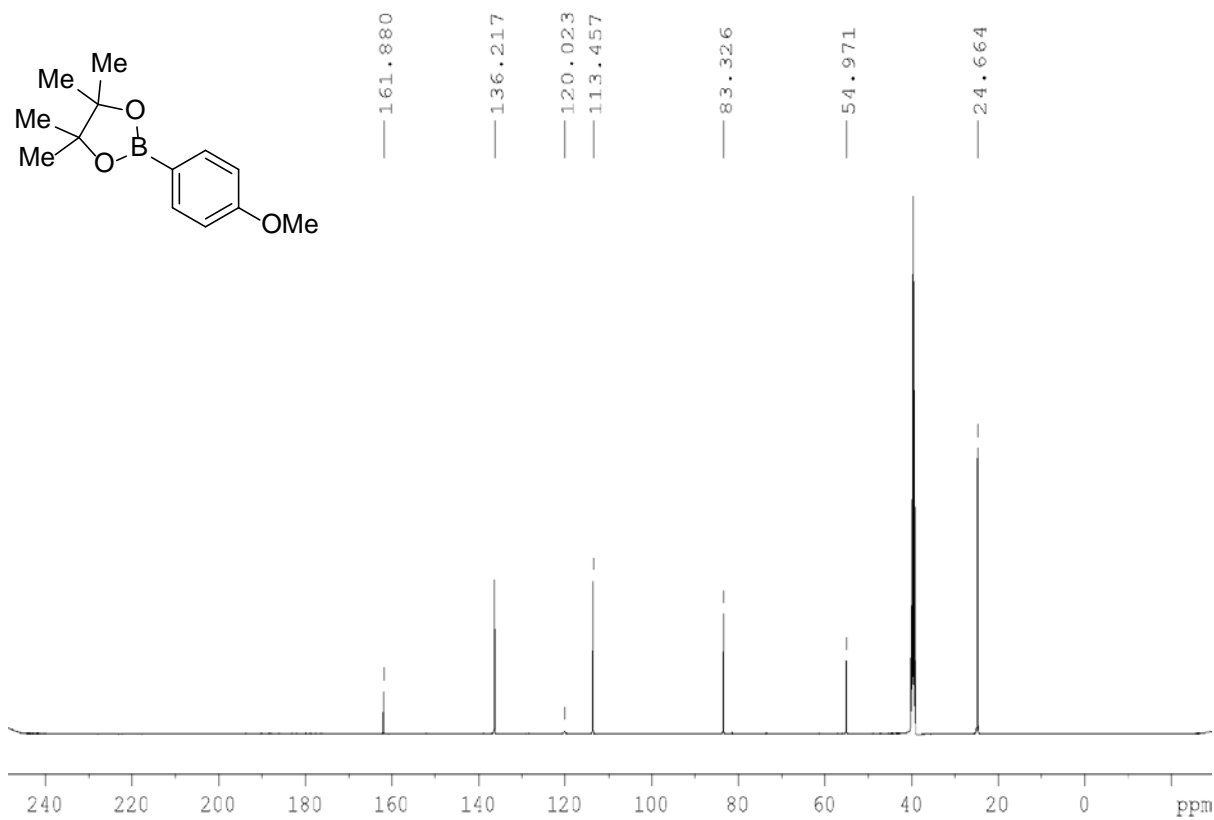
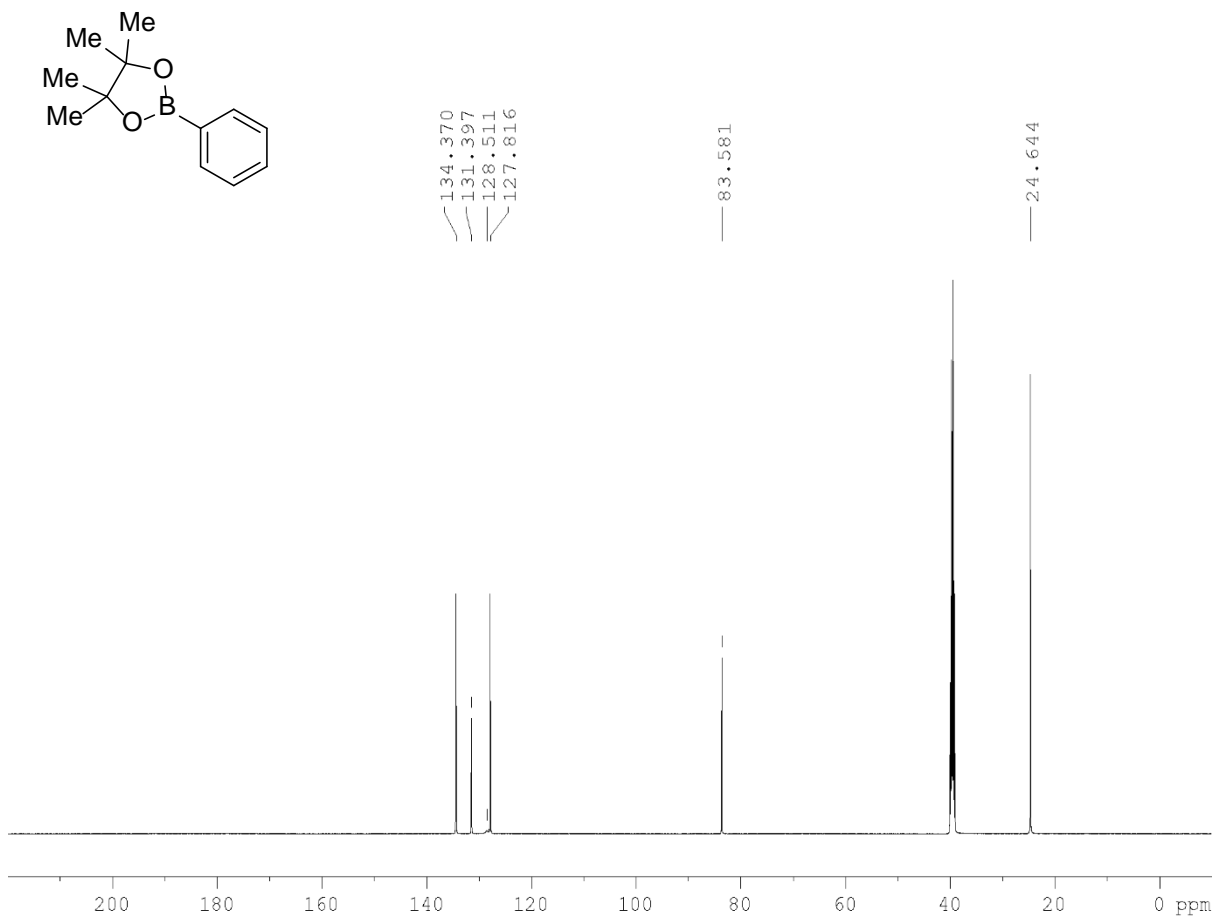


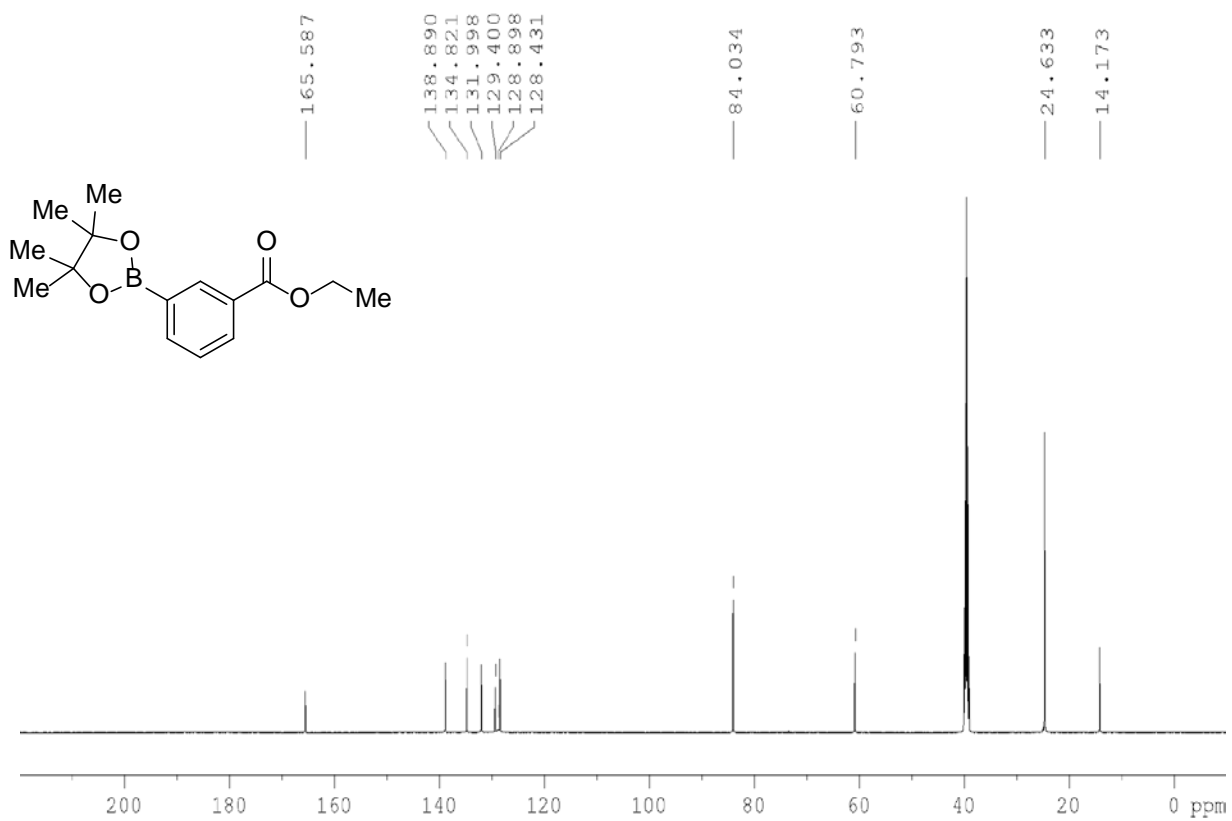
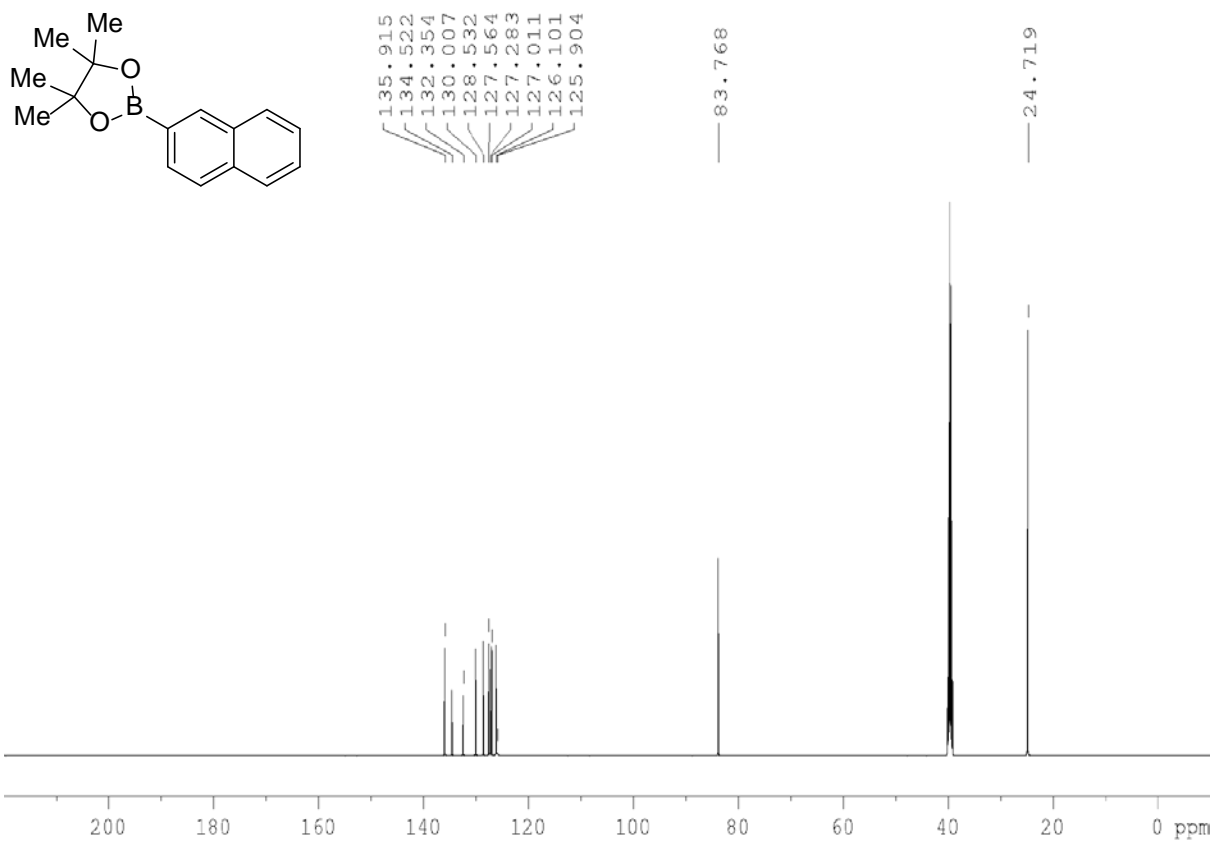
Mass spectra of key peak

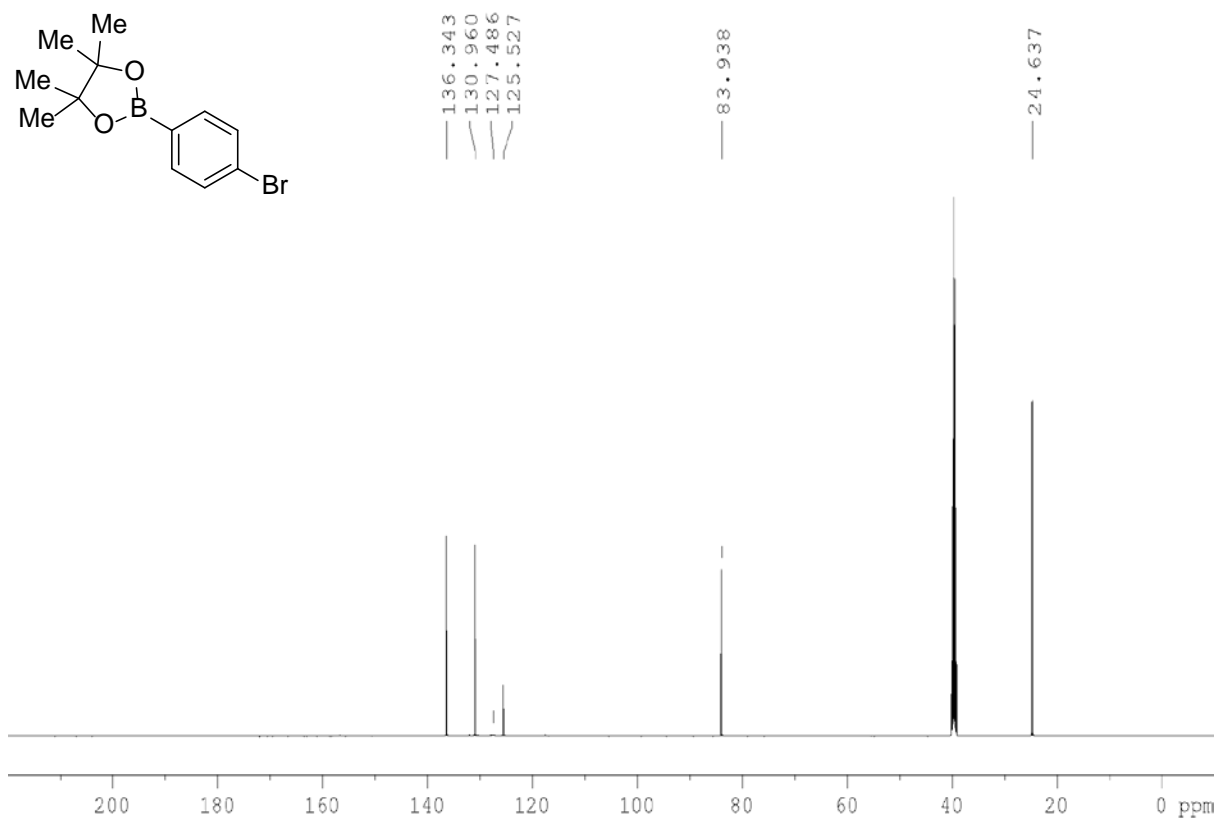
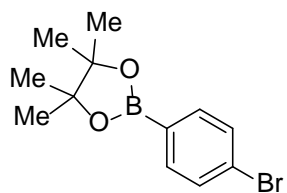
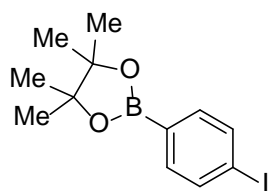


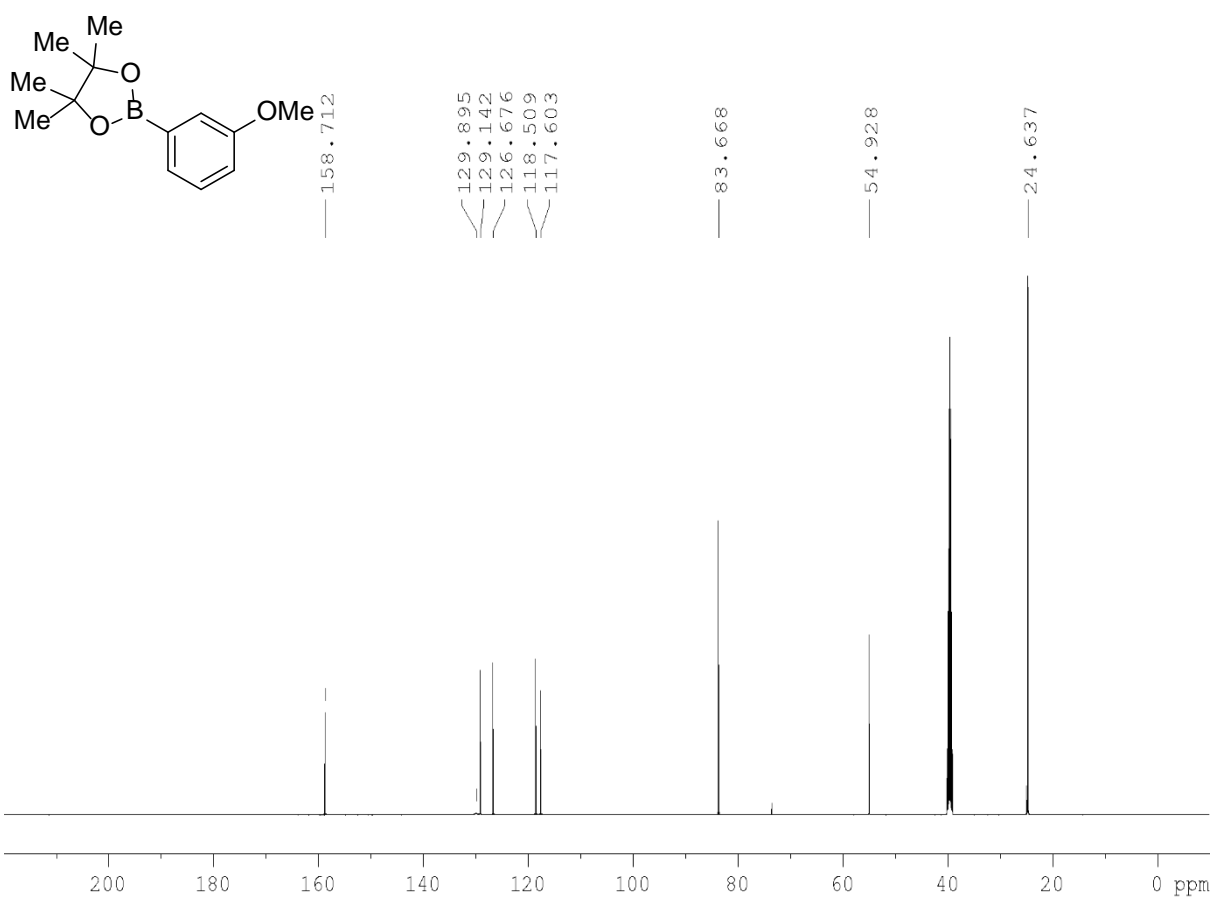
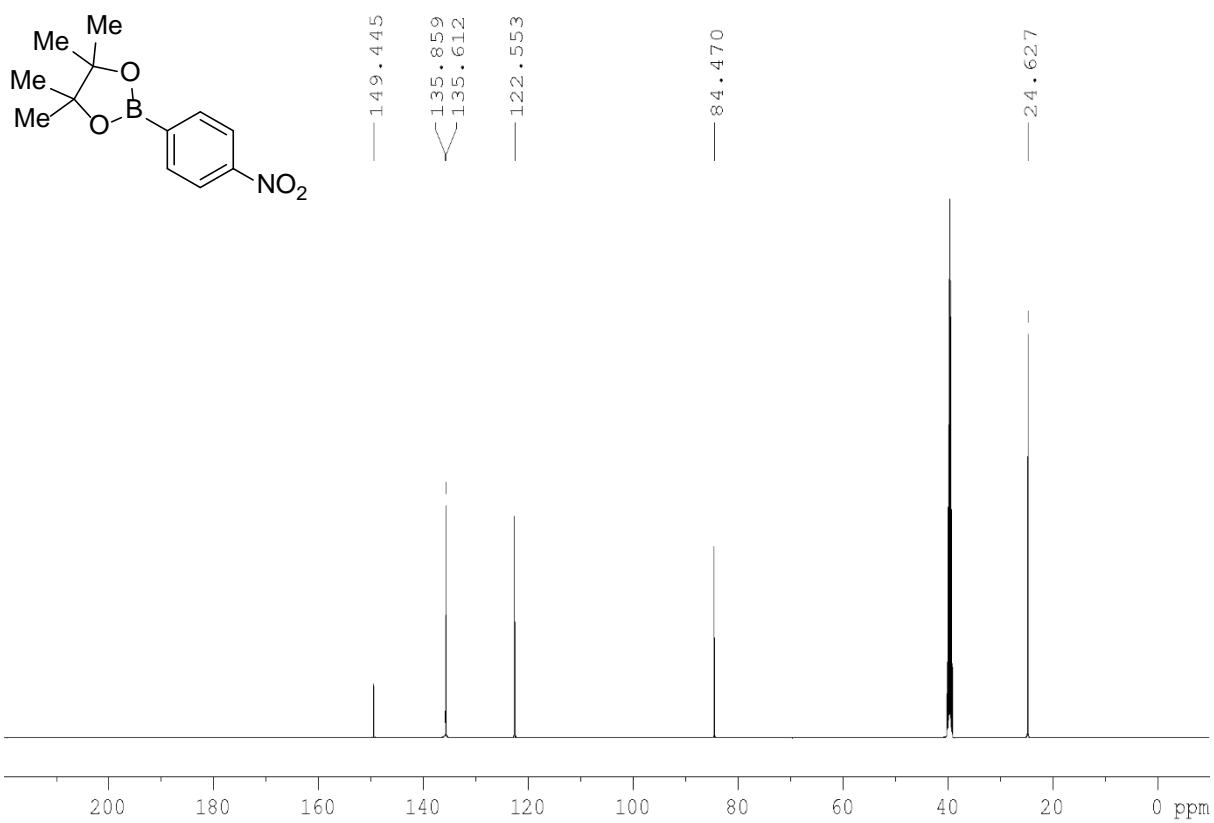
Appendix 1: Spectra

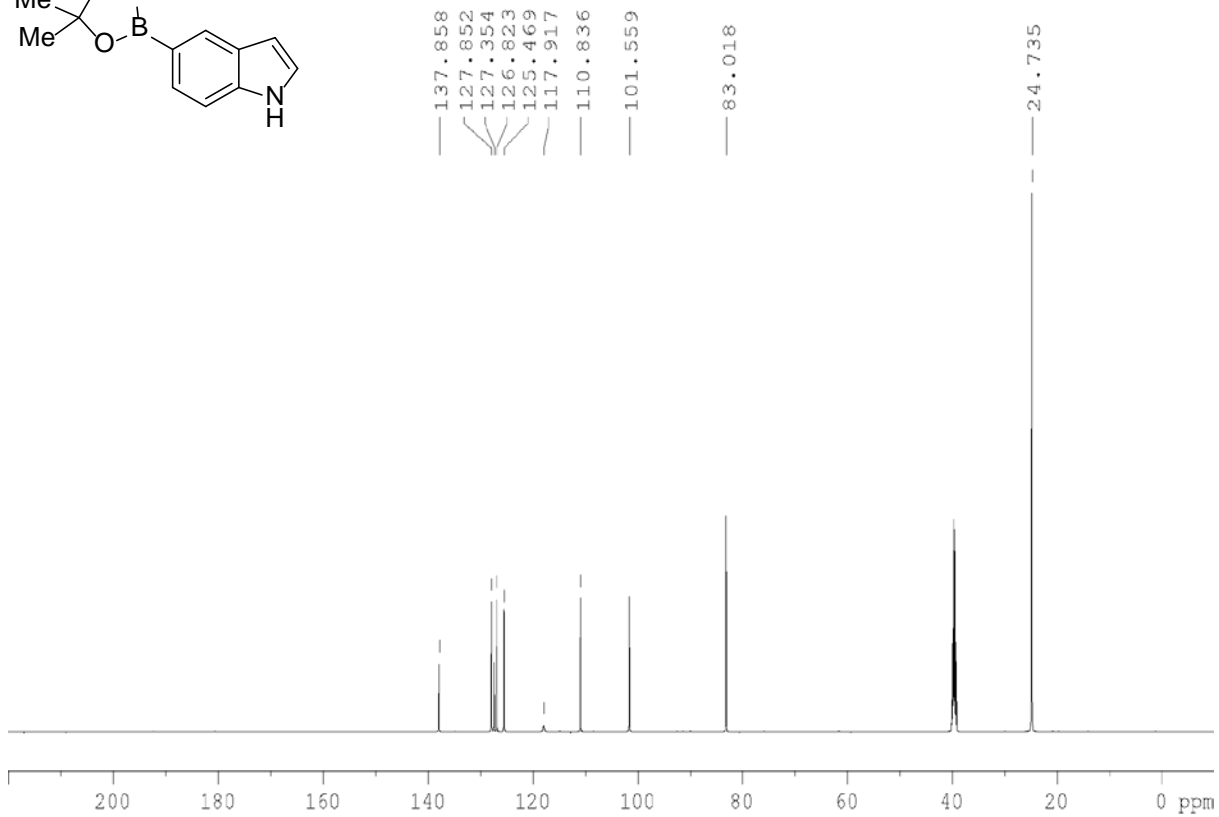
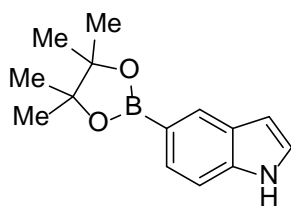
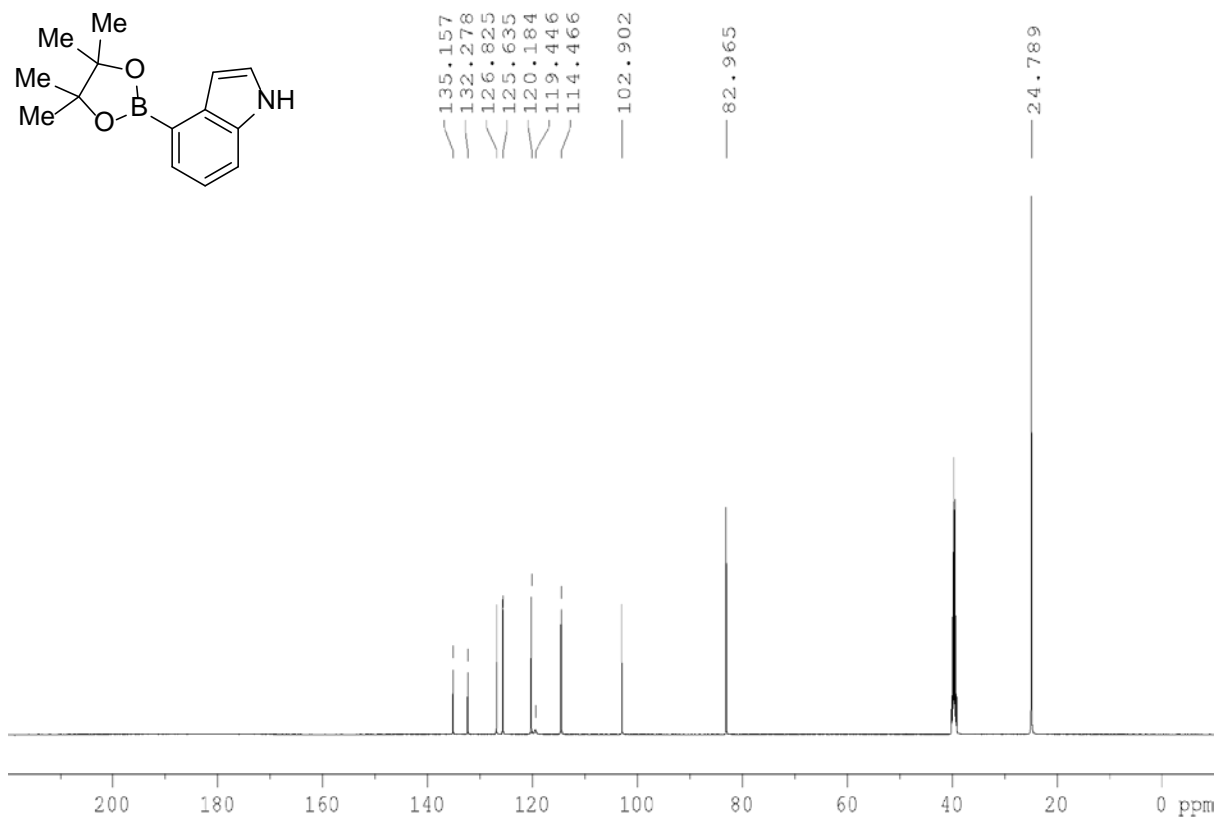
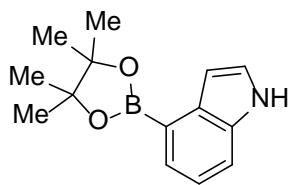
Chan-Lam Spectra

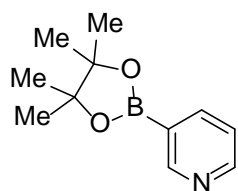








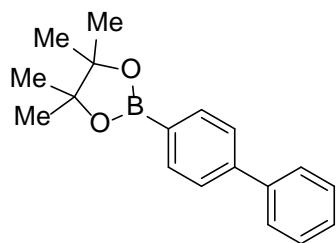
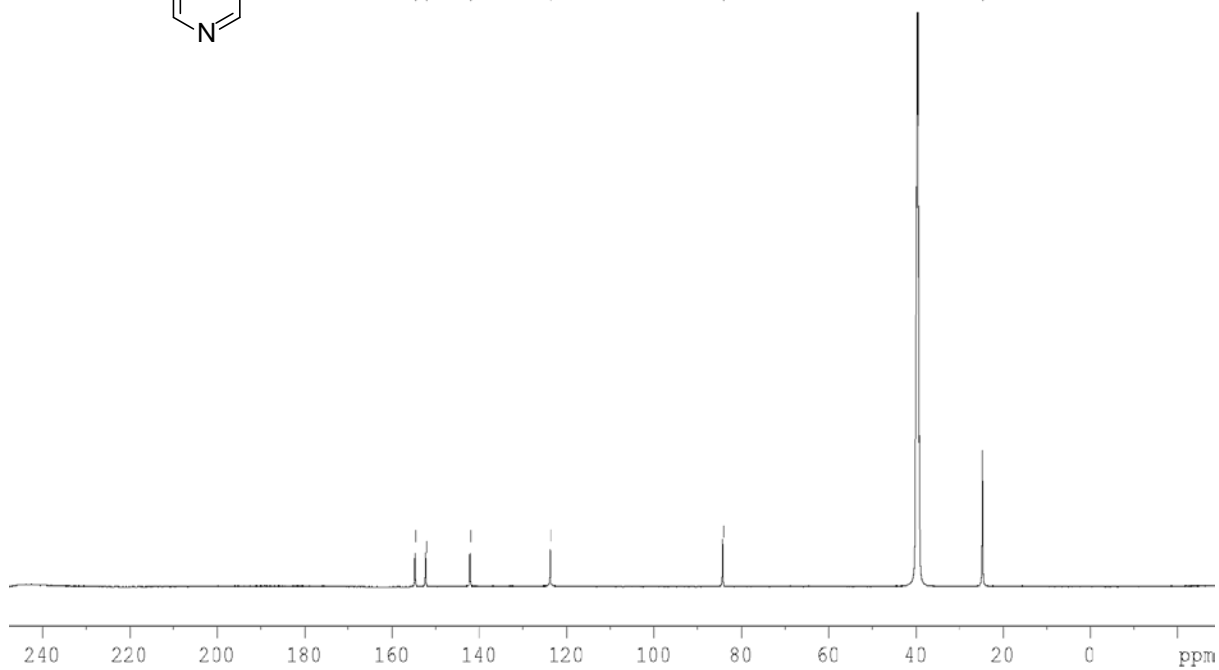




154.546
152.134
141.872
123.542

84.085

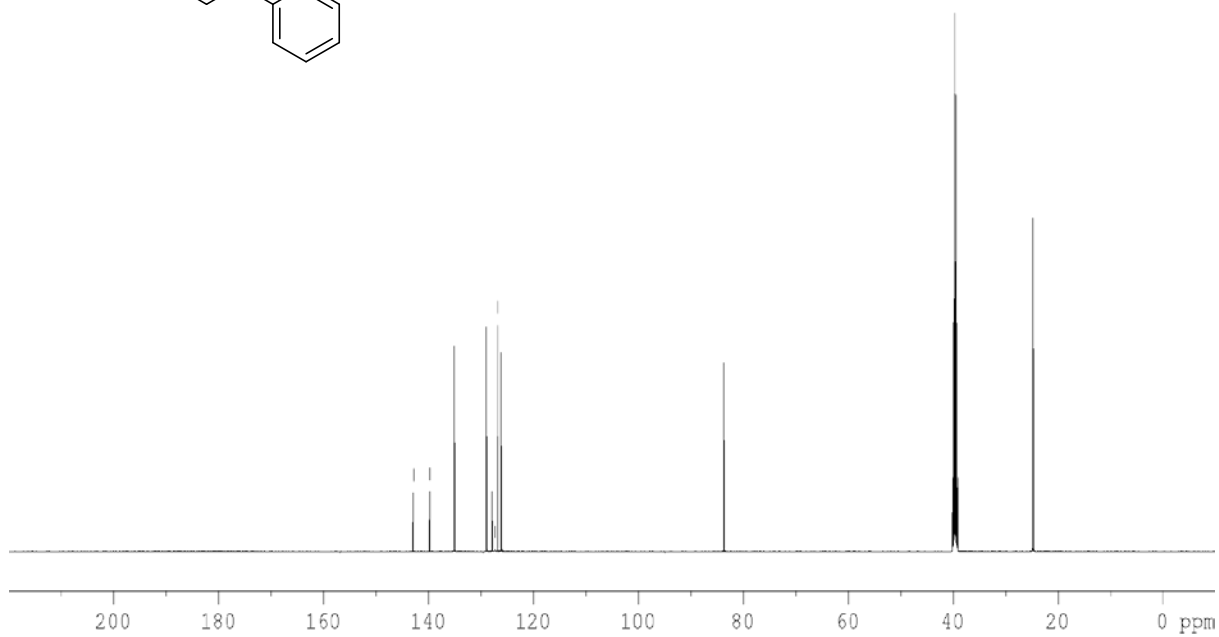
24.629

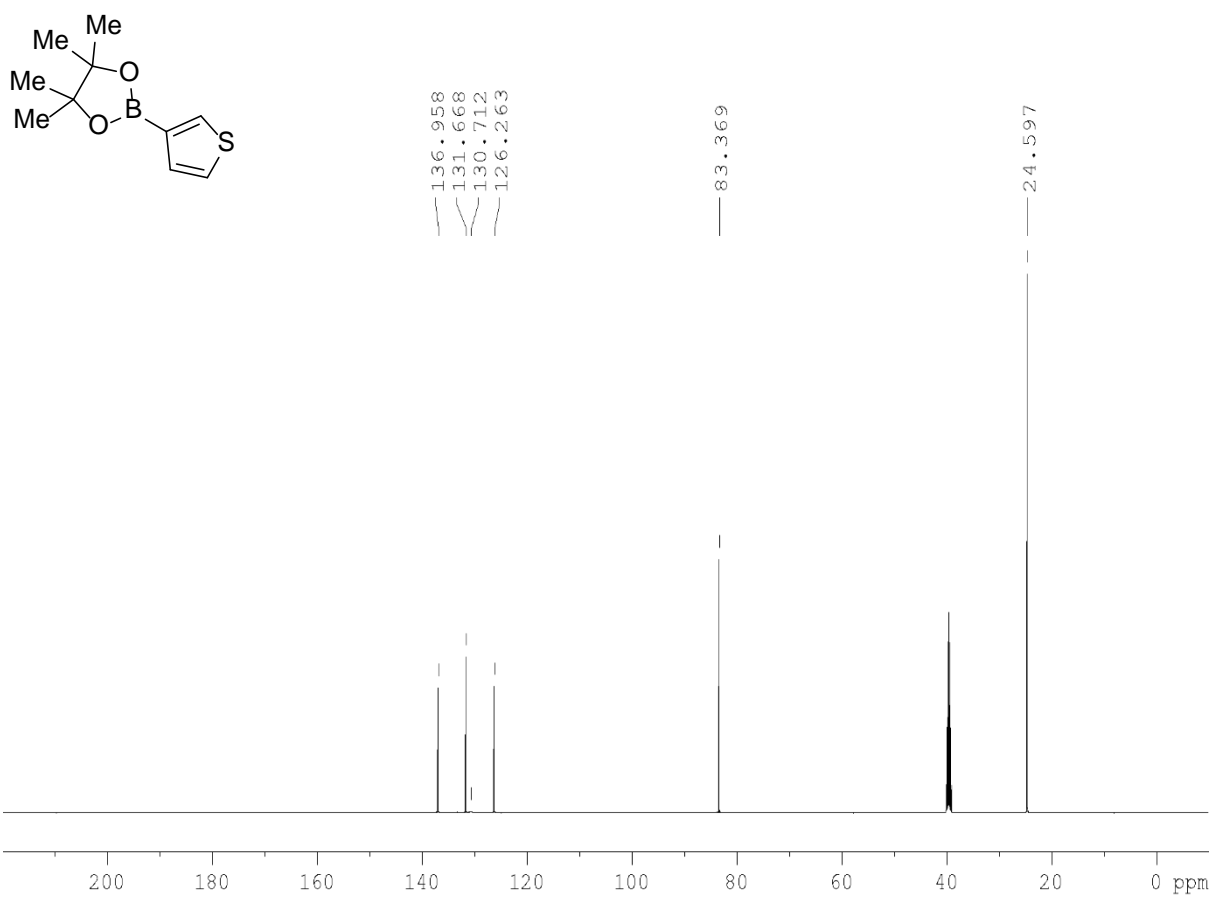
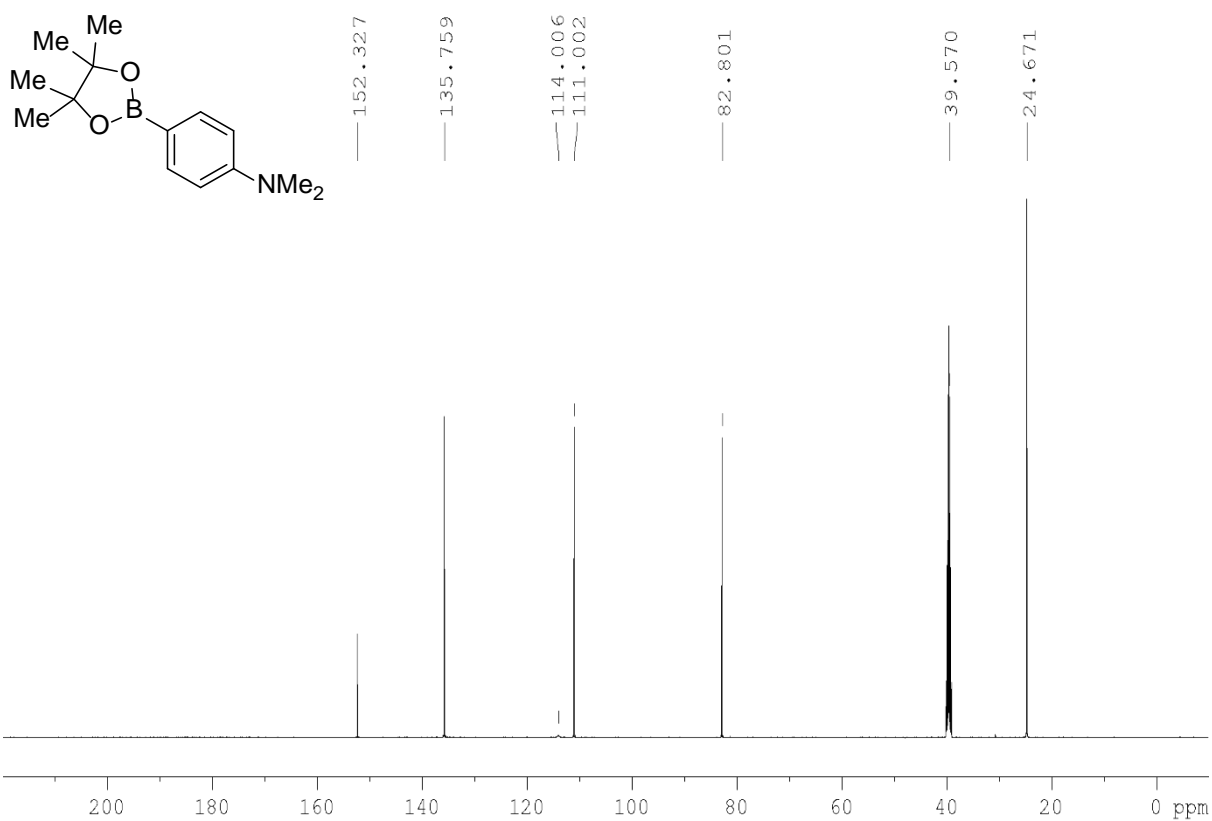


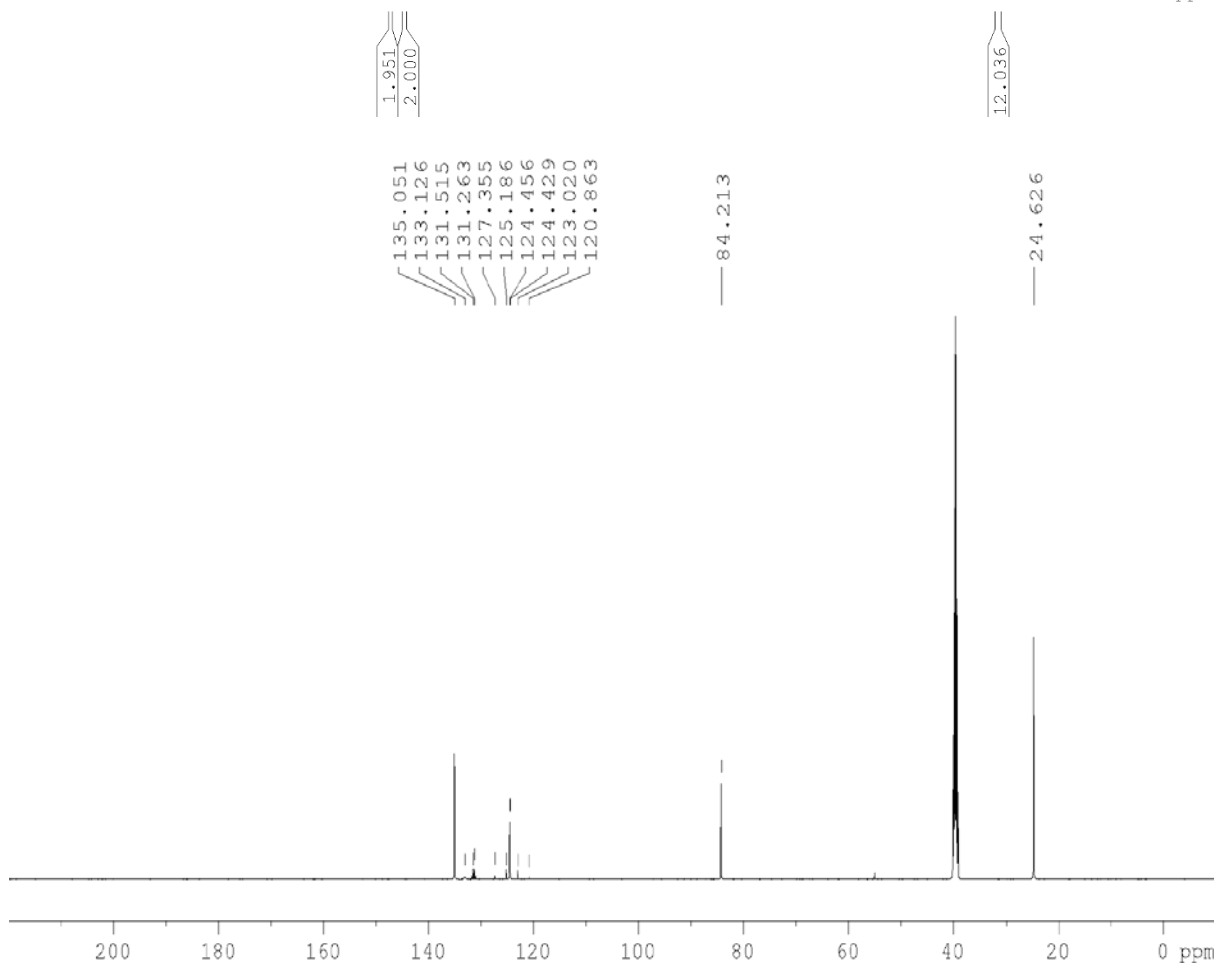
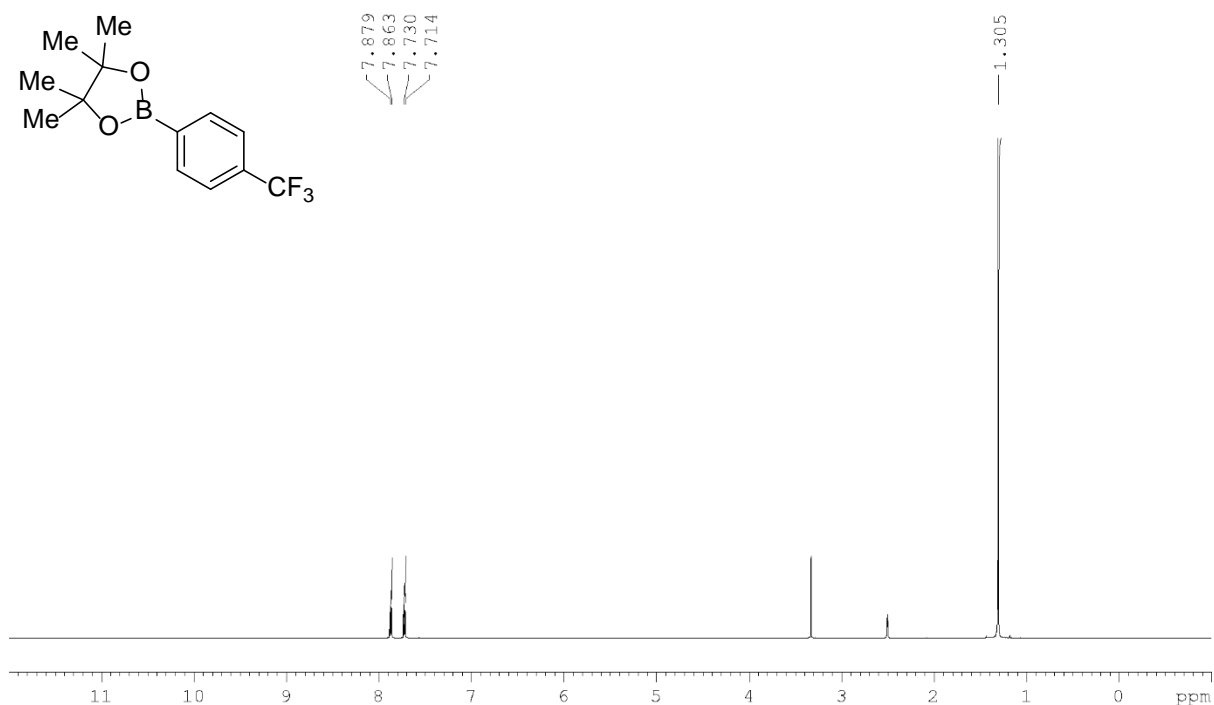
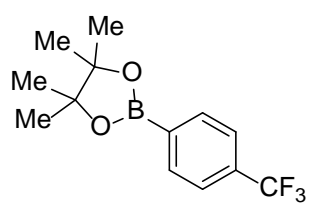
142.927
139.748
135.069
128.982
127.854
127.315
126.743
126.100

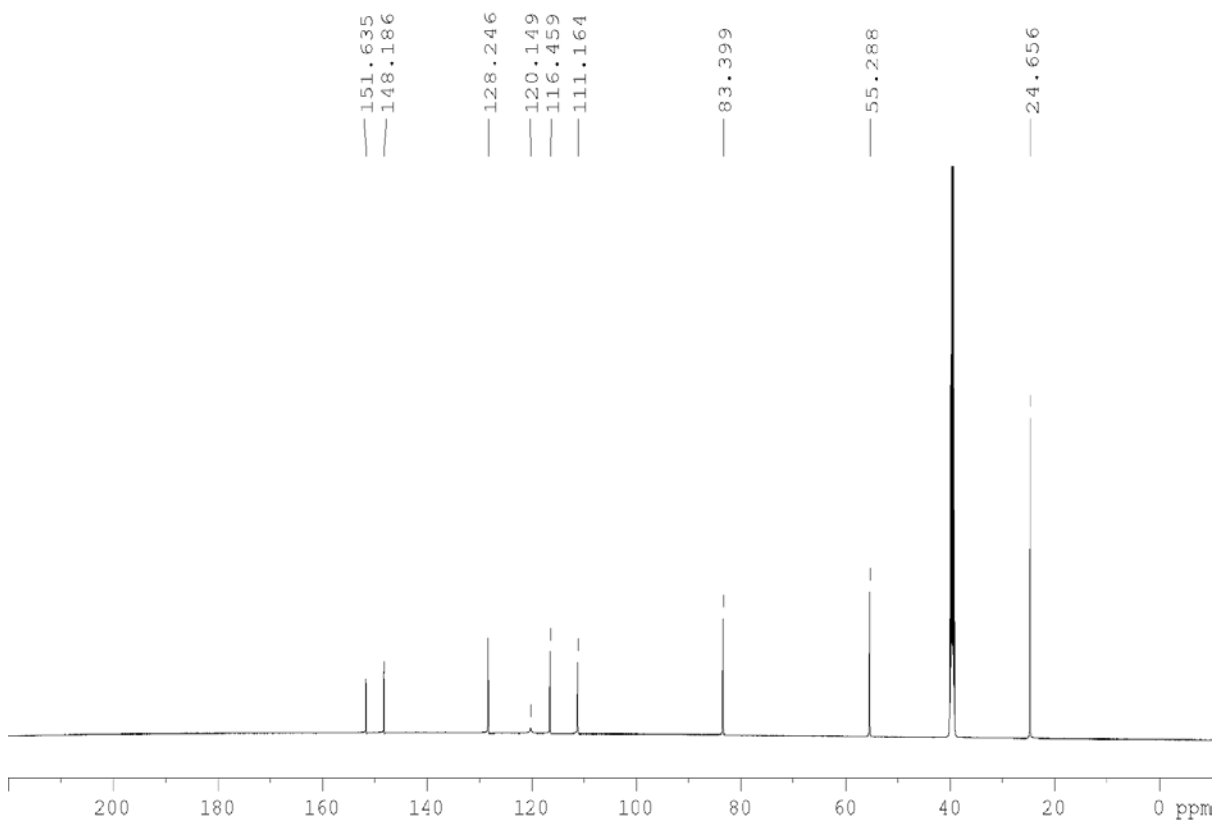
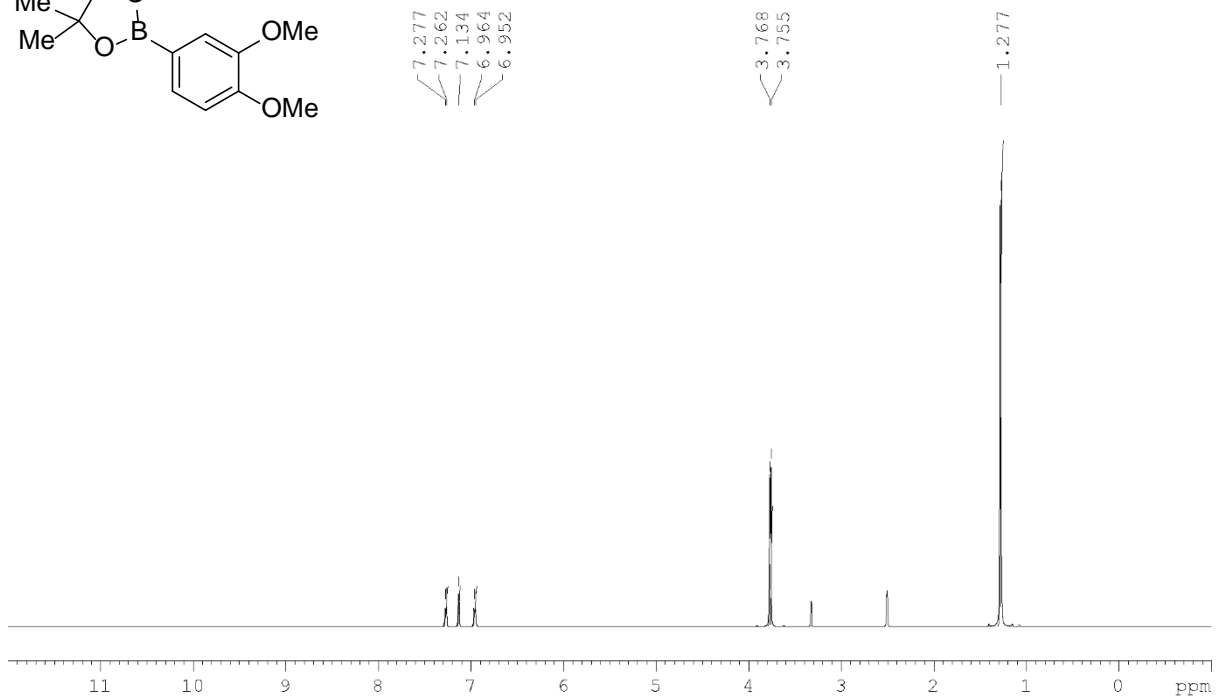
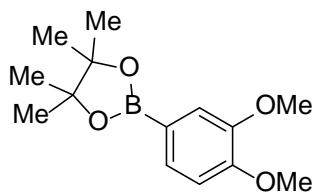
83.653

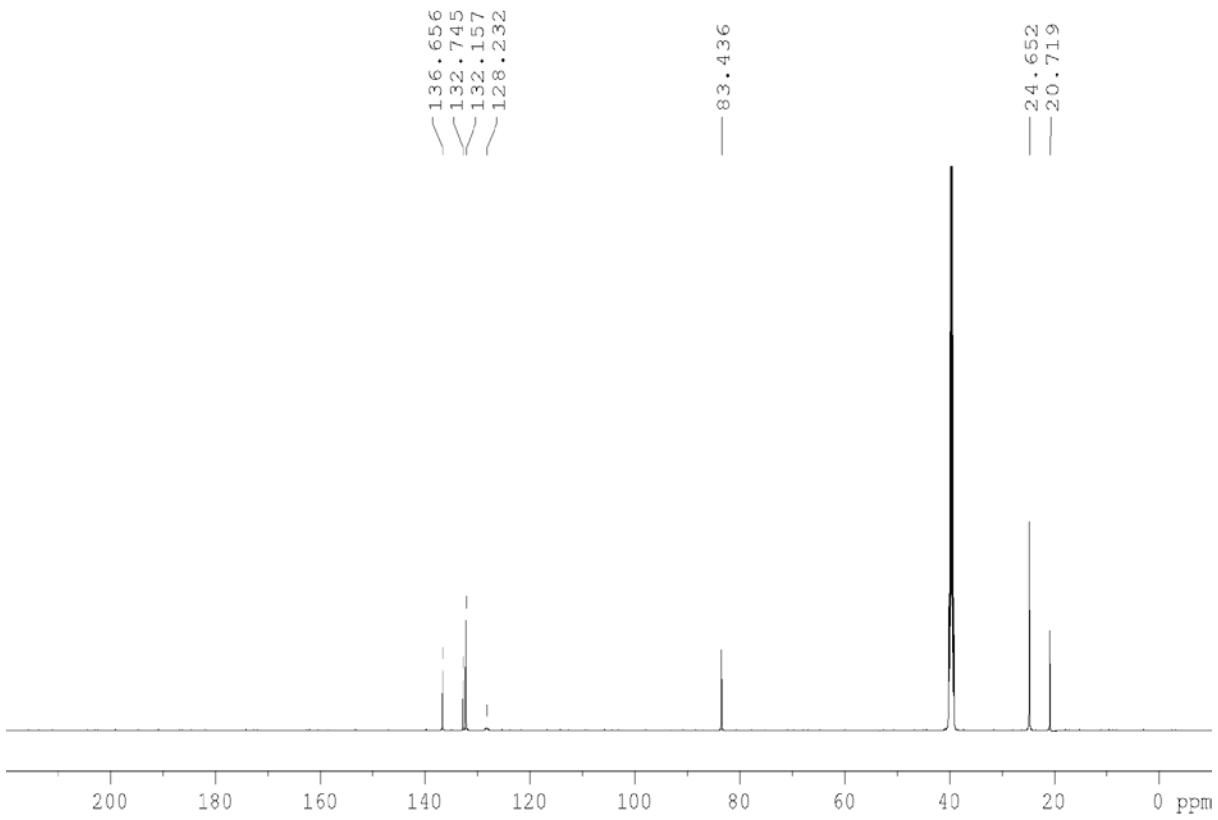
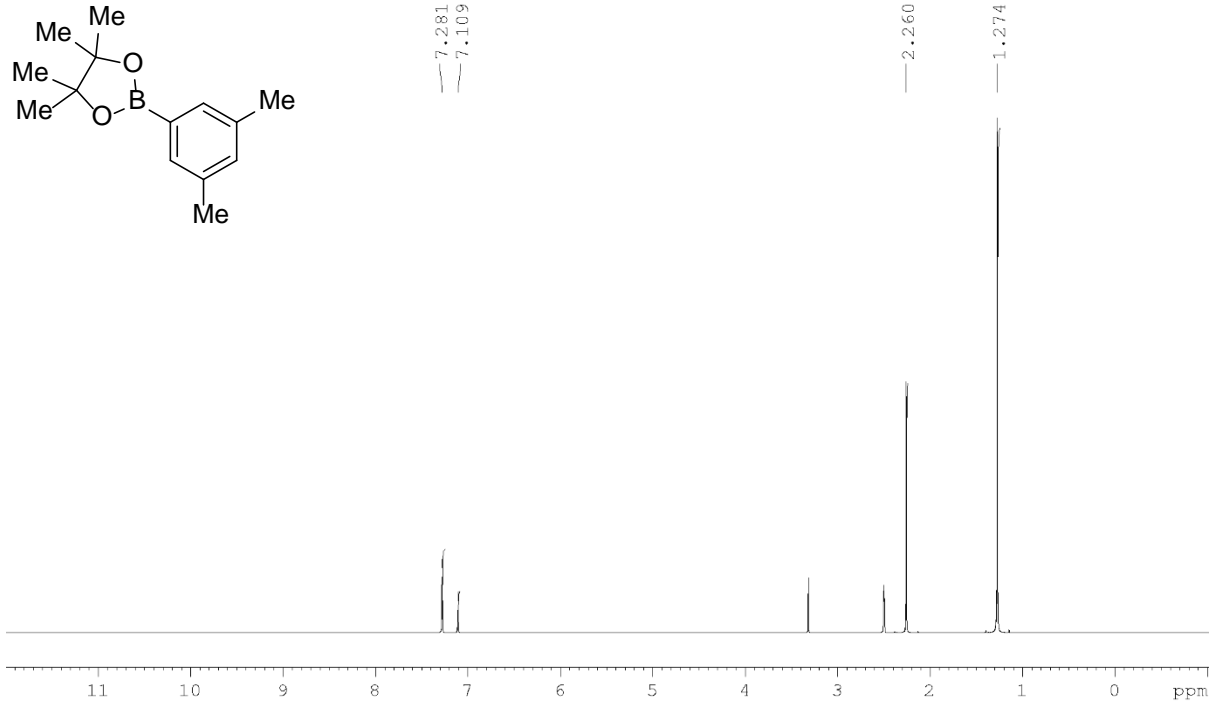
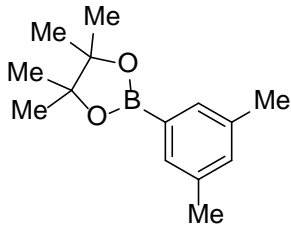
24.663

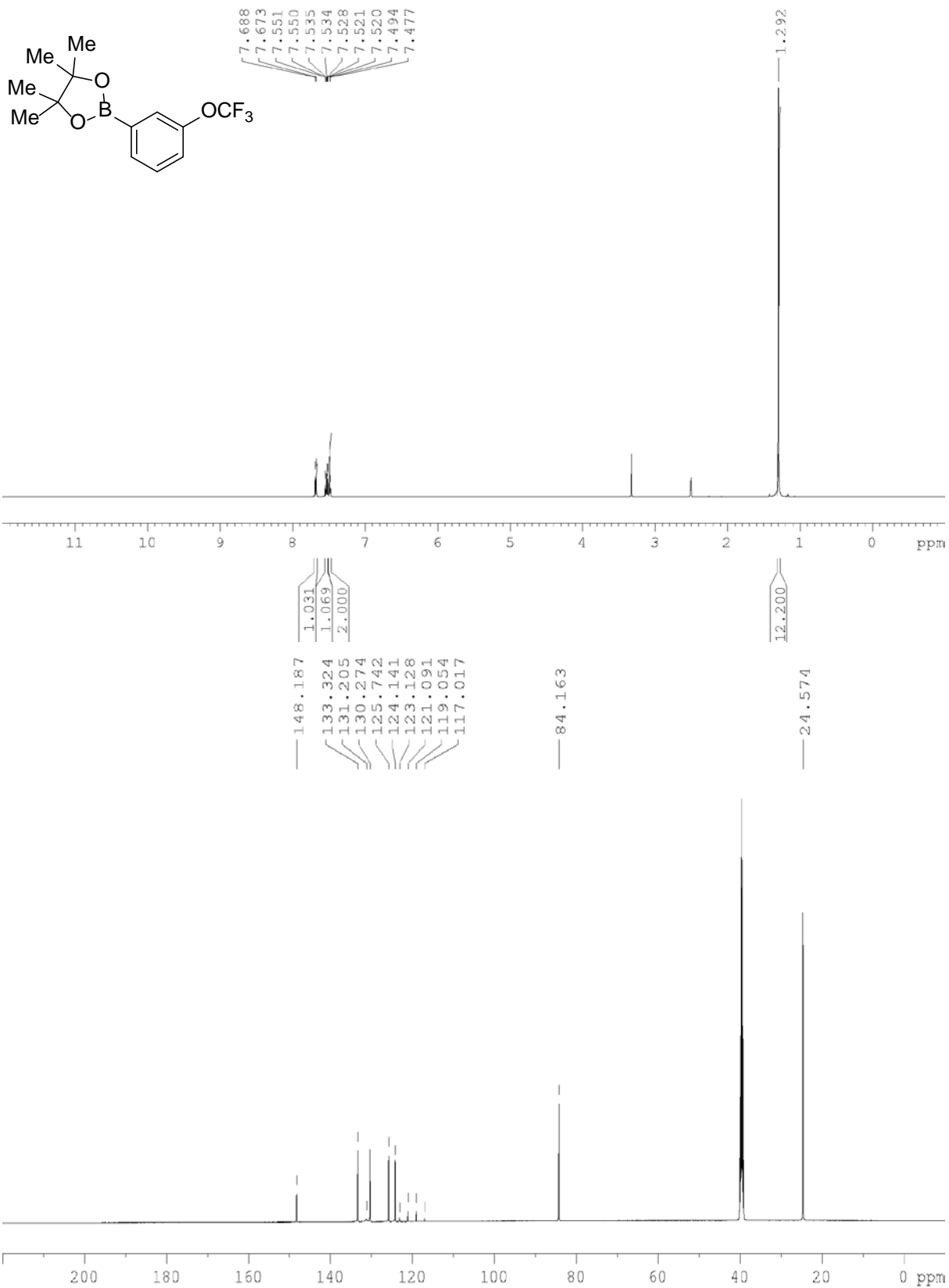


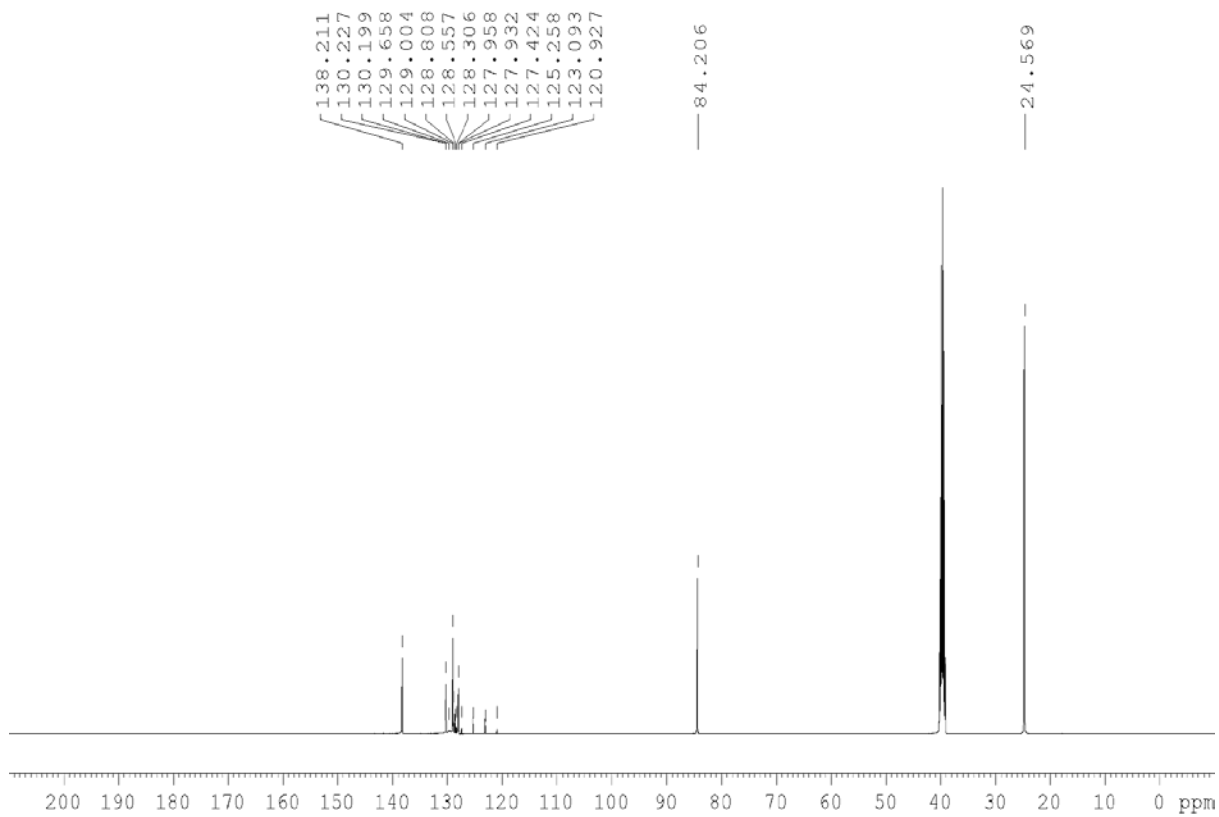
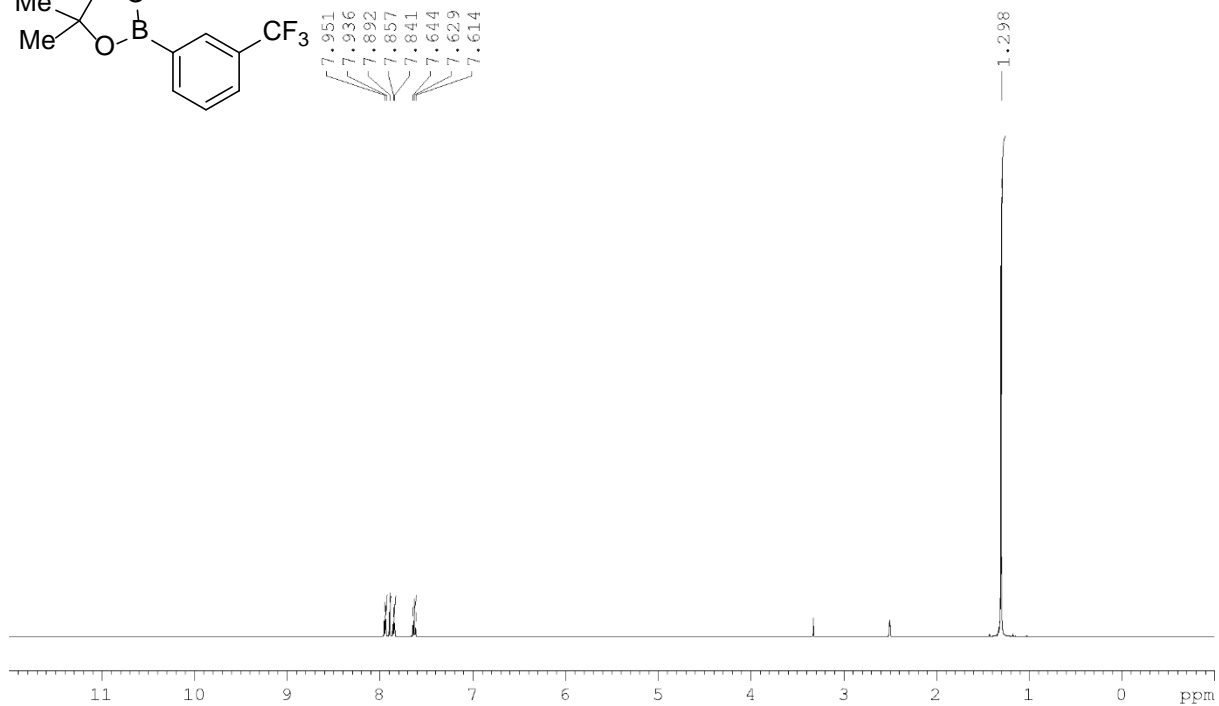
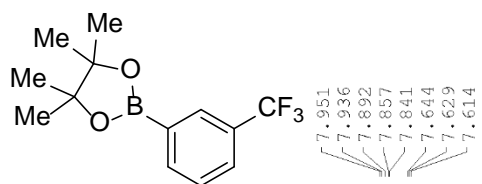


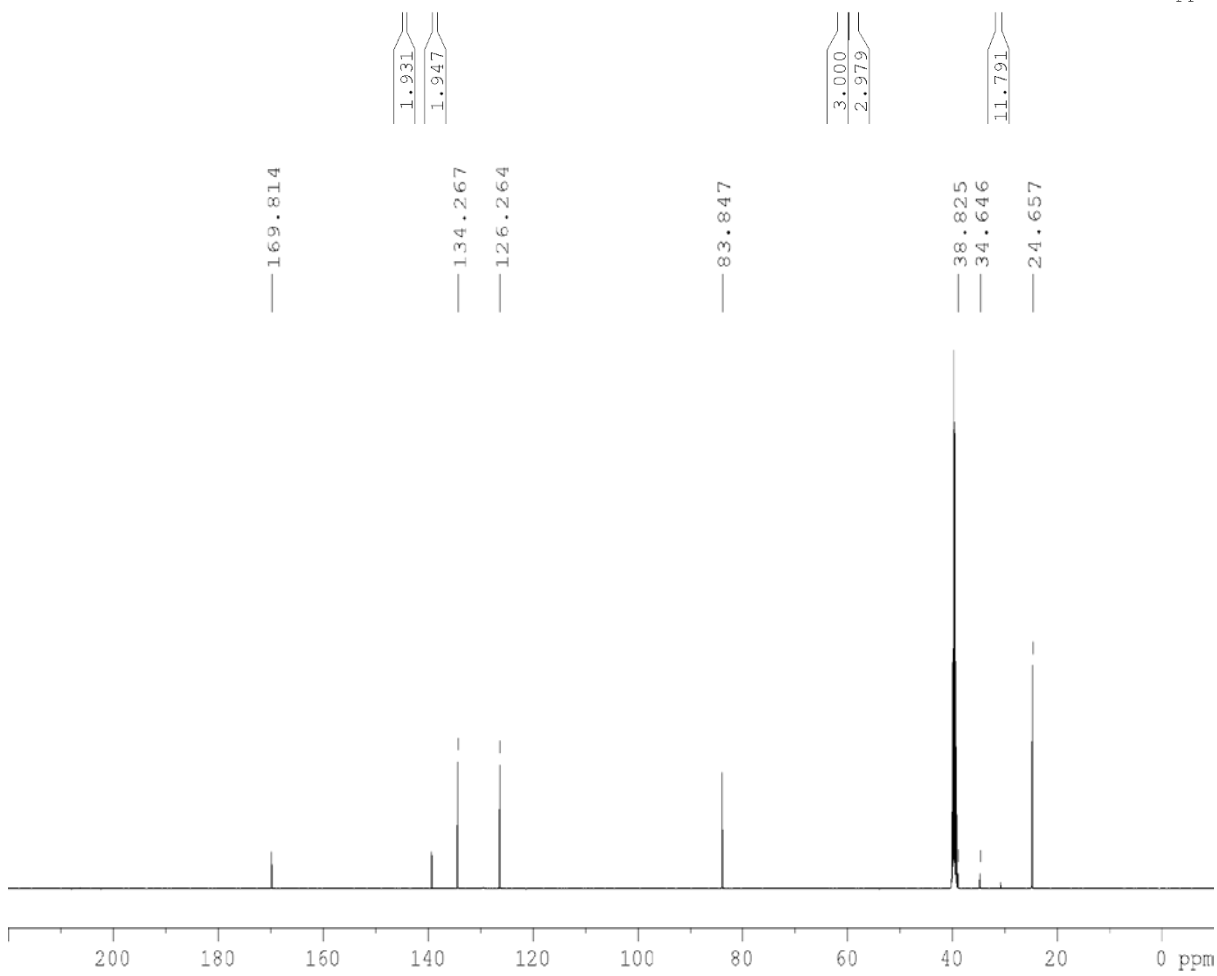
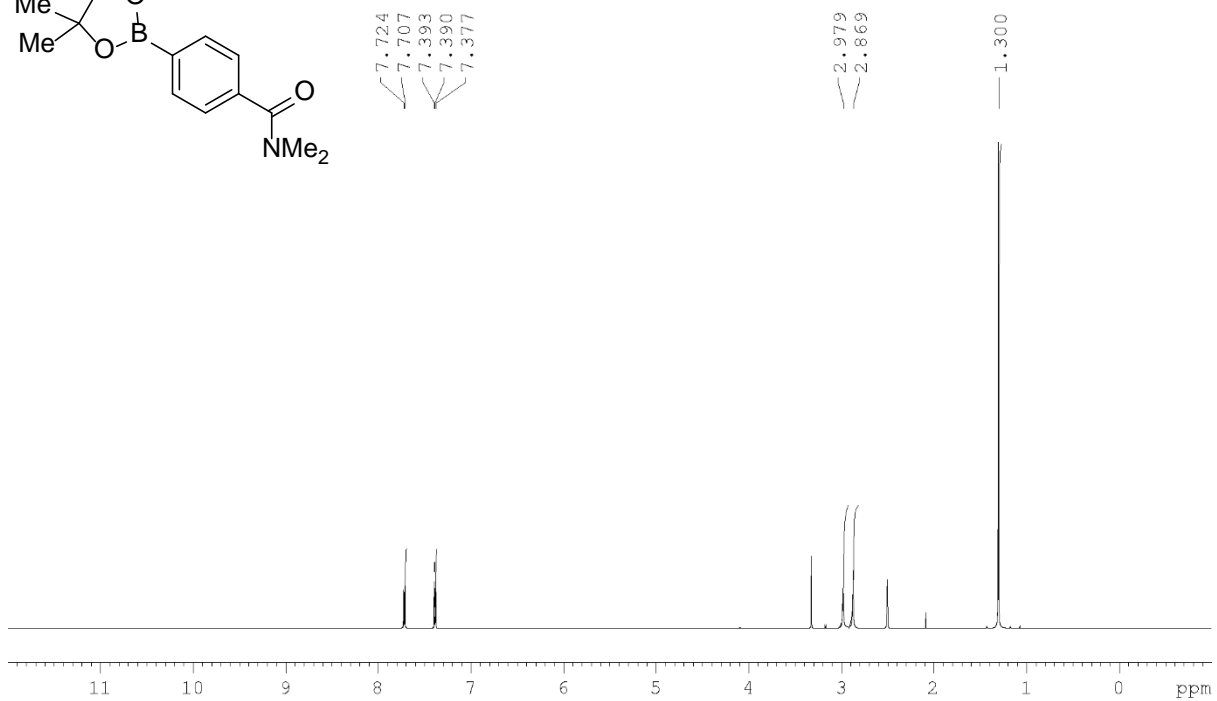
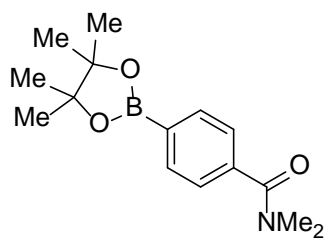


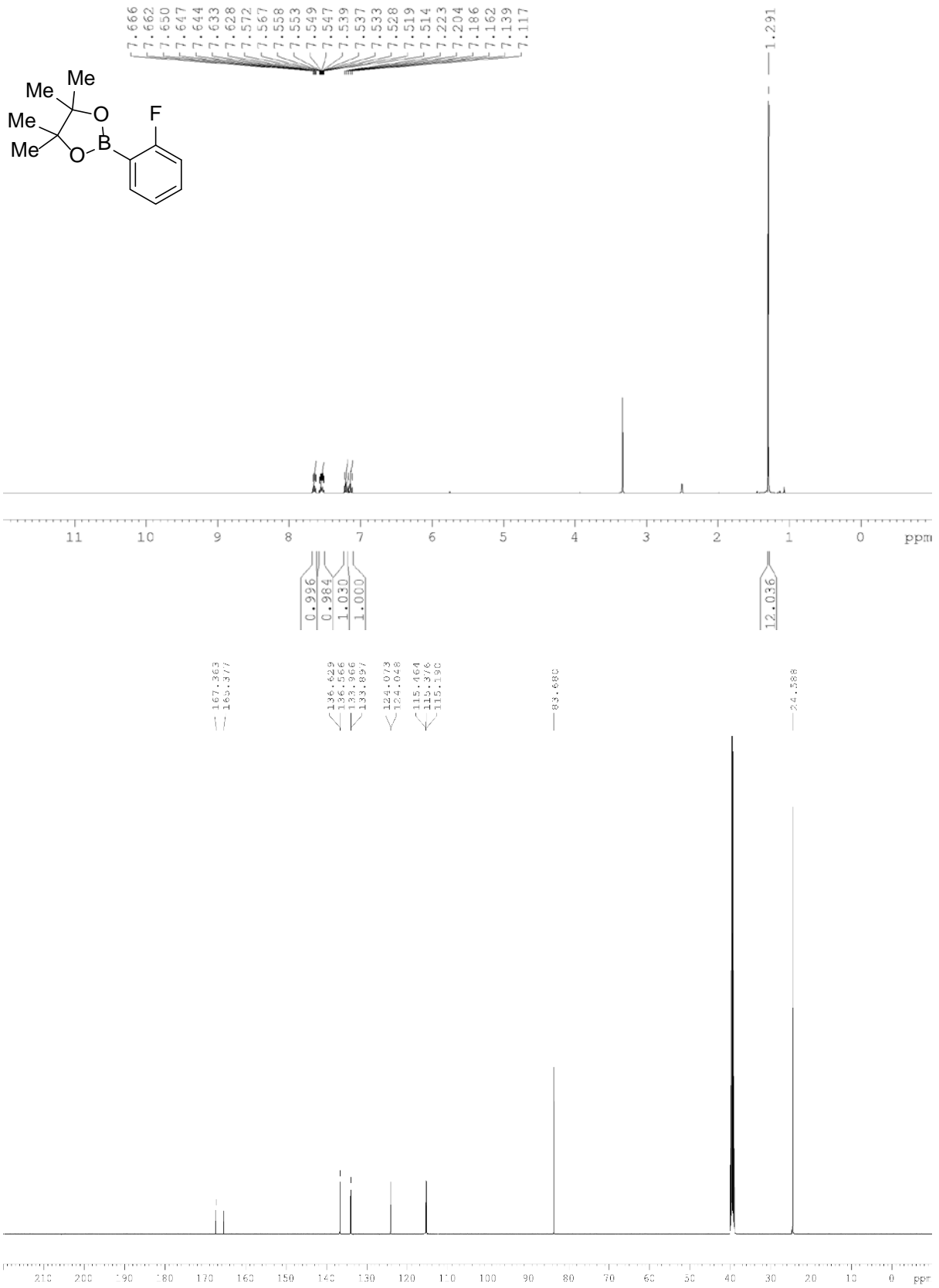


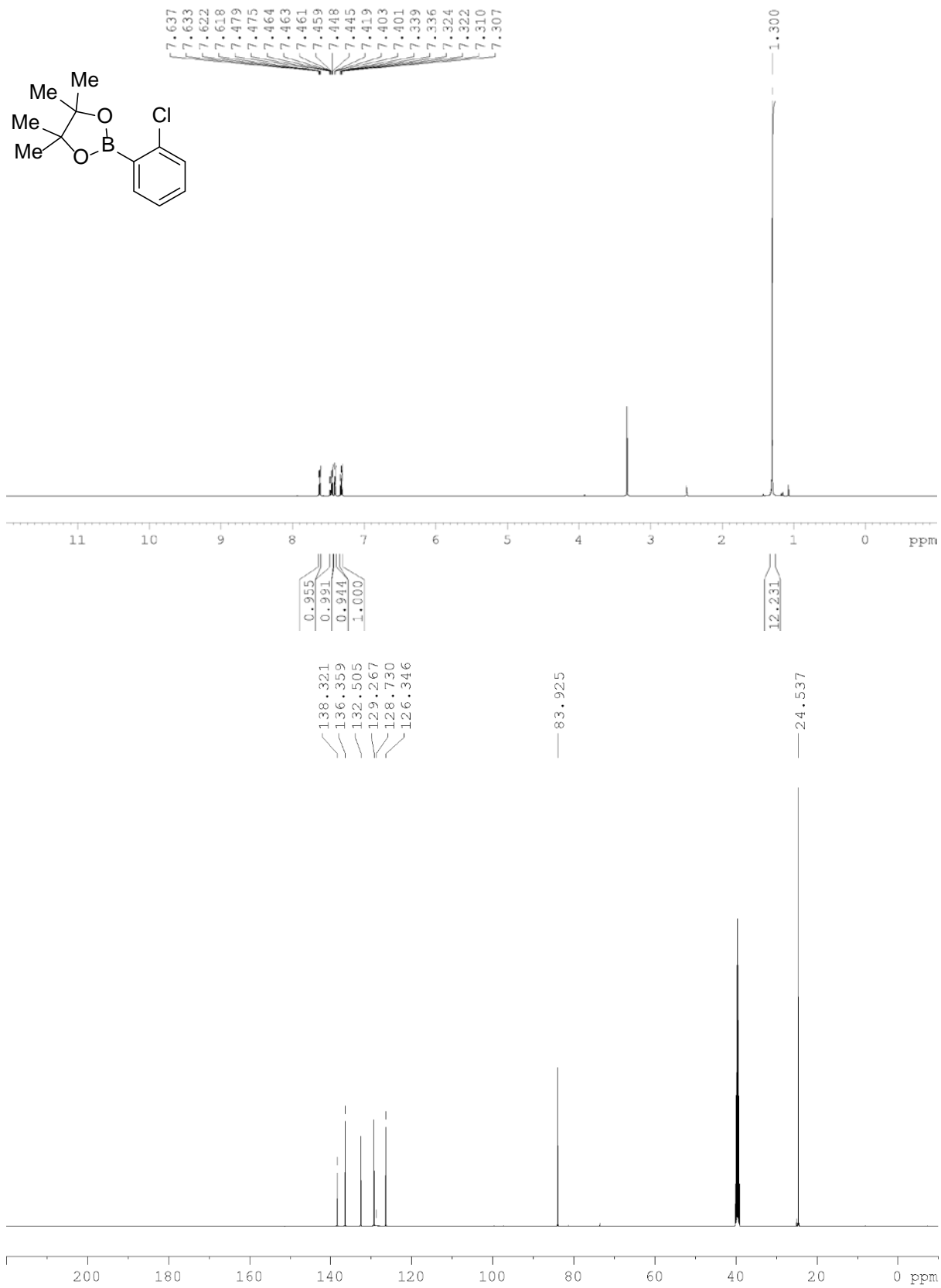


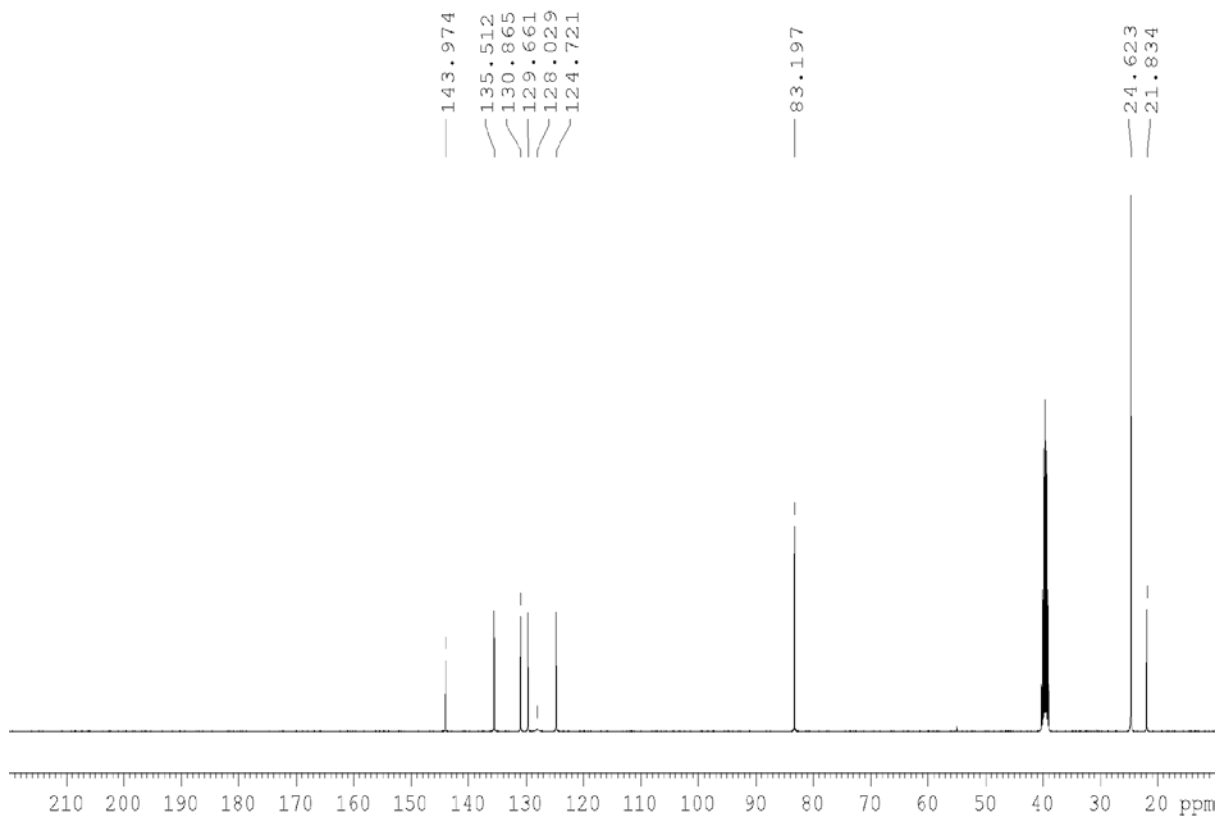
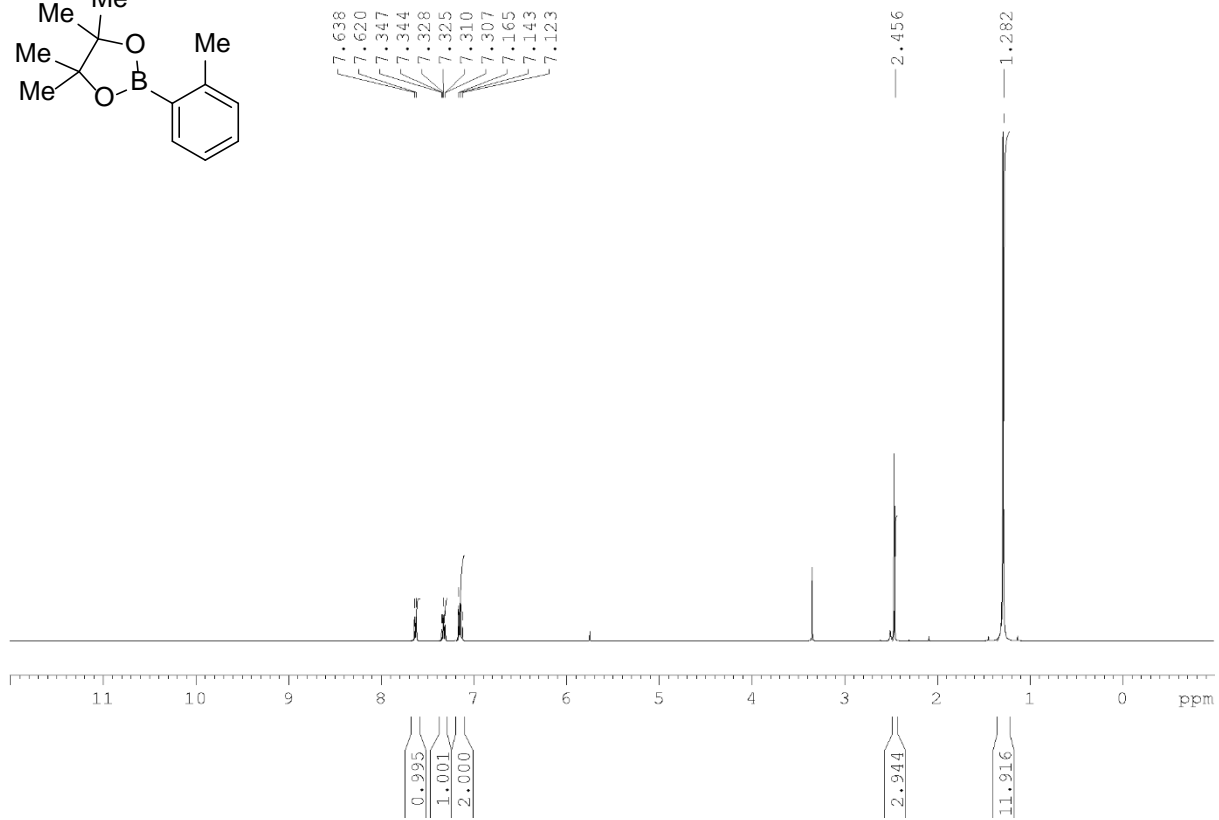
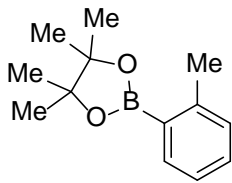


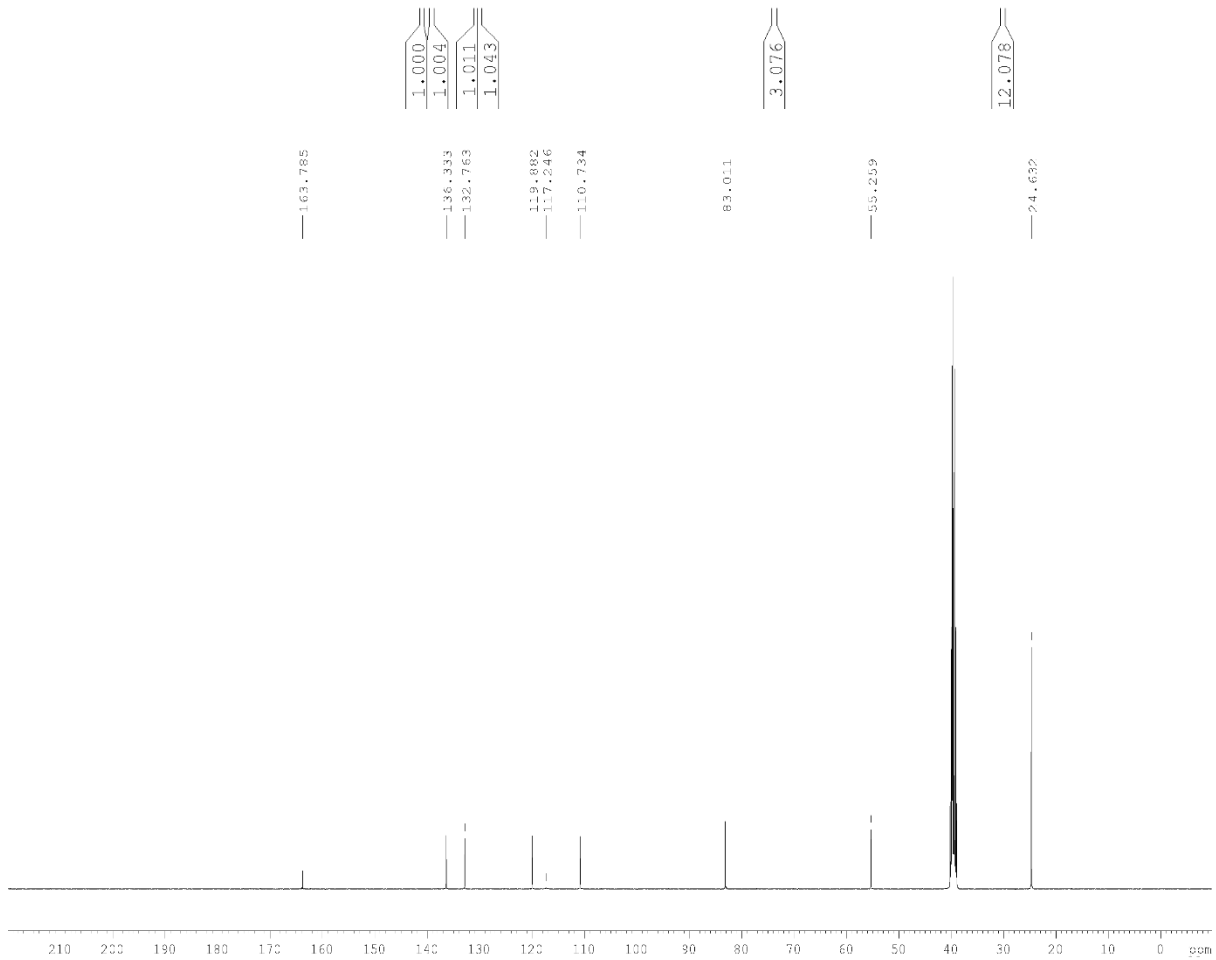
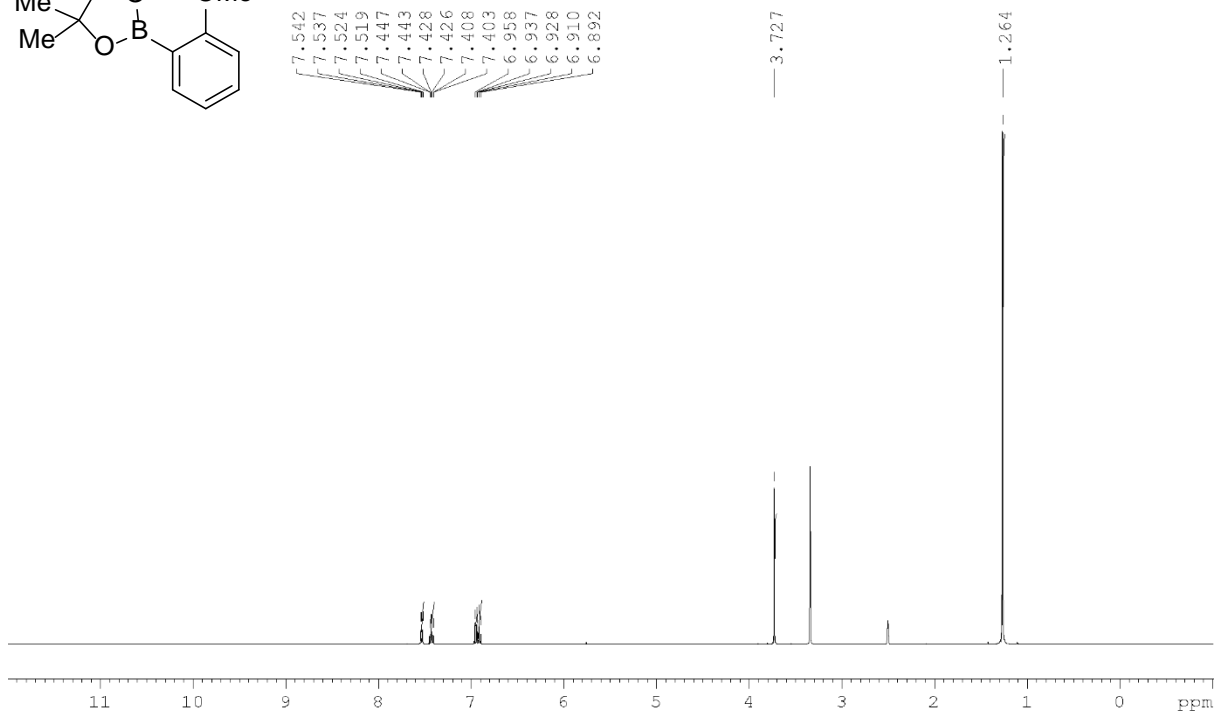
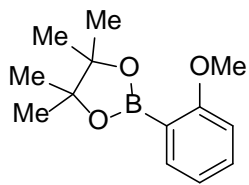


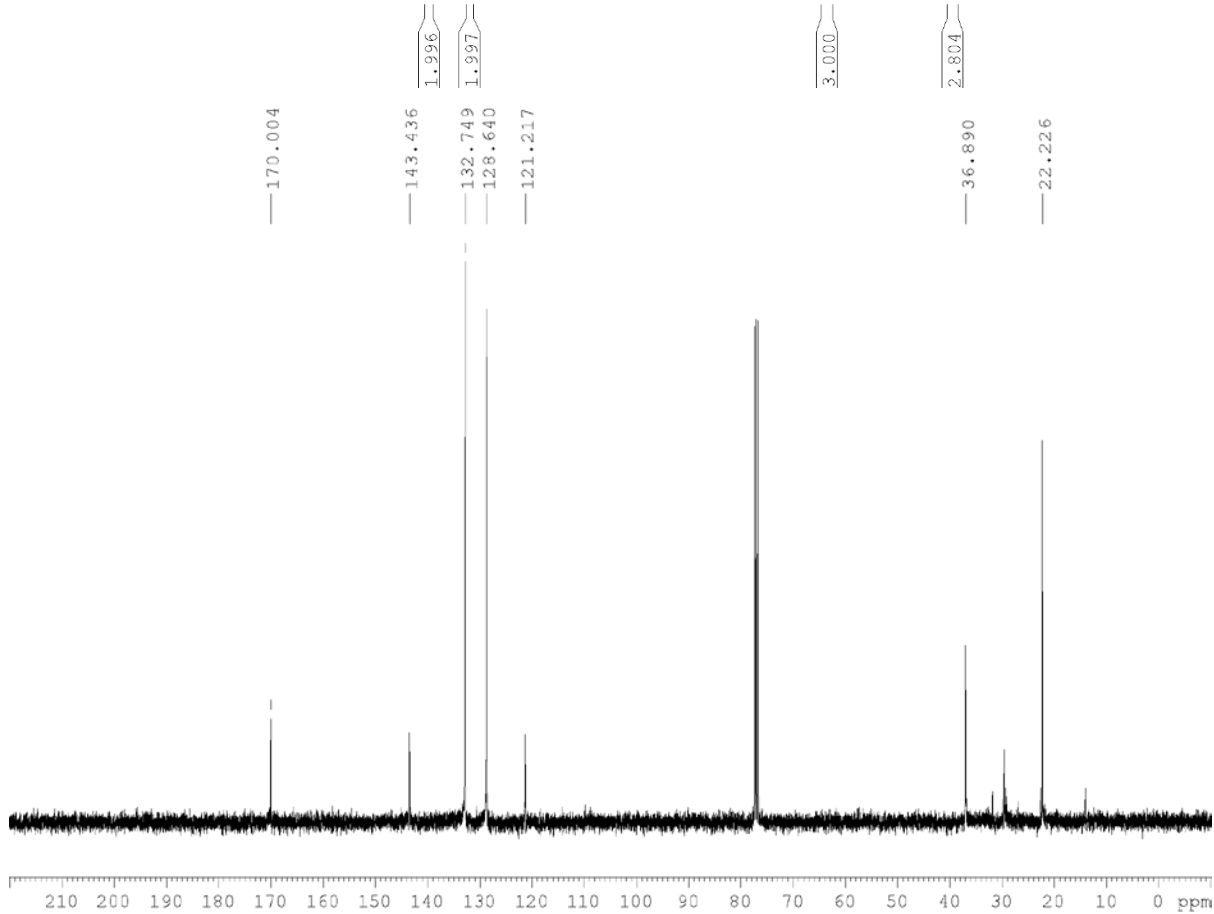
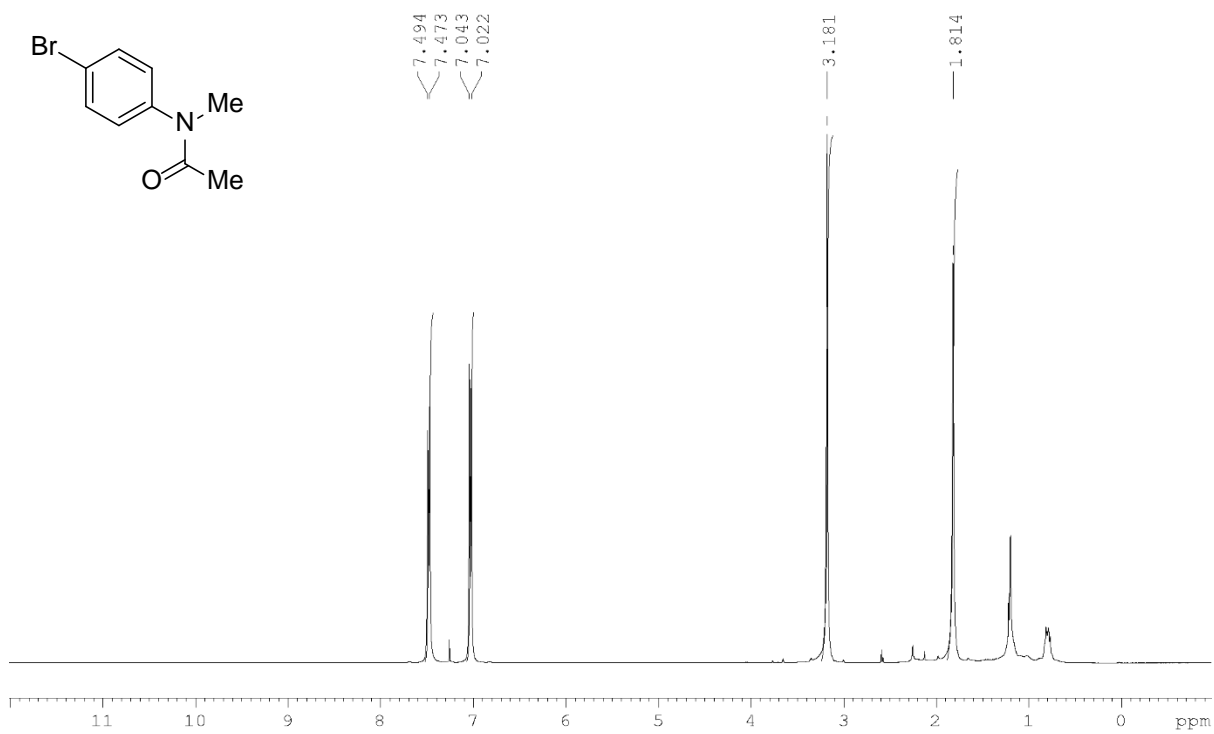
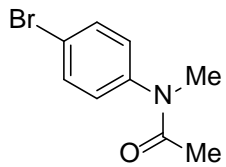


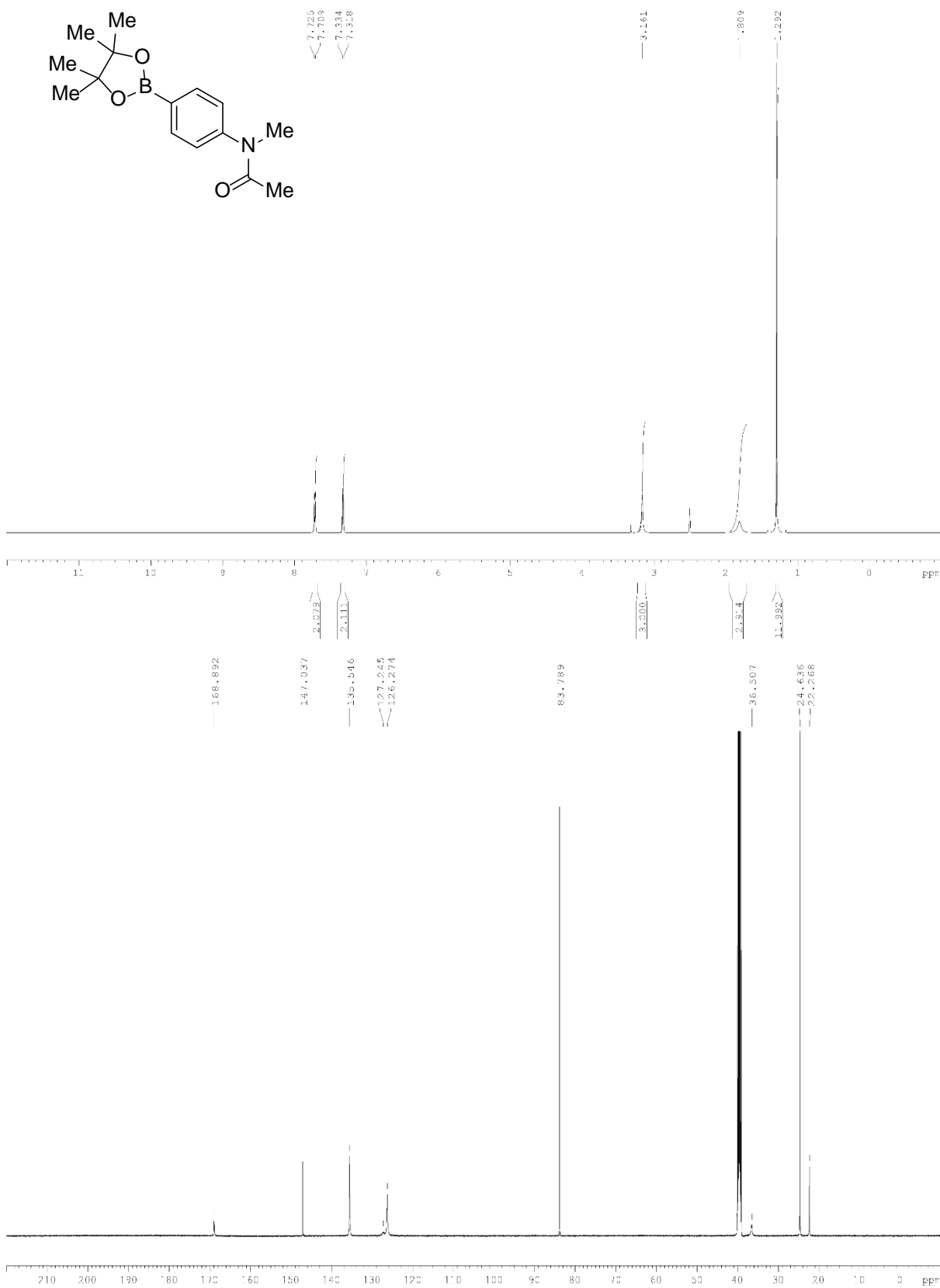


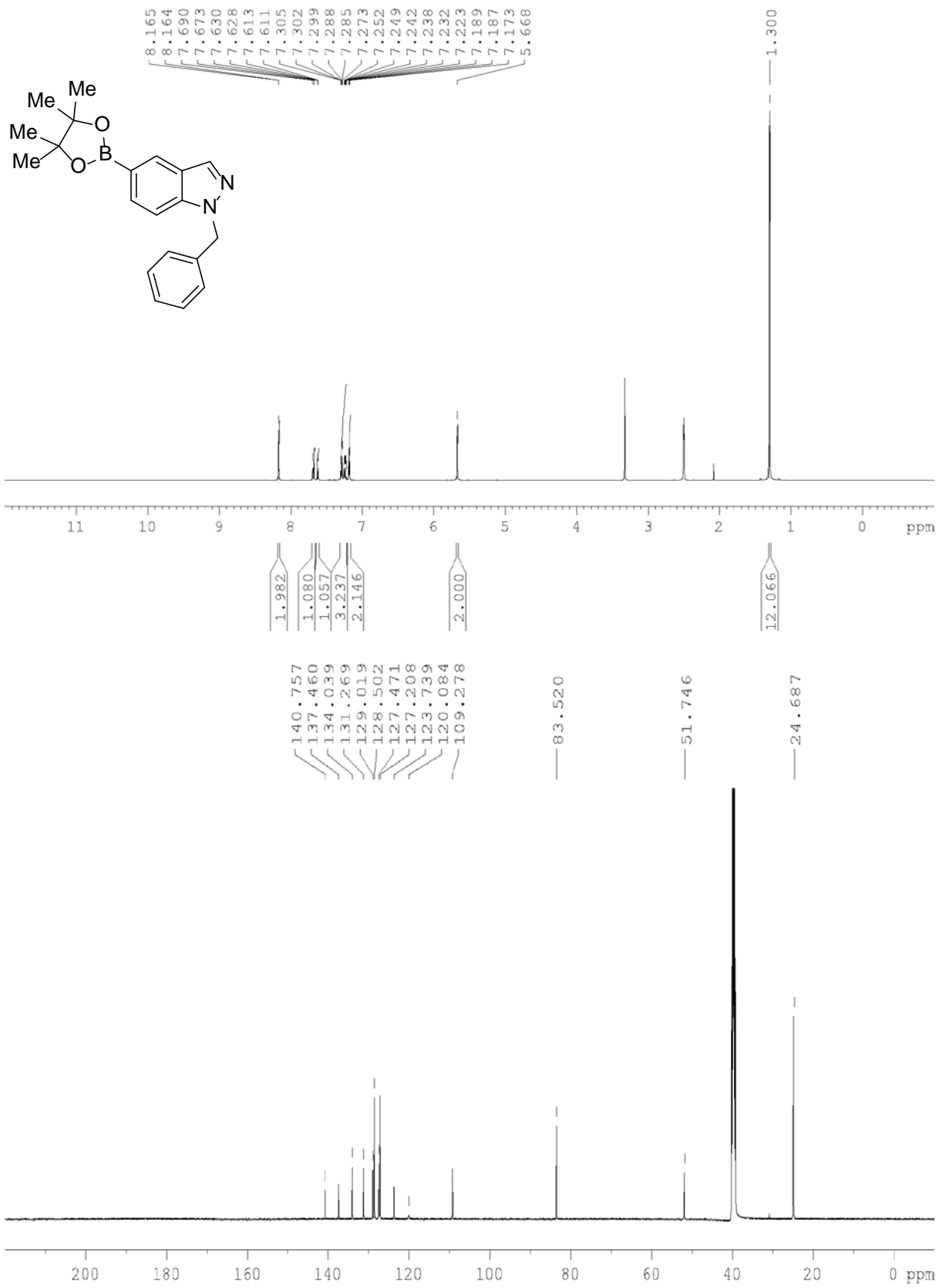


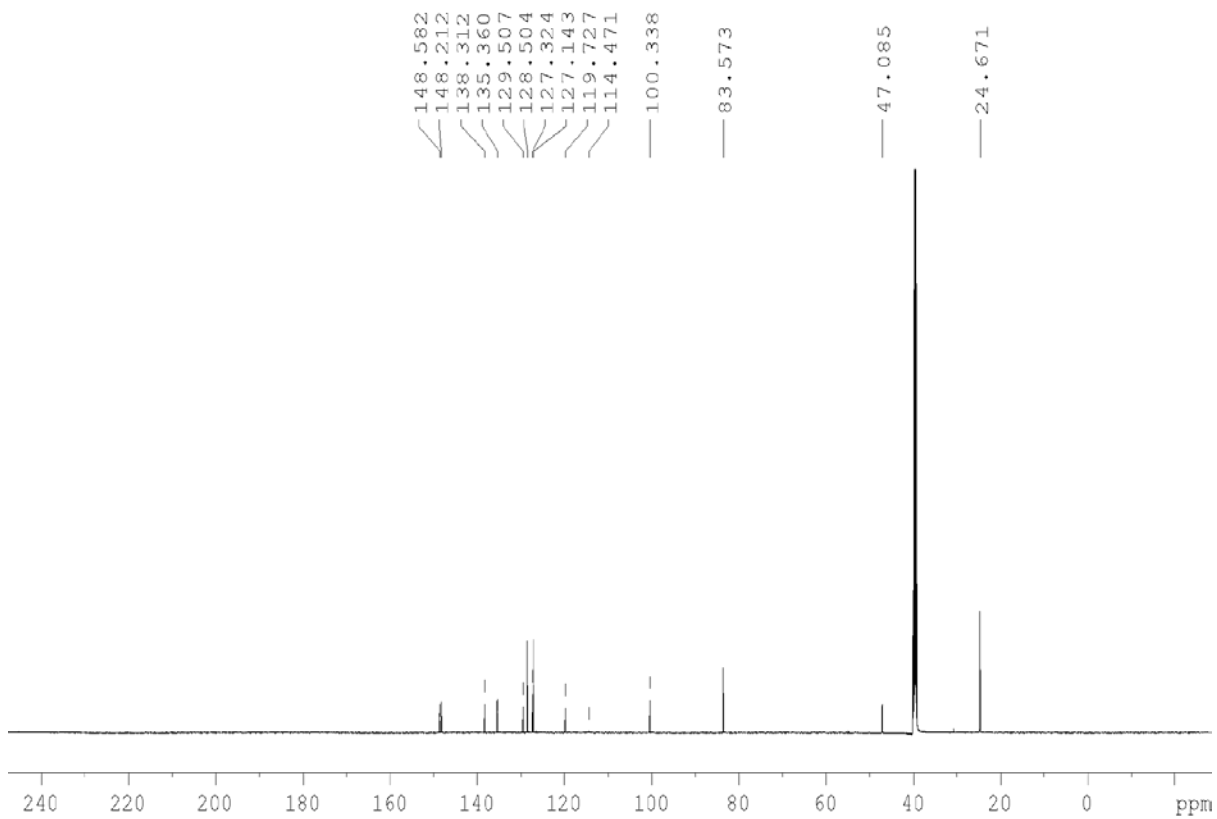
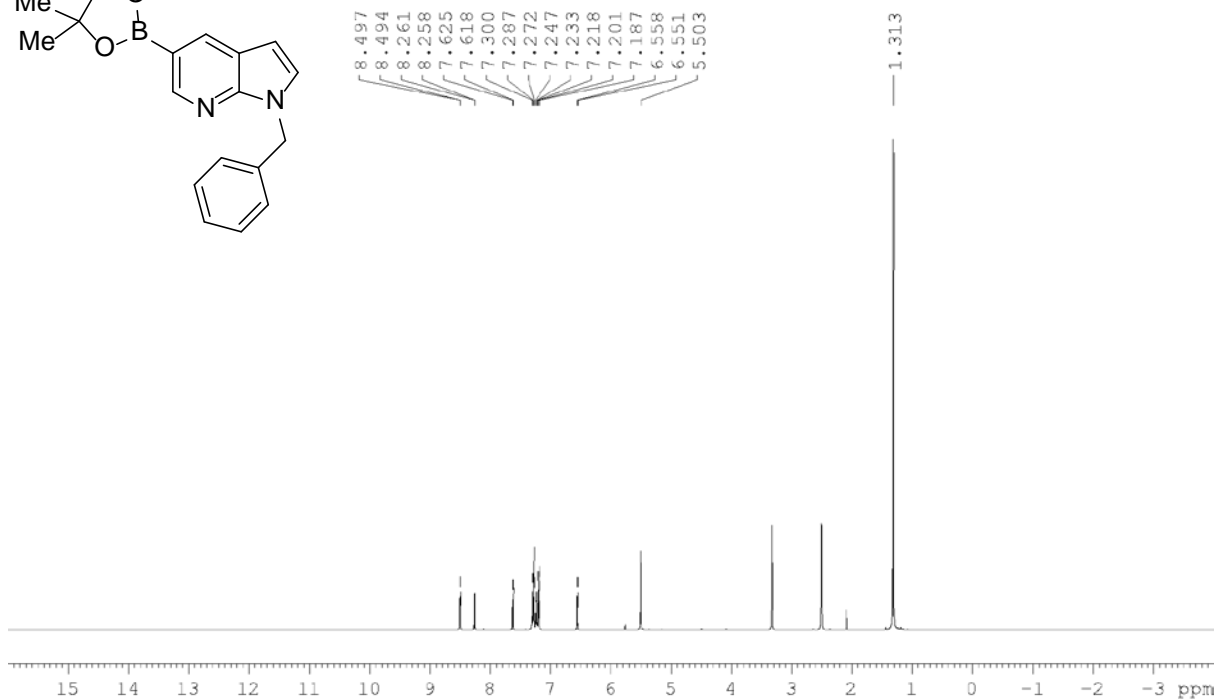
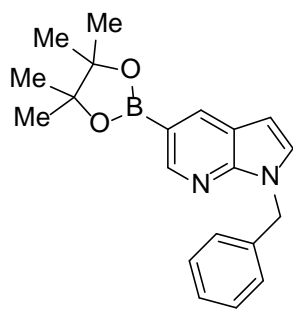


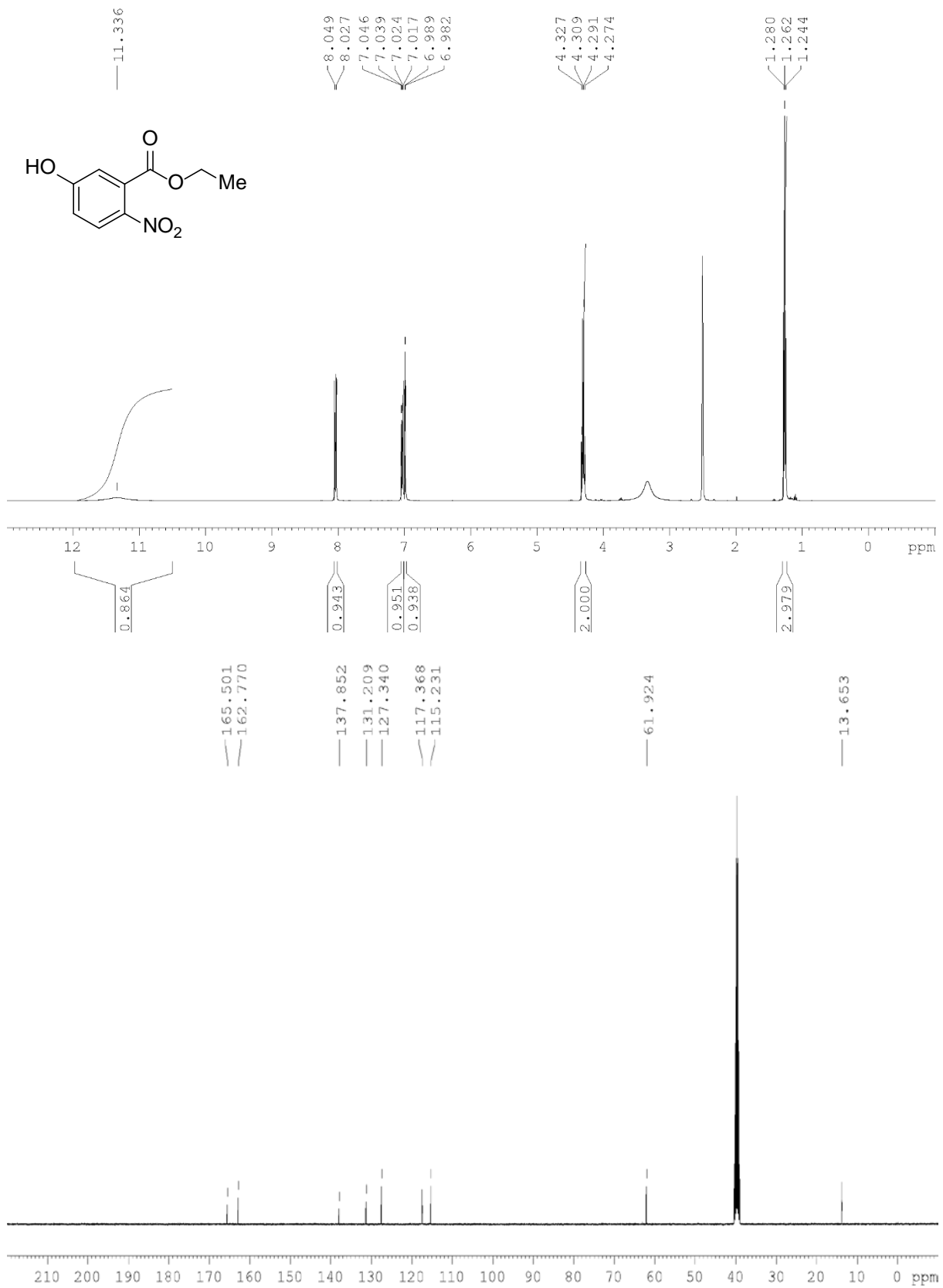


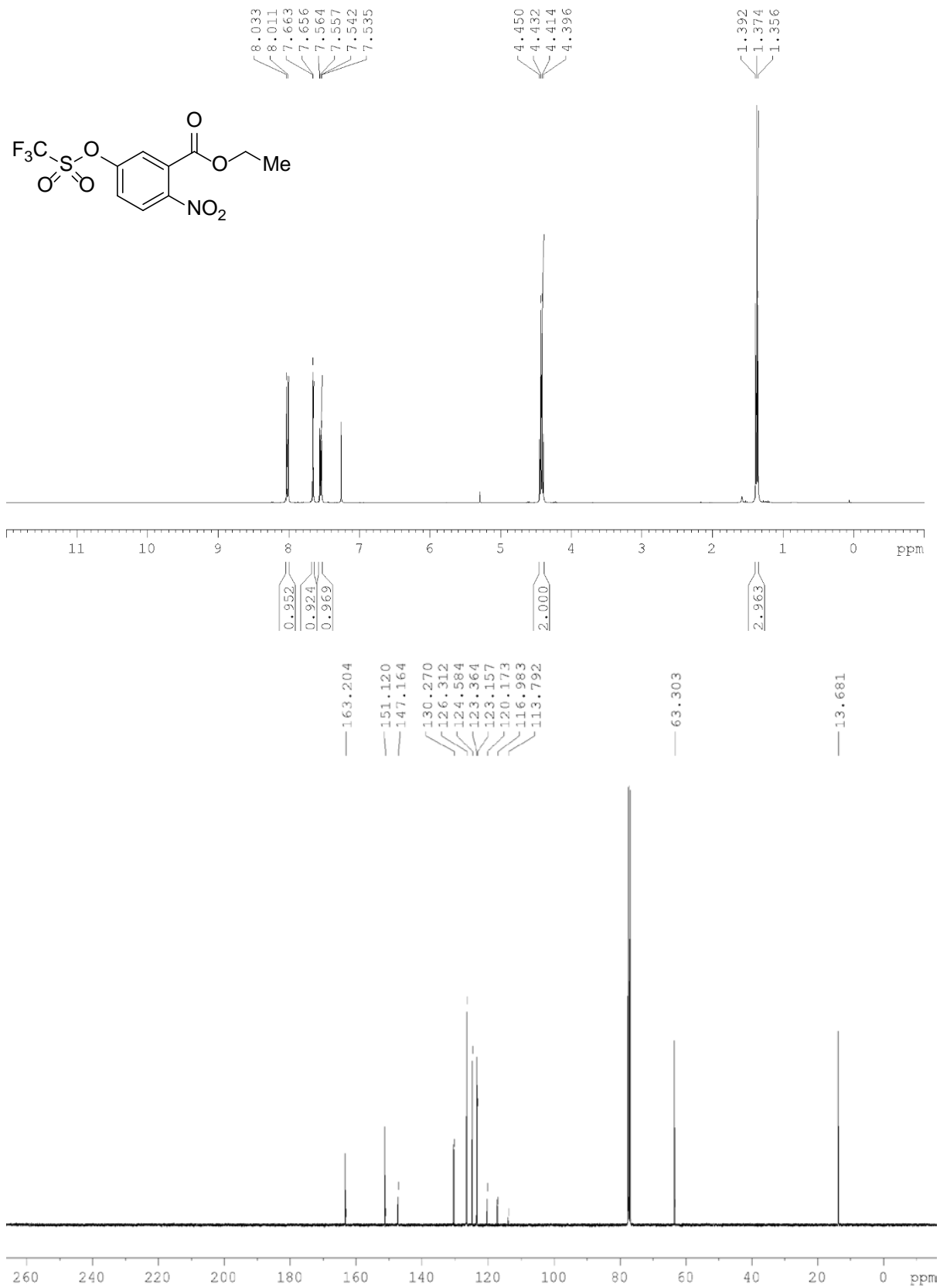


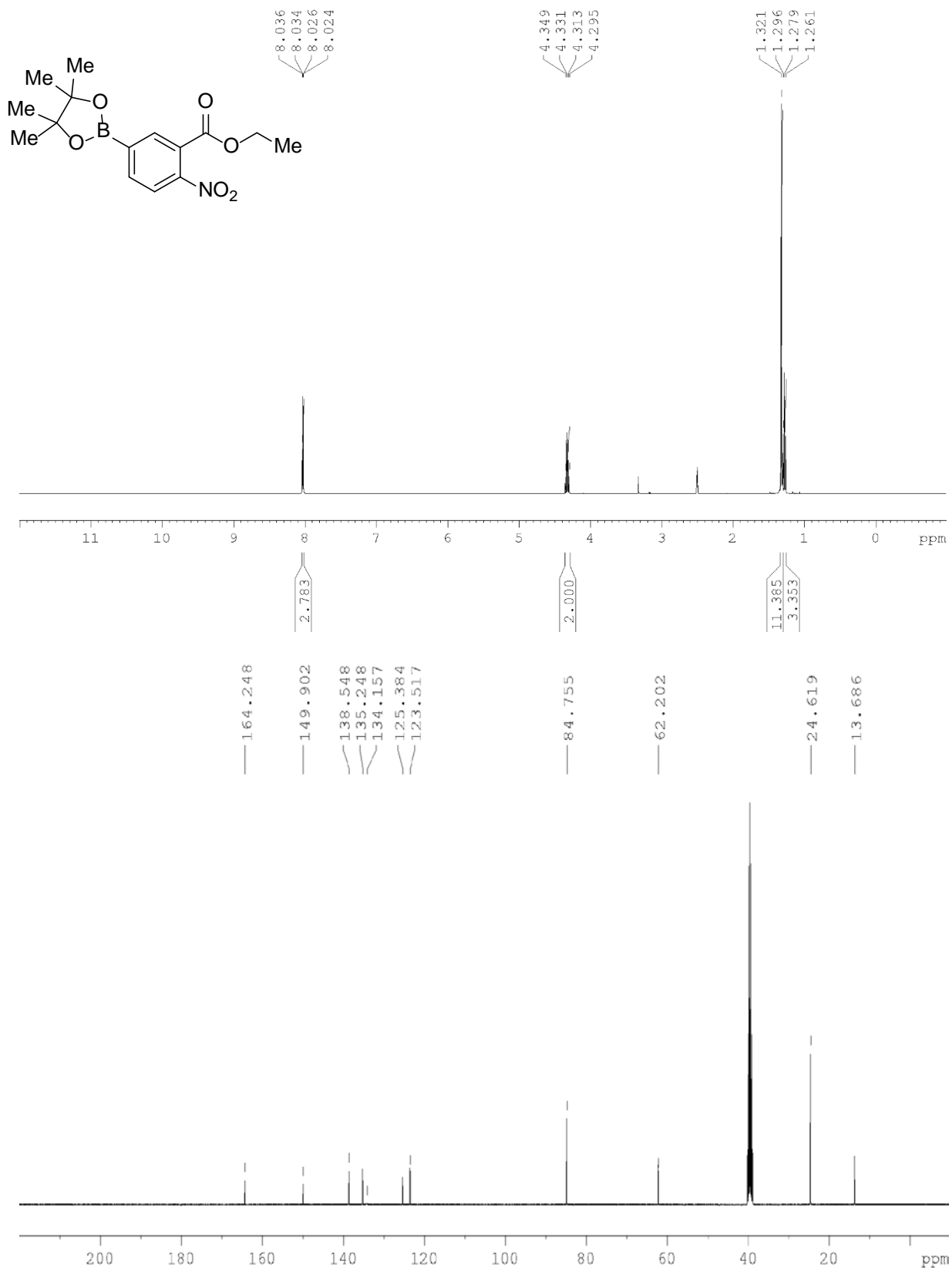


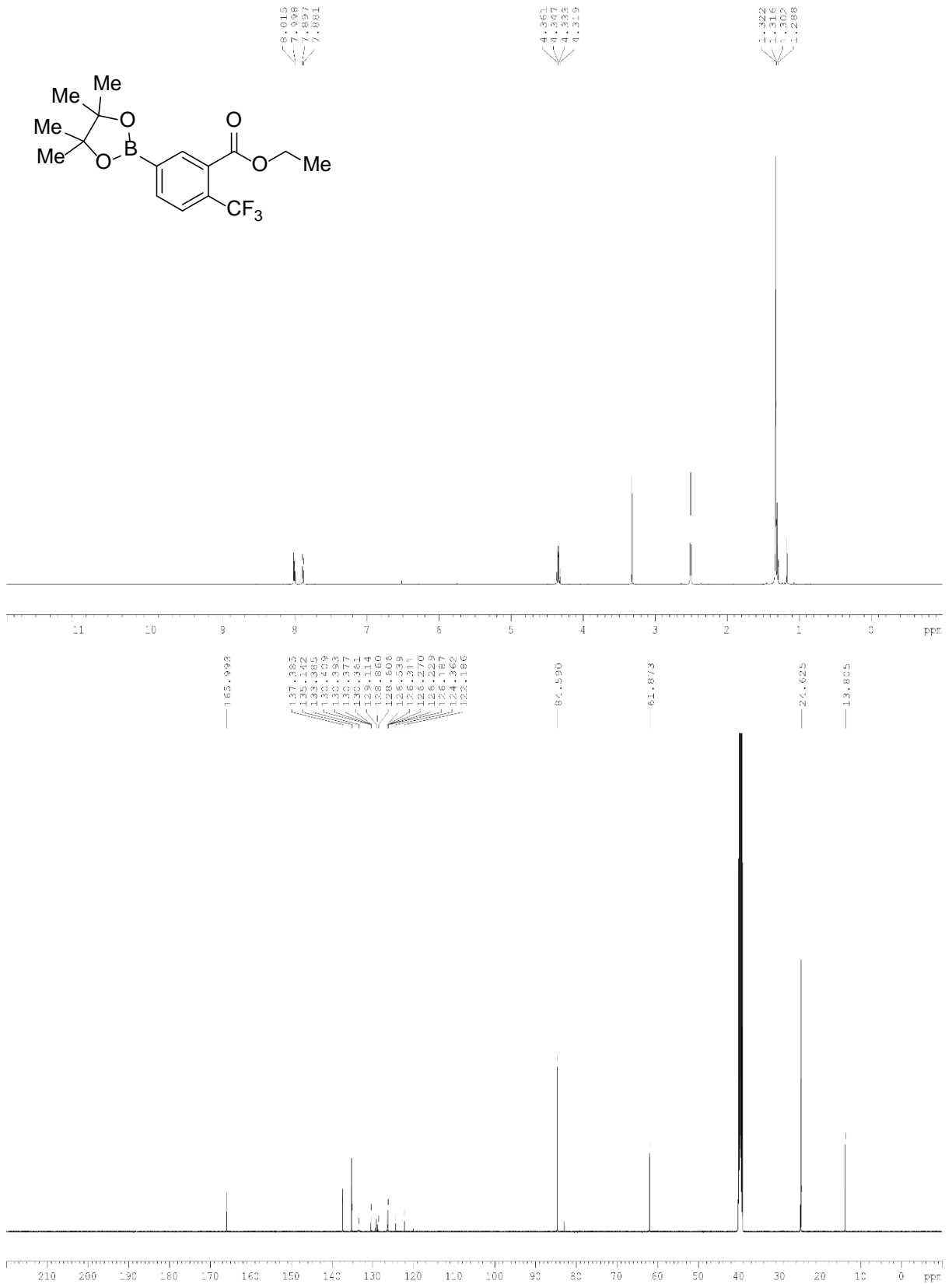


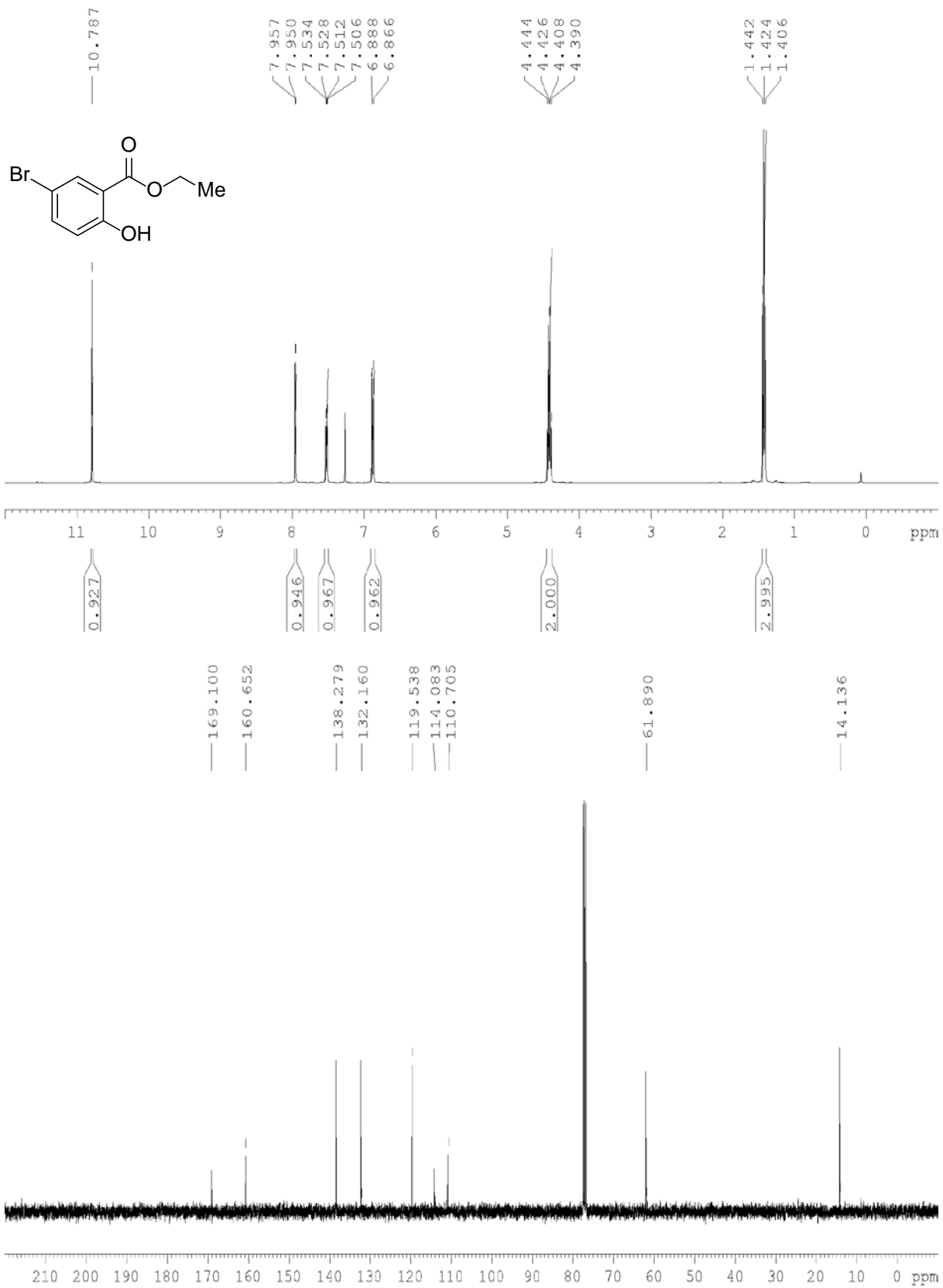


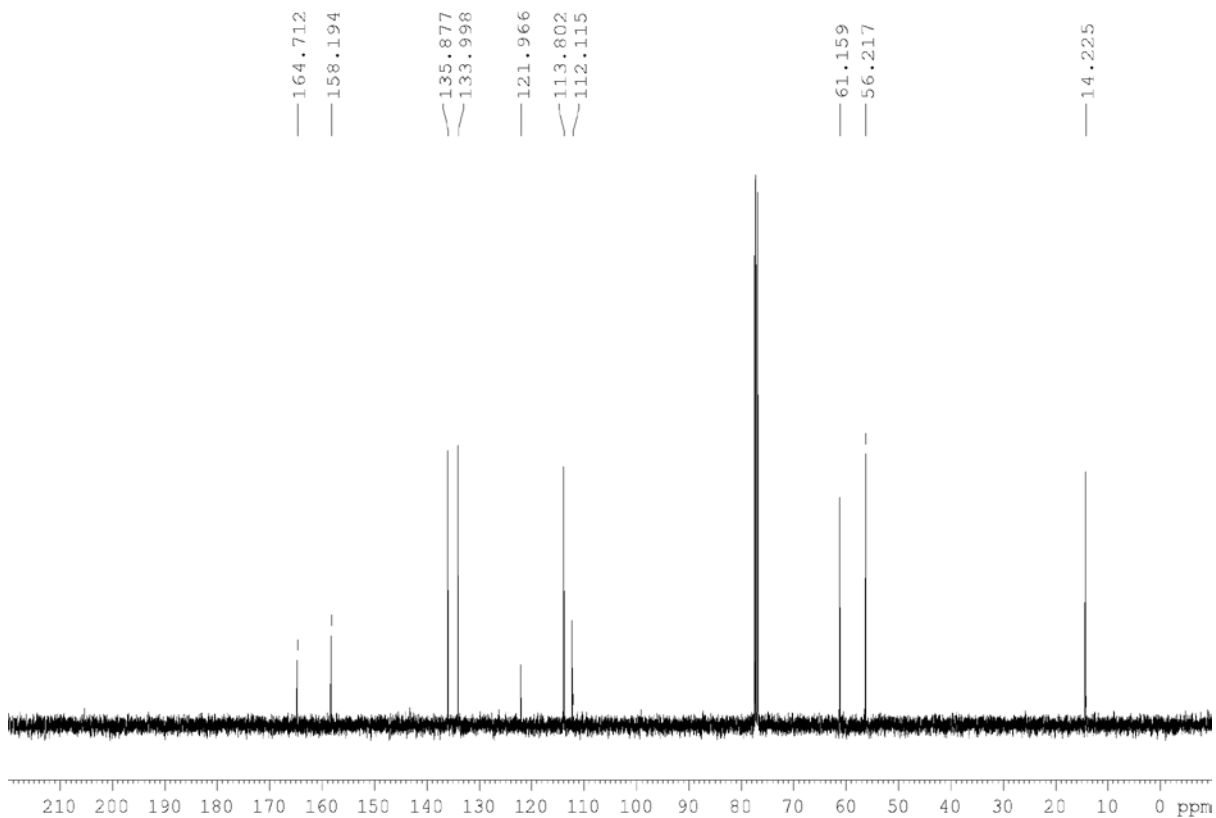
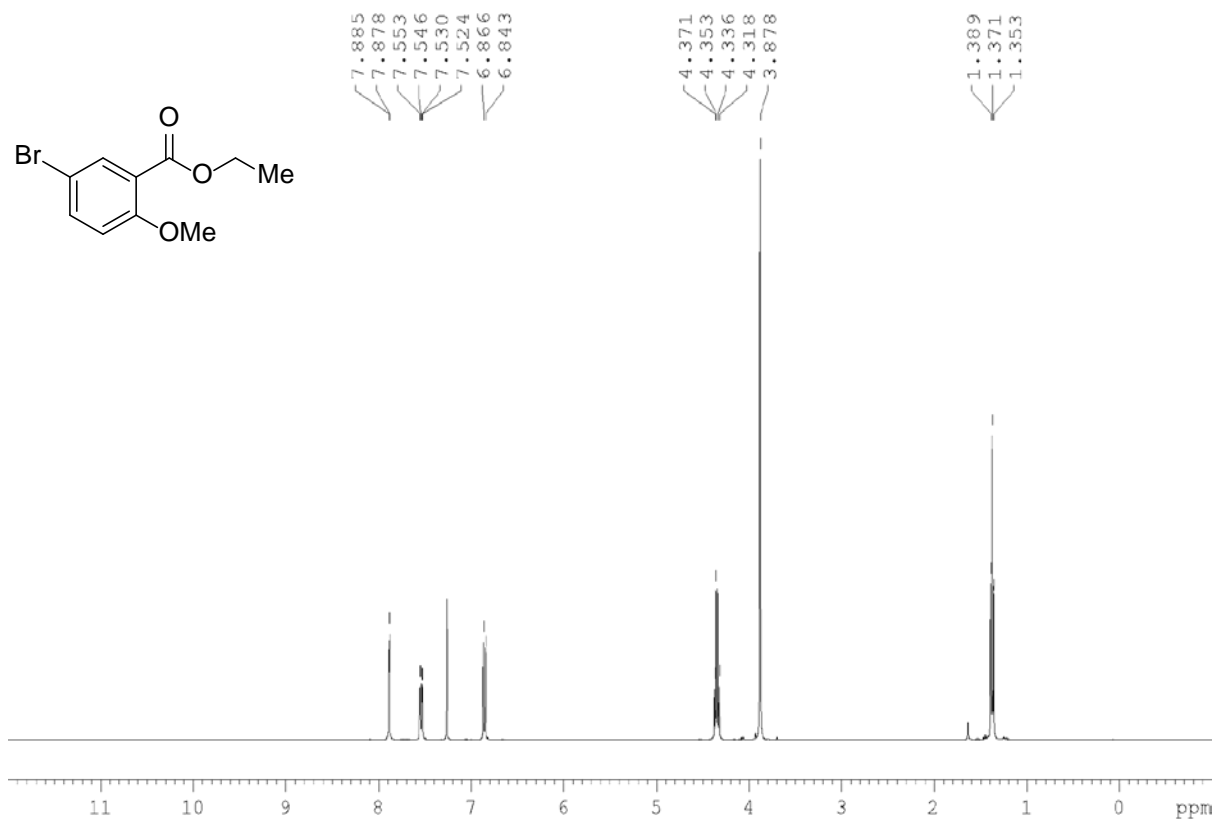
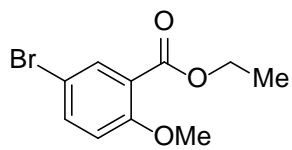


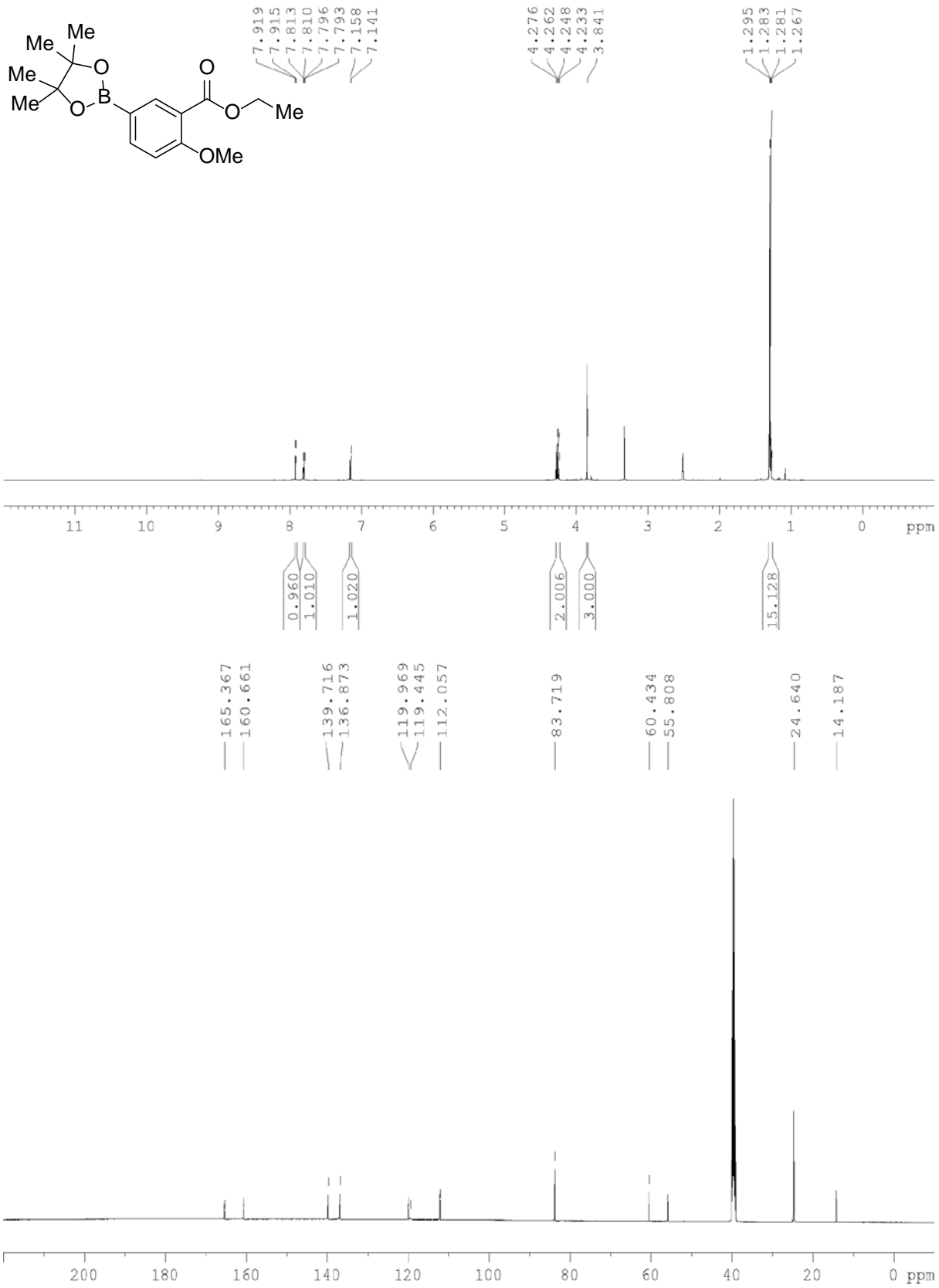


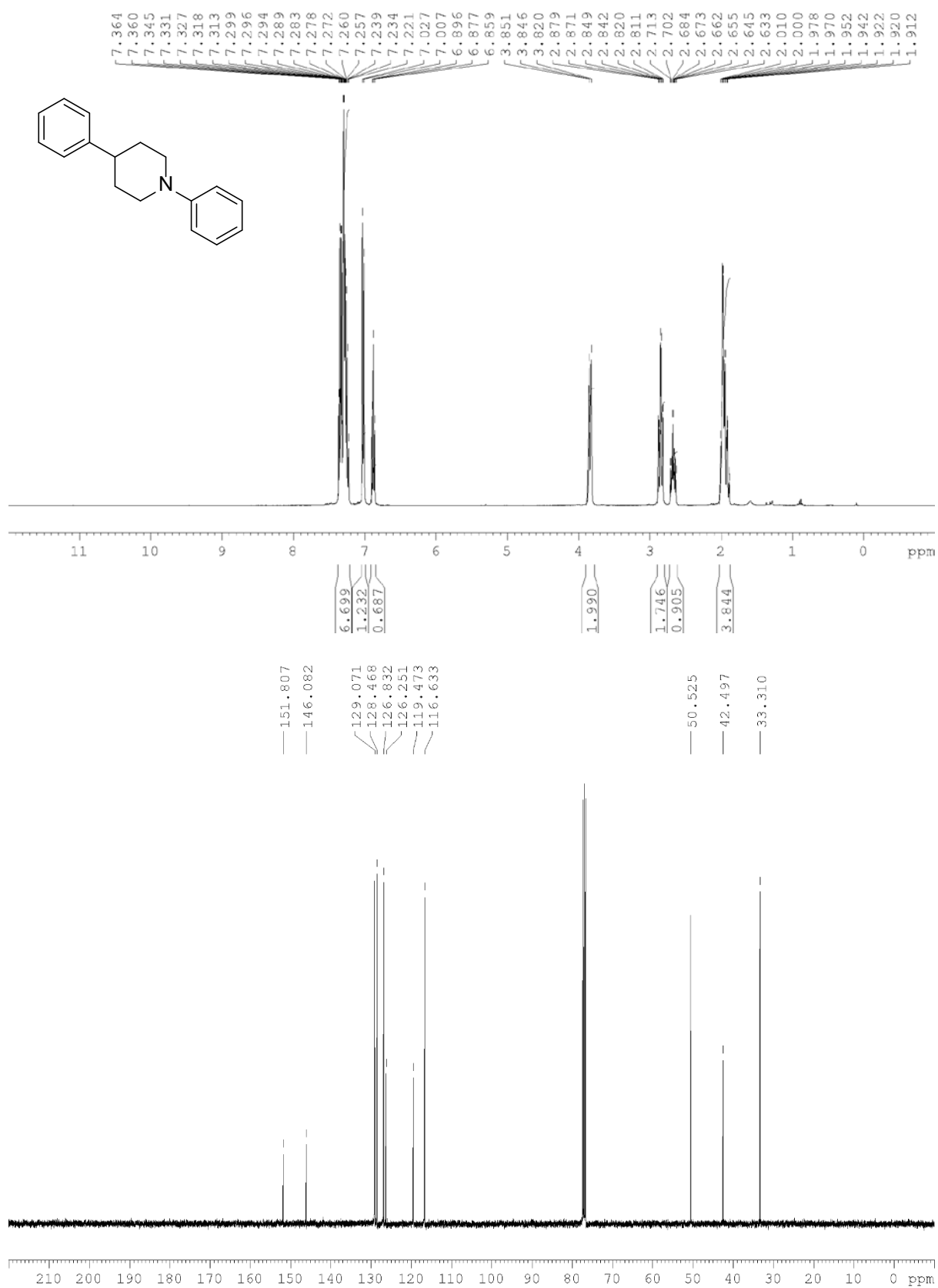


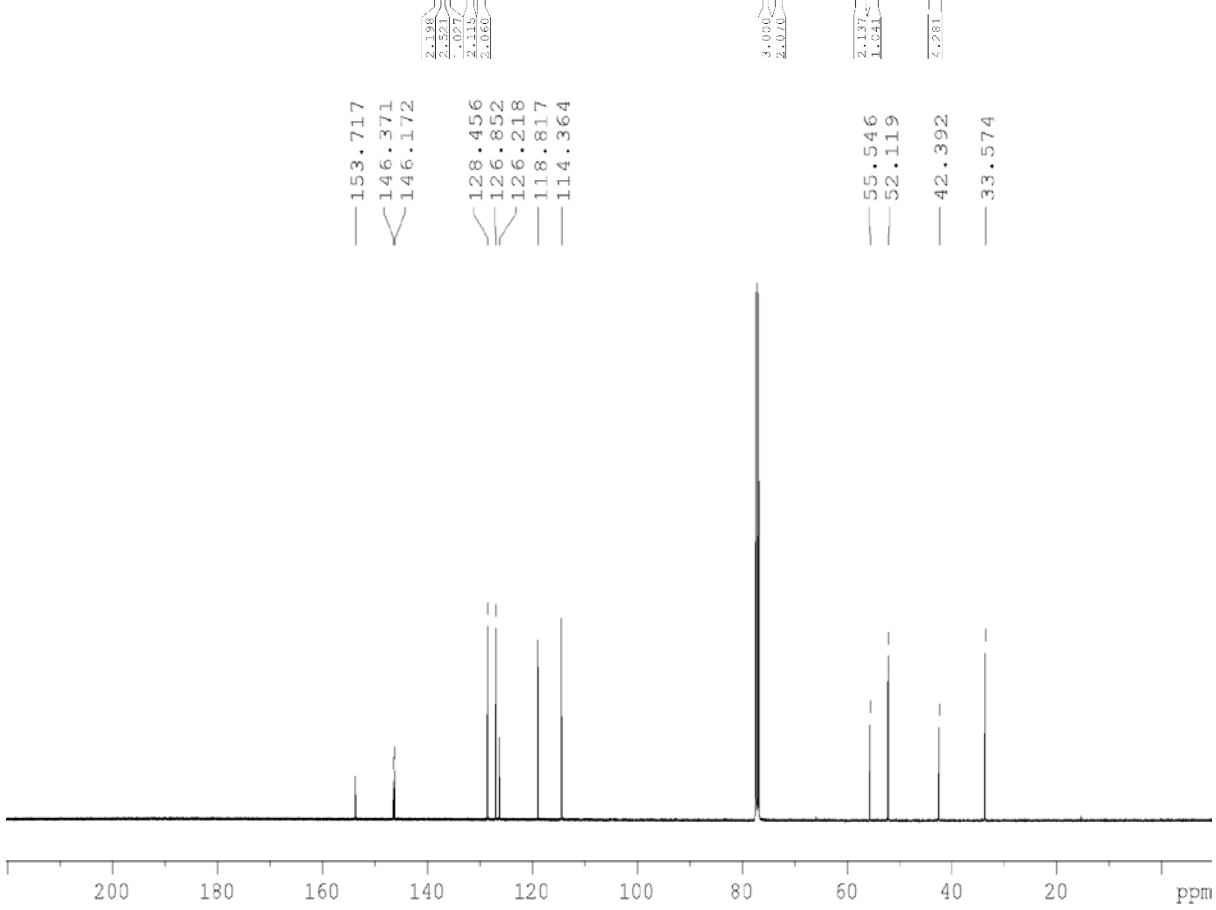
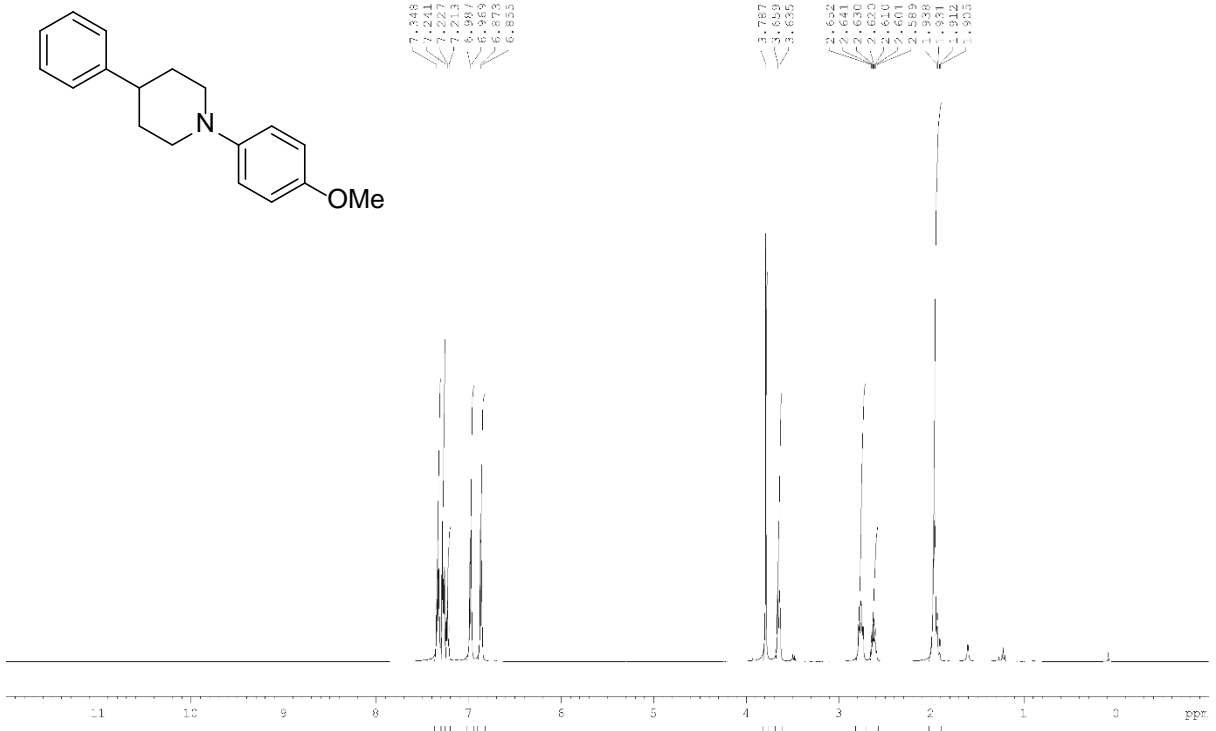
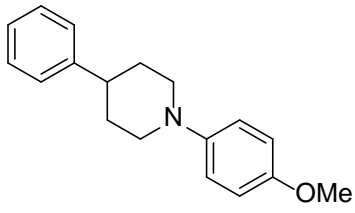


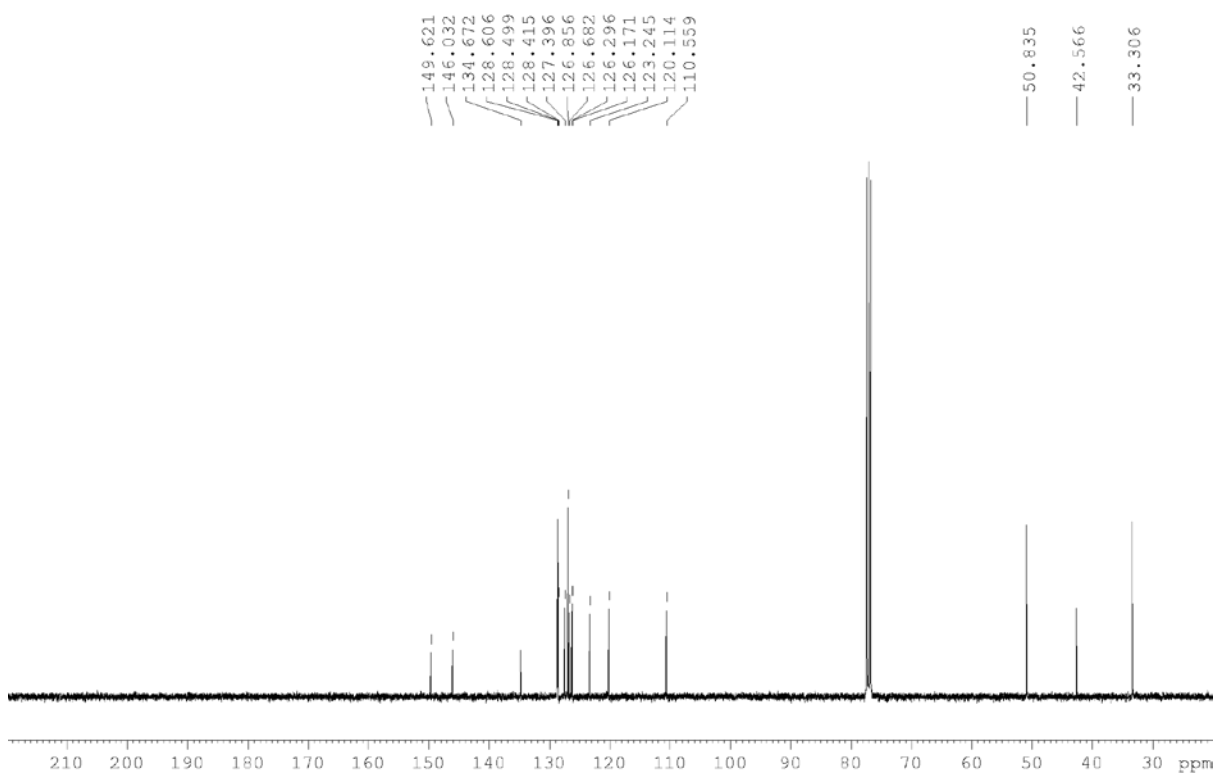
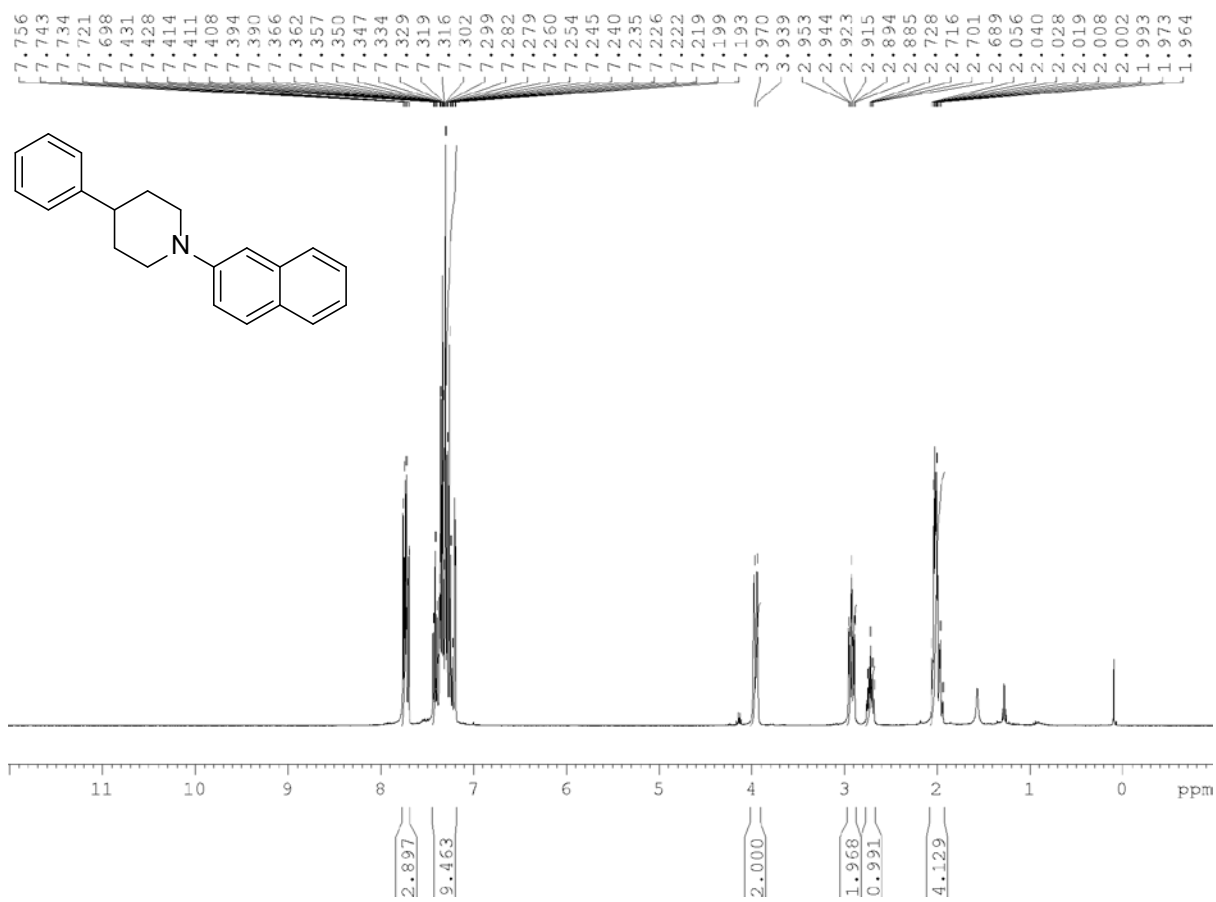


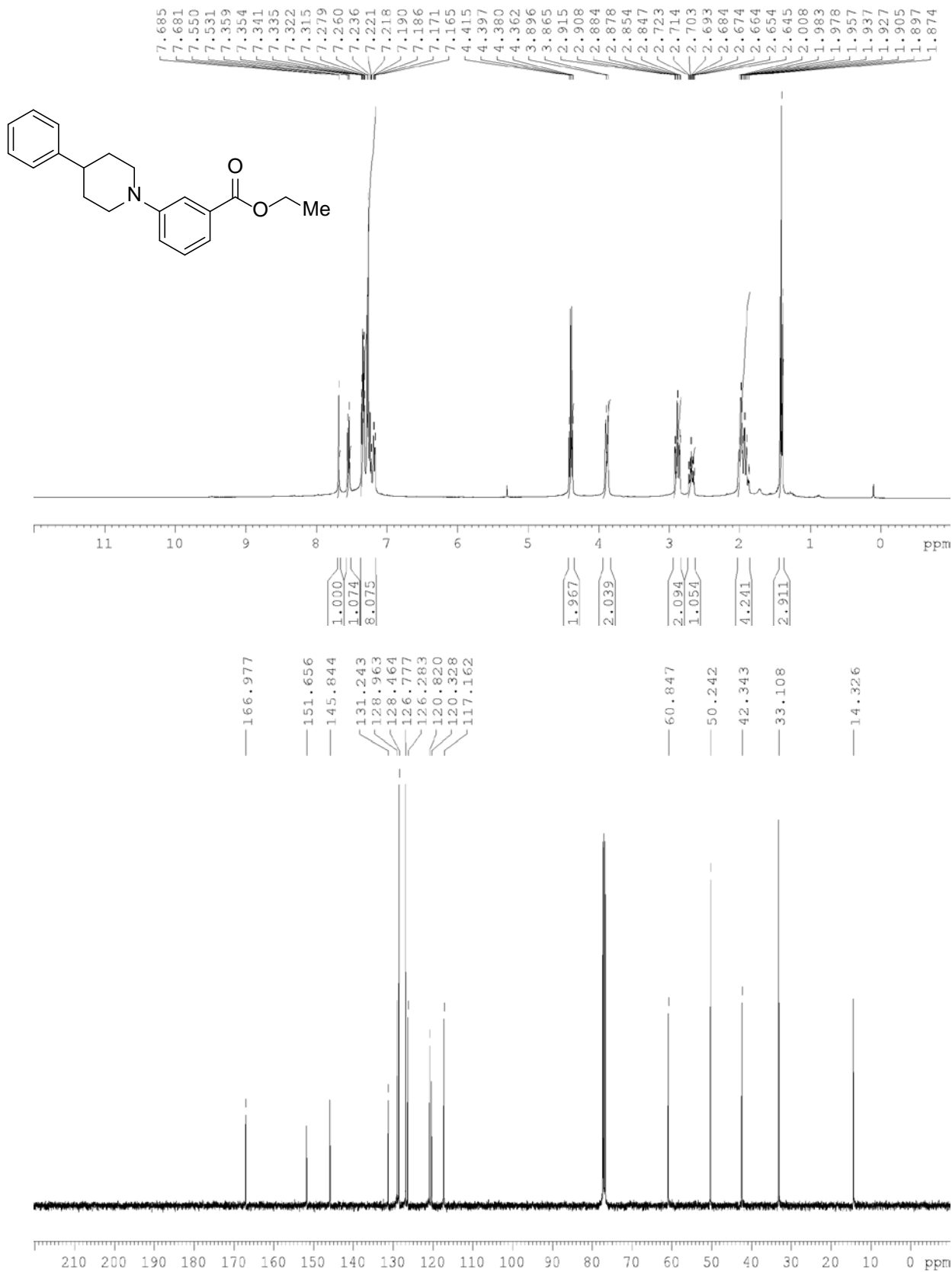


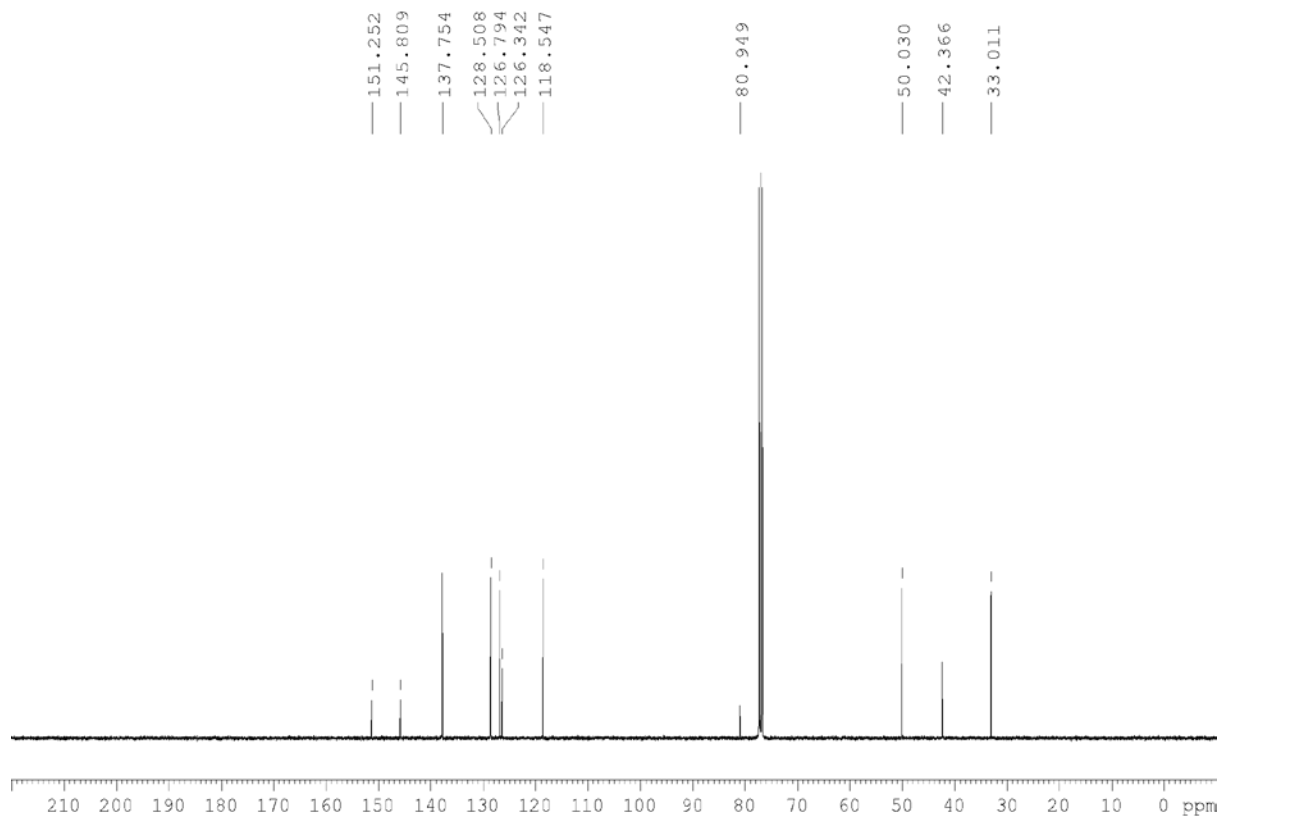
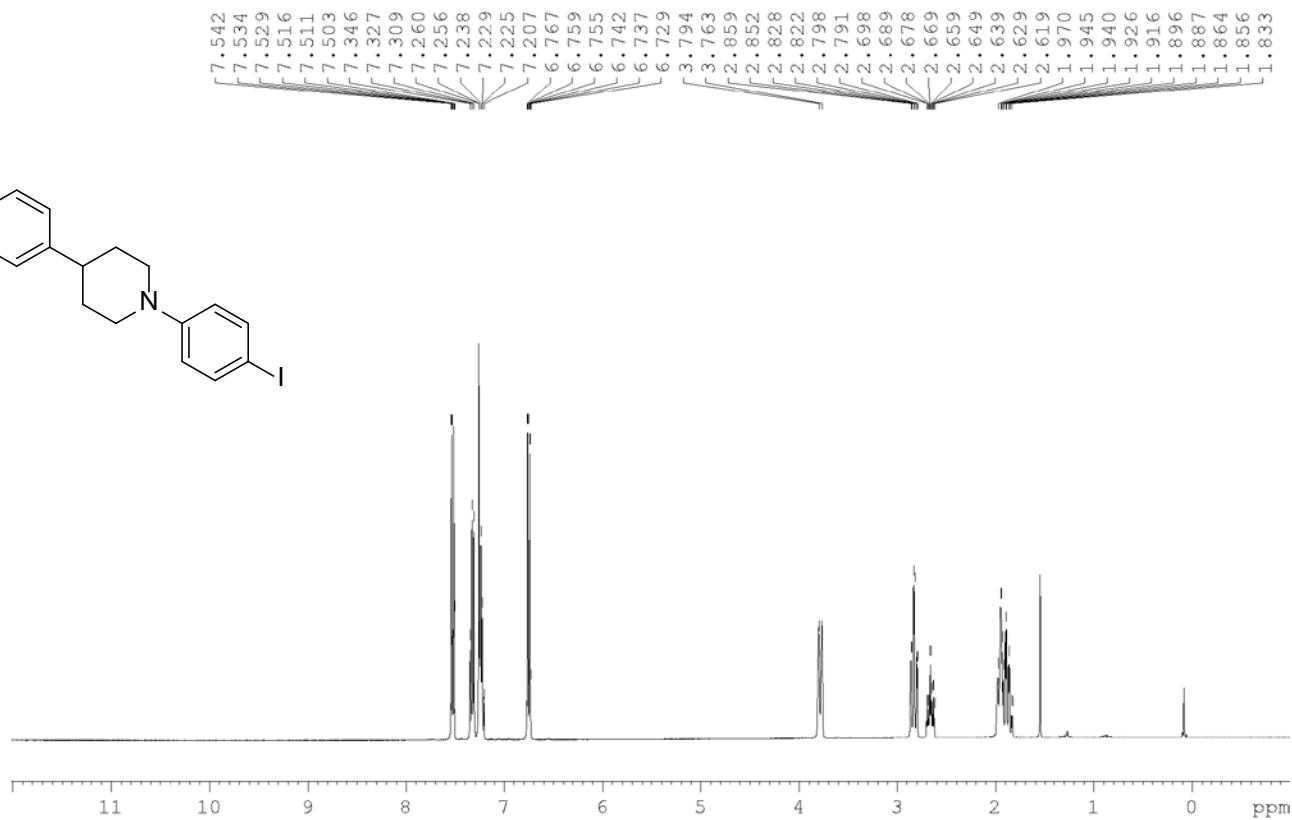
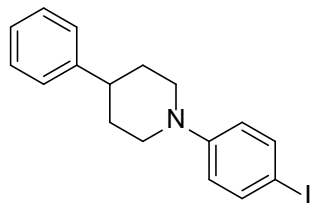


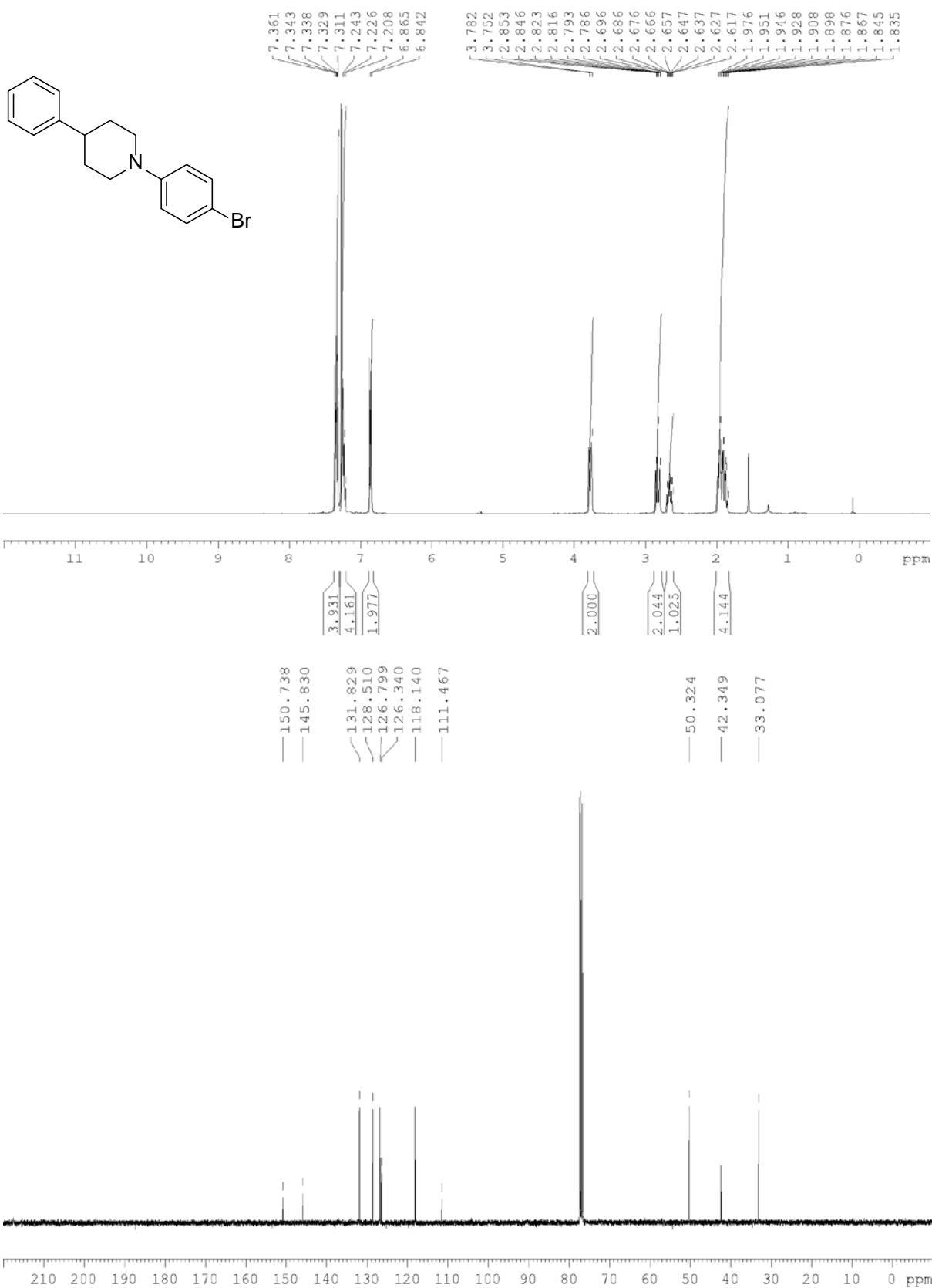


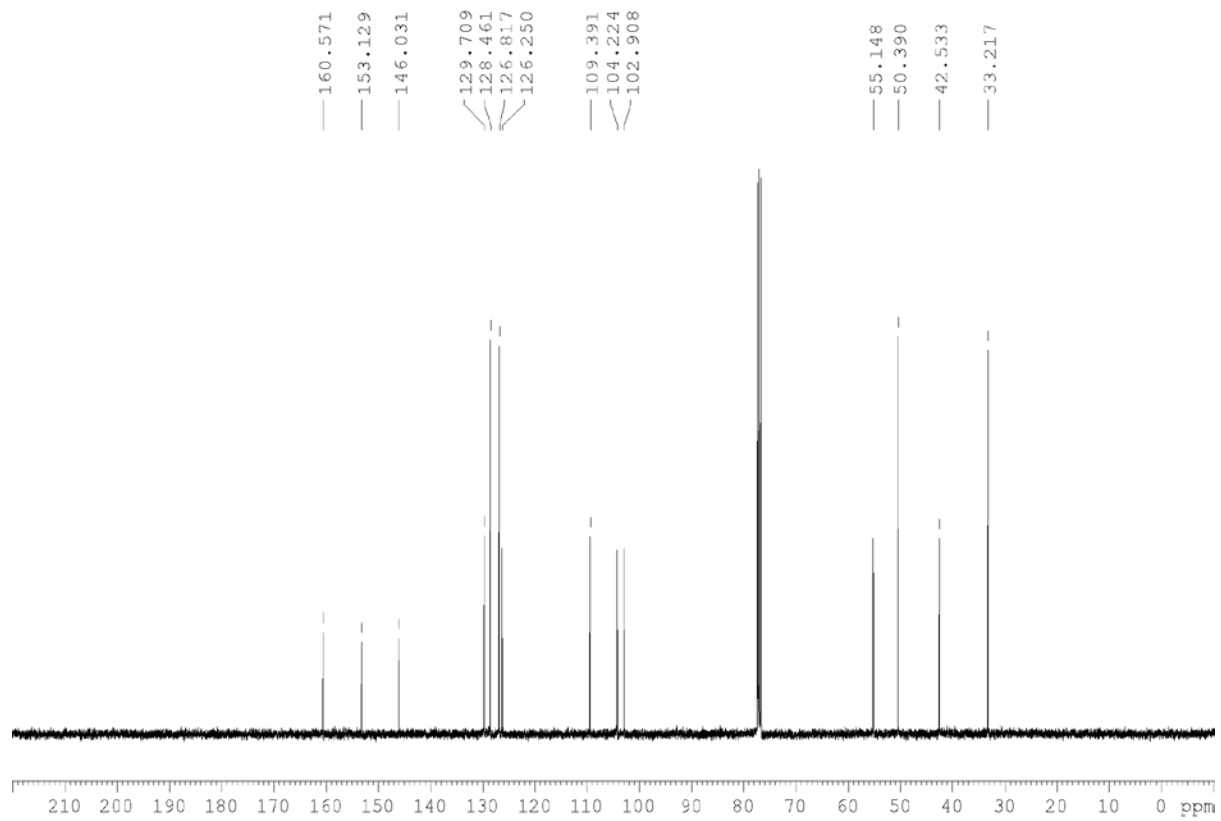
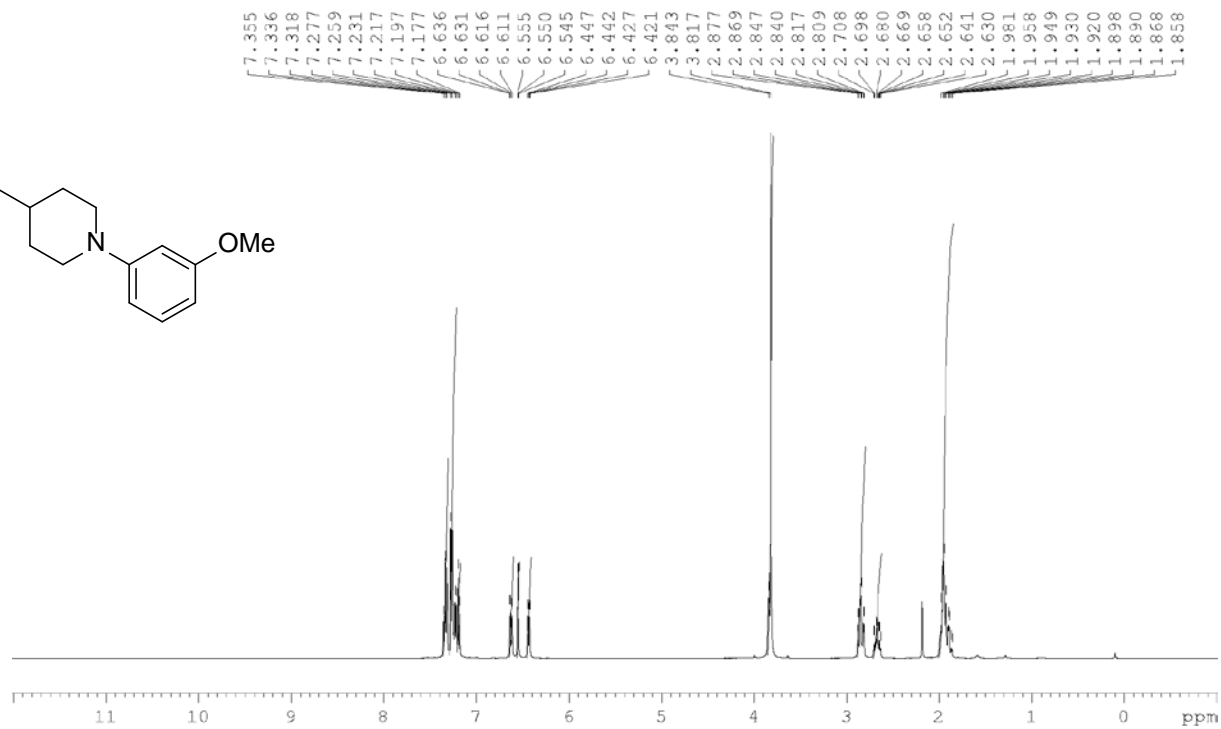
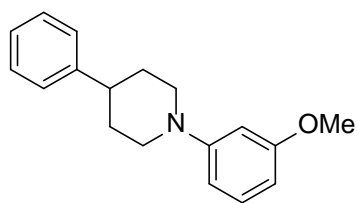


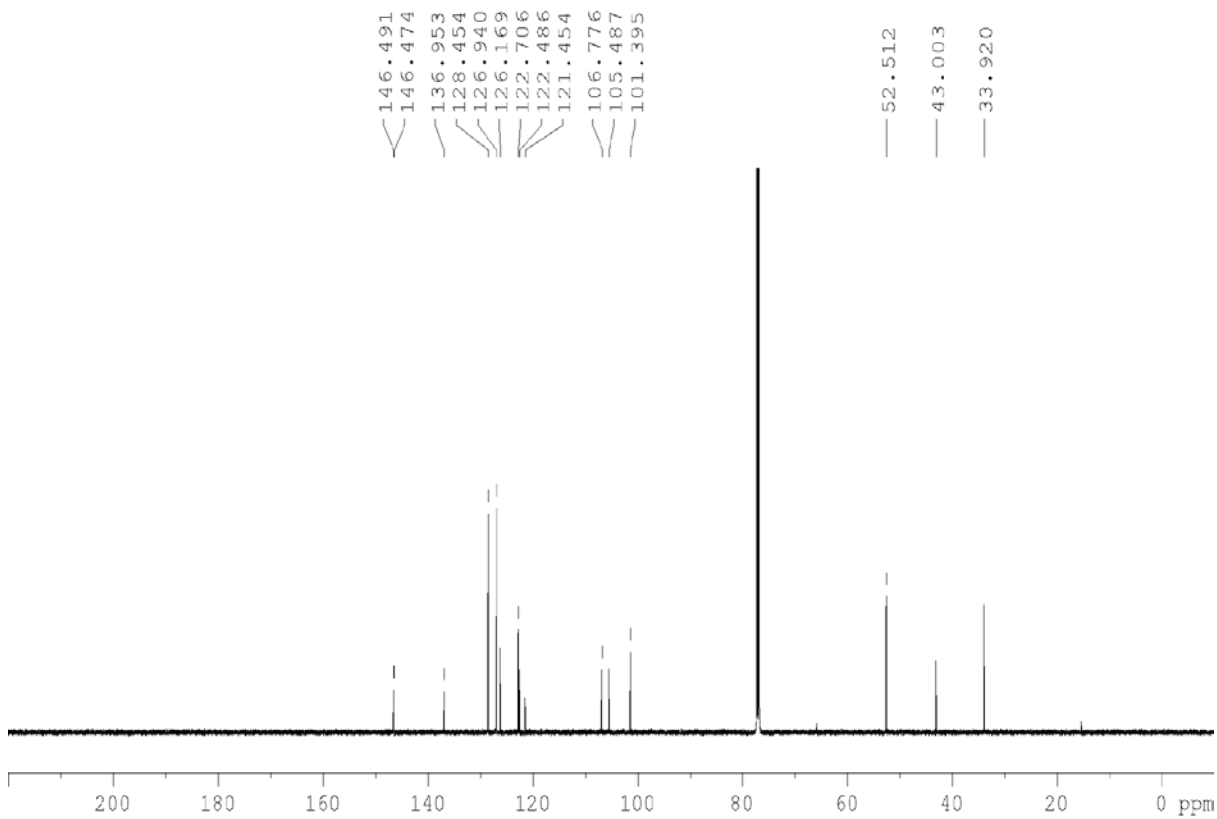
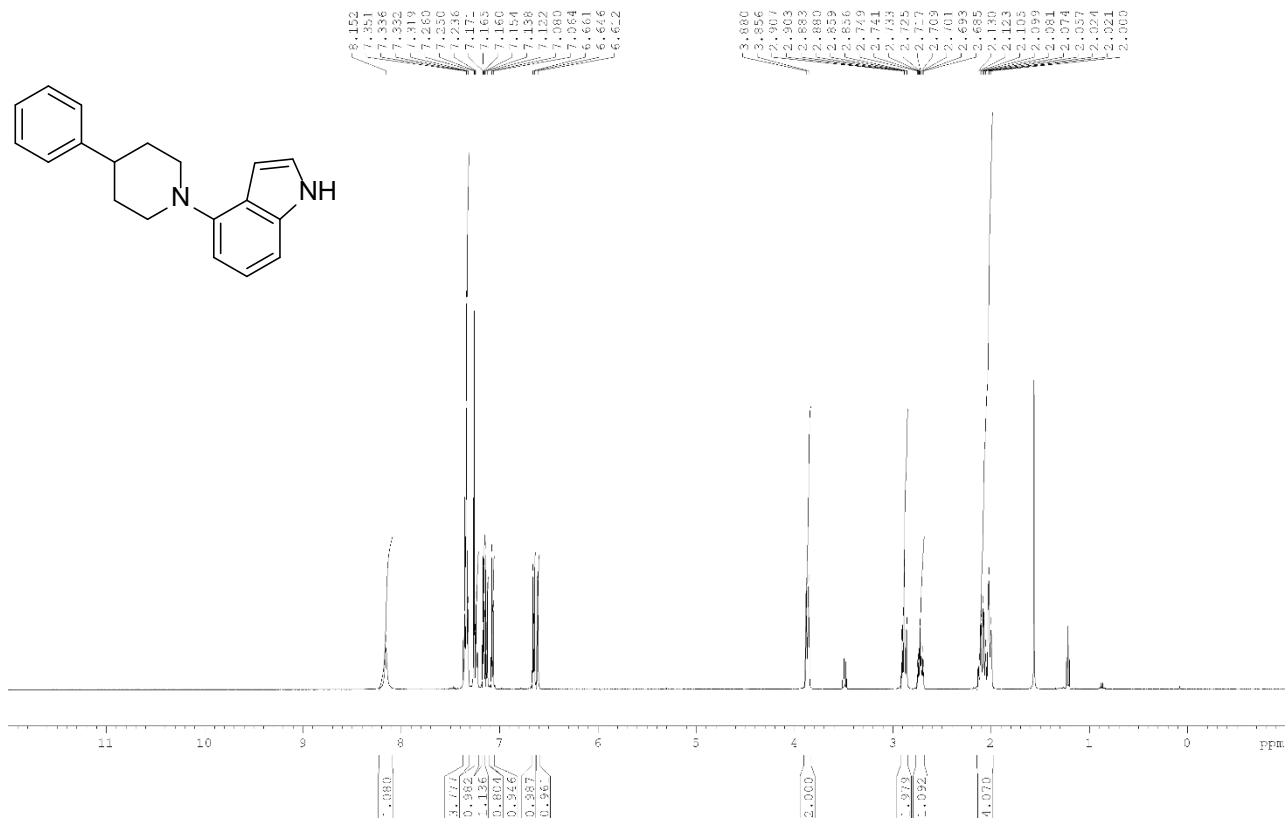
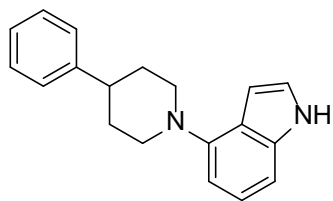


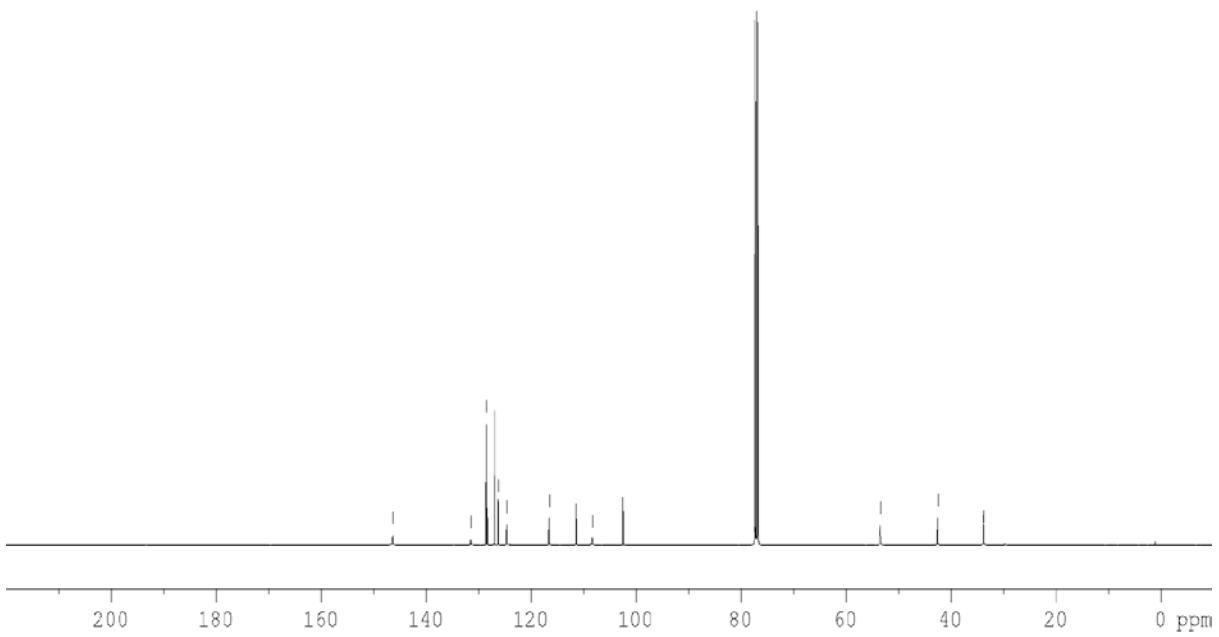
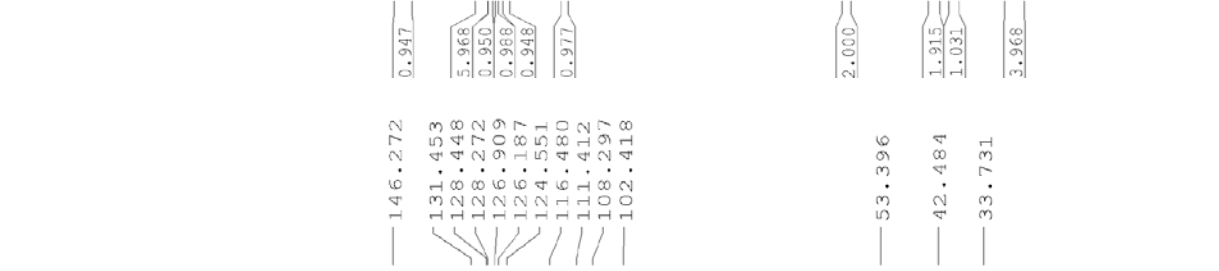
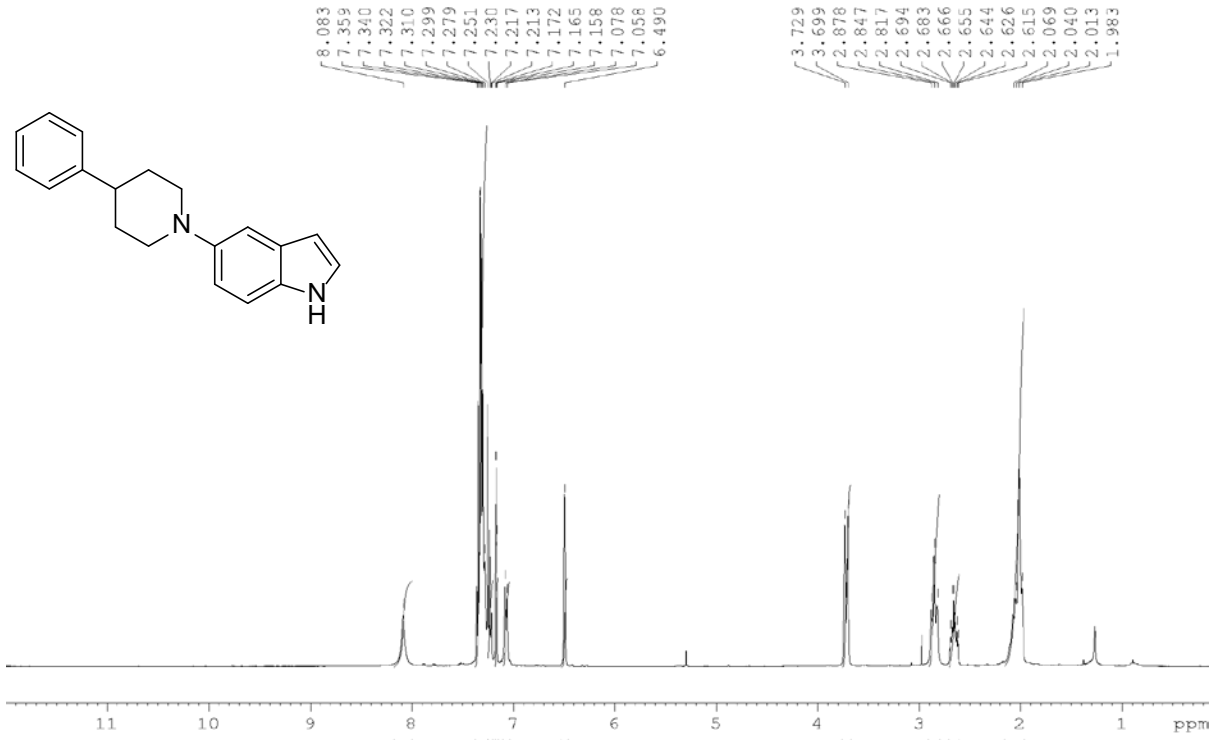
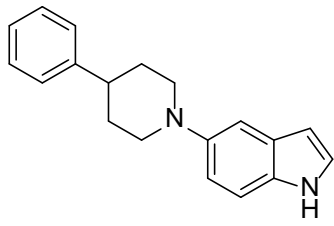


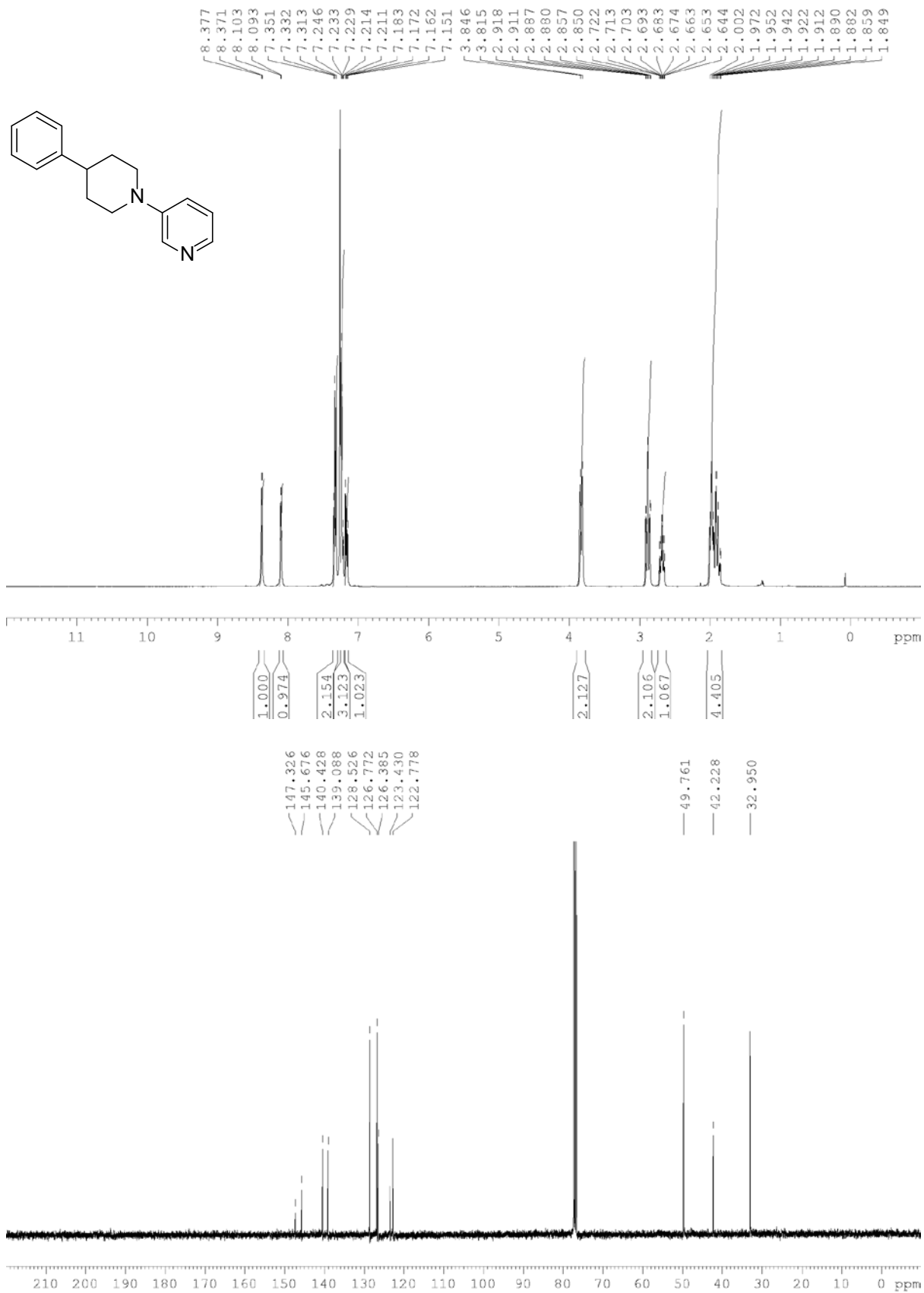


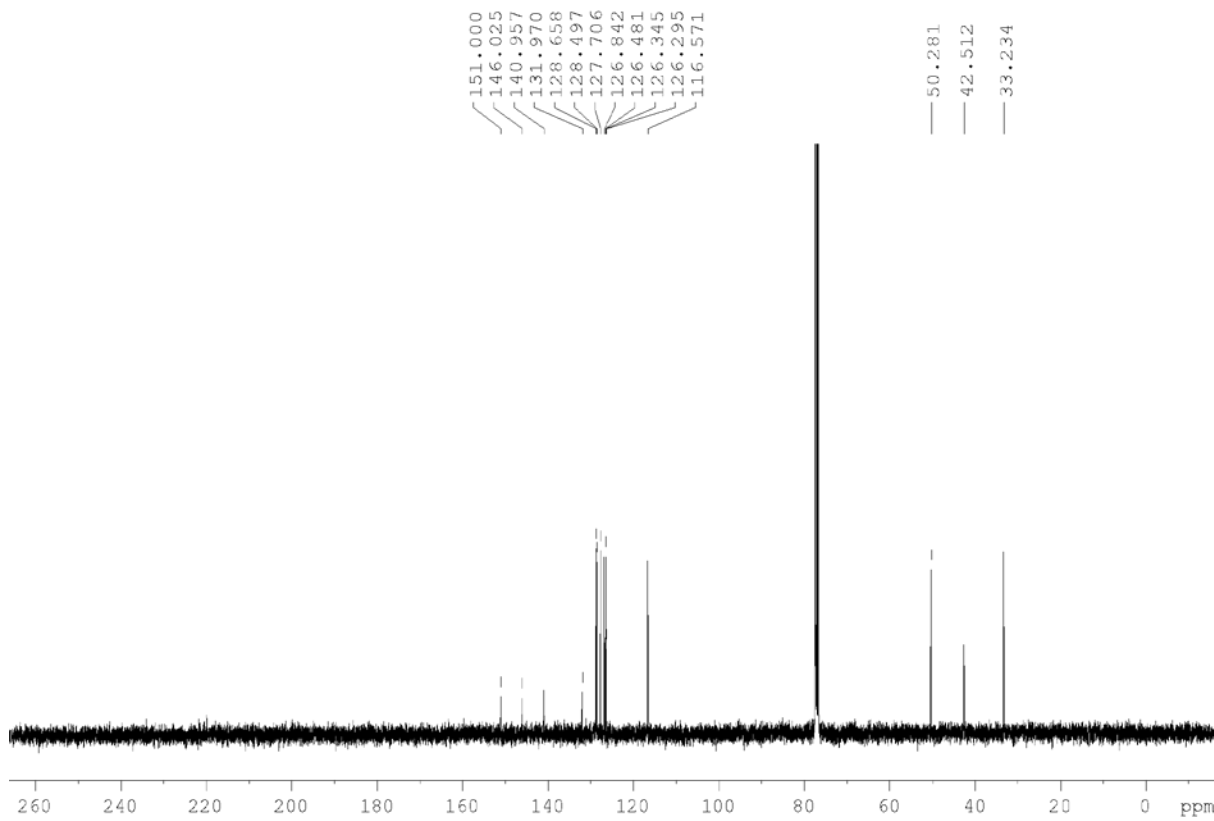
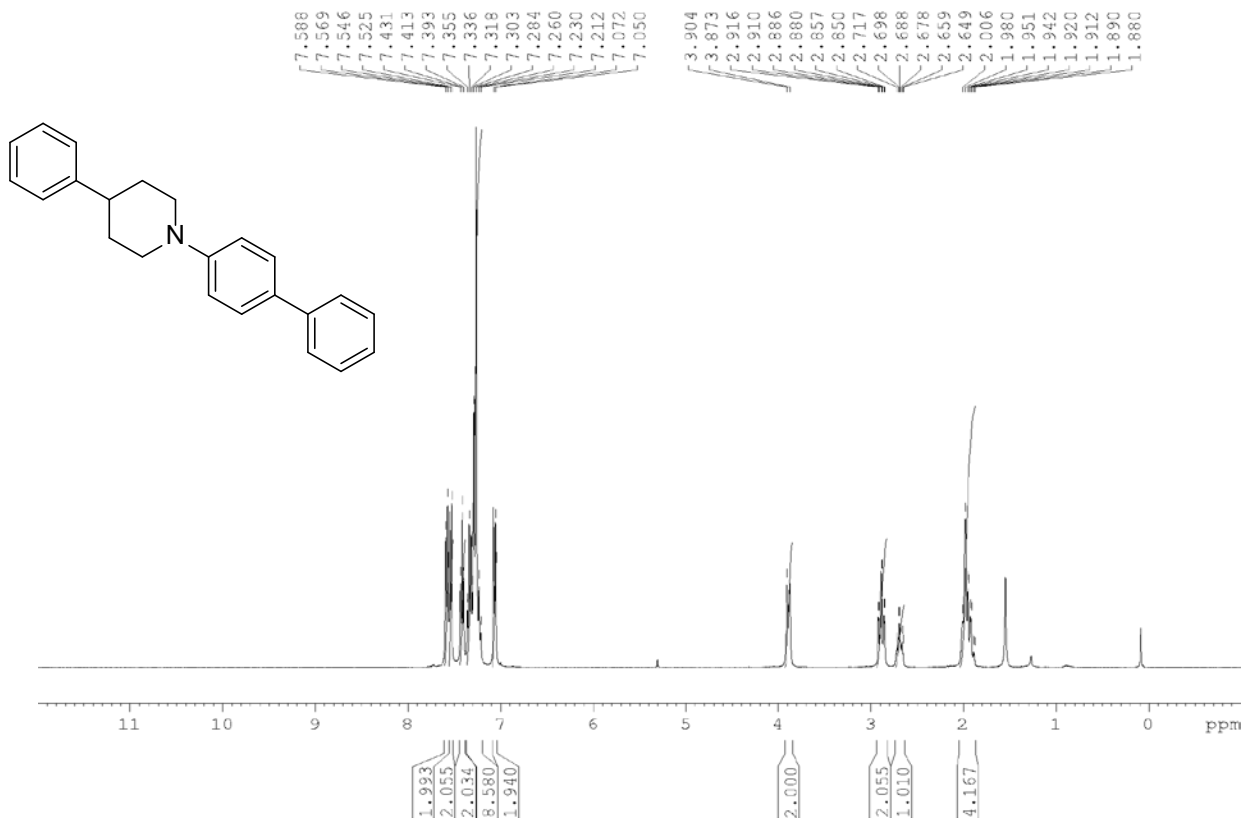


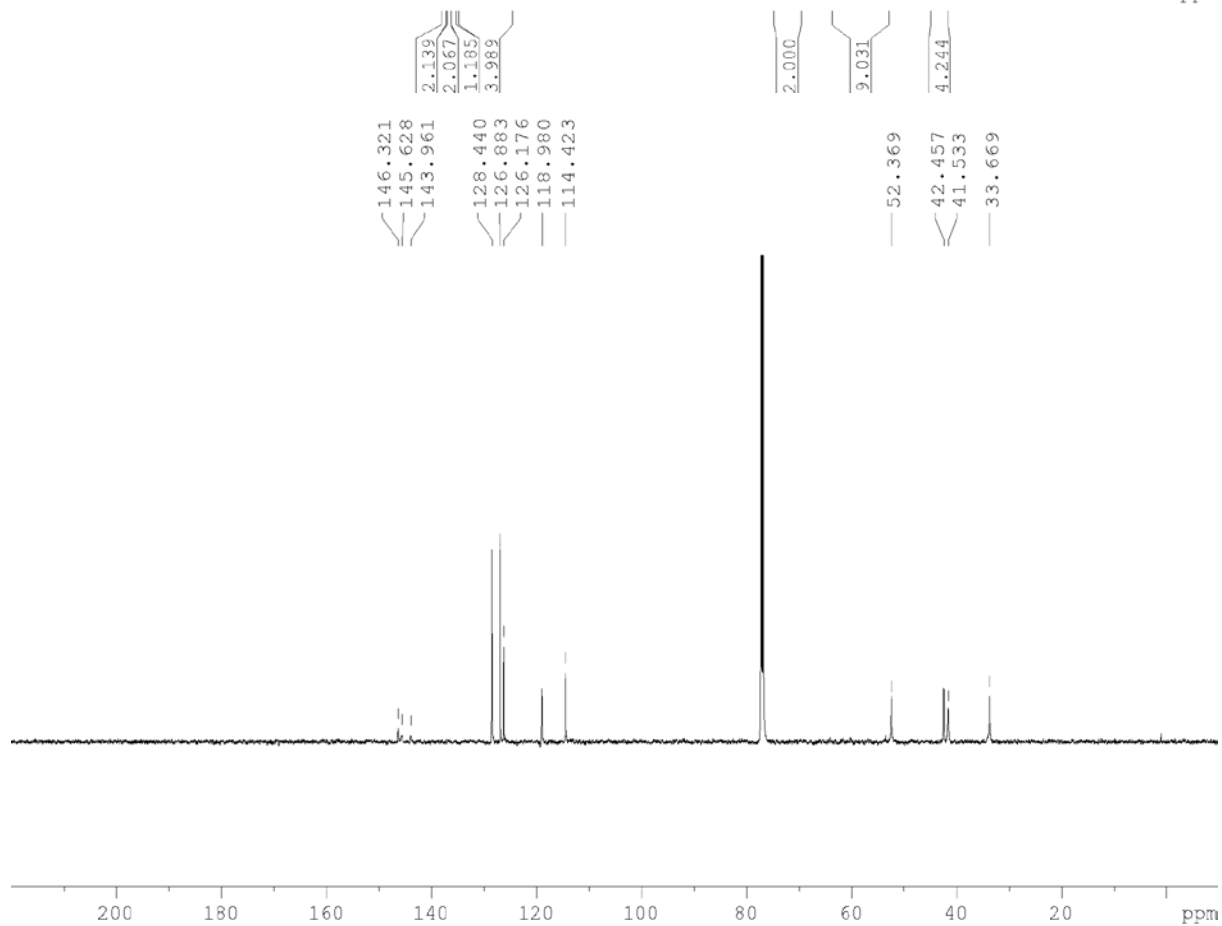
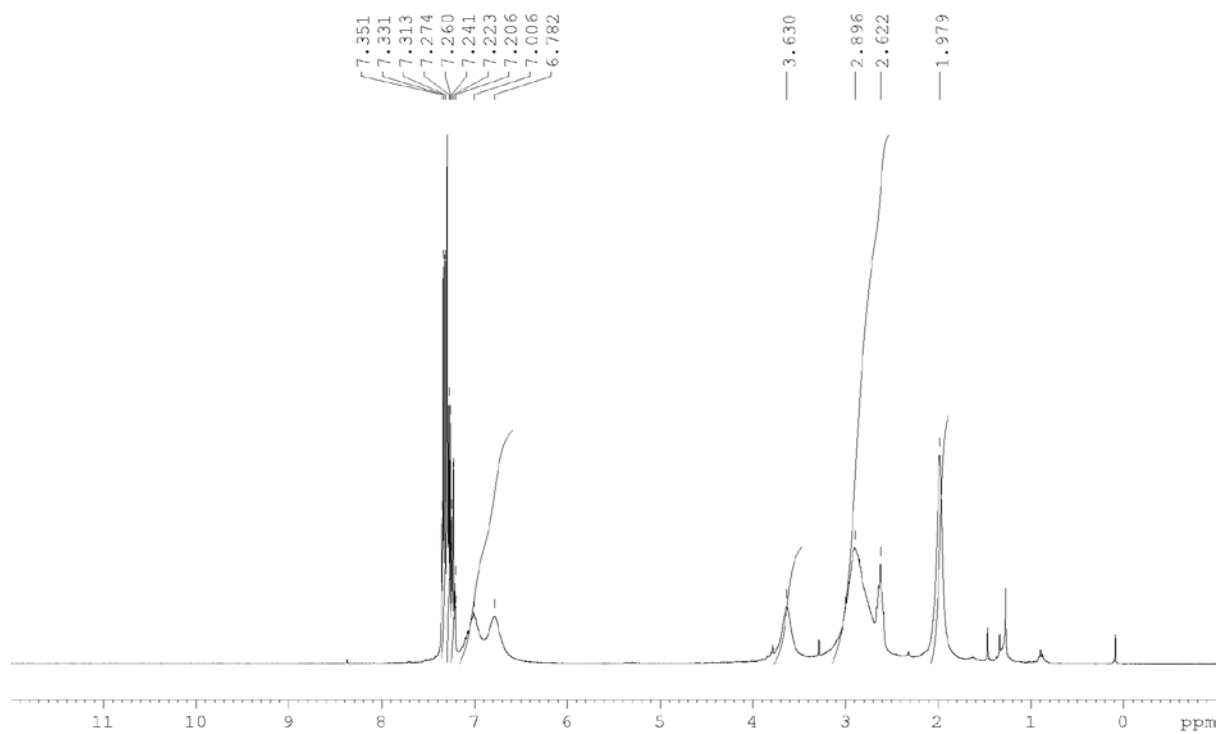


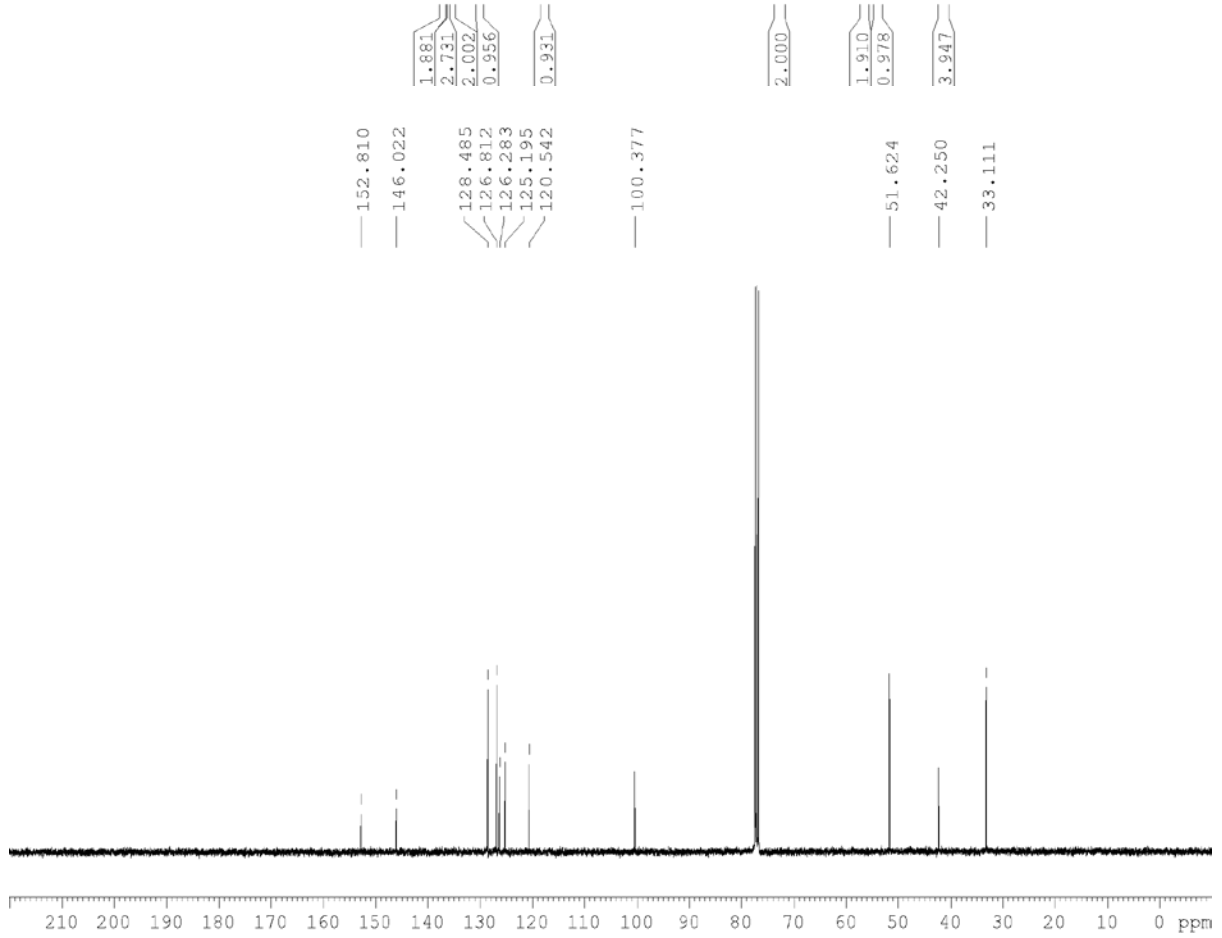
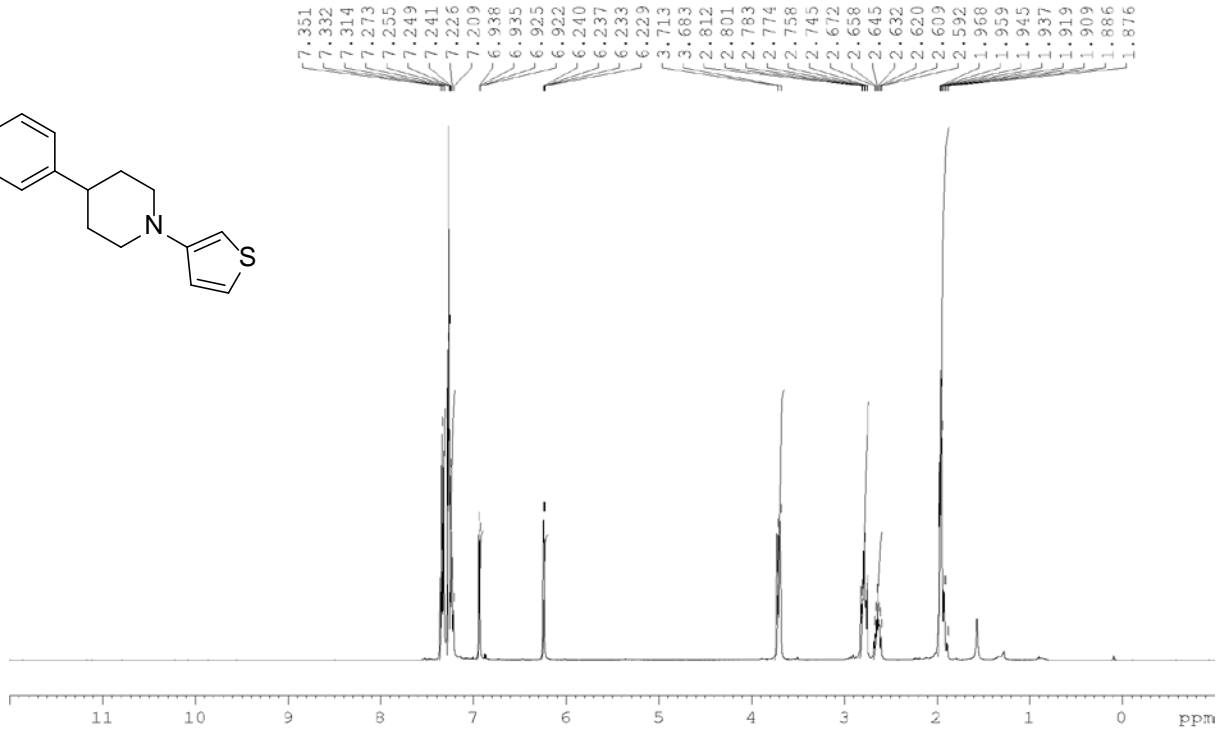
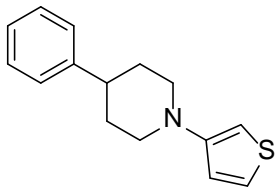


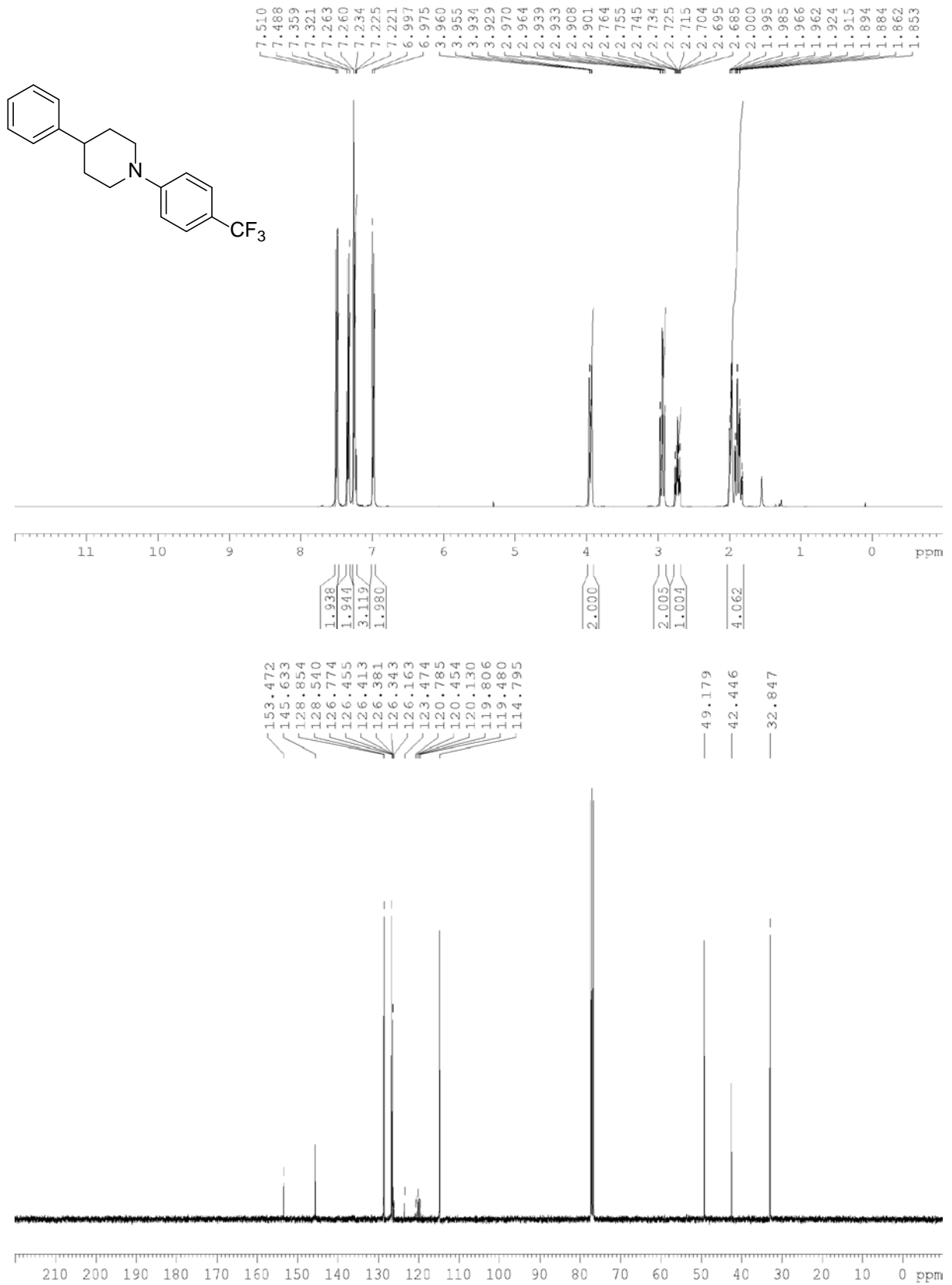


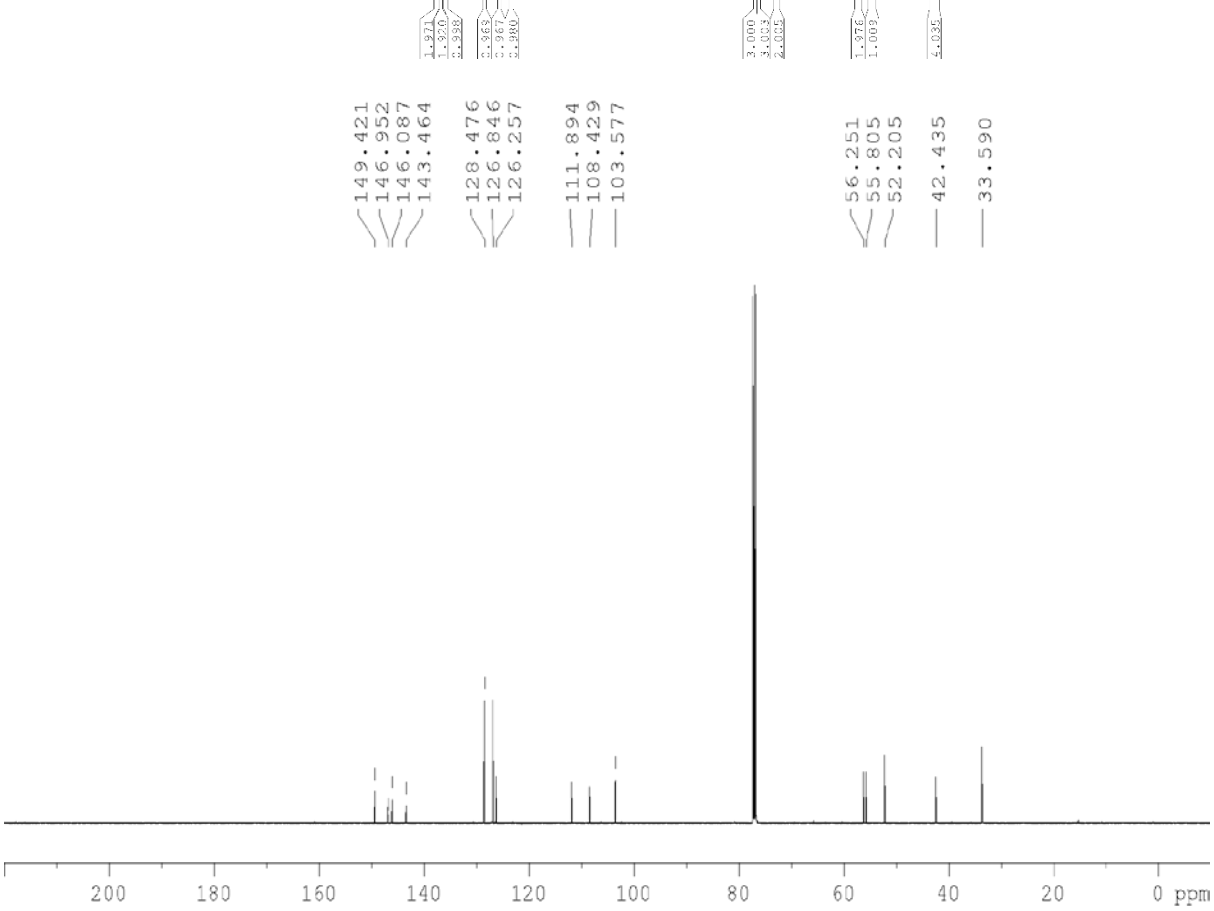
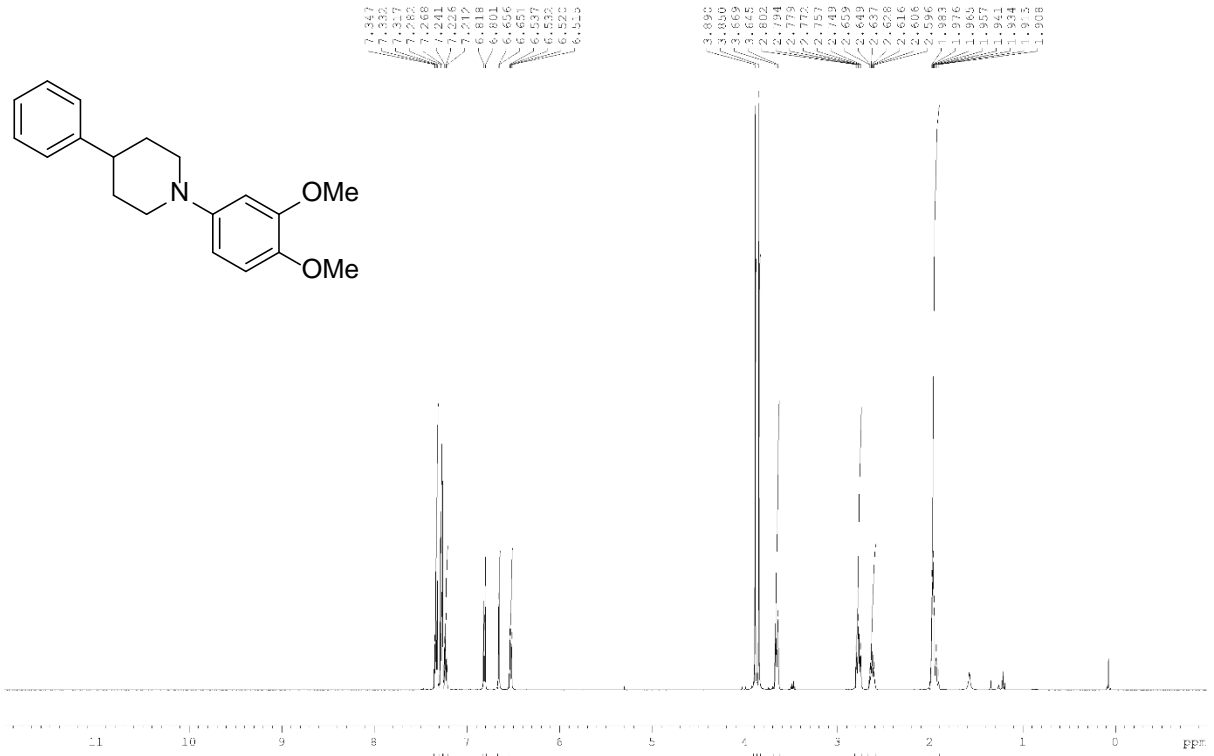
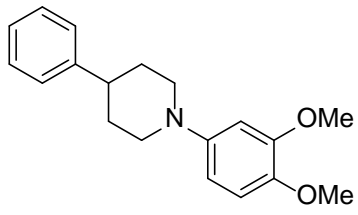


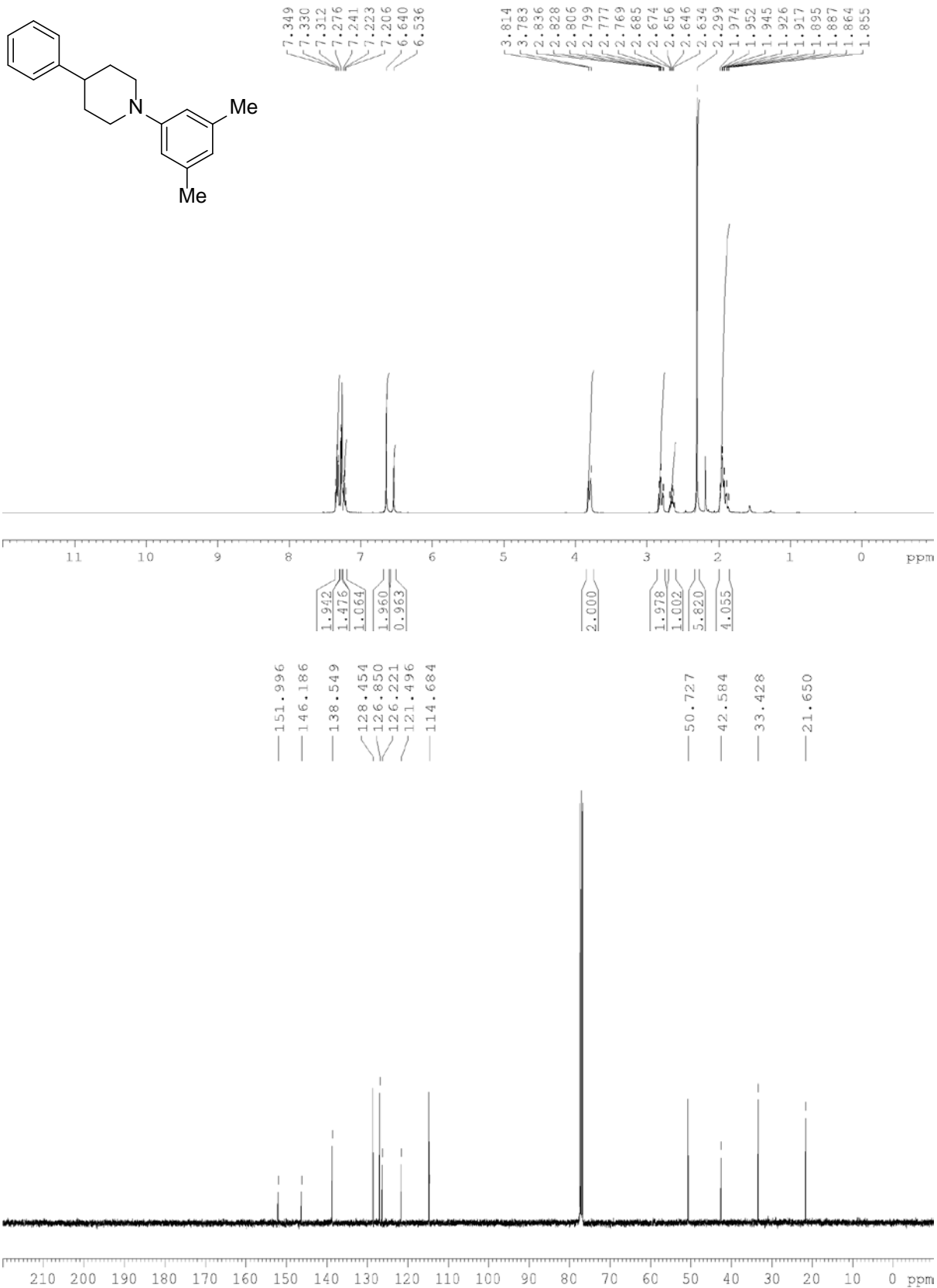


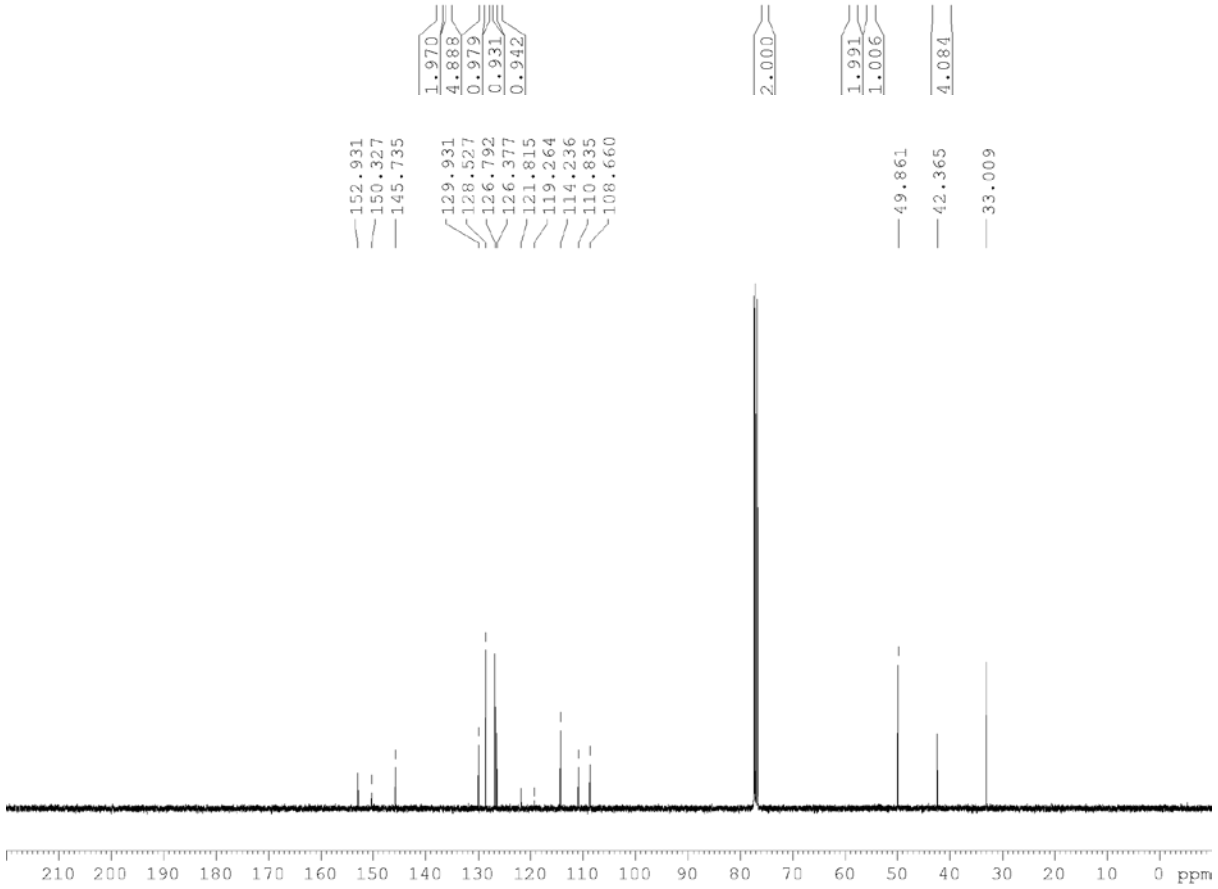
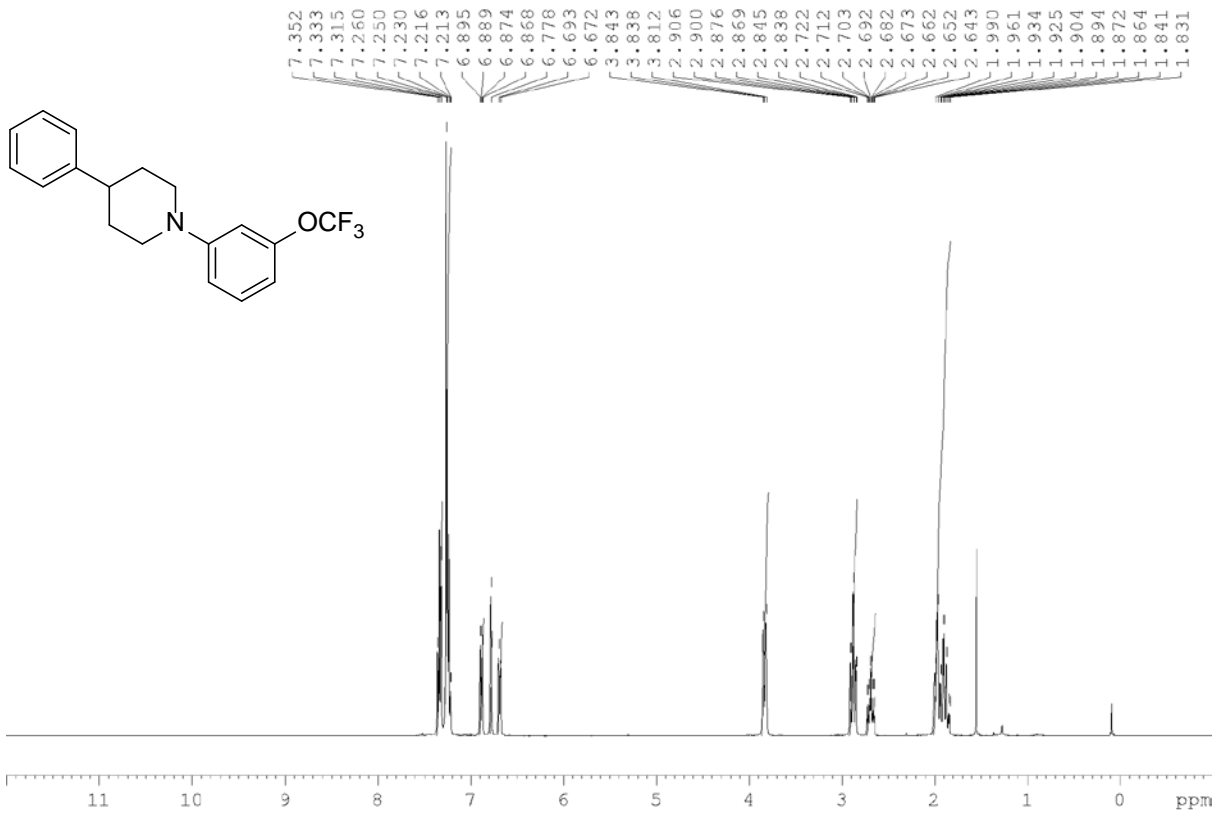


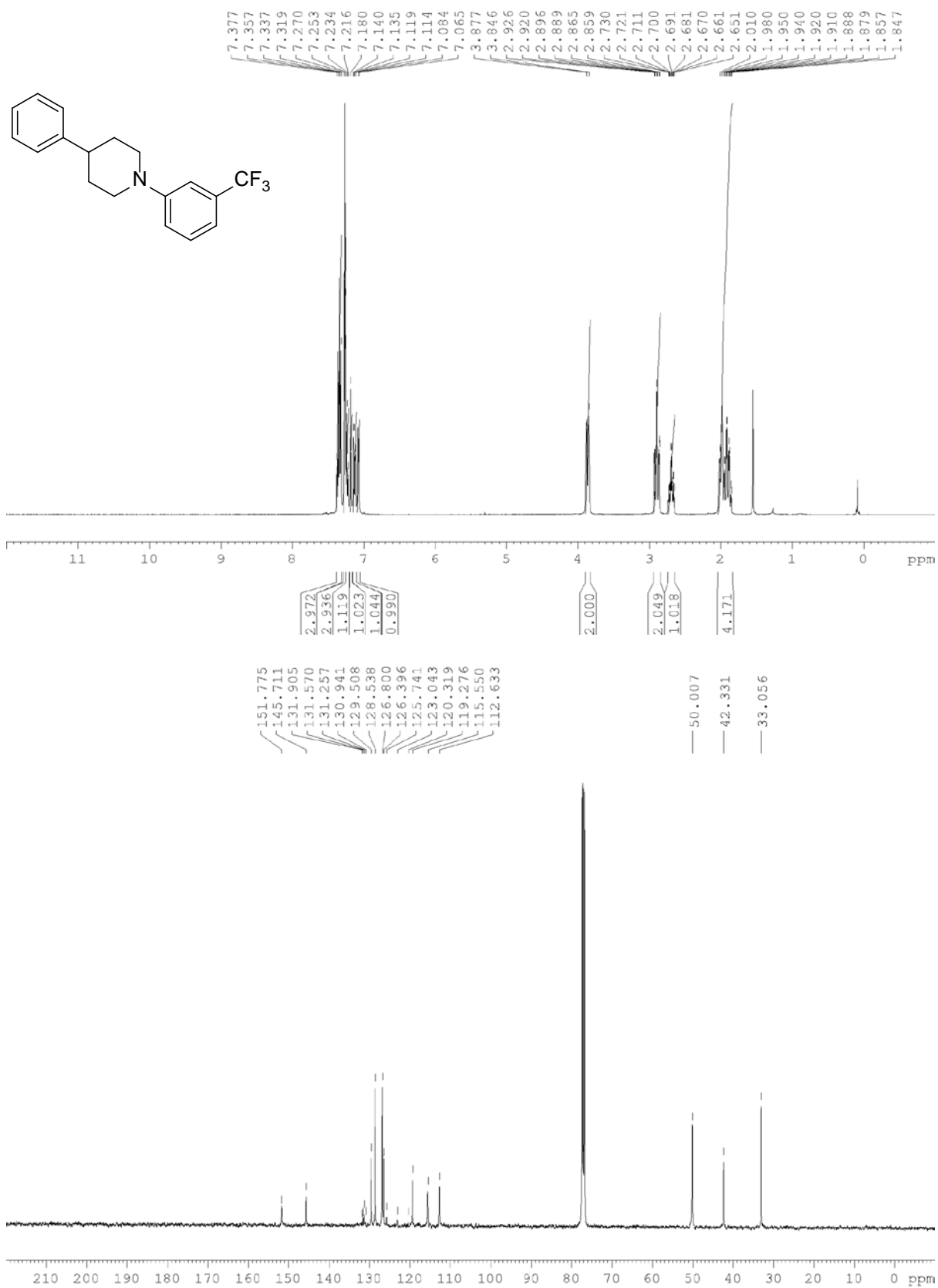


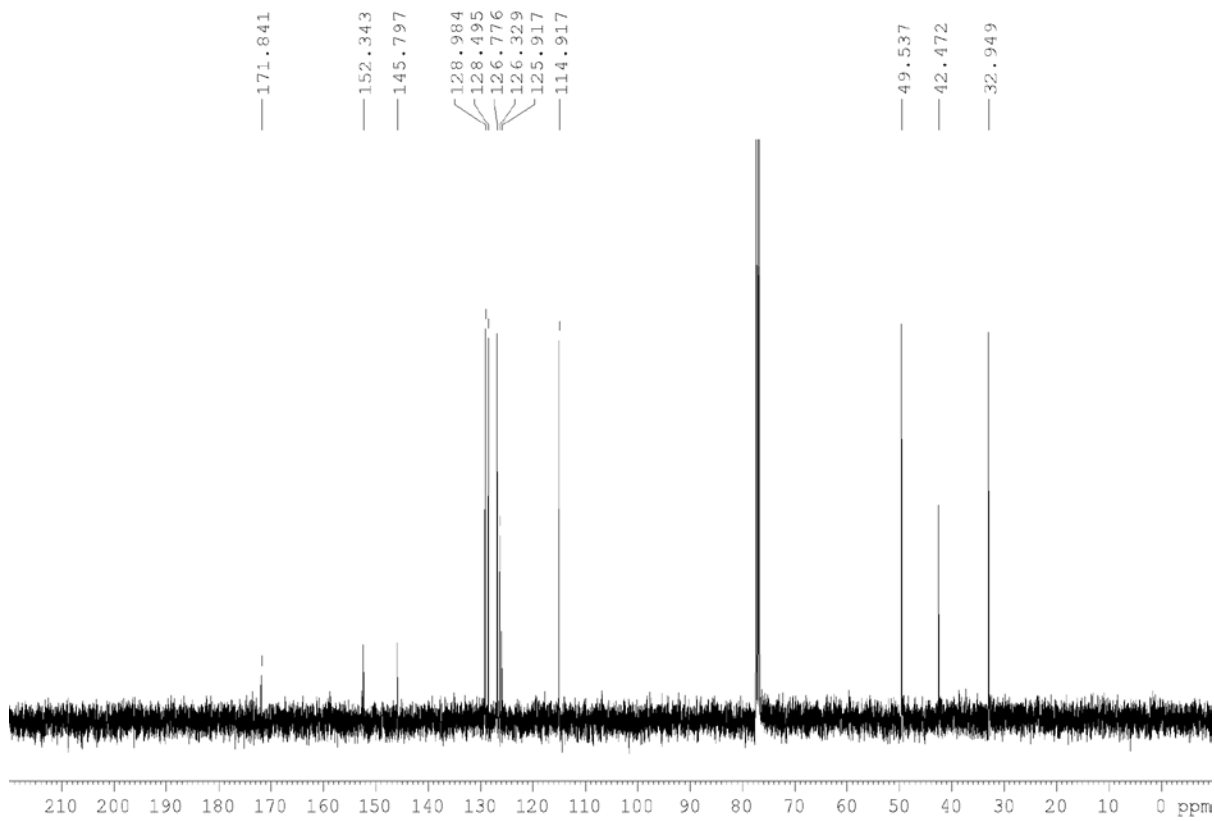
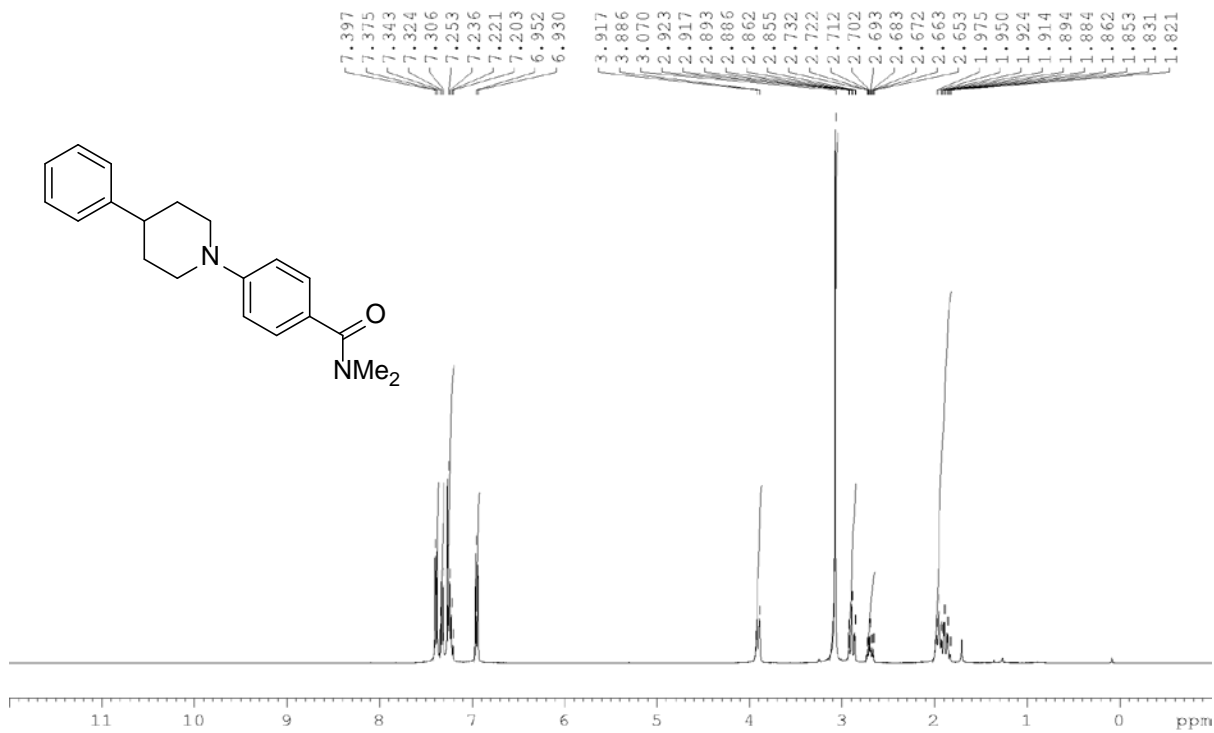


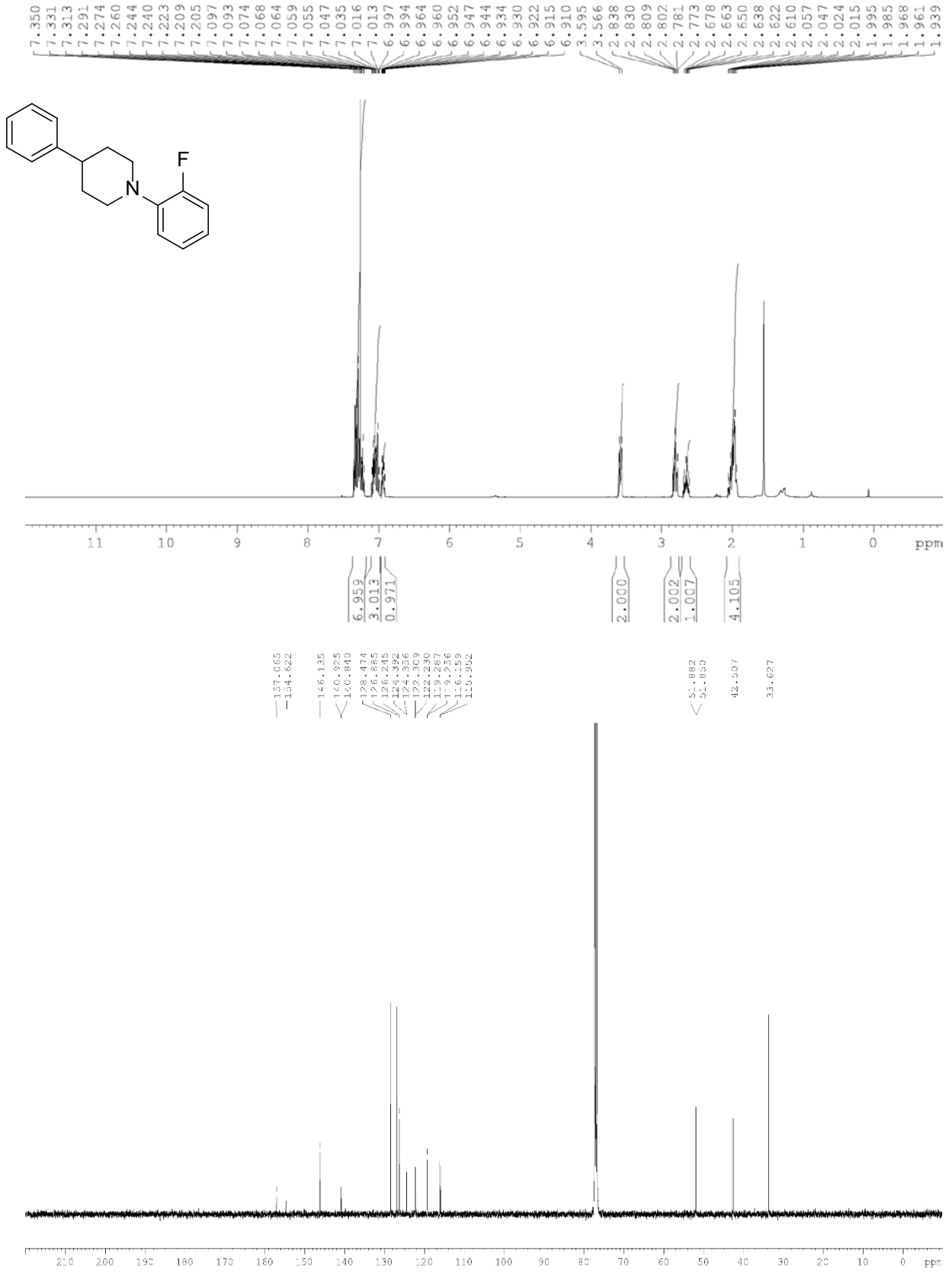


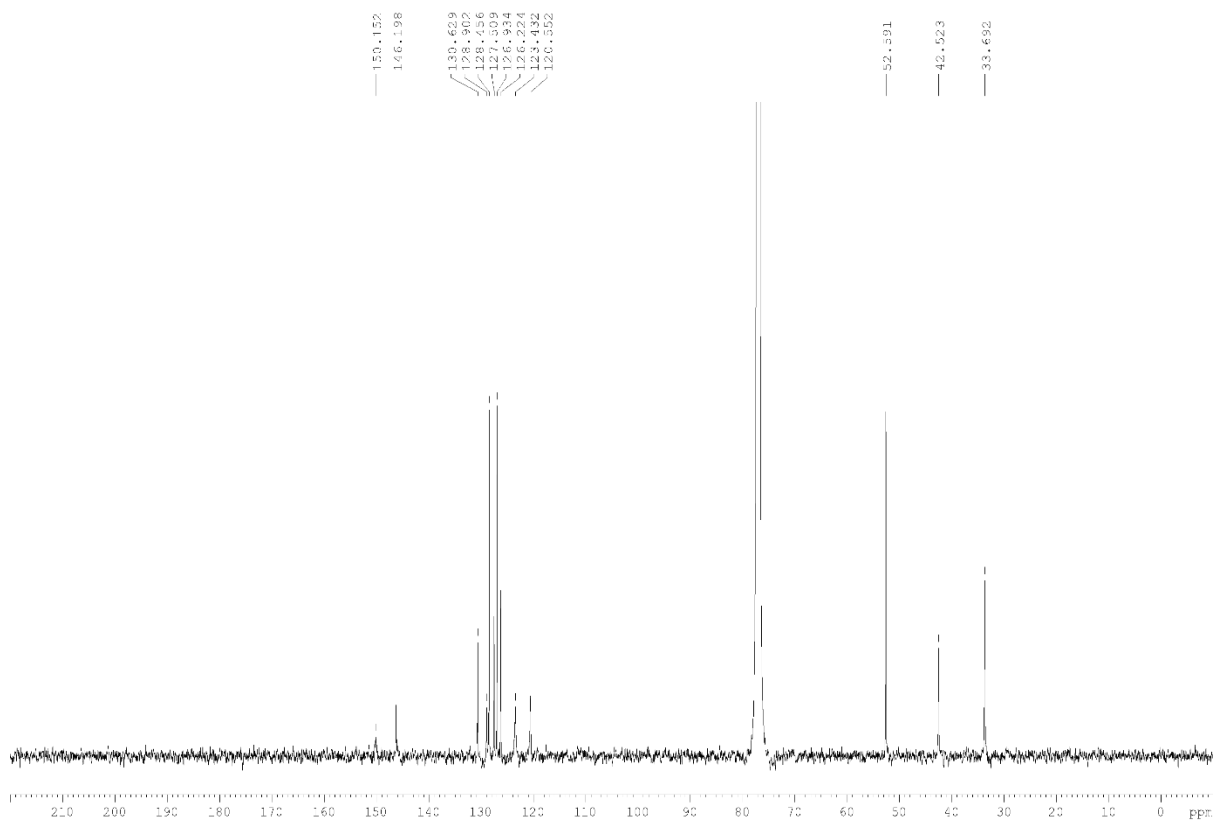
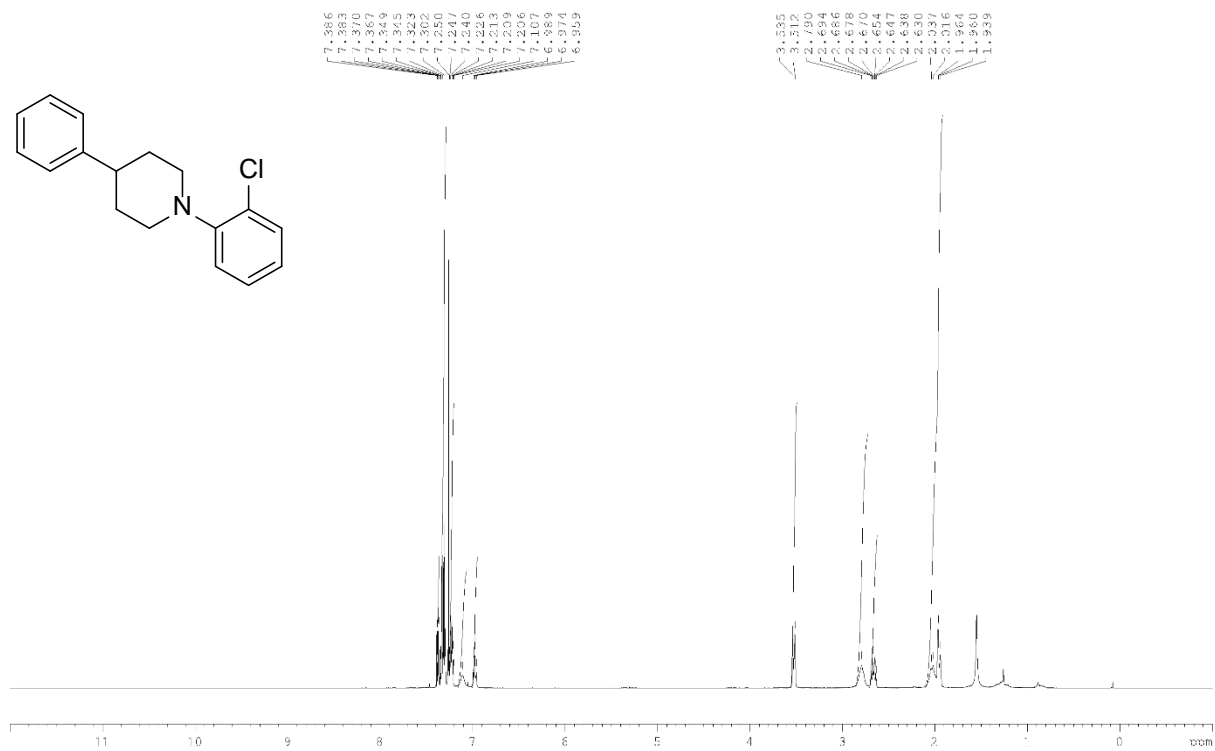
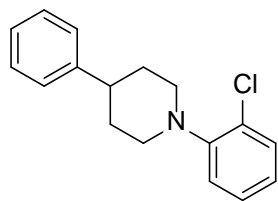


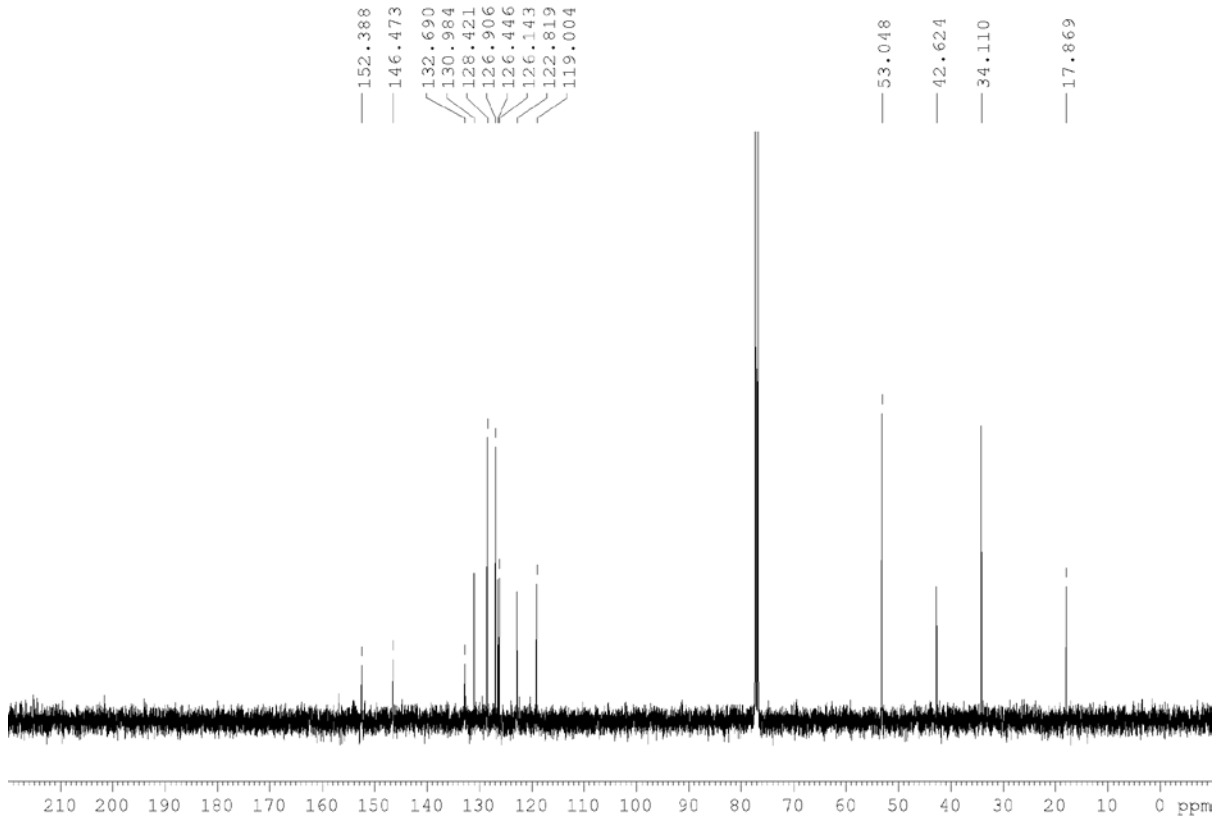
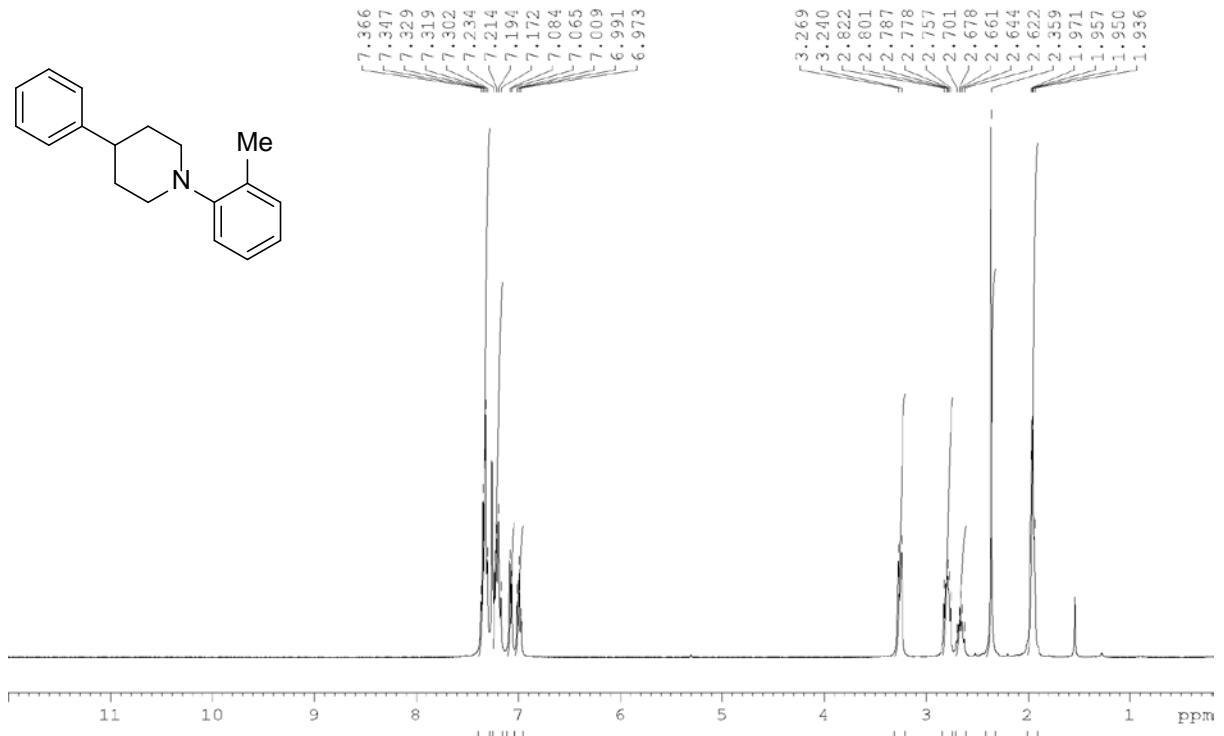
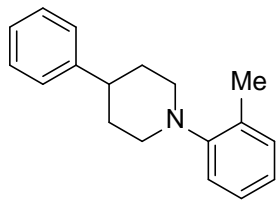


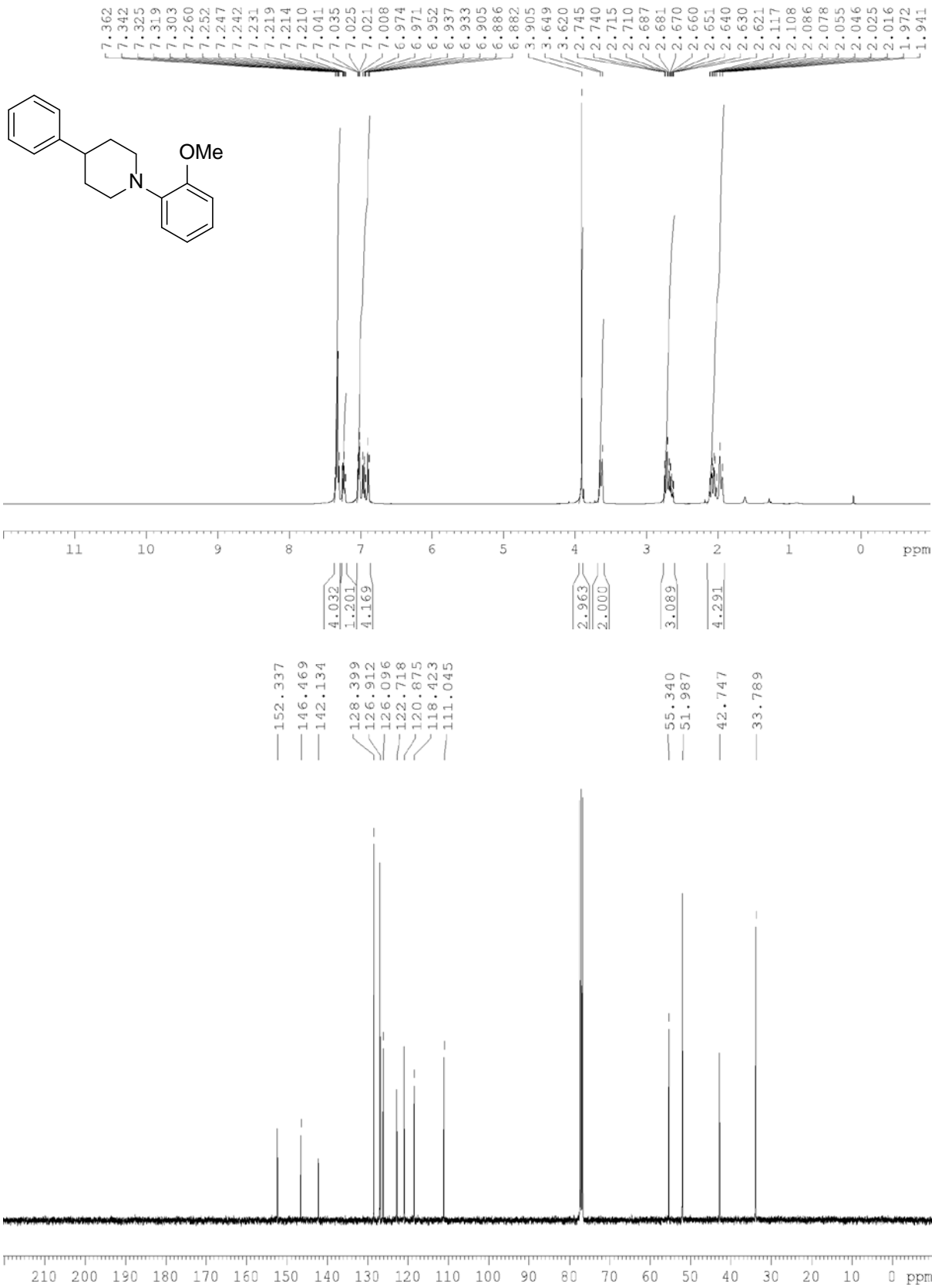


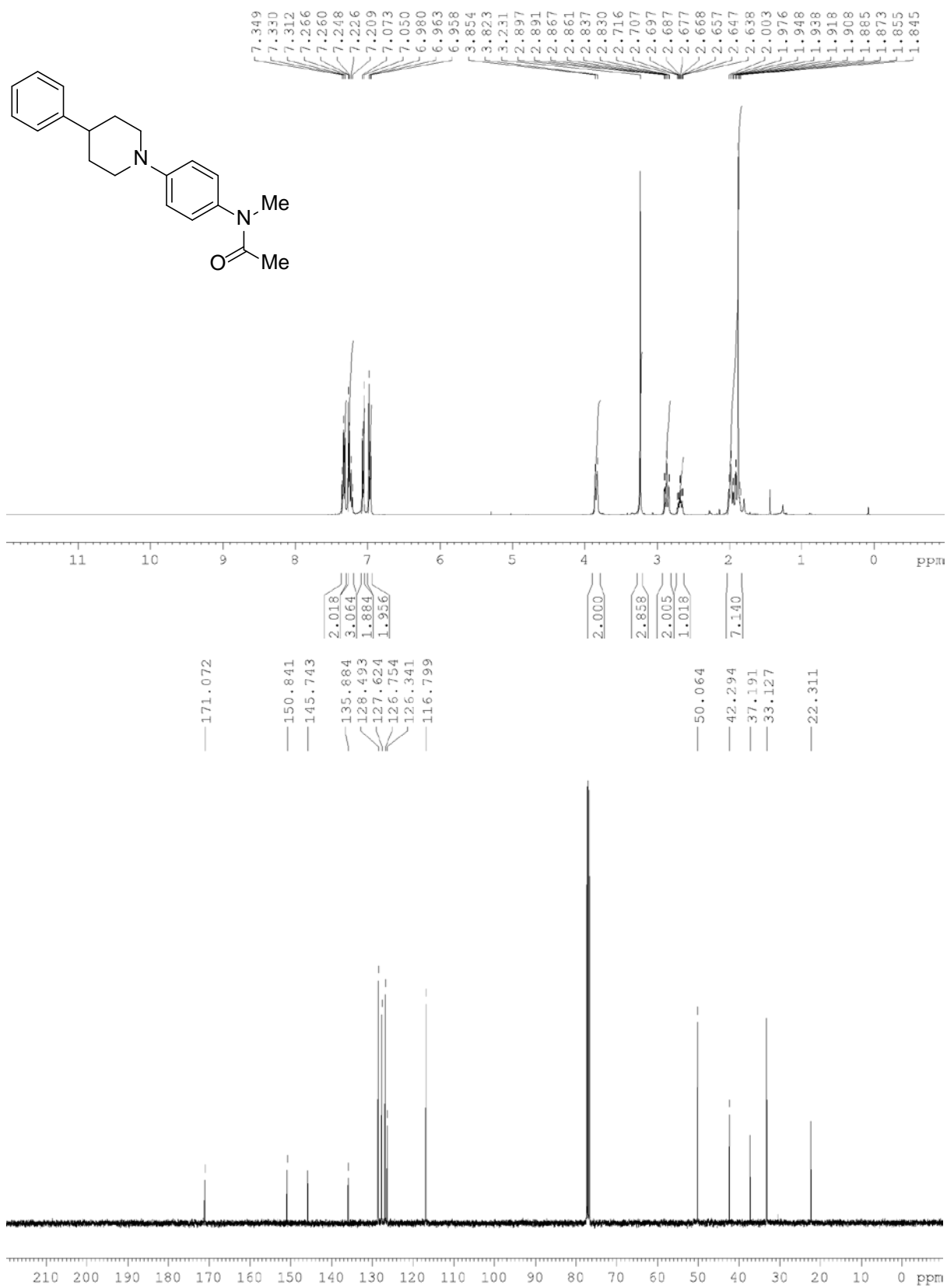


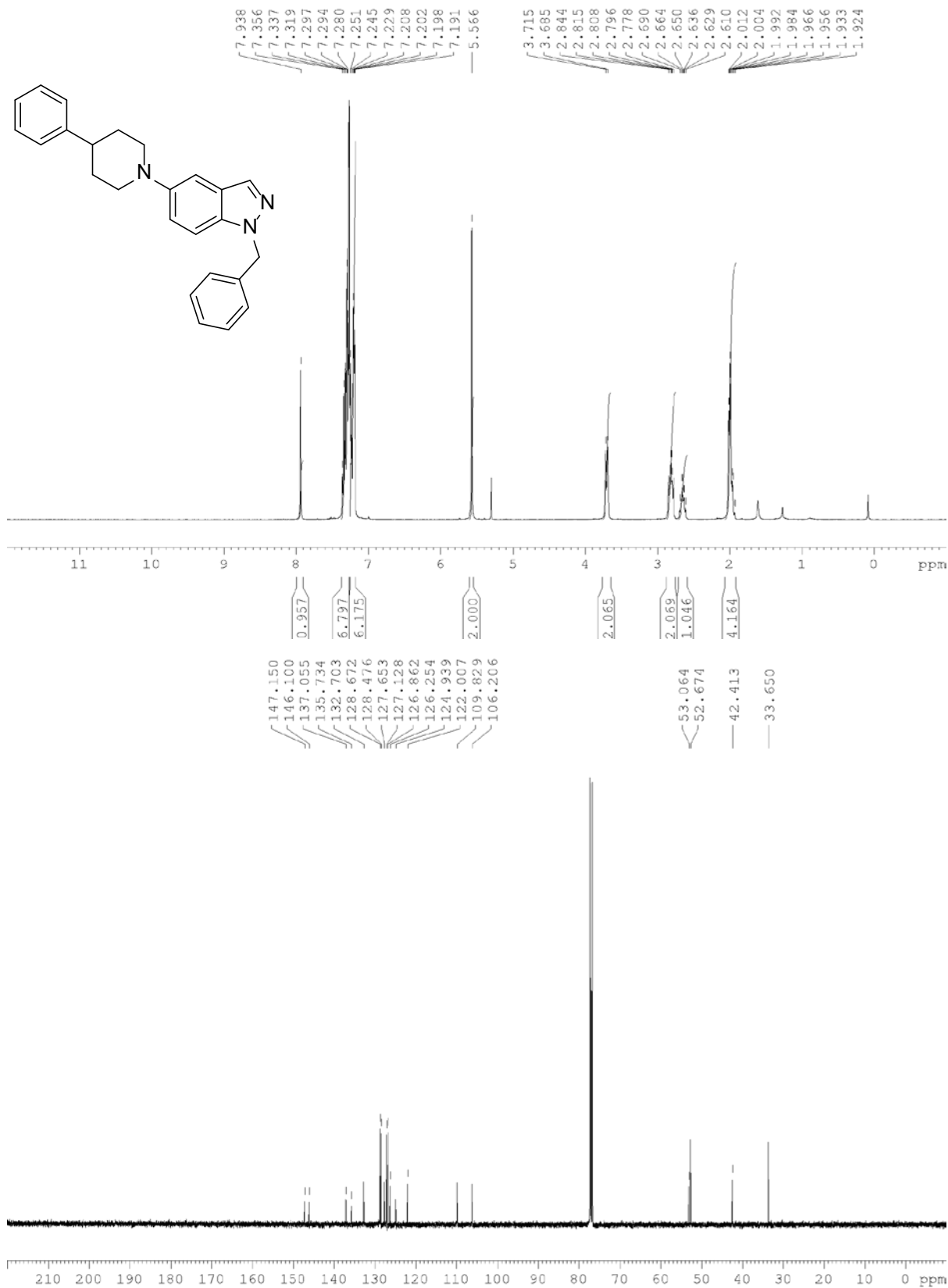


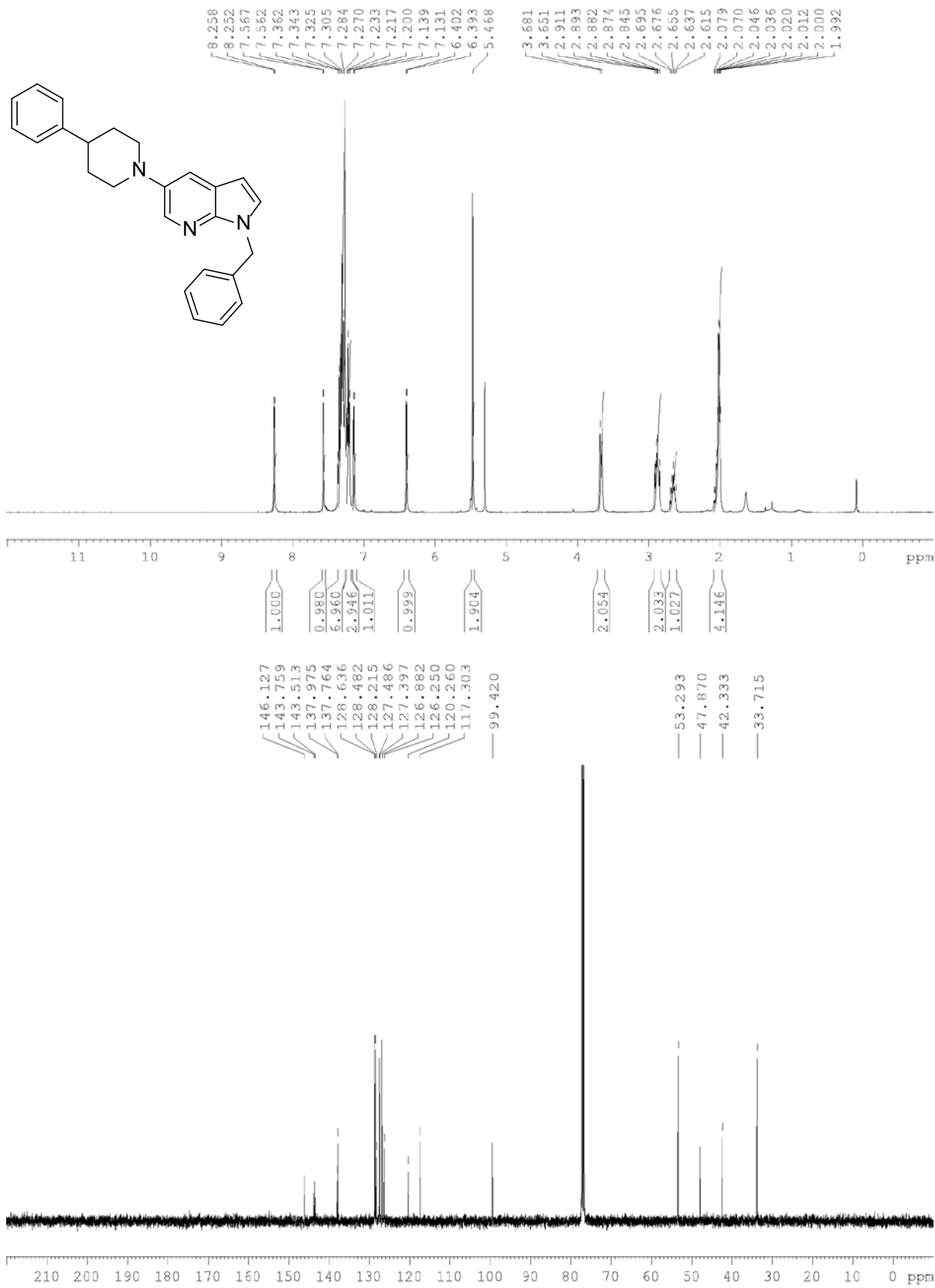


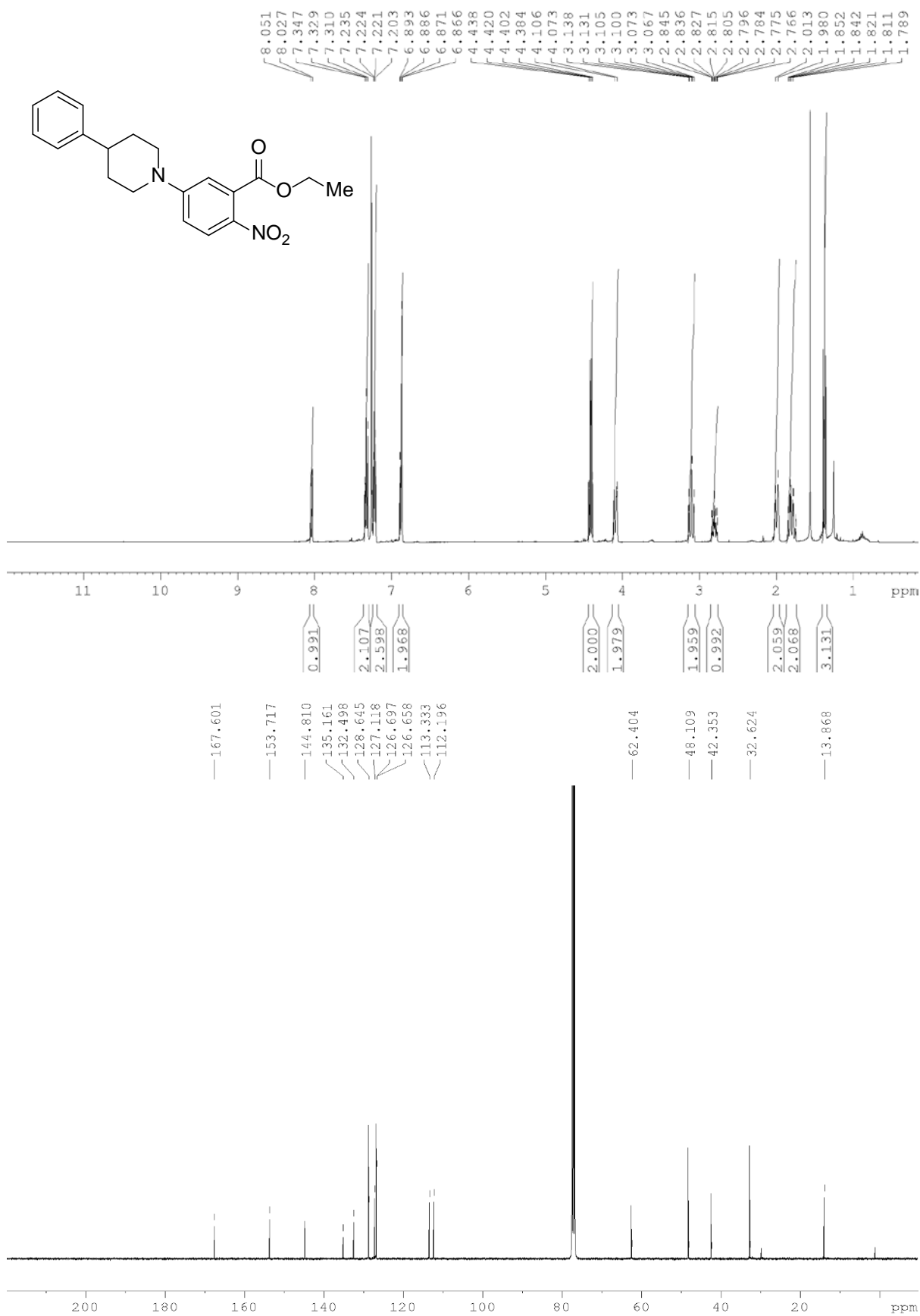


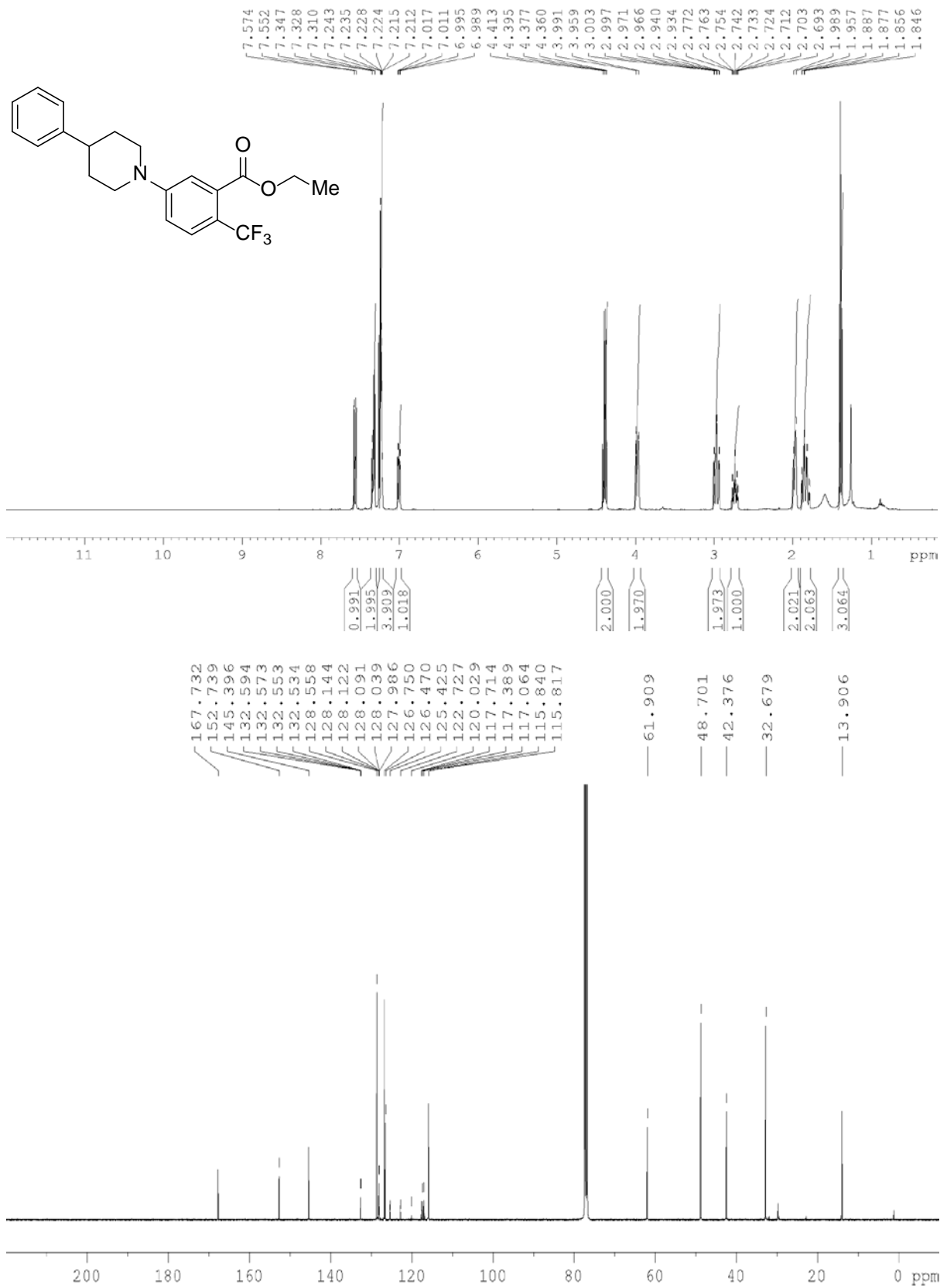


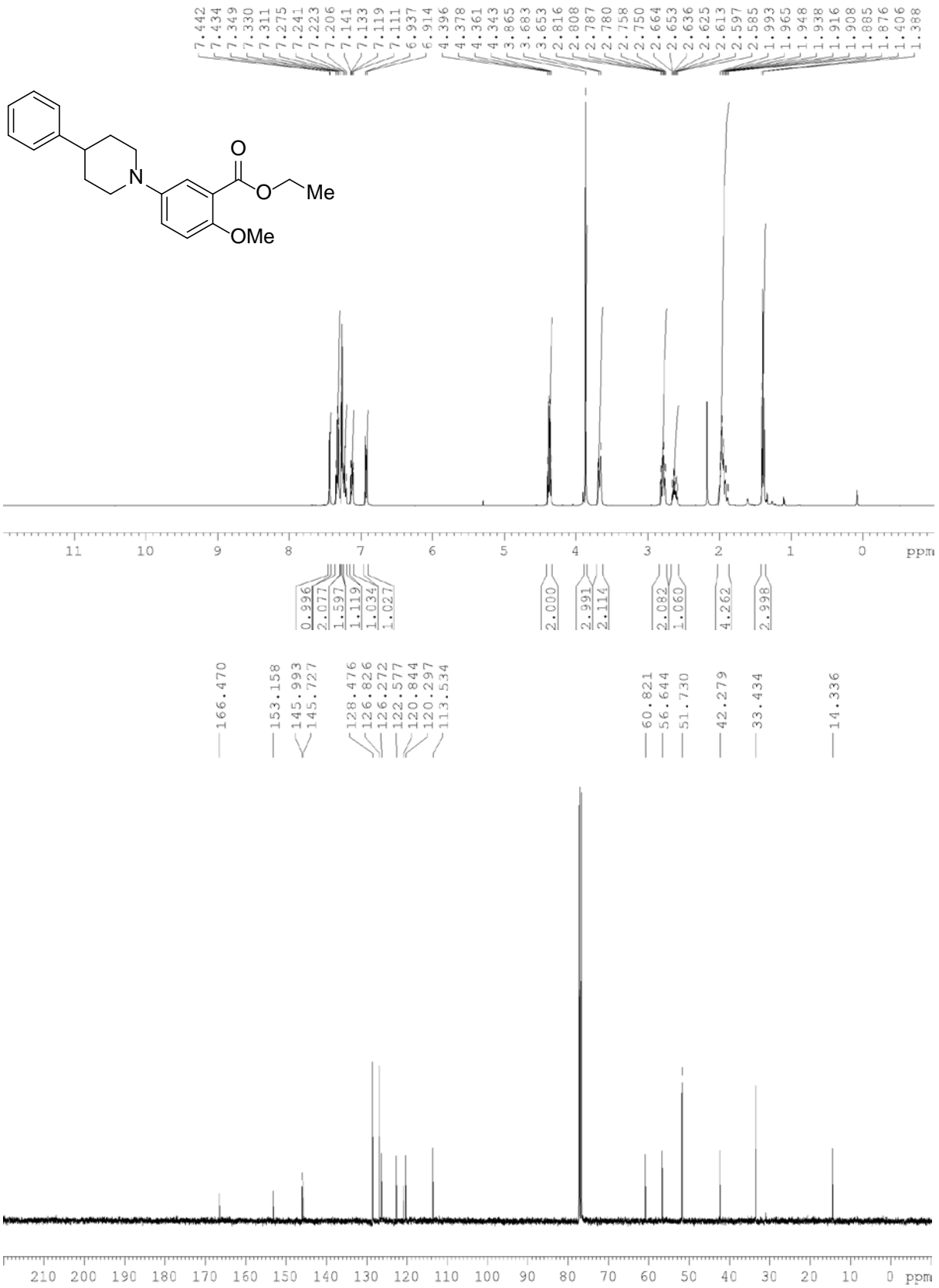




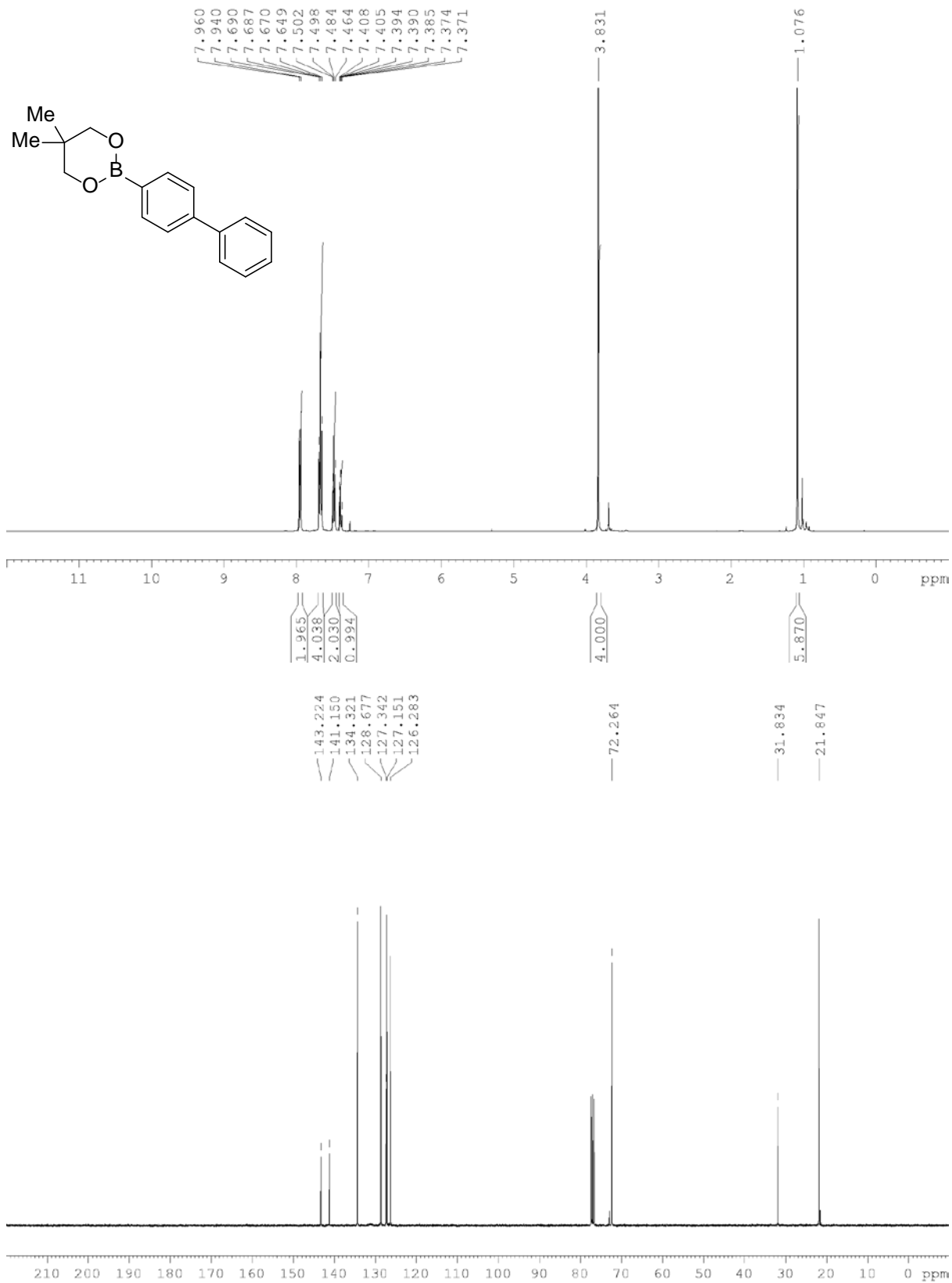








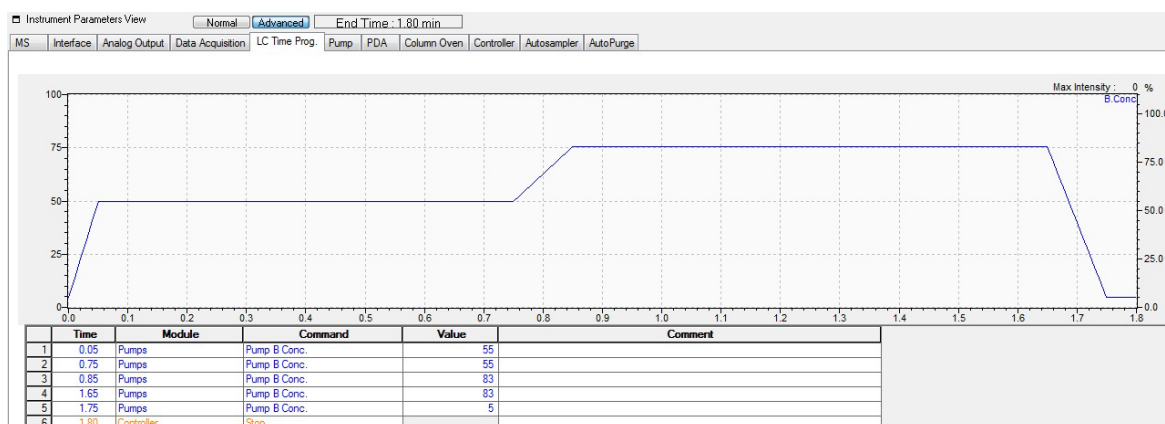
Reaction Discovery Spectra



Appendix 2: LCMS method files

1,4-Diphenylpiperidine 314

LCMS mobile phase assay graph



Mass spectrum parameters

Instrument Parameters View Normal **Advanced** End Time: 1.80 min

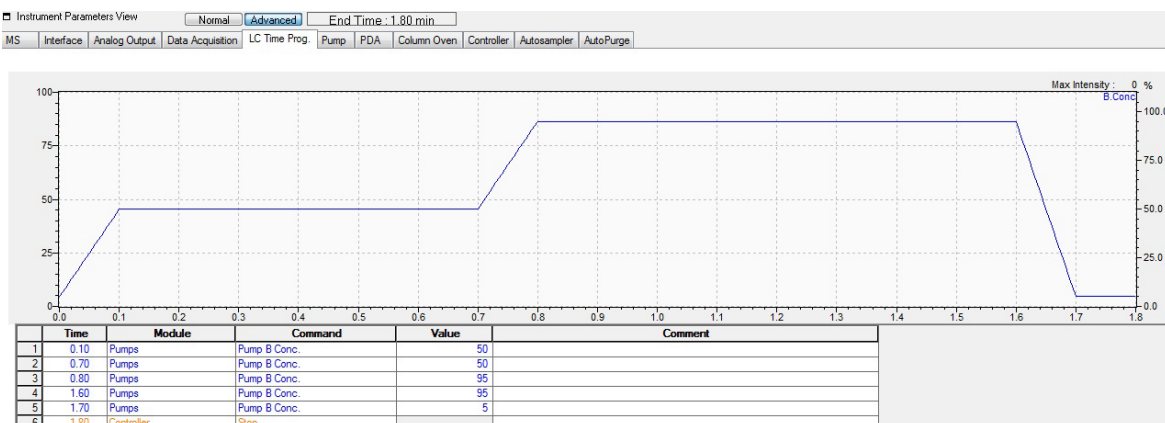
MS Interface Analog Output Data Acquisition LC Time Prog. Pump PDA Column Oven Controller Autosampler AutoPurge

Segment#1

Start Time (min)	End Time (min)	Acquisition Mode	Polarity	Event Time (sec)	SIM m/z	Scan Speed	Detector Volt. Mode	Micro Scan(s)	Interface Volt. Mode	DL Volt. Mode	Qarray DC Mode	Qarray RF Mode	
1	0	1.8	SIM	Positive	0.02	274.00,238.00	15000	Relative to the Tuning Result	0	Tuning File	Default (0V)	Default (0V)	Tuning File

1-(4-Methoxyphenyl)-4-phenylpiperidine 315

LCMS mobile phase assay graph



Mass spectrum parameters

Instrument Parameters View Normal **Advanced** End Time: 1.80 min

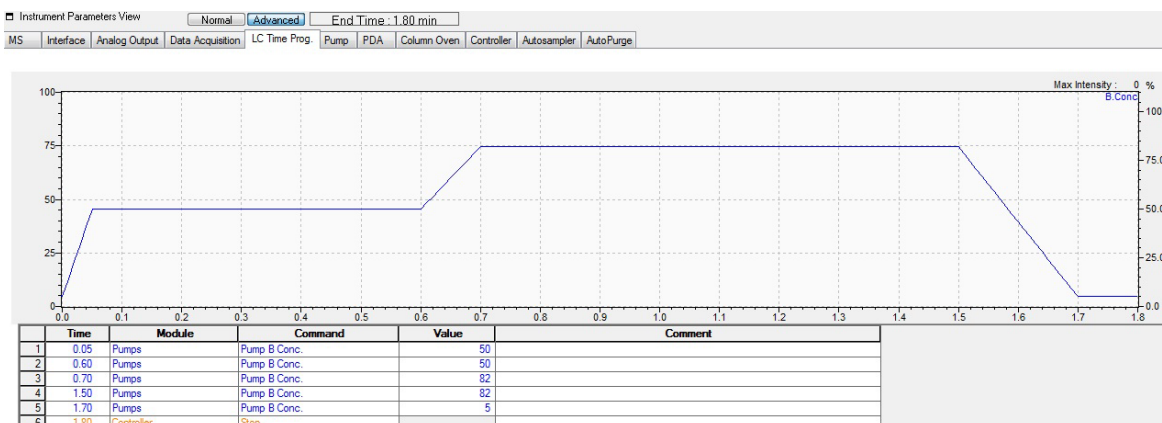
MS Interface Analog Output Data Acquisition LC Time Prog. Pump PDA Column Oven Controller Autosampler AutoPurge

Segment#1

Start Time (min)	End Time (min)	Acquisition Mode	Polarity	Event Time (sec)	SIM m/z	Scan Speed	Detector Volt. Mode	Micro Scan(s)	Interface Volt. Mode	DL Volt. Mode	Qarray DC Mode	Qarray RF Mode	
1	0	1.8	SIM	Positive	0.02	274.00,268.00	15000	Relative to the Tuning Result	0	Tuning File	Default (0V)	Default (0V)	Tuning File

1-(Naphthalen-2-yl)-4-phenylpiperidine 372

LCMS mobile phase assay graph



Mass spectrum parameters

Instrument Parameters View: Normal | **Advanced** | End Time: 1.80 min

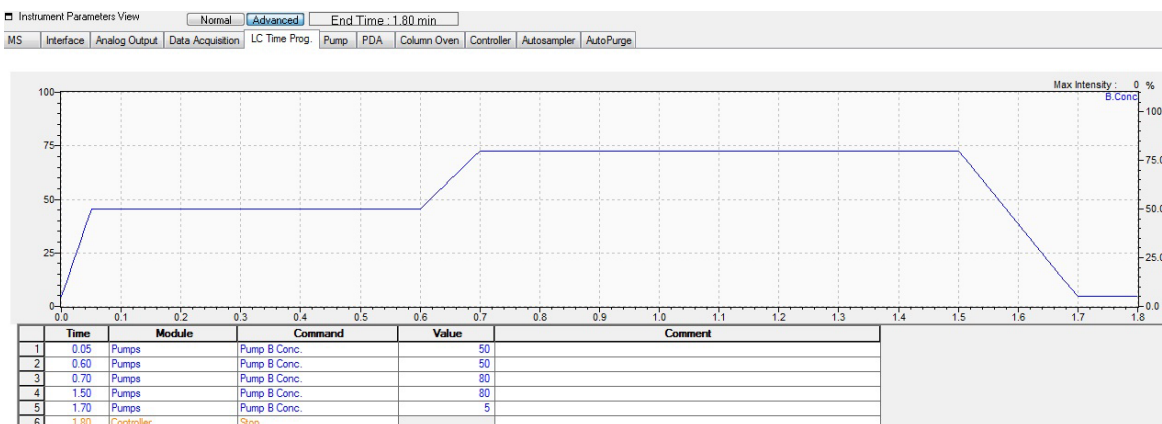
MS | Interface | Analog Output | Data Acquisition | LC Time Prog. | Pump | PDA | Column Oven | Controller | Autosampler | AutoPurge

Segment#1

Start Time (min)	End Time (min)	Acquisition Mode	Polarity	Event Time (sec)	SIM m/z	Scan Speed	Detector Volt. Mode	Micro Scan(s)	Interface Volt. Mode	DL Volt. Mode	Qarray DC Mode	Qarray RF Mode	
1	0	1.8	SIM	Positive	0.02	274.00,288.00	15000	Relative to the Tuning Result	0	Tuning File	Default (0V)	Default (0V)	Tuning File

Ethyl 3-(4-phenylpiperidin-1-yl)benzoate, 369

LCMS mobile phase assay graph



Mass spectrum parameters

Instrument Parameters View: Normal | **Advanced** | End Time: 1.80 min

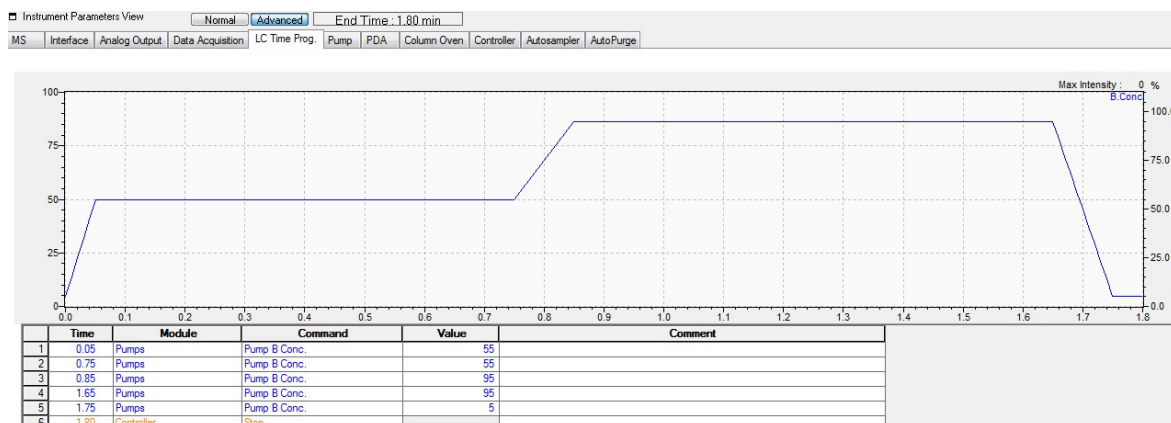
MS | Interface | Analog Output | Data Acquisition | LC Time Prog. | Pump | PDA | Column Oven | Controller | Autosampler | AutoPurge

Segment#1

Start Time (min)	End Time (min)	Acquisition Mode	Polarity	Event Time (sec)	SIM m/z	Scan Speed	Detector Volt. Mode	Micro Scan(s)	Interface Volt. Mode	DL Volt. Mode	Qarray DC Mode	Qarray RF Mode	
1	0	1.8	SIM	Positive	0.02	274.00,310.00	15000	Relative to the Tuning Result	0	Tuning File	Default (0V)	Default (0V)	Tuning File

1-(4-Iodophenyl)-4-phenylpiperidine, 373

LCMS mobile phase assay graph



Mass spectrum parameters

Instrument Parameters View: Normal | **Advanced** | End Time: 1.80 min

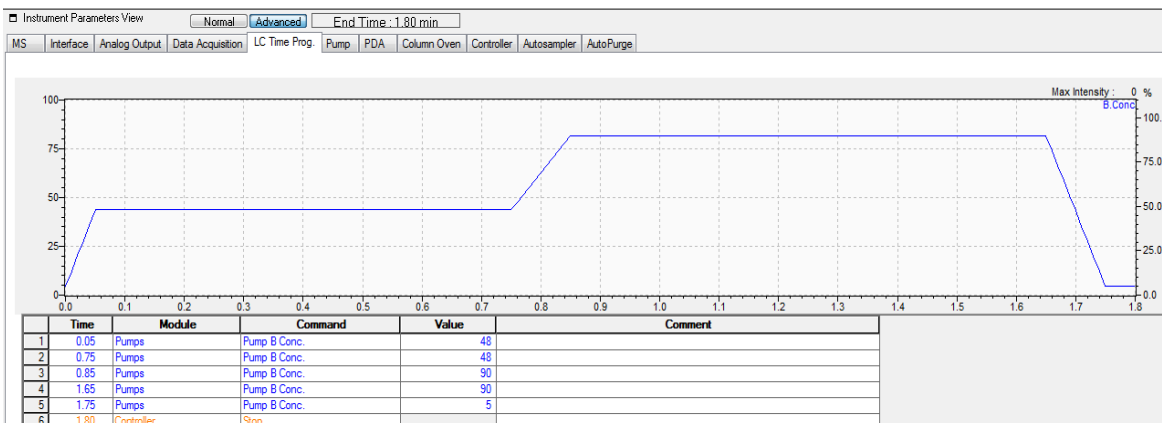
MS | Interface | Analog Output | Data Acquisition | LC Time Prog. | Pump | PDA | Column Oven | Controller | Autosampler | AutoPurge

Segment#1

Start Time (min)	End Time (min)	Acquisition Mode	Polarity	Event Time (sec)	SIM m/z	Scan Speed	Detector Volt. Mode	Micro Scan(s)	Interface Volt. Mode	DL Volt. Mode	Qarray DC Mode	Qarray RF Mode	
1	0	1.8	SIM	Positive	0.02	274.00.364.00	15000	Relative to the Tuning Result	0	Tuning File	Default (0V)	Default (0V)	Tuning File

1-(4-Bromophenyl)-4-phenylpiperidine, 418

LCMS mobile phase assay graph



Mass spectrum parameters

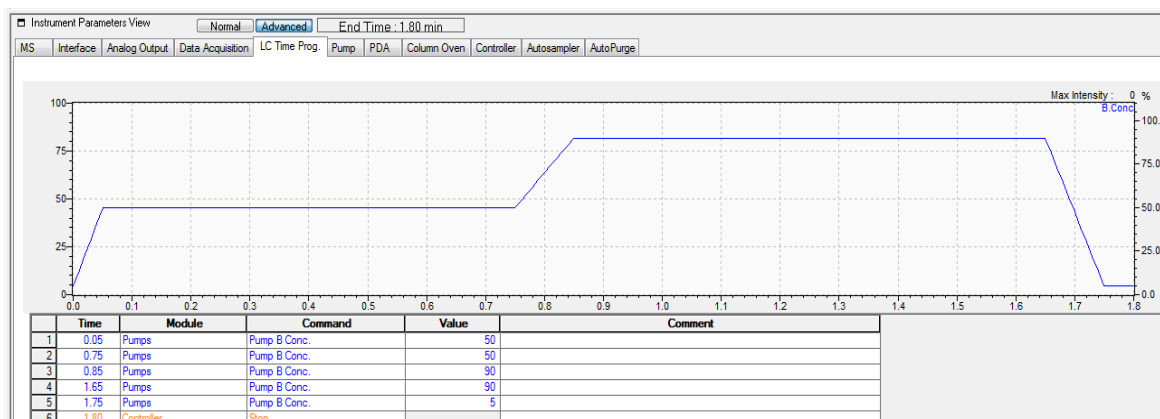
MS | Interface | Analog Output | Data Acquisition | LC Time Prog. | Pump | PDA | Column Oven | Controller | Autosampler | AutoPurge

Segment#1

Start Time (min)	End Time (min)	Acquisition Mode	Polarity	Event Time (sec)	SIM m/z	Scan Speed	Detector Volt. Mode	Detector Volt. (kV)	Micro Scan(s)	Interface Volt. Mode	DL Volt. Mode	Qarray DC Mode	Qarray RF Mode	
1	0	1.8	SIM	Positive	0.02	274.00.317.00	15000	Relative to the Tuning Result	0	0	Tuning File	Default (0)	Default (0V)	Tuning File

1-(4-Nitrophenyl)-4-phenylpiperidine, 417

LCMS mobile phase assay graph



Mass spectrum parameters

Instrument Parameters View Normal **Advanced** End Time: 1.80 min

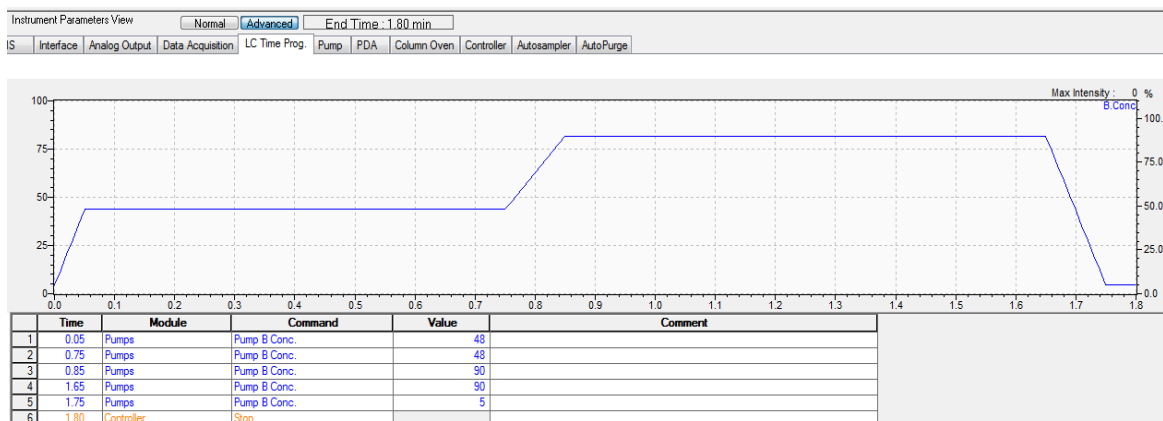
MS Interface Analog Output Data Acquisition LC Time Prog Pump PDA Column Oven Controller Autosampler AutoPurge

Segment#1

Start Time (min)	End Time (min)	Acquisition Mode	Polarity	Event Time (sec)	SIM m/z	Scan Speed	Detector Volt. Mode	Detector Volt. (kV)	Micro Scan(s)	Interface Volt. Mode	DI Volt. Mode	Garvey DC Mode	Garvey RF Mode
1	0	1.8	SIM	Positive	0.02	274.00,268.00	15000	Relative to the Tuning Res	0	Tuning File	Default(DV)	Default(DV)	Tuning File

1-(3-Methoxyphenyl)-4-phenylpiperidine, 428

LCMS mobile phase assay graph



Mass spectrum parameters

Instrument Parameters View Normal **Advanced** End Time: 1.80 min

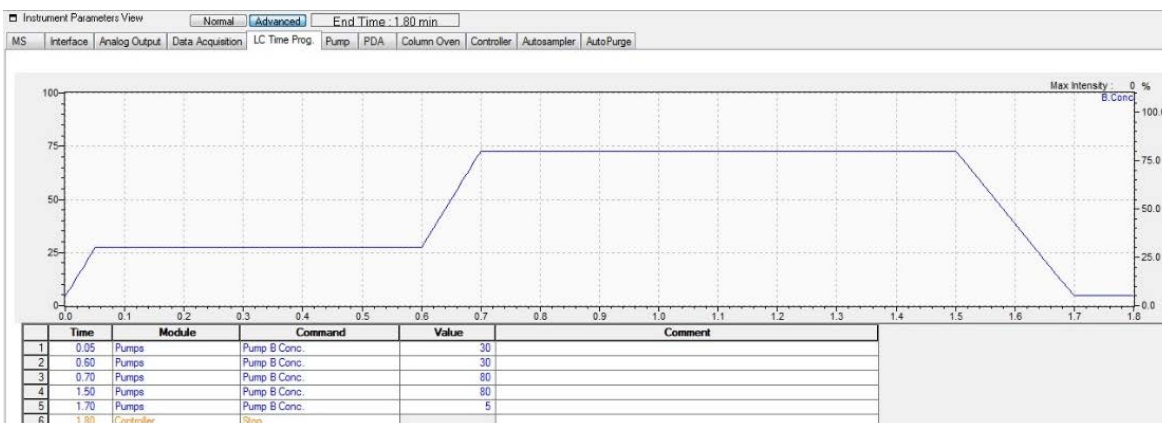
MS Interface Analog Output Data Acquisition LC Time Prog Pump PDA Column Oven Controller Autosampler AutoPurge

Segment#1

Start Time (min)	End Time (min)	Acquisition Mode	Polarity	Event Time (sec)	SIM m/z	Scan Speed	Detector Volt. Mode	Detector Volt. (kV)	Micro Scan(s)	Interface Volt. Mode	DI Volt. Mode	Garvey DC Mode	Garvey RF Mode
1	0	1.8	SIM	Positive	0.02	274.00,268.00	15000	Relative to the Tuning Result	0	Tuning File	Default(D)	Default(DV)	Tuning File

4-(4-Phenylpiperidin-1-yl)-1H-indole, 371

LCMS mobile phase assay graph

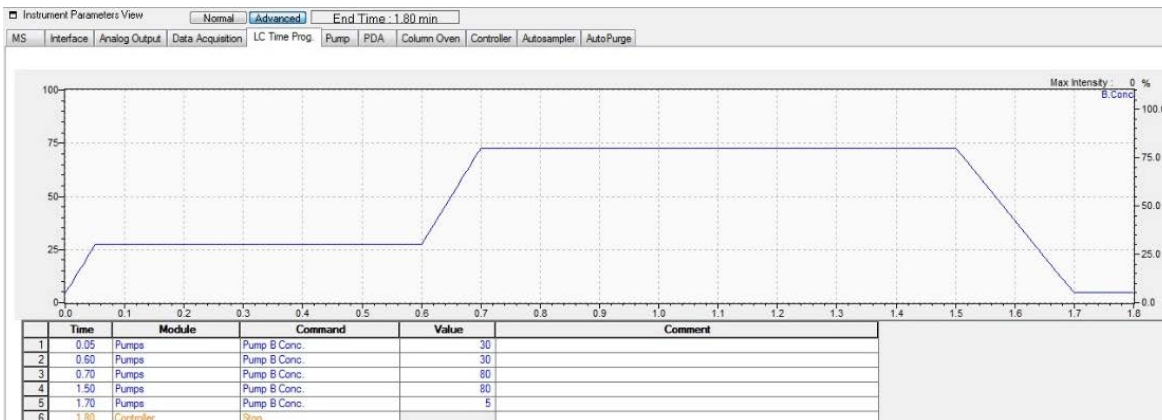


Mass spectrum parameters

Start Time (min)	End Time (min)	Acquisition Mode	Polarity	Event Time (sec)	SIM m/z	Scan Speed	Detector Volt. Mode	Detector Volt. (kV)	Micro Scan(s)	Interface Volt. Mode	DL Volt. Mode	Qarray DC Mode	Qarray RF Mode	
1	0	1.8	SIM	Positive	0.02	274.00,277.00	15000	Relative to the Tuning Result	0	0	Tuning File	Default(0V)	Default(0V)	Tuning File

5-(4-Phenylpiperidin-1-yl)-1H-indole, 431

LCMS mobile phase assay graph

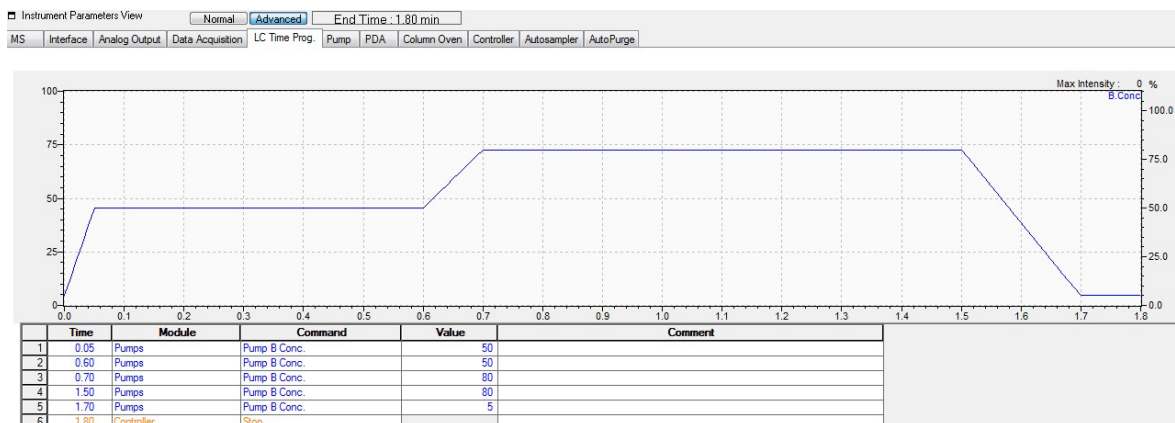


Mass spectrum parameters

Start Time (min)	End Time (min)	Acquisition Mode	Polarity	Event Time (sec)	SIM m/z	Scan Speed	Detector Volt. Mode	Detector Volt. (kV)	Micro Scan(s)	Interface Volt. Mode	DL Volt. Mode	Qarray DC Mode	Qarray RF Mode	
1	0	1.8	SIM	Positive	0.02	274.00,277.00	15000	Relative to the Tuning Result	0	0	Tuning File	Default(0V)	Default(0V)	Tuning File

3-(4-Phenylpiperidin-1-yl)pyridine, 370

LCMS mobile phase assay graph



Mass spectrum parameters

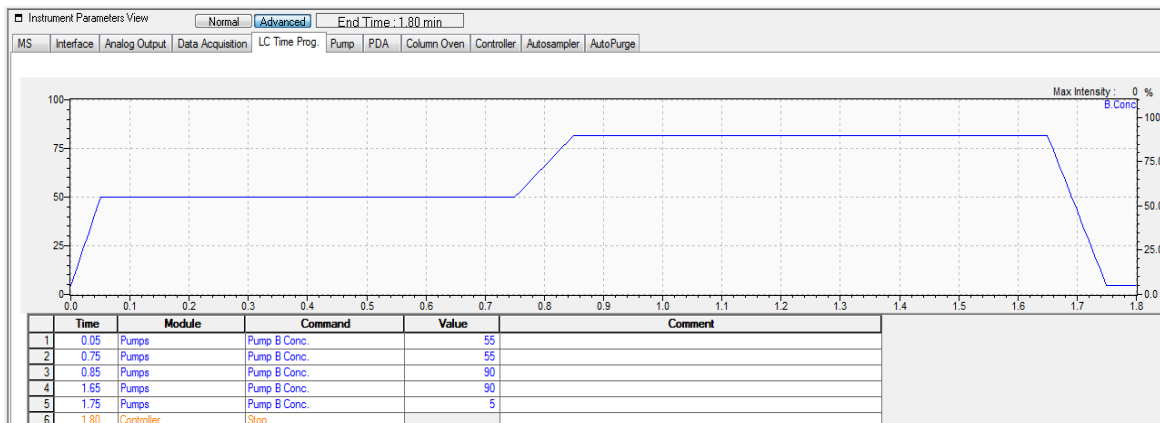
Instrument Parameters View: Normal | **Advanced** | End Time: 1.80 min

MS | Interface | Analog Output | Data Acquisition | LC Time Prog. | Pump | PDA | Column Oven | Controller | Autosampler | AutoPurge

Start Time (min)	End Time (min)	Acquisition Mode	Polarity	Event Time (sec)	SIM m/z	Scan Speed	Detector Volt. Mode	Micro Scan(s)	Interface Volt. Mode	DL Volt. Mode	Garay DC Mode	Garay RF Mode	
1	0	1.8	SIM	Positive	0.02	274.00,239.00	15000	Relative to the Tuning Result	0	Tuning File	Default(0V)	Default(0V)	Tuning File

1-([1,1'-biphenyl]-4-yl)-4-phenylpiperidine, 423

LCMS mobile phase assay graph



Mass spectrum parameters

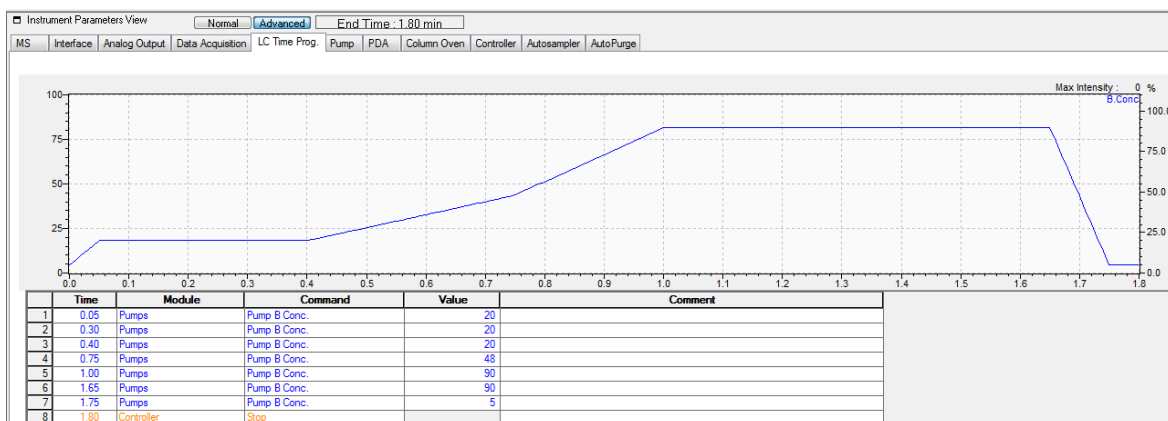
Instrument Parameters View: Normal | **Advanced** | End Time: 1.80 min

MS | Interface | Analog Output | Data Acquisition | LC Time Prog. | Pump | PDA | Column Oven | Controller | Autosampler | AutoPurge

Start Time (min)	End Time (min)	Acquisition Mode	Polarity	Event Time (sec)	SIM m/z	Scan Speed	Detector Volt. Mode	Detector Volt. (kV)	Micro Scan(s)	Interface Volt. Mode	DL Volt. Mode	Garay DC Mode	Garay RF Mode	
1	0	1.8	SIM	Positive	0.02	274.00,314.00	15000	Relative to the Tuning Result	0	0	Tuning File	Default(0)	Default(0)	Tuning

N,N-dimethyl-4-(4-phenylpiperidin-1-yl)aniline, 424

LCMS mobile phase assay graph

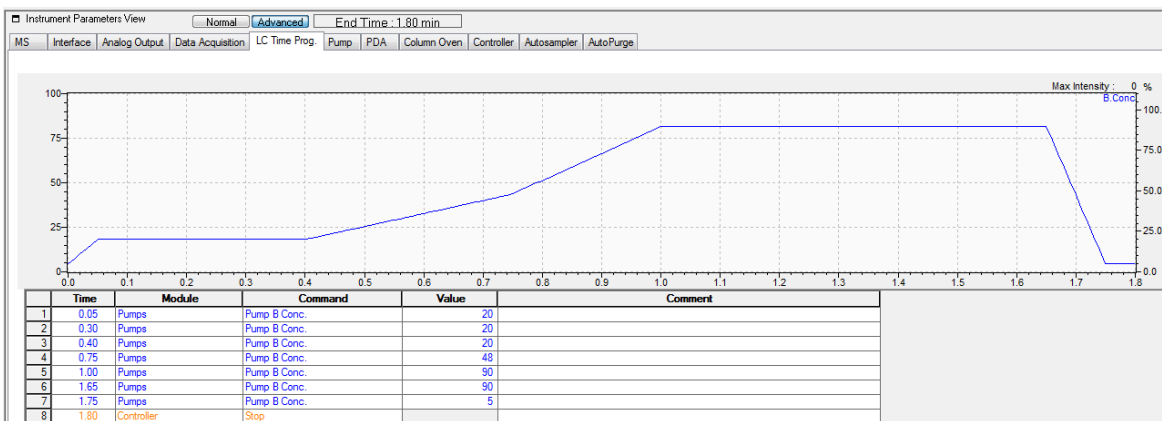


Mass spectrum parameters

Start Time (min)	End Time (min)	Acquisition Mode	Polarity	Event Time (sec)	SIM m/z	Scan Speed	Detector Volt. Mode	Detector Volt. (kV)	Micro Scan(u)	Interface Volt. Mode	DL Volt. Mode	Qarray DC Mode	Qarray RF Mode	
1	0	1.8	SIM	Positive	0.02	274.00,281.00	15000	Relative to the Tuning Result	0	0	Tuning File	Default(IV)	Default(IV)	Tuning File

4-Phenyl-1-(thiophen-3-yl)piperidine, 427

LCMS mobile phase assay graph

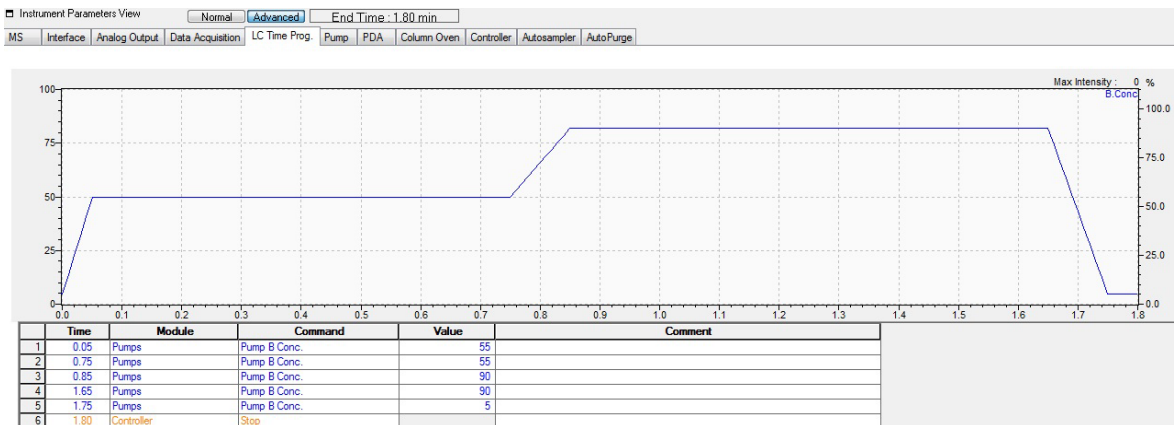


Mass spectrum parameters

Start Time (min)	End Time (min)	Acquisition Mode	Polarity	Event Time (sec)	SIM m/z	Scan Speed	Detector Volt. Mode	Detector Volt. (kV)	Micro Scan(u)	Interface Volt. Mode	DL Volt. Mode	Qarray DC Mode	Qarray RF Mode	
1	0	1.8	SIM	Positive	0.02	274.00,244.00	15000	Relative to the Tuning Result	0	0	Tuning File	Default(IV)	Default(IV)	Tuning F

4-Phenyl-1-(4-(trifluoromethyl)phenyl)piperidine, 316

LCMS mobile phase assay graph



Mass spectrum parameters

Instrument Parameters View Normal **Advanced** End Time : 1.80 min

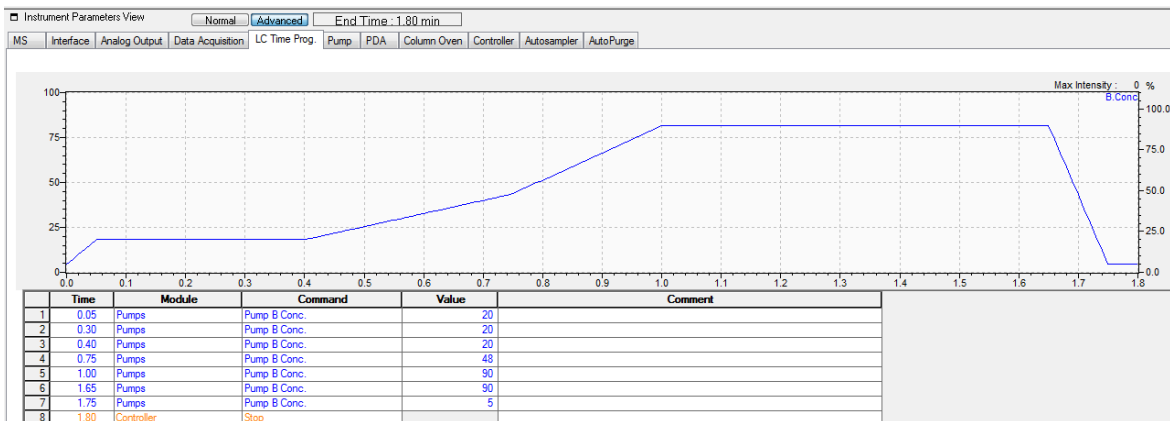
MS Interface Analog Output Data Acquisition LC Time Prog. Pump PDA Column Oven Controller Autosampler AutoPurge

Segment#1

Start Time (min)	End Time (min)	Acquisition Mode	Polarity	Event Time (sec)	SIM m/z	Scan Speed	Detector Volt. Mode	Micro Scan(s)	Interface Volt. Mode	DL Volt. Mode	Qarray DC Mode	Qarray RF Mode	
1	0	1.8	SIM	Positive	0.02	274.00.306.00	15000	Relative to the Tuning Result	0	Tuning File	Default (0V)	Default (0V)	Tuning File

1-(3,4-Dimethoxyphenyl)-4-phenylpiperidine, 425

LCMS mobile phase assay graph



Mass spectrum parameters

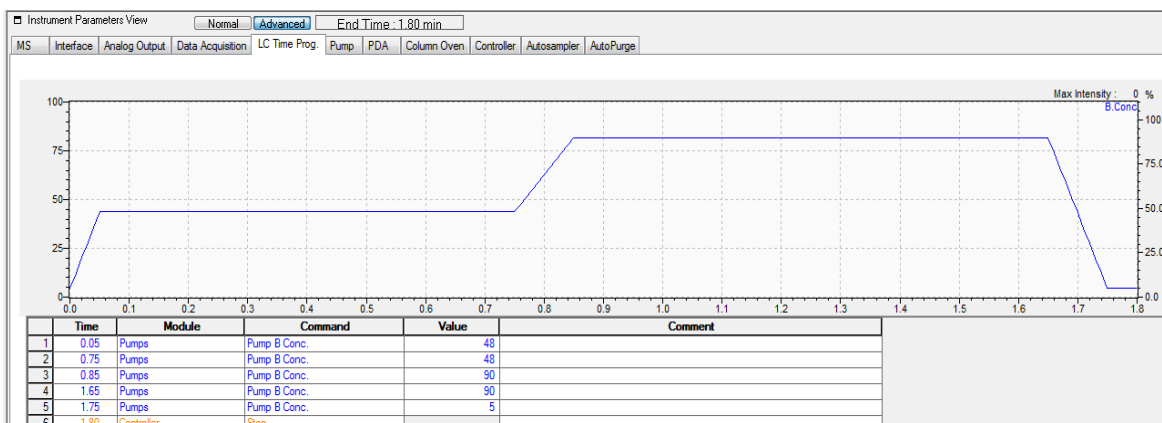
MS Interface Analog Output Data Acquisition LC Time Prog. Pump PDA Column Oven Controller Autosampler AutoPurge

Segment#1

Start Time (min)	End Time (min)	Acquisition Mode	Polarity	Event Time (sec)	SIM m/z	Scan Speed	Detector Volt. Mode	Detector Volt. (kV)	Micro Scan(s)	Interface Volt. Mode	DL Volt. Mode	Qarray DC Mode	Qarray RF Mode
1	0	1.8	SIM	Positive	0.02	274.00.298.00	15000	Relative to the Tuning Result	0	Tuning File	Default (0	Default (Tuning File

1-(3,5-Dimethylphenyl)-4-phenylpiperidine, 420

LCMS mobile phase assay graph

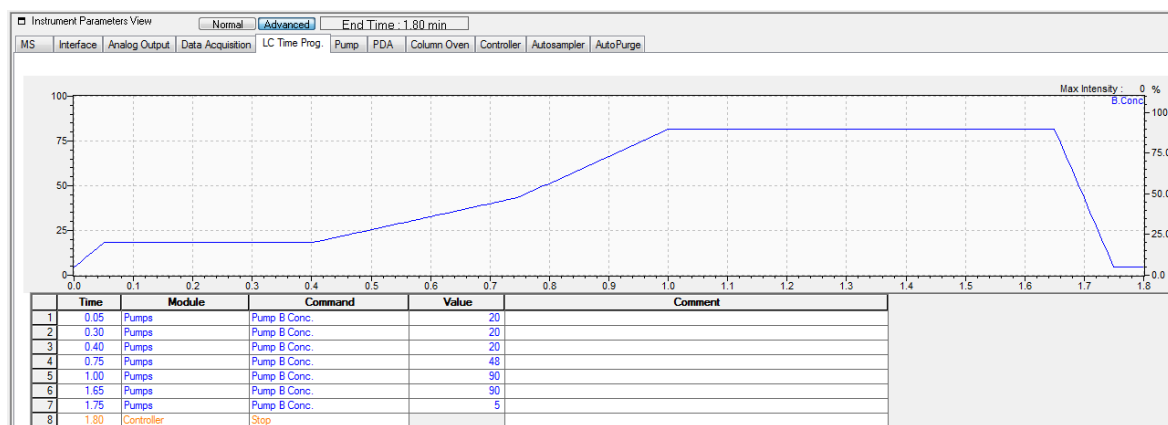


Mass spectrum parameters

Start Time (min)	End Time (min)	Acquisition Mode	Polarity	Event Time (sec)	SIM m/z	Scan Speed	Detector Volt. Mode	Detector Volt. (kV)	Micro Scan(s)	Interface Volt. Mode	DL Volt. Mode	Qarray DC Mode	Qarray RF Mode	
1	0	1.8	SIM	Positive	0.02	274.00,296.00	15000	Relative to the Tuning Res	0	0	Tuning File	Default (0V)	Default (0V)	Tuning File

4-Phenyl-1-(3-(trifluoromethoxy)phenyl)piperidine, 426

LCMS mobile phase assay graph

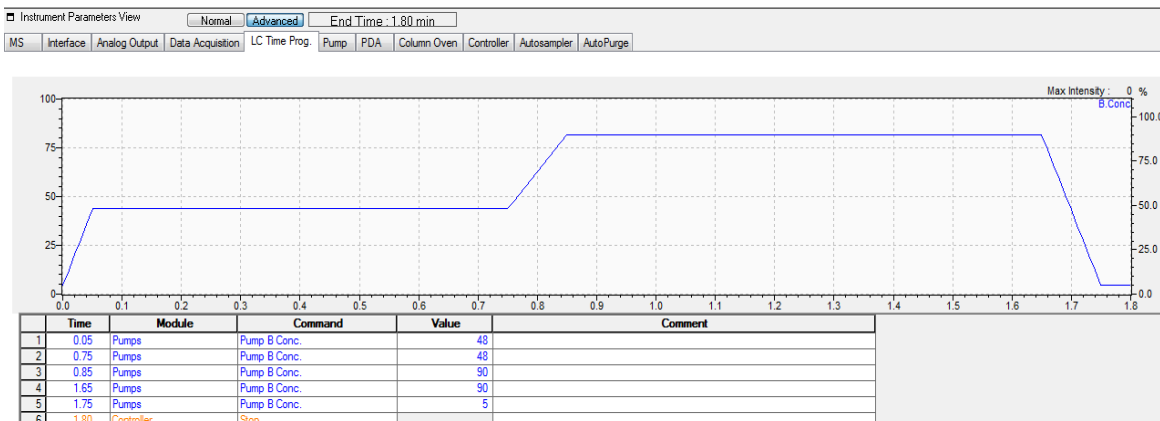


Mass spectrum parameters

Start Time (min)	End Time (min)	Acquisition Mode	Polarity	Event Time (sec)	SIM m/z	Scan Speed	Detector Volt. Mode	Detector Volt. (kV)	Micro Scan(s)	Interface Volt. Mode	DL Volt. Mode	Qarray DC Mode	Qarray RF Mode	
1	0	1.8	SIM	Positive	0.02	274.00,322.00	15000	Relative to the Tuning Result	0	0	Tuning File	Default (0)	Default (0)	Tuning File

4-Phenyl-1-(3-(trifluoromethyl)phenyl)piperidine, 419

LCMS mobile phase assay graph



Mass spectrum parameters

Instrument Parameters View: Normal | **Advanced** | End Time: 1.80 min

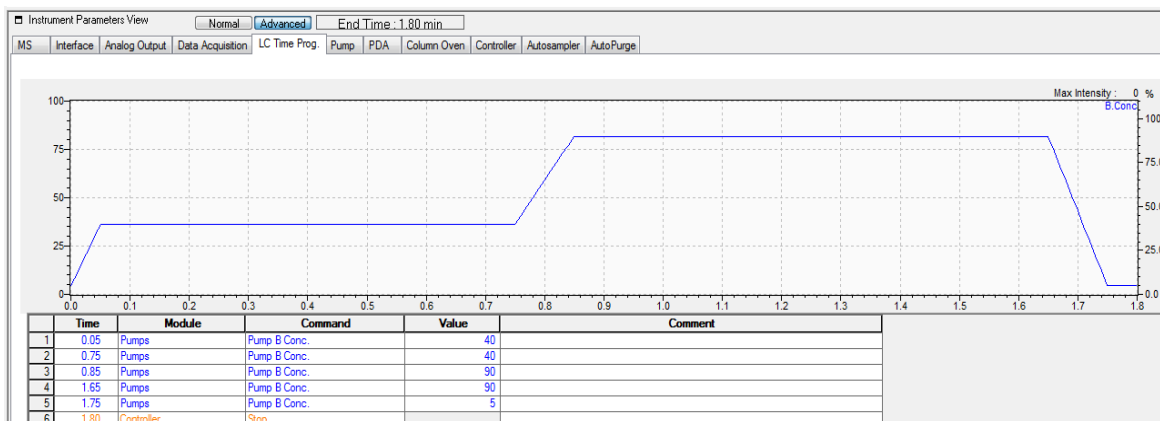
MS | Interface | Analog Output | Data Acquisition | LC Time Prog. | Pump | PDA | Column Oven | Controller | Autosampler | AutoPurge

Segment#1

Start Time (min)	End Time (min)	Acquisition Mode	Polarity	Event Time (sec)	SIM m/z	Scan Speed	Detector Volt. Mode	Detector Volt. (kV)	Micro Scan(s)	Interface Volt. Mode	DL Volt. Mode	Qarray DC Mode	Qarray RF Mode	
1	0	1.8	SIM	Positive	0.02	274.00,306.00	15000	Relative to the Tuning Result	0	0	Tuning File	Default (0V)	Default (0V)	Tuning File

N,N-Dimethyl-4-(4-phenylpiperidin-1-yl)benzamide, 438

LCMS mobile phase assay graph



Mass spectrum parameters

Instrument Parameters View: Normal | **Advanced** | End Time: 1.80 min

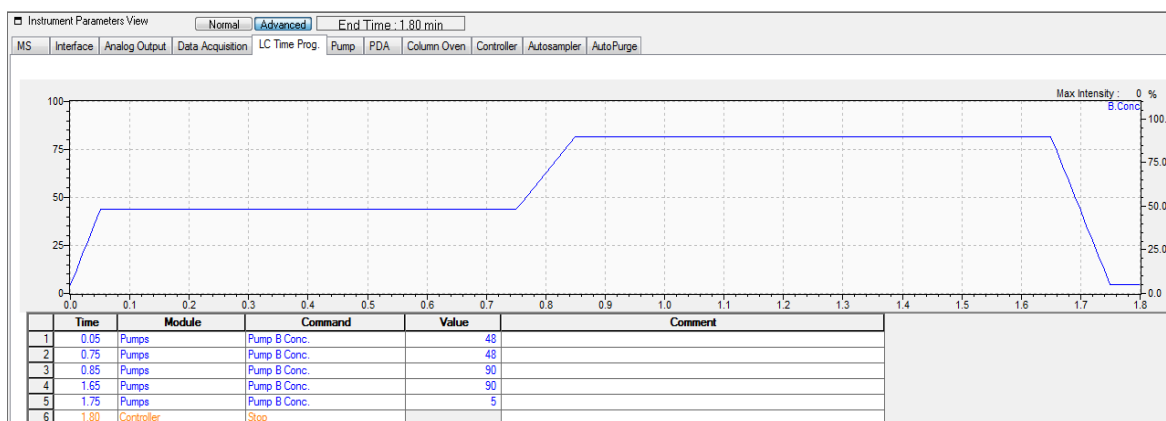
MS | Interface | Analog Output | Data Acquisition | LC Time Prog. | Pump | PDA | Column Oven | Controller | Autosampler | AutoPurge

Segment#1

Start Time (min)	End Time (min)	Acquisition Mode	Polarity	Event Time (sec)	SIM m/z	Scan Speed	Detector Volt. Mode	Detector Volt. (kV)	Micro Scan(s)	Interface Volt. Mode	DL Volt. Mode	Qarray DC Mode	Qarray RF Mode	
1	0	1.8	SIM	Positive	0.02	274.00,309.00	15000	Relative to the Tuning Result	0	0	Tuning File	Default (0)	Default (0V)	Tuning File

1-(2-Fluorophenyl)-4-phenylpiperidine, 434

LCMS mobile phase assay graph



Mass spectrum parameters

Instrument Parameters View: Normal (Advanced) End Time: 1.80 min

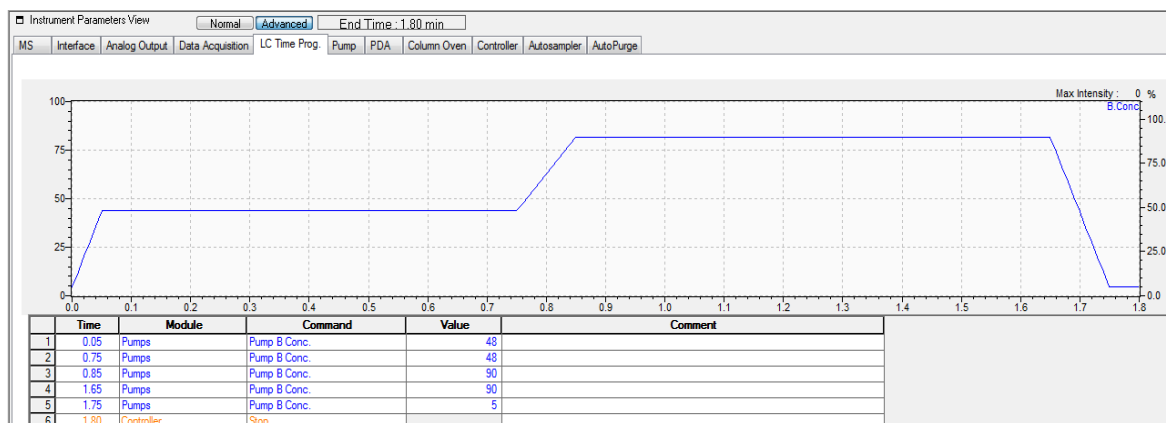
MS Interface Analog Output Data Acquisition LC Time Prog Pump PDA Column Oven Controller Autosampler AutoPurge

Segment#1

Start Time (min)	End Time (min)	Acquisition Mode	Polarity	Event Time (sec)	SIM m/z	Scan Speed	Detector Volt. Mode	Interface Volt. Mode	DL Volt. Mode	Qarray DC Mode	Qarray RF Mode	
1	0	1.8	SIM	Positive	0.02	274.00,256.00	15000	Relative to the Tuning Result	Tuning File	Default (0V)	Default (0V)	Tuning File

1-(2-Chlorophenyl)-4-phenylpiperidine, 433

LCMS mobile phase assay graph



Mass spectrum parameters

Instrument Parameters View: Normal (Advanced) End Time: 1.80 min

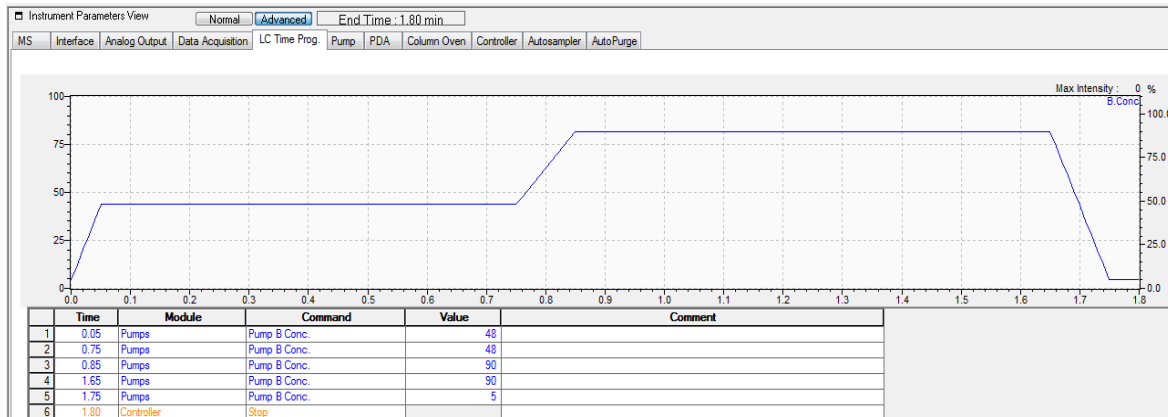
MS Interface Analog Output Data Acquisition LC Time Prog Pump PDA Column Oven Controller Autosampler AutoPurge

Segment#1

Start Time (min)	End Time (min)	Acquisition Mode	Polarity	Event Time (sec)	SIM m/z	Scan Speed	Detector Volt. Mode	DL Volt. Mode	Qarray DC Mode	Qarray RF Mode	
1	0	1.8	SIM	Positive	0.02	274.00,272.00	15000	Relative to the Tuning Result	Default (0V)	Default (0V)	Tuning File

4-Phenyl-1-(o-tolyl)piperidine, 432

LCMS mobile phase assay graph

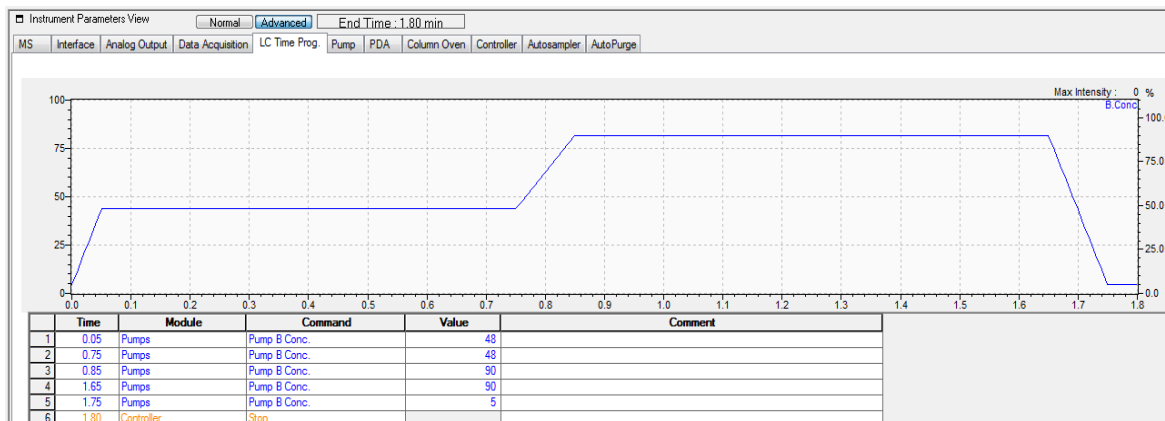


Mass spectrum parameters

Start Time (min)	End Time (min)	Acquisition Mode	Polarity	Event Time (sec)	SIM m/z	Scan Speed	Detector Volt. Mode	Interface Volt. Mode	DL Volt. Mode	Qarray DC Mode	Qarray RF Mode
1	0	1.8 SIM	Positive	0.02	274.00,252.00	15000	Relative to the Tuning Result	Tuning File	Default (0V)	Default (0V)	Tuning File

1-(2-Methoxyphenyl)-4-phenylpiperidine, 435

LCMS mobile phase assay graph

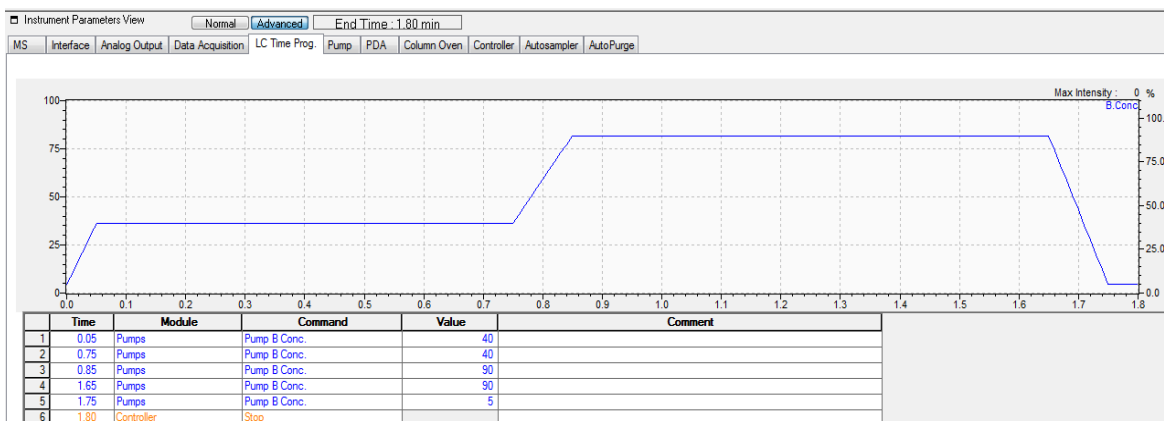


Mass spectrum parameters

Start Time (min)	End Time (min)	Acquisition Mode	Polarity	Event Time (sec)	SIM m/z	Scan Speed	Detector Volt. Mode	Interface Volt. Mode	DL Volt. Mode	Qarray DC Mode	Qarray RF Mode
1	0	1.8 SIM	Positive	0.02	274.00,268.00	15000	Relative to the Tuning Result	Tuning File	Default (0V)	Default (0V)	Tuning File

N-Methyl-N-(4-(4-phenylpiperidin-1-yl)phenyl)acetamide, 440

LCMS mobile phase assay graph



Mass spectrum parameters

Instrument Parameters View: Normal | **Advanced** | End Time: 1.80 min

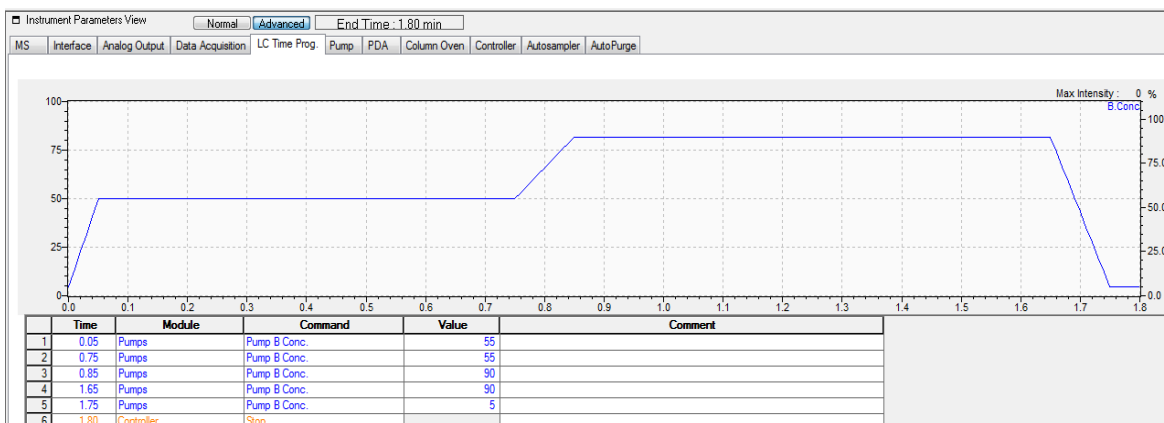
MS | Interface | Analog Output | Data Acquisition | LC Time Prog. | Pump | PDA | Column Oven | Controller | Autosampler | AutoPurge

Segment#1

Start Time (min)	End Time (min)	Acquisition Mode	Polarity	Event Time (sec)	SIM m/z	Scan Speed	Detector Volt. Mode	Interface Volt. Mode	DL Volt. Mode	Qarray DC Mode	Qarray RF Mode	
1	0	1.8	SIM	Positive	0.02	274.00,309.00	15000	Relative to the Tuning Result	Tuning File	Default (0V)	Default (0V)	Tuning File

1-Benzyl-5-(4-phenylpiperidin-1-yl)-1H-indazole, 429

LCMS mobile phase assay graph



Mass spectrum parameters

Instrument Parameters View: Normal | **Advanced** | End Time: 1.80 min

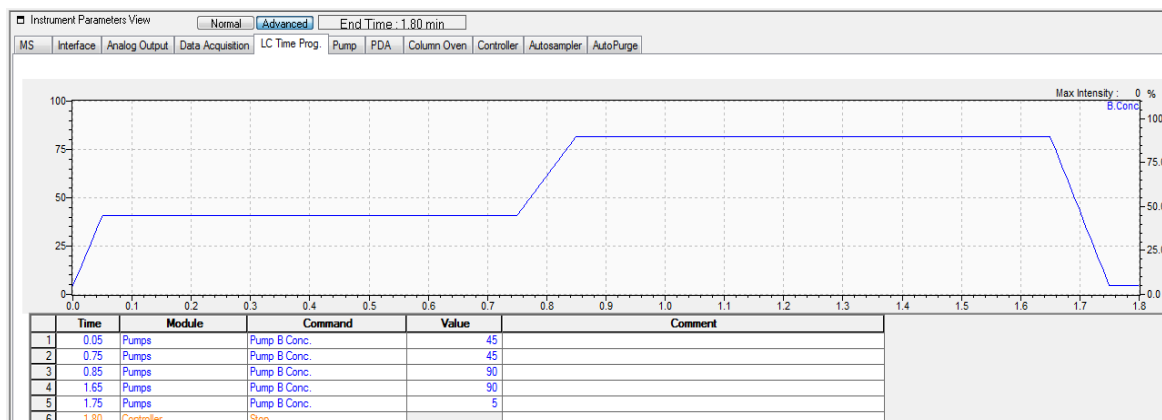
MS | Interface | Analog Output | Data Acquisition | LC Time Prog. | Pump | PDA | Column Oven | Controller | Autosampler | AutoPurge

Segment#1

Start Time (min)	End Time (min)	Acquisition Mode	Polarity	Event Time (sec)	SIM m/z	Scan Speed	Detector Volt. Mode	Detector Volt. (kV)	Micro Scan(s)	Interface Volt. Mode	DL Volt. Mode	Qarray DC Mode	Qarray RF Mode	
1	0	1.8	SIM	Positive	0.02	274.00,368.00	15000	Relative to the Tuning Result	0	0	Tuning File	Default	Default(0)	Tuning File

1-Benzyl-5-(4-phenylpiperidin-1-yl)-1H-pyrrolo[2,3-b]pyridine, 430

LCMS mobile phase assay graph

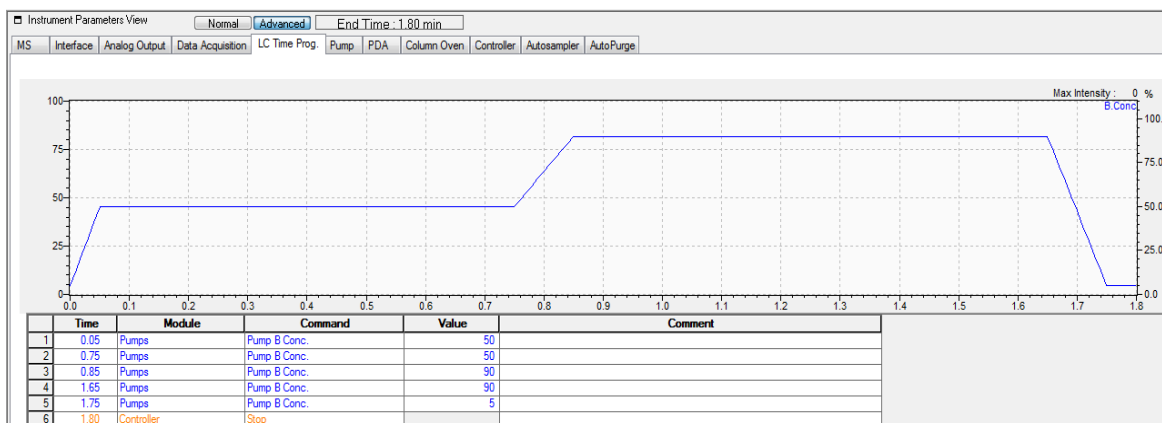


Mass spectrum parameters

Start Time (min)	End Time (min)	Acquisition Mode	Polarity	Event Time (sec)	SIM m/z	Scan Speed	Detector Volt. Mode	Detector Volt. (kV)	Micro Scan(s)	Interface Volt. Mode	DL Volt. Mode	Qarray DC Mode	Qarray RF Mode	
1	0	1.8	SIM	Positive	0.02	274.00,368.00	15000	Relative to the Tuning Result	0	0	Tuning File	Default(0)	Default(0)	Tuning File

Ethyl 2-nitro-5-(4-phenylpiperidin-1-yl)benzoate, 436

LCMS mobile phase assay graph

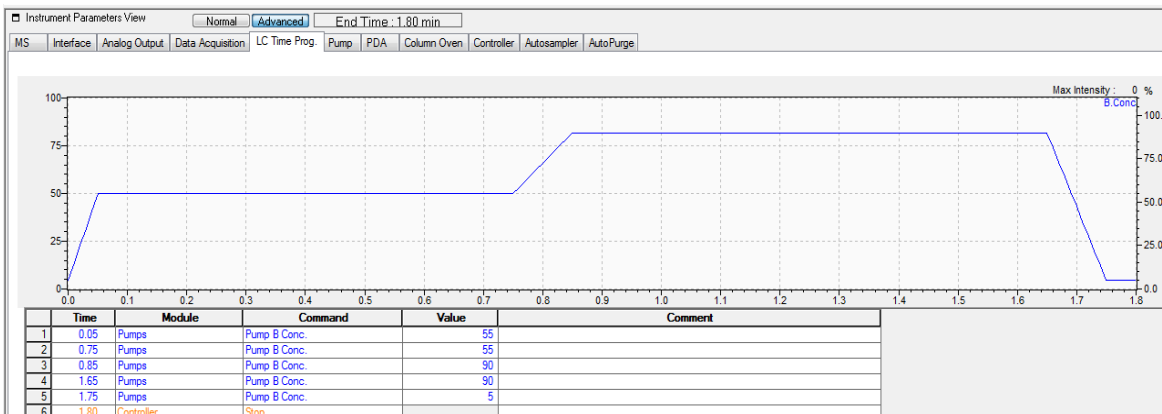


Mass spectrum parameters

Start Time (min)	End Time (min)	Acquisition Mode	Polarity	Event Time (sec)	SIM m/z	Scan Speed	Detector Volt. Mode	Interface Volt. Mode	DL Volt. Mode	Qarray DC Mode	Qarray RF Mode	
1	0	1.8	SIM	Positive	0.02	274.00,365.00	15000	Relative to the Tuning Res	Tuning File	Default(IV)	Default(IV)	Tuning File

Ethyl 5-(4-phenylpiperidin-1-yl)-2-(trifluoromethyl)benzoate, 437

LCMS mobile phase assay graph



Mass spectrum parameters

Instrument Parameters View Normal **Advanced** End Time: 1.80 min

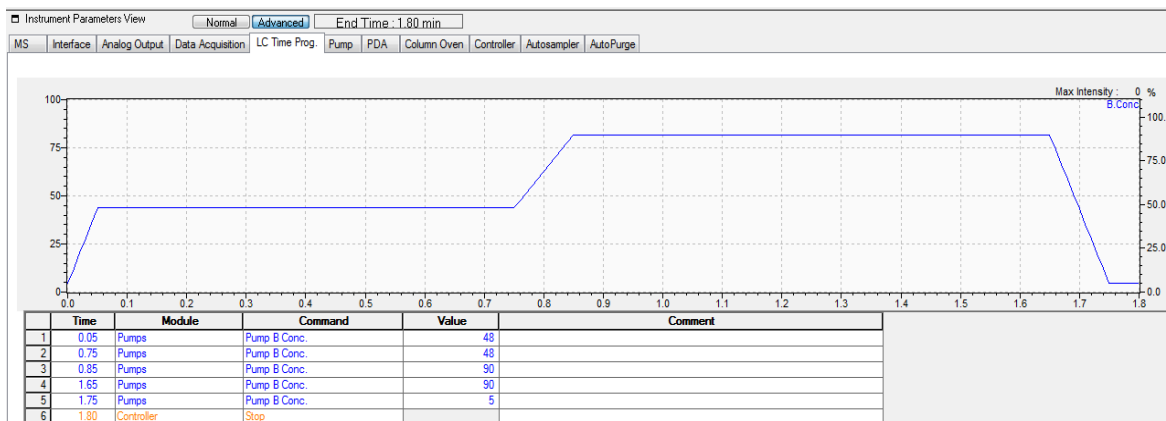
MS Interface Analog Output Data Acquisition LC Time Prog Pump PDA Column Oven Controller Autosampler AutoPurge

Segment#1

Start Time (min)	End Time (min)	Acquisition Mode	Polarity	Event Time (sec)	SIM m/z	Scan Speed	Detector Volt. Mode	Interface Volt. Mode	DL Volt. Mode	Qarray DC Mode	Qarray RF Mode
1	0	1.8 SIM	Positive	0.02	274.00,378.00	15000	Relative to the Tuning Result	Tuning File	Default (0V)	Default (0V)	Tuning File

Ethyl 2-methoxy-5-(4-phenylpiperidin-1-yl)benzoate, 422

LCMS mobile phase assay graph



Mass spectrum parameters

Instrument Parameters View Normal **Advanced** End Time: 1.80 min

MS Interface Analog Output Data Acquisition LC Time Prog Pump PDA Column Oven Controller Autosampler AutoPurge

Segment#1

Start Time (min)	End Time (min)	Acquisition Mode	Polarity	Event Time (sec)	SIM m/z	Scan Speed	Detector Volt. Mode	Detector Volt (kV)	Micro Scan(s)	Interface Volt. Mode	DL Volt. Mode	Qarray DC Mode	Qarray RF Mode
1	0	1.8 SIM	Positive	0.02	274.00,340.00	15000	Relative to the Tuning Result	0	0	Tuning	Default (0V)	Default (0V)	Tuning File